ASB American Society of Biomechanics

FOUNDED IN 1977

ABSTRACT BOOK

ASB Annual Meeting

AUGUST 13 - 16 2025

David L. Lawrence Convention Center **Pittsburgh, PA**

www.asbweb.org

#ASB2025

THE IMPACT OF CARPOMETACARPAL OSTEOARTHRITIS ON THUMB-TIP FORCE, MOVEMENT-EVOKED PAIN, AND SELF-REPORTED DISABILITY

*Troy F. Kelly Jr[1], Benjamin J. Nowak[1], Alexis R. Benoit[1], Jessica E. Molina[1], Victor E. Akpaloo[1], Jennifer A. Nichols[1]
[1]J. Crayton Pruitt Family Department of Biomedical Engineering, University of Florida, Gainesville, FL
*troy.kelly@ufl.edu

Introduction: Functional impairments are commonly assessed using both biomechanical and clinical measures.[1] For example, when examining hand pathologies, such as carpometacarpal osteoarthritis (CMC OA), thumb-tip force is a biomechanical measure that evaluates strength, while the Disabilities of the Arm, Shoulder, and Hand (DASH) questionnaire is a clinical measure that captures self-reported disability.[2] Importantly, both biomechanical and clinical measures are evaluated in the context of activities of daily living (ADLs). Quantified strength deficits are interpreted in the context of whether the generated thumb-tip force is sufficient for ADLs, such as grasping a jar, inserting and removing keys (key pinch task), and picking up coins (tip pinch task). Similarly, the DASH explicitly asks questions associated with how difficult it is to perform ADLs. Unfortunately, ADLs can evoke pain in individuals suffering from CMC OA. How chronic and acute pain influence biomechanical and clinical measures of function is not well understood in the context of CMC OA. As a step toward filling this gap, we examined how severity of CMC OA (defined as early- vs. late-stage) influences maximum thumb-tip force, movement-evoked pain (MEP), and self-reported disability. We also explored the interaction between these variables and conducted a secondary analysis to assess how acute pain from fine-wire electromyography (EMG) influenced our findings.

Methods: To date, this IRB-approved study includes 20 participants across three cohorts defined by radiographic severity: healthy (n = 5), early-stage CMC OA (n = 4), and late-stage CMC OA (n = 11). Each participant completed 9 tasks. This analysis focuses on three: tip pinch, key pinch, and jar grasp. The complete task set was performed twice, once prior to placement of any sensors (termed pre-insertion) and once following placement of motion capture markers and fine-wire EMG in 8 thumb muscles (termed post-insertion). Participants reported MEP ratings before, during, and after each task using a 101-point visual analog scale (VAS). Participants also completed a comprehensive clinical battery, including the DASH questionnaire, which measures the level of disability related to musculoskeletal disorders affecting the upper limb on a scale from 0 to 100, where higher scores indicate greater disability. ANOVAs were used to separately explore the relationship between DASH scores and MEP ratings, cohort and MEP ratings, and cohort and force. Paired t-tests were used to identify significant differences in thumb-tip force or MEP ratings between pre- and post-insertion.

Results & Discussion: When examining thumb-tip force, observed trends differ when examining pre- versus post-insertion data (Fig. 1A). Notably, individuals with early-stage CMC OA produced the largest thumb-tip force pre-insertion, while individuals with end-stage CMC OA produced the largest force post-insertion. Increased force during pre-insertion tasks in early-stage CMC OA may suggest heightened neuromuscular activity and compensatory stabilization, while individuals with late-stage CMC OA may exert high forces both pre- and post-insertion due to neuropathic adaptation, reduced sensory feedback, and/or desensitization.

Differences in MEP ratings between individuals with early- versus late-stage CMC OA held regardless of task or insertion status (Fig. 1B). With the exception of healthy individuals' pre-insertion who reported no pain, individuals with late-stage CMC OA reported the lowest MEP ratings across all tasks. MEP ratings between pre- and post-insertion were significantly different for the healthy cohort but not for either CMC OA cohort. This suggests that CMC OA pain is the dominant factor modulating MEP for individuals with CMC OA, whereas the needle insertion modulated the pain experience of the healthy controls. Specifically, pre/post-insertion MEP changes in healthy controls were >4, while within the CMC OA groups, the difference in magnitude was ~2. This finding may reflect neuropathic adaptation or a reduction in sensory feedback in CMC OA.

The analysis of before-task MEP ratings in relation to DASH scores revealed a significant relationship, indicating that higher baseline pain levels contribute to greater self-reported functional impairment (DASH scores: healthy 9.0±12.9, early-stage 22.5±18.0, late-stage 13.3±16.6). The significant relationship held across all tasks ($p<0.05$), suggesting that baseline (or chronic) pain plays a crucial role in disability severity. No significant relationships were found between force and cohort, indicating that force-generating ability is preserved in individuals with CMC OA. Together, these findings suggest that participants may be functionally limiting themselves due to pain rather than deficits in strength. Thus, biomechanical measures alone may not fully capture self-reported disability in CMC OA.

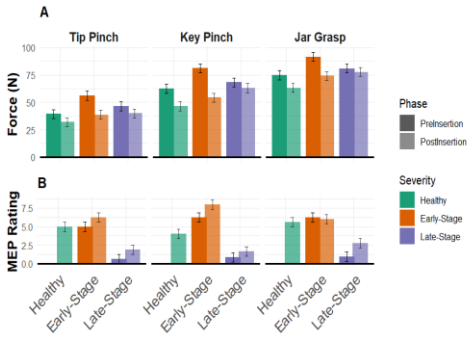

Figure 1: Bar plots showing average (b) thumb-tip force and (b) movement-evoked pain rating. Three functional tasks are shown for healthy (green), early- (orange), and late-stage (purple) cohorts pre- (dark shading) and post- (light shading) insertion.

Significance: This study highlights the importance of assessing pain and disability in the CMC OA population to contextualize biomechanical measures. Additionally, it highlights the need for caution when interpreting force data from fine wire EMG studies, particularly when comparing pre- and post-insertion measurements.

Acknowledgments: Funding from the National Institutes of Health (R01 AR078817) is gratefully acknowledged.

References: [1] Davis et al. (2022), *Osteoarthritis and Cartilage* 30(6):775-785; [2] Gillis et al. (2011), *Can J Plast Surg.* 2011;19(4):134-138

THE RELATIONSHIP BETWEEN 3D SCAPULAR MORPHOLOGY AND GLENOHUMERAL OSTEOARTHRITIS

*Rebekah L. Lawrence,[1,2] Lindsey G. Kahan,[2] Jay D. Keener,[2] Alexander Aleem[2]; Benjamin M. Zmistowski[2]
[1]Program in Physical Therapy, Washington University School of Medicine, St. Louis, MO, USA
[2]Department of Orthopaedic Surgery, Washington University School of Medicine, St. Louis, MO, USA
*Corresponding author's email: r.lawrence@wustl.edu

Introduction: Glenohumeral osteoarthritis (GH OA) is prevalent and, as total shoulder arthroplasty (TSA) has become more widely utilized, surgeons are recognizing different patterns of GH OA that may influence surgical outcomes. Specifically, Walch et al. defined subtypes of GH OA based on glenoid wear patterns with symmetric wear classified as concentric OA (Walch A glenoids), while asymmetric posterior wear classified as eccentric OA (Walch B glenoids) [1]. Although the etiology of eccentric GH OA remains unclear, acromial morphology has been implicated as a potential contributor [2] and has led to the development of corrective osteotomies [3]. However, acromial morphology calculations informing these procedures use the glenoid as a base of reference, which may be confounded by joint degenerative changes. Therefore, our purpose was to assess the relationship between scapular morphology and GH OA patterns using 3D morphology analysis and a scapular reference frame less likely to be confounded by joint degeneration.

Methods: Patients were retrospectively included if they had symptomatic GH OA, were being evaluated for TSA, had in intact rotator cuff, and had a pre-operative CT scan that included the full scapula (n=98, 65±9 years, 26% female). The Walch criteria was used to classify patients into concentric OA (COA) or eccentric OA (EOA) groups [1,4]. A control group consisted of participants from an ongoing study who did not have GH OA (per CT) or a rotator cuff tear (per ultrasound) (n=40, 55±3 years, 65% female). Scapular morphology was calculated on CT-derived 3D bone models as follows. First, a scapular reference frame was defined based on landmarks on the scapular body unlikely to be affected by degenerative changes (juncture of scapular spine and medial border, spinoglenonid notch, inferior angle) [5]. Second, the 3D anatomical axes of the acromion and glenoid were defined via principal components [5]. Third, acromial sagittal, coronal, and axial tilt and glenoid inclination and version were calculated by relating the axes of the acromion or glenoid, respectively, to the scapular reference frame. The lateral acromial ratio was calculated as the ratio of the width of the lateral acromion and scapular body. Anterior and posterior acromial coverage was calculated as the degree of acromial extension relative to the glenoid center [2]. Finally, morphology was compared between groups using ANCOVA to adjust for group differences in sex.

Results & Discussion: Of the 98 patients with GH OA, 26 were classified as having COA and 72 were classified as having EOA. Significant differences in glenoid morphology were observed between groups, particularly between patients with EOA and healthy controls (Table). Specifically, the glenoid in patients with EOA was oriented an average (±SE) of 14.9° ± 1.6° more posterior (i.e., retroverted) compared to patients with COA ($p<0.01$) and 15.0°±1.4° more posterior compared to than healthy controls ($p<0.01$). These findings are consistent with what would be expected based on the Walch classification [1]. Further, the glenoid was 4.4°±1.7° more inferiorly oriented in patients with EOA compared to those with COA, and both groups had a more inferiorly oriented glenoid compared to controls ($p\leq0.03$). Significant group differences in acromial morphology were also observed (Table 1). Specifically, the acromion was 6.9°±1.6° flatter in the sagittal plane (i.e., sagittal tilt) in patients with EOA compared to healthy controls ($p<0.01$), while no differences were found between groups in coronal or axial tilt. The acromion in patients with EOA extended less laterally compared to those with COA and healthy controls (lower lateral acromial ratio; $p<0.01$). Regardless of classification, the acromion in patients with GH OA extended less posteriorly than healthy controls (lower posterior acromial coverage; $p<0.01$). Ultimately, the use of a scapular reference frame resulted in less pronounced differences in acromial morphology than what has been previously reported [2]. Although still unclear, the variations in acromial morphology associated with EOA may alter the line of action of the deltoid [6] and prevent posterior humeral escape [2].

Variable	COA (Walch A) (n=26)	EOA (Walch B) (n=72)	Controls (n=40)	ANCOVA p-value
Glenoid version	-3.2° ± 1.4° (a)	-18.1° ± 0.9° (b)	-3.1° ± 1.1° (a)	<0.01
Glenoid inclination	-4.1° ± 1.5° (a)	-8.5° ± 0.9° (b)	1.3° ± 1.2° (c)	<0.01
Anterior coverage	7.2° ± 1.6°	7.8° ± 1.0°	7.3° ± 1.3°	0.94
Posterior coverage	55.7° ± 1.4° (a)	55.3° ± 0.8° (a)	62.7° ± 1.1° (b)	<0.01
Overall coverage	62.9° ± 1.3° (a)	63.0° ± 0.8° (a)	70.1° ± 1.0° (b)	<0.01
Acromial sagittal tilt	68.2° ± 1.6° (ab)	71.3° ± 1.0° (a)	64.4° ± 1.2° (b)	<0.01
Acromial coronal tilt	75.8° ± 1.9°	79.4° ± 1.2°	78.5° ± 1.5°	0.26
Acromial axial tilt	26.2° ± 1.8°	25.5° ± 1.1°	22.5° ± 1.4°	0.19
Lateral acromial ratio	31.5% ± 1.0% (a)	27.5% ± 0.6% (b)	31.1% ± 0.8% (a)	<0.01

Table: Comparison of scapular morphology variables between groups. Data are presented as adjusted means ± standard error. Letters are used to indicate significant differences between groups within a variable (i.e., groups within a row that share the same letter are not statistically different).

Significance: EOA appears to represent a distinct morphological phenotype characterized by a shorter, flatter acromion and significant glenoid retroversion. EOA is associated with higher complication rates after shoulder arthroplasty [6]; thus, understanding the factors associated with EOA may help inform the development of more robust surgical techniques and conservative prevention strategies.

Acknowledgments: The investigation that provided data for the healthy control group was funded by the NIH (K99/R00-AR075876).

References: [1] Walch et al., *J Arthroplasty*, 1999;14(6); [2] Beeler et al., *J Shoulder Elbow Surg,* 2018;27(12); [3] Gerber et al., *J Bone Joint Surg Cases*, 2023;13(2); [4] Bercik et al., *J Shoulder Elbow Surg, 2*016;25(10); [5] Lawrence et al., *J Orthop Res*, 2024;42(3); [6] Viehöfer et al., *J Orthop Res*, 2016;34(6); [7] Iannotti et al., *J Bone Joint Surg*, 2003;85(2).

MUSCLE AND ADIPOSE ELASTIC MODULUS FOLLOWING ELECTIVE TOTAL HIP ARTHROPLASTY

Alyssa M. Tondat[1], Emiko Arshard[1], Sheryl Bourgaize[1], Marina Mourtzakis[1], Tina Mah[2], Matthew Snider[3], Paul Grosso[3], Brandon Girardi[3], Oliver Gauthier-Kwan[3], Stephanie Nemirov[3], Carla Girolametto[3], Kailyn Clarke[3], & Andrew C. Laing[1*]
[1]Department of Kinesiology and Health Sciences, University of Waterloo, Waterloo, ON, Canada. [2] Schlegel-UW Research Institute for Aging, Waterloo, ON, Canada. [3]Grand River Hospital, Kitchener, ON, Canada
*Corresponding author's email: actlaing@uwaterloo.ca

Introduction: Total Hip Arthroplasty (THA) is an orthopedic procedure to improve pain, mobility, and quality of life in people with hip osteoarthritis (OA) [1]. There is a loss of muscle strength in people with OA [2], and muscle strength improves following THA [3]. However, there is limited evidence on how THA affects the mechanical properties of local soft tissues. These mechanical properties are important to consider as they have implications for post-operative recovery and functional outcomes, and also influence impact dynamics during falls on the hip. Accordingly, the primary objective of this research was to determine the influence of elective THA on shear wave elastography (SWE) measured elastic modulus (E, a metric of resistance to deformation under applied stress) of the muscle and adipose tissues over the lateral proximal femur. Based on the premise that E is more modifiable for active contractile vs. passive tissues, it was hypothesized that muscle E would increase following surgery while there would be no changes in adipose E following THA. The secondary objective was to qualitatively examine changes in muscle and adipose tissue morphology pre- versus post-elective THA.

Methods: Ten adults (4 females) aged 66.2 ± 8.7 years participated. Ultrasound (GE LOGIQ E10 with a L2-9VN-D linear array transducer) obtained SWE measurements of muscle and adipose E from the surgical and non-surgical limbs of participants at three time points (within one week prior to THA, 6 weeks post THA, and 6 months post THA). Measurements were taken directly over the greater trochanter (GT), and at a location 3 cm posterior and 6 cm distal to the GT (location of peak pressure during a lateral fall [4]), called PD). As appropriate based on normality of data, one-way repeated measures ANOVAs with post-hoc pairwise comparisons (or Friedman ANOVA with post-hoc Wilcoxon signed rank tests) were performed for each tissue at each location.

Results & Discussion: *Adipose.* In the surgical limb, adipose E at the GT location was significantly greater following THA ($Q = 9.8$, $p = 0.007$), with E being 45.7% greater 6 weeks and 56.2% 6 months post-surgery (both $p < 0.05$) (Figure 1). In contrast, there was no significant changes in adipose E at the PD location ($F = 0.743$, $p = 0.49$). *Muscle.* There were no significant differences in muscle E across time points in either limb (all $p > 0.05$). However, there was a trend of decreasing muscle E post-THA in the non-surgical limb (Figure 1). Qualitative analysis of ultrasound B-mode images revealed substantial tissue-level changes following THA over the GT, but not over the PD location in the surgical limb. These changes include alterations in the appearance of the subcutaneous fat tissues and the presence of edema.

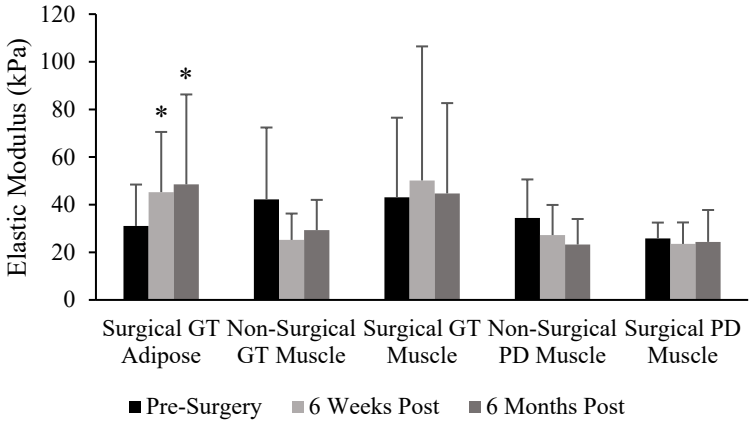

Figure 1: Elastic modulus (E) of muscle and adipose at the greater trochanter (GT) and posterior-distal (PD) locations before surgery, 6 weeks post-surgery, and 6 months post-surgery in the surgical and non-surgical limbs. * indicates significant changes from pre-surgery values.

There are several possible explanations for these findings. The increase in adipose E over the GT in the surgical limb is likely due to direct consequences of the surgical processes including edema and scar tissue. In retrospect, the lack of changes in surgical limb muscle E are perhaps not surprising. While E derived from shear wave elastography has been shown to increase in response to increased muscle activation, it has not been validated as a metric of muscle functional capacity. Despite this, the trends of decreasing muscle E in the non-surgical limb following THA are intriguing and may be indicative of more balanced muscle recruitment patterns across limbs following surgery. Ongoing work is assessing whether these soft tissue properties, derived from ultrasound (an accessible, well-tolerated imaging modality), are associated with functional outcomes including pain and mobility post-THA.

Significance: This is the first study to evaluate changes in soft tissue elastic modulus (E) following THA. As the changes in adipose E over the surgical site correspond to qualitative morphological changes, there is potential value in ultrasound SWE as a tool to quantify post-surgical tissue alterations. The trend towards more equivalent PD muscle E across limbs following THA may suggest more symmetrical muscle utilization patterns and capacity – this has implications for both prehabilitation and rehabilitation programs. There is value in further research to evaluate soft tissue properties beyond 6-month post-THA, whether these changes influence impact attenuation in the event of a fall, and whether E derived from ultrasound SWE is associated with muscle capacity and functional outcomes post-THA.

Acknowledgments: Funding provided by Ontario Ministry of Health / Natural Sciences Engineering Research Council of Canada.

References: [1] CIHI (2022). Hip and Knee Replacements in Canada: CJRR Annual Report; [2] Loureiro et al. (2018), *BMC Musculoskelet Disord* 19(1):303; [3] Winther et al. (2019), *HIP Int* 29(4):405-411; [4] Choi et al. (2010), *Clin Biomech* 25(1):63-69.

BIOFEEDBACK MODIFIES LOWER EXTREMITY LOADING WITHOUT INCREASED PAIN IN PATIENTS WITH KNEE OSTEOARTHRITIS

*Elizabeth Bjornsen[1], Todd A. Schwartz[2], Brian Pietrosimone[3], Jason R. Franz[1]
[1]Lampe Joint Department of Biomedical Engineering, University of North Carolina at Chapel Hill and North Carolina State University
[2]Department of Biostatistics, Gillings School of Global Public Health, University of North Carolina at Chapel Hill
[3]Department of Exercise and Sport Science, University of North Carolina at Chapel Hill
*Corresponding author's email: ebjornse@email.unc.edu

Introduction: Knee osteoarthritis (KOA) patients exhibit maladaptive limb-level loading during walking [1], with vertical ground reaction force (vGRF) profiles worsening as the disease-state progresses [2,3]. Standard of care rehabilitation protocols for KOA patients do not address altered limb-level loading [4]. Interventions that target gait, a modifiable risk factor for KOA progression, are needed to improve loading profiles and thereby long-term function. Therefore, the purpose of this study was to determine the efficacy of prescribing acute differences in peak vGRF during treadmill walking [i.e., four visual biofeedback conditions (i.e., -3%, +3%, +6%, 9% habitual vGRF peak) relative to habitual walking]. Secondly, we determined whether acutely modifying peak vGRF would be accompanied by changes in self-reported pain that would preclude the clinical utility of visual, vGRF-driven gait biofeedback in KOA patients. We hypothesized that KOA patients would demonstrate decreased peak vGRF during the cued -3% BW condition compared to the habitual walking condition, and, conversely, exhibit increased magnitudes of peak vGRF corresponding with prescribed biofeedback increases (i.e., +3%, +6%, 9%) compared to habitual walking without accompanying changes in self-reported knee pain.

Methods: Individuals with mild and moderate KOA were included in this repeated-measures experiment. In randomized order, participants completed four 2-min biofeedback conditions that visually cued peak vGRF targets (i.e., -3%, +3%, +6%, +9%) relative to habitual walking vGRF on a dual-belt instrumented treadmill and self-reported knee pain (1-100 pts.) on the Visual Analog Scale following each trial. All trials were performed at the participants' self-selected overground walking speed, and participants were blinded to biofeedback condition. Peak vGRF was extracted bilaterally during the first 50% of stance phase for each step, averaged across the duration of the trial separately for each limb, and normalized to body weight (%). In the case that participants had bilateral KOA, participants self-reported the limb that was most symptomatic. Separate general linear mixed effects models assessed within-subject changes in 1) peak vGRF across conditions and between limbs; and 2) pain across conditions. Model-estimated marginal means and standard errors were calculated, and pairwise comparisons were assessed with a Tukey correction if a significant overall condition or limb effect existed.

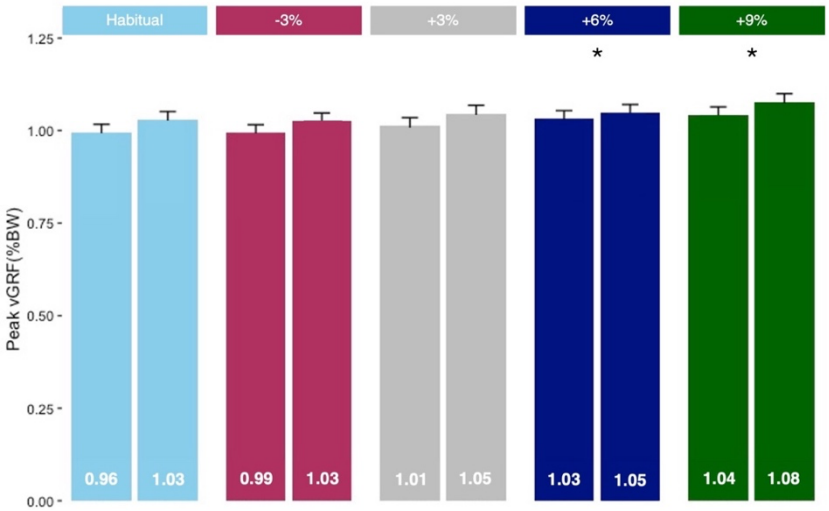

Figure 1. Peak vGRF model-estimated marginal means for condition and limb pairwise comparisons. Asterisks (*) denote statistically significant differences compared to habitual walking (p=0.05).

Results and Discussion: We have thus far included 11 participants in our sample [28.4±2.9 kg/m^2, 45% female, 1.22 ± 0.19 m/s, 55% bilateral KOA (n=6), 66.1 ± 7.9 yrs]. We observed a significant, overall condition effect on peak vGRF (p<0.001; Fig.1). Here, peak vGRF was greater during the +6% (p<0.001) and +9% (p<0.001) conditions compared to habitual walking. The same was not found for the -3% (p=0.996) and +3% (p=0.067) conditions. Overall effects of limb (p=0.059) and the condition×limb interaction (p=0.060) were notable though not statistically significant at the 0.05 level. No effect of condition on self-reported pain (p=0.238) was identified. Real-time biofeedback can successfully modify peak vGRF during walking in individuals with KOA, with the most notable changes observed when prescribing targets of +6% and +9%. For clinical context, using biofeedback to prescribe a +9% difference in vGRF produced a measured increase of approximately +5% peak habitual vGRF, narrowing the gap between insufficient limb loading observed in KOA patients compared to healthy controls [1,3]. Further, the ability to respond to peak vGRF visual biofeedback without changes in self-reported pain provides promise for the future development of long-term, vGRF-driven biofeedback interventions in KOA patients.

Significance: KOA patients may benefit from gait retraining using real-time biofeedback to modify limb-level loading. We have also shown promise to move this work outside the lab using wearable sensing and machine learning [5]. Future studies should assess the feasibility of implementing a large-scale, clinical trial in the KOA population to normalize vGRF loading profiles during walking.

Acknowledgments: Research presented in this abstract was supported by the North Carolina Biotechnology Center (TRG-0024).

References: [1] Childs et al., *Clin Biomech* (2004); [2] Bjornsen et al., *Arthritis Rheum* (2023); [3] Costello et al., *Osteoarthritis Cartilage* (2021); [4] Mikeskey et al., *Arthritis Care Res* (2006). [5] Pimentel et al., *PLOS Digital Health* (2024)

LOADING ASYMMETRY PERSISTS DESPITE PHYSICAL ACTIVITY AND SYMMETRY INTERVENTION AFTER TOTAL KNEE ARTHROPLASTY

*Renoa Choudhury[1], Liubov Arbeeva[2], Carla Hill[3], Katie F. Huffman[2], Todd A. Schwartz[2], Kelli D. Allen[2,3], Robin M. Queen[1]
[1]Department of Biomedical Engineering and Mechanics, Virginia Tech, Blacksburg, VA; [2]Thurston Arthritis Research Center, University of North Carolina at Chapel Hill, [3]Department of Medicine, University of North Carolina at Chapel Hill
*Corresponding author's email: renoac@vt.edu

Introduction: Total Knee Arthroplasty (TKA) is one of the most prevalent surgeries in the United States and is projected to rise to 3.48 million procedures annually by 2030 [1]. While TKA reduces pain and improves patient-reported function, many patients exhibit persistent limb loading asymmetry after surgery and subsequent rehabilitation. Research suggests that preoperative asymmetries arise as compensatory mechanisms to reduce pain and load in the arthritic limb [2]. However, following TKA, patients continue to place greater loads on the non-surgical limb despite pain reduction, increasing the risk of progressing to a contralateral TKA [3]. Studies show that current post-TKA rehabilitation paradigms do not adequately address these loading deficits [4], highlighting the need for targeted interventions. To address this gap, this study examined the effect of a novel Physical Activity and Symmetry (PAS) intervention [5] on post-TKA loading asymmetry during walking compared to an attention (ATT) control cohort and assessed the degree of loading asymmetry in both patient cohorts (PAS and ATT) compared to healthy controls (HC). Given the balance exercise component of the PAS intervention, it was hypothesized that PAS participants would show decreased load asymmetry post-intervention compared to ATT participants, and both patient cohorts would have greater asymmetry compared to the HC participants.

Methods: 60 patients post-TKA were enrolled and randomly assigned to the PAS intervention (n=30) or ATT (n=30) group. The PAS intervention included physical activity counseling and balance exercises over two sessions at the end of routine physical therapy (PT), followed by supplemental sessions at 4- and 8-weeks post-PT. The ATT group participated in supplemental sessions discussing surgical recovery benchmarks at 4- and 8-weeks post-PT [5]. Additionally, 70 healthy participants (HC) matched for age and sex to TKA cohorts were enrolled. All participants completed three 10-meter walking trials at a self-selected speed, while plantar loading data was collected using an in-shoe load sensor (loadsol®, novel Electronics). Patient cohorts were tested within 4–8 weeks post-surgery (pre-intervention) and again 3 months after the intervention (post-intervention), while HC participants were tested during a single session. The Normalized Symmetry Index (NSI) [6] was calculated for peak impact force (PIF) and peak propulsive force (PPF). A general linear mixed-effects model (GLMM) was used to examine the main effects of intervention (PAS vs. ATT), time (pre- vs. post-intervention), and their interaction on each outcome variable. Another GLMM assessed the main effects of group (post-intervention PAS, post-intervention ATT, HC) on each outcome variable at a single time-point (i.e., post-intervention). In both models, age, sex, and gait speed were included as fixed effects, with participant as a random effect.

Results & Discussion: For the patient cohorts, no significant intervention (PAS, ATT) by time (pre-, post-intervention) interaction (p=0.52) or significant main effect of intervention (p=0.38) and time (p=0.07) were found for the PIF NSI. A significant interaction (p<0.001) was found for the PPF NSI. Post-hoc comparison showed pre- and post-intervention PPF NSI was similar in the ATT (pre-: NSI = 7.88 ± 0.991, post-: NSI = 7.81 ± 1.050, p=0.49), but the PAS group showed higher PPF NSI post-intervention (pre-intervention NSI = 6.69 ± 0.982, post-intervention NSI = 9.27 ± 1.040, p<0.001). Prior research suggested that patients post-TKA demonstrate a high level of movement asymmetry in the early stages of recovery [5]. However, the pre-intervention loading asymmetry was lower in the PAS group, which could have an impact on the intervention outcome. In addition, the length of the PAS intervention may need to be longer or started later in the recovery period to have the desired symmetry changes. When compared to healthy controls, both ATT and PAS cohorts demonstrated significantly greater asymmetry in PIF and PPF at the post-intervention assessment (Figure 1). In these models, gait speed was a significant explanatory variable for both PIF NSI (p<0.001) and PPF NSI (p=0.014), and age was only significant for PIF NSI (p=0.009). These findings indicate biomechanical impairments persist at least 3 months post-TKA compared to healthy age-matched adults. This suggests that an intervention focused on restoring gait symmetry may be necessary to elicit clinically meaningful improvements in limb loading patterns beyond standard PT.

Significance: Given the rapidly increasing rate of TKA procedures and the progression of disease in the contralateral limb, it is essential to address the key deficits of post-TKA rehabilitation. This study highlights the likely need for targeted interventions beyond standard PT and balance exercises to improve post-TKA joint loading symmetry. Also, it indicates the potential use of in-shoe load sensors to objectively quantify loading symmetry during clinical care and establishes a baseline for future studies to improve loading symmetry following TKA.

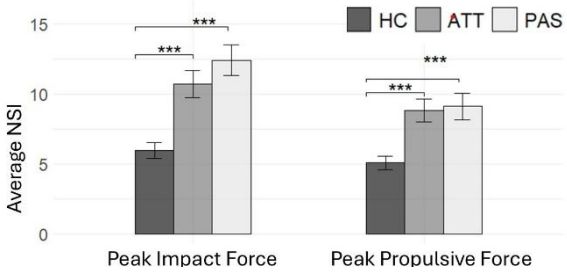

Figure 1: Average NSI between healthy controls (HC), post-intervention ATT and post-intervention TKA

Acknowledgments: This study was funded by NIAMS (R21AR074149). We would like to acknowledge the contributions of physical therapists in the UNC Healthcare System.

References: [1] Feng et al. (2018), *J Multidiscip Healthc*. 11; [2] Jones et al. (2016), *BMC Health Serv. Res.,* 16 (1); [3] Meier et al., (2008), J. Orthop. Sports Phys. Ther., 38 (5), [4] Alnahdi et al., (2011), *J. Orthop. Res.* 29 (5); [5] Queen et al., 2024, Osteoarthritis and Cartilage Open, 6(4), [6] Queen et al. (2020), *J Biomech 99*.

Effects of Age and Lateral Ankle Sprain History on Talar Cartilage Characteristics

Amin Mohammadi[1], *Ryan McCann[1]
[1] Ellmer College of Health Sciences, Macon & Joan Brock Virginia Health Sciences at Old Dominion University
*Corresponding author's email: rmccann@odu.edu

Introduction: Lateral ankle sprain (LAS) is a common musculoskeletal injury among physically active individuals [1]. LAS increases the risk of post-traumatic osteoarthritis (PTOA) over time [2]. LAS-related mechanical stress accelerates talar cartilage degeneration, increasing PTOA risk [3]. Additionally, age-related cartilage degeneration, such as the loss of proteoglycan content, further compounds these risks by reducing the cartilage's ability to withstand compressive forces, resulting in altered loading patterns and microtrauma [4]. Individuals with a history of LAS are particularly susceptible to degenerative changes in the medial talar dome, where joint stress is most pronounced [5, 6].

Due to the high cost and limited accessibility of magnetic resonance (MR) imaging, repeated assessments in clinical settings are often impractical. Ultrasonography (US) has emerged as a promising alternative for evaluating lower extremity cartilage thickness, with studies demonstrating a strong correlation between US-based measurements and MR-based femoral cartilage thickness assessments [7]. Few studies have assessed US imaging for detecting cartilage changes post-LAS. This study aims to examine the effects of LAS history and age on talar cartilage characteristics. By utilizing ultrasonography, we aim to determine whether a history of LAS and aging contribute to cartilage degeneration and whether their combined effects accelerate structural and compositional changes in the talar cartilage.

Methods: A total of 40 participants were evenly divided into four groups: young ankle sprain (YAS), young control (YC), middle-ankle sprain (MAS), and middle-control (MC) groups. Young participants were between 20 and 35 years old, while middle-aged participants were between 40 and 55 years old at the time of participation. Talar cartilage properties were assessed using a diagnostic ultrasound unit (Sonosite M-MSK; FujiFilm, Bothell, WA), measuring medial and lateral talar cartilage cross-sectional area (CSA), echointensity (EI), and echogenicity (EG). A two-way ANOVA analyzed the effects of LAS history and age on each outcome, with statistical significance set at $P < 0.05$.

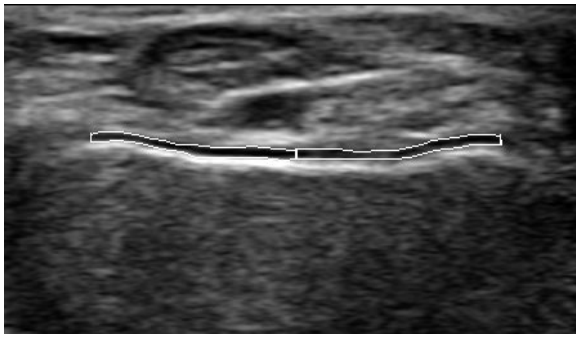

Figure 1: Medial and Lateral cross-sectional areas (CSA) of ankle joint were divided and analyzed using ImageJ software. Cartilage echo intensity (EI) which refers to the brightness of the cartilage, was calculated from the mean of the CSA and the echogenicity (EG) was calculated as the standard deviation of the EI value.

Results & Discussion: A significant age by LAS history interaction was observed for lateral EI ($F = 6.41$, $P = 0.016$) and medial EI ($F = 8.06$, $P = 0.007$). Large effect sizes for lateral EI ($d = 0.88$ [-0.07, 1.76]) and medial EI ($d = 0.91$ [-0.05, 1.78]) indicate YAS had higher EIs than MAS. Moderate to large effect sizes also indicate MC had higher lateral EI ($d = 1.24$ [0.24, 2.14]) and medial EI ($d = 0.72$ [-0.21, 1.59]) than YC. A significant age main effect for medial CSA ($F = 7.684$, $P = 0.009$, $d = 0.82$ [0.16, 1.45]), indicates young participants had thicker talar cartilage than middle-aged participants. Additionally, there was a significant LAS history main effect on lateral CSA ($F = 7.97$, $P = 0.008$, $d = 0.62$ [-0.30, 1.49]) and medial CSA ($F = 6.23$, $p = 0.017$, $d = 1.50$, [0.45, 2.42]), indicating thicker talar cartilage in participants with a previous LAS. A significant LAS history main effect for lateral EG ($F = 7.68$, $P = 0.009$, $d = 0.78$, [-1.65, 0.16]) indicates participants with a previous LAS had lower EG. No significant interaction or main effect was observed for medial EG ($F = 0.49$, $P = 0.488$, $d = 0.26$, [-0.63, 1.13]).

The observation of thicker CSA in individuals with a history of LAS contradicts our hypothesis that cartilage thickness would be reduced following injury. Lower EI values in individuals with LAS, suggest early cartilage degeneration characterized by increased water content and proteoglycan loss, rather than increased cartilage density. This finding aligns with previous findings indicating that early degenerative changes, such as proteoglycan loss and increased water content, can lead to reduced EI values [8]. Similarly, lower EG values may indicate a reduction in normal cartilage structural variability, potentially due to cartilage softening or a more uniform degenerative process. These results suggest that aging and a history of LAS together contribute to early signs of talar cartilage degeneration in middle aged adults, but not necessarily reductions in cartilage thickness.

Significance: This study examines the long-term impact of ankle sprains on talar cartilage health. While MR imaging remains the gold standard, diagnostic ultrasound might provide a cost-effective alternative for early detection of cartilage degeneration in middle-aged individuals with a history of ankle sprains.

References: 1. Herzog, M.M., et al., 2019. 54(6): p. 603-610. **2**. Gribble, P.A., et al., Br J Sports Med, 2016. 50(24): p. 1496-1505. **3**. Martin, J.A. and J.A. Buckwalter, Iowa Orthop J, 2001. 21: p. 1-7. **4**. Rahmati, M., et al., Ageing Research Reviews, 2017. 40: p. 20-30. **5.** Sugimoto, K., et al., JBJS, 2009. 91(1): p. 99-106. **6**. Lee, M., et al., Foot & Ankle International, 2015. 36(9): p. 1050-1057. **7.** Schmitz, R.J., et al., Knee, 2017. 24(2): p. 217-223. **8**. Harkey, M.S., et al., Ultrasound in Medicine & Biology, 2021. 47(1): p. 43-50.

PERSONALIZED EXOSKELETON CONTROL FOR OPTIMIZING GAIT ECONOMY IN STROKE SURVIVORS

Daniel Rodriguez-Jorge[1*], Gregory Sawicki[1], Aaron Young[1]
[1]Georgia Tech, Atlanta, Georgia
*Corresponding author's email: djorge8@gatech.edu

Introduction: Stroke survivors often experience impaired gait mechanics and reduced walking economy, which significantly impact their mobility and quality of life [1]. Wearable exoskeletons targeting specific joints, such as the hip and ankle, have shown promise in improving ambulation. Current systems often lack adaptability to individual needs and fail to address real-world challenges, limiting their clinical relevance and user adoption. This study aims at developing personalized exoskeleton systems with end-to-end controllers and Bayesian optimization to reduce metabolic cost and potentially improve gait mechanics for stroke survivors. Our control system for hip exoskeletons uses neural networks to estimate joint moment and power. Scale, delay, and shape parameters were optimized by the Bayesian algorithm to minimize joint positive biological power across all three lower limb joints. By reaching a personalized control paradigm for stroke survivors, we aim to create adaptive systems that support long-term community ambulation.

Methods: We developed a hip joint exoskeleton equipped with a personalized control system based on temporal convolutional neural networks trained with an n=12 dataset collected specifically in stroke survivors, encompassing both paretic and non-paretic legs. The controller uses two neural networks to estimate hip joint torque and hip, knee, and ankle joint power. These power estimates feed into a Bayesian optimization algorithm designed to minimize biological joint positive power by shaping, scaling, and delaying the hip torque estimates, as in figure 1. This deep learning-based control system, designed to mimic human biological movement and introduced in [2], can harmonize control across different locomotion modes, and proved to reduce metabolic cost and joint work compared to operating without an exoskeleton in [3] with device-specific training data. Now, device-agnostic data were used to re-train the TCNs that can potentially be used in different devices, predicting current and future torque values in both paretic and non-paretic limbs. In addition, the second TCN model trained to predict power at all joints serves as a cost function estimator for the Bayesian optimizer. The optimizer identified personalized, optimal scale, delay, and shape parameters for the assistive torque profile for previously collected data (offline).

Results & Discussion: Our personalized control system demonstrated promising results: (i) both TCNs achieved low RMSE values, including joint torque estimates with an RMSE of ~0.15 Nm/kg, and 0.19, 0.26, and 0.34W/kg for joint power at the hip, knee, and ankle respectively, indicating reliable predictions for stroke survivors; (ii) the offline Bayesian optimizer consistently identified high scale factors, low shape factors, and delays between 120–180ms as optimal for minimizing joint positive biological power utilizing offline data collected previously in a limited time frame, consistent with results found in [2]; (iii) expected outcomes: by minimizing positive biological power at the joints, we anticipate reductions in metabolic cost during walking for stroke survivors, although the identified optimal parameters may vary during the human-in-the-loop online optimization. These findings highlight the potential of combining neural networks with Bayesian optimization to create adaptive control systems tailored to individual stroke community ambulators.

Significance: This study represents a step forward in developing personalized exoskeleton technologies for stroke survivors. By leveraging AI-based controllers and optimization algorithms, we can create adaptive systems that enhance gait mechanics while ensuring clinical relevance and user adoption. Future work will focus on real-world testing of both hip and ankle exoskeletons to evaluate their effectiveness in community ambulation settings.

Acknowledgments: This work was funded by NIH R01 Award #R01HD113598-01.

References: [1] Murray et al. (2007), *Reviews in Clinical Gerontology* 17(4); [2] Molinaro et al. (2024), *Science Robotics* 9; [3] Molinaro et al. (2024), *Nature* 635.

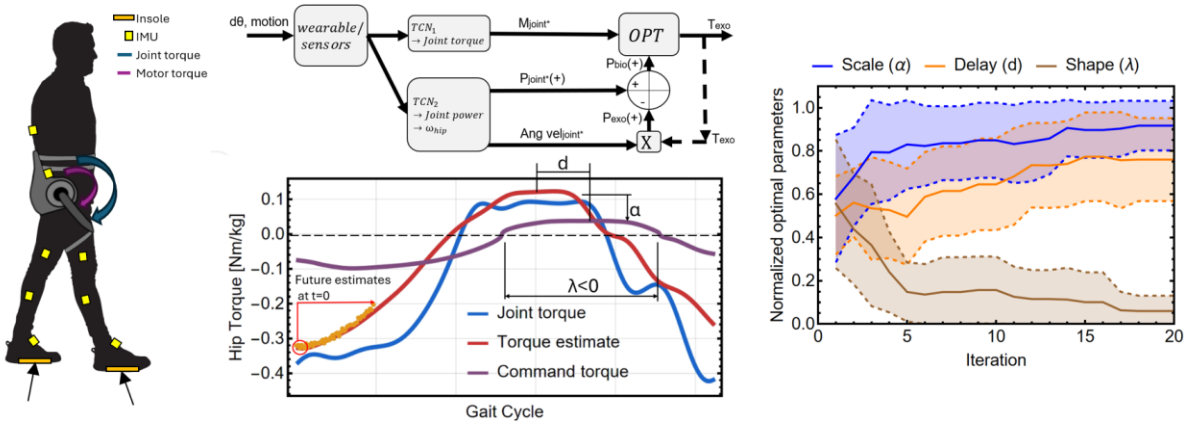

Figure 1: Evolution of the three optimization parameters throughout the optimization process and the resulting command torque versus hip joint torque. Biological work is estimated by subtracting motor power to hip power and integrating over a 25s window utilizing offline data collected previously and assuming unchanged biological power at the knee and ankle joints. Optimization boundaries: α: 0.05-0.3, d: 0-200ms, λ: 0.5-3.

Automatic Segmentation of Abductor Hallucis in Ultrasound Images: Development of Deep Neural Networks with Healthy People

Halime Gulle[1*], Furkan Mumcu[2], Austin Goodrich[3], Lokman Bekit[2], A. Wayne Johnson[3], Yasin Yilmaz[2], Irene S. Davis, FACSM[1]
[1]School of Physical Therapy and Rehabilitation Science, University of South Florida, FL, USA
[2]Colleage of engineering, University of South Florida, FL, USA
[3] Exercises Science, Brigham Young University, Utah, USA

Introduction: Plantar foot intrinsic muscles (PIMs) are essential for arch support, balance, and overall foot stability, playing a critical role in gait mechanics and injury prevention. While MRI-based cross-sectional area (CSA) estimation provides detailed muscle assessment, it is costly and time-intensive, limiting its clinical utility. Ultrasound offers a more accessible and cost-effective alternative but requires significant manual effort for image digitization. Recent advancements in machine learning (ML), particularly in Deep Neural Networks (DNNs), have shown promise in automating musculoskeletal segmentation, reducing the demand for clinician expertise[1]. Despite this progress, ML-driven segmentation techniques have not yet been applied to the PIMs. This study aims to develop an automated segmentation framework for PIMs using DNNs, beginning with the Abductor Hallucis (ABDH) muscle. We plan to expand the model to include additional PIMs, such as the Flexor Hallucis Longus, Quadratus Plantae, and Abductor Digiti Minimi. We hypothesize that DNN-based automatic segmentation of ABDH will achieve comparable accuracy to manual segmentation, demonstrating the feasibility of ML-driven ultrasound analysis for PIM assessment.

Methods: To date, we utilized ultrasound images of the ABDH muscle from 83 participants, capturing both right and left sides. Out of the 166 images (83x2), one random image from each patient was selected for testing and validation, while the remaining images were used for training. Specifically, 123 images were allocated for training, 31 for testing, and 12 for validation.

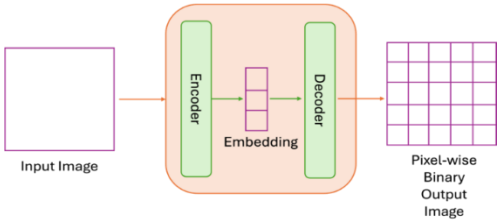

Figure 1. Encoder-Decoder Network Architecture for Pixel-wise Binary Classification.

We used two DNN models, U-Net and Feature Pyramid Network (FPN) with Mix Vision Transformer (MiT) backbone, to perform semantic segmentation on pre-processed ultrasound images. Both models utilize an encoder-decoder architecture (**Figure 1**). The images were first labeled with muscle boundaries to train the DNN models to distinguish the target muscle from the background. The raw images, paired with their labeled versions, served as the input and desired output, respectively, for training the DNN models. The models were then trained using the Dice loss function, which is widely employed in segmentation tasks to measure overlaps between predicted and ground truth segmentation masks. After training, the model predictions were used to compute the CSA. For training, images were normalized to a scale between 0 and 1, and resized to 224x224 pixels, as larger image sizes resulted in inferior performance. Preprocessing included contrast-limited adaptive histogram equalization to enhance the contrast between the aponeurosis and the muscle tissue. The performance of UNet and FPN were evaluated using the commonly used Intersection over Union (IoU) and F1 (or Dice coefficient) scores, which both range between 0 and 1 with higher scores indicating a better alignment between the prediction and ground truth. IoU and F1 scores differ in the weights used for true positive (correctly detected muscle region), false positive (region falsely detected as muscle), and false negative (missed muscle region).

Results & Discussion:
The results of both models are presented in Table 1 using Mean IoU and Mean F1 scores averaged over all test images. Both models achieved highly successful alignment with the ground truth labels from manual segmentation while FPN slightly outperformed U-Net. With Mean IoU and Mean F1 scores above 0.9, either approach works well for detecting ABDH muscle. This is further illustrated in the visual comparison of the ground truth mask and the predictions generated by the FPN and U-Net algorithms **(Figure 2).**

Table 1: Mean IoU and F1 Scores for U-Net and FPN models

Models	Mean IoU	Mean F1
U-Net	0.9097	0.9345
FPN	0.9207	0.9404

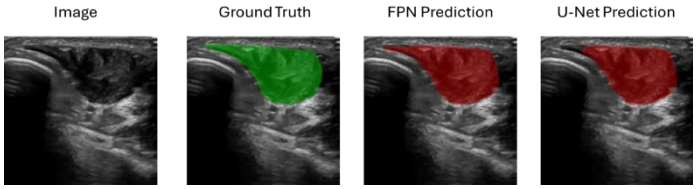

Figure 2. Visualization of ground truth mask and the predictions on the image with FPN and U-Net algorithms.

Significance: These preliminary findings show promising results for the automatic segmentation process. To enhance performance, we will train six separate models for ABDH, as well as other intrinsic foot muscles, including the Flexor Hallucis Brevis, Quadratus Plantae, and Abductor Digiti Minimi, using data from 100 participants. The most accurate model will be selected for the final segmentation of the full muscle set. Future work will also assess the accuracy of determining muscle volumes from these automated cross-sectional slices.

References:

1. Xiao, H., L. Li, Q. Liu, X. Zhu, and Q. Zhang, Transformers in medical image segmentation: A review. Biomedical Signal Processing and Control, 2023. 84: p. 104791

Neural Network for Reconstruction of Intact Tibia Shapes from Post-Fracture Bone CT Scans

*Alireza Ariyanfar[1], Hannah Dailey[1]
[1]Department of Mechanical Engineering and Mechanics, Lehigh University, Bethlehem, PA
*Corresponding author's email: hlr3@lehigh.edu

Introduction: Virtual mechanical testing is a technique for assessing the mechanical rigidity of a healing bone fracture using an image-based finite element (FE) model built from a computed tomography (CT) scan. Morphometric and bone density variations between individuals are common, so the torsional rigidity of the fractured bone is often normalized to the value for the intact contralateral. This can be accomplished easily in animals, but not in humans because only the injured tibia is imaged to minimize radiation exposure. To model the missing intact bone, we previously developed a manual technique for segmenting cortical bone fragments from the injured leg CT and reconstructing them into an intact shape.[1] This method is tedious, requires extensive user training, and cannot be automated for scalable clinical use. Hence, it is of interest to develop an algorithm for automatic reconstruction of an accurate intact bone shape from the post-fracture CT scan. The goal of this study was to train a multi-layer perceptron (MLP) neural network to predict missing cortical bone contours from the midshaft near a diaphyseal fracture using contours detected further away. We hypothesized that the shapes of MLP-reconstructed intact tibiae agree with shapes taken directly from ground-truth imaging of the full contralateral bones.

Methods: Adult female Swiss alpine sheep were used for this study due to the availability of intact and operated CT scans from a previously completed osteotomy fracture study.[2] Data from 26 intact tibiae and 3 operated tibiae were used in this study. Intact bones were randomly assigned to MLP training and validation (N = 21) and testing (N = 5) groups. To train the MLP, the pericortical contours of intact bones were detected by a snake model, downsampled to 100 contours, and were divided into "known" sections (30% on each bone end) and "unknown" sections (middle 40% of each bone). The contours of both sections were transformed to a cylindrical coordinate system. Contour points were arranged at regular angles creating a "string" at each angle that stretched from proximal to distal end. Radii of all the strings in each bone were standardized and normalized with respect to the known section. The MLP with 50, 40, and 30 neurons in its hidden layers was trained (65%) and validated (35%) on 5376 strings by minimizing the loss, which was defined as the mean square error (MSE) of predicted contours with respect to the targets. The MSE was calculated similarly for testing set. Additionally, the outputs were reverse normalized, reverse standardized, and converted to the initial cartesian coordinate system to calculate Dice Similarity Index (DSI) between the outputs and targets.

As a proof of principle, MLP-reconstructed contours were used to build intact bone FE models from three operated images. Ground truth endocortical and pericortical contours were detected for 30% of the ends of the operated bones using histogram equalization, Otsu's adaptive thresholding, and the snake model. Unknown contours in the middle 40% of each bone were predicted by the MLP that had been trained on the intact bone scans. From the resulting bone shapes (pericortical and endocortical contours), binary masks were meshed with hexahedral elements using an in-house code. The meshes were imported into Abaqus and assigned a homogeneous Young's modulus of 14 GPa [3] and Poisson's ratio of 0.3. The models were twisted by 1° at one end and fixed at the other end. Virtual torsional rigidity (VTR) was calculated and compared to the ground-truth VTR obtained from a model created from the image of the originally intact pair.

Results & Discussion: The MLP had comparable loss values of 0.00090 and 0.00101 at the end of training and validation, indicating that it captured general trends without overfitting. The losses and DSIs calculated for the testing set were smaller than 0.00024 and higher than 97.33%, respectively, indicating geometric fidelity with MLP reconstruction. The MLP-reconstructed pericortical contours for one bone from the testing set and for an operated bone are shown in Figure 1. The VTRs of the 3 MLP-reconstructed intact bones derived from fractured bone scans had <6% error relative to ground truth VTR values taken from the scans of the intact bones, even without accounting for individual animal BMD when assigning the Young's modulus. Inaccuracy in the known contour detection due to bone remodeling [4], training of MLP using only pericortical contours, inherent geometrical differences between the right/left limb pairs, the assumption of homogeneous material property, and the selection of Young's modulus from the literature are the sources of error and the limitations of the methodology, that could be partially addressed in future.

Significance: The proposed method for reconstructing the pre-fracture shape of a tibia from post-fracture CT scans may enhance the objectivity of virtual mechanical testing by recreating the intact bone without user input. Additionally, robust estimation of pre-op cortical contours in an osteotomized bone would allow the study of density variations inside the cortex during the remodeling stage of fracture healing.

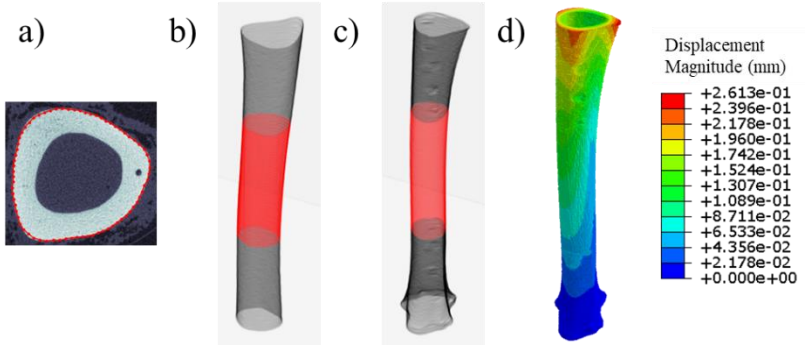

Figure 1. a) An example pericortical contour used as input in training the MLP neural network that was used for reconstructing missing portions (red) of b) an intact bone during MLP testing and c) an operated bone leading to d) virtual torsion testing of the reconstructed intact shape (contours show model displacement).

References: [1] Schwarzenberg et al (2019), *J Biomech.*; [2] Schwarzenberg et al (2021), *J Orthop. Res.*; [3] Orassi et al. (2021), *Front. Bioeng. Biotechnol.*; [4] Ariyanfar et al (2024), *CMBBE: Imaging & Vis*.

DOWNHILL WALKING CLASSIFICATION FOR GAIT-ASSISTIVE WEARABLE ROBOT: A MACHINE LEARNING AND DEEP LEARNING APPROACH

Chihyeoung Lee[1], Eunsik Choi[1], Minhye Kim[1], *Jooeun Ahn[1, 2]
[1]Department of Physical Education, Seoul National University, South Korea
[2]Institute of Sports Science, Seoul National University, South Korea
*Corresponding author's email: ahnjooeun@snu.ac.kr

Introduction: Gait-assistive wearable robots have been developed to improve mobility for individuals with gait impairments. These robots are becoming lighter and more comfortable to wear, enhancing their practicality for real-world use. A key challenge is that many current robots do not automatically adjust their assistance modes based on walking conditions, requiring users to switch modes manually. Downhill walking, in particular, has distinct biomechanical characteristics compared to level-ground and uphill walking [1], requiring adjustments in assistance timing and force profiles. Therefore, this study aims to develop a method for distinguishing downhill walking from level-ground and uphill walking using data that can be collected from a wearable robotic system.

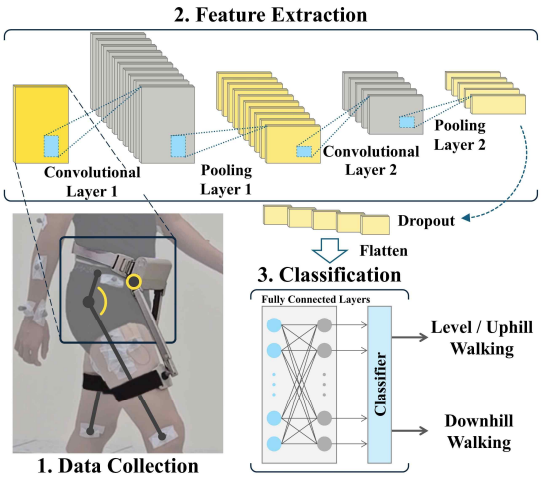

Figure 1. A Participant wearing Robot 1, the structure of the convolutional neural network (CNN) consisting of two convolutional layers and two pooling layers, and fully connected layers for classification.

Methods: Twenty-six healthy young adults (14 males; age: 27.3 ± 2 yrs; height: 170.8 ± 6.9 cm; mass: 66 ± 11.4 kg) participated in this study. Each performed a 2-minute walking task under three slope conditions: level-ground, uphill (+5°), and downhill (-5°), repeating each condition twice. Fourteen participants wore Robot 1 (WIM, WIRobotics, Korea) on the anterior waist, while 12 wore Robot 2 (H10, Angel Robotics, Korea) on the posterior waist. Kinematic data were collected using reflective markers and processed using Opensim software (Simbios, USA). To ensure applicability to wearable robotic systems, hip angular velocity and marker accelerations attached on anterior/posterior superior iliac spine or the robot were selected as features. These were chosen based on data that could be measured by common sensors like inertial measurement units or encoders. For machine learning (ML) methods, 6 features were extracted from each gait cycle (Table 1) [2]. The ML models used were logistic regression (LR), k-nearest neighbors (K-NN), support vector machines (SVM), random forests (RF), and extreme gradient boosting (XGB). For deep learning (DL) methods, gait cycle data were time-normalized to 100% and used as input for a CNN (Fig. 1) [3].

Table 1. The accuracy and calculation time for machine learning and deep learning classification

	Machine learning (ML)										Deep learning (DL)	
	{Mean, minimum, maximum, variance, skewness, and kurtosis} of gait cycle										Time-normalized gait cycle	
	LR		K-NN		SVM		RF		XGB		CNN	
	A	C	A	C	A	C	A	C	A	C	A	C
Hip angular vel.	88.93	0.98	94.40	4.21	89.20	34.38	82.24	1.95	95.41	1.76	**99.46**	**0.16**
Anterior acc.	88.71	0.47	92.54	3.05	88.97	34.26	83.05	1.46	93.92	1.99	65.24	0.16
Posterior acc.	91.22	0.33	95.72	4.72	91.54	26.75	90.16	1.40	96.92	1.41	65.25	0.23
All included.	98.23	1.44	98.45	6.96	98.36	36.28	91.76	1.98	99.15	3.34	65.25	0.23

A: Accuracy (%); C: Calculation time (sec).

Results & Discussion: A total of 40,710 samples were collected, including 14,122 from downhill walking. The CNN-based DL model using hip joint angular velocity achieved the highest accuracy (99.46 %) with a calculation time of only 0.16 s. In comparison, the ML-XGB model reached a similarly high accuracy of 99.15% when incorporating all feature set. However, despite its accuracy, it required 3.34 s for calculation, which is more than twice the average downhill gait cycle duration (1.36 ± 0.1 s), making it impractical for real-time applications. These findings suggest that the CNN-based DL approach with hip joint angular velocity is the most effective method for distinguishing downhill walking. Future research should validate these findings using real sensor data from an actual robotic system and assess the model's robustness during active robot assistance.

Significance: This study contributes to real-time detection of downhill walking. Our findings will help a wearable device to enhance the ability to distinguish diverse walking conditions more effectively using a DL approach. Improving adaptability in gait-assistive wearable robots will ultimately provide greater support and mobility benefits for individuals with gait impairments.

Acknowledgments: The study was supported in part by the grant of the Korea Health Technology R&D Project through the Korea Health Industry Development Institute (KHIDI), funded by the Ministry of Health & Welfare (no. HK23C0071), and the National Research Foundation of Korea (NRF) grants funded by the Korean Government (MSIT) (No. RS-2023-00208052).

References: [1] Lay et al. (2006), *J Biomech*, 39(9); [2] Özdemir et al. (2014), *Sensors*, 14(6); [3] Cronin. (2021), *J Biomech*, 123.

DEEP LEARNING BIOLOGICAL STATE ESTIMATION ENABLES JOINT WORK OPTIMIZATION ACROSS TASKS

*Matthew T. Lerner[1], Ethan B. Schonhaut[1], Aaron J. Young[1]
[1]Georgia Institute of Technology, Atlanta, GA
*Corresponding author's email: matthew.lerner@gatech.edu

Introduction: Assistive wearable robotics have increasingly demonstrated the capability to reduce the metabolic cost of walking and running [1]. Recent work that directly estimates biological information of the user via deep learning has enabled unified control across tasks [2]. However, current unified control frameworks do not provide optimal energetic cost reduction. Currently, the largest metabolic cost reductions are provided by controllers optimized for individual tasks such as walking or running [3]. The standard wearable robotics optimization method, human-in-the-loop optimization (HILO) of metabolic cost measured via indirect calorimetry, requires at least two minutes of data to evaluate a single combination of parameters [4], creating challenges for optimizing across a range of tasks. Additionally, highly dynamic, tiring, and non-cyclic tasks are difficult to complete repeatedly, making metabolic optimization of such tasks intractable. To address this, we propose the direct optimization of joint work estimated via deep learning to reduce the mechanical energy exerted by exoskeleton users. In this study, we hypothesize that a Bayesian optimization procedure can determine exoskeleton control parameters that reduce the user's exerted joint work compared to a no actuation condition.

Methods: We completed an optimization experiment (N=1) to minimize user exerted hip joint energy for different movements while wearing a clothing-integrated research-grade exoskeleton capable of applying 18 Nm of torque at the hip and knee joints developed at X, the moonshot factory [2]. We applied hip joint assistance based on a linear combination of instantaneously estimated joint moment and joint power for level ground walking (1.25 m/s) and for sit to stands (15 repetitions/minute) (Fig. 1A). We determined the combination of parameters which maximally reduced user exerted joint energy using Bayesian optimization, a sample-efficient optimization framework previously used in wearable robotics [5]. We estimated user joint moment from wearable sensors and temporal convolutional neural networks [2], determined net joint power from estimated moment and measured joint velocity, calculated user joint power by subtracting applied exoskeleton power from net joint power, and calculated user joint work by integrating user joint power over the last 10 seconds of each condition for walking and during the last 4 repetitions of sit-to-stands. The user experienced each control condition for 30 seconds during walking and for 10 repetitions during sit-to-stands.

Results & Discussion: The combined joint moment and joint power controller optimization successfully reduced the user's positive joint work by 20.3% and 22.6% for walking and sit-to-stands respectively compared to the no actuation condition (Fig. 1B). Additionally, the Bayesian optimization procedure converged to the optimum for both walking and sit to stands within 20 iterations, demonstrating the capability to directly optimize joint work. The best parameter combinations tested were in the same region for walking and sit to stands (Fig. 1C). This indicates that a single parameter combination may be nearly optimal across these tasks, however, different controller parameterizations and additional task exploration could discover parameters that provide additional improvement but are not shared across tasks. The entire optimization procedure involved 10 and 13.3 minutes of movement with exoskeleton actuation for walking and sit to stands respectively. A similar metabolic optimization would require at least 40 minutes of movement under actuation for a single task optimization. In the same allotted time, joint work optimizations can explore additional tasks or more complex control parametrizations. Future work is required to compare metabolically optimized and joint work optimized control parameters.

Significance: We demonstrate the ability to reduce user joint energy expenditure by optimizing deep-learning joint state estimates. These metrics are much faster to measure than metabolic cost, enabling the optimization of a wider variety of tasks in shorter experimental paradigms. We also demonstrate the promise of combining joint-level biological states as a basis of exoskeleton control. This new optimization metric and control framework has the potential to provide improved generalizable assistance.

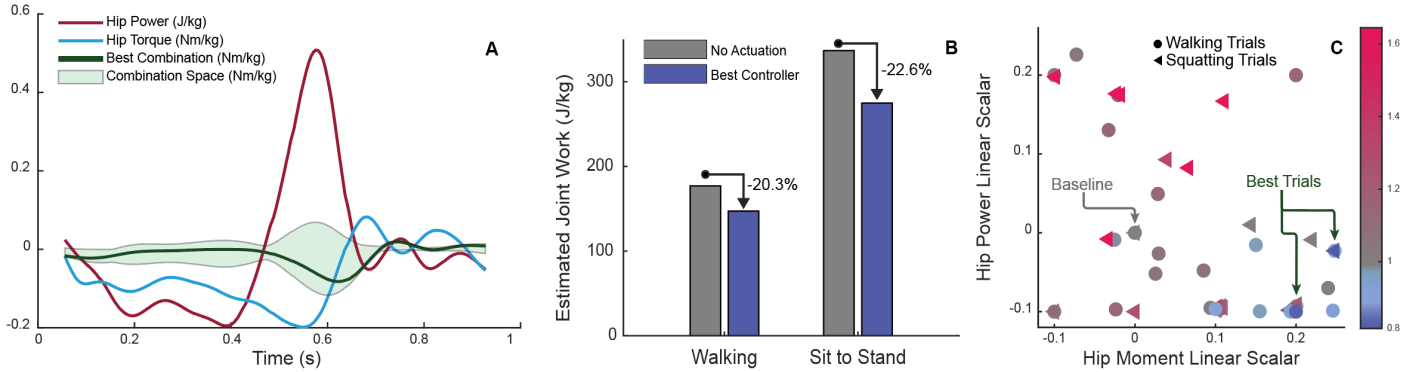

Figure 1: Deep-learning estimates of joint moment and power, the applied torque from the optimized linear combination of joint moment and power, and the space of possible combinations (A). The best combination reduced joint work compared to no actuation across tasks (B). Joint work cost landscape from walking and sit to stand optimizations, where the joint work value for each trial is normalized by no actuation cost (C).

Acknowledgments: This work is supported by NSF FRR Award #2233164.

References: [1] Sawicki et al. (2020), *J NeuroEngineeringRehabil* 17(1); [2] Molinaro et al. (2024), *Nature* 635(8038); [3] Franks et al. (2021), *Wearable Technol.* 2(16); [4] Zhang et al. (2017), *Science* 356(5344); [5] Kim et al. (2017), *Plos One* 12(9);

GAIT DIFFERENCES IN ACL INJURIES: MACHINE LEARNING FOR UNCOVERING PATIENT CLUSTERS 2 YEARS AFTER RECONSTRUCTION

Jingyu Hu[1]*, Bret Freemyer[2], Andrew A. Takata[3], Christopher Stickley[1]
[1]University of Hawaii at Mānoa, Kinesiology and Rehabilitation Science
[2]Punahou School, Honolulu, HI
*Corresponding author's email: hujingyu@hawaii.edu

Introduction: Anterior cruciate ligament (ACL) injuries are common in sports, particularly among high school and college aged people[1].Young adults who have undergone ACL reconstruction (ACLR) are at a higher risk of developing post-traumatic osteoarthritis (PTOA) at a younger age compared to those without a history of ACL injuries.[2-3] However, gait changes after ACLR and their contribution to PTOA remain complex, therefore identifying different patterns in the years after ACLR may help elucidate how varying patient clusters may progress towards early PTOA. Machine learning algorithms may help identify gait data phenotypes and reveal distinct movement patterns associated with PTOA in ACL-injured individuals. Therefore, the purpose of this study was to categorize knee loading patterns using the K-means clustering method.

Methods: Fifty-one ACLR patients (age: 27.0 ± 6.6 years; height: 169.8 ± 10.4 cm; mass: 75.4 ± 21.5 kg), a minimum of two years post-operatively (mean: 8.2 ± 5.3 years post-ACLR), participated in this study. Gait biomechanics were collected at the University of Hawaii at Mānoa using a Vicon Nexus motion capture system (Nexus 2.5.0, Vicon Motion Systems, Vicon LA, Culver City, CA, USA). Participants walked barefoot at a self-selected velocity. Kinetic data were collected using a force plate (Advanced Mechanical Technology, Inc., Massachusetts, MA, USA) embedded in the laboratory floor. Kinematic and kinetic gait variables for the knee were processed using Visual3D (C-Motion, Inc., Germantown, MD, USA). Uniform Manifold Approximation and Projection (UMAP) was used to reduce the dimensions of the biomechanical knee gait variables. The K-means clustering (Python Version 3.10.12), an unsupervised machine learning algorithm, was then applied to group participants based on similar gait characteristics. Finally, independent t-tests (SPSS Version 26.0, with an alpha level of $p < 0.05$) were conducted to analyse differences between the clusters.

Results & Discussion: The K-means clustering resulted in two groups of ACLR participants (Cluster 1, n=26 (13 females & 13 males); Cluster 2, n=25 (23 females & 2 males)). The independent t-test results are shown in Table 1. Cluster 1 exhibited more vertical centre of mass (COM) displacement, higher peak vertical COM, greater second peak vertical GRF, loading rate, and peak knee flexion moment (KFM) and KFM impulse compared to Cluster 2. Conversely, Cluster 2 exhibited a greater peak knee adduction angle during stance, peak first knee adduction moment (KAM) rate, and peak first KAM. In conclusion, participants in Cluster 1 relied more on increased knee flexion moments with greater vertical impact loading, whereas participants in Cluster 2 exhibited an increased frontal plane loading.

Table 1. T-test Results for GRF and knee variables.

Variables	Cluster 1		Cluster 2		t-value	P-value	Effect Size
	Mean	SD	Mean	SD			
Vert COM DISP (m)	0.031	0.01	0.025	0.01	4.25	<0.01	1.19
Peak Vertical COM (m)	0.89	0.06	0.83	0.04	4.37	<0.01	1.22
Peak KAD Angle IC to Midstance (∘)	-0.44	3.68	2.29	2.50	-3.11	<0.01	-0.87
Peak KAD Angle Midstance to Toe Off (∘)	0.62	4.23	5.15	3.16	-4.34	<0.01	-1.21
Peak KER Angle IC to Midstance (∘)	5.02	7.74	15.25	6.31	5.18	<0.01	1.45
2nd Peak Vertical GRF (N)	909.6	202.7	616.3	100.1	6.59	<0.01	1.84
Vertical GRF Loading Rate (N/s)	5912.6	1934.0	4274.6	1029.4	3.80	<0.01	1.06
1st Peak KAM Rate (Nm/kg/s)	2.46	1.00	3.13	1.05	-2.30	0.03	-0.64
Peak KAM IC To Midstance (Nm/kg)	0.37	0.12	0.44	0.10	-2.39	0.02	-0.67
Peak KFM (Nm/kg)	0.54	0.24	0.38	0.13	3.03	<0.01	0.85
KFM Impulse Stance (Nm·s/kg)	0.059	0.05	0.02	0.062	2.90	0.01	0.81
* COM: Center of Mass; DISP: Displacement; GRF: Ground Reaction Force; IC: Initial Contact; KAM: Knee Adduction Moment; KAD: Knee Adduction; KER: Knee External Rotation; KFM: Knee Flexion Moment; VERT: Vertical;							

Significance: Half of our sample clustered with greater peak KFM and vertical GRF and less frontal plane knee medial compartment loading, indicating a greater sagittal loading after ACLR compared to the other cluster. Consistently decreased loading on knee cartilage over years could contribute to PTOA due to the insufficient compression on medial cartilage, leading to degeneration.[4] These results may demonstrate that altered loading across planes could be a risk factor that should studied prospectively in ACLR patients across the lifespan.

References: [1] Schilaty, ND. et al. (2008), Orthop J Sports Med, 6(5). [2] Miko SC. et al. (2021), J Sci Med Sport, 24(2). [3] Wellsandt E. et. al (2017) Journal of orthop Res, 35(3). [4] Caroline Michele Lisee et. al. (2022), J Athletic training, 57(0/10).

DATA-DRIVEN DEEP LEARNING OF HUMAN BIOLOGY ENABLES TASK AGNOSTIC CONTROL FOR WEARABLE ROBOTS

Aaron. J Young[1*], Dean Molinaro[1], Keaton Scherpereel[1]
[1]Georgia Institute of Technology, Atlanta, GA
*Corresponding author's email: aaron.young@me.gatech.edu

Introduction: One of the biggest challenges in deploying exoskeleton technology in the real-world to solve human needs is the lack of a control system that is universally helpful across the many types of activities humans perform daily. Realizing lower-limb exoskeleton technology in the real world would enable human mobility to reach new feats, making heavy boxes feel lighter in the warehouse, increasing the success rate of search and rescue operations, or even enabling new innovations in athletic performance and injury reduction. Many controllers have been developed that assist level-ground walking but fall short of providing meaningful assistance on the myriad of other activities such as stair climbing, sitting, standing squatting, running, jumping, lifting, cutting, stepping over an obstacle, navigating hills and slopes, and dozens of other tasks that humans regularly perform. We have engineered a new class of training datasets for exoskeleton users focused on estimating physiological states, such as biological joint moments, which enable task agnostic control [1].

In this study, we test the hypothesis that a deep learning-based control system trained to human biological moment can unify control across both cyclic and non-cyclic locomotion to reduce metabolic cost and joint work compared to not using an exoskeleton.

Methods: We first collected a series of training data (N=15) which consisted of exoskeleton users walking in robotic trousers weighing ~7kg in total that bilaterally assisted the hip and knee by up to 14Nm (Fig 1A) [1]. Users completed trials consisting of 29 activities including both 11 cyclic tasks and 18 non-cyclic tasks which have been previously published in our open source dataset [2]. Motion capture and force plate data were collected for all these tasks and standard inverse dynamics was run to compute net joint torques. We trained a temporal convolutional network (TCN) [3] to estimate joint torques in real time and scale assistant to 20% biological moment at the hip [4] and 15% at the knee. We performed tests in a separate group (N=10) to test the accuracy and efficacy of the unified deep learning system in real-time. Accuracy testing was conducted across all tasks, while metabolic testing was conducted in 4 cyclic tasks and joint work testing in 6 non-cyclic tests. We compared our system to a zero-impedance condition and a no exoskeleton condition.

Results & Discussion: The unified control system enabled by deep learning human physiological state provided reliable and accurate assistance to novel tasks. Average real-time R^2 values for estimating biological moment was 0.79 at the hip and 0.86 at the knee for cyclic tasks and 0.81 at the hip and 0.87 at the knee for non-cyclic tasks (representative tracking curves shown in Fig. 1B), which enabled a highly controllable system for all testing subjects during real-time operation. Human outcomes largely matched our hypothesis with the task agnostic controller significantly ($p<0.05$) reducing metabolic cost on repetitive lifts and running compared to no exoskeleton and additionally on level walking and inclined walking compared to zero impedance. Similarly, the task agnostic controller reduced ($p<0.05$) joint work on sit-to-stand, squatting, lunging, and lift and place weight compared to no exoskeleton and on stair ascent and single step up compared to zero impedance.

Significance: We demonstrate, for the first time, a task agnostic control system based on deep learning of human physiological state capable of real-time estimation and control for exoskeletons across numerous tasks [3]. The key innovation is the reliance on learning human internal biomechanical states to unify exoskeleton control with human movement dynamics. Key significance is that we can now enable reliable and useful control across dozens of locomotion tasks without the need for estimating tasks explicitly (typically achieved through either a state machine or mode classifier) or the need to estimate gait phase for control. In addition, all deployments were user-independent (no training data from the test subject) and no heuristic hand tuning or user-specific configurations were needed. This new style of control has the potential to enable exoskeleton technology to be deployed in real-world and community ambulatory environments.

Acknowledgements: This project was funded by Google X and NSF.

References: [1] Molinaro and Scherpereel et al., (2024), *Nature* 635. [2] Scherpereel et al. (2023) *Scientific Data* 10(1). [3] Molinaro et al., (2022). *IEEE TMRB* 4(1). [4] Molinaro et al. (2024), *Science Robotics* 9(8).

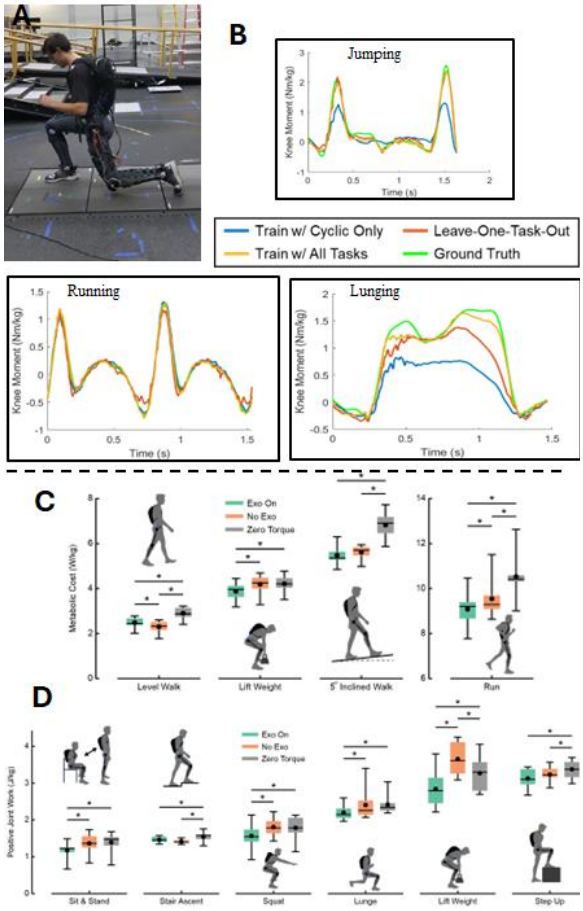

Figure 1: This N=25 study was conducted with flexible robotic-integrated pants that supports the hip and knee bilaterally (A). Representative tracking of the deep learning system across jumping, lunging and running showed excellent tracking to the ground truth (B). Our task agnostic system control system reduced both metabolic cost (C) and joint work (D) significantly compared to the the zero impedance condition and on the majority of tasks compared to no exoskeleton.

SOFT EXOSUIT REDUCES FREEZING-OF-GAIT IN AN INDIVIDUAL WITH PARKINSON'S DISEASE BY APPLYING BILATERAL HIP FLEXION ASSISTANCE DURING PERSONALIZED HOTSPOT

Sukirat K. Bhullar[1], Chih-Kang Chang[1], Christina Lee[1], Nicole Eklund[2], Teresa Baker[2], Nicholas Wendel[2], Andrew Chin[1], Franchino Porciuncula[2], Terry Ellis[2*], Conor Welsh[1*]
[1]John A. Paulson School of Engineering and Applied Sciences, Harvard University, Boston, MA
[2]College of Health and Rehabilitation Sciences, Sargent College, Boston University, Boston, MA
*Dr. Conor Walsh: walsh@seas.harvard.edu; Dr. Terry Ellis: tellis@bu.edu

Introduction: Parkinson's disease (PD) is one of the leading causes of disability worldwide [1,2], with individuals experiencing a range of motor impairments, including freezing-of-gait (FoG). FoG is characterized by an inability to move forward despite an intention to walk. Individuals experience a breakdown in their spatiotemporal gait metrics before FoG occurs [3]. Activities that provoke FoG are individual-specific and may include turning, obstacles, and other environmental factors. Current pharmacological and surgical interventions for PD provide only modest reductions in FoG that diminish as the disease progresses [4]. Recently, a bilateral hip-flexion assisting soft wearable device, i.e., exosuit, has been shown to eliminate FoG for an individual during straight-line walking [5]. However, many participants have hotspots that trigger FoG, such as changes in floor surfaces and tight turns around obstacles. Subsequently, this case study investigates the effectiveness of the exosuit during a personalized hotspot for one participant during four different visits.

Methods: A personalized hotspot for one participant with PD (69 years, male) was identified as them rushing to answer their doorbell. This scenario was replicated in the three lab visits and one home visit with the exosuit. The participant completed randomized trials with and without assistance from the exosuit. The cable connecting the thigh and the waist belt provided bilateral hip flexion assistance. A tensional force of 7.5% body weight was applied at maximum hip extension detected using thigh-mounted inertial measurement units (IMU; XSens, Netherlands). Data was also collected using pressure insoles (XSENSOR, Canada) and IMUs mounted on the bilateral shanks and feet.

Total time spent freezing (s) was used as an objective measure of freeze severity. It was obtained by identifying FoG episodes using pressure insoles and shank IMUs, and validated by a physical therapist. We compared the total completion time (s) of the personalized hotspot as a functional outcome. We calculated spatiotemporal gait metrics, stride length (m) and stride frequency (strides/min), using foot IMUs and pressure insoles. Considering the small sample sizes, hedge's g effect size was used to evaluate the effect of the exosuit assistance on total time spent freezing and total completion time. Hedge's g effect sizes were considered small ($g \geq 0.2$), medium ($g \geq 0.5$), or large ($g \geq 0.8$) [6]. Given the larger sample sizes, Cliff's δ effect sizes were used for stride length and stride frequency. Cliff's δ effect sizes were considered small ($\delta \geq 0.15$), medium ($\delta \geq 0.33$), and large ($\delta \geq 0.47$) [7].

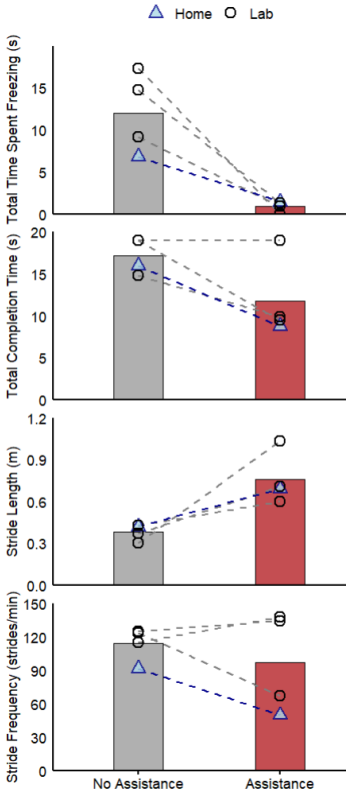

Figure 1: Total time spent freezing, total completion time, and spatiotemporal gait metrics with and without exosuit assistance during the participant's personalized hotspot.

Results & Discussion: On average, the total time spent freezing decreased from 11.95 ± 4.45 s to 0.90 ± 0.64 s (mean ± stdev) with assistance (g = 1.19). The total completion time decreased from 21.22 ± 9.45 s to 15.39 ± 12.08 s with assistance (g = 0.99). The stride length increased from 0.37 ± 0.22 m to 0.72 ± 0.31 m with assistance (δ = -0.62), while the stride frequency decreased from 114.36 ± 66.59 strides/min to 94.36 ± 99.93 strides/min with assistance (δ = 0.45).

The assistance reduced the participant's freezing severity and the total completion time during the personalized hotspot, which is challenging due to FoG. The assistance also had a large effect on increasing their stride length and a medium effect on decreasing their stride frequency, which can be interpreted as an improvement in spatiotemporal gait metrics. Further investigation is required to explore the effectiveness of the exosuit on a larger sample size and additional hotspots.

Significance: A bilateral hip-flexion exosuit reduces FoG during a personalized hotspot for one participant across multiple visits. The exosuit enhanced the spatiotemporal gait metrics that tend to deteriorate during walking in individuals with PD, specifically during their activities of daily living.

Acknowledgments: This work was supported by the Michael J. Fox Foundation (MJFF-024589; T.E. 554 and C.W.), the National Science Foundation (CMMI-1925085; C.W.), the National Institutes of 555 Health (U01 TR002775; C.W. and T.E.), the Massachusetts Technology Collaborative (C.W.), 556, the Social Technology for Global Aging Research Initiative at Harvard University (C.W.), and the Raj Bhattacharyya and Samantha Heller Assistive Technology Initiative Fund.

References: [1] Dorsey, E. R. et al. (2018), *Lancet Neurol.* [2] Feigin, V. L. et al. (2017), *Lancet Neurol.* [3] Chee et al. (2009), *Brain.* [4] Cui et al. (2021), *Front. Hum. Neurosci.* [5] Kim, Porciuncula et al. (2024), *Nat Med.* [6] Hedges et al. (1985), *J. Educ. Stat.* [7] Cliff, N. (1993), *Psychol. Bull.*

NEURAL ADAPTATION TO EXOSKELETON ASSISTANCE DURING WALKING

Banu Abdikadirova[1*], Paul McDonnell[2], Molly Fabrizio[1], Wouter Hoogkamer[2], Douglas N. Martini[2] & Meghan E. Huber[1]
Departments of [1]Mechanical and Industrial Engineering and [2]Kinesiology, University of Massachusetts Amherst
*Corresponding author's email: babdikadirov@umass.edu

Introduction: Wearable robotic exoskeletons hold great promise for assisting gait across diverse populations, including able-bodied individuals [1], aging adults [2], and those with gait impairments [3]. Advances in exoskeleton control personalization, such as human-in-the-loop optimization, have further improved performance [4]. However, a recent finding showed that such personalization accounts for only a quarter of the improvement in gait efficiency, while human adaptation contributes more than half [5]. This highlights the critical role of human adaptation in shaping the performance of the coupled human-exoskeleton system, underscoring the need for a deeper understanding of its mechanisms [6]. To address this, the present study examined changes in metabolic energy expenditure and prefrontal cortex (PFC) activity using functional near-infrared spectroscopy (fNIRS) (**Fig. 1A**) while participants learned to walk with an assistive hip exoskeleton (**Fig. 1B**). We hypothesized that both measures would decrease with practice, reflecting reduced effort and cognitive demand. Prior neuroimaging studies of novel motor skill learning show high initial PFC activity that decreases with practice, coinciding with improved performance [7,8].

Methods: Eight individuals (24.3 ± 3.5 years, 4 females and 4 males) practiced walking on a treadmill at 1.3 m/s with a hip exoskeleton that provided time-based assistance in hip flexion, which was triggered by the detection of maximum hip extension (**Fig. 1D**). The experimental protocol consisted of six sessions: pre-training assessment, three training sessions, post-training assessment, and retention assessment (**Fig. 1C**). In all sessions except the post-assessment, participants walked with the exoskeleton powered for 20 minutes, during which the metabolic cost of walking was measured. In the pre, post, and retention assessments, participants walked for 9 minutes with the exoskeleton switching from powered to unpowered mode every 90 seconds, during which relative concentration changes (from baseline standing) of oxygenated hemoglobin (ΔHbO_2) in the PFC were quantified. A one-way repeated measures analysis of variance (ANOVA) tested the effect of session on the reduction in metabolic cost while walking with the exoskeleton powered compared to unpowered. A two-way repeated measures ANOVA tested the effect of session and exoskeleton mode (powered vs. unpowered) on PFC activity. The significance level was set to $\alpha = .05$, and significant effects/interactions were assessed post-hoc with pairwise *t*-tests.

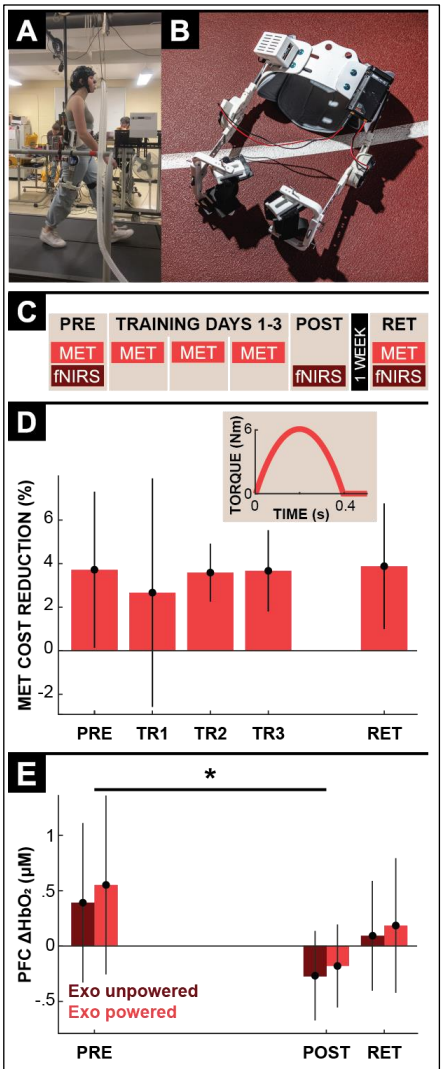

Figure 1. A. Experimental setup, **B.** Portable HRSL hip exoskeleton, **C.** Experimental protocol, **D.** Average reduction in metabolic cost across sessions, **E.** Average PFC activity change across sessions. * indicates a statistically significant effect. Error bars represent ± SD.

Results & Discussion: Walking with the powered exoskeleton reduced metabolic cost (**Fig. 1D**). Due to excessive noise, one participant's metabolic data was excluded from analysis. However, contrary to our hypothesis, session had no significant effect on metabolic cost reduction ($F(4,24) = 0.13, p = 0.97$), suggesting that training did not further improve metabolic savings. In contrast, session did have a significant effect on ΔHbO_2 ($F(2,14) = 4.44$, $p = 0.03$) (**Fig. 1E**). Specifically, ΔHbO_2 decreased from pre- to post-assessment ($t(7) = 3.20$, $p = 0.02$), indicating reduced PFC activity following training. This reduction represents a shift away from executive control of gait, suggesting increased automaticity (i.e., motor learning). While ΔHbO_2 values remained lower at retention compared to pre-training, the reduction was not statistically significant ($t(7) = 1.42$, $p = 0.20$). Exoskeleton mode also had a significant effect on ΔHbO_2 ($F(1,7) = 9.69$, $p = 0.02$). Walking with the exoskeleton powered resulted in more positive ΔHbO_2, indicating greater PFC activation, and thus cognitive load, than walking with the device unpowered. The condition × session interaction was not significant ($F(2,14) = 0.83$, $p = 0.46$).

Significance: Although training did not reduce the metabolic cost of exoskeleton-assisted walking, the decrease in PFC activity suggests that learning still occurred. This implies that fully leveraging mechanical assistance of an assistive exoskeleton is a complex locomotor skill, similar to learning to ice skate or ski, which are also devices designed to enhance locomotor efficiency. These results underscore the need for a deeper understanding of the mechanisms and time scales involved in learning to walk with assistive exoskeletons to more effectively evaluate and improve their design.

References: [1] G. Sawicki et al. (2020), *J Neuro Eng and Rehab*. [2] S. Galle et al. (2017), *Gait & Posture*. [3] K. Takahashi et al. (2015), *J Neuro Eng and Rehab*. [4] P. Slade et al. (2024), *Nature.* [5] K. L. Poggensee et al. (2021), *Science Robotics*. [6] R. Hybart and D.P. Ferris (2023), *IEEE Trans. Neural Syst. Rehabil. Eng.* [7] H. Ayaz et al. (2012), *Neuroimage.* [8] V. Puttemans et al. (2005), *J Neurosc*.

KINEMATIC COUPLING RELATIONSHIPS BETWEEN HIP AND KNEE JOINTS WHEN WALKING WITH A HIP EXOSKELETON

Chihyeong Lee[1], Hyeonwoo Kim[2], Chae Lynne Kim[1], Jooeun Ahn[1,3], Keewon Kim[4], *Yujin Kwon[4]
[1]Department of Physical Education, Seoul National University, South Korea,
[2]College of Medicine, Seoul National University, South Korea
[3]Institute of Sport Science, Seoul National University, South Korea
[4]Department of Rehabilitation Medicine, Seoul National University Hospital, South Korea
*Corresponding author's email: yujinkwon@snu.ac.kr

Introduction: Flexible wearable robots are transforming mobility assistance devices, which feature lightweight designs and improved wearability, making them suitable for daily integration. These innovations have the potential to enhance the quality of life for elderly individuals, those recovering from injuries, and even healthy users seeking to increase their physical activity. Despite their potential, research on flexible wearable robots is still limited. A deeper understanding of their interaction with human motion is necessary to ensure natural gait patterns, reduce user discomfort, and optimize mobility support. Thus, this study aims to quantitatively evaluate differences in joint coordination patterns between robotic and human motion using a vector coding technique when walking with a hip assist robot.

Methods: Eleven healthy young adults (age: 25.1 ± 1.8 yrs, height: 1.70 ± 0.07 m, mass: 65.7 ± 11.8 kg) participated in this study. This study utilized a flexible wearable hip robot (1.4 kg; WIM, WIRobotics, South Korea) to assist participants during the experimental tasks. Each participant performed 2-min treadmill walking in three conditions in a randomized order: (1) normal walking (*None*), (2) walking with a robot worn but inactive (*Off*), and (3) walking with a robot worn and active (*On*). All tasks were conducted at each participant's preferred walking speed (mean: 1.06 ± 0.09 m/s). Whole body kinematic data recorded using a 3D motion capture system were used to compute joint angles via an inverse kinematics approach in OpenSim. Then, we used a vector coding technique to calculate coupling angles at each time point. At each time point of the angle-angle plot (Fig 1A), we calculated coupling angle by applying the arctangent function and mean coupling angle for each gait cycle phase (early, mid, late stance and terminal swing) [1,2]. We then calculated mean coupling angles across all gait cycles and categorized them into one of four coordination phases [1] – proximal phase (hip joint rotates exclusively), in-phase (hip and knee joints rotate in the same direction), distal phase (knee joint rotates exclusively), and anti-phase (hip and knee joints rotate in the opposite directions). We performed repeated measures ANOVA to evaluate the effect of walking conditions on the mean coupling angle.

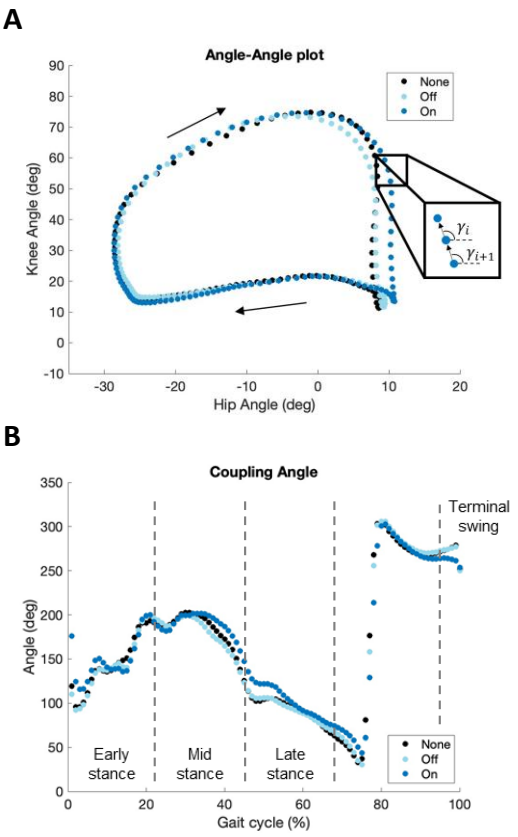

Figure 1: Mean sagittal plane hip-knee angle-angle plot and coupling angle (γ) calculation method (A) and mean hip-knee coupling angle in three walking conditions (B).

Results & Discussion: A significant effect of walking condition was observed in the mean coupling angle during the mid stance phase (None: 183.0º, Off: 178.4º, On: 188.0º; p=0.012) and the late stance phase (None: 92.1º, Off: 92.4º, On: 102.5º; p=0.035) (Fig 1B). Although pairwise differences were not statistically significant after adjustment, the mean coupling angle in the mid and late stance phases tended to increase in the On condition. The mean coupling angle during the mid stance phase near 180° suggests a proximal phase coordination pattern where hip extension predominates. The slightly increased values above 180° in the On condition suggest a shift toward the in-phase coordination pattern, which was driven by slightly increased knee extension during the mid stance phase while the difference in the hip joint angle between conditions was not noticeable. For the late stance phase, the result of mean coupling angle (92.1 ~ 102.5º) indicates a distal phase pattern dominated by knee flexion. However, coupling angles exceeding 90° reflect a tendency toward the anti-phase coordination within the distal phase, which aligns with the greater knee extension in the On condition. The results suggest that the hip-based robot may influence knee joint movement, specifically knee extension in the mid to late stance phase although the robot was designed to mainly assist hip flexion and extension.

Significance: The study findings suggest that a vector coding technique can detect differences in hip-knee joint coordination patterns in the mid and late stance phases between non-assisted and assisted walking with a hip assist robot and that coupling angle can be used as a measure for evaluating kinematics of assisted walking.

Acknowledgments: This work was supported in part by the grant of the Korea Health Technology R&D Project through the Korea Health Industry Development Institute (KHIDI), funded by the Ministry of Health & Welfare, Republic of Korea (no. HK23C0071).

References: [1] Chang et al. (2008), *J Biomech* 41(14); [2] Hafer and Boyer (2017), *Gait Posture* 51.

QUANTITATIVE AND QUALITATIVE EFFECTS OF BIOLOGICAL TORQUE ASSISTANCE PARAMETERS USING A HIP EXOSKELETON DURING DECLINE WALKING

Katherine Peterka[1*], Jelovy Djaja [1*], Keya Ghonasgi[1,2], Aaron Young[1]
[1]Georgia Institute of Technology, Atlanta, GA, USA, [2]Rice University, Houston, TX, USA
*Corresponding author's email: kpeterka3@gatech.edu, jdjaja7@gatech.edu

Introduction: Robotic exoskeletons offer a compelling solution for targeted gait assistance. The hip exoskeleton developed at the Exoskeleton and Prosthesis Intelligent Controls Lab features a joint moment-driven Temporal Convolution Network (TCN) controller, addressing gait imbalance [1]. The exoskeleton provides torque assistance at varying magnitudes and timing delays relative to estimated biological torque, improving movement efficiency in everyday ambulatory tasks. Prior studies have explored the effects of modulating assistance in spline-based control for able-bodied and hemiparetic participants [2]. However, no exhaustive study has examined biologically driven assistance's effects on quantitative and qualitative performance metrics. We hypothesize that as assistance magnitude and timing are increased, so will step lengths and peak ground reaction forces for decline walking. Prior works have suggested a bowl-shaped change in metabolic cost relative to assistance timing (lowest cost at mid-level delay). We expect to see a corresponding inverted bowl in user preference.

Methods: 6 able-bodied (AB, Georgia Institute of Technology IRB H22051) participants utilized the hip exoskeleton during decline walking (Fig 1A). Participants walked under the exoskeleton off and 12 assistance conditions (10% and 20% assistance magnitude, and 0, 40, 80, 120, 160, and 200ms assistance delay) in a randomized order (Fig 1B). Pairwise preference ratings were collected by comparing the current condition to the previous one (better: +1, worse: -1, similar: 0). Additionally, motion capture and force plate data were collected for all control modes to compute step length and peak ground reaction force (Fig 1 A). The Davidson-Bradley Terry Model [3], [4] was used to determine each participant's rankings. Using 2-way repeated measures ANOVA, was performed on all step metric data and preference data normalized by the S0D0 (exoskeleton off) data.

Results & Discussion: Step length was the only gait parameter significantly affected by both assistance magnitude and timing delay. ANOVA revealed significant effects for assistance magnitude ($p = 0.017$) and timing delay ($p = 0.002$) on step length, with no significant interaction ($p = 0.448$), indicating independent effects. Longer delays (160–200 ms) increased step length, particularly at 10% assistance, while 20% assistance initially reduced step length before recovering at later delays (Fig 1C). User preference during decline walking (Fig 1D) was significantly influenced by timing delay ($p = 0.016$) but not by assistance magnitude ($p = 0.609$). Mid-range delays (80–120 ms) had the lowest preference scores, suggesting that assistance timing plays a key role in user preference.

The step length results matched our original hypothesis, though peak ground reaction forces did not. Preference results showed the opposite trend than what we expected, with lower preferences at mid-level delays and higher preferences at higher delays. Further, we observed an alignment between step length increases and higher preference scores at later delays, suggesting that biomechanical efficiency may drive user perception, at least for decline walking in AB individuals.

Significance: While we saw the expected trend in step length increasing with increased delay, we did not see expected results for ground reaction forces and preference. Our preference results, in fact, were exactly the inverse of our expectation from level-walking hip exoskeleton assistance effects on metabolic cost. These trends suggest that assistance timing can significantly affect user perception while both magnitude and timing affect step length, and that these effects may be vary across walking tasks. The current population, able-bodied individuals, may have different responses to exoskeleton assistance than individuals with gait impairments. It should be noted that these surprising results could be due to a small population size or the chosen decline walking condition. Our results indicate a need for further experiments to confirm these trends in decline walking hip exoskeleton assistance with larger subject populations and in individuals with hemiparesis.

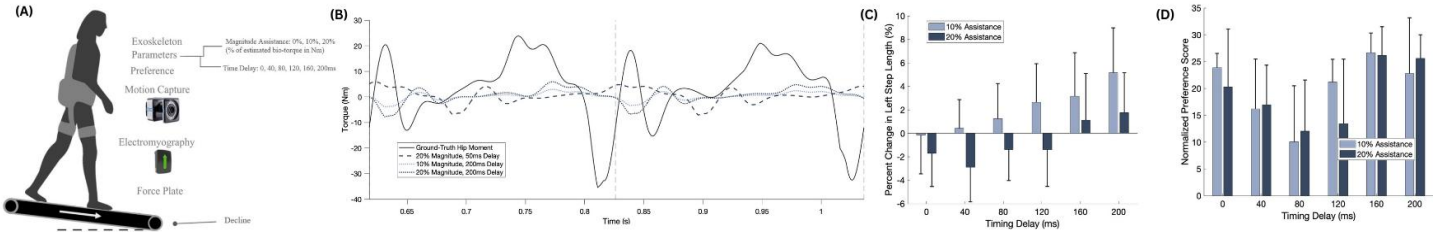

Figure 1. Experimental Setup and Decline Walking Results (A) illustrates the experimental setup, where participants walked on a treadmill under decline walking conditions while wearing a powered exoskeleton. Motion capture, EMG, and force plates were used to assess gait mechanics, while user preference was recorded. (B) Shows applied hip joint torque across the gait cycle, illustrating the effects of assistance magnitude and timing delay on torque delivery for a representative participant. (C) shows the percent change in left step length during decline walking. (D) presents normalized preference scores for decline walking.

Acknowledgments: This research was partially supported by National Institutes of Health Grant No. 1DP2HD111709-01.

References: [1] Molinaro, D., et al. (2024), *Sci. Rob*. 9 (88), [2] Pan, Y., et al. (2022), *Annls. Biomed Eng.* 51 (410), [3] Davidson (2012) *J Am. Stat. Assoc.* 65 (329), [4] Bradley, R., Terry. M., *Biometricka* 39(3/4) (1952).

THE EFFECTS OF ANKLE EXOSKELETON ASSISTANCE ON GAIT CAPACITY IN YOUNGER ADULTS

Ethan Simaitis[1*], Oluranti Olatosi[1], Michael D. Lewek[1,2], Jason R. Franz[1]
[1] Lampe Joint Department of Biomedical Engineering, UNC Chapel Hill & NC State University, Chapel Hill, NC, USA,
[2] Division of Physical Therapy, Department of Health Sciences, UNC Chapel Hill, Chapel Hill, NC, USA
*Corresponding author's email: simaitis@email.unc.edu

Introduction: Extensor muscles spanning the ankle perform more than 50% of the mechanical work needed to power walking, which includes their pivotal role in forward propulsion. Unfortunately, these muscles experience disproportionate declines in function with age and disease which can be resistant to conventional intervention [1]. Ankle exoskeletons (EXOs) are a promising solution designed to augment the function of these muscles by providing adaptive plantarflexion torque assistance to restore ankle power output. Prior research has shown that walking with ankle EXOs can reduce metabolic energy cost, increase speed, and increase habitual propulsion; these outcomes have been used to suggest an improved capacity for independent mobility [2]. However, no study to date has objectively quantified the extent to which ankle EXOs can improve users' maximum capacity to generate propulsion during walking. Thus, the purpose of this study was to investigate the effects of ankle EXO assistance on performance of a 'biomechanical stress test' designed in previous studies [e.g., 3] to quantify maximum propulsive capacity during walking. We hypothesized that ankle EXO assistance would increase walking duration in the biomechanical stress test while also increasing maximum positive propulsive impulse.

Methods: Thus far, 6 healthy younger adults (age: 22.8±2.6 yrs) have participated. We first used overground walking trials to determine each participant's preferred walking speed (1.39±0.14 m/s). Participants then completed a series of treadmill walking trials at their preferred walking speed while wearing a bilateral powered ankle exoskeleton (Biomotum SPARK). In a fully randomized order, participants walked with four levels of ankle EXO assistance: none (0% body weight [BW]), low (5% BW), medium (15% BW), and high (25% BW). Values represent maximum assistance, prescribed proportional to biological ankle moment. Following a 60-s acclimation period at the respective assistance level, participants responded to a horizontal impeding force delivered to a waist belt via a motor-driven system that increased linearly at a rate of +1 %BW/s. This biomechanical stress test continued until measuring an inexorable posterior sacrum displacement of 0.5 m, indicating that participants had reached their maximum propulsive capacity. We measured ground reaction forces using a split-belt treadmill and collected kinematic data of the pelvis and lower extremities using 3D motion capture. A repeated measures analysis of variance (ANOVA) tested for the effects of ankle EXO assistance on the maximum impeding force withstood during the biomechanical stress test.

Results & Discussion: We have thus far found that, for 6 of 6 participants, ankle EXO assistance increased performance during our biomechanical stress test, demonstrating the ability of these wearable robotic devices to objectively enhance maximum propulsive capacity in walking. However, assistance levels capable of conveying those benefits were not one-size-fits-all. In fact, on average, data thus far show no repeated measures main effect of ankle assistance level ($p=0.70$). Conversely, a participant-specific analysis revealed that assistance values of low (n=3), medium (n=1), and high (n=2) conveyed an average increase of 14.7% in the maximum capacity to generate propulsion compared to completing the stress test without assistance ($p<0.01$) (Fig. 1A). Biomechanical outcomes provide a likely explanation for these observations; those performance gains were accompanied by – on average – a 12% increase in maximum anterior GRF (i.e., "propulsive") impulse (Fig. 1B). Indeed, relative to unassisted walking, changes in positive propulsive impulse elicited by ankle EXO assistance have thus far exhibited moderate-to-strong correlations with those in biomechanical stress test performance (e.g., 25% BW: $R^2 = 0.664$, blue symbols; participant-specific maximum: $R^2 = 0.328$, green symbols) (Fig. 1C).

Significance: Our findings provide objective evidence that powered ankle exoskeletons can enhance maximum propulsive capacity in walking. Beyond prior reports of their metabolic benefits, improved propulsive capacity has the potential to enhance community accessibility for individuals with walking impairment.

Acknowledgments: Funded in part by a grant from NIH (R01AG058615)

References: [1] Franz (2016) *ESSR*. [2] Chuang et al. (2023) *Biomed Eng Online*. [3] Conway et al. (2018) *J Appl Biomech.*

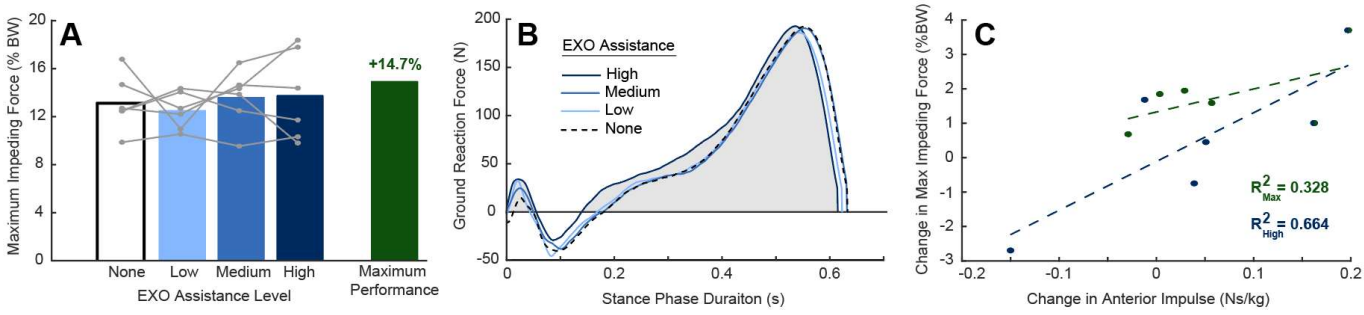

Figure 1: (A) Blue bars represent group-average results of performance on the biomechanical stress test across EXO conditions. Green bar is the average of each participant's maximum performance independent of assistance level. (B) Group-average results of the maximum ground reaction force profile across EXO conditions. (C) Scatterplot displaying the correlation between changes in maximum impeding force and anterior impulse from no assistance to high assistance (R^2_{High}) and from no assistance to maximum performance (R^2_{Max}).

FOREARM FLEXOR MUSCLE STRENGTH & ELBOW JOINT GAP CHANGES WHEN UTILIZING FLEXPRO GRIP

*Jessica K. Geiger[1,2], Brett S. Pexa[3], Blake W. Jones[1], Kristen F. Nicholson[2]
[1]Wake Forest University School of Medicine, Winston-Salem, NC, [2]Department of Orthopaedic Surgery & Rehabilitation, Wake Forest University School of Medicine, [3]Department of Athletic Training, High Point University, High Point, NC
*Corresponding author's email: jkgeiger@wakehealth.edu

Introduction: The overarm throwing motion is one of the fastest human movements, generating elbow valgus stress that can exceed the ulnar collateral ligament's (UCL) tensile strength [1]. With pitchers throwing harder and more frequently, UCL injuries are rising [2]. The pitching motion creates a maximum valgus stress of 64 Nm in the elbow, with an average ultimate moment of 34 Nm for the UCL [3]. This discrepancy between the valgus stress in pitching and the ultimate moment of the UCL is believed to be due to the flexor-pronator muscles acting as dynamic stabilizers to the UCL [4]. These muscles are often injured in congruence with UCL injuries [3]. To combat these injuries, a unique training device was created. The FlexPro Grip (FlexPro Grip 'FPG', LLC, Toledo, OH) allows for isometric applications of force in four directions: flexion, extension, ulnar deviation, and radial deviation. The FPG claims to optimally target and strengthen the muscles and tendons throughout the forearm for rehabilitating and preventing UCL injuries. The purpose of this study is to investigate changes in flexor muscle strength, cross-sectional area, and ulnohumeral joint (UHJ) space gapping before and after baseball pitchers complete a 10-week program using the FPG training device. This cohort (FPG group) will be compared to a control group of participants who do not complete the program. We hypothesized that there will be a significant increase in flexor muscle cross-sectional area (MCSA) and significant decrease in joint loaded UHJ gapping in participants who complete the 10-week FlexPro Grip program and no significant changes in those who do not use FPG.

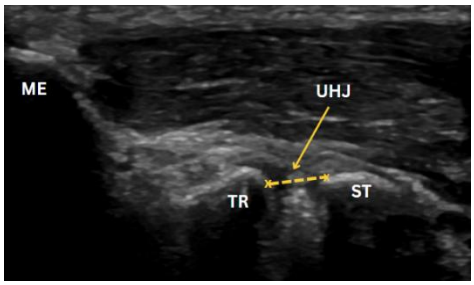

Figure 1: US UHJ Gapping – Medial Elbow unloaded at 30°. ME: Medial epicondyle; TR: Trochanter; ST: Sublime tubercle

Methods: This study was a prospective cohort study approved by the University's Institutional Review Board. Participants were healthy Division I male baseball pitchers (18 FPG group, 18 control group) from two local universities who reported having no pain and full participation in all games and practices. Participants were excluded if they violated compliance, had an injury or pain, or were not throwing. Participants' UHJ gaps (mm) were measured using ultrasound (US) in both unloaded and loaded conditions. UHJ gapping was defined as the shortest distance from the distal-medial corner of the trochlea to the proximal edge of the sublime tubercle (Fig. 1). Measurements were taken with participants lying supine, arm abducted to 90°, and elbow flexed at 30° and 90°. Loaded testing was performed by strapping a 2.5-kg weight to the wrist to induce valgus stress while remaining in a relaxed position. The MCSA (mm^2) of the flexor digitorum profundus (FDP), flexor carpi ulnaris (FCU), and flexor digitorum superficialis (FDS) were measured using ultrasound in the supine testing position with 30° of elbow flexion, unloaded, and at rest. The difference in UHJ gapping between the loaded and unloaded conditions at 30° (D30) and 90° (D90) of flexion were calculated. The FPG training protocol consisted of a periodized ramp up training protocol to increase forearm flexor muscle strength. Participants followed coaches' instructions on training frequency and intensity. Training days included variations of ulnar deviation, fingertip flexion, mid finger flexion, finger extension, and radial deviation. After 10 weeks, all variables were remeasured for both cohorts. A two-way (Between Group, Within Time) mixed ANOVA ($\alpha = 0.05$) for each variable was performed to assess changes in UHJ gap and MCSA before (pre) and after (post) the 10-week period.

Results & Discussion: Significant interactions between group and time were present for all conditions, excluding unloaded UHJ gapping (Table 1). The FPG pre to post displayed a significant decrease in UHJ gapping for all conditions and a significant increase in MCSA. The control group presented almost no significant change except for an increased UHJ gap which was opposed to the desired decrease. Decreases in UHJ gapping and an increase in MCSA are beneficial towards protecting the UCL by enhancing the elbow's ability to withstand stress and providing functional stability to the elbow joint. Smaller UHJ gaps are associated with improved stability of the medial elbow joint and reducing the risk of injury, which is critical when placing stress on the elbow [5]. Additionally, higher elbow stability signifies a more secure and less lax joint structure. The FPG group presenting decreased UHJ gapping under all conditions after the 10-week protocol allows us to deduce FPG is effective in reducing injury risk due to UCL stress. The FDP, FDS, and FCU play a critical role in protecting the UCL by providing dynamic support to the UHJ, especially during movements that involve high valgus stress like pitching. The FPG group presenting significant increases in their MCSA further indicates that FPG is an effective tool for protecting and stabilizing the UCL as these muscles provide critical stabilization and resistance to valgus forces.

Table 1: Interaction Effects

Condition	P-Value
30° Loaded	<.001
90° Loaded	<.001
D30	<.001
D90	<.001
FDS	<.001
FCU	.003
FCU	.003

ANOVA Group x Time significant interaction effects ($p<0.05$) for tested conditions.

Significance: This study identifies that the UHJ gapping decreases (unloaded and loaded) and MCSA increases after training with a 10-week FlexPro Grip program. Utilizing this training protocol may help more baseball pitchers prevent and recover from UCL injuries more effectively by training the extrinsic protective muscles to the elbow under valgus loads.

References: [1] Werner et al. (2001), *Am J Sports Med*, 29(3); [2] Mahure et al. (2016), *J Shoulder Elbow Surg* 25(6); [3] Izeku et al. (2022), *J. Shoulder Elbow Surg*., 31(8); [4] Udall et al. (2009), *Am J Sports Med*, 46(9); [5] Hitoshi et al. (2021), *J. Shoulder Elbow Surg*., 30(9)

WEIGHT TRANSFER AND PITCH VELOCITY: A COMPARATIVE STUDY OF YOUTH AND PROFESSIONAL BASEBALL PITCHERS

Zyanya Burgos Resendiz[1], Julia Dunn[2], Michelle Sabick[3*]
[1]Department of Mechanical and Materials Engineering, University of Denver, Denver, CO
z.burgosresendiz@du.edu

Introduction: Baseball pitching is a complex skill requiring full-body coordination [1]. During the foot contact phase of pitching, both the stride and drive legs generate forces that contribute to pitch velocity. Vertical ground reaction forces (GRF) are the largest components affecting pitch velocity [2]. Energy generated by the legs flows upward through the body to the arm, with weight transfer from one leg to another occurring between 56-66% of the pitch duration for youth baseball pitchers [3]. Although this has been studied in youth pitchers, a deeper examination of the vertical GRF in professional pitchers is needed [2, 3]. This study aims to compare the timing of weight transfer from the drive leg to the stride leg in two groups of baseball pitchers: youth pitchers and collegiate/professional pitchers to understand how weight transfer relates to pitch velocity. A deeper understanding of this transition may help us provide critical information to players and coaches to increase pitch velocity while protecting developing athletes from injury.

Methods: Motion capture data from the three fastest strike pitches were collected from 23 male youth baseball pitchers between the ages of 9-13 (weight = 46.19 ± 11.71 kg, height = 1.56 ± 0.12 m, pitch velocity = 27.71 ± 3.71 mph) and 5 male professional baseball pitchers between the ages of 19-21 (weight = 88.77± 14.37 kg, height = 1.88 ± 0.07 m, pitch velocity = 83.42 ± 4.12 mph). The youth baseball pitchers' whole-body kinematics were collected using a 14-camera motion capture system operating at 250 Hz (Vicon Motion Systems, Oxford, UK) [3]. Data from professional pitchers were collected using a portable 10-camera motion capture system (Qualisys Motion Capture, Goteborg, Sweden) operating at 250 Hz. For both groups, GRF data were collected at 1000 Hz using two portable force platforms (Kistler, Winterthur, Switzerland), embedded in a custom pitching mound that allowed the location of the forward force platform to be adjusted depending on the pitcher's stride length [3]. The duration of the pitching motion was normalized from maximum stride leg knee height (0%) to maximum internal rotation of the shoulder after ball release (100%). Data analysis was performed using MATLAB (The MathWorks, Inc., Natick, MA) to determine the instant when stride foot contact (SFC) occurred. Weight transfer was assumed to have occurred after 10% of the pitcher's body weight was transferred from the drive leg to the stride leg. Pitch velocity and SFC timing were then compared for each group of pitchers. An unpaired t-test was performed to compare mean pitch velocity between the professional and youth pitchers.

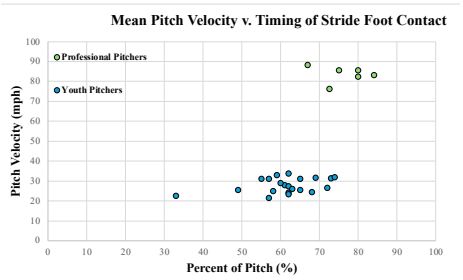

Figure 1: Pitch velocity generated vs. timing of weight transfer. Youth pitchers achieved pitch velocities of 20-35mph while professional pitchers ranged from approximately70-90mph.

Results & Discussion: The youth pitchers made SFC at 61.24% ± 8.93 of their pitch, whereas professional pitchers made SFC significantly later at 74.42% ± 6.15, p = 0.004 (Figure 1). This may indicate differences in weight transfer strategy associated with skill or experience. In both youth and professional pitchers, no significant relationships between pitch velocity and the timing of SFC were found. However, previous research suggests that correlations between SFC and timing of ball release could affect pitch velocities [2, 4]. On average, professional pitchers initiated SFC later in the pitch than youth pitchers (Figure 2), and much later than the optimal timing agreed upon by youth coaches, 56-66% [3]. None of the professional pitchers we studied had a weight transfer within that window. Interestingly, the fastest pitch velocity recorded was close to the proposed optimal range. Although this study evaluated the timing of SFC and pitch velocity, there are many other factors in the pitching motion that likely influence pitch velocity.

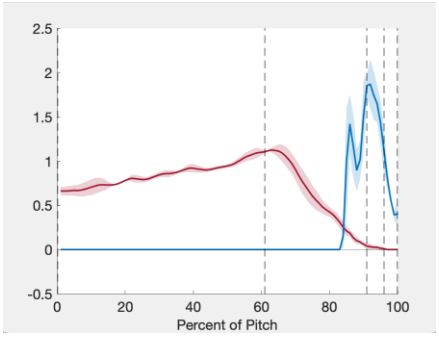

Figure 2: Mean ± SD vertical ground reaction forces for an exemplar professional pitcher. Red curve represents the drive leg while blue curve represents the stride leg.

Significance: This study analysed how the timing of the weight transfer from the drive leg to the stride leg during the baseball pitch affects pitch velocity in both youth and professional pitchers. These findings may indicate that coaching youth pitchers to initiate SFC later in their pitch may help to increase pitch velocity from power generated in the lower extremities, rather than putting additional strain on the upper body. We will continue to investigate coordination and timing during the pitching motion in a wider variety of pitchers to help coaches and pitchers to understand the optimal timings for stride foot to help athletes achieve their greatest performance.

Acknowledgments: The authors would like to thank Moira Pryhoda, Jacob Howenstein, Andrew Bryan, and Kristof Kipp for their contributions to project conceptualization and data collection for the youth pitchers' group.

References: [1] MacWilliams, B. A., Choi, T., Perezous, M. K., Chao, E. Y., & McFarland, E. G. (1998). *AJSM*, *26*(1), 66–71 [2] Wasserberger, K. W., & Giordano, K. A. (2023). *Sports Biomechanics*, 1–15. [3] Pryhoda, M. K., & Sabick, M. B. (2022) *Frontiers in Sports and Active Living*, *4*. [4] Elliott, B., Grove, J. R., & Gibson, B. (1988). *Int J Sport Biomechanics*, *4*(1), 59–67.

Pitchers Show Bilateral Lower Extremity Neuromuscular Decline in a Simulated Baseball Game: An RMS Analysis

*Thomas Demirjian[1], Adam Barrack[2], Jeremy Praski[3], Zachary Domire[1], Nicholas Murray[1]
[1]East Carolina University, Department of Kinesiology, Greenville NC
[2]University of Southern California, Division of Biokinesiology and Physical Therapy, Los Angeles CA
[3]University of Tennessee, Department of Kinesiology, Recreation, and Sport Studies, Knoxville TN
*Corresponding author's email: demirjiant25@ecu.edu

Introduction: Baseball pitching is a complex movement that involves a coalescence of lower and upper extremity movements. Previous research has identified that an increase in pitching volume is associated with elbow and shoulder injury. Increase in pitching volume has also been studied in the context of neuromuscular capacity [1-5]. While neuromuscular activation and muscular capacity has been categorized during the pitching movement [2,6-7], prior work has not used root mean square (RMS) analysis to evaluate the electromyographic changes in both the stride and drive leg after a simulated baseball game. Therefore, our purpose was to quantify changes in RMS values in lower extremity musculature of the drive and stride leg, hypothesizing that pitchers would have decreased RMS values post-game.

Methods: Nine high school and collegiate pitchers (16.67±0.86 yrs, 1.78±0.08 m, 74.6±14.82 kg) were included in this analysis. Electromyographic sensors sampling at 2000 Hz were placed on the muscle bellies of the biceps femoris, medial gastrocnemius, semitendinosus, vastus lateralis/medialis of the stride leg as well as the gluteus maximus, and vastus lateralis/medialis of the drive leg. Prior to starting the first inning, each pitcher underwent maximal voluntary contractions of each muscle in both stride and drive legs. Each pitcher then threw up to 7 simulated innings consisting of 14-18 pitches randomized for type (fastballs, offspeed, breaking balls). The final inning was determined when the pitcher reported that they could not complete another inning. Electromyographic data were filtered using a fourth order butterworth filter with a high cutoff of 5 Hz and a low cutoff at 500 Hz, rectified, and then smoothed with a second order lowpass filter at 10 Hz. Each muscle signal from each pitch in the first and last inning were then normalized to their respective maximal voluntary contractions. Finally, a RMS analysis was performed on each muscle during each pitch, and then averaged by inning. One participant registered a poor maximal voluntary contraction for the gluteus maximus and was removed from the analysis for this muscle. For statistical analysis, two-way repeated measures analysis of variances were performed for each individual muscle with the independent variables being inning (first and last). All statistical analyses were performed in Rstudio with the significance level set to 0.05.

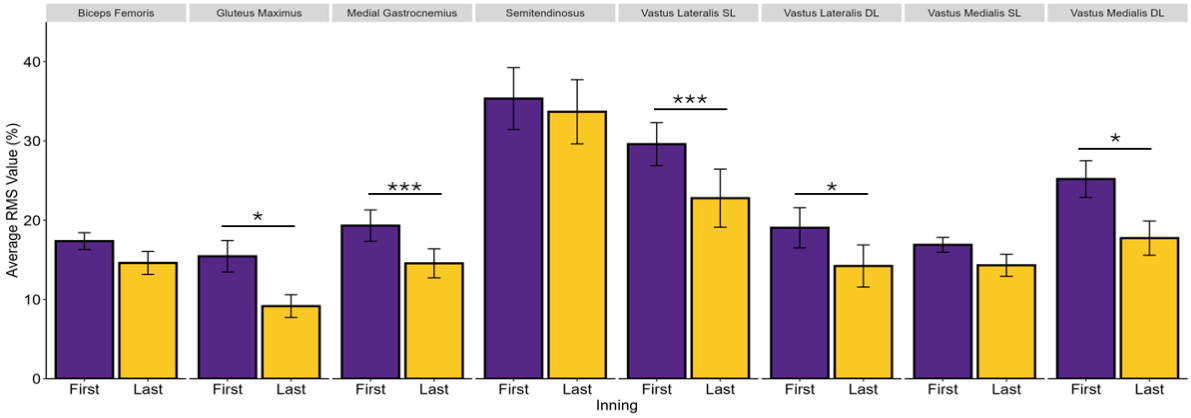

Figure: Comparison of average RMS values between innings. *<0.05, ***<0.001, DL: Drive Leg, SL: Stride Leg

Results & Discussion: After the simulated game, a significant main effect for inning was observed for the vastus lateralis ($F(1,8) = 6.07$, $p<0.001$) and medial gastrocnemius ($F(1,8) = 30.22$, $p < 0.001$) of the stride leg as well as the vastus lateralis ($F(1,8) = 6.82$, $p = 0.031$), vastus medialis ($F(1,8) = 7.49$, $p = 0.026$), and gluteus maximus ($F(1,7) = 17.23$, $p = 0.002$) of the drive leg **(Figure)**. No significant main effects were observed for the vastus medialis, biceps femoris, and semitendinosus of the stride leg. The stride leg vastus lateralis and medial gastrocnemius experienced a decrease in RMS of 9.16% and 5.52%, respectively. Likewise, the drive leg vastus lateralis, vastus medialis, and gluteus maximus experienced a decrease in RMS of 9.57% , 8.30%, and 7.54% respectively. In agreement with strength outcomes reported in simulated games [2,6-7], our RMS analysis provided strong indication that pitch volume contributed to a decrease in neuromuscular capacity. Interestingly, regardless of leg, the quadriceps experienced the greatest RMS degradation compared to the gastrocnemius and gluteus maximus. Reduced drive leg quadriceps and gluteus maximus capacity may impact the pitcher's propulsive capacity during stride phase. Similarly, reduced stride limb quadriceps and medial gastrocnemius capacity may compromise the timing-sensitive action of the stride limb during the arm cocking and arm acceleration phases of the pitch.

Significance: Bilateral reduction in lower extremity RMS values over the span of a simulated game may underpin capacity-related adjustments to pitching mechanics with implications for injury risk and performance. Future research should explore how time-series kinematics and electromyographical parameters of both the stride and drive leg evolve under the stress of high pitching volumes.

References: [1] Birfer, Sonne, Holmes (2019) *PeerJ* ; [2] Yanagisawa & Taniguchi (2018) *JER* 14(3); [3] Escamila et al., (2007) *Am J Sports Med* 35(1) ;[4] Wang et al., (2024) *Sports Health* [5] Agresta et al., (2017) *Orthop J Sports Med* 7(2); [6] Kokott et al., (2023) *ISBS Proceedings* 41(1); [7] Mullaney et al., (2006) *Am J Sports Med* 33(1)

"AN OUNCE OF PREVENTION"
HOW INCREASING BALL WEIGHT AND SIZE DECREASE ELBOW VARUS TORQUE IN BASEBALL PITCHING

*Glenn S. Fleisig[1], Jonathan S. Slowik[1], Brad Hall[1], David P. Beason[1], E. Lyle Cain, Jr[1]
[1]American Sports Medicine Institute, Birmingham, AL
*Corresponding author's email: glennf@asmi.org

Introduction: With the rate of ulnar collateral ligament (UCL) injuries in professional baseball continuing to rise, Major League Baseball conducted a survey of more than 200 experts to understand the problem. The consensus was that the continued increase in pitch velocity and pitchers throwing more often at maximal effort are associated with high loads within the elbow and the high rate of UCL injuries.[1] This theory is supported by biomechanical research, showing that (a) higher fastball velocity correlates with greater elbow varus torque, especially within-pitcher [2,3] and (b) higher elbow varus torque leads to higher risk of UCL injury.[4] Thus, reducing elbow varus torque may be key for reducing the rate of UCL injuries. Previous research indicated that increased ball weight may correlate with decreased arm torque.[5,6] Thus, the purpose of the current study was to investigate if elbow varus torque is affected by ball weight and size in professional and high-level collegiate pitchers. It was hypothesized that slightly increased ball weight and/or size would decrease elbow varus torque.

Methods: Twenty healthy professional and high-level collegiate baseball pitchers were recruited for the study. Participants were tested in pairs, like pitchers facing each other in a game. After 47 reflective markers were adhered to each pitcher, the pair alternated pitching seven full-effort fastballs for four innings from an indoor mound to a strike zone over a home plate the regulation 18.44 m distance away. The pair used a different type of ball for each inning. The order of the four types of ball was randomized for each pair of participants and the participants were blinded to what ball they were using. The weight and circumference of the four types of balls were: (A) 5 oz, 9.1 in (i.e. regulation baseball); (B) 5 oz, 9.4 in; (C) 6 oz, 9.1 in; and (D) 6 oz, 9.4 in.

Ball speed, horizontal break, and vertical break were recorded with a PITCHf/x system (Sports Media Technology). Motions of the reflective markers were captured at 240 Hz with a 12-camera automated digitizing motion analysis system (Motion Analysis Corporation). Raw data of the markers were filtered using a fourth-order Butterworth low-pass filter with a cut-off frequency of 13.4 Hz. Five kinetic parameters, 25 kinematic parameters, and five ball movement parameters were calculated for each trial.[2,6-9] For each participant, the data from his first two pitches with each ball were excluded from analysis to allow for any acclimation to the ball. Mean values were then computed and compared among the four ball types using two-way (ball weight x ball size) repeated measures ANOVA ($p<0.05$).

Results & Discussion: As hypothesized, increased ball weight and increased ball size correlated with less elbow varus torque. The current study showed a 4% decrease in torque from the 5 oz, 9.1 in ball to 6 oz, 9.4 in ball. In comparison, two previous studies each showed a 3% decrease in torque from 5 oz to 6 oz standard size (9.1 in) balls.[5,6] The current study also found correlations with increased ball weight and/or size and decreased shoulder internal rotation torque, shoulder horizontal adduction torque, and shoulder proximal force. Shoulder internal rotation velocity and elbow extension velocity were significantly less with heavier balls and larger balls. Statistically significant differences were found for several angles, but these differences were less than 1°. Fastball pitch speed and ball break were significantly less with the heavier and/or larger balls.

Key Parameter	5 oz, 9.1 in	5 oz, 9.4 in	6 oz, 9.1 in	6 oz, 9.4 in	Standard Error
Elbow varus torque (Nm)^{W,S}	99.5	97.3	98.2	95.6	3.1
Shoulder internal rotation velocity (°/s)^{W,S}	6718	6622	6546	6516	184
Ball velocity (mph)^{W,S}	85.1	83.9	82.3	81.3	0.6
Ball break (in)^{W}	17.4	17.1	13.4	13.4	0.6

W: Significant difference ($p<0.05$) between 5 oz and 6 oz weight; S: Significant difference ($p<0.05$) between 9.1 in and 9.4 in ball size

The current study suggests that a slightly bigger and heavier baseball might be more appropriate for today's bigger and stronger pitchers and may reduce elbow varus torque. However, there are several unknown factors about how changing the baseball may affect the rates of UCL injuries. Ball weight and size may affect various pitch types and skill levels differently. Pitchers may also adapt to bigger/heavier balls over time modifying their mechanics and strategy. Decreased pitch velocity and break with heavier/bigger balls may lead to more balls hit into play. Ball tackiness and hardness, as well as the height of seams, also affect pitched and batted balls.

Significance: Increasing the weight of baseballs from 5 oz to 6 oz and the circumference from 9.1 in to 9.4 in may reduce elbow varus torque and the risk of elbow injury for pitchers. Future research in league play or simulated play is warranted.

Acknowledgments: This study was funded by a grant from Major League Baseball.

References: [1] Adler D (2025), MLB releases Report on Pitcher Injuries. MLB.com; [2] Slowik JS et al. (2019), J Athl Train 54(3); [3] Sakurai M et al. (2024), Sports Biomech 23(12); [4] Anz AW et al. (2010), Am J Sports Med 38(7); [5] O'Connell ME et al. (2022), J Appl Biomech 38(5); [6] Fleisig GS et al (2017), Sports Health 9(3); [7] Escamilla RF et al (2023), Am J Sports Med 51(4); [8] Fleisig GS et al. (2024), Sports Biomech 23(12); [9] Fleisig GS et al (2024), Am J Sports Med 52(7).

SEGMENTAL CONTRIBUTION TO WHOLE-BODY ANGULAR MOMENTUM IN BASEBALL PITCHING

Jun Ming Liu[1], Christopher Knowlton, Mathew Gauthier, Zach Tropp, Nikhil Verma, Gregory Nicholson, Anthony Romeo, Antonia Zaferiou[1*]
[1]Stevens Institute of Technology
*Corresponding author's email: Antonia.Zaferiou@stevens.edu

Introduction: Baseball pitching involves sequential rotations of body segments from the ground up [1]. The generation of whole-body momenta is a major mechanical objective of pitching [2]. Angular momentum (H) about the body's center of mass (COM) can characterize of how segmental dynamics contribute to whole-body rotation. There is a lack of prior direct investigations of whole-body and segmental H in pitching, despite the stated importance of the timing of H transfer [3]. In a prior study, the trunk was described as the largest contributor towards whole-body H during the double support phase prior to ball release, though the H computational method was limited [4]. Thus, we aimed to investigate the relative contributions of each upper body segmental H to whole-body H.

Methods: High school male pitchers (n=20; mean (S.D.) age of 15.3 (1.0) years) volunteered for this study in accordance with the IRB. Pitchers self-reported an ability to throw 75-mph fastballs. They pitched at least five fastballs on a regulation practice mound at regulation distance (18.44 m) with optical motion capture (Optitrack; 250 fps). Markers and rigid-body clusters were attached to body segments. All variables are expressed in a global coordinate system with a horizontal forward axis defined from mound to home plate, an upward axis as global vertical, and a leftward axis as a cross product of upward and forward axes. The phase of interest began at the time of the maximum front leg knee height and ended at ball release and is normalized from 0-100%. Whole-body H was calculated as the sum of all segments H. Segment H is the sum of (1) the 'local term': the segment's angular velocity multiplied by its moment of inertia, and (2) the 'remote term': the cross product of (a) the vector from the body's COM to the segment's COM and (b) the segment's COM linear momentum relative to the body's COM. Segment and whole-body COM position were calculated using prior methods [1,5]. Segmental maximum H (H_{max}), the time of H_{max}, the contributions of the local and remote terms at the time of H_{max}, and Segmental H_{max} as a percentage of whole-body H were computed for each segment about each global axis.

Results & Discussion: Whole-body H_{max} was the largest about the leftward axis, and it became positive at around 60% of the phase of interest prior to double support (**Figure 1**). All upper body segments except the pelvis had the largest segmental H_{max} about the leftward axis compared to the other axes, signifying the generation of whole-body and segmental rotation in this plane being an important aspect of pitching. Of the upper body segments, the trunk H_{max} was the largest contributor towards whole-body H, followed by the forearm and upper arm at their respective time of H_{max} (**Table 1**). The trunk's importance in rotation generation is consistent with prior research [4,6], and the emergence of the forearm as the next major contributor near ball release is consistent with the objectives of accruing high momentum for the arm segments that are close to the ball. The remote term H was the primary contributor (at least 70%) of segmental H for all upper body segments, meaning that the segments' linear momenta relative to the body's COM are more responsible for the rotational behaviours of the body segments than are the rotations of the segments about their own COMs (**Table 1**). Relatedly, the timing sequences of max segmental H follow a proximal-to-distal sequence, which relates to sequential increases in the segment's linear momentum towards ball release (**Table 1**).

Table 1: Discrete values of segmental H_{max} about the leftward axis.

	Pelvis	Trunk	Upper Arm	Forearm	Hand
Local H ($kg{\cdot}m^2/s$)	0.25 (0.21)	4.28 (1.62)	0.13 (0.05)	0.22 (0.13)	0.00 (0.01)
Remote H ($kg{\cdot}m^2/s$)	0.54 (0.31)	8.66 (1.61)	6.42 (1.45)	9.48 (2.72)	4.61 (0.99)
Max H ($kg{\cdot}m^2/s$)	0.79 (0.39)	12.94 (2.48)	6.55 (1.48)	9.70 (2.83)	4.61 (0.99)
% of Whole-body H	2.06 (0.96)	33.07 (4.16)	17.42 (2.59)	25.87 (7.01)	12.24 (1.42)
Time of Max *H* (%)	95.34 (4.21)	95.88 (1.04)	99.14 (0.85)	99.53 (0.61)	99.83 (0.14)

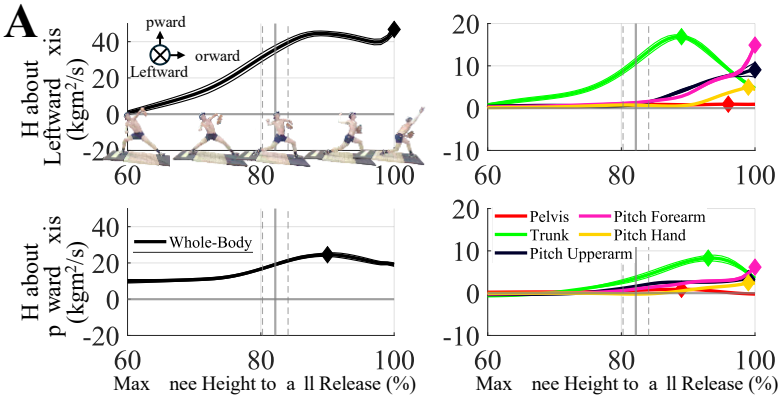

Figure 1: Mean (± 1 standard deviation) whole-body and upper body segmental H time-series about the leftward and upward axes. Time was normalized from max knee height to ball release (0-100%). Colored diamonds indicate H_{max}. Images and data are from the participant with fastest fastball speed of the cohort.

Significance: Baseball pitching involves the generation of whole-body and segmental H about the leftward and upward axes, and H are built up and transferred from the trunk into the throwing arm segments, resulting in H_{max} near or at ball release. Segmental H are primarily due to the segment's linear momentum relative to the body's COM, despite much prior research having focused on segmental angular velocities [5]. These findings build upon our research that identified relationships between ball speed and segmental H_{max}.

Acknowledgments: We thank the pitchers for volunteering and financial support from a Major League Baseball research grant.

References: [1] Betzel (2010) *Thesis Indiana. U.* [2] Liu et al. (2022), *Sports Biomech.* [3] Aguinaldo et al. (2007), *J. Applied Biomech* [4] Lin et al (2003) *J Chinese Inst. of Eng.* [5] de Leva (1996) *J. Biomech* [6] Orishimo et al. (2023) *J. Strength Cond. Res.*

COMPARING THE PERFORMANCE OF MODERN COLLEGIATE NON-WOOD BASEBALL BATS TO HISTORIC WOOD BAT DATA

Joseph J. Crisco*[1], Amy M. Morton[1], Kristen F. Nicholson[2], Richard M. Greenwald[3]
[1]Department of Orthopaedics, Warren Alpert Medical School of Brown University, Providence, RI
[2]Wake Forest University School of Medicine, Winston-Salem, NC [3]Thayer School of Engineering Dartmouth College, Hanover NH
*Corresponding author's email: joseph_crisco@brown.edu

Introduction: Performance of baseball bats has been an intriguing question since the traditional wood bat was first doctored or "corked" by a player. Currently, wood bats are used almost exclusively by Major and Minor League Baseball, while in high school and college play, they have been replaced by metal and composite bats. Metal bats were originally introduced in the early 1970's as a cost saving alternative to wood bats that were prone to break. By the early 1980's, however, there was a consensus among players and coaches that metal bats could largely outperform wood ones. The concerns for increased bat performance over wood are generally twofold: the potential for increased injuries from the batted ball to the pitcher and infield players and an imbalance between offense and defense. Presently, non-wood bat performance is regulated with laboratory-based testing using criteria that vary with the level of play and league. These laboratory-based tests were validated through field performance studies and computational analysis. The last published field performance study was in 2014 [1]. This and similar studies [2] were well-controlled batting cage studies, but due to the associated costs, reproducing these rigorous studies with more modern baseball bats has been challenging. With the advent of markerless-tracking systems now installed in many baseball stadiums that capture player and batter kinematic data, we sought to investigate if data from these systems could be used to evaluate modern collegiate baseball bat performance. Bat performance, as was done previously, was defined as batted ball speed after accounting for bat swing speed at the location of the ball-bat impact.

Methods: 4,318 at bats were analysed from data collected with a KinaTrax system (300 Hz) at Wake Forest University. All data was de-identified, and only the 3D coordinates of the tracked baseball and the knob and tip of the bat were analysed under a Data Transfer and Use Agreement. Previous algorithms for calculating baseball bat performance from optical motion capture data [1,2] were revised and applied. With the bat modelled as a 3D line segment (tip to knob), the ball-to-bat distance was computed at each frame. The ball-bat impact frame was defined as that with the minimum ball-bat distance and a reversal of the ball trajectory. This point on the bat defined the bat impact location, referenced from the bat tip. Batted ball speed (mean and SD) was computed using finite difference methods from two frames after ball-bat impact to the last frame the ball was tracked. Bat swing speed was computed as the magnitude of the linear velocity of the bat impact location using finite difference method from the prior frame. Bat lengths were computed from the data to yield a mean of 32 inches with a SD of 0.7 inches. Player performance was intentionally excluded from these calculations. Data analysis was limited to descriptive statistics and graphical evaluation by plotting batted ball speed as a function of bat swing speed and bat impact location from the bat tip. Units are reported in mph and inches reflecting their historical use in baseball.

Results & Discussion: From the dataset, 3,170 hits were successfully analysed. Of these, no attempts were made to remove foul tips, grounders, or other non-ideal hits. The maximum batted ball speed was 123 mph, median was 88 mph, with 25% of the hits over 97 mph. When examining batted ball speed as a function of bat swing speed (**Fig. 1**) it is important to note the character of the plot. For wood bats, at any given bat swing speed there is only a single value of maximum batted ball speed. Over the range of bat speeds these values produce a maximum performance "front" of data points that lie along a line oriented from bottom left to top right in **Fig. 1**. Balls hit outside the "sweet spot" or not squarely on the central axis of the bat, result in lower batted ball speeds, and hence lie below this front. The performance front for modern collegiate bats is clearly elevated compared to wood and its offset ranges from approximately 10 mph to 15 mph. Meaning that at any given bat speed, modern collegiate baseball bats hit the ball faster than wood by these values. We also notice that the front of maximum performance is not as well defined for modern collegiate bats as it is with the two wood bat studies. We speculate that this is due the larger variability in computing batted ball speed in the current analysis. An estimate of the sweet spot, the location on the bat associated with maximum batted ball speeds, was approximately 3" to 9" from the tip (**Fig. 2**).

Significance: Ensuring non-wood baseball bats comply to regulations necessitates laboratory-based testing for efficiency. However, it is important to ensure that these laboratory-based methods are a valid representation of field performance. This study is not a validation of those laboratory-based tests because the bats were not identified. Rather, this data is critical from a broader perspective because it provides a refences for investigators and governing bodies as to the current field performance of modern collegiate baseball bats.

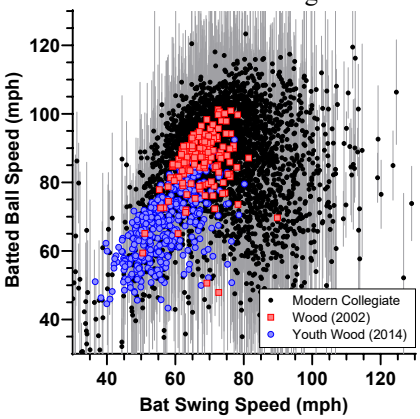

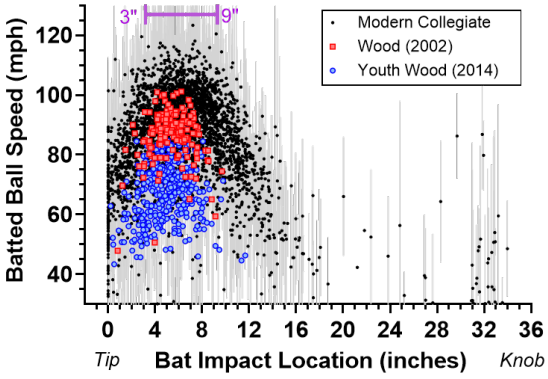

Figure 1. (*left*) Batted ball speed as a function of bat swing speed, defined as the linear speed of the bat at the point of impact. Error bars (gray) are SD in finite difference method for ball speed. **Figure 2**. (*right*). The "sweet spot" is the location on the bat that produces the fastest batted ball speeds. For the modern collegiate bats, the sweet spot is approximately from 3" to 9" from the tip. For the wood bats, the sweet spot is narrower and appears to drop-off faster along the length of the bat.

References: [1] Crisco et al. (2014), *J Applied Biomech* 30(2); [2] Crisco et al. (2002), *MSSE* 34(10).

EFFECTS OF PASSIVE STRETCHING ON MUSCLE-TENDON UNIT VISCOELASTICITY

*Skylar Taylor[1], Kristen L. Jakubowski[1], Madison Gaines[1], Young-Hui Chang[1], Gregory Sawicki[1]
[1]Georgia Institute of Technology, Atlanta, GA
*Corresponding author's email: staylor314@gatech.edu

Introduction: The viscoelastic properties of the muscle-tendon unit are highly influential in animal locomotion. Highly elastic tendons, such as the kangaroo's Achilles tendon, store and release energy efficiently, reducing the amount of muscular effort required for the hopping motion they are known for. In contrast, inelastic tendons, like that of the kangaroo rat, cannot store elastic energy and require greater muscular effort to maintain hopping [1]. In these examples, both animals use a similar hopping gait, but they adopt different strategies due to differences in the viscoelastic properties of their Achilles tendons. Given the critical role of tendons during locomotion, it is important to understand how actions like static stretching—known to decrease joint stiffness—impact both muscle and tendon properties [2]. Both humans and other animals have been observed to passively stretch their muscle-tendon units across varying contexts, yet its impact on the viscoelastic properties of the muscle-tendon unit (MTU) remain unclear. The purpose of this study was to identify the effects of passive stretch on the *in vivo* viscoelastic properties of the human Achilles tendon-triceps surae muscle-tendon unit. We hypothesize that static stretching will make the muscle tendon unit more compliant by modulating tendon viscoelastic properties, specifically: (1) decreasing tendon stiffness, (2) increasing tendon hysteresis.

Methods: All participants provided informed consent according to the protocol approved by the Georgia Tech IRB. Preliminary data were collected on six human subjects (22.8 ± 2.6 years). Subjects entered the lab and completed the following protocol in one session. Subjects began by performing three ankle maximum voluntary contractions (MVC) on a dynamometer where the dynamometer plate was locked in place. Between each contraction subjects were given 3 minutes of rest. After finishing the MVC block, subjects rested for 10 minutes. Subjects then had their ankle passively dorsiflexed until they reported "discomfort"; the dynamometer plate was then locked in this position for 6 minutes of passive stretching. At the end of this period, the ankle was returned to a neutral position (90° of flexion), and subjects performed another round of MVCs. The stretch MVC cycle was completed once more for a total of three MVC blocks (Pre, Mid, and Post), and two stretching blocks. Throughout all data collection, ultrasound imaging of the medial gastrocnemius-Achillies tendon junction were taken, along with muscle electromyography, and ankle joint torque from the dynamometer. Viscoelastic properties of the MTU were estimated by producing "work loops" that were derived from MVC tests.

Results & Discussion: Passive ankle torque declined by a mean of 13% from the initial torque during stretching, with no observed muscle activity from ankle flexors or extensors (**Figure 1**). This suggests that stress relaxation occurred during the period of stretching, which may be explained by changes in the stiffness of the muscle or tendon during the period of stretching. Stress relaxation has been shown to occur in other *in vivo* studies and explains the increase in range of motion seen in joints after stretching [3].

Despite the observed decline in passive torque, there were no significant changes in tendon hysteresis (Repeated Measures Anova $p = 0.72$) or tendon stiffness during MVC trials (Linear Mixed Effects Anova $p >> 0.05$). The stiffness and hysteresis values obtained in this study agree with those found in previous research using similar methodology [4].

Other studies attempting to identify the effects of stretching on muscle-tendon properties have yielded varying results. Kay and Blazevitch [5] reported no changes in Achillies tendon stiffness, but observed decreases in Gastrocnemius stiffness, while Kubo et al. found decreased tendon stiffness and hysteresis while observing Soleus muscle aponeurosis [6]. The discrepancies across these studies may arise from different strain patterns across the triceps surae muscle group, possibly leading to differential effects of stretching on each muscle-tendon unit in the group.

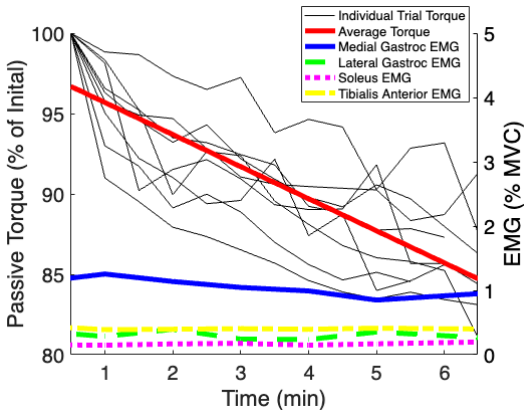

Figure 1: Passive ankle torque during stretching (red line displays average torque) coupled with EMG results of the ankle flexor and extensor muscles.

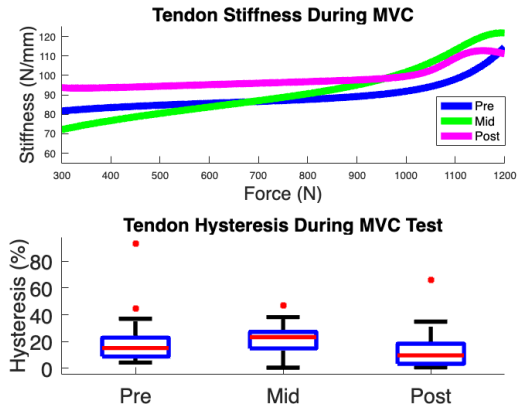

Figure 2: Tendon stiffness and hysteresis during MVC tests.

Significance: Our data suggest that stretching did not impact the viscoelastic properties of the Achilles tendon, despite a clear decline in passive ankle torque during the static stretching period. This may be explained by changes in the passive viscoelastic properties of the triceps surae muscles rather than the Achilles itself. Understanding these mechanisms will provide insight into the functional role of stretching related to both animal and human locomotion.

References: [1] Biewener & et al. (1981) *J Zool Lond*; [2] Amri-Khorasani et al. (2011) *J Strength Cond Research*; [3] Ker R. F. (1981) *J Exp Bio*; [4] Jakubowski et al. (2024) *Ann Biomed Eng*; [5] Kay & Blazevitch (2009) *J Appl Physiol*; [6] Kubo et al. (2001) *J Appl Physiol*

DEFINING THE RELATIONSHIP BETWEEN TEAR SEVERITY AND MECHANICAL PROPERTIES IN A RABBIT MUSCLE-TENDON UNIT

Kathryn T. Rex[1], Joshua Pataky[1], Zoe M. Moore[1], Meghan E. Vidt[1,2]
[1]Department of Biomedical Engineering, Pennsylvania State University, University Park, PA, USA
[2]Department of Physical Medicine & Rehabilitation, Penn State College of Medicine, Hershey, PA, USA
Email: ktr5133@psu.edu

Introduction: Computational modeling is a common method for examining the musculoskeletal response to external factors that are unable to be experimentally determined. Previous work modeling the effects of rotator cuff tears assumed that increased tendon tear size was linearly related to decreased peak isometric muscle force, as the linear actuators in the model represent the combined muscle-tendon unit [1]. However, the actual relationship between muscle-tendon unit mechanical properties, including muscle force and tendon tear size, is currently unknown. The objective of this study was to define the relationship between tendon tear size and changes in muscle mechanical properties to better define injury in a musculoskeletal model. We hypothesized that as tendon tear severity increased, the mechanical properties of the tendon-muscle unit would decrease linearly.

Methods: Bilateral Achilles tendons from 12 New Zealand White rabbits (N=24) were randomly assigned to 1 of 4 groups (n=6; 3M/3F) representing amount of injury severity (0%, 25%, 50%, 75%), with tears defined as a percentage of the tendon thickness in the anterior-posterior direction. Prior to testing, the thickness of the midpoint of the tendon long axis (anterior to posterior) was measured using digital callipers. The muscle-tendon unit was laid flat on the table and an incision was made on the posterior side of the tendon to introduce a tear by sharp dissection that corresponded with the group tear size. Samples were potted and underwent uniaxial mechanical testing. Cross-sectional area (CSA) was calculated as an ellipse using the width of the tendon and the new thickness after injury. Muscle-tendon units were dyed with methylene blue and 4 evenly spaced Verhoeff stain lines were applied. An MTS 858 Mini Bionix (MTS Systems Corp., Eden Prairie, MN) and previously reported protocol were used to perform uniaxial tensile testing [2]. Briefly, samples underwent cyclic loading, stress-relaxation, and load-to-failure tests. Strain was calculated using Harris Corner Detection [3] with a custom MATLAB (MathWorks Inc., Natick, MA) script. Elastic modulus, stiffness, yield stress, maximum force, and maximum stress were calculated. Two 1-way ANCOVAs, with sex as a covariate, were used to separately examine differences in mechanical properties across groups, and between small (0%, 25%) and massive (50%, 75%) tendon injuries, Linear regression was used to separately assess the relationship between each mechanical property and tendon tear severity. All analyses were performed with SAS OnDemand (SAS Institute, Cary, NC), with significance set to $p<0.05$.

Results & Discussion: Results showed that yield stress and maximum stress for the 75% tear group was greater than the lesser tear severities, while the maximum force was reduced compared to groups with lesser tear severity (Fig. 1). The massive tear group (50%, 75%) had increased yield stress (p=0.0012) and maximum stress (p=0.0002), and decreased maximum force (p=0.019) compared to the small tear group (0%, 25%). Elastic modulus and stiffness were not different between any tear severity groups (all $p>0.1421$), or between the small and massive tear groups (all $p>0.0624$). Yield stress (p=0.0003) and maximum stress ($p<0.0001$) had a positive linear relationship with tear severity, while maximum force (p=0.0196) had a negative linear relationship. Maximum force results support our hypothesis of a negative linear relationship, while yield stress and maximum stress did not support the hypothesis. The positive linear relationship for yield stress and maximum stress may be caused by decreased tendon CSA post-tear. When calculating stresses with the CSA computed before introduction of a tendon tear, both yield stress and maximum stress decreased with increased tendon tear size. This suggests that defining the dimensions of the injury is important to consider in modeling applications. Additionally, when testing the 0% tear group, failure was seen at the aponeurosis region of the muscle-tendon unit, while failure generally occurred at the tendon tear site for the other injury groups. The different failure locations within the muscle-tendon unit, possibly driven by the different mechanical properties for muscle and tendon tissue, may explain the lower maximum force values seen for the 0% group.

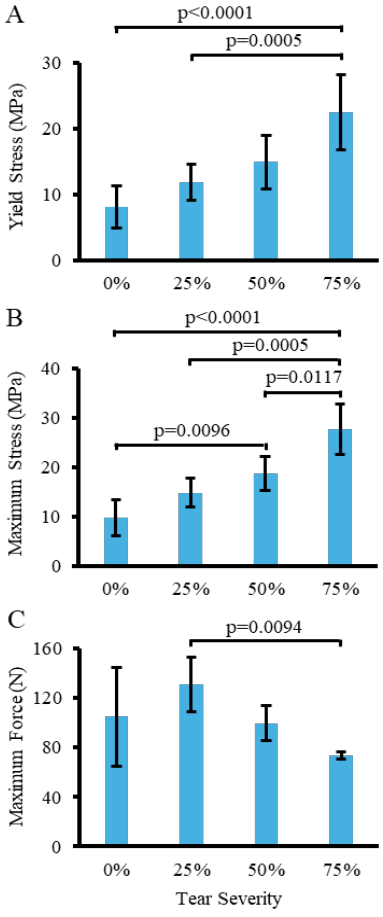

Figure 1: Mean A) yield stress, B) maximum stress, and C) maximum force across varying injury severity.

Significance: This work experimentally tested and confirmed the assumption describing the linear relationship between tendon tear size and maximal muscle-tendon force, which has been used in prior modeling applications. This work also highlights the importance of defining the injury dimensions, as this can influence force definitions.

Acknowledgments: NIH-R01AR079999; Start-up funds (Vidt)

References: [1] Pataky et al. (2021), *Clin Biomech* 90; [2] Khandare et al. (2022), *J Biomech* 132; [3] Elliott et al. (2022), *Ann Biomed Eng* 50(5).

INVESTIGATING THE ROLE OF FAT INFILTRATION PATTERNS ON MECHANICAL STRAIN IN FACIOSCAPULOHUMERAL DYSTROPHY

Kimberly M. Steininger[1]*, Allison N. McCrady, PhD[1], Seth Friedman, PhD[2], Silvia S. Blemker, PhD[1]
[1]Multiscale Muscle Mechanophysiology Lab, University of Virginia, Charlottesville, VA, USA
[2]FSHD MOVE+ Imaging Core, Seattle Children's Hospital, Seattle, WA, USA
*Corresponding author's email: fma5br@virginia.edu

Introduction: Facioscapulohumeral dystrophy (FSHD) is the third most common form of muscular dystrophy, causing progressive muscle weakness via fat infiltration in face, shoulder, upper arm, trunk, and lower limb [1]. Disease progression varies widely across muscles and patients, and the underlying mechanisms are poorly understood. Despite clinical trials [2-5], traditional biomarkers, including clinical exams, MRIs, and biopsies [6-8], do not explain the link between fatty infiltration and muscle strain in FSHD progression. However, finite element models (FEM) offer us the ability to map detailed, element-based anatomical fat patterns to predict regions of abnormal strain and have been validated through clinical metrics [9]. **This study thus leverages MRI data and FEM to investigate the correlation between intramuscular tensile force and strain distributions due to fat infiltration in the tibialis anterior (TA) in FSHD.**

Methods: MRI T1 Dixon scans (3T Siemens scanner: E1=1.35 ms, TE2=2.58 ms, TR=4.12 ms, matrix=448x266, voxel size=1.1×1.1×4.0 mm, 104 slices) were obtained from 7 FSHD patients (56.9 ± 17.0 years). Muscle segmentation: TA muscles were segmented from axial slices using a combination of deep convolutional neural network-based and manual review (Springbok Analytics, Charlottesville, VA) [10]. The central aponeurosis and distal tendon were manually segmented and converted into 3D CAD models (3D Slicer, Autodesk Inventor). Model building: TA volume and central and proximal aponeurosis were meshed using tetrahedron elements (Coreform Cubit), and fascicle orientations were defined using Laplacian fluid flow simulations (Autodesk CFD) [11]. Fat fraction values were assigned to each element by averaging voxel-level fat content within the corresponding region (MATLAB) [9]. Muscle was represented as an uncoupled solid mixture, using a transversely isotropic, nearly incompressible, hyperelastic constitutive model. Fat was modeled as an incompressible Neo-Hookean material [12,13]. The ratio of these materials was governed by the fat fraction. The aponeuroses were modeled as an uncoupled solid mixture with a Mooney-Rivlin ground matrix and fibers following an exponential power law, aligned parallel to the muscle's proximal-distal axis. Boundary conditions simulated bony attachments during isometric contraction [9]. Analysis: Lagrangian strain tensors for each element were output and element strain was calculated. Adjacent regions of fat and strain were correlated by calculating the fat fraction gradient and strain gradient. Spearman correlations between these gradients were performed to determine whether changes in fat predict changes in strain (MATLAB).

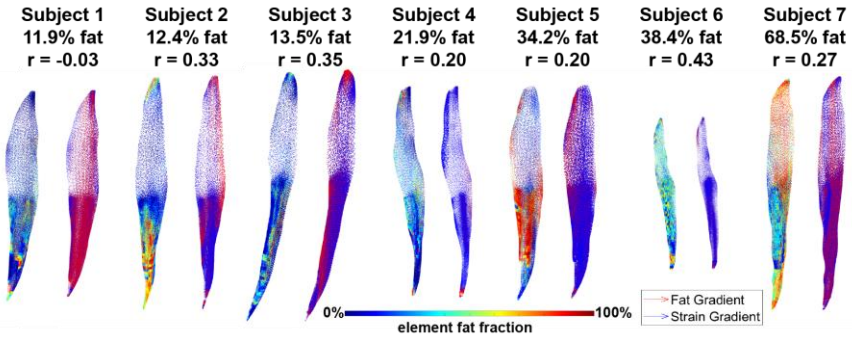

Figure 1: Total muscle percent fat and Spearman correlation between gradients (above), element fat fraction (left), and fat and strain gradients (right) for each FSHD patient.

Results & Discussion: Low correlations were found between fat and strain gradients across all subjects. Subject 6 had the strongest correlation (r = 0.43), with a moderate overall percent fat but whose fat was primarily concentrated in the distal aponeurosis region. In contrast, subjects 1, 6, and 7, whose fat infiltrations were spread along the length of the muscle, experienced much lower correlations (r = -0.03, r = 0.2, and r = 0.27), respectively (**Fig. 1**). These results suggest that a non-uniform strain response may be linked to subject-specific regional fat infiltration patterns. Future work will use pseudomaps to systematically vary fat location to examine the functional implications of abnormal strain gradients and better assess non-uniform and cascading effects of FSHD-related muscle dysfunction.

Significance: These results provide new insights into how mechanical forces may influence spatial progression of fat within affected muscles. The low correlation between fat infiltration and strain gradients suggests that while high fat regions may alter local strain distribution, mechanical loading alone does not fully explain fat propagation. Further analysis is required to identify additional factors that modulate mechanical loading in these regions. As the longitudinal mechanical effects of fat infiltration in FSHD have not previously been studied, this work establishes a foundation for studying how mechanical processes drive fat infiltration and disease progression.

Acknowledgments: Research funded by the Biotechnology Training Program at UVA (5T32GM136615-05).

References: [1] Rijken, NHM et al. (2014). *J. Neuro Dis*; [2] Avidity Bioscience. (2024). NCT05747924; [3] Arrowhead Pharma. (2024). NCT06131983; [4] Hoffmann-La Roche. (2024). NCT05548556; [5] U. Kansas Med Center. (2024). NCT04635891; [6] Eichinger, K et al. (2018). *Musc & Nerve*; [7] Leung, DG (2018). *Musc & Nerve*; [8] Statland, JM, et al. (2015). *Musc & Nerve*; [9] McCrady, AN et al. (2025). *medRxiv*. https://doi.org/10.1101/2025.02.15.25322140; [10] Ni et al. (2019), *J. Med Imaging*. [11] Choi, HF et al. (2013). *PLoS ONE*; [12] Blemker, SS et al. (2005). *J. Biomech*; [13] Criscione, JC et al. (2001). *J. Mech & Physics*.

IN-VIVO HUMAN GRACILIS MUSCLE ACTIVE FORCE-LENGTH RELATIONSHIP IS EXPLAINED BY THE SLIDING FILAMENT THEORY

Zheng Wang[1], Lomas S. Persad[1], Benjamin I. Binder-Markey[2], Ernest M. Hoffman[3], William J. Litchy[3], Alexander Y. Shin[1], Kenton R. Kaufman[1], and Richard L. Lieber[4]

1 Department of Orthopedic Surgery, Mayo Clinic, Rochester, MN, USA.

2 Departments of Physical Therapy and Biomedical Engineering, Drexel University, Philadelphia, PA, USA

3 Department of Neurology, Mayo Clinic, Rochester, MN, USA.

4 Shirley Ryan Ability Lab, Chicago, IL, USA.

*Correspondence: rlieber@sralab.org

Introduction: The skeletal muscle isometric length-tension (LT) relationship describes how muscle force varies with length, a concept explained by the sliding filament theory [1]. This theory, based on actin-myosin overlap, was originally demonstrated in frog muscles [2] and has since been validated in small animal models [3]. Models based on this theory have been developed and widely applied although it has never been validated in human muscles. In this study, we determined if the human whole muscle LT relationship can be modelled by the sliding filament theory given extensive data on appropriate actin and myosin filament length, fiber length, and estimated sarcomere shortening from tendon compliance.

Methods: Nineteen patients undergoing free-functioning muscle transfer surgery were recruited. After the gracilis was isolated intraoperatively, maximal tetanic force and muscle-tendon lengths were measured using a buckle force transducer [4] and electrical stimulation of the obturator nerve at four joint configurations (JC1–JC4). Length parameters were normalized by both literature-based fiber length (Lf:Lm ratio = 0.79) [5] and subject-specific fiber length derived from full-width-at-half-maximum (FWHM) analysis [3]. Gracilis tendon compliance was characterized from six cadaveric specimens (n=6), with an exponential stress-strain model applied to estimate in-vivo sarcomere shortening for further length parameter adjustment. The sarcomere LT curve was constructed using reported human myofilament dimensions [6] and normalized to an optimal sarcomere length of 2.7 µm. Model performance was evaluated using the coefficient of determination (R^2) between experimental data and sarcomere LT model.

Results & Discussion: The sarcomere LT model, constructed using human filament lengths, is different from the widely implemented frog LT model (Fig 1A). There was no obvious relationship between the muscle length and force in the raw experimental data (Fig 1B). With normalization to the optimal fascicle length and peak force (Fig 1C), experimental data still exhibited a poor fit to the model with only 13.7% of the variance ($r^2 = 0.137$) explained. Incorporating subject-specific fiber lengths derived from full-width-at-half-maximum (FWHM) analysis, along with estimated sarcomere shortening, significantly improved the model fit (Fig 1D), capturing 79.7% of the variance ($r^2 = 0.797$). The improvement in the model with subject-specific fiber lengths and tendon compliance underscores the limitations of using general architectural assumptions. These results also highlight accurate measurement of human muscle fiber length is the key to modeling the human LT relationship.

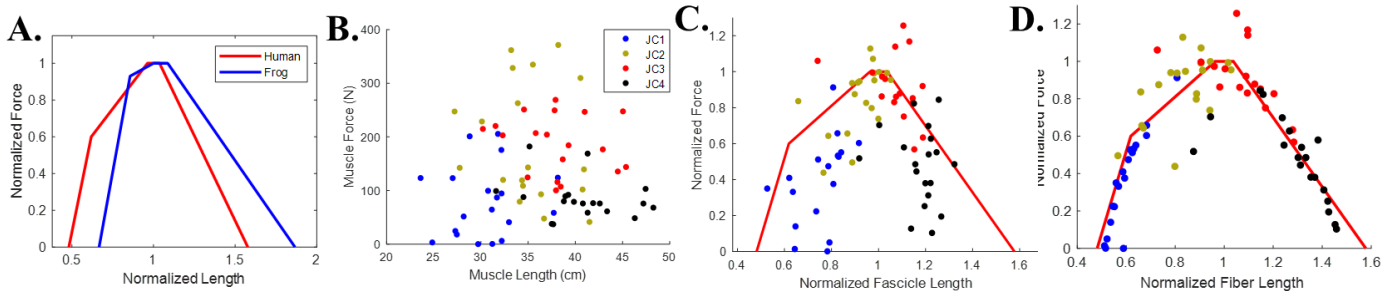

FIGURE 1: (**A**) Normalized human (red) and frog (blue) sarcomere LT curves. Human sarcomere length is normalized to an optimal length of 2.7 µm while frog sarcomere length is normalized to an optimal length of 2.05 µm. (**B**) Experimental muscle force (measured in N) and length (measured in cm) at the four different JCs using raw data. No apparent form of this relationship is observed. (**C**) Muscle LT relationship calculated from data in (B) by normalizing to a fiber length to muscle length ratio of 0.79 (r^2=0.137) and peak muscle force compared to the human LT relationship. (**D**) Muscle LT relationship calculated from data in (B) by normalizing to subject-specific fiber length with tendon strain adjustment (r^2=0.797) compared to the human LT relationship.

Significance: The in-vivo human active length-tension relationship is accurately represented by the sliding filament theory when using human filament dimensions and subject-specific measurement of fiber length. The assumption that muscle fascicle length is a surrogate for muscle fiber length is not accurate in long human muscles.

Acknowledgments: This work was supported by VA funding 1 I01 RX002462 and Research Career Scientist Award Number IK6 RX003351 from the United States (U.S.) Department of Veterans Affairs Rehabilitation R&D (Rehab RD) Service.

References:

[1] Huxley & Niedergerke (1954), Nature 173:971.
[2] Gordon et al. (1966), J Physiol 184:170.
[3] Winters et al. (2011), J Biomech 44:109.
[4] An et al. (1990), J Biomech 23:1269.
[5] Ward et al. (2009), Clin Orthop Relat Res 467:1074.
[6] Lieber et al. (1994), J Neurophysiol 71:874.

INCREASED TENDON COMPLIANCE CAN INCREASE MUSCLE POWER AND WORK OUTPUT

*David Lin[1,2], Austin Au[2], Bertrand Tanner[2]
[1]School of Chem. Eng. and Bioengineering and [2]Dept. of Integrative Physiol. & Neurosci., Washington State University
*Corresponding author's email: davidlin@wsu.edu

Introduction: Series compliance in the form of a tendon is important for increasing skeletal muscle power and work output that ultimately produce ballistic movements [1]. The mechanism responsible for this observation is that a tendon allows for muscle shortening and stores the muscle work done in the form of elastic energy, especially during the initial phase of the movement when the body's inertia is just beginning to accelerate. The objective of this study was twofold: experimentally measure how muscle power and work output is determined by the magnitude of a linear tendon compliance; and how the relationship between tendon compliance and muscle output changes with the introduction of the nonlinearity of a tendon toe region. We used a novel experimental setup with single muscle fibers to manipulate tendon compliance through real-time physical simulations using a feedback system. The significance of our results is we were able to determine how well tuned tendons in vivo are for generating optimal power and work during a ballistic movement.

Methods: Skinned single muscle fibers were obtained from the medial gastrocnemius (MG) of adult white rats by gross dissection of the muscle and followed by immersion in a skinning solution. Single fibers were mounted on the experimental setup and bathed in a relaxing solution. After setting the sarcomere length to 2.7 μm, activation was achieved by moving the fiber to a solution with pCa=4.0. Four activations were sequentially performed: an isometric contraction; two activations with a simulated tendon that either had a linear compliance ranging from 0.02 to 0.2 L_o/F_o, where L_o is the initial fiber length and F_o is the isometric force, or had a toe region before a linear region, while the total musculotendon length was isometric (i.e., muscle shortening equalled tendon lengthening); and a final isometric contraction. A tendon was simulated by feeding back force to the length servo. For a linear tendon, force was multiplied by the desired compliance to determine fiber length. For a nonlinear tendon, toe compliance was set to be twice the linear compliance and the transition between the toe and linear regions occurred when fiber force reached a predefined value in the range of 0.1 to 0.5 F_o. Fiber length and force were recorded at 2 kHz.

For quality control, the final isometric contraction was compared to the initial isometric contraction in terms of maximal stress and time derivative of force (i.e., the variable "yank"). If the comparison did not pass set criteria, we did not use the fiber's data in the final analyses. Lastly, we used gel electrophoresis to identify the fiber type of each fiber tested. Due to the predominance of type IIb fibers in our samples, we limited our analyses to only type IIb fibers. For analyses, we calculated the work done by a muscle fiber by integrating force with respect to change in length for a 5 second interval after the initiation of activation. Power over time was calculated from the product of fiber velocity and force.

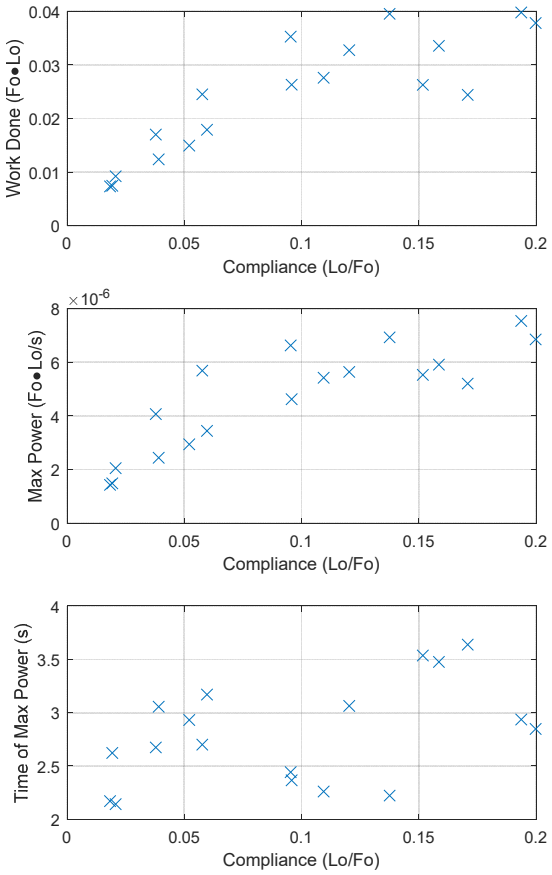

Figure 1. Muscle work, maximum power, and time to maximum power as a function of tendon compliance.

Results & Discussion: After applying the quality control criteria and excluding non-type IIb fibers, we used 22 type IIb fibers in our analyses. For the simulated tendon trials, as fiber force increased following the switch to the activating solution, the fiber shortened, doing work on the simulated tendon. To determine the relationship between linear compliance and muscle output, we plotted tendon compliance against the variables of work, maximum power, and time to maximum power (Fig. 1). We found that for lower compliance values, an increase in compliance enabled the muscle to do more work, but the effect was diminished for higher compliance values. Peak power followed a similar trend. The time to maximum power did not change with compliance. Note that we estimated in vivo compliance for the rat MG to be 0.06 L_o/F_o, which is less than the compliance values that resulted in more work and power. For nonlinear compliances, expanding the toe region also increased work done and maximum power but did not change time to maximum power.

Significance: In this study, we found that changing the linear tendon compliance or the extent of the toe region influenced muscle mechanical output, but the effect was less when the compliance was larger. Functionally, the optimal compliance was found to be more than the estimated in vivo value. However, our experimental conditions were different than in vivo conditions with respect to temperature (experiments conducted at room temperature) and the calcium delivery system (diffusion in experiments versus the sarcoplasmic reticulum), both of which slowed the activation dynamics. In the future, we explore how changes in activation dynamics alter the relationship between tendon properties and muscle mechanical output.

Acknowledgments: This work was supported by NSF grants #2128545 (DCL) and # 2312925 (BWCT and DCL), AHA 23TPA1074093 and NIH HL149164 (BWCT).
References: [1] Roberts and Marsh (2003), *J Exp Biol,* 206.

Measuring whole and sectioned skeletal muscle stiffness with microindentation

Gianni A. Valentine[1] & Benjamin B. Wheatley[2*]
[1]Program in Cell Biology/Biochemistry, Bucknell University, Lewisburg, PA
[2]Department of Mechanical Engineering, Bucknell University, Lewisburg, PA
*Corresponding author's email: b.wheatley@bucknell.edu

Introduction: Microindentation is a technique used to measure material properties in a non-destructive manner [1,2]. Briefly, a cylindrical test probe attached to an instrumented load cell is displaced into a material, enabling the measurement of local material stiffness. Skeletal muscle tissue is the most abundant tissue in the human body and comprises approximately 40% of total body weight [3]. It is composed of multiple hierarchical layers including muscle fibers and muscle fiber bundles, organized by the collagen-rich extracellular matrix. The outer layer of the extracellular matrix – the epimysium – is a protective sheath the surrounds the entire muscle. Prior research has shown that fluid pressurization in muscle tissue plays a role in muscle force and muscle stiffness, and this fluid is likely retained by the epimysium [4,5]. However, the extent to which the epimysium contributes to the material properties of muscle tissue remains largely unexplored. Therefore, we seek to measure differences in stiffness of muscle tissue between whole (epimysium intact) and sectioned passive and healthy muscle tissue with the use of micro-indentation.

Methods: Lapine lower limb skeletal muscle tissue was harvested, dissected, and tested within eight hours of euthanization in order to avoid the onset of rigor mortis. An equal number of muscles from the gastrocnemius lateral head, gastrocnemius medial head, and vastus intermedius were used [6]. Muscles from each category were randomly assigned as either whole (epimysium intact) or sectioned. Sectioned samples were cut using a custom drop cutter to ensure precision and repeatability in slicing the muscle midbelly. Three to five indents were performed on each muscle sample depending on size of muscle. Equal spacing was utilized between indents to minimize variability. Requirements for indentation included that the indent probe evenly contacted the muscle sample. Each indent was manually preloaded with a cylindrical sheath to ~30mN. The test probe was then inserted 0.4mm into the muscle over a ramp time of one second, held at the inserted position for 30 seconds for stress relaxation analysis, and retracted over a ramp time of one second. Raw force-displacement and force-time data were smoothed using a Savitsky Golay filter, and the peak force value was extracted from each test. The ramp and relaxation phases were then fit with an exponential function $y = a * \exp(b * x)$ to characterize the tissue stiffness nonlinearity and tissue relaxation rate, respectively. Groups were compared using unpaired t-tests ($\alpha = 0.05$). All data processing and analysis was performed using MATLAB.

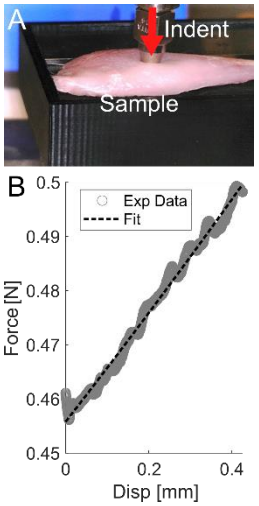

Figure 1. A) Experimental micro indentation of a whole muscle. B) Representative fit to experimental force data of indentation.

Results & Discussion: A total of 120 muscles were tested, including n=40 from each muscle. With multiple indentations per muscle, a total of 505 indents to the gastrocnemius lateralis, gastrocnemius medialis, and vastus intermedius were performed. Whole muscle samples had a lower peak force ($p<0.001$) and a faster relaxation rate ($p<0.001$) than sectioned muscle samples. These results contradict our hypothesis that sectioned samples would be less stiff and exhibit faster relaxation due to the disruption of the epimysium, which may be due to differences in sample geometries between groups but the same preloading condition. While these differences were statistically significant, they were also rather small (in each case smaller than standard deviation). Future work to develop and implement finite element models of the microindentation experiment, and thus link tissue structure to tissue function, would greatly enhance the ability to interpret these results and enhance our understanding of impairments such as pressure ulcers.

Table 1. Mean and standard deviation values for the peak force (in mN), the exponential parameter b for the loading phase (stiffness nonlinearity) and the b parameter for the relaxation phase (relaxation rate).

	Peak	Stiffness Nonlinearity	Relaxation Rate
Whole Muscle	511 (13.8) mN	0.219 (0.0480) mm^{-1}	-0.00793 (0.00160) sec^{-1}
Sectioned Muscle	520 (18.6) mN	0.227 (0.0710) mm^{-1}	-0.00737 (0.00170) sec^{-1}
p-value	< 0.001*	0.163	< 0.001*

Significance: The understanding of the epimysium's contribution to skeletal muscle tissue stiffness is essential for identifying and combatting impairments such as pressure ulcers. Novel microindentation data of passive muscle tissue will assist in the development of methods, such as patient specific physics based or statistical models, to detect and prevent such conditions.

Acknowledgments: This material is based upon work supported by the National Science Foundation under Grant No. 2301653.

References: [1] Camy, C., et al. (2024). *Bone Reports*, 20(3), 101734; [2] Tang, S. et. Al. (2010). *Polymer Testing*, 29(2), 159–163. [3] Frontera, W. r., & Ochala, J. (2015), *PubMed* 96(3); [4] Sleboda, D. A., & Roberts, T. J. (2020). *Proceedings of the National Academy of Sciences*, *117*(3), 1772–1778; [5] Lavigne, T. et. Al. (2022). *Clinical Biomechanics*, *93*; [6] Lieber, R. L., & Blevins, F. T. (1989). *Journal of Morphology*, *199*(1), 93–101.

EFFECTS OF TRIPPING TYPES AND REPETITIONS ON REACTIVE BALANCE CONTROL DURING WALKING AND CARRYING TASKS

Ling Li[1], Kaden Valkenburg[2], Ben Geske[2], Carly Palmer[2], *Boyi Dai[3]
[1] Department of Health & Human Performance, College of Idaho, Caldwell, ID, USA
[2] Division of Kinesiology and Health, University of Wyoming, Laramie, WY, USA
[3] Department of Rehabilitation and Movement Science, University of Vermont, Burlington, VT, USA
*Corresponding author's email: boyi.dai@med.uvm.edu

Introduction: Slips, trips, and falls are major occupational hazards, causing 21,400 injuries annually in construction and extraction in the United States [1]. Reactive balance control, the ability to restore stability after a perturbation, is critical in preventing falls [2]. Load carrying may further challenge balance by shifting the center of mass and limiting arm movement [3]. While previous studies have studied tripping types and load carriage in tripping and obstacle negotiation tasks, their combined effects of and the potential learning effects through repetition remain unclear. This study examined stepping and trunk kinematics between surface-tripping and cord-tripping during walking and carrying tasks across 6 repetitions. These findings may help understand different trips and falls and develop prevention strategies for occupational falls.

Methods: Twenty participants (11 males, 9 females; Age: 22.87 ± 4.06 ys; Height: 1.70 ± 0.08 m; Mass: 71.13 ± 12.44 kg) with at least 500 hours of experience in occupational environments with elevated risk of falls performed walking and carrying a 15-lb box while wearing a safety harness (Figure 1). Each participant completed six trials for each of the four conditions: walking or carrying with surface-tripping (19-cm obstacle) or cord-tripping (retractable cord), with 0-2 non-tripping trials between two tripping trials. Dependent variables included recovery step time, recovery step length, trunk flexion angles at recovery step touch-down, and maximum trunk flexion angles 100 ms after touch-down. Paired t-tests assessed differences between the two tripping types, the walking and carrying tasks, and the first and sixth trials ($p < 0.05$).

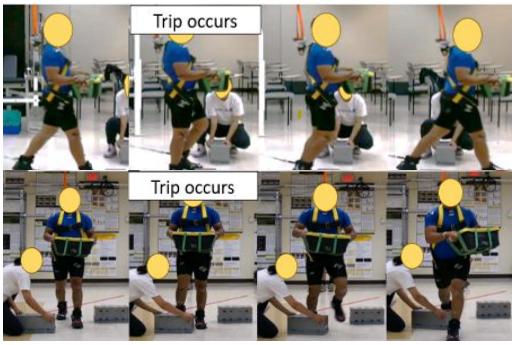

Figure 1. Top: cord-tripping with load ;Bottom: surface-tripping with load carrying.

Results & Discussion: Cord-tripping resulted in significantly better control patterns, indicated by shorter recovery step times, smaller step lengths, and reduced trunk flexion angles compared to surface-tripping for most tasks and trials(Table 1). Surface-tripping, partially blocking the placement of the tripping foot, presented a more challenging tripping situation than cord-tripping, in which individuals could immediately place their tripping foot downward. Carrying tasks did not significantly affect any dependent variables, indicating a relatively light load did not impair reactive balance control after tripping in young workers. Compared to the first trials, the sixth trials showed some improvement in recovery mechanics, mostly in surface-tripping with carrying tasks, suggesting that the experience of tripping may promote reactive balance for challenging tripping situation.

Table 1. Means and standard deviations of dependent variables for the two perturbation strategies and two tasks in 1st and 6th trials

			Surface-Tripping	Cord-Tripping
Step Time (seconds)	Walking	1st trial	0.61±0.08**A**	0.50±0.09**B**
		6th trial	0.60±0.07**A**	0.51±0.09**B**
	Carrying	1st trial	0.64±0.07**AI**	0.51±0.09**B**
		6th trial	0.60±0.06**AII**	0.49±0.09**B**
Step Length (m)	Walking	1st trial	1.08±0.24**A**	0.89±0.19**B**
		6th trial	1.05±0.19**A**	0.92±0.14**B**
	Carrying	1st trial	1.15±0.21**AI**	0.92±0.17**B**
		6th trial	1.03±0.17**AII**	0.92±0.13**B**
Trunk Flexion Angle at Touch-Down (°)	Walking	1st trial	20.08±11.81	15.76±8.00
		6th trial	17.76±11.86	16.32±7.41
	Carrying	1st trial	19.31±12.91**AI**	13.34±10.97**B**
		6th trial	14.40±9.53**II**	13.66±9.13
Peak Trunk Flexion Angle 100 ms after Touch-Down (°)	Walking	1st trial	23.38±13.01**AI**	17.58±9.53**B**
		6th trial	19.52±13.40**II**	16.88±7.92
	Carrying	1st trial	21.87±12.91**I**	15.59±12.97
		6th trial	16.80±12.33**II**	14.56±10.54

Note: The effect of tripping conditions for each tripping task was grouped by A>B. The effect of trials for each tripping condition was grouped by I>II. Indicated group differences are statistically significant at $p < 0.05$.

Significance: These findings highlight the different challenges of surface- and cord-tripping, emphasizing the need to consider different tripping types to understand falls. Exposing workers to trips in a safe environment may promote the exploration of effective recovery strategies.

References: [1] Helmick & Petosa. (2022), The U.S. Bureau of Labor Statistics; [2] Grabiner & Kaufman. (2021), Front. Sports Act. Living, 3; [3] Roos et al. (2008), Gait & posture, 27(2).

ANKLE AND HIP MUSCLE ACTIVATION IN RESPONSE TO GROUND SLIDE PERTURBATIONS

*Theresa Hardin[1], Jennifer K. Leestma[2], Gregory S. Sawicki[1], Aaron J. Young[1]
[1]Georgia Institute of Technology, Atlanta GA
[2]Harvard University, Cambridge MA
*Corresponding author's email: thardin9@gatech.edu

Introduction: Humans are excellent at maintaining balance during steady state walking and in response to perturbations. When someone is perturbed, there are two main strategies to deal with the perturbation: (1) an ankle strategy, which involves modulating the center of pressure underneath the foot and (2) a hip strategy, which involves changing where the foot is placed during walking. It has been shown that in healthy young adults, as perturbation magnitude increases, step placement changes are more often used to correct for instability. The role of these two strategies and how different muscles contribute in response to varying magnitude and direction perturbations in both the stance and swing leg has not been extensively investigated [1,2]. We hypothesized that as perturbation magnitude increases, increases in hip muscle activity will be more pronounced than ankle muscles as individuals switch from ankle strategy to hip strategy.

Methods: Eleven healthy participants walked at 1.25 m/s on a 6 degree-of-freedom instrumented treadmill while being exposed to translational perturbations of varying directions magnitudes and timings (Figure 1). Surface electromyography (sEMG) was collected at 2000 Hz on the Tibialis Anterior (TA), Medial Gastrocnemius (MG), Rectus Femoris (RF), and Biceps Femoris (BF). The full experimental protocol has been previously described by Leestma et al. [3]. This analysis will focus on anterior and posterior perturbations at 50% double support (Fig 1). We will compare hip and ankle response in the sagittal plane using muscle activation patterns from the above-mentioned muscles. sEMG signals were processed using a 4th order Butterworth filtered between 10 and 450 Hz and smoothed with a 100ms root mean square (RMS). The integrated signal was computed over one stride.

Results & Discussion: As hypothesized, we observed there were larger increases in hip muscle activation vs. ankle muscle activation for the larger magnitude perturbations (Fig. 2). This is expected for two reasons. First, larger perturbations are more destabilizing and thus necessitate alterations in step placement to produce the external moments needed to restore baseline fluctuations in angular momentum. Second, smaller perturbations (5cm) remain within the foot's lever arm, allowing for center of pressure adjustments without the need for hip involvement. We observed that as perturbation magnitude increased, *all* muscles - both agonists and antagonists with respect to the perturbation direction - had higher activation. This suggests a limb-wide co-activation strategy as part of the repertoire used to restore balance, especially at the higher perturbation magnitudes, Presence of co-activation also suggests the ankle strategy remains essential for balance recovery during larger perturbations, perhaps because the step placement is not precise for achieving immediate stability, requiring continued ankle adjustments to compensate for any residual instability after the step.

Significance: Young- healthy adults shift muscle coordination to rely more on proximal vs. distal muscles for large pitch-perturbations in the sagittal plane – indicating that hip driven step placement is critical to recover from perturbations large enough to elicit falls. This finding could help improve our understanding of balance deficits in clinical populations, such as older adults or individuals' post-stroke that suffer localized (asymmetric) muscle weakness. In addition – focusing therapies and assistive technologies to strengthen proximal rather than distal joints may be a key to preventing falls in scenarios where altering foot placement restores balance.

Acknowledgments: This project was funded by NIH R01 Award #R01HD113598-01

References: [1] Rankin et al. (2014) J. neurophysiology; [2] Stimpson et al. (2018) J. Biomechanics; [3]Leestma et al. (2023), J. Exp Biol.

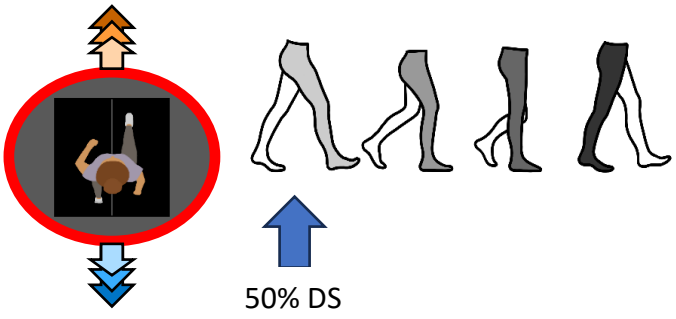

Figure 1: Perturbation conditions with varying magnitudes (hue) following DS perturbations

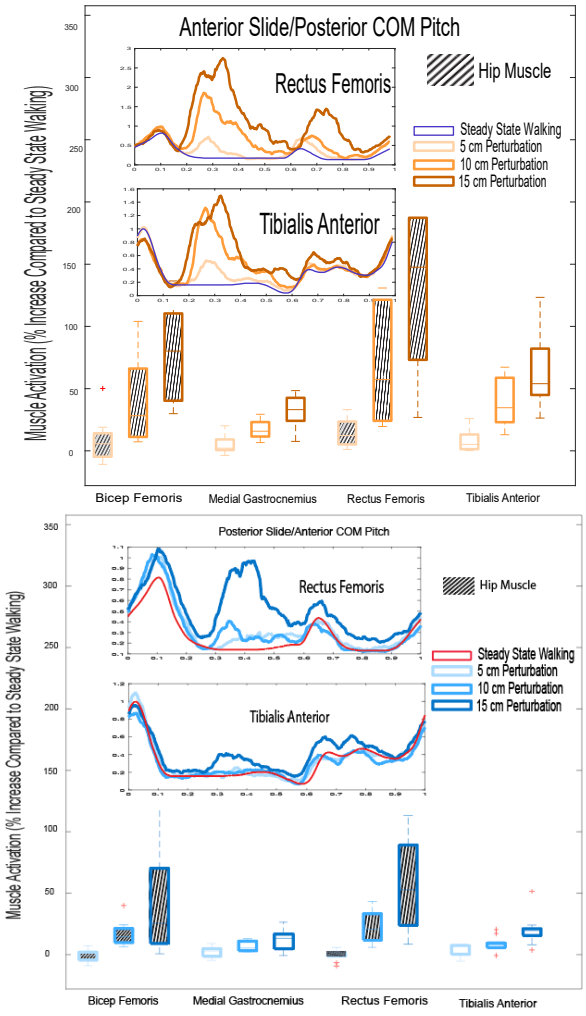

Figure 2: Averaged sEMG curve over a gait cycle for steady state and perturbation conditions. Increase in muscle activation compared to steady state walking for Anterior (top) and Posterior (bottom) ground slide Perturbation Condtitions

REACTIVE STEPPING RESPONSES TO LATERAL PERTURBATIONS IN INDIVIDUALS WITH TRANSFEMORAL AMPUTATION

*Hiva Razavi[1], Kristin A. Perrin[1], Boer Chen[1], Kayla Russell-Bertucci[1], Noah J. Rosenblatt[2], Deanna H. Gates[1]
[1]School of Kinesiology, University of Michigan, Ann Arbor, MI
[2]Dr. William M. Scholl College of Podiatric Medicine, Rosalind Franklin University of Medicine and Science, North Chicago, IL
*Corresponding author's email: razavih@umich.edu

Introduction: People with lower limb amputation have a high risk of falls [1], with higher rates in those with transfemoral amputation (TFA) compared to those with transtibial amputation (TTA) [1]. In order to prevent falls after a postural perturbation, individuals must employ reactive balance strategies such as foot-in-place responses (i.e. using ankle and hip) or compensatory stepping responses [2]. While there has been some research on reactive balance responses in individuals with TTA, with a primary focus on and anterior-posterior (AP) perturbations [3-5], no studies have assessed medio-lateral (ML) balance recovery in individuals with TFA. ML perturbations are particularly important to study because, unlike sagittal plane perturbations such as tripping or slipping, they do not allow the sound limb to compensate for the prosthetic limb's limitations [6]. Therefore, this study aimed to investigate how individuals with TFA respond to ML perturbations toward and away from their prosthetic limb during standing.

Methods: Three male participants with unilateral TFA (age: 36.7±26.3 yrs, 2-K4, and 1K2) have thus far provided written informed consent to participate. Participants stood quietly while wearing a waist belt connected to two equally loaded weight stacks (Fig 1). Perturbations were initiated by randomly releasing one load via disengagement of an electromagnet. This applied a pulling force in the opposite direction of the dropped load, passively loading the limb on that side of the pull. Participants were instructed to try and maintain their balance without stepping. We determined the step threshold (ST) by increasing the weights on each side by 2.5% body weight (BW) until participants stepped in two consecutive trials at the same magnitude. Participants then experienced four perturbations at magnitudes 2.5% BW higher than their ST, which were expected to force stepping responses. We qualitatively assessed stepping strategies during stepping trials (2 at ST and 4 at a higher magnitude) based on whether the loaded leg or unloaded leg was used to take the initial step [7, 8]. The former case includes the loaded leg step (LLS) which requires the loaded leg to initiate a step, which first necessitates an active weight shift onto the unloaded leg. The latter case included three sub-classifications: medial side step (MSS), crossover step (COS), and unloaded leg step (ULS). MSS strategy involves the unloaded leg taking a small, quick step toward the loaded leg, narrowing the base of support, and often requiring a follow-up lateral step with the loaded leg. In COS strategy, the unloaded leg crosses in front of or behind the loaded leg, typically followed by a second step to restore balance. ULS strategy consists of a step taken with the unloaded leg only, including a side step, medial step, or leg lift, without additional steps from the loaded leg.

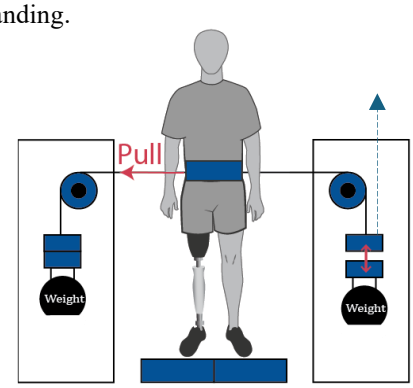

Figure 1. Waist-Pull System; When perturbation is toward the prosthetic side, the prosthetic limb bears the load, while the sound limb is unloaded.

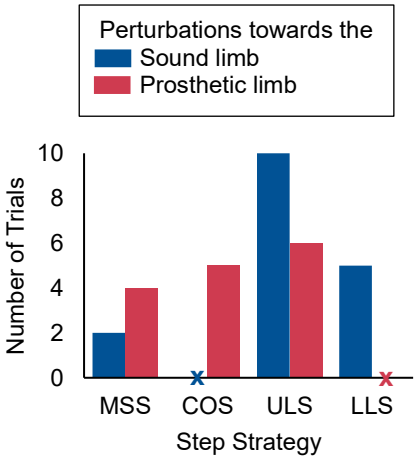

Figure 2. Number of trials in which participants used unloaded (MSS, COS, ULS) or loaded limb strategies during perturbations toward the sound or prosthetic limb. Trials where no step strategy was used are marked with an "X" on the axis.

Results & Discussion: One participant stepped during one perturbation below ST, but a consecutive step at that magnitude was not observed, so the trial was not included in the analysis. On four of the 36 trials, one toward the sound side and three toward the prosthetic side, participants did not step. Across the 32 stepping responses observed, 84% were unloaded limb strategies (Fig. 2). Among these, 59% were ULS 22% were MSS, and 19% were COS. Notably, COS were only used during perturbations toward the prosthetic limb. Conversely, loaded leg stepping (LLS) occurred exclusively during perturbations toward the sound limb. Taking a step with the loaded sound limb involves a weight shift from the sound to the prosthetic limb, requiring considerably more time, coordination, and strong abductors on the residual limb side compared to unloaded limb strategies, although the resultant step may be more stable.

Significance: These findings underscore the need to understand direction-dependent stepping in TFA, as it aids fall prevention and balance recovery. Identifying step strategies can inform rehab programs to improve weight-shifting, prosthetic use, and decrease fall risk.

Acknowledgments: This work was supported by the Orthotics and Prosthetics Outcomes Research Program under Award W81XWH-22-1-0140

References: [1] Miller et al. (2001), Arch Phys Med Rehabil 82(8); [2] Hof (2007), J Biomech 40(2); [3] Molina-Rueda et al. (2016), PM&R 8(3); [4] Kolářová et al. (2021), Sensors 21(21); [5] Vanicek et al. (2009), Arch Phys Med Rehabil 90(6); [6] Curtze et al. (2012), Gait Posture 36(2); [7] Batcir et al. (2020), BMC Geriatr 20(1); [8] Handelzalts et al. (n.d.), Reactive Balance Strategies after Stroke;

GOAL-DIRECTED LATERAL STEPPING SHEDS LIGHT ON MUSCLE COORDINATION STRATEGIES IN WALKING BALANCE CHALLENGES

Grant T Maddox[1*], Andrew D Shelton[2,3], Vicki S Mercer[2], Jeremy R Crenshaw[4], Jason R Franz[2,3], Jessica L Allen[1]
[1] University of Florida, USA, [2] UNC Chapel Hill, USA, [3] NC State University, USA, [4] University of Delaware, USA
email: grantmaddox@ufl.edu

Introduction: Older adults are at an exceptionally high risk of falls, with the majority of falls occurring during walking. Many previous studies focus on habitual walking to understand biomechanical factors behind poor balance and fall risk; however, the demands of habitual walking may not adequately reflect the balance required for walking challenges. In contrast, goal-directed lateral stepping [1] is a daily activity that requires control of both foot placement and balance, demands that are also required when responding to walking balance challenges. Achieving these demands requires individuals to modulate their muscle coordination. This study aimed to determine if the change in muscle coordination complexity from habitual walking to a goal-directed lateral stepping task better reflects an individual's ability to respond to walking balance challenges than habitual walking alone. We hypothesized that greater modulation of muscle coordination complexity from habitual walking to goal-directed lateral stepping, quantified using motor module analysis [2] would better predict vulnerability to perturbations to walking than habitual treadmill walking as measured by whole-body angular momentum (WBAM) [3].

Methods: 25 older adults (13F; 72.6±6.2yrs) walked on a split-belt treadmill at their preferred walking speed (1.21±0.16 m/s) under five different conditions. Muscle coordination complexity was extracted during two voluntary tasks: (1) habitual treadmill walking and (2) goal-directed lateral stepping [1]. WBAM was analyzed during three perturbation tasks: (3) treadmill-induced slip perturbations (200 m/s duration, 6 m/s^2) applied randomly 5 times bilaterally at heel strike, (4) impulsive lateral waist pulls (100 m/s duration, 5% body weight) applied bilaterally toward the swing leg at toe-off, and (5) two minutes of continuous mediolateral optical flow perturbations using a nominal amplitude of 35 cm. Surface electromyography (EMG) was collected from eight lower-limb muscles on the right leg spanning the hip, knee, and ankle. Muscle coordination complexity was quantified using motor module (a.k.a. muscle synergy) analysis. Motor modules were extracted from EMG data using non-negative matrix factorization, and muscle coordination complexity was defined as the variance accounted for by one motor module (VAFby1) [2]. The modulation of muscle coordination complexity was defined as VAFby1 in habitual treadmill walking minus VAFby1 in goal-directed lateral stepping, where a positive value indicates a decrease in muscle coordination complexity in the goal-directed lateral stepping condition. Subjects also wore 36 motion capture markers on their feet, legs, pelvis, and trunk from which we calculated WBAM during the perturbation conditions. Peak-to-peak WBAM was calculated in both the sagittal ($WBAM_{AP}$) and the frontal ($WBAM_{ML}$) planes. For the optical flow perturbation, WBAM was averaged across all strides, while for the impulsive lateral waist pull and treadmill-induced slip perturbations, WBAM was averaged over the immediate recovery step [4]. To test our hypothesis that the modulation of muscle coordination complexity between a goal-directed lateral stepping task and habitual treadmill walking would more closely predict WBAM than the muscle coordination complexity of habitual treadmill walking, we performed a linear regression between our measures of modulation of muscle coordination complexity and both $WBAM_{AP}$ and $WBAM_{ML}$ in the three different perturbation conditions. The fitted regression model was: WBAM = β_1 x Modulation of Stance leg Complexity + β_2 x Modulation of Stepping leg Complexity + β_3 x Complexity of Habitual Treadmill Walking.

Results & Discussion: We identified a significant association between the modulation of muscle coordination complexity and WBAM for lateral waist-pull and optical flow perturbations, but only in the direction of the perturbation. The modulation of muscle coordination complexity from habitual treadmill walking to goal-directed lateral stepping in the stance leg was a significant predictor of $WBAM_{ML}$ for both the lateral waist pulls ($\beta = 0.0011$, $p = 0.023$) and optical flow ($\beta = 0.00073$, $p = 0.031$) perturbations (Fig. 1 A and B). Specifically, individuals who had a larger reduction in muscle coordination complexity had a smaller range of $WBAM_{ML}$, which is considered representative of better balance. There were no such relations for $WBAM_{ML}$ or $WBAM_{AP}$ measured from treadmill-induced slip perturbations. These results suggest that decreasing muscle coordination complexity in the stance leg during goal-directed lateral stepping may reflect increased coactivation of muscles for improved regulation of angular momentum around the center of mass during a perturbation to walking.

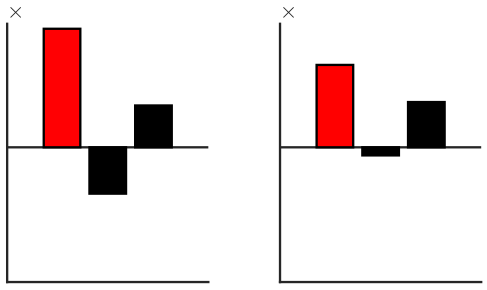

Figure 1 Linear regression to predict (A) $WBAM_{ML}$ in lateral waist pull and (B) $WBAM_{ML}$ in optical flow perturbations. (β_1 – modulation of muscle coordination complexity of stance leg; β_2 - modulation of muscle coordination complexity of stepping leg; β_3 – muscle coordination complexity of habitual treadmill walking; red bar = $p<0.05$)

Significance: We found that a decrease in muscle coordination complexity from habitual walking to goal-directed lateral stepping in the stance leg is associated with better walking balance control in response to mediolaterally demanding perturbations. These findings suggest that voluntary tasks that introduce varying demands on both stepping and balance control may provide valuable insight into an individual's ability and strategy to accommodate walking balance challenges.

Acknowledgments: Supported by a grant from NIH R21AG067388.

References: [1] Selgrade et al. (2020), *J. of Biomechanics* 109710(104), [2] Steele et al. (2015), *Dev Med Child Neurol* 57(2), [3] Herr et al. (2008), *J. Exp. Biol.* 211(467), [4] Franz et al. (2025), *J. Neuroeng. Rehabilitat* 22(11)

SHOE-RUNG COEFFICIENT OF FRICTION AS A PREDICTOR OF SLIPS IN LADDER CLIMBING

*Violet M. Williams[1], Sarah C. Griffin[1], Richard W. Smith[1], Jassi S. Chera[1], Mark S. Redfern[1], Kurt E. Beschorner[1]
[1]Department of Bioengineering, University of Pittsburgh, Pittsburgh, PA, USA.
*Corresponding author's email: Violet.Williams@pitt.edu

Introduction: Falls from height are a common occupational hazard, accounting for 82% of all fall-related fatalities (725 deaths in 2023) [1]. Ladder falls are one of the most common causes of falls from height with 30% of falls from height involving ladders [2]. Slips are a common initiating event of ladder falls, with 14% of ladder fall accidents involving a slip [3]. Available coefficient of friction (ACOF) is a metric that quantifies the friction generated between shoes and walking surfaces related to slip risk. While ACOF is known to predict slip outcomes during level walking [4], validated methods for ladder climbing are lacking. Thus, the purpose of this study was to quantify the ability of ACOF to predict slip outcomes in ladder climbing.

Methods: An instrumented ladder apparatus that could be oriented to 3 angles and 8 sets of interchangeable rungs was used for human subject testing. The ladder's 3rd rung was rigidly attached to a force plate (AMTI). Motion tracking cameras (Vicon) collected kinematic data. 84 participants (42 F, 42 M; 43.4 ± 12.3 years old; 80.1 ± 16.9 kg; 170.9 ± 91.6 cm) were instructed to climb up to the 5th rung of the ladder at an urgent pace that would reflect a busy work environment. After a pause, they climbed back down at a similar pace. Prior to the participant's final climb, a liquid contaminant (90% glycerol + 10% water) was applied to the 3rd rung. Some participants (n = 46) encountered the contaminant during only the descent while the remainder (n = 42) had the chance to slip during both ascent and descent. Slip outcomes were categorized using a k-means cluster analysis (slip distance & slip velocity) where clusters with high slip distance and slip velocities were classified as slips. Classifications were confirmed by two independent reviewers.

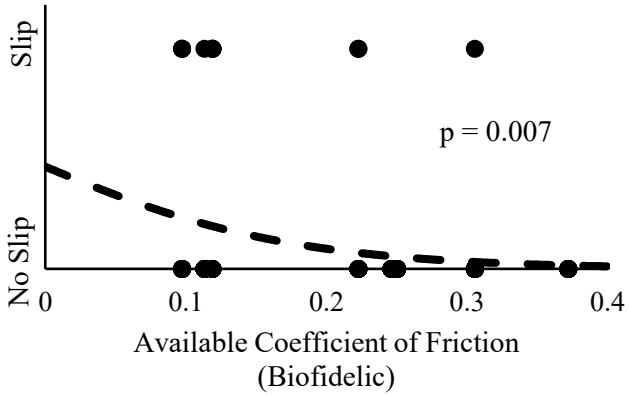

Figure 1: Logistic regression of slip outcomes against available coefficient of friction (ACOF) obtained with biofidelic testing conditions where lower $ACOF_B$ values predict higher odds of a slip when exposed to a liquid contaminant during ladder climbing. Filled circles represent the slip outcomes from participant testing, and the dashed line represents the logistic equations

ACOF was measured for each of the 8 rungs using a mechanical slip tester with a custom mount for the different rungs. Testing was conducted using two sets of testing conditions (slip speed; normal force; foot angle): generic and biofidelic. The generic conditions (0.3 m/s; 500 ± 50 N; 0°) [5,6] were created by adapting COF test methods from level-walking COF test methods and their results are reported as $ACOF_G$. The biofidelic conditions were based on the slips found in this study (0.35 m/s; 300 ± 50 N; 7° dorsiflexion) and their results are reported as $ACOF_B$. 5 trials were collected for each rung in each set of testing conditions and the ACOF was calculated as the ratio of resultant shear and normal forces. Two logistic regressions were run with slip outcome as the dependent variable while the independent variables were $ACOF_G$ and $ACOF_B$. Receiver operating curves were generated for each logistic regression and the area under the curve (AUC) was quantified.

Results & Discussion: $ACOF_G$ ($p = 0.003$; $\chi^2_1 = 8.64$; pseudo-$R^2 = 0.126$) and $ACOF_B$ ($p = 0.007$; $\chi^2_1 = 7.42$; pseudo-$R^2 = 0.108$) were both found to be significant predictors of slip outcomes in unexpected ladder slipping events. Higher ACOF values were associated with a decreased risk of slipping when exposed to the liquid contaminant in both models. An increase of 0.01 in ACOF would result in 15% reduced odds of a slip in the generic model while it would result in 10% reduced odds of a slip in the biofidelic model. The generic model had an AUC of 0.742 while the biofidelic model had an AUC of 0.723, indicating that both models can moderately discriminate slip outcomes based upon ACOF values alone. Thus, these regressions support the use of ACOF and mechanical slip testing as a method for assessing the slip risk of different ladder rung designs, with higher ACOF values corresponding to lower slip risks.

Significance: The relationship between slip outcomes and ACOF values demonstrate the importance of rung design in ladder safety. The ability of ACOF to predict slip outcomes supports changes to footwear and rung design that result in higher ACOF values. Further, the results seen in these models indicate that improvements in ACOF, through ladder rung design, would help reduce slip risk during ladder climbing.

Acknowledgments: The authors would like to acknowledge Jenna Trout and the undergraduate students who assisted with this work. This work was supported by NIOSH R01OH011799, NSF GRFP 2139321, and NCRR S10RR027102.

References: [1] U.S. BLS (2024), *Fatal Occupational Injuries,* U.S. DOL; [2] U.S. BLS (2024), *Nonfatal Occupational Injuries,* U.S. DOL; [3] Cohen et al. (1991), J. Saf. Res. 22(1); [4] Iraqi et al. (2018), J. Biomech. 74; [5] ASTM F2913-19 (2024); [6] ISO 13287 (2019);

PRELIMINARY DESIGN AND VALIDATION OF THE GLIDIATOR: A NOVEL MEANS OF ELICITING UNEXPECTED AND REPEATED LARGE AMPLITUDE SLIPS

Gaspard Diotalevi[1,2], Chantal Gauvin[4], Denis Rancourt[2,3], Cécile Smeesters[1,2]*
[1]Research Centre on Aging, Sherbrooke, QC, Canada
[2]Department of Mechanical Engineering, Université de Sherbrooke, Sherbrooke, QC, Canada
[3]Centre for Research in Acoustics-Signal-Human of the Université de Sherbrooke (CRASH-UdeS), Sherbrooke, QC, Canada
[4]Institut de recherche Robert-Sauvé en santé et en sécurité du travail (IRSST), Montreal, QC, Canada
*Corresponding author's email: Cecile.Smeesters@USherbrooke.ca

Introduction: Spreading lubricant on a force platform to slip participants in the lab, as has been done for over 50 years [1], proves inefficient at collecting unexpected and repeated slipping data [2]. Indeed, many calibration, training and dummy trials are required to hopefully collect a single anticipation-free slippery trial [2]. This abstract presents the Glidiator, a novel means of eliciting unexpected and repeated large amplitude true slips [3] of human participants in the laboratory, allowing for better gait and anticipation control. Preliminary mechanical characterization results of the manually triggered device will pave the way for optimized computer-controlled experiments and further development of the Glidiator.

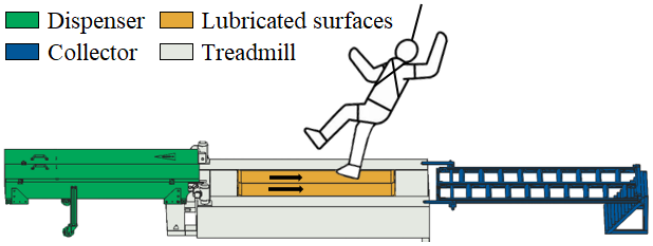

Figure 1: A hypothetical slippery trial using the Glidiator.

Methods: The Glidiator is composed of a dispenser, a split-belt treadmill instrumented with 2 AMTI force platforms, lubricated surfaces and a collector (Fig. 1). The dispenser propels one or two lubricated surfaces onto the treadmill by way of a spring-loaded mechanism. These lubricated surfaces are currently composed of stainless steel on rubber, 1/8 in thick and brushed with canola oil, but other flooring material and lubricants could also be used. The lubricated surfaces must match the treadmill's speed upon landing, so as to be carried away by the split belts without slippage. In slipping experiments, these surfaces would then elicit a slip of the participant before being recovered by the rollers on the collector. 10 trials without participants nor any treadmill movement were repeated at four even intervals of the spring's expected working compression range to characterize the manually triggered Glidiator. Rigid bodies, each composed of three OptiTrack passive markers (200 Hz), were placed on the hand pulling the triggering mechanism and on each lubricated surface, and then tracked by 10 cameras to measure triggering, propulsion and landing elapsed times from lubricated surface movement initiation. Triggering time was measured to hand movement initiation and is thus negative. Propulsion time was measured to maximal speed of the lubricated surface. Landing time on the treadmill was measured to when the lubricated surface reached minimal altitude, at which point lubricated surface speed and position were recorded.

Results & Discussion: A change in the operator's posture after the 60% compression rate trials and increasing triggering resistance from higher loads may explain the trend and high variability of triggering times (Fig. 2, red). Propulsion times (blue) remain surprisingly constant across trials at 65 ± 15 ms (mean ± standard deviation). Crucially, landing times (orange) across all trials were less than 80 ± 17 ms with excellent repeatability. As elite sprinters react to a starting gun in 140 ms at best [4], participants will certainly set foot on the lubricant before reacting to any audio clue from the Glidiator, preserving normal gait. Landing speeds increased with a linear trend from 1.24 ± 0.15 m/s to 2.21 ± 0.13 m/s (both surfaces combined). This suggests that the spring could be operated at lower and safer compression rates. Excess energy might also help with adherence to the belt upon landing. Landing positions were repeatable within 6 cm (min to max position), except at 90% compression rate for the right surface which had a higher variability of its landing time.

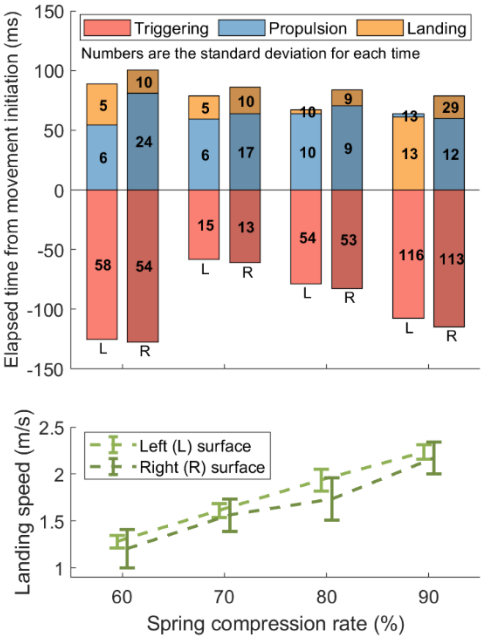

Figure 2: Mechanical delays and landing speeds upon manually triggering the Glidiator for both lubricated surfaces.

Significance: Results from the manually triggered Glidiator are encouraging for the eventual computer-controlled triggering based on participants' gait, anticipation levels and electro-mechanical delays. Preliminary dry trials within the team also proved that triggering the Glidiator based on a participant's gait is feasible, to ensure that heel strike position on the lubricated surfaces allows for full range slips. Moreover, preliminary trials within the team on a conceptual prototype using a lubricated acrylic sheet manually dispensed on the treadmill immediately resulted in large slips (and one fall).

Acknowledgments: The Fonds de recherche du Québec – Nature et Technologies (FRQNT, 315311) and the Natural Sciences and Engineering Research Council of Canada (NSERC, ALLRP 570347-21) for their financial support. G. Aubut, A. Beaudry and M.-J. Laliberté for their technical assistance. A. Caron-Laramée, C. Dessureault, F. Martel and N. Zabjesky for experimental assistance.

References: [1] Son (1990), PhD Dissertation, Texas Tech University; [2] Diotalevi et al. (2024), *ASB2024*; [3] Diotalevi and Smeesters (2023), *ASB2023*; [4] Tønnessen et al. (2013), *J Strength Cond Res* 27(4).

MUSICAL FEEDBACK FOR GAIT RETRAINING IN ORTHOPEDIC REHABILITATION

*Luisa Cedin[1], Camilla Antognini[1], Christopher Ferrigno[2], Christopher Knowlton[1], Markus Wimmer[1]
[1]Department of Orthopedic Surgery, Rush University Medical Center, Chicago, IL
[2]Department of Anatomy and Cell Biology, Rush University Medical Center, Chicago, IL
*Corresponding author's email: luisa_cedin@rush.edu

Introduction: Several orthopedic rehabilitation programs utilize gait retraining to address deficient walking patterns. [1,2] However, several key barriers such as accessibility and cost limit the full implementation and utility of gait retraining. Home-based feedback training can facilitate motor learning [3] and possibly retention. This study presents a personalized real-time musical feedback system designed to improve loading conditions in the knee joint by promoting a center of foot pressure shift. Further, we evaluated the biomechanical strategies employed to accomplish the gait adjustment.

Methods: Healthy subjects were recruited and underwent informed consent. After warming up, they performed single walking trials recorded simultaneously by a marker-based multi-camera motion analysis system (Qualysis AB) and wireless 16-sensor insoles (Insole3, Moticon ReGo AG). Following baseline trials, subjects practiced using a musical feedback protocol based on the real-time center of pressure (COP) designed to promote medialization of foot pressure and to reduce the knee adduction moment (KAM). Data from the insoles were processed in Max 8 (Cycling '74). Popular music was played during the gait training with auditory feedback. A lowpass filter muffled the music when the subject's COP was unable to medialize their COP across a spatial threshold (25% shift in average peak lateral COP from baseline). Subjects were instructed to avoid the muffling of music by shifting their plantar pressure medially while maintaining an otherwise natural gait. All trials were averaged since no significant differences were found between the right and left sides. Spatiotemporal parameters and COP were compared between baseline and after-training conditions using paired t-tests ($\alpha < 0.05$). Statistical Parametric Mapping analyzed differences in kinetics and kinematics parameters.

Results & Discussion: All 12 participants (6/6 women/men, 31.4 ± 5.28 years, 75.4 ± 10.9 Kg, 1.71 ± 0.07 m) significantly medialized their COP with musical feedback (-11% ± 0.04, range -6.21% to -19.19%). After training, KAM peaks were significantly reduced (Table 1). Surprisingly, walking speed, stride length, and cadence remained unchanged, despite the feedback being designed to introduce a modified gait pattern. Kinematic analysis revealed increased hip external rotation (Fig. 1a) and knee flexion during stance facilitate COP medialization. Additionally, the ankle exhibited an increased dorsiflexion near heel strike and at mid-stance with a more pronounced external rotation throughout the entire gait cycle (Fig. 1b). Notably, the frontal plane knee angle remained unchanged post-training, despite the reduction in KAM peaks. SPM analysis detected no significant changes in knee flexion or rotation moments, except for a reduction in KAM near the second peak. Further analysis revealed that step width remained consistent before and after training (Table 1). Although the foot progression angle did not significantly change, a slight tendency toward toe-out was observed, aligning with the increased hip external rotation during stance. In conclusion, musical feedback effectively cued participants to medialize their gait line, reducing KAM. While hip and knee kinematics adapted to support this shift in the COP, overall gait parameters—including speed, stride, cadence, and foot progression angle—remained unchanged.

Table 1: Spatiotemporal parameters and kinetics

	Baseline	Post-Training
Speed (m/s)	1.25 ± 0.18	1.26 ± 0.15
Cadence (strides/min)	54.14 ± 3.41	54.80 ± 3.68
Stride length (m)	1.40 ± 0.13	1.39 ± 0.11
Stride width (m)	0.10 ± 0.02	0.11 ± 0.03
Foot Progression Angle (°)	2.33 ± 4.04	3.77 ± 4.18
KAM 1st Peak	-2.47 ± 0.71	-2.29 ± 0.63**
KAM 2nd Peak	-2.26 ± 0.40	-1.94 ± 0.38**

KAM: Knee Adduction Moment. *p < 0.05 **p < 0.01

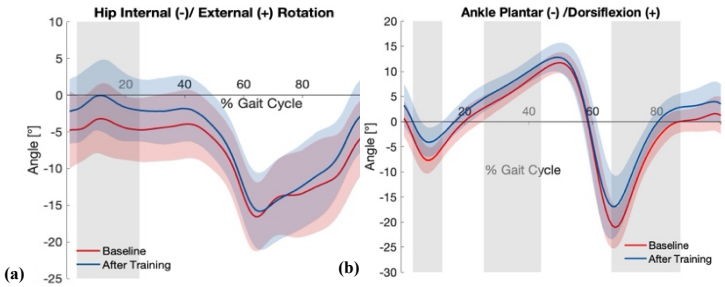

Figure 1: Hip rotation (a) and knee flexion (b) at baseline and after training with the musical feedback. Shaded regions represent +/- SD. Gray areas show significant differences between conditions.

Significance: This study demonstrates the potential of real-time musical feedback as an innovative intervention for shifting the gait line and reducing knee adduction moments (KAM). By leveraging auditory cues, this approach facilitates gait adjustments without disrupting overall walking patterns, offering a novel strategy for movement retraining. The observed biomechanical adaptations highlight the effectiveness of music-driven feedback in promoting targeted gait modifications, which could be applied in various settings, including sports performance, injury prevention, and rehabilitation. Furthermore, the accessibility and adaptability of this feedback system suggest its potential for home-based training, making gait retraining more scalable and engaging.

Acknowledgments: Supported by Grant T32AR 073157 from the NIAMS.

References: [1] Reh et al. (2021) Front. Sports Act. Living, 3, [2] Cedin et al. (2025) Healthcare, 13(2), [3] Forman et al. (2021) Frontiers, 2.

ESTIMATING METABOLIC ENERGY COST USING WEARABLE SENSORS

*Katherine M. Butler[1], Rachel V. Vitali[1]
[1]University of Iowa, Department of Mechanical Engineering
*Corresponding author's email: katherine-butler@uiowa.edu

Introduction: The US Navy utilizes different protective equipment depending on a given situation. This protective equipment, typically worn by damage control (i.e., emergency response) teams, potentially limits mobility and incurs a significant physiological burden on the human body. One measure of physiological burden is metabolic cost – a measure of the energy expended to perform a specific task. Metabolic cost is most often estimated via indirect calorimetry, which involves measuring the volumes of oxygen consumption (V_{O_2}) and carbon dioxide production (V_{CO_2}) on a breath-by-breath basis. A common model (Eqn. 1) for relating these volumes to metabolic cost was offered in [1] and is widely used today, though the expression below is normalized by the participant's mass (m).

$$EE = \frac{16.58 * V_{O_2} + 4.15 * V_{CO_2}}{m} \quad (1)$$

Despite its advantages and widespread use, indirect calorimetry requires participants to wear a mask, which is uncomfortable, usually restricts measurements to a lab setting, and produces noisy, low frequency data. Also, when considering protective equipment, it is often not possible to use a mask due to preexisting protective equipment covering the face. This study proposes using wearable sensors as an alternative approach. Wearable sensors provide many benefits including their relatively small size, enables faster data collection, and is compatible with protective gear. Existing studies using wearable sensors either use the raw data to directly predict metabolic cost or apply machine learning algorithms, which may lack generalizability [2]. This study aims to estimate metabolic cost by combining sensor metrics to derive new features such as kinetic energy to develop a more generalizable algorithm to predict metabolic cost.

Methods: This study consists of validating a computational method for estimating metabolic cost with the goal of quantifying the physiological burden of protective equipment during operationally relevant tasks. A dataset consisting of 10 subjects performing 6 exercises along with individual characteristics of each subject were used to develop the wearable sensor-based method [3]. Each trial consisted of the participant completed the exercise for a 6-minute interval across different conditions (e.g., speed and incline). The first metric utilized in the metabolic cost prediction is the raw heart rate (HR), which was collected via a heart rate monitor and then averaged over the last 3 minutes at each exercise speed and incline. A novel feature proposed here is a proxy for kinetic energy, which was derived from the angular velocity obtained by inertial measurement units (IMUs). Since individual body segment moments of inertia were not available, the NASA standard for the body segment moment of inertia (I_b) was used by multiplying it by ratio of the subject's mass to that of the NASA standard [4]. Next, the angular velocity (ω) magnitude was computed such that the kinetic energy could be calculated for each body segment at each sampling point ($I_b\,\omega^2$). Each body segment's kinetic energy (KE) was summed and averaged over the course of the last 3 minutes at each speed and incline of the exercise. Linear regression analyses were performed, from which the root mean squared error (RMSE) and coefficients of determination (R^2) were computed. The first linear regression model (EE ~ 1 + KE + HR) assessed the impact of using kinetic energy and heart rate on metabolic cost. To improve the model's accuracy, the subjects' height, mass, age, and sex were incorporated into an updated liner regression model: EE ~ 1 + KE + HR + height + mass + age + sex.

Results & Discussion: Figure 1 illustrates the relationship between KE and EE. The solid blue line indicates the KE calculated at each time step. The solid black (yellow) line indicates the 3-minute average for KE (EE) for that walking speed. The preliminary results illustrate the potential for using KE and HR to predict EE. This model yielded an RMSE of 1.66 and R^2 of 0.70. With the additional participant data, the RMSE decreased to 1.38 and the R^2 increased to 0.80, indicating a better fit. These findings are comparable to those reported in [3], which achieved an RMSE of ~1 when all wearable sensor data were used. Future work will continue to refine and expand the features used to predict EE by deriving other features from the HR and IMU data as well as potentially adding surface electromyography data.

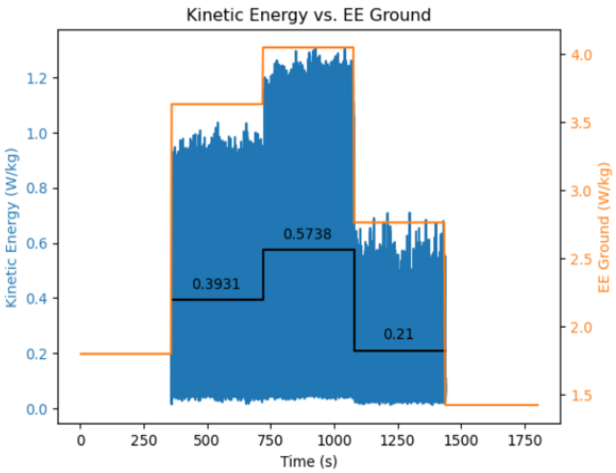

Figure 1: Plot of kinetic energy (blue, left vertical axis), the 3-minute average (solid black), and ground truth metabolic cost (yellow, right vertical axis) for a participant walking at 3 different speeds.

Significance: Quantifying the physiological burden incurred during tasks performed by damage control teams is critical to ensuring their safety and optimal performance in high-risk environments. This study proposed a method of estimating metabolic cost using wearable sensors, with the overall goal of reducing physiological burden of protective equipment on the user. By utilizing wearable sensors, data collection becomes more feasible across various environments. The findings of this study can provide insights to inform equipment design and training protocols.

Acknowledgments: This material is based upon work supported by DoD Navy (NEEC) Grant No. N00178-24-1-0006.

References: [1] Brockway, J. M., (1987), Clinical Nutrition, 41(6), 463-471. [2] Lopes, J. M., et. Al., (2022), Sensors. [3] Ingraham, K., et al., (2019), J. of Applied Physiology, 126(3). [4] McConville, J., (n.d.), A/F Aerospace Medical Res.

ACCURACY OF A TIBIAL MOUNTED ACCELEROMETER AT IDENTIFYING TAKE-OFF AND LANDING OF A SINGLE-LEGGED VERTICAL JUMP

*Jean L. McCrory[1], Millissia Murro[1], Marcus Marpoe[2], Matthew Fleshman[1], and Michelle A. Sandrey[1]
[1]School of Medicine, [2]Statler College of Engineering, West Virginia University, Morgantown, WV
*Corresponding author's email: jlmccrory@hsc.wvu.edu

Introduction: The countermovement vertical jump (CVJ) is frequently utilized to assess lower extremity performance. Historically, force plates have been used to identify take-off (TO) and landing (LAND) times for the CVJ [1]. Accurate determination of these events is essential to determine jump height and EMG muscle activation latencies. Technological developments in accelerometers and inertial measurement units (IMUs) have allowed the study of movement in 'real-world' environments [2]. Elvin et al. [3] examined ground reaction forces (GRFs) and axial tibial acceleration of the single-legged CVJ. Using principles of projectile motion, they purported the first and last negative accelerations defined TO and LAND, respectively. However, the shank may not follow the rules of projectile motion because it is subject to knee torques during the jump. Errors for TO and LAND event time determination were not reported. The **purpose** of this study was to evaluate the accuracy of the criteria first/last negative axial acceleration of a tibial placed accelerometer for detecting TO and LAND events [3] and to develop and evaluate alternative formulae for identifying these events in single-legged CVJs.

Methods: Twenty young healthy individuals participated (21.7±3.7yrs, 1.67±0.13m, 70.5±14.1kg, 10M/10F). Following consent, a triaxial accelerometer was secured on the proximal anterior tibia of the subject's preferred leg. The accelerometer was aligned with the cardinal axes of the leg. Each subject performed five single-legged CVJs on a force plate. Acceleration and GRF were synchronously collected (1000Hz) and filtered with a 4th order dual-pass Butterworth filter (f_c=100Hz). GRF data were used as the gold-standard in our event time determinations. Data from three subjects (15 jumps) were used to develop criteria to identify TO and LAND. Force plate TO and LAND were defined as when the vertical GRF dropped below 5N (TO) and then exceeded 5N (LAND) [3]. 3D and resultant acceleration data were graphed with GRF-defined TO and LAND events. Based on visual inspection and the work of Elvin [3], we developed the following possible criteria to define TO from the acceleration data: peak anteroposterior acceleration, peak resultant acceleration, and first negative axial tibial acceleration [3]. Criteria to define LAND included last negative axial acceleration [3] and slope of axial acceleration >15K m/s^2. The remaining 85 jumps were used to evaluate the accuracy of the above acceleration-based criteria. Agreements were quantified using root mean square error (RMSE) and intraclass correlation coefficients (two-way mixed model for absolute agreement; α=0.05) between the GRF data and each accelerometer criterion. Skewness was assessed to determine if a certain method over- or underestimated true TO and LAND times. The range of error was calculated for each criterion.

Results and Discussion: All criteria detected TO and LAND from all single-legged CVJs. Results are shown in Table 1. All measures exhibited strong correlations with the GRF data (ICC>0.99, p<0.001). In determining the time of TO, the first negative axial tibial acceleration produced the smallest RMSE (error range -25.7ms to 55.2ms) and no skewness compared to the GRF data. Conversely, the RMSEs and ranges of error using the anteroposterior and resultant acceleration peaks to determine TO were much greater. The positive skewness of using peak anteroposterior acceleration indicated that it tended to underestimate the TO time or determined TO earlier than the force plate. The point at which the slope of the axial acceleration exceeded 15K m/s^2 was the most accurate at determining LAND. However, the skewness value of 1.233 indicated this method was likely to identify the event earlier than the force plate. Using the first positive axial acceleration following TO detected the moment of LAND with an error of ~24ms and was not likely to be skewed compared to force plate LAND.

Using an accelerometer to detect TO and LAND will result in acceptable errors in jump height determination. If TO is defined as the first negative axial tibial acceleration [3], a RMSE of 17.6ms would result in an estimated jump height error of 0.15cm. If detecting LAND using the slope of axial acceleration >15k m/s^2, the expected error in jump height determination would be 0.06cm. Elvin et al. [3] reported an ICC of 0.828 of jump height assessed with an accelerometer vs the force plate. The accuracy of accelerometry may not be sufficient to assess EMG muscle activation latencies in landing, as our RMSE to detect LAND was 24ms.

Significance: In conclusion, wearable-technology, such as IMUs, can identify TO and LAND of a single-legged CVJ with sufficient accuracy to determine jump height but not muscle activation latencies in field-based research.

Table 1: Accuracy of accelerometry-determined take-off and landing times compared to force plate determined times.

Variable	Method	RMSE (ms)	Error range (ms)	Skewness*	ICC (CI, 95%)**
Take off	First Negative Axial Accel [3]	17.6	-25.7 to +55.2	0.021	1.000 (0.999, 1.000)
	Peak Ant-Post Accel	106.1	-179.0 to +394.3	1.188	0.991 (0.986, 0.994)
	Peak Resultant Accel	49.1	-166.7 to +107.6	-0.841	0.998 (0.997, 0.999)
Landing	First Positive Axial Accel [3]	24.0	-35.2 to +2.9	0.922	1.000 (0.875, 1.000)
	Slope of Axial Accel > 15K m/s^2	10.7	-25.7 to +40.0	1.233	1.000 (1.000, 1.000)

* Skewness values >1.0 indicate data skewed to the left (early compared to force plate data). **p<0.001.

References: [1] Warr et al. (2020) *Cogent Soc Sci* 6; [2] Camomilla et al. (2018) *Sensors-Basel* 18; [3] Elvin et al. (2007) *J Appl Biomech*, 23, 180-189.

HOW MUCH INSOLE SENSOR DATA IS ENOUGH TO IDENTIFY HABITUAL ACHILLES TENDON LOADING?

*Ke Song[1], Michelle P. Kwon[1], Andy K. Smith[2], Ryan T. Pohlig[2], Karin Grävare Silbernagel[2], Josh R. Baxter[1]
[1]University of Pennsylvania, Philadelphia, PA; [2]University of Delaware, Newark, DE
*Corresponding author's email: ke.song@pennmedicine.upenn.edu

Introduction: Exercise with loading progression is a standard treatment for Achilles tendinopathy [1,2], yet recovery outcomes vary greatly among patients [3]. Notably, most rehabilitation programs do not account for tendon loading outside of the prescribed exercises, despite that underloading and overloading in daily life can both be detrimental to tendon health [4]. This suggests an unmet clinical need to monitor Achilles tendon load during daily living. Wearable sensors are increasingly common for tracking real-world biomarkers, and researchers have used instrumented insole sensors to monitor biomechanical loading [5,6]. In our ongoing parent study, we used insole sensors to quantify 2 weeks of cumulative tendon loading in individuals with Achilles tendinopathy and found it associated with plantar flexor function. Despite this clinical relevance, practical and technical challenges with insole sensors both limit their feasibility for long-duration usage. Therefore, in this ancillary study, we aimed to determine the minimal insole sensor data needed to represent habitual 2-week tendon loading in patients with Achilles tendinopathy. We hypothesized that compared to cumulative tendon loads estimated from 2-week insole data, subsamples on a reduced number of days would lead to increasing error and decreasing agreement with the full data.

Methods: In our IRB-approved parent study, 15 participants with Achilles tendinopathy provided informed consent and completed a 2-week insole monitoring program. They wore a 3-sensor instrumented insole (heel, midfoot, forefoot) as much as possible for at least 6 days and up to 14 days, which recorded their plantar contact forces during daily living. We applied our validated algorithm on the insole data [6] to compute Achilles tendon load and its cumulative impulse. We stratified this cumulative tendon load at 2 thresholds: "overall" load ≥ 0.3 times Body Weight (×BW) that includes all general daily living activities [1], and "high-level" load ≥ 3.0×BW that is beyond gait and mainly related to dynamic movements [1]. We divided these cumulative overall and high-level loads by overall loading time ≥ 0.3×BW to account for the insole wear time variability. We iteratively quantified the errors when estimating from extracted insole data subsamples with reduced number of monitoring days, using the 2 week-based overall and high-level loads as reference. Specifically, we computed Mean Absolute Percent Error (MAPE: % difference from 2 week-based) [7] and Pearson correlation to 2 week-based estimates when estimating from 6 (first six days of insole data), 5 (omit day-1, … omit day-6), 4, 3, 2, or 1 day of data (day-1 only, … day-6 only).

Results: Using less days of insole data led to increased error in estimating the overall cumulative and high-level Achilles tendon loads (**Fig. 1**). Estimated overall Achilles tendon load *per hour* were relatively robust with subsampling, as MAPE remained <10% even when only using 1 day of insole data (**Fig. 1A, 1C**). In contrast, using 1 day of data led to mis-estimated high-level load *per hour* for some participants on multiple days, resulting in a >60% MAPE across the group (**Fig. 1B, 1C**). This error gradually lowered when increasing the number of insole sensor monitoring days. When using the first 6 days of insole data from each participant, MAPE of the high-level tendon load was 25.1% (**Fig. 1C**) with correlation r = 0.95 against the full dataset-based estimate (**Fig. 1D**).

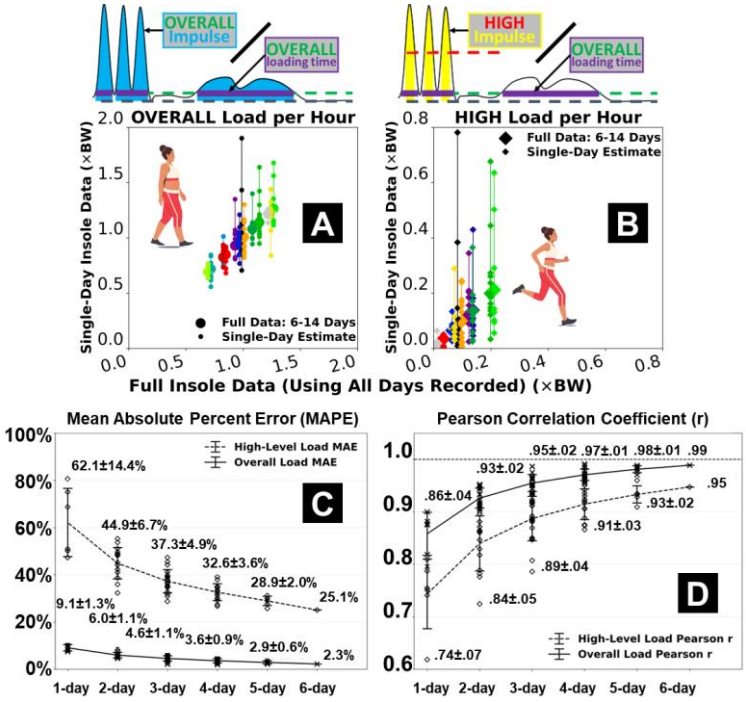

Figure 1: Effects of subsampling on estimated cumulative Achilles tendon load. Compared to 2-week data, 1-day data often under- or over-estimated overall load **(A)** and especially high-level load *per hour* **(B)**. MAPE for 1 day-based estimate was small (<10%) for the overall load but larger (up to >60%) for high-level load with more day-to-day variations **(C)**. Using more days of insole data gradually reduced this MAPE and increased correlation to the 2 week-based estimates **(D)**.

Discussion: When only using 1 day of insole data, error against the full 2-week dataset remained low for overall tendon load (<10%) but was higher for the high-level load (>60%) (**Fig. 1**). One day of insole sensor data may thus be sufficient to reliably characterize habitual tendon loading required for daily living mobility. Instead, multi-day insole monitoring may be necessary to ascertain the high-level tendon loading status, including its day-to-day variations, that are unique to sports and dynamic activity.

Significance: This subsampling analysis is important due to the practical challenges of using insole sensors and useful for establishing the best practices that future studies can leverage to balance data fidelity with participant burden. We recommend researchers select insole monitoring durations based on the population studied to maximize cohort size and assessing clinically relevant loading parameters with better confidence.

Acknowledgments: NIH R01AR078898, P50AR080581, R01AR072034. We thank Devyn Russo for assisting with data collection.

References: [1] Baxter+ *Med Sci Sports Exerc* 2021. [2] Silbernagel+ *Am J Sports Med* 2007. [3] van der Plas+ *Br J Sports Med* 2012. [4] Aicale+ *J Orthop Surg Res* 2018. [5] Elstub+ *J Sports Sci* 2022. [6] Hullfish+ *Gait Post* 2020. [7] de Myttenaere+ *Neurocomputing* 2016.

ARM MOVEMENT IN REACTION TO EMOTIONAL STIMULI REVEAL POTENTIAL BIOMARKERS FOR CHILDHOOD MENTAL HEALTH DIAGNOSES

Jenna G. Cohen[1*], Bryn C. Loftness, Julia Halvorson-Phelan, Ellen W. McGinnis, Ryan S. McGinnis
[1]Biomedical Engineering, University of Vermont
*jenna.g.cohen@uvm.edu

Introduction: More than one in five children have a mental health diagnosis, including ADHD, anxiety, and depression [1]. Since children cannot reliably articulate their emotions, current screening relies on parent reports [2]. As many symptoms are unobservable, even the most attentive caregivers may underreport [1]. Child behaviors (i.e., startle response) during stressful laboratory tasks have been found to indicate mental health risk [3], however coding videos by hand leaves room for subjectivity. Wearable sensors can offer feasible, objective metrics of behavioral stress responses in children. In this analysis, we consider child arm movement in reaction to two startling buzzers during a stressful laboratory task as a behavioral measure of reactivity. We hypothesized there would be differential behavioral stress reactivity by child mental health diagnosis. Results will identify potential new movement biomarkers that could improve detection of mental health diagnoses in young children.

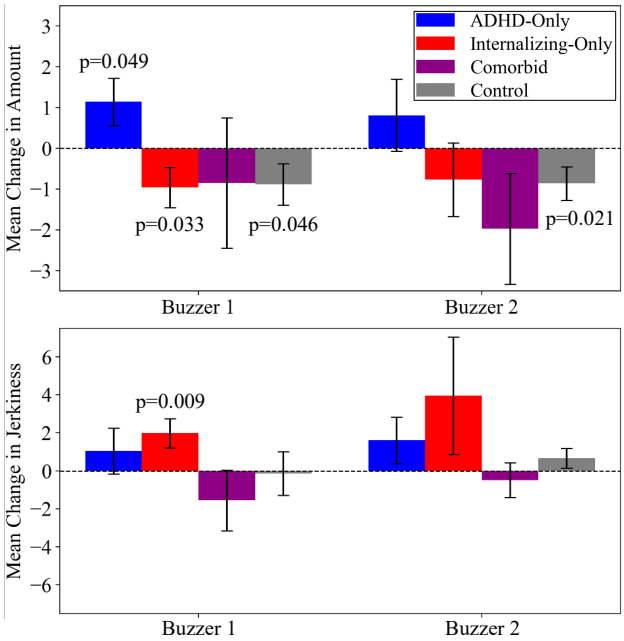

Figure 1: Mean and standard error of the change in arm movement factors in reaction to buzzers for children in each diagnostic group.

Methods: We present arm movement data from children ages 4-8 (N=82, 41% female) during the widely used Trier Social Stress Task adapted for children [2]. In this task, children were told they would be judged while telling an impromptu 3-minute story. A startling buzzer sounded halfway through and with 30 seconds remaining, inducing additional fear. Accelerometer data extracted from a BioStamp® sensor located on the child's forearm yielded 16 features that were condensed into meaningful factors via exploratory factor analysis characterizing the 'Amount' and the 'Jerkiness' of arm movement. To measure buzzer reactivity, a change score was calculated from the data 15 seconds before and after each buzzer for both factors. Child mental health diagnoses were determined via a gold-standard semi-structured interview (KSADS-PL). We examine arm movement buzzer reactivity across child participants with ADHD (ADHD-Only, n=7), anxiety or depression (collectively called Internalizing-Only, n=23), comorbid ADHD and anxiety or depression (Comorbid, n=10), and without any mental health diagnoses (Control, n=42). T-tests were conducted to demonstrate significant buzzer reactivity compared to zero (no change).

Results & Discussion: Buzzer reactivity, defined as a significant increase or decrease in arm movement, revealed differentiation by diagnosis (Fig. 1). For movement 'Amount', the ADHD-Only group (p=0.049) had a significant increase in reaction to the first buzzer, whereas the Internalizing-Only (p=0.033) and Control (p=0.046) groups each had a significant decrease. These trends were also observed in reaction to the second buzzer, however only the Control group's change was significant (p=0.021). For movement 'Jerkiness', the Internalizing-Only group had a significant increase in reaction to the first buzzer (p = 0.009), with similar non-significant trends to the second buzzer. Results for children with ADHD are consistent with previous findings demonstrating higher overall activity as measured by wrist-worn sensors [4], but add to mixed literature on startle response [5], showing both increased and decreased startle compared to controls depending on stimuli. Results for children with internalizing diagnoses suggest a jerky, abrupt quality of movement resulting in stilling, perhaps consistent with increased startle [6] and "freezing" behaviors [7] seen in anxiety. Children with no diagnosis also stilled, but without the abrupt quality, potentially characterizing a less intensive reaction to stressful stimuli than those with an internalizing diagnosis. Children with comorbid ADHD *and* internalizing diagnoses never had a significant reaction to a buzzer, potentially due to duelling symptom types masking one another's response, and thus these children may be overlooked using this indicator of mental health. There is a dearth of literature that is inclusive of children with comorbidities, however, null results are surprising given this subgroup, by definition, often exhibits the most symptoms and impairment.

Significance: Changes in arm movement factors, derived via exploratory factor analysis, in reaction to startling buzzers during a short anxiety-induction task provide potential biomarkers of mental health conditions in young children.

Acknowledgments: Research supported by the US National Institutes of Health (MH123031) and the US National Science Foundation (2046440).

References: [1] K. B. Madsen et al. (2018), *Eur Child Adolesc Psychiatry*; [2] B. C. Loftness et al. (2023), *IEEE JBHI*; [3] L. S. Wakschlag et al. (2005), *Clin Child Fam Psychol Rev,* 8(3); [4] F. De Crescenzo et al. (2016), *Sleep Medicine Reviews*; [5] A. Conzelmann et al. (2008), *Biological Psychiatry* 65(7); [6] L. M. McTeague et al. (2012), *Depression and anxiety* 29(4); [7] C. Borkar et al. (2021), *J Vis Exp*

DETECTING SHOULDER RANGE OF MOTION CHANGES FOLLOWING BREAST RECONSTRUCTION USING A NOVEL SMARTPHONE APP

*Kayla Russell-Bertucci[1], Smarika Khadka[2], Stephen M. Cain[3], Daniel L. Hertz[4], David B. Lipps[1]
[1]School of Kinesiology, University of Michigan, Ann Arbor, MI
[2]Department of Biomedical Engineering, University of Michigan, Ann Arbor, MI
[3]Department of Chemical and Biomedical Engineering, West Virginia University, Morgantown, WV
[4]College of Pharmacy, University of Michigan, Ann Arbor, MI
*Corresponding author's email: kaylarb@umich.edu

Introduction: There is a need to quantify the functional deficits associated with mastectomy and breast reconstruction procedures as more breast cancer patients elect to undergo these surgeries to manage future cancer recurrence and improve aesthetics. Breast cancer patients commonly report shoulder pain and restricted arm mobility in the months and years following surgery [1]. Shoulder strength reductions up to 20-26% through adduction, flexion, and internal rotation [2,3] and decreases of 20° in flexion following surgery [4] paired with more sedentary lifestyles after treatment [5] may explain these arm mobility restrictions. Currently, clinicians do not have the resources to assess upper extremity range of motion (UEROM) due to the needed additional clinic time and specialized equipment. Earlier detection of UEROM limitations can help clinicians target rehabilitation efforts sooner to reduce severity [6], thus improving quality of life by improving UEROM sooner after treatment [7]. One promising strategy to improve the accessibility of collecting this key measurement of physical function is using an iPhone application. We hypothesize that there will be decreases in shoulder abduction and flexion range of motion following surgery since previous studies reported arm mobility restrictions. We further hypothesize that the iPhone app will detect similar reductions in UEROM after surgery as wearable inertial measurement units (IMUs) and reveal a strong correlation between the two measurements.

Methods: 13 female breast cancer patients (45.5(8.5) years old; 96(20) kg, 1.66(0.05) m) performed an at-home UEROM assessment simultaneously using OPAL APDM IMUs and an iPhone app before breast reconstruction surgery and 6-12 weeks after their surgery. The IMU set consists of 5 sensors: sternal, right upper arm, left upper arm, right forearm and left forearm. The iPhone application (MyDataHelps platform, CareEvolution) provided video and verbal instructions for donning the IMU sensors and holding their iPhone for reliable comparisons, including keeping their elbow and wrist locked while moving their arms upward. IMU measurements of UEROM are measured as the change in upper arm elevation angle from the neutral position using accelerometers. The iPhone application used the Apple ResearchKit toolbox to measure the change in phone orientation (in quaternions) between when the phone is held at the patient's side and when the patient reached their maximum elevation angle in flexion or abduction movements. The IMU and iPhone app maximum shoulder elevation angle of the breast cancer-affected side's changes pre- and post-surgery were assessed using paired t-tests. To determine the validity and correlation of the iPhone app's measurements to IMU-derived measures, the difference in pre-post UEROM was compared between IMU and smartphone elevation angles using paired t-tests and Pearson correlations.

Results & Discussion: Participants exhibited decreased UEROM of their affected limb in both the plane of abduction and flexion following surgery, with the iPhone app detecting these changes with non-significant differences from the IMUs. IMU-derived maximum shoulder elevation revealed a significant decrease in shoulder abduction (p=0.007) and flexion (p=0.007) after breast reconstruction surgery (Figure 1a). The iPhone app detected significant decreases in flexion (p=0.004), and a trend towards a decrease in abduction (p=0.08) after surgery (Figure 1b). The pre-post difference in UEROM between the elevation angles derived by the IMUs and the iPhone app were statistically similar (both $p > 0.15$), with medium-to-large correlations between the measures in abduction (r=0.58) and flexion (r=0.78) (Figure 1c).

These findings indicate post-operative decreases in UEROM after breast reconstruction and similar results between IMU- and iPhone app-derived UEROM measures. The IMU results indicate a greater reduction in shoulder abduction (-22°) than shoulder flexion (-15°) following breast reconstruction surgery. The iPhone app had similar performance as the IMUs and may be sensitive enough to remotely assess UEROM without the burden of donning multiple IMU sensors. One limitation is the iPhone-measured UEROM measures may have larger error due to wrist movements occurring independently of the shoulder. Future studies should continue validating the iPhone app with other kinematic methods to better understand this variance.

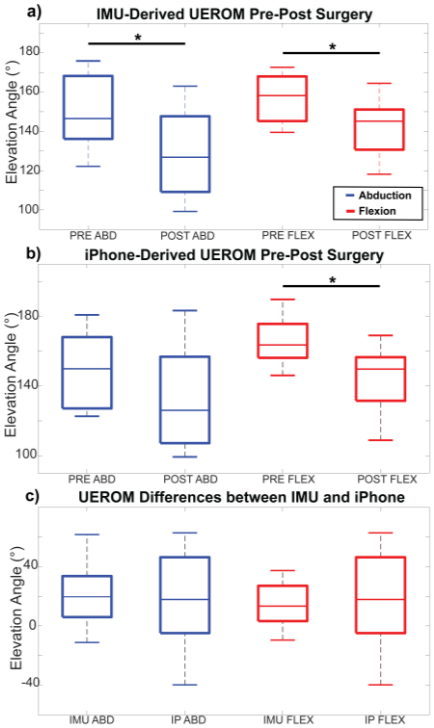

Figure 1: Boxplots of maximum shoulder elevation angles in abduction (blue) and flexion (red) measured by IMU or iPhone app (IP). **a)** IMU measured; **b)** IP measured; **c)** comparison of pre-post-surgery difference between IMU and IP.

Significance: These findings indicate mobile technologies can detect UEROM deficits in breast cancer survivors after breast reconstruction. Adopting this smartphone app can assist clinicians in remotely detecting these deficits sooner to improve post-operative quality of life.

Acknowledgments: American Cancer Society TLC-22-191-01; Anna Lamport

References: [1] Tarantino et al. (2006), *Plast Reconst Surg*, 117(5); [2] de Haan et al. (2007), *Ann Plast Surg*, 59(6); [3] Hage et al. (2014), *Ann Plast Surg*, 72(6); [4] Min et al. 2021, *J Clin. Med,* 10(15) [5] Phillips et al. (2015), *Gynecol Oncol*, 138(2); [6] Lai et al. (2016), *Ann Surg Oncol*, 23(10); [7] Chrischilles et al. (2019), *Breast Cancer Res Treat*, 175(3)

STEPPING INTO THE FLOW: MECHANICAL WORK INFLUENCES WALKING-INDUCED HYPEREMIA

*Jose G Anguiano-Hernandez[1], Jenna K Burnett[1], Cody P Anderson[2], Song-Young Park[2], Kota Z Takahashi[1]
[1]Department of Health and Kinesiology, University of Utah, Salt Lake City, UT
[2]School of Health and Kinesiology, University of Nebraska at Omaha, Omaha, NE
*Corresponding author's email: jose.anguianohernandez@utah.edu

Introduction: The human body needs synergistic actions of the vascular and musculoskeletal systems so that oxygen is delivered to the muscles to produce work. Yet, the vascular and musculoskeletal systems are often studied in isolation in many locomotion studies. Understanding the interactions between the two systems is crucial to elucidating how locomotion is affected in those with impaired leg blood flow (e.g., diabetes, peripheral artery disease, aging) [1]. We have developed a novel ultrasound technique to quantify leg hyperemia (i.e., increase in leg blood flow) induced by walking [2], opening the door to quantify the previously elusive vascular-musculoskeletal interactions. The purpose of this study is to use our novel ultrasound technique to examine the relationship between leg work and walking-induced leg skeletal muscle hyperemia on different slopes. We hypothesize that net leg work will positively correlate with walking-induced hyperemia because of increased oxygen demand in the leg muscles. We also hypothesize positive leg work (surrogate for concentric contractions) will correlate more strongly with leg skeletal muscle hyperemia than negative leg work (surrogate for eccentric contractions), because of the higher oxygen demand of concentric contractions [3].

Methods: Ten healthy young adults (5 females, 28.4 ± 3.8 years old, 68.5 ± 9.2 kg) participated in this study. Participants rested for at least 15 minutes before walking on an instrumented treadmill (FIT5, Bertec, USA) for 10 minutes at 1.2 m/s on a 0° slope. They then walked at a -5° and 5° slope in random order at the same speed. Fifty-four reflective markers and twelve infrared cameras were used to record motion capture at 250 Hz (Nexus v2.16, Vicon, UK). Ground reaction force was recorded at 1000 Hz. Dominant-side common femoral artery blood flow was measured with Doppler ultrasound (Terason uSmart 3300 NexGen, USA) using a 3D printed bracket. Thirty-second ultrasound recordings were taken during quiet standing immediately before and after walking. A validated open-source software (FloWave.US, USA) was used to extract artery diameter (cm) and blood flow velocity (cm/s) from ultrasound videos to calculate (LBF) in L/min [4]. Six degree-of-freedom power done by the dominant-side hip, knee, ankle, and foot [5] was calculated in Visual3D (v11.2, HAS-Motion, USA). Joint (or segment) power curves were integrated to find positive and negative work and summed to find total positive and negative leg work. Positive and negative leg work were summed to find net leg work. MATLAB (R2023A, MathWorks, USA) was used to calculate LBF during pre- and post-walking periods. Walking-induced leg hyperemia was calculated as the change in LBF from baseline. A Repeated Measures ANOVA compared leg skeletal muscle hyperemia across conditions. A linear mixed model was used to determine the relationship between net leg work and leg hyperemia. A second linear mixed model was used to determine the influence of positive and negative leg work on leg hyperemia. All statistical tests were done at $\alpha = 0.05$.

Results & Discussion: Incline walking caused the greatest increase in LBF compared to level ($p = 0.01$) and decline ($p = 0.004$) walking, suggesting that the oxygen demand of uphill walking was greater than level and downhill walking (Figure 1A). Net leg work positively associated with leg hyperemia ($p = 0.002$), where a 1 J/kg increase in net leg work increased leg hyperemia by 0.51 L/min (Figure 1B). Positive leg work was significantly associated with leg hyperemia ($p = 0.015$), with a 1 J/kg increase in positive leg work increased leg hyperemia by 1.03 L/min (Figure 1C). Negative leg work did not associate with leg hyperemia ($p = 0.978$), suggesting that leg hyperemia is likely driven by positive work done by concentric leg muscle contractions during walking as opposed to negative leg work done by eccentric contractions.

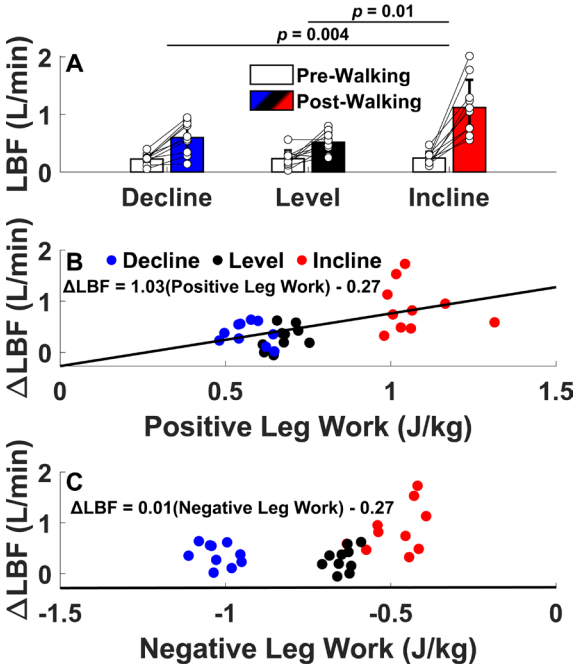

Figure 1: A) Leg hyperemia (i.e., increase in leg blood flow [LBF]) was greatest during uphill walking. B) Positive leg work associated with leg hyperemia during walking, but C) negative leg work did not. Regression lines were taken from linear mixed model results.

Significance: We demonstrated the musculoskeletal system's dependence on the vascular system to do positive leg work. Our novel experimental framework will be valuable for understanding the mechanisms of mobility outcomes in people with healthy and compromised vascular function, which may ultimately guide future interventions to enhance vascular and musculoskeletal functions in the legs.

Acknowledgments: This work was supported by NIH R01HD106911 awarded to KZT and SYP, and NIH 1T32DK11096601 awarded to JKB.

References: [1] Adam et al. (2017), *Computers in Biology and Medicine* 91; [2] Anguiano-Hernandez et al. (in review), *J Appl Physiol*; [3] Abbott et al. (1952), *J Physiol* 117(3); [4] Coolbaugh et al. (2016), *J Appl Physiol* 121(4); [5] Zelik et al. (2015), *J Exp Biol* 218(6)

NOT ALL MUSLCES ARE CREATED EQUAL: EXPLORING TORQUE DENSITY, A MEASURE OF MUSCLE TORQUE GENERATING EFFICIENCY

*Mario E. Garcia[1], Emily M. McCain[1], Xiao Hu[1], Shawn D. Russell[1], Silvia S. Blemker[1]
[1]University of Virginia, Charlottesville, VA, USA
*Corresponding author's email: nfq3bd@virginia.edu

Introduction: Understanding muscle architecture and joint mechanics is often limited in size and coverage, resulting in piecewise analysis and necessitating a metric of muscle efficiency. Imaging and machine learning advancements now enable large-scale biomechanical studies of lower limb muscles [1,2]. By pairing MRI-derived muscle volumes with isometric joint exertions across angles, we assess muscle size contributions to torque differences between sexes. This study introduces **torque density** (joint torque per unit muscle volume) as a metric for evaluating muscle efficiency across exertion-angle combinations (**Fig. 1**). We investigate whether torque density 1) differs between sexes, 2) varies with body size (mass, height), and 3) depends on muscle size relative to body size. By quantifying these relationships, we aim to uncover how relationships between muscle size and strength vary across the population.

Methods: Seventy-five active adults (39 female, 36 male), aged 20–49 (27.79±7.49 years), were recruited with representative heights (female: 1.64±0.052m, male: 1.76±0.056m) and masses (female: 62.1±10.5kg, male: 80.4±12.4kg) based on a U.S. population study [3]. Dynamometry: After a self-selected walking trial, subjects performed two unilateral three-second maximal voluntary isometric exertions using a Biodex System 4 dynamometer (Biodex Medical Systems Inc., Shirley, NY) for ankle plantar/dorsiflexion (PF/DF), knee flexion/extension (KF/KE), hip flexion/extension (HF/HE), and hip abduction/adduction (HAB/HAD). Joint, exertion, and angles were randomized to reduce bias. Hip trials were performed with a custom rigid frame and Donjoy T-ROM brace while standing. Peak isometric torques were extracted using custom MATLAB (MathWorks, Natick, MA) functions correcting for gravity [4]. Muscle Volumes: Subjects underwent a 3T MRI (Prisma, Siemens, Munich, Germany) two-point Dixon sequence (FOV: 366mm×450mm, slice thickness: 5mm, in-plane resolution: 1.76mm×1.76mm, TR: 4ms, TE: 1.23ms). Muscle and bone volumes were calculated using an automated segmentation method [1] with manual vetting (Springbok Analytics, Charlottesville, VA). Muscle group volume z-scores were determined for each sex. Analysis: Normality of height and mass distributions were assessed using Shapiro-Wilk tests. Torque density (peak isometric exertion torque/muscle volume) was analyzed through repeated-measures ANOVA with Bonferroni-corrected post-hoc comparisons. Pearson correlations evaluated relationships between torque density and size metrics (height, mass, height-mass product, and volume z-score). All statistical analyses were conducted in R, with $\alpha<0.05$ indicating significance.

subject	S01		S02	
sex	F		M	
height (m)	1.73		1.63	
mass (kg)	68.49		83.00	
volume (cm^3)	210.61		211.96	
torque (Nm)	25.21		46.47	

Figure 1: Example subjects' dorsiflexors at 15° PF.

Results & Discussion: Heights and masses were normally distributed for each sex. In DF, sex ($F(1,73)=13.63$, $p=4.26E-4$, $ges=0.098$) and angle ($F(1,73)=48.35$, $p=4.78E-16$, $ges=0.218$) were significant main effects on torque density (**Fig. 2A**). Similar effects were observed in KF (sex: $F(1,73)=4.87$, $p=0.03$, $ges=0.044$; angle: $F(1,73)=6.07$, $p=0.007$, $ges=0.025$) and HE (sex: $F(1,73)=4.80$, $p=0.032$, $ges=0.053$; angle: $F(1,73)=11.44$, $p=1.77E-4$, $ges=0.022$) torque densities but not in PF, KE, HF, HAB, or HAD. DF torque density positively correlated with height at 15° PF ($p=0.026$), mass at 0°, 15°, and 30° PF ($p=0.043$; $p=0.002$; $p=0.013$, **Fig. 2B, C**), and height-mass product at 0°, 15°, and 30° PF ($p=0.042$; $p=0.002$; $p=0.020$). PF torque density was negatively correlated with mass at 30° and 45° PF ($p=0.042$; $p=0.048$) and height-mass product at 30° PF ($p=0.046$). HF and HAD torque density positively correlated with muscle volume z-score at 15° HF ($p=0.040$) and 10° HAB ($p=0.023$). Notably, intramuscular fat fraction did not correlate with torque density in any condition and did significantly alter trends.

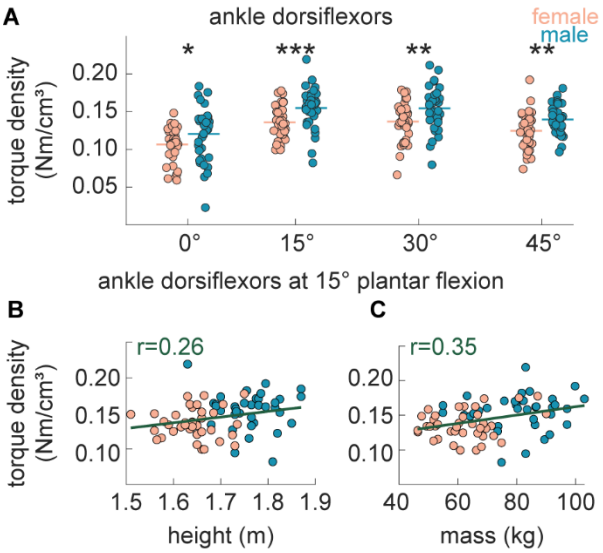

Figure 2: A) DF torque density (female: peach, male: blue) and significant correlations (green) with **B)** height and **C)** mass. (sex: *$\alpha<0.05$, **$\alpha<0.01$, ***$\alpha<0.005$).

Significance: This study examines functional and structural characteristics across a representative population of males and females and introduces a concept to investigate factors that influence the volume-torque relationship across sexes. Additional factors such as internal muscle architecture and neuromuscular factors may have greater influence on muscle efficacy than volume alone. Future work will use statistical shape modeling and fiber orientations to assess how sex-based internal architecture differences influence torque generation.

Acknowledgments: Research funded by NIH Grant #R01AR078396, NIH Award T32GM145443, and the Wallace H. Coulter Center for Translational Research.

References: [1] Ni et al. (2019), *J Med Imaging* [2] Damon et al. (2017), *NMR Biomed* [3] Fryar et al. (2016), *Vital Health Stat* [4] Keating et al. (1996), *J Orth Sport PT*

THE IMPACT OF MANUAL WHEELCHAIR USE DURING CHILDHOOD AND ADOLESCENCE ON SHOULDER JOINT COMPLEX MUSCLE ELASTICITY

Denali Hutzelmann[1], Colleen Vogel[1], Savanna Rudy[1], Heath Henninger[2], Joshua Leonardis[1]
[1]University of Illinois Urbana-Champaign, IL, [2]University of Utah, UT
Email: denalih2@illinois.edu

Introduction: The prevalence of shoulder pain among manual wheelchair users (MWUs) with pediatric-onset disabilities increases significantly during the transition from childhood to adulthood [2,5]. This period of significant growth presents an optimal environment for musculoskeletal adaptations. For example, adolescent tennis players develop greater muscle mass in their playing arm compared to the non-playing arm, and competitive sprinting increases passive medial gastrocnemius elasticity changes that persist into adulthood [1, 6]. Similarly, MWU places substantial demands on the shoulder joint complex, likely driving musculoskeletal adaptations that offer insight into the mechanisms underlying pain and pathology. Shear wave elastography (SWE), a non-invasive ultrasound technique, estimates muscle elasticity through shear wave velocity (SWV) [4]. This measure is sensitive to changes resulting from MWU in childhood and adolescence, as well as adaptations seen in individuals with rotator cuff pathologies [3]. Therefore, this study aimed to assess the impact of MWU in childhood and adolescence on shoulder joint complex muscle elasticity.

Methods: Bilateral passive SWE images were collected from 15 MWU (5F/10M, ages 18-23 yrs) without pain or pathology in a seated posture supported by the wheelchair backrest with unloaded shoulders and pronated palms resting on their lap. Eleven muscles were imaged (neck-shoulder muscles: sternocleidomastoid (SCM), 3 upper trapezius fiber regions (UT1, UT2, UT3); glenohumeral primary movers: posterior deltoid (PD), middle deltoid (MD), pectoralis major-clavicular (PCV), pectoralis major-sternocostal (PSC); dynamic glenohumeral stabilizers: infraspinatus (INF), supraspinatus (SUP), biceps brachii (BB)). Mean SWV was calculated from a region of interest (ROI) capturing the muscle on each image. Linear regression evaluated the relationship between SWV and total years of MWU (TYU) and years of use during peak development (YUPD), which was defined as the number of years of use between the ages of 10-17 in females and 10-20 in males. The critical alpha was set at 0.05.

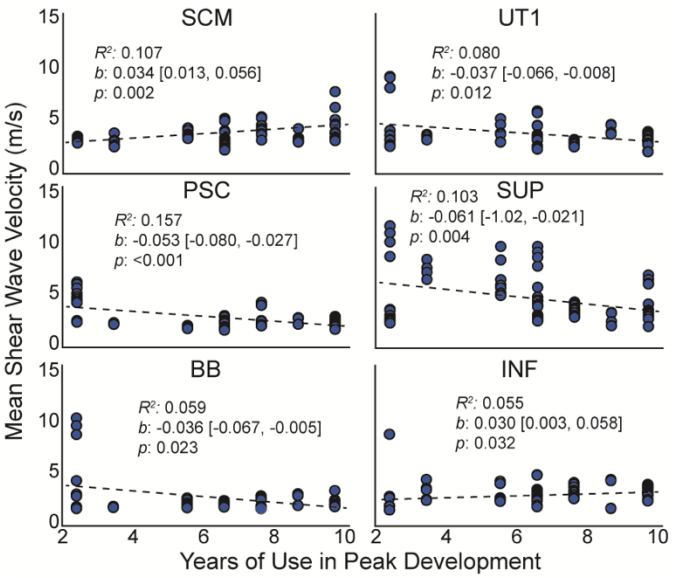

Figure 1. Noteworthy relationships between YUPD and muscle SWV. Dashed lines represent least-squares lines of best fit. Unstandardized betas are reported with 95% intervals.

Results & Discussion: Both TYU and YUPD were associated with neck-shoulder muscle SWV. TYU was associated with SCM SWV (R^2 = 0.002, *b* [95% CI]: -0.017 [-0.031, -0.003] p = 0.017), showing that as TYU increased, SCM SWV decreased. YUPD was associated with SCM and UT1 SWV (Fig. 1), showing that as YUPD increased, SCM SWV increased, which contrasts with our findings regarding the relationship between TYU and SCM SWV. As YUPD increased, UT1 SWV decreased. These findings reveal an interesting contradiction in the impact of YUPD on neck-shoulder musculature. Opposing relationships were revealed in anterior and posterior musculature, which may be attributed to region-specific adaptions, like length changes, due to the prolonged seated forward head posture related to MWU.

Glenohumeral primary mover SWV was also impacted by TYU and YUPD. TYU was associated with PSC SWV (**R^2** = .085, *b* [95% CI] = -0.021 [-0.036, -0.006], p = 0.006) showing that as TYU increased, PSC SWV decreased. Similarly, as YUPD increased, PSC SWV decreased (Fig. 1). Both TYU and YUPD (Fig. 1) were associated with dynamic glenohumeral stabilizer SWV, including SUP SWV (TYU: R^2 = 0.136, *b* [95% CI] = -0.039 [-0.062, -0.017], p = 0.001) and BB SWV (TYU: R^2 = 0.056, *b* [95% CI] = -0.018 [-0.034, -0.002], p = 0.027), showing that as TYU and YUPD increased, SUP and BB SWV decreased. Contrary to these findings, as YUPD increased, INF SWV increased (Fig. 1). These results suggest that TYU and YUPD increases compliance in anterior glenohumeral primary movers (PSC) and anterior/superior dynamic glenohumeral stabilizers (SUP, BB). Wheelchair propulsion requires repetitive glenohumeral flexion and internal rotation, facilitated by muscles like the PSC, alongside constant dynamic glenohumeral stabilization facilitated by the SUP and BB. Their increased compliance may reflect an adaptation to withstand the mechanical demands of wheelchair propulsion.

Significance: Our results provide the first evidence that MWU during childhood and adolescence impacts shoulder complex muscle elasticity, potentially revealing adaptations to MWU that precede pain or pathology. These findings highlight differential responses between anterior and posterior musculature, suggesting that targeted interventions addressing musculoskeletal imbalances may be helpful in mitigating shoulder pain and pathology in MWU. Our ongoing research will draw the link between musculoskeletal adaptations in MWU and the lifetime risk of shoulder pain and pathology.

Acknowledgments: We thank the Eunice Kennedy Shriver National Institute of Child Health and Human Development of the National Institutes of Health for their support (R03HD114181).

References: [1] Daly, R. (2004). *Bone*. [2] Hwang, M. (2014). *J Spinal Cord Med.* [3] Ishith, S. (2023). *J Shoulder and Elbow Surg.* [4] Leonardis J. (2017). *J Biomech* [5] Schottler, J. (2019). *Top Spinal Cord Inj Rehabil.* [6] Yamazaki K. (2022). *Eur J Appl Phys*

LEVERAGING ULTRASOUND IMAGING TO PERSONALIZE MUSCULOSKELETAL THUMB MODELS

* Victor E. Akpaloo[1], Alexis R. Benoit[1], Jennifer A. Nichols[1]
[1]J. Crayton Pruitt Family Department of Biomedical Engineering, University of Florida, Gainesville, FL
*Corresponding author's email: ve.akpaloo@ufl.edu

Introduction: Musculoskeletal models are vital for understanding and predicting muscle forces and joint mechanics. Traditionally, generic models are constructed by averaging data from cadaveric studies and/or small *in vivo* studies. Generic models can then be scaled to match an individual's anthropometry. Although scaled models have broad utility, they often neglect inter-individual variability in muscle architecture, leading to inaccuracies in simulating muscle function. In contrast, personalized models integrate subject-specific muscle parameters – typically derived from *in vivo* imaging – to improve simulation accuracy. Extended field-of-view ultrasound (EFOV-US) offers a non-invasive means to capture muscle fascicles *in vivo* in one continuous panoramic scan, enabling the development of personalized models that more accurately reflect individual muscle parameters. The overarching goal of this study is to understand to what extent incorporating personalized muscle parameters derived from EFOV-US affects estimated thumb muscle forces. We focus on the thumb, as there are many small muscles in the hand that work together to enable grasp and other dexterous motor tasks, and we expect that this complexity will make the muscles sensitive to minor variations in muscle parameters.

Methods: This analysis is based on an ongoing IRB-approved study using data from 15 healthy adults (10 males, 5 females; age: 22.8 ± 2.2 years, weight: 81.8 ± 16. 7 kg, height: 174.0 ± 8.3 cm) with no history of musculoskeletal injuries. Six thumb muscles [abductor pollicis brevis (APB) and longus (APL), extensor pollicis brevis (EPB) and longus (EPL), flexor pollicis brevis (FPB) and longus (FPL)] in each participant were imaged using EFOV-US (Supersonic Imagine Mach 30), with five high-quality images acquired per muscle.

All images were analyzed in ImageJ by manually measuring fascicle length (traced as the longest distance between proximal and distal aponeuroses), pennation angle (angle between identified fascicle and aponeurosis), and PCSA (approximated by the maximum muscle height perpendicular to the fascicles). Measurements from the five images were averaged for each muscle in each participant. The ARMS Wrist and Hand model [2] with 23 degrees of freedom was considered the generic model for this study. For each participant, a personalized model was created by first scaling the model to the participant's anthropometry and then updating its muscle parameters (maximum isometric force, optimal fiber length and pennation angle) to reflect the measured values. A thumb abduction–adduction motion was simulated in OpenSim 4.4 using identical input motion for the 1 generic and the 15 personalized models. Muscle forces were estimated using computed muscle control, and the individual as well as mean muscle forces from the personalized models were compared to those from the generic model. Paired t-tests and independent samples t-tests were performed in Python.

Results & Discussion: The personalized models produced significantly greater muscle forces than the generic model across all muscles (Fig. 1). With the exception of APL, the personalized models produced mean muscle forces at least twice the magnitude of those in the generic model. The largest differences were observed in the extrinsic muscles, particularly FPL, which have longer fiber lengths compared to intrinsic muscles, like APB and FPB. This suggests that the magnitude of the difference between the personalized models and the generic model is muscle specific. The large range of participants' forces suggest muscle parameters vary substantially across participants, where participants with longer fascicles or larger PCSA produced higher forces than generic models. Inter-participant variability is also illustrated by the large standard deviations observed.

The muscle forces generated by the personalized models were not significantly influenced by either biological sex or participant height. Although male participants tend to have higher personalized forces than the generic model (e.g. FPL, EPL, & APL in Fig. 1A), there is considerable overlap between muscle forces in male and female participants (e.g. APB & EPB in Fig. 1A). This implies that some females can match or exceed male force generation. Thus, factors like muscle size or training level may be more important to force generation than biological sex. Similarly, while increased height typically correlates with larger muscle dimensions and potential higher force generation [3], some short participants produced greater muscle forces than tall participants (Fig. 1B). This emphasizes that muscle force generation depends on more than height alone.

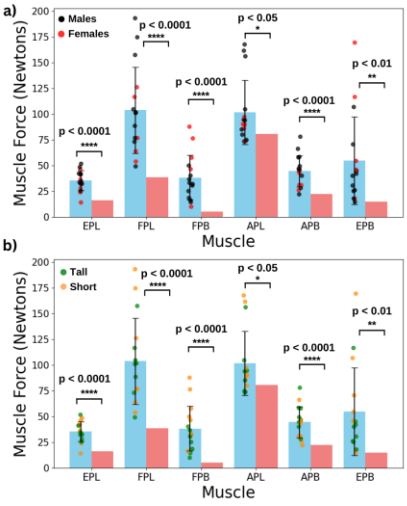

Figure 1: Comparison of muscle forces generated during simulations of thumb abduction-adduction with generic (coral) versus personalized (blue) models. Dots represent each personalized model (one per participant), separated by **a) biological sex** and **b) height** (tall participants ≥ median height). Error bars indicate standard deviation.

Significance: This study demonstrates that generic models underestimate muscle forces in the thumb and incorporating subject-specific parameters can capture individual variability. These findings establish a foundation for more precise musculoskeletal assessments of hand function and advance development of predictive simulations of the hand.

Acknowledgments: Funding from NIH NIAMS (R01 AR078817) is gratefully acknowledged.

References: [1] Charles et al. (2022), *J Anatomy* 237(5); [2] McFarland et al. (2023), *IEEE Trans Biomed Eng*.70(5); [3] Son et al. (2024), *J Exp Biol.* 227(6).

CLINICAL APPLICATION OF VIRTUAL MECHANICAL TESTING OF TIBIAL FRACTURE HEALING AND NONUNION

Mehran Bahrami[1], *Hannah L. Dailey[1]
[1]Mechanical Engineering & Mechanics, Lehigh University, Bethlehem, PA, USA
*Corresponding author's email: hlr3@lehigh.edu

Introduction: Tibial fractures treated with intramedullary nailing have a 12% chance of developing nonunion (failure to heal). Nonunion is usually diagnosed 6-9 months after the initial injury, yet the mechanical characteristics of these long-term cases remain poorly understood because nonunions present with a wide range of healing patterns from minimal (atrophic) to excessive (hypertrophic) callus formation. To study these cases, we applied our previously developed methods for measuring tibial fracture healing using finite element models built from computed tomography (CT) scans [1]. The objective of this study was to analyze the mechanical characteristics of late-stage tibial nonunions and compare them to normally healing fractures. We hypothesized that hypertrophic nonunions are more rigid than all other nonunion types and have higher strain concentrations than normally healing fractures.

Methods: Two datasets were used in this analysis: human tibial nonunions, and normally healing human tibial fractures. The nonunions were retrospectively identified at four Level I trauma centers. The normally healing fractures (N = 29) were prospectively recruited from a single Level I trauma center and CT scanned at 12 weeks post-op. All patients were treated by intramedullary (IM) nailing. The clinical study protocol was reviewed and approved by the local Institutional Review Boards prior to initiation in each center. Scan were processed in Mimics Innovation Suite (Materialise Inc.) to reconstruct 3D models of the fractures (Fig. 1). Regions of cortical bone and callus (if present) were thresholded, reconstructed, and meshed with quadratic tetrahedral (tet10) elements. A voxel-based density scaling method was used to assign tissue elastic moduli values in an elementwise fashion. Fracture models were then imported to ANSYS Workbench Mechanical (ANSYS Inc.) to perform virtual torsion testing. Virtual torsional rigidity (VTR) was calculated as: $VTR = ML/\phi$ [N-m^2/°], where M is the calculated reaction torque, L is the working length of the tibial diaphysis model, and ϕ is the applied angle of twist. Statistical analysis was performed in R Studio.

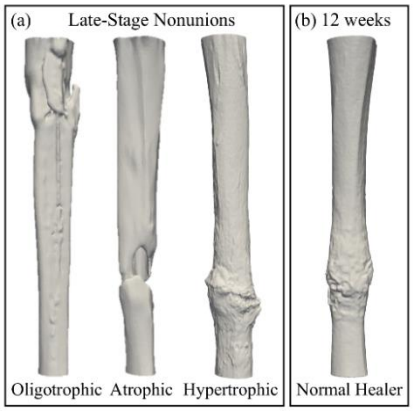

Figure 1: Representative cases of **a)** tibial nonunion, and **b)** normal healer.

Results & Discussion: Nonunion scans were taken at a median of 54 weeks from injury. Some patients were scanned before the first major surgical intervention to treat the nonunion (e.g., exchange nailing) and some were scanned after one or more reoperations. Of the 24 nonunions, 4 patients were atrophic with no callus and evidence of bone resorption. These all had very low torsional rigidity (0.228 ± 0.111 N-m^2/°). The oligotrophic (10 patients, 2.288 ± 1.138 N-m^2/°) and hypertrophic (10 patients, 2.953 ± 1.237 N-m^2/°) cases had torsional rigidities comparable to the combined group of normal healers who were scanned at only 12 weeks post-op (2.459 ± 0.966 N-m^2/°). VTR in atrophic group was significantly lower than the hypertrophic and oligotrophic groups (ANOVA; $p \leq 0.017$), which were not different from each other ($p = 0.421$). The observed high rigidity for many hypertrophic and oligotrophic nonunions arose from extensive mineralization in the irregularly bridged callus. Yet, von Mises (equivalent) strain contours also revealed patterns of strain "hot spots" in the nonunion defect sites that had failed to resolve over time. This suggests that late-stage nonunions can have high rigidity, but with persistent high local strains.

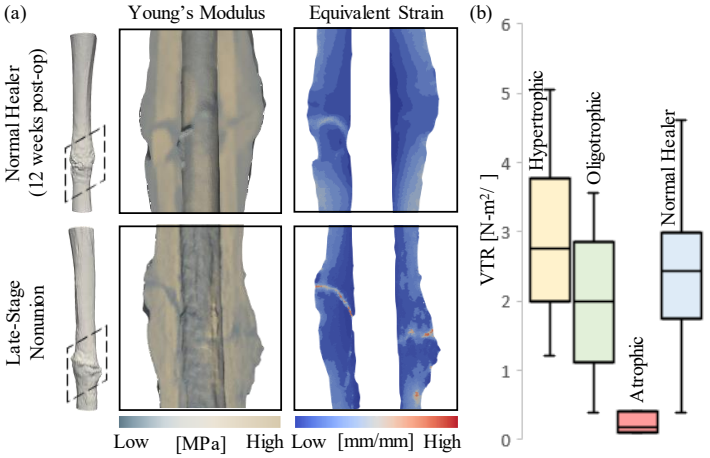

Figure 2: a) Young's modulus and equivalent strain distribution at the fracture line for two representative cases: a normal healer scanned at 12 weeks and a late-stage hypertrophic nonunion case scanned at 65 weeks. b) Virtual mechanical testing revealed deficiencies in mechanical healing in the atrophic group.

Significance: When at least some callus is present, late-stage nonunions can become highly mineralized and mechanically stable, but with localized high strains that could be mediating pain and delayed healing in other parts of the fracture. This suggests that nonunion intervention may be more effective if undertaken as early as possible, before rigidity has been achieved. A clinically symptomatic nonunion that exhibits mechanical stability may require more aggressive debridement and correction osteotomy to achieve a more uniformly bridged union.

Acknowledgments: Thanks to James Harty, Meir Marmor, Henry Boateng, and Chinenye Nwachuku for clinical data collection. This project was supported in part by the National Science Foundation under Grant Number CMMI-1943287.

References: [1] Dailey+. Virtual Mechanical Testing Based on Low-Dose Computed Tomography Scans for Tibial Fracture. *J Bone Jt Surg*. 2019.

PATELLOFEMORAL JOINT STRESS IS ASSOCIATED WITH CARTILAGE COMPOSITION SEVEN YEARS AFTER ANTERIOR CRUCIATE LIGAMENT RECONSTRUCTION

Riley J. Starr[1], Richard E. Magony[1], Dianne M. Bryant[1], Alan M. J. Getgood[1], Derek N. Pamukoff[1]
[1]School of Kinesiology, Faculty of Health Sciences Western University, London, ON
*Corresponding author's email: rstarr3@uwo.ca

Introduction: Individuals with anterior cruciate ligament reconstruction (ACLR) are at a greater risk for knee osteoarthritis (OA), partially due to aberrant biomechanics [1]. ACLR influences sagittal plane knee mechanics, which may contribute to cartilage degeneration and OA development [2]. Early stages of OA include proteoglycan loss, collagen loss, which can be detected by T1rho and T2 magnetic resonance imaging (MRI) relaxation times [3], respectively. Cartilage composition can also be imaged using ultrasound echo intensity (EI) [4], which describes the average gray scale of a traced region of interest and may provide an alternative imaging method. Current studies are mixed on the role of loading in the development of OA following ACLR, with many studies using joint moments as surrogates of loading rather than more robust estimates of internal joint loading [5]. While persistent biomechanical changes within the tibiofemoral joint (TFJ) have been well-documented, the patellofemoral joint (PFJ) articulation remains understudied despite its functional role in ambulation and knee extension. Patellofemoral joint stress (PFJS) provides a more precise estimate of internal joint loading, which offers insight into biomechanical factors that contribute to cartilage degeneration. We compared PFJS and trochlea cartilage composition between ACLR and contralateral limbs and assessed the associations between PFJS and cartilage outcomes. We hypothesized that greater PFJS would be associated with longer T1rho and T2 relaxation times, higher echo intensity, and that EI would be associated with MRI outcomes, supporting its potential as an alternative imaging method.

Methods: Forty-eight participants (58.3% female, Age= 25.79 ± 2.63 years, BMI= 25.79 ± 5.03 kg/m²) from the STABILITY I [6] cohort performed walking trials seven years post-ACLR. Participants with contralateral injury were excluded to permit the contralateral limb to serve as control. Kinematic and kinetic data during self-selected speed gait were collected using a 12-camera motion capture system and an in-ground force plate along a 10m walkway (5 trials per limb). Marker position and force plate data were combined using Cortex (Motion Analysis Corp, Santa Rosa CA) and exported for model construction (Visual 3D, Germantown, MD). Kinematic and force plate data were low-pass filtered at 6Hz. We used an inverse dynamics musculoskeletal model to calculate PFJS accounting for hamstrings and gastrocnemius muscle co-contraction. Quadriceps force was derived as the quotient of adjusted net knee extensor moment over the quadriceps moment arm. Patellofemoral joint reaction force was calculated using quadriceps force as a function of the knee joint angle and normalized by sex-specific patellofemoral contact area to estimate PFJS [7]. Cartilage composition was assessed using MRI to measure T1rho and T2 relaxation times and ultrasound to quantify average cartilage echo-intensity. Between limb comparisons compared cartilage and biomechanical outcomes between limbs using paired samples t-tests (α=0.05). Pearson's correlation evaluated associations between PFJS and cartilage outcomes in each limb (α=0.05).

Results & Discussion: No differences were found in imaging or biomechanical outcomes between limbs (PFJS: $p = 0.870$, EI AVG: $p = 0.862$, T1rho Trochlea Ultrasound: $p = 0.554$). In the affected limb, higher PFJS was correlated with longer T1rho ($r = 0.634$, $p < 0.001$), and higher EI ($r = 0.460$, $p < 0.001$). In the unaffected limb, higher PFJS was correlated with longer T1rho ($r = 0.667$, $p < 0.001$) and higher EI ($r = 0.535$, $p < 0.001$). Longer T1rho times, indicative of reduced proteoglycan content, suggest early cartilage degeneration that may reduce resistance to compression [8], [9]. Higher EI was associated with longer T1rho but not with T2 times in either limb ($r = 0.483$ and 0.629, $p < 0.001$) suggesting that EI may capture similar proteoglycan characteristics detectable by T1rho. These findings demonstrate that greater PFJS is associated with compositional differences in trochlea cartilage, possibly preceding OA development.

Table 1 Between-limb comparisons of Patellofemoral Joint Stress (PFJS), Average Echo Intensity (EI), T1rho Trochlea Ultrasound (T1rho), and T2 Trochlea Ultrasound (T2) in ACLR and Contralateral Limbs.

Variable	ACLR Limb	Contralateral Limb	p	d
PFJS (MPa)	4.05±1.56	4.08±1.78	0.870	-0.026
EI (0-255 a.u.)	78.19±24.69	77.87±22.90	0.862	0.027
T1rho (ms)	65.05±9.69	65.23±10.47	0.828	-0.035
T2 (ms)	57.29±6.91	56.61±5.84	0.554	0.094

Significance: Higher PFJS during gait may contribute to alterations in trochlear cartilage composition, potentially preceding OA development seven years post-ACLR. Ultrasound EI may be a valuable and accessible tool for measuring proteoglycan loss and cartilage composition, enabling the detection of early degenerative changes. These insights could enhance load modification strategies to mitigate OA development after ACLR.

Acknowledgements: This study was conducted with funding support from the Lawson Internal Research Fund and the Ontario Graduate Scholarship program.

References: [1] Wellsandt et al. (2016), *AJSM* 44(1); [2] Van De Velde et al. (2008), *AJSM* 36(6); [3] Guermazi et al. (2015)**,** *OARS* 23(10); [4] Okada et al. (2023), *KSSTA* 31(9); [5] Wellsandt et al. (2015), *AJMS* 44(1); [6] Getgood et al. (2019), *BMC Musculoskelet Disord* 20(1); [7] Messier et al. (2011), *OARS* 19(3); Henao-Murillo et al. (2019), *Cartilage* 13(2); Duvvuri et al. (2002). *OARS* 10(11)

TRANSIENT SADNESS IS ASSOCIATED WITH ALTERED GAIT AND BALANCE IN PEOPLE WITH GLAUCOMA

Natalie Bick[1*], Helmet T. Karim[2,1], Howard Aizenstein[2,1], Mark S. Redfern[1], Subashan Perera[3,1], and Rakié Cham[1,4]
[1]Department of Bioengineering, University of Pittsburgh, Pittsburgh, PA
[2]Department of Psychiatry, University of Pittsburgh, Pittsburgh, PA
[3]Department of Medicine, University of Pittsburgh, Pittsburgh, PA
[4]Department of Ophthalmology, University of Pittsburgh, Pittsburgh, PA
*Corresponding author's email: natalie.bick@pitt.edu

Introduction: Glaucoma is a complex disease with ophthalmological, neurological, sensorimotor, and psychological changes [1]. Though previous work has identified many fall risk factors such as depressive symptoms, balance and gait deficits, and visual impairments, it is unclear how these factors contribute to the increased fall rate in people with glaucoma. Specifically, *the impact of mood on gait and balance in glaucoma has not been studied*. Our goal was to understand how transient mood induction induces gait and balance changes in this population. We hypothesized that gait and balance would be worse while participants reflected on sad memories compared to happy or neutral memories, and that individuals with glaucoma would be more impacted than those without.

Methods: Twenty-one adults with glaucoma (G) between the ages of 65 and 85 years and seventeen similarly aged adults without (nG) were enrolled after screenings to exclude any vestibular, somatosensory, or neurological condition. Based on previous research on mood and gait [2] and worry-rumination [3], participants were asked to "Think of a time in your life when you felt extremely [happy or sad]," then rate how strongly they felt emotion during each memory on a scale of 1-5, where 1=no emotion and 5=extreme emotion. Participants recalled 4 happy and 4 sad personalized memories, termed induced transient mood (ITM) cues, each with a rating ≥3. Participants walked at a comfortable pace along a straight walkway during 4 floor/lighting conditions: floor conditions were a hard and a soft floor; lighting conditions were bright and dim. Gait data were collected using a Vicon motion capture system. Gait speed was calculated from a marker on C7. Balance testing was performed using the Bertec® CDP/IVR™ during 4 proprioception/vision conditions: proprioception conditions were fixed and sway-referenced (SR) floor; vision conditions were eyes open (EO) and closed (EC). Sway magnitude in the anterior-posterior direction was computed. For each gait/balance condition, participants were asked to focus on a happy and sad memory (randomized), separated by a neutral fact. Each condition lasted 6 minutes, with the participant focusing on each ITM cue for 2 minutes (Fig. 1-A). Mixed linear regression models were constructed within each gait/balance condition, with fixed effects ITM, participant group, and the first order interactions, with subject as a random effect. The hypotheses were investigated using post-hoc means contrasts tests. The dependent variable for gait was gait speed and for balance was sway magnitude. Statistical significance was set at α=0.05.

Results & Discussion: Gait Speed: During hard floor/bright, the two groups had statistically different gait-mood relationships: the glaucoma group walked significantly slower during sad moods compared to happy, whereas the group without glaucoma had the opposite relationship (Fig. 1-B).
Sway Magnitude: During SR/eyes closed, the glaucoma group had statistically significantly larger sway magnitudes (RMS) during sad compared to happy while those without glaucoma had smaller sway during sad compared to happy (Fig. 1-C).

Gait speed and sway magnitude were sensitive to glaucoma-specific motor changes that occur during sad emotional states, demonstrated by people with glaucoma walking slower and having worse balance during sad moods. Together, these results suggest that the emotional state may be a contributing factor in fall risk in adults with glaucoma.

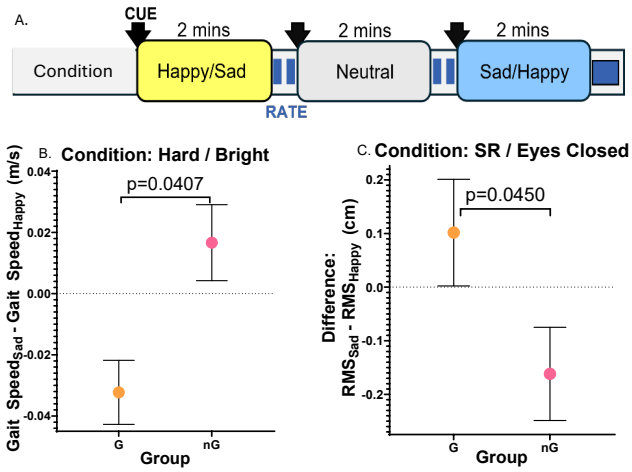

Fig. 1: (A) The induced transient mood task methodology used for gait and balance testing. (B) Group differences in gait-mood relationship on hard floor/bright condition. (C) Group differences in balance-mood relationship during sway-referenced/eyes-closed. Error bars are standard error of the mean.

Significance: By further understanding the role of psychological factors in gait and balance changes in people with glaucoma, we may ultimately find ways to reduce their fall risk related to mental health by developing alternate methods for gait rehabilitation, such as incorporating strategies from cognitive behavioral therapy.

Acknowledgements: Bioengineering in Psychiatry T32 Fellowship (5T32MH119168-02) & Lendvay-Newton Balance Disorder Research Philanthropic Gift

References: [1]O'Hare et al., 2012. *Clin Exp Ophthalmol*, 40(9). [2] Kang and Gross, 2016. *J Biomech*. 49(16). [3] Andreescu et al., 2011. *Depress Anxiety*. 28(3).

Changes in Posture of Clinicians during VR Designed to Elicit Implicit Biases

Thomas H. Rossi[1], Connor Delaney[1], Tiphanie Raffegeau[1], Brandon Patterson[2], Stephen Trapp[2], Kerri Shaffer[2], Samuel Acuña[1]*
[1]George Mason University, Fairfax, VA, USA
[2]University of Utah, Salt Lake City, UT, USA
*Corresponding author's email: sacuna2@gmu.edu

Introduction: Disparities in health outcomes, including increased patient mortality, have been well-documented among individuals from minority groups [1, 2]. While multiple factors contribute to these disparities, implicit biases among healthcare providers (HCPs) are one potential underlying mechanism [3]. Implicit biases are unconscious, unrecognized thoughts that influence behaviors and actions toward a target group, such as a specific patient population [4]. These biases can subtly manifest in a person's movements and nonverbal behaviors [5]. Patients presenting with characteristics associated with minority groups—such as lower socioeconomic status, obesity, drug use, or sexual identities—may elicit biases in HCPs, which could, in turn, impact patient-provider interactions and clinical decision-making [6-8]. Given the influence of implicit biases on treatment decisions, patient adherence, and health outcomes, it is critical to understand how these biases manifest and how to identify them.

The purpose of this study was to determine if changes in posture during HCP-patient interactions could serve as measurable indicators of implicit bias. Postural sway characteristics may reflect subtle, unconscious motor responses associated with bias—imperceptible to the individual but observable by others. We hypothesized that postural sway at the hip would differ based on interactions with different patient stereotypes. To test this hypothesis, we conducted an experiment in which medical students engaged in HCP-patient interactions through a virtual reality display while their postural responses were recorded.

Methods: 20 HCPs from the School of Medicine at the University of Utah participated in the study, including residents, fellows, and medical students at various stages of their training. Participants viewed 5 mock patient interactions as 360^{O} videos presented through an HTC Vive virtual reality system designed to elicit varying degrees of implicit bias (**Fig. 1**). Each video was preceded by a waiting screen presenting a description, which was written in a manner to further evoke any potential biases, of why the patient was seeing a clinician. For each video, the participant played the role of the attending clinician for the patient in the video. Scripts for the videos were written in conjunction with Community Health Workers, who operate as patient advocates in underserved communities. Video 1 featured an older male adult with back pain. Videos 2 and 3 featured a female and male adult drug user. Video 4 featured a trans nonbinary patient looking for gender-affirming care. Video 5 featured a non-native English-speaking female adult. To extract measures of postural sway from participants during these videos, participants had motion capture trackers placed on their hips and on the HTC Vive Headset. These sensors captured positional data at a 12.5Hz sampling rate. Our outcome measure was the average velocity of the sway (AP direction) for the duration of the video.

Figure 1: Screenshots of videos 3 and 4 seen in VR.

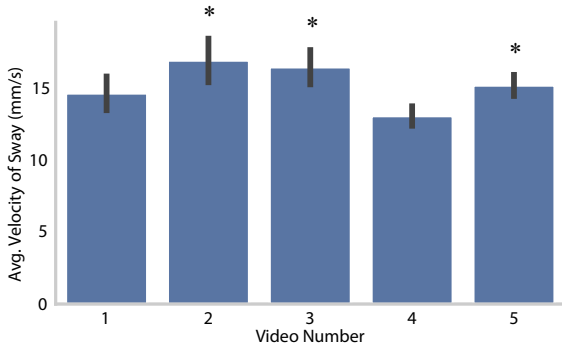

Figure 2: Average velocity was significantly higher when participants watched videos 2, 3, and 5 (comp. to video 4).

Results & Discussion: A repeated measures ANOVA revealed significant differences existed between the sway velocity for the 5 videos ($F = 3.84$, $p = 0.007$). Post hoc pairwise comparisons found that the sway velocity for videos 2, 3, and 5 were significantly higher than video 4. These early findings support our hypothesis that implicit biases may subtly influence postural control during HCP-patient interactions, with variations in sway velocity potentially serving as a measurable indicator of these biases. Although there are many potential reasons to explain the observed differences in sway velocity across patient scenarios, certain patient presentations may elicit greater subconscious physiological responses from HCPs, possibly reflecting discomfort, cognitive load, or underlying biases. If bias is a source of these differences, one possible explanation for these results is that increased postural sway may reflect an avoidance response, aligning with prior research suggesting that nonverbal cues, such as movement and body orientation, can unconsciously communicate discomfort or bias in social interactions. Future work will explore whether these sway variations correlate with other physiological or behavioral indicators of bias, such as eye tracking, heart rate variability, or speech patterns.

Significance: This study provides early evidence in support of our hypothesis that biases among healthcare providers can be detected through subtle variations in postural sway during patient interactions. By exploring postural responses as an objective marker of potential biases, such as sway velocity, this approach may have utility in for real-time bias detection and intervention for clinicians.

References: [1] Haider et al. (2008), *Arch Surg* 143(10); [2] Nelson et al. (2002), *J Natl Med Assoc* 94(8); [3] Chapman et al. (2013), *J Gen Internal Med* 28(11); [4] Greenwald & Banaji (1995), *Psych Review* 102(1); [5] Maina et al. (2018), *Soc Sci & Med* 199 [6] Geller & Watkins (2018), *AMA J Ethics* 20(10); [7] Harris et al. (2016), *BMC Med Educ* 16(1); [8] Leslie et al. (2018), *Med Teach* 40(4)

VISUAL CONTEXT AFFECTS LATERAL STEPPING REGULATION ON WINDING PATHS

Anna C. Render[1], Tarkeshwar Singh[1], Joseph P. Cusumano[2], Jonathan B. Dingwell[1*]
[1] Department of Kinesiology, Pennsylvania State University, University Park, PA, USA
[2] Department of Engineering Science & Mechanics, Pennsylvania State University, University Park, PA, USA
*Corresponding author's email: dingwell@psu.edu

Introduction: Visual information is essential for guiding locomotion [1], but how do changes in visual context affect stepping regulation when the inherent walking task remains unchanged? To investigate how perception shapes action during goal-direct walking, we examined asked how environment richness and path contrast affect gaze and lateral stepping regulation on straight and winding paths. We hypothesized that altering available visual information would modify gaze behavior, but may or may not disrupt stepping regulation.

Methods: Twenty-eight participants (16F/12M; age 26.2±4.2) walked on straight and winding 0.45m wide virtual paths [2] projected onto a 1.2m wide treadmill (Motek M-Gait). Each path was presented in high contrast (HC) or low contrast (LC) color combinations, combined with each of two distinct virtual environments: a dense forest (Rich) or open grassy plain (Sparse). Participants were instructed to "walk on the path" and minimize steps off the path. Hence, on either path (straight or winding), the biomechanical requirements were fixed – only the visual context was systematically manipulated. Each participant completed two 3-minute trials per condition.

For each condition, we analyzed the first 250 steps of each trial. We computed participants' sagittal plane head pitch angles, where negative (or positive) pitch indicated downward (or upward) head movement. Head pitch reasonably approximates general gaze direction [3]. We calculated within-trial means and standard deviations of head pitch angle at each step.

To quantify lateral stepping regulation, we calculated lateral body position (z_B) and step width (w) relative to the walking path at each step. We performed direct control analyses, computing stepping error-correction slopes (M) (e.g., Figs. 1A, 2A) to quantify the degree to which deviations from the average w and z_B were corrected on the next step [2]. Slope values of $M = -1$ indicated that deviations were completely corrected at the next step. Slope values of $M = 0$ indicated that deviations went uncorrected [2].

Dependent measures were compared using 2×2 (contrast × environment) ANOVA for each path (straight v. winding) separately.

Results & Discussion: Participants exhibited lower average head pitch and decreased head pitch variability on winding paths compared to straight paths ($p < 0.001$), indicating a more consistent and downward gaze [3]. On straight paths, participants lowered head pitch in Sparse environments ($p < 0.001$) and LC paths ($p = 0.03$) and exhibited less head pitch variability in Sparse environments ($p = 0.028$). On winding paths, participants lowered head when walking on LC paths ($p = 0.021$) and exhibited less head pitch variability in Sparse environments ($p = 0.011$). People thus changed where they looked depending both on the task (i.e., path) and the visual context.

On straight paths (Fig. 1), participants corrected z_B deviations more in Sparse environments ($p < 0.001$) and less on LC paths ($p < 0.001$). However, they corrected w deviations similarly across all visual contexts ($p \geq 0.167$). On winding paths (Fig. 2), participants corrected z_B deviations less ($p < 0.001$) and w deviations more ($p < 0.001$) on LC paths. However, they corrected both z_B and w deviations similarly in Rich and Sparse environments ($p \geq 0.112$). People thus changed how they regulated their stepping movements depending on visual context (environment and/or path contrast), even for the same biomechanical task requirements (i.e., same walking path).

Significance: Visual context influenced both gaze (head tilt) and lateral stepping regulation when participants walked on straight or winding paths. Hence, even though the biomechanical requirements of each task remained the same (i.e., "walk on the path"), visual context none the less altered how people *performed* these tasks.

These results demonstrate the dynamic interplay between perception, action, and goal-directed movement, where path shape influences how visual information is used [1]. That stepping regulation remains robust even when visual context is degraded, suggests that visual context refines, rather than determines, motor planning.

Acknowledgments: NIH / NIA Grants # R01-AG049735 & R21-AG053470, and Sloan Foundation Grant # G-2020-14067.

References: [1] Drew & Marigold (2015), *Curr Opin Neurobiol* 33; [2] Render et al. (2025), *J Biomech* 180; [3] Thomas et al (2020), *PeerJ* Apr 3:8:e8838.

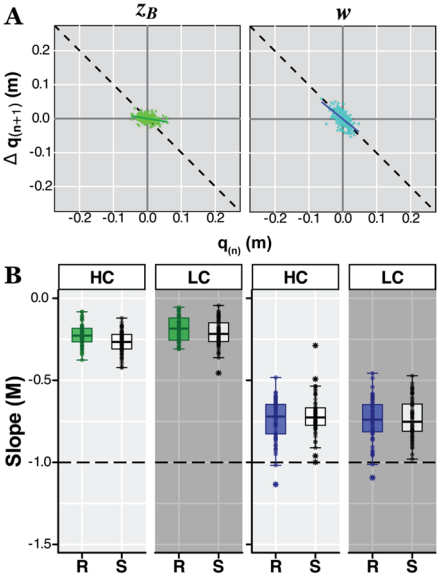

Figure 1: Straight Paths – Stepping Error-Correction. **A)** Example direct control plots for position (z_B) and step width (w). **B)** Box plots of direct control plot slopes for z_B and w for high & low contrast (HC/LC) paths in Rich and Sparse (R/S) environments.

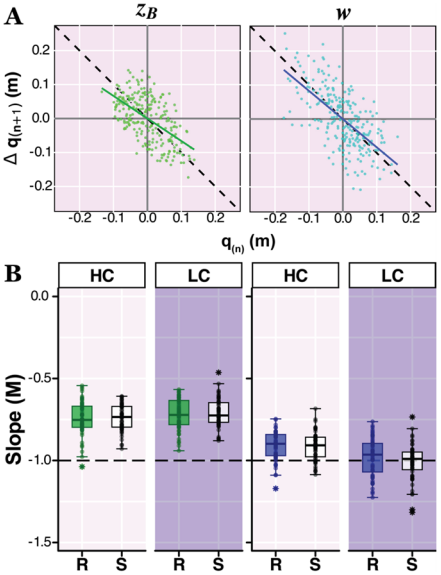

Figure 2: Winding Paths – Stepping Error-Correction. **A)** Example direct control plots for position (z_B) and step width (w). **B)** Box plots of direct control plot slopes for z_B and w for high & low contrast (HC/LC) paths in Rich and Sparse (R/S) environments.

INFLUENCE OF THREAT-INDUCED ANXIETY ON MUSCLE COORDINATION BETWEEN UPPER AND LOWER LIMBS DURING REACTIVE BALANCE

Anke Hua[1], Katherine Dudek[1], Kelly Westlake[1]
[1] Department of Physical Therapy & Rehabilitation Science, University of Maryland School of Medicine, Baltimore, MD 21201, USA
*Corresponding author's email: ahua@som.umaryland.edu

Introduction: Since fear of falling is associated with the occurrence of falls, it is important to understand how threat-induced factors (such as state anxiety) affect the reactive balance response to perturbations. Reactive balance response generally involves coordinated movements between rapid arm and lower limb reactions. Threat-induced factors can influence reactive balance response to unexpected perturbations, characterized by higher co-contraction between agonist-antagonist lower-limb muscles, larger arm responses, and earlier and larger muscle activity in upper- and lower-limb muscles [1]. However, it is still unclear how threat-induced anxiety influences the muscle coordination between the upper and lower limbs in response to unexpected perturbations. The purpose of this study is to explore the effect of threat-induced anxiety on muscle coordination through intermuscular coherence (IMC) analyses between bilateral deltoid muscles and lower-limb muscles during reactive response to an unexpected slip-perturbation. Due to threat-induced factors increased corticospinal excitability [2] and IMC at beta (13-30Hz) and gamma (30-45Hz) bands probably reflect a shared cortico-muscular drive originating from the motor cortex [3], we expected that threat-induced anxiety would increase IMC between arm and lower-limb muscles, especially at beta- and gamma-bands.

Methods: In this study, ten participants were exposed to a virtual environment either under a ground condition or a height condition. Each participant stood on the ActiveStep treadmill, wearing a virtual reality head-mounted display and a safety harness. Participants first underwent two slip perturbations (i.e., a forward perturbation of the treadmill) (1.26m/s, 10cm, 7.88m/s2) under the ground condition as the habituation. Then, participants underwent one slip perturbation under the ground condition and, subsequently, one slip perturbation under the height condition. Participants were instructed to restore balance naturally. To reduce anticipation, the perturbation test trial occurred after two or three no-perturbation trials. After each trial, participants completed a subjective unit of distress scale (SUDS) as subjective anxiety. A sEMG system ((Noraxon, Scottsdale, AZ)) was used to collect EMG data from ten muscles, including bilateral tibialis anterior (TA), medial gastrocnemius (MG), rectus femoris (RF), semitendinosus (ST), deltoid lateral. Recorded sEMG raw data was filtered using a 20-500Hz band-pass, 4th-order Butterworth filter, and subsequently filtered using a 20Hz high-pass, 4th-order Butterworth filter, and then rectified using Hilbert transform. As we focused on the reactive balance response, we used EMG data from 100ms-400ms after slip-perturbation onset to calculate IMC using the "mscohere" function in MATLAB. The analysis focused on the anterior muscles of the lower limb as these muscles are the primary agonists for a forward perturbation of the support surface. To compare the IMC, a paired *t*-test was performed for the area under the curve for the beta (13-30Hz) and gamma (30-45Hz) frequency bands. *P* value <0.05 was defined as a significant level, and all p-values were corrected with the false discovery rate (FDR) method.

Results & Discussion: Self-reported anxiety (i.e., SUDS) was higher under the height condition compared to the ground condition (31.1 ±16.6 vs. 46.6±18.8, p=0.004). This confirms the success of the anxiety manipulation. There were several significant differences related to threat-induced anxiety in IMC between the shoulder and lower-limb muscles. Compared to the ground condition, gamma-band IMC between the bilateral deltoid and RF on the stance side increased by 91% (p=0.01), while IMC between the bilateral deltoid and TA on the stance side increased by 72% (p=0.04) under the height condition. Two potential mechanisms may contribute to the observed threat-induced changes in IMC between upper and lower limbs during reactive responses to unexpected slip-perturbation. First, threat-related increases in corticospinal excitability probably cause earlier and larger muscle activity in upper and lower limbs in response to unexpected perturbation. Consistently, our results showed that threat-induced anxiety increased gamma-band IMC between upper and lower limbs during reactive response to the slip perturbation, as gamma-band IMC may reflect supra-spinal projections that modulate muscle activation by a coordinated and shared neural drive originating from the motor cortex [3]. Second, the threat increases spindle sensitivity and stretched muscles (i.e., TA and RF) due to the perturbation of the support surface will contribute more to corrective torques. Changes in spindle gain could influence the neuromuscular coupling through supraspinal pathways, characterized by the larger gamma-band IMC between the deltoid and TA/RF on the stance side. These findings are consistent with previous research, where the increase in gamma-band IMC was observed when the somatosensory feedback of muscle spindles increased [4].

Significance: Our present study found that threat-induced anxiety increased the IMC (gamma-band) between the upper and lower limbs during the reactive balance response to unexpected perturbation. This suggests that threat-related increases in corticospinal excitability further influence the muscle coordination between upper- and lower-limb responses to balance perturbations. This helps improve understanding of the neural mechanisms contributing to upper- and lower-limb coordination among older adults with fear of falling and balance deficits.

References: [1] Cleworth et al. (2016), *Gait & Posture* 47; [2] Tanaka et al. (2013), *J. Psychophysiol 2*7; [3] Boonstra. (2013), *Frontiers in human neuroscience* 7; [4] Nguyen et al. (2017) *J Neurophysiol* 117.

HOW DO INDIVIDUALS WITH CHRONIC STROKE ADAPT WALKING BALANCE CONTROL TO TASK DEMANDS?

*Grace K. Kellaher[1], Elisa S. Arch[1], Jason R. Franz[2], Darcy S. Reisman[1], Jeremy R. Crenshaw[1]
[1]Biomechanics & Movement Science Program, University of Delaware, Newark, DE, USA; [2]Lampe Joint Department of Biomedical Engineering, University of North Carolina at Chapel Hill and North Carolina State University, Chapel Hill, NC, USA
*Corresponding author's email: gkk@udel.edu

Introduction: Post-stroke balance and gait impairments are a barrier to safe community ambulation [1-2] as they limit walking adaptability for people with chronic stroke [3]. Walking adaptability is the ability to modify gait to meet the ambulatory demands of an environment [3]. Our premise is that walking adaptability and frontal-plane balance control during walking are interrelated factors that, when addressed together, may benefit post-stroke mobility. Studies of post-stroke walking adaptability, however, have largely ignored the mechanisms by which balance is controlled when faced with different environmental demands [4-6]. Mechanisms that control the lateral acceleration of the center of mass (a_{com}), an aspect directly influencing walking balance performance, include foot placement ($a_{Foot\text{-}Placement}$) and push-off ($a_{Push\text{-}Off}$). [7-8]. These mechanisms are quantified as mediolateral accelerations that are a function of the distance between the center of pressure (COP) and the vertical projection of the COM on the ground (COM'), as well as the magnitude of the vertical ground reaction force (GRF) under the lead limb from foot-strike through single-limb support ($a_{Foot\text{-}Placement}$) and under the trail limb during double-limb support ($a_{Push\text{-}Off}$) (Figure 1). Different environments may place either demands or constraints on the $a_{Foot\text{-}Placement}$ and $a_{Push\text{-}Off}$ mechanisms, which could alter their contribution to a_{com}. Thus, we believe that the capacity to adapt balance control mechanisms may underlie walking adaptability in individuals with chronic stroke. The purpose of this study was to characterize the foot placement and push-off mechanisms in individuals with chronic stroke during preferred walking, fast walking, and narrow-path walking tasks.

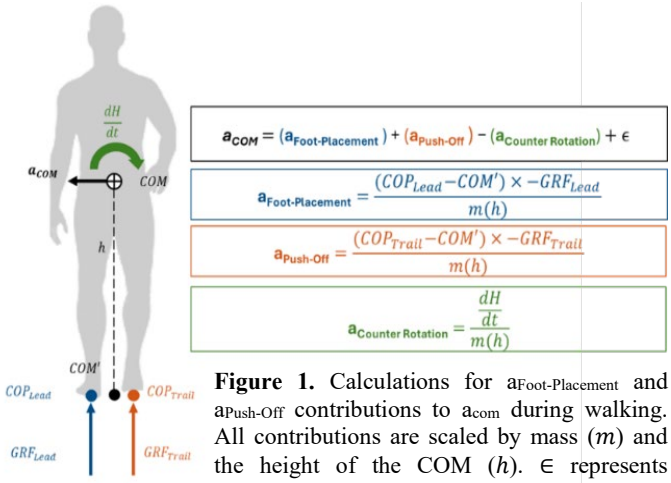

Figure 1. Calculations for $a_{Foot\text{-}Placement}$ and $a_{Push\text{-}Off}$ contributions to a_{com} during walking. All contributions are scaled by mass (m) and the height of the COM (h). $\in$ represents measurement error or other mechanisms that are not directly measurable.

Methods: Three individuals with chronic stroke (1M/2F; age: 59±14 years; BMI: 32.6±7.6; time since stroke: 63±43 months) have thus far participated in this study. Kinematic (Qualisys, 200 Hz) and force (Bertec, 2000 Hz) data were recorded while participants walked on an instrumented, split-belt treadmill for 60 seconds under three conditions in a fixed order: 1) preferred walking (self-selected speed and step width), 2) narrow-path walking (self-selected speed and narrow step width), and 3) fast walking (fast speed and self-selected step width). We calculated $a_{Push\text{-}Off}$ and $a_{Foot\text{-}Placement}$ according to methods described in Figure 1. Descriptive statistics were calculated for this preliminary data set.

Results & Discussion: The mean $a_{Push\text{-}Off}$ and $a_{Foot\text{-}Placement}$ contributions per step were calculated for the paretic and non-paretic limbs during each walking condition (Figure 2). The largest changes in contribution to a_{com} were an 11% increase in non-paretic (Figure 2, Panel C) and a 12% increase in paretic (Figure 2, Panel D) $a_{Foot\text{-}Placement}$ contribution when comparing preferred and fast walking This trend may suggest that the role of the foot-placement mechanisms for controlling a_{com} may be more pronounced at fast walking speeds. There are not yet any other strong trends evident from this preliminary data set. We will explore how these results develop with a larger sample, with comparisons to individuals without chronic stroke, and we will investigate how lower-extremity functional mobility and gait speed relate to our results.

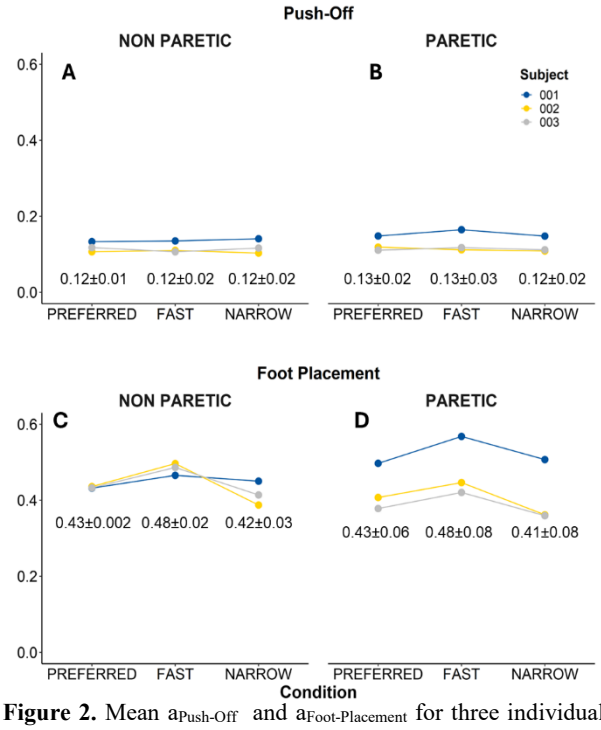

Figure 2. Mean $a_{Push\text{-}Off}$ and $a_{Foot\text{-}Placement}$ for three individuals with chronic stroke for each walking condition.

Significance: Understanding how walking adaptability is linked to balance control may allow us to address critical barriers to community ambulation for those with chronic stroke. Balance control mechanisms such as foot placement and push-off, then, could serve as targets for interventions aimed at enabling safe community ambulation in individuals with chronic stroke.

Acknowledgments: This work was supported by the American Society of Biomechanics Graduate Student Grant-in-Aid Award and the University of Delaware Department of Kinesiology & Applied Physiology Doctoral Dissertation Award.

References: Hill et al. (1997), *Aus J Phys Ther* 43(173-180); [2] Balaban & Tok (2014), *PM&R* 6(635-642); [3] Balasubramanian et al. (2014), *Stroke Res & Treat* 2014(1-21); [4] Vistamehr et al. (2018), *J Biomech* 74(106-115); [5] Bansal et al. (2022), *Top Stroke Rehab* 2022(1-10); [6] Schrager et al. (2008), *Gait & Pos* 28(466-471); [7] Reimann et al. (2017), *PLoS ONE* 12(0172215); [8] van den Bogaart et al. (2022), *J Biomech* 136(111073)

THE IMPACT OF DOG WALKING ON GAIT KINEMATICS AND VARIABILITY

Alex Peebles[1, 2*], Michael Bennett[1], Samantha Morison[2], Ji Chen[1, 2], and Lara Thompson[1, 2]
[1]Department of Mechanical Engineering, University of the District of Columbia
[2]Biomedical Engineering Program, University of the District of Columbia
*Corresponding author's email: alexander.peebles@udc.edu

Introduction: Between 2001 and 2020, it was estimated that 422,659 adults visited an emergency department in the US for an injury they sustained while walking their dog, with 55% of injuries being the direct result of an accidental fall [1]. Living with a dog and taking them on frequent walks can provide a myriad of mental and physical health benefits [2]. Therefore, adopting a dog may help to improve the function and quality of life of older adults and various patient populations. However, there is currently no way to assess one's risk of injury while walking their dog. To address this gap, we recently developed a system which simultaneously measures leash tension and accelerations of the waist. We found peak leash tension in a single bout of dog-walk to be about 153 +/- 79 N across 20 participants, which is much higher than forces which are typically applied in laboratory environments to study the effects of perturbations on dynamic balance [3, 4]. The purpose of this study is to determine the impact that walking a dog has on gait kinematics and variability. We hypothesized that walking with a dog increases gait acceleration and temporal variability relative to walking alone.

Methods: Twenty human subject participants signed informed consent and participated in this IRB approved study. All participants were healthy, 18 to 60 years old, and lived with a dog who they walked routinely. Participants were asked to use our custom dog walking measurement system while they took their dog on a routine walk, then to repeat the same route without their dog on a separate day. The system measured leash tension and triaxial waist acceleration simultaneously at 100 Hz (Figure 1). Acceleration signals were first used to split trials into periods of gait and not-gait, then to identify time points of initial contact bouts of continuous gait. Root mean square (RMS) of vertical and anterior acceleration were computed during each stride and averaged across strides. Standard deviation of stride time and sample entropy of step time were used to quantify gait variability. Outcomes were compared between conditions (walking with dog vs walking alone) using paired t-tests and Cohen's d effect size, with an alpha level of 0.05.

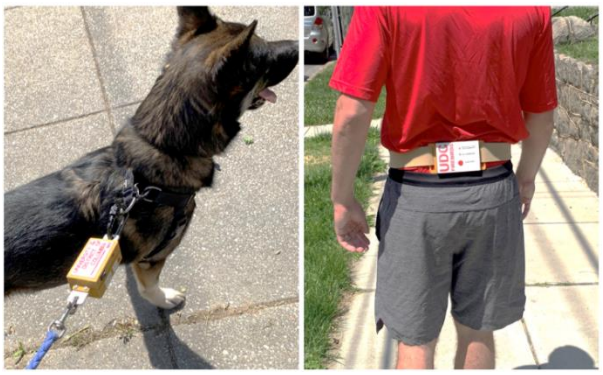

Figure 1: Leash tension (left) and gait kinematics (right) measurement systems.

Results & Discussion: Comparisons between the two test conditions are shown in Table 1. There was no significant effect of walking a dog on stride time ($p = 0.21$), which suggests that walking with a dog does not systematically influence cadence or gait speed. We also found no significant effect of condition on RMS of accelerations in the anterior ($p = 0.32$) or vertical directions ($p = 0.33$). RMS is a measure of dispersion relative to zero which has been widely used to assess the magnitude of waist and trunk accelerations in gait analysis research [5]. While some studies have found acceleration RMS to be altered in clinical populations relative to healthy controls [6], there is a positive correlation between acceleration RMS and walking speed [5].

Table 1: Between-condition comparisons. *Significant difference ($p<0.05$).

	Walking with dog	Walking alone	p value	Effect size (d)
Stride time (s)	1.04 ± 0.06	1.06 ± 0.06	0.21	0.41
AP RMS (g)	0.31 ± 0.08	0.34 ± 0.09	0.32	0.33
VT RMS (g)	1.02 ± 0.03	1.01 ± 0.04	0.33	0.32
Stride time SD (s)	0.092 ± 0.044	0.063 ± 0.037	**0.03***	**0.71**
Step Time SaEn	1.73 ± 0.27	1.55 ± 0.34	0.08	0.58

Walking with a dog significantly increased stride time variability relative to walking alone ($p = 0.03$) with a medium effect size, which supports our second hypothesis. Stride time variability has been widely shown to be increased in clinical populations relative to controls [7] and in older adults with a history of falls relative to those without a fall history [8]. While step time sample entropy was increased when walking with a dog relative to walking alone, this comparison was not statistically significant ($p = 0.08$). Increased sample entropy is interpreted to reflect a decrease in the repeatability and predictability of gait patterns [9]. While we speculate that the increased gait variability reflects worse dynamic balance and an increased risk of falling while walking with a dog, it is important to note that fluctuations in gait speed could also contribute to the observed differences. Future work should investigate the effects of leash tension on more sensitive measures of dynamic balance.

Significance: Our goal is to identify individuals with a heightened risk for dog walking injuries, so that appropriate interventions can be administered. This initial study provides evidence that dog walking impairs balance and motivation for further research.

Acknowledgments: Funding support was received from NIH (Award Number R25AG067896) and NSF (Award Number: 2229575).

References: [1] Maxson et al. (2023), *MSSE*; [2] Dall et al. (2017), *BMC Pub Health*; [3] Wu et al. (2017), *Gait & Posture*; [4] Bucklin et al. (2019), *J of Biomechanics*; [5] Kavanagh and Menz (2008), *Gait & Posture*; [6] Huisinga et al. (2012), *Annals of BME*; [7] Socie et al. (2013), *Gait & Posture*; [8] Hausdorff et al. (2001), *Archives of PMR*; [9] Yentes et al. (2013), *Annals of BME*.

EFFECTS OF ASYMMETRIC SURFACE STIFFNESS WALKING ON WEIGHT BEARING AND LOWER LIMB MUSCLE EXCITATION SYMMETRY

Elena Schell[1], Jonaz Moreno Jaramillo[1], Leah Metsker[2], Jenna Chiasson[1], Meghan Huber[3], Mark Price[1,3], Wouter Hoogkamer[1]
[1] Department of Kinesiology, University of Massachusetts, Amherst
[2] Department of Biomedical Engineering, University of Massachusetts, Amherst
[3] Department of Mechanical and Industrial Engineering, University of Massachusetts, Amherst

*Corresponding author's email: eschell@umass.edu

Introduction: Stroke is a leading cause of long-term adult disability in the United States, leaving about 80% of survivors with gait impairments and an estimated 55% of chronic stroke survivors with gait asymmetries [1, 2]. Decreased plantarflexion during push off is prevalent in post-stroke gait, which has been shown to in turn decrease walking speed [3]. Chronic hemiparetic stroke often manifests as asymmetric weight bearing, with individuals bearing more weight on their paretic limb [4]. Previous literature using asymmetric speed treadmill walking has been shown to improve select temporal gait outcomes, however effects on weight bearing symmetry are unreported and reported changes in muscle activation are small [1, 5, 6]. Alternatively, asymmetric surface stiffness treadmill walking has the potential improve these gait outcomes. Previous results from our lab indicate that weight bearing during weight-acceptance can be shifted towards the side exposed to a low stiffness condition. This study aimed to assess if changes in weight bearing come with changes in lower limb muscle excitation symmetry. We hypothesized that the plantarflexor muscle excitation asymmetry would increase during push off during asymmetric stiffness walking to account for vertical deflection under weight, and that this asymmetry will persist when participants return to symmetric high stiffness walking.

Methods: 11 individuals (age: 18-42; mass: 68.25 ± 8.82kg) with no musculoskeletal or neurological injuries completed 3 walking bouts in a single session at 1.25 m/s. Participants completed a 5-minute baseline on a dual-belt instrumented treadmill (Bertec, Columbus, OH, USA), then 10 minutes on an adjustable surface stiffness treadmill (AdjuSST [7]) with one side at 15 kN/m (L), and the other side rigid (300 kN/m) (H). We assessed aftereffects for muscle excitations during a 5-minute post condition on the dual-belt treadmill. Asymmetry ratios (AR) were calculated over 10-stride windows during each condition (baseline (BL), early adaptation (EA), late adaptation (LA), and early post (EP)) for muscle excitation (M) using the following formula: $AR = ((M_L - M_H)/(M_L + M_H)) * 100$. To assess muscle excitation changes during adaptation, we ran a one-way repeated measures ANOVA on all muscles collected (vastus lateralis, tibialis anterior, lateral gastrocnemius, soleus, and biceps femoris) for 9 participants. We ran a post hoc analysis with Bonferroni correction when the within-subjects effect was significant to determine significant differences among all four conditions. To determine if the muscle excitations of the plantarflexors were significantly different from BL to EP we performed one sample t-tests as against 0 (the BL condition was symmetric for all participants for these muscles).

Results & Discussion: Statistics revealed a significant change in the asymmetry ratio of the lateral gastrocnemius during push off in EA, LA, and EP compared to BL asymmetry ratios (AR_{BL}=0, AR_{EA}=36.1, AR_{LA}=49.1, AR_{EP}=17.3), and a significant increase in soleus excitation during EA, LA and EP (AR_{BL}=0, AR_{EA}=16.0 AR_{LA}=25.1, AR_{EP}=10.8) (Fig. 1). In support of our hypothesis, our results indicate that a single bout of asymmetric surface stiffness walking can increase plantarflexor muscle excitation during and after asymmetric surface stiffness walking. This neuromuscular adaptation in plantarflexor muscle excitation can be beneficial in post stroke gait, improving paretic propulsion [3].

Significance: Asymmetric stiffness walking can produce aftereffects that indicate the presence of neuromuscular adaptation. Previous literature has not reported muscle excitation changes throughout the adaptation period, and this data provides useful insight about neuromuscular adaptation strategies. Hemiparetic stroke rehabilitation requires a tailored approach, and these results show that asymmetric stiffness walking has the potential for targeted intervention aimed to improve common manifestations of post-stroke gait.

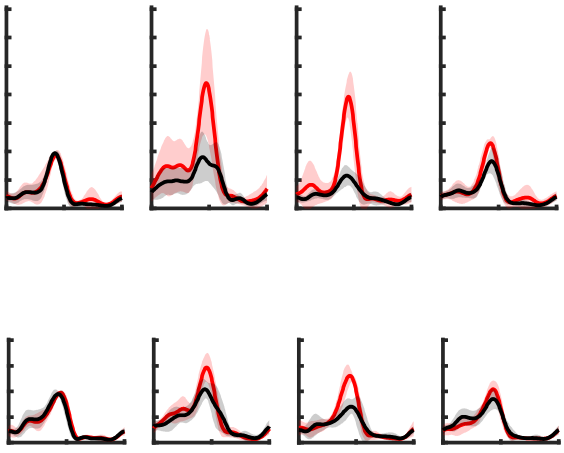

Figure 1: Low stiffness (red) and high stiffness (black) traces for gastrocnemius (top) and soleus (bottom) for a single stride averaged over 10-stride-windows. P-values are shown for comparisons for EA, LA, and EP relative to baseline. Shaded regions represent 1 standard deviation from the mean.

References: [1] Duncan et al. (2005) *Stroke* 36(9); [2] Hendrickson et al. (2014). *Gait & posture,* 39(1); [3] Roelker et al 2019, *Gait & Posture*, 68(6); [4] Sackley (1990). *Physiother Theo and Pract*, 6(4); [5] Rozanski et al (2020) *Disabil Rehabil*, 42(5); [6] Hoogkamer (2017). *Exerc Sport Sci Rev*, 45(1); [7] Price et al., 2024 *IEEE/ASME Trans Mechatron.*

HEADS UP! ALTERED HEAD MOVEMENT IN WALKING TASKS IN PEOPLE WITH GLAUCOMA

*Michelle J. Harter[1], Galen Holland[1], Amanda Bicket[2], Mark S. Redfern[3], Rakié Cham[1]
[1]Dept. of Ophthalmology, University of Pittsburgh [2]Dept. of Ophthalmology & Visual Sciences, University of Michigan
[3]Dept. of Bioengineering, University of Pittsburgh *Corresponding author's email: mjk160@pitt.edu

Introduction: Vision loss is associated with poor mobility and increased fall risk [1,2]. Mobility is particularly challenging for people with glaucoma who experience visual field loss [1]. Visual field loss can be partially compensated for by adopting a head scanning strategy in order to capture visual information that would otherwise remain outside of an individual's field of view [3]. Guidelines for evaluating orientation and mobility in people with low vision recommend monitoring head movement [3], as this could give more insight into one's functional abilities throughout disease progression or interventions. Despite this guideline, there is limited research on head movement during mobility tasks in people with glaucoma and no standardized outcome for objectively tracking head movement in this population. The purpose of this work was to identify how measures of head movement differ between healthy adults and those with glaucoma across a set of walking tasks. We hypothesized that people with glaucoma would show increased magnitude and frequency of head movement in walking tasks, particularly when navigating around obstacles, reflective of a head scanning strategy to compensate for visual field loss. The long term goal is to establish an objective measure of head movement that can be used to assess mobility performance in people with glaucoma.

Methods: Eight healthy adults (62±7 years; 5F) and 5 people with glaucoma (68±4 years; 4F; visual field mean deviation better/worse eye: -6.6±5.4/-9.0±4.3 dB) performed walking tasks while head accelerations were measured using an inertial measurement unit (Opal, Clario) on the forehead. Participants completed a two-minute walk (2MW), tandem walks with eyes open (EO) and eyes closed (EC), and an obstacle course. The obstacle course required participants to step over boxes and walk around cones. The head acceleration magnitude was evaluated by the root-mean-square (*RMS*). The frequency content of the head acceleration was evaluated by the frequency below which 90% of the signal power was contained (*90% cut-off frequency*) [4]. Magnitude and frequency measures were calculated in the vertical (V), anteroposterior (AP), and mediolateral (ML) directions. Differences in head movement were identified between the healthy and glaucoma groups across tasks using separate two-way ANOVAs for each outcome with fixed effects of group, task, and their interaction and a random effect for subject (Software: JMP Pro 17). Box Cox transformations were used to meet normality assumptions.

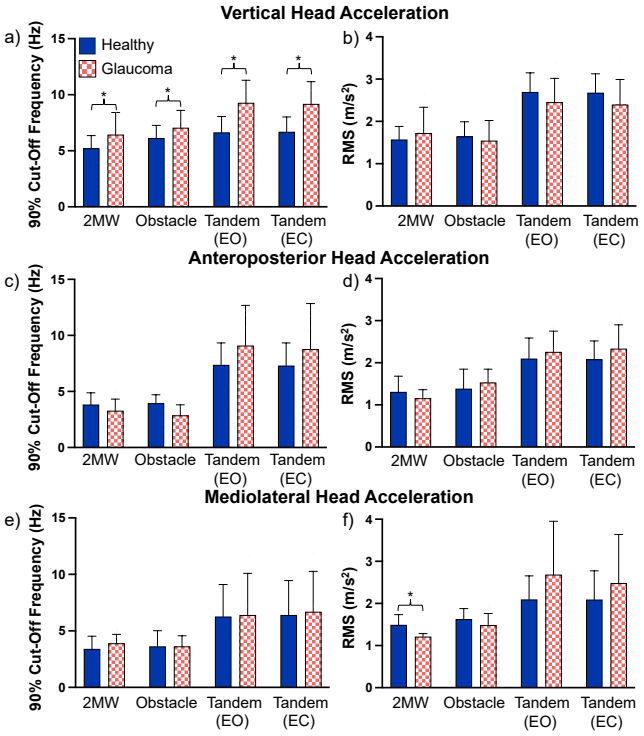

Figure 1: Head acceleration frequency and magnitude for healthy adults and people with glaucoma across walking tasks.

Results & Discussion: There were differences in head acceleration outcomes across tasks, with tandem walking (EO and EC) eliciting larger magnitude and higher frequency content than the 2MW or obstacle course (**Fig. 1a-f**, significance not pictured), but we instead focus on group differences. Contrary to our hypothesis that people with glaucoma would show increased magnitude of head movement due to scanning, there were no differences between groups, apart for decreased ML RMS head acceleration in the glaucoma group for the 2MW ($p = 0.04$) (**Fig. 1f**). While people with glaucoma did not have larger magnitude of head movement, they showed higher frequency content of vertical head acceleration than healthy adults (group effect: $p = 0.02$) (**Fig. 1a**). The increased frequency of vertical head movement was particularly notable in tandem walking (**Fig. 1a**). Although tandem walking is frequently used to identify vestibular or balance disorders, these results indicate that tandem walking may be useful for evaluating mobility in people with low vision. The increased frequency could reflect 1) greater effort from the postural control effort to maintain head posture or 2) could indicate smaller, faster head movements that allow for sufficient scanning of the visual field. As there was increased frequency content of the vertical head movement even when walking tandem with eyes closed, these results favour the former interpretation that the differences in head movement indicate greater control effort in maintaining head stability in people with glaucoma compared to healthy adults, rather than intentional or unintentional compensation for visual field loss.

Significance: These results demonstrate control of head posture is different in those with glaucoma compared to healthy adults during various walking tasks. The differences in head movement found here are likely not indicative of a scanning strategy, but rather of increased effort for head stabilization. The findings motivate future work examining differences in head movement in mobility in people with glaucoma. Alternate tasks and outcome measures (e.g. head posture) should be considered to identify ways to objectively track head scanning during walking in people with glaucoma throughout disease progression and interventions.

Acknowledgments: Hillman Foundation, Department of Ophthalmology, University of Pittsburgh

References: [1] Turano et al. (2004), *Opt. & Vision Sci.* 81(5); [2] Freeman et al. (2007), *Investigative Ophthalmology & Visual Science* 48(10); [3] Ayton et al. (2020), *Trans Vis Sci Tech.* 9(8); [4] Kavanagh et al. (2005), *Eur J Appl Physiol* 94: 468–475

LONG-TERM ADAPTATION IN STEP WIDTH AND SHORT-TERM ADAPTATION IN STEPPING COORDINATION.

Seongwoo Mun[1], Corbin M. Rasmussen[2], *Nathaniel H. Hunt[1]
[1]Department of Biomechanics, University of Nebraska at Omaha, Omaha, NE, USA
[2]Department of Exercise Science and Pre-Health Professions, Creighton University, Omaha, NE, USA
*Corresponding author's email: nhunt@unomaha.edu

Introduction: Foot placement control particularly in the mediolateral direction plays a crucial role in walking balance [1]. Humans exhibit a preferred step width, and step width variability occurs naturally with each step. The preferred step width is determined by mechanical and metabolic costs [2]. But step-by-step control compensates for the center of mass (CoM) mediolateral motion, with 80% of step width variability explained by the CoM dynamics at the previous mid stance [3]. However, our understanding of the adaptation of these step width controls remains limited. Using the CAREN system, we introduced mediolateral platform movements at specific timings during treadmill walking to enforce either a wider or narrower step width. The aim of this study is to examine how step width and its coordination with CoM (CoM-SW coordination) adapt over short and long time scales.

Methods: Nine young and healthy participants took part in the study. 15 reflective markers were attached to the pelvis and feet. Kinematic data were collected using a 10-camera motion capture system (Vicon, Oxford Metrics, Oxford, UK). Participants completed a single 40-minute walking session on CAREN system (Motek Medical B.V., Amsterdam, Netherlands), which was divided into five periods: three 10-minute periods of normal walking interspersed with two 5-minute perturbation periods. During the perturbation periods, participants were exposed to either step width widening (WP) or narrowing perturbations (NP) on every step. Throughout the perturbation periods, the treadmill platform introduced lateral movements to modify participants' step width. In the WP condition, the platform shifted 5 cm to the right immediately after toe-off of the left foot during right single stance, and 5 cm to the left during left single stance, effectively forcing participants to take wider steps than intended. Conversely, in the NP condition, the platform moved 5 cm to the left during right single stance and 5 cm to the right during left single stance, causing participants to take narrower steps than intended. To examine gradual adaptation in gait patterns, catch steps, steps without perturbation, were randomly inserted every 20 steps. Changes in step width and CoM-SW coordination were analyzed both during perturbation periods and the normal walking periods immediately afterward.

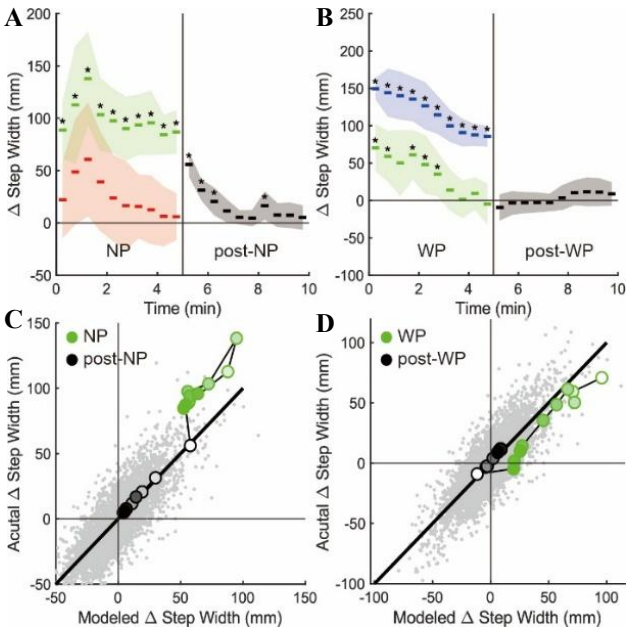

Figure 1. Changes in step width (A, B) and CoM-SW coordination (C, D) during and after perturbation for NP (A, C) and WP (B, D). Each data point represents the mean value within a 30-second window. Red and blue data points indicate perturbed steps, green data points represent catch steps, and black data points denote normal walking steps after perturbation. In (C) and (D), darker shades indicate later time points.

Results & Discussion: Participants quickly widened their step width at the onset of perturbation, showing a step width wider than baseline within the first 30-second window (Figure 1A, 1B). This suggests that they quickly adjust their walking pattern to enhance stability. In NP, participants exhibited a persistent widening of step width, even after the perturbation ended, suggesting a lasting aftereffect and motor adaptation in step width adjustment (Figure 1A). In contrast, in WP, step width gradually narrowed but did not fall below baseline, indicating a tendency to avoid excessively narrow steps (Figure 1B). Consequently, WP did not produce an aftereffect of changed step width.

CoM-SW coordination adapted rapidly during perturbation. In NP, participants took wider steps than predicted by their baseline model, whereas in WP, they took narrower steps (Figure 1C, 1D). Despite these deviations, coordination returned to baseline almost immediately post-perturbation. Interestingly, the first step after perturbation followed its direction, while the second step corrected significantly in the opposite direction, indicating an overshooting effect. This rapid recalibration demonstrates that the CoM-SW coordination was adjusted much faster than expected, within just one or two steps, to maintain stability.

Significance: This study reveals two distinct adaptation mechanisms in gait control: step width adapts slowly with lasting aftereffects, particularly in the widening direction, while CoM-SW coordination recalibrates rapidly for immediate stability. These findings highlight the multi-timescale nature of step width control, which can inform the design of assistive devices and bipedal robots to improve balance control and enable more human-like gait adaptations.

Acknowledgments: This study is funded by GRACA award from UCRCA at UNO and by NIH grants R15AG063106, P20GM109090, and 1P20GM152301

References: [1] Bruijn et al. (2018), *J R Soc Interface* 15(143); [2] Donelan et al. (2001), *Proc R Soc B* 268(1480); [3] Wang et al. (2014), *Biol Lett* 10(9)

THE EFFECTS OF WALKING SPEED ON MULTI-SEGMENT FOOT RIGIDITY AND COORDINATION

Megan Weaver[1], Ross Smith[1], Shyam Patel[1], Kota Z. Takahashi[2], Jason R. Franz[1]
[1]Lampe Joint Department of Biomedical Engineering, UNC Chapel Hill & NC State University, Chapel Hill, NC, USA
[2]Department of Health and Kinesiology, University of Utah, Salt Lake City, UT, USA
*Corresponding author's email: megweav@unc.edu

Introduction: The foot plays a critical role in dispersing forces, absorbing shock, and generating power, all of which are necessary for providing leverage against external forces and facilitating an effective and economical push-off [1,2]. We can quantify that leverage via foot rigidity, defined herein and previously as lesser foot segment range of motion. However, more sophisticated analyses of multi-segment foot coordination during gait may provide additional insight into the control of rearfoot, midfoot, and forefoot kinematics. While foot rigidity and coordination have been quantified during walking [3,4], no study to date has quantified how these outcomes change to meet the greater muscular force requirements and biomechanical demands of walking faster [5]. Therefore, the purpose of this study was to investigate how foot rigidity and multi-segment coordination vary with increased walking speed. We hypothesized that rigidity and coordination would reflect more tightly regulated multi-segment foot kinematics at faster speed.

Methods: 16 young adult (6 M / 10 F, age: 26.9 ± 5.2 years, height: 1.73 ± 0.1 m; mass: 79.2 ± 15.4 kg) completed two 2-minute barefoot walking trials, one at 1.0 m/s and one at 1.4 m/s, on a split-belt instrumented treadmill. We placed 12 retroreflective markers to define calcaneus, metatarsal, and phalangeal segments on the right foot [6]. Marker trajectories were recorded at 100 Hz using a 15-camera motion capture system. We used Visual 3D to calculated foot joint angles**:** 1) Rearfoot: calcaneus orientation relative to the shank, 2) Midfoot: metatarsal orientation relative to the calcaneus, and 3) Forefoot: phalangeal orientation relative to the metatarsus. We analyzed 10 consecutive stance phases from each participant, from which we calculated: (i) "foot rigidity" from 3D ranges of motion and (ii) intersegmental coordination using a modified vector technique for each joint [7] considering thus far only the sagittal plane. For the latter, we calculated the coupling angles, describing the relationship between two distinct joint angles using the Needham classification, and coupling angle variability which quantifies the degree of fluctuation in this relationship. According to Needham et al. [7], we interpret movement phases (in-phase or anti-phase) along with angular amplitude, which reveals which segment is dominant during movement based on coordination angles. We divided stance into early (0-33%), middle (34-66%), and late (67-100%), corresponding to loading response, midstance, and propulsion, respectively.

Results & Discussion: We first found that foot rigidity significantly decreased when walking faster for all foot segments (rearfoot: $p = 0.035$, midfoot: $p = 0.026$, forefoot: $p < 0.001$). An earlier transition from anti-phase proximal to in-phase distal rearfoot-midfoot coupling was observed with increasing speed during late stance (78-81%, Fig. 1A). However, no differences in coupling variability were found. We found no significant differences in the distribution of rearfoot-midfoot coupling designations; however, midstance showed a statistical trend towards significance, with a decrease in in-phase proximal coupling ($p = 0.075$) and an increase in anti-phase distal coupling ($p = 0.063$) for 1.4 m/s vs. 1.0 m/s (Fig. 1B). Forefoot-midfoot coupling angles increased with speed during late stance (i.e., 79-81%, 89-94%) (Fig. 1C). Walking faster also decreased coupling variability during late stance (i.e., 68-69%, 71-79%, and 94-95%). We found no significant differences in the distribution of forefoot-midfoot coupling designations. However, we found notable trends. During midstance, in-phase distal coupling tended to increase (p=0.075) and anti-phase proximal coupling tended to decrease (p=0.088) when walking faster; during late stance, in-phase proximal coupling tended to decrease (p-value) when walking faster.

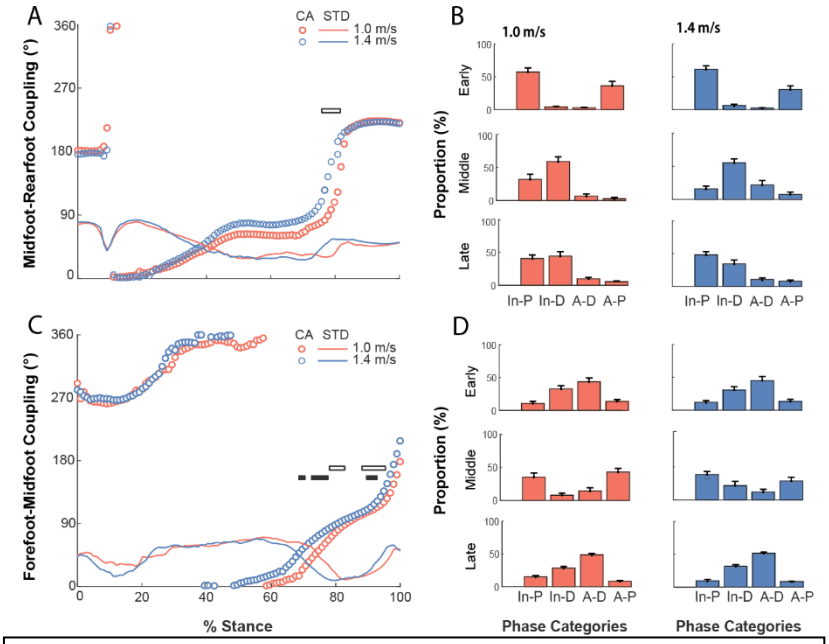

Figure 1: Average coupling angles (CA) and step-to-step variabilities (STD) for midfoot-rearfoot (**A**) and forefoot-midfoot (**C**). Coupling distribution proportion designations for midfoot-rearfoot (**B**) and forefoot-midfoot (**D**). Designations defined using in-phase (In), anti-phase (A), proximal dominant (P) and distal dominant (D).

Significance: Despite increases in ranges of motion (and thus lesser rigidity), multi-segment foot coordination appears to be highly resilient to requisite increases in neuromuscular demand when walking faster. However, decreases in forefoot-midfoot coordination variability throughout late stance implies more tightly regulated control of those distal foot segments when walking faster.

Acknowledgments: This work was supported by a grant from the National Institutes of Health (R01AR081287) and an NSF GRFP.

References. [1] Salathe Jr. et al.(1990) *J Biomech,* 23(7) ; [2] Yamagiwa et al. (2024) *J Body & Mvmt Therapies,* 37(1); [3] Challis et al. (2022) *J PLoS ONE,* 17(9); [4] Takabayashi et al. (2017) *J Foot Ankle Res.,*10(1) ; [5] Neptune et al. (2008) *J Gait Post,* 28(1); [6] Bruening et al. (2012) *Gait & Posture,* 35(4); [7] Needham et al. (2015) *Footwear Science,* 7(1).

QUANTIFYING PREDICTIVE AND REACTIVE CONTROL STRATEGIES DURING STEPPING MANEUVERS

Allison Kenney[1*], Francis Grover[2], Anna Shafer[3], Keith E. Gordon[2,3]
[1]Department of Biomedical Engineering, Northwestern University, [2]Physical Therapy and Human Movement Sciences, Northwestern University, [3]Research Service, Edward Hines Jr. VA Hospital
*Corresponding author's email: allisonkenney2025@u.northwestern.edu

Introduction: People use both predictive and reactive control strategies to effectively maneuver during walking. Predictive control strategies are preplanned movements in anticipation of a walking maneuver. Reactive control strategies are walking maneuvers initiated in response to an environmental cue. Quantifying the contributions of predictive and reactive control strategies during walking maneuvers would be valuable for understanding and addressing mobility impairments in neurological populations. However, current methods, based on kinematic measures, have not been able to clearly differentiate between these strategies. Kinetic measures have been used effectively to quantify predictive and reactive control strategies during reaching [1,2] but have not been applied to walking maneuvers. Here we use ground reaction forces (GRF) to quantify the contributions of predictive and reactive control strategies during walking maneuvers. We hypothesized that GRFs would reveal force profiles indicating predictive control when likelihood of maneuvering was high, and reveal force profiles indicating reactive control when likelihood of maneuvering was low.

Methods: Ten young healthy adults performed 280 discrete stepping trials, moving from a set of start targets to a set of end targets (either **straight** ahead or requiring a **maneuver**) 1.5 leg lengths away (3 total steps) (Fig. 1A). Participants initiated each trial with a right step to a set location on a force plate. On select trials, an audio cue occurring 125 msec after the first step initial contact was used to signal the participant to step to the maneuver end targets. Participants performed four blocks of trials: Straight Baseline (20 straight trials with explicit knowledge of trial type); Maneuver Baseline (20 maneuver trials with explicit knowledge of trial type); Frequent Maneuvers (120 trials, maneuvers cued randomly 5 out of every 6 trials, no prior knowledge of trial type); Infrequent Maneuvers (120 trials, maneuvers cued randomly 1 out of every 6 trials, no prior knowledge of trial type). We calculated mediolateral GRF impulse from the first step during three time windows, **Total Stance**; **Predictive** (initial contact until the 95% confidence intervals of maneuver GRFs diverged from straight GRFs during the Infrequent Maneuver block); **Reactive** (end of Predictive Window to end of stance). We calculated the relative contribution of Predictive and Reactive Control Strategies during lateral maneuvers by subtracting the Straight Baseline GRF from the Maneuver GRFs and then calculating the mediolateral impulse during the Predictive and Reactive windows as a percentage of Total Stance mediolateral impulse.

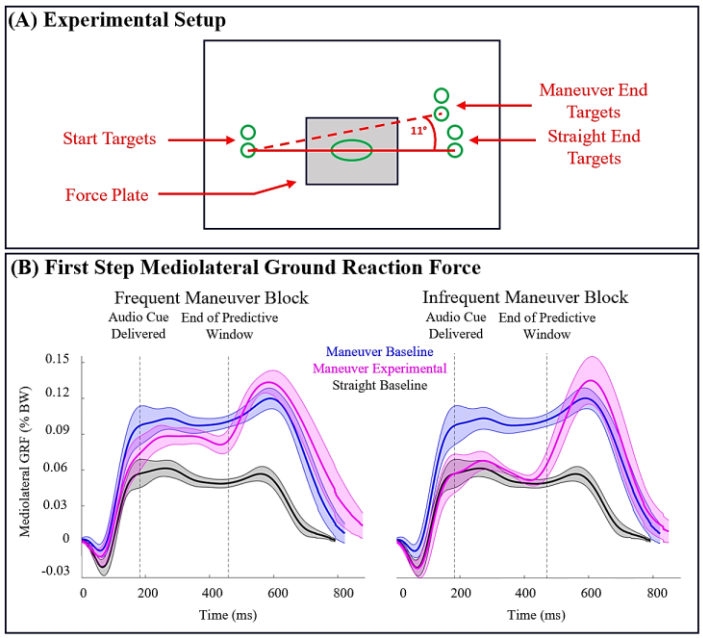

Figure 1: (A) Experimental setup. (B) Mediolateral GRF during the first step. Data shown are average and 95% confidence intervals of all participants.

Results & Discussion: GRF analysis revealed distinct force profiles between Frequent and Infrequent Maneuver blocks (Fig. 1B). In the Frequent Maneuver block, maneuver GRFs were greater than Straight Baseline trials and somewhat similar to Maneuver Baseline trials during the Predictive window, indicating that participants were anticipating the maneuver. Conversely, in the Infrequent Maneuver block, maneuver GRFs were similar in magnitude to Straight Baseline trials during the Predictive window, indicating that participants were not anticipating the maneuver. During the Frequent Maneuver Block we calculated that the contribution of Predictive and Reactive control strategies to lateral maneuvers was 27.43% to 72.57% respectively. These contributions changed significantly (paired t-test; $p < 0.05$) during the Infrequent Maneuver Block where the contribution of Predictive and Reactive control strategies to lateral maneuvers was 13.33% to 86.67% respectively.

Significance: This study established a novel and simple approach for quantifying the relative contributions of predictive and reactive control strategies during walking maneuvers within our specific experimental setup. This methodology can now be applied to advance our understanding of the challenges people with neurological impairments experience when maneuvering. Knowing how specific deficits in predictive and/or reactive control strategies impacts the ability to maneuver will allow clinicians to appropriately tailor interventions to optimize motor function and rehabilitation outcomes.

Acknowledgments: Supported in part by the U.S. Department of Veterans Affairs, RR&D Service #I01RX003371 and the National Institutes of Health's National Center for Advancing Translational Sciences, #UM1TR005121.

References: [1] Ludvig, Kearney. (2010), *Annu Int Conf IEEE Eng Med Biol Soc.* 2010:4914-7; [2] Ludvig et al. (2007) *Exp Brain Res.* 183(2).

HUMAN BRAIN AND BODY DYNAMICS DURING VISUAL TRACKING AND STEPPING OVER VIRTUAL OBJECTS

*Andrew D. Nordin, Yu-Po Cheng[2]
[1]University of Houston, Department of Biomedical Engineering, Houston, TX, 77204
[2]Texas A&M University, Texas A&M Institute for Neuroscience, College Station, 77840
*Corresponding author's email: adnordin@uh.edu

Introduction: Detecting and visually monitoring objects in the environment is critical for making anticipatory gait adjustments. Mobile electroencephalography (EEG) has been used to identify electrocortical spectral power dynamics while healthy individuals detected and stepped over unexpected obstacles that appeared on a treadmill belt within close proximity to the feet [1]. Supplementary motor area, premotor cortex, and posterior parietal cortex showed transient spectral power increases involved in interrupting and planning foot placement ahead of overstepping unexpected obstacles [1]. Navigating complex environments frequently involves visually tracking fixed or moving objects over longer durations and distances. Our aim was to identify eye gaze behavior, gait biomechanics, and electrical spectral power dynamics during visual tracking and stepping over fixed and moving objects in a projected virtual reality environment. We hypothesized that visuospatial processing during object tracking would show reduced alpha (8-13 Hz) and beta band (13-30 Hz) spectral power from visual and parietal cortex, and gait adjustments in the steps leading up to the virtual objects would show transient increases in alpha and beta band spectral power from supplementary motor area and sensorimotor cortex, indicative step planning. We anticipated that mismatches between gait speed and obstacle approach speed would further reduce visual and parietal electrocortical spectral power during object tracking and increase spectral power from supplementary motor area and sensorimotor cortex compared to matched gait and obstacle speed, reflecting greater cortical processing in response to environmental complexity.

Methods: We recorded eye gaze behavior (Tobii Pro Glasses 3), lower limb biomechanics (Vicon), and electrical brain activity (Brain Products LiveAmp) while 18 healthy individuals (8F, 10M) walked on a dual belt-force instrumented treadmill (DIH M-Gait). Subjects completed 12 conditions lasting 3-4 minutes each, including walking at 1.0 m/s, 1.25 m/s, and 1.5 m/s, and walking at each gait speed with virtual objects in the environment approaching at 0.75x, 1.0x, and 1.25x gait speed. We calculated the distance between the approaching obstacles and the location of the subject on the treadmill to extract the distance to contact, when the individual stepped over the obstacle. We identified stepping events from the ground reaction force data and foot marker trajectories and synchronized the biomechanical data and EEG data to extract electrical brain activity during visual tracking and stepping over the obstacles. We used EEGLab [2] and custom MATLAB scripts to remove noise (motion, eye, and muscle activity) from the channel recordings and extracted source brain activity as independent components that we modeled as equivalent current dipoles fit to cortical structures [1]. We calculated power spectral density and time-frequency spectral power fluctuations tied to the biomechanical events in each condition. Independent component power spectral density and time-frequency spectral power fluctuations were aggregated among subjects using clustering techniques and conditions comparisons were evaluated using bootstrapped analysis of variance methods in EEGLab ($\alpha = 0.05$).

Results & Discussion: We identified source activity from visual, parietal, sensorimotor, and frontal cortex, and supplementary motor area. Distinct changes in spectral power among brain structures were tied to the gait cycle and distance of the virtual obstacles relative to the body. Sustained alpha band spectral power decreases occurred from parietal (**Fig. 1**) and sensorimotor cortex, along with reduced alpha, beta, and gamma band (>30 Hz) power from visual cortex as subjects tracked and approached obstacles. Matching previous results, delta (3-4 Hz), theta (4-8 Hz), and alpha power from supplementary motor area increased as obstacles approached within 1.2 m of subjects, along with transient spectral power increases in theta and alpha power from sensorimotor and parietal cortex in the steps nearest obstacles [1].

Significance: We identified the cortical structures, timing, and spectral content of brainwave activity during visual object tracking and step planning among healthy individuals. Our findings improve our understanding of how the human brain transforms visual information into motor adjustments during gait. Identifying healthy electrical brain dynamics can help to determine neural pathways underlying gait deficits due to aging or neurological disorder and can serve as the basis for developing assistive locomotor brain computer interfaces.

Acknowledgments: Sponsored by the American Society of Biomechanics, 2024 Junior Faculty Research Grant.

References: [1] Nordin et al. (2019), *Sci Reports* 9(4693); [2] Delorme et al. (2004), *J Neurosci Methods* 134(1).

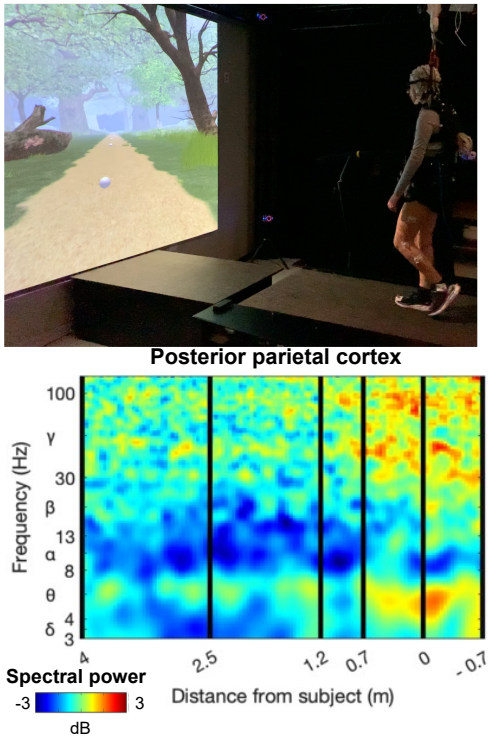

Figure 1: (**top**) Subject walking in a projected virtual reality environment while visually tracking an approaching object (white sphere) to step over. Virtual objects were projected onto the treadmill belt. (**bottom**) Time-frequency electrocortical spectral power from posterior parietal cortex, showing reduced delta (3-4 Hz) and alpha (8-13 Hz) band power while visually tracking the approaching object (4-0.7 m from the subject), and increased theta (4–8 Hz) and gamma band (>30 Hz) power while planning steps over the obstacle (0.7-0 m from the subject).

SAGITTAL PLANE MOMENT AND IMPULSE 1 MONTH POST-ACL RECONSTRUCTION ARE ASSOCIATED WITH CARTILAGE DEGENERATION 12 MONTHS POST-ACL RECONSTRUCTION

Justin D. Dennis[1*], Alex E. Nilius[1], Thomas Birchmeier[1], J. Troy Blackburn[1]
[1]University of North Carolina at Chapel Hill
*Corresponding author's email: jddennis@unc.edu

Introduction: Patellofemoral and tibiofemoral post-traumatic osteoarthritis (PTOA) are evident via magnetic resonance imaging (MRI) within the first year after anterior cruciate ligament reconstruction surgery (ACLR).[1] As such, identifying early intervention targets is imperative to mitigate cartilage degeneration. Greater sagittal plane angles[2] and moments[2] but lesser vertical ground reaction force (vGRF)[3] during walking 6 months post-ACLR are associated with declines in tibiofemoral cartilage health (i.e., increased T1ρ relaxation times indicating less proteoglycan density) within the first year post-ACLR. However, it is unclear if aberrant gait biomechanics 1 month post-ACLR are associated with cartilage degeneration 12 months post-ACLR. Consistent with the literature, we hypothesized that greater sagittal plane angles, moments, and impulses but lesser vGRF 1 month post-ACLR would be associated with larger changes in patellofemoral and tibiofemoral T1ρ relaxation times (i.e., declines in proteoglycan density) 12 months post-ACLR.

Methods: Fourteen individuals with primary unilateral ACLR (50% female; age: 22±5 years; height: 1.75±0.10 m; mass: 72.3±14.3 kg; patellar tendon autograft: 11; quadriceps tendon autograft: 3) underwent MRI with a 3T scanner and 4-channel knee coil 1 and 12 months post-ACLR. Voxel-by-voxel T1ρ relaxation times were calculated using a five-image sequence in MATLAB and images were manually segmented in ITK-SNAP software. Cartilage was divided into lateral and medial regions based on the peak of the tibial intercondylar eminence and was further subdivided into posterior, middle, and anterior weight-bearing as well as femoral trochlea regions based on the anterior and posterior horns of the meniscus (Figure 1). Participants completed five barefoot walking trials at their preferred speed with a 10-camera motion capture system synchronized with 3 floor embedded force platforms 1 month post-ACLR. Peak sagittal plane angles and moments, sagittal plane impulse, and peak vGRF were extracted from heel strike to 50% of stance. Moments and impulses were multiplied by 100 and normalized to body weight and height (%BW×Ht and %BW×Ht×S, respectively), and vGRF was normalized to body weight (BW). Percent changes in T1ρ relaxation times from 1 to 12 months were calculated to normalize values for each participant. Partial Pearson correlations while controlling for preferred gait speed were performed to determine the associations between changes in T1ρ relaxation times and gait biomechanics in the ACLR limb (α=0.05).

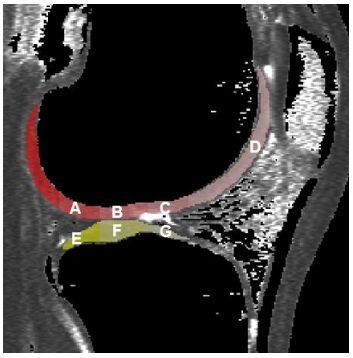

Figure 1: Segmented T1ρ relaxation time map of the lateral posterior femur (A), middle femur (B), anterior femur (C), femoral trochlea (D), posterior tibia (E), middle tibia (F), and anterior tibia (G).

Results: Peak knee flexion angle and vGRF at 1 month were not associated with T1ρ percent change from 1 month to 12 months post-ACLR. Lesser knee extension moment at 1 month was associated with greater T1ρ percent change from 1 month to 12 months in the lateral femoral trochlea (ρ = -0.622, p = 0.023) (Figure 2A). Greater sagittal plane impulse at 1 month was associated with greater T1ρ percent change from 1 month to 12 months in the middle medial tibia (ρ = 0.628, p = 0.021) (Figure 2B).

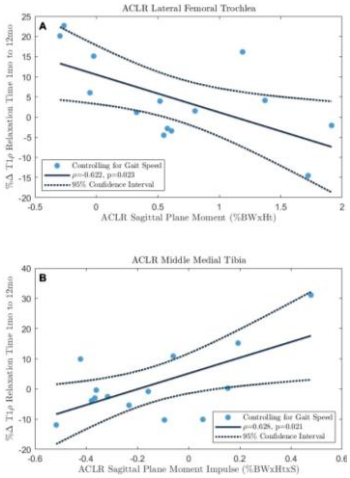

Figure 2: Associations between sagittal plane moment (A) and impulse (B) at 1 month and T1ρ percent change from 1 to 12 months post-ACLR.

Discussion: The magnitude and duration of sagittal plane knee loading 1 month post-ACLR are associated with reduced tibiofemoral cartilage proteoglycan density 12 months post-ACLR. Contrary to our hypothesis, lesser peak sagittal plane loading at 1 month is associated with worse lateral femoral trochlear cartilage health at 12 months. Supporting our hypothesis, greater cumulative sagittal plane loading (i.e., impulse) at 1 month is associated with worse middle medial tibia cartilage health at 12 months.

Significance: This study elucidated gait biomechanics that may serve as intervention targets to preserve cartilage health while patients are still undergoing rehabilitation. During gait, an internal knee flexion moment at heel strike is generally followed by an internal extension moment. Interestingly, those who walked with an internal knee flexion moment throughout stance at 1 month post-ACLR displayed declines in lateral femoral trochlea cartilage health while those who had an internal knee extension moment displayed improvements in cartilage health. Moreover, sustained knee loading (i.e., larger sagittal impulse) 1 month post-ACLR may contribute to declines in medial tibia cartilage health 12 months post-ACLR by preventing nutrient exchange and water influx. Future research should investigate how the magnitude and duration of sagittal plane knee loading at 1 month influences cartilage health and PTOA development at later timepoints post-ACLR.

Acknowledgments: This study was supported by the Department of Defence Award Number W81XWH21C00490011582719.

References: [1] Culvenor et al. (2015), *Arthritis Rheumatol* 67(4); [2] Teng et al. (2017), *Am J Sports Med.* 45(14); [3] Pfeiffer et al. (2019), *Med Sci Sports Exerc.* 51(4).

ARTHROKINEMATICS ANALYSIS OF HIGH IMPACT AND LARGE ROTATION ACTIVITIES 1-2 YEARS POST-ACLR+M

*Sadegh Khodabandeloo[1], John Ramsdell, Bruce Beynnon, Mathew Failla, Mathew Geeslin, Mickey Krug, Michael DeSarno, Niccolo Fiorentino[1]
[1]Department of Mechanical Engineering, University of Vermont, Burlington, VT, USA
*Corresponding author's email: sadegh.khodabandeloo@uvm.edu

Introduction: Risk of post-traumatic osteoarthritis (PTOA) following anterior cruciate ligament reconstruction (ACLR) is increased when ACLR is combined with a meniscus lesion (ACLR+M), affecting 50% of patients 10-20 years after the surgery [1]. Alterations in joint biomechanics have been implicated as one of the contributing factors to the degenerative pathway of PTOA [2]. Given that even minor alterations in joint angle and translations (osteokinematics) following ACLR+M can significantly impact cartilage contact mechanics, gaining a deeper understanding of cartilage arthrokinematics – relative position of the articulating surfaces – in-vivo during the early postoperative stages is crucial. Such insights will enhance our knowledge of changes in joint loading and their role in the onset and progression of PTOA. Because the majority of ACLR+M patients return to sport and engage in high demanding activities as early as 12 months after the surgery, this study aimed to quantify abnormal joint arthrokinematics (surgical vs contralateral) during demanding activities in the high PTOA risk population (ACLR+M) at an early-stage post-surgery [3]. Therefore, the objective of this study was to determine the effect of ACLR+M surgery on joint osteokinematics and articular cartilage arthrokinematics 1-2 years after surgery during three demanding dynamic activities: single-legged landing, single-legged lunging, and pivoting.

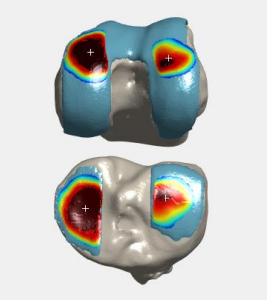

Figure 1: An example of the contact overlap (dark red area) and the weighted centroid of contact area (white markers) between two cartilage surfaces.

Methods: Twelve patients were recruited 1-2 years after ACL reconstruction with either a concomitant meniscal repair and/or partial meniscectomy. All patients reported having an uninjured, normal contralateral limb. Each participant performed three activities (landing, lunging, and pivoting) three times on each side (surgical and contralateral). Patient-specific tissue models from MRI, and a validated MBT method [4], were used to measure the side-to-side (surgical vs contralateral) differences of the 1- six degrees of freedom osteokinematics, 2- overlapping area of tibial and femoral cartilage (contact overlap), 3- the weighted centroid of contact area between the cartilage surfaces (contact point) (**Figure 1**), 4- the length of contact path, and 5- the excursion of contact path. Results were time-normalized to the percentage of maximum ground reaction force for single-legged landing, maximum degree of flexion for single-legged lunging, and maximum forward position of the knee lateral marker (FKLM) for pivoting.

Results & Discussion: During single-legged landing, the ACLR+M knee compared to the contralateral knee showed less flexion at the last timepoint (8°, P<0.001) (**Figure 2A**, top left), increased anterior tibial translation reaching 3.6 mm (P=0.01) at peak loading (**Figure 2A**, bottom center), and a posterior shift in the medial compartment's contact centroid reaching 2.5 mm (P=0.02) at peak loading (**Figure 2B**, left). During single-legged lunging, it exhibited less maximum flexion (4.5°, P=0.05), greater tibial external rotation (2°, P=0.05), and increased AP contact path excursion (0.4 mm, P=0.02). During pivoting, it showed an anterior tibial translation reaching a 3 mm side-to-side difference at peak FKLM and increased contact overlap. The posterior shift and anterior tibial translation during landing and pivoting suggest that reconstruction and rehabilitation fail to restore anteroposterior tibial positioning compared to the normal knee, potentially altering cartilage loading and promoting PTOA. Less flexion during landing and lunging may serve as a strategy to enhance joint stabilization in knees post-ACL reconstruction [5]. Increased medial compartment contact overlap suggests reduced shock absorption, post-ACLR+M.

Significance: This study is the first to quantify abnormal joint arthrokinematics in ACLR+M patients during demanding activities 1-2 years post-surgery, a critical period coinciding with return-to-sport clearance. Increased tibial translation and reduced shock absorption capacity indicate persistent mechanical deficits that may accelerate cartilage degeneration and PTOA risk. These findings offer novel insights into early joint changes, with potential to guide targeted rehabilitation strategies for this high-risk population.

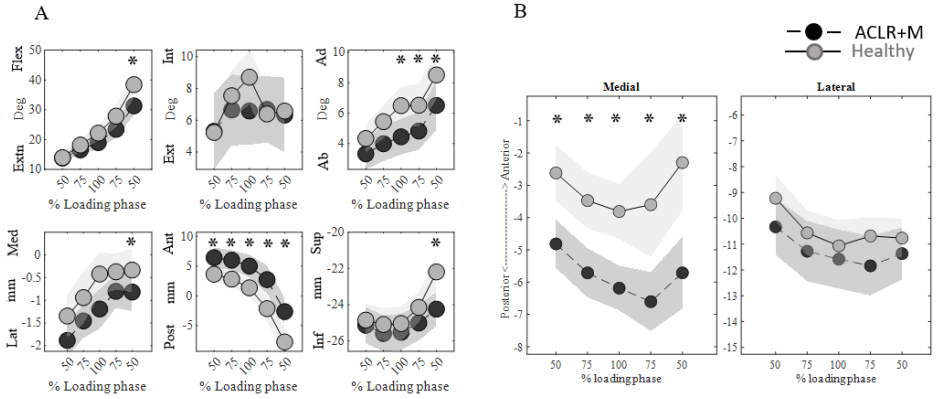

Figure 2: (A) 6 degree of freedom osteokineamtics and (B) anteroposterior centroid of contact during single-legged landing. Shading areas represent standard error. *P<0.05

Acknowledgments and References: Rebecca Choquette for coordination of the study, and Melissa Cuke for regulatory. [1] Lohmander et al. (2007), J Sports Med 35(10). [2] Chaudhari et al. (2008), MSSE 40(2). [3] Swirtun et al. (2006), Med Sci Sports 16(6). [4] Ramsdell et al. (2023), Med Eng Phys 114. [5] Rudolph et al. (2000), Knee Surg Sports Traumatol Art.

SEX-BASED VARIATIONS IN MENISCAL MORPHOLOGY AND CONTACT MECHANICS FOLLOWING ACL RECONSTRUCTION

Dominique A. Barnes*[1,2], Ata M. Kiapour[3], Jillian E. Beveridge[1,2], Mohammadreza Movahhedi[3], Crystal J. Murray[1,2], Martha M. Murray[3], Braden C. Fleming[1,2]

[1]Brown University, Providence, RI, [2]Rhode Island Hospital, Providence, RI, [3]Boston Children's Hospital, Boston, MA

*Corresponding author's email: dominique_barnes@brown.edu

Introduction: The meniscus' primary function, which is dependent on its shape and size, is to distribute load [1]. Meniscal injuries often occur concurrently with ACL injuries and increase the risk of early-onset osteoarthritis [2]. These injuries can compromise the morphological structure of the meniscus, which may impair its ability to distribute axial tibiofemoral forces, a key function in stabilizing the joint during articulation [3]. Therefore, this study aimed to compare the cross-sectional area (CSA) profiles of the medial and lateral menisci between male and female subjects using statistical parametric mapping (SPM). Furthermore, we investigate whether differences in CSA correspond to variations in contact areas and pressures experienced during static loading. We hypothesized that the female medial and lateral menisci CSA profiles, even when normalized by knee size, are smaller than male profiles following ACL surgery.

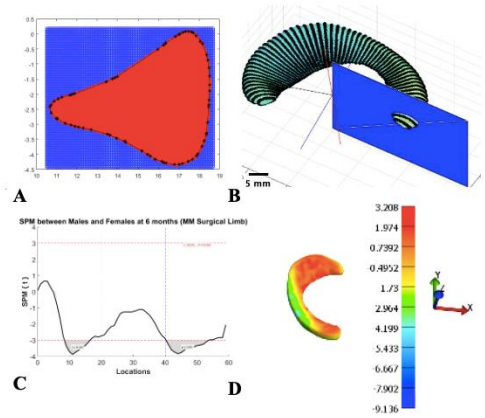

Figure 1: 1A. Meniscal Cross Section profile; 1B. 60 intersections between the plane and the meniscal 3D model; 1C. SPM of the surgical limb's CSA. The t-value of the difference between male and female average CSA profiles of the medial meniscus (MM) is shown on the y-axis; 1D. FE analysis of femur-meniscus contact: The heatmap shows gap distance (mm), with high-contact regions visualized in red.

Methods: Data were collected from 105 subjects (70 females and 35 males, median age 17.6) who underwent unilateral ACL surgery and magnetic resonance imaging (MRI) at six months post-surgery. The medial and lateral menisci of the surgical knee were automatically segmented from Constructive Interference in Steady State sequence (CISS) image stack using custom software [4]. Cross-sectional profiles that describe the changes throughout the menisci were generated by rotating an intersecting plane around the meniscus (Fig. 1A). Sixty CSA measurements, equally spaced about the rotational axis, were made ranging from the anterior root (0%) to the posterior root (100%) (Fig. 1B). Each CSA values were normalized to the mediolateral bicondylar width of the knee to account for differences due to knee size. SPM was used to conduct two-tailed t-tests at each of the sixty positions to compare the CSA profile differences between sexes. A finite element (FE) model was developed in FEBio using the automatically segmented geometry from an MRI of a randomly selected female subject included in our cohort [5]. The model consisted of the femur and tibia represented as rigid bodies, with the tibia fixed in 6 degrees of freedom and the femur fixed in 5 degrees of freedom with axial displacement (z-axis) not fixed. No ligaments were included in the model, however, the menisci and articular cartilages were modeled as a hyperelastic material. The femoral cartilage was rigidly fixed to the femur, and the tibial cartilages and menisci were rigidly fixed to the tibia. Sliding contacts were applied between the articular cartilages and the menisci. Axial displacement in the z-axis was placed to the femur in full extension to identify the peak contact areas between the femur and menisci, specifically the medial meniscus.

Results & Discussion: No significant differences were found between the normalized lateral meniscus CSA of the surgical knee in males and females. However, in the medial meniscus, females exhibited a mean percent difference of 12.9% and 13.1% CSA compared to males in the anterior and posterior regions respectively ($p<.001$) (Fig. 1C). The FE model revealed that peak contact between the femur and medial meniscus during static axial displacement occurs in the same region where we identified significant CSA differences (Fig. 1D). This spatial overlap emphasizes the biomechanical relationship between load distribution and meniscal morphology. The similarities between the significant differences in the medial meniscus CSA and high-contact area may indicate altered load distribution in female patients post-ACL surgery, potentially increasing the risk of early osteoarthritic changes. Identifying the specific regions of the meniscus that undergo changes after surgery, particularly in female patients, may inform the development of targeted rehabilitation strategies aimed at reducing post-surgical OA risk. Future research should focus on incorporating dynamic loading conditions to the subject-specific FE models to better capture the complex biomechanics of the femur-meniscus interaction. By integrating patient-specific geometries and loading scenarios, we can improve the accuracy of contact stresses and better understand how post-ACL surgery morphological changes influence joint mechanics over time.

Significance: This study provides important insights into meniscal morphometry post-ACL surgery, which may contribute to understanding the sex-based differences in OA risk. Additionally, our FE analysis highlights the biomechanical link between meniscal morphology and joint contact loading. Understanding these differences could guide treatment strategies and improve long-term joint health outcomes, particularly for female patients who are at a higher risk of early on-set OA.

Acknowledgments: Funded by the NIH (NIAMS R01-AR065462), the National Football League Players Association, the Lucy Lippitt Endowment, the RIH Orthopaedic Foundation, and the Boston Children's Hospital Orthopaedic Surgery Foundation.

References: [1] Vrancken et al (2014), *J. Anat,* 225(4); [2] Pruneski et al. (2024), *Am. J. Sports Med* 52(1); [3] Luczkiewicz et al. (2015), *J. Biomech.* 48(8); [4] Singh et al. (2024), *ORS*; [5] Maas et al. (2012), *J. Biomech. Eng.* 134(1)

Comparison of musculoskeletal modeling methods to estimate tibiofemoral contact force in individuals post-ACL reconstruction

*Willa Ma[1], Russell T. Johnson[2], Susan Sigward[1]
[1]University of Southern California, Division of Biokinesiology and Physical Therapy
[2]Northwestern University, Department of Physical Medicine and Rehabilitation
*Corresponding author's email: willama@usc.edu

Introduction: Altered gait mechanics following anterior cruciate ligament reconstruction (ACLr) is thought to contribute to early onset and progression of knee osteoarthritis.[1] Reduced surgical knee extensor moments (KEM) during loading response and limited knee flexion excursion across the stance phase are interpreted as underloading of the surgical knee.[2] However, it is not clear how these gait mechanics translate to joint contact forces. Since inverse dynamics computes net joint moments, which account for all external forces, these moments exclude the individual contribution of agonist and antagonist muscles; therefore, knee extensor moments may be underestimated in the presence of co-contractions between the knee flexors and extensors.[3] Musculoskeletal modeling approaches estimate joint contact forces using optimization techniques incorporating kinematics, kinetics, and biomechanical constraints to determine individual muscle forces and their contributions to joint loading. Electromyography (EMG) can also be included as an input to inform the musculoskeletal simulations about the timing and magnitude of muscle activations recorded during the trial.[4,5] EMG inputs can be particularly useful to account for potential co-contractions that are thought to be present, in individuals post-ACLr.[6,7] Since quadriceps dysfunction and weakness are well-established in individuals post-ACLr, it is unclear how the inclusion of EMG would influence the estimation of joint contact force in this population. Therefore, the purpose of this study is to compare between-limb tibiofemoral contact forces (TFCF) estimated from dynamic optimization with and without EMG. We hypothesized lesser TFCF in the surgical compared to the non-surgical knee and that including EMG input will highlight the variability in patterns of TFCF in this population.

Methods: Fourteen individuals 111.9 ± 17 days post-ACLr (8 Male/6 Female, age: 26 ± 6 years) were included. We collected marker trajectory, ground reaction force, and EMG data (3D motion capture system) while individuals walked 10 meters overground at a self-selected speed. EMG probes were placed on the following muscles bilaterally: medial and lateral gastrocnemius, semitendinosus, biceps femoris long head, vastus lateralis and medialis, and rectus femoris. These inputs were used for musculoskeletal modeling in OpenSim (version 4.4). We scaled a generic musculoskeletal model to participant anthropometrics. To estimate muscle forces and TFCF, we used a dynamic optimization technique via the OpenSim MocoInverse toolbox.[8] MocoInverse solves the muscle redundancy problem by directly prescribing the kinematics and external reaction forces, while minimizing an objective function that distributes the muscle forces in a way that maximizes muscle endurance. The dynamic optimization was run using two different objective functions: 1) to minimize the sum of activations squared (without EMG) and 2) to minimize the sum of activations squared plus a weighted function that seeks to track measured EMG signals normalized to a peak maximum voluntary contraction (with EMG). Peak TFCF at loading response and terminal stance, as well as the minimum at midstance, were compared between limbs. Effect size (ES) was used to indicate the strength of between-limb differences.

Results & Discussion: Differences in TFCF ensemble waveforms are observed between the two optimization methods (Fig. 1). Without EMG, peak TFCF at loading response was lesser in the surgical limb compared to the non-surgical ($p = 0.0016$; ES: 1.04), and peak TFCF at terminal stance was lesser in the surgical limb compared to the non-surgical, but this difference was not significant ($p = 0.051$; ES: 0.56). No between-limb differences were observed for TFCF estimated with EMG. The inclusion of EMG influences the estimation of TFCF across the stance phase. The use of EMG may remove the assumption of idealized muscle activity; however, a limitation of EMG, particularly in this post-ACLr population, is that quadriceps dysfunction is known, so maximum voluntary isometric contraction and EMG can be highly variable. Therefore, EMG of quadriceps muscles may not be a true representation of muscle activation and assumed muscle dynamics may not accurately model a dysfunctional muscle.

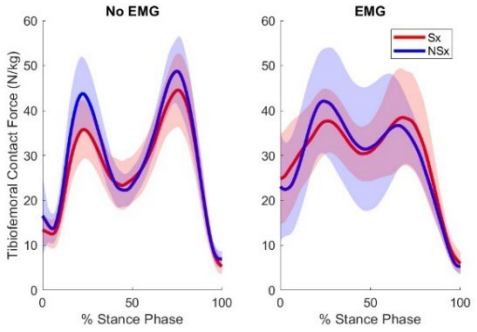

Figure 1: Tibiofemoral contact force between surgical (Sx, red) and non-surgical (NSx, blue) limbs in individuals post-ACLr across the stance phase with and without EMG.

Significance: Our current understanding of tibiofemoral joint loading is limited, especially at this early time point post-ACLr (approximately 3 months post-surgery). Early recovery is a critical window to address deficits as biomechanical alterations that lead to osteoarthritis may be modifiable. Estimating TFCF allows for an enhanced understanding of what is happening at the joint level. Musculoskeletal modeling is a valuable tool that requires important decisions, such as using additional inputs like EMG. These decisions affect the overall outcome and interpretation of knee contact forces for individuals post-ACLr. This study highlights that despite the large variability in TFCF across the stance phase, EMG may help better quantify individualized loading patterns, allowing for exploration of a more personalized understanding of recovery and risk for knee osteoarthritis.

Acknowledgments: N/A

References: [1] Luc-Harkey et al. (2014), *J Athl Train* 49(6); [2] Kaur et al. (2016), *Sport Med* 46.; [3] Lin & Sigward. (2016), *J Orthop Res* 38. [4] Manal & Buchanan. (2013), *J Biomech Eng* 135(2).; [5] Lloyd & Besier. (2003), *J Biomech* 35(6). [6] Tsai et al. (2012), *J Orthop Res* 30(12).; [7] Paredes et al. (2024), *Knee* 48(109).; [8] Dembia et al. (2020), *PLoS Comput Biol*. 16(12).

IMPACT OF TARGETED NEUROMUSCULAR TRAINING ON CLINICAL PERFORMANCE TESTING IN ATHLETES RETURNING TO SPORT AFTER ACL RECONSTRUCTION

*Nathaniel A Bates[1], Nathan D Schilaty, Kim D Barber Foss, April L McPherson, Gregory D Myer, Aaron J Krych
[1]The Ohio State University Wexner Medical Center, Columbus, OH, USA
*Corresponding author's email: nathaniel.bates@sosumc.edu

Introduction: Clinical surrogates for complex biomechanical metrics have been utilized to predict relative risk of ACL injury in healthy populations. [1] Further, clinical metrics are often implemented in return to sport decision making as athletes rehab from ACL reconstruction (ACLR). Prior investigations in patients following ACLR indicate that targeted neuromuscular training (TNMT) can improve biomechanics and decrease relative injury risk. [2] However, it remains unknown as to what influence TNMT has on clinical metrics following rehabilitation from ACLR.

Methods: Clinical strength and performance metrics were assessed in patients following ACLR (N=109) as part of a randomized clinical trial. All study participants had completed ACLR rehabilitation and were cleared to return to sport at time of enrollment. Subjects were randomized in 3 groups (STAN – standard of care, 6 weeks of no additive intervention; HOME – 6 week prescribed home-based cardiovascular training; TNMT – 6 week progressive targeted neuromuscular training [3]). Study participants were assessed for standard clinical performance variables of knee flexion/extension strength on an isokinetic dynamometer, isometric hip abduction strength on a custom device, and single-leg hop performance battery both pre- and post-intervention. Deltas in performance metrics were calculated by subtracting pre-test values from post-test values. Student T-tests were used to assess pre- vs post-intervention differences within each group. 3x1 ANOVA assessed differences in deltas between groups. Significance was set at $\alpha \leq 0.05$.

Results & Discussion: A total of 36, 33, and 39 study participants completed pre- and post-intervention strength assessments in the STAN, HOME, and TNMT groups, respectively. Strength testing did not exhibit pre/post differences in the STAN and HOME groups ($p \geq 0.08$; Table 1). Isokinetic knee extension strength was greater at post-testing than pre-testing for the TNMT group for both the 180°/sec and 300°/sec tests ($p \leq 0.05$). There were no significant differences in pre/post strength deltas between groups ($p \geq 0.15$). Pre- and post-intervention Hamstrings:Quadriceps ratio at 180°/sec were 0.59 (0.19) and 0.62 (0.18) for STAN, 0.56 (0.27) and 0.61 (0.26) for HOME, and 0.56 (0.11) and 0.60 (0.20) for TNMT. There were no ratio differences between pre- and post-intervention ($p \geq 0.11$), group ($p \geq 0.44$), or deltas ($p \geq 0.66$).

A total of 34, 33, and 38 study participants completed hop testing assessments in the STAN, HOME, and TNMT groups, respectively. Hop testing for single, triple, triple crossover, and 6-meter-timed hop expressed no significant differences between pre- and post-intervention within any group ($p \geq 0.17$); except for triple crossover hop which approached significance in the TNMT group ($p = 0.06$). Pre/post deltas between groups indicated that the TNMT group had a larger pre/post improvement in crossover hopping than STAN or HOME groups ($p = 0.01$).

Though muscle strengthening can certainly be a by-product of TNMT, TNMT is not explicitly targeted towards increasing muscle strength of the lower extremity. Rather, TNMT programs are targeted towards altering neuromuscular activation to decrease deleterious knee kinetics and kinematics during athletic tasks. The predominant focus of TNMT is constraining knee motion in the frontal plane. Relative to clinical metrics, the current data demonstrated that TNMT only influenced change in the dynamic hopping variable that invited frontal plane motion, by asking the subject to crossover the centerline of their body with each jump (triple crossover hop).

Significance: TNMT demonstrated improved extension strength and crossover hop performance whereas untrained groups did not, even though most return to sport clinical performance metrics remained unaffected. Further research is needed to directly correlate how these improvements in clinical metrics associate with 3D motion analysis-derived kinetics and kinematics metrics.

Acknowledgments: NIH NIAMS R01-055563; Florida Department of State Center for Neuromusculoskeletal Research.

References: [1] Myer et al. (2010), *AJSM* 38(10); [2] Hewett et al. (2017), *AJSM* 45(9); [3] Di Stasi et al. (2013), *JOSPT* 43(11).

	STAN				HOME				TNMT				DELTA
	Pre-Testing	Post-Testing	p-value	DELTA	Pre-Testing	Post-Testing	p-value	DELTA	Pre-Testing	Post-Testing	p-value	DELTA	p-value
Isokinetic Flex 180 (Nm)	47 (15)	48 (17)	0.57	2 (10)	46 (17)	46 (21)	0.98	0 (12)	45 (14)	48 (13)	0.21	3 (10)	0.29
Isokinetic Flex 300 (Nm)	37 (14)	39 (15)	0.59	1 (11)	36 (15)	36 (18)	0.92	0 (11)	35 (13)	37 (13)	0.42	2 (10)	0.71
Isokinetic Ext 180 (Nm)	80 (24)	85 (32)	0.32	6 (21)	81 (34)	86 (33)	0.40	5 (15)	78 (24)	87 (24)	0.02*	9 (13)	0.31
Isokinetic Ext 300 (Nm)	67 (29)	61 (21)	0.12	7 (15)	61 (24)	64 (24)	0.53	3 (12)	59 (19)	65 (20)	0.05*	6 (13)	0.15
Hip Isometric (N)	253 (90)	294 (114)	0.08	41 (85)	253 (104)	273 (89)	0.41	20 (85)	276 (125)	314 (123)	0.20	38 (90)	0.57
Single Hop (cm)	125 (35)	133 (33)	0.17	8 (22)	142 (30)	141 (24)	0.71	-2 (27)	136 (29)	134 (31)	0.75	2 (26)	0.07
Triple Hop (cm)	399 (103)	404 (102)	0.75	6 (46)	448 (81)	440 (75)	0.54	-8 (58)	405 (79)	414 (87)	0.54	8 (42)	0.10
Crossover Hop (cm)	355 (99)	367 (100)	0.50	12 (41)	401 (88)	402 (78)	0.91	2 (56)	358 (78)	384 (86)	0.06	25 (42)	0.01*
6-meter Hop (cm)	2.55 (0.81)	2.42 (0.75)	0.31	-0.1 (0.4)	2.35 (0.58)	2.24 (0.34)	0.18	-0.1 (0.5)	2.42 (0.66)	2.31 (0.56)	0.26	-0.1 (0.4)	0.93

Table 1: Means (standard deviation) of pre- and post-intervention assessments of clinical strength and hop testing performance separated by intervention group, along with the mean (standard deviation) delta between pre- and post-assessment differences. Relative to clinical return to sport measures, only the TNMT group demonstrated differences and they were limited to knee extension and crossover hopping.

ADOLESCENT ATHLETES POST-ACL RECONSTRUCTION DEMONSTRATE GENDER AND LIMB DIFFERENCES IN STRUT AND SPRING BEHAVIORS

Katelyn S. Campbell[1*], Sierra D. Hastings[1], Eric L. Dugan[1,2]
[1] Motion Analysis Laboratory, Texas Children's Hospital, The Woodlands, TX, USA
[2] Department of Orthopaedic Surgery, Baylor College of Medicine, Houston, TX, USA
*Corresponding author's email: kscampbe@texaschildrens.org

Introduction: Understanding the biomechanical effects of limb injury and gender on movement patterns is crucial for optimizing rehabilitation strategies, particularly in adolescent athletes. Knee injuries, especially those requiring surgical intervention, can significantly alter joint biomechanics, impacting rehabilitation and return-to-sport decisions. This study aimed to assess biomechanical differences between injured and uninjured limbs in adolescent patients post-ACL reconstruction surgery, focusing on the Strut, Spring, Damper, and Motor indices. We hypothesized that injured limbs would exhibit higher Strut Index values compared to non-injured limbs.

Methods: Forty-three adolescents (Age: 15.86 ± 1.61 years; Height: 170.32 ± 9.53 cm; Weight: 74.31 ± 16.02 kg; Days post-surgery: 187.07 ± 46.82) ran on a treadmill at a self-selected pace. Kinematic and ground reaction force data were collected simultaneously using a 10-camera system (200 Hz; Vicon, Oxford, UK) and tandem-belt force-instrumented treadmill (1200 Hz; AMTI, Watertown, MA). Gender distribution was 37.2% female and 62.8% male. Data were processed and analysed using Visual 3D (HAS Motion, Kingston, ON), Matlab (MathWorks Inc., Natick, MA), and R (4.3.1). Kinematic and ground reaction force data were filtered using low-pass Butterworth filters with cut-off frequencies of 6 and 20 Hz, respectively.

For each subject, the Strut, Spring, Damper, and Motor indices were calculated bilaterally during the stance phase of running [1,2]. Linear mixed-effects models were used to evaluate the effects of limb injury and gender on each index, adjusting for repeated measures within subjects. Given the compositional nature of the indices, a centered log-ratio (clr) transformation was applied to normalize the data. Bonferroni correction was applied to adjust for multiple comparisons.

Results: The injured limb demonstrated an increase in Strut behavior and a decrease in Spring behavior relative to the uninjured limb. Specifically, the Strut Index showed a significant difference between limb types ($p < 0.001$), with the injured limb exhibiting higher Strut values. Similarly, the Spring Index also showed a significant difference ($p < 0.001$), with the injured limb showing lower Spring values. In contrast, Damper ($p = 0.99$) and Motor ($p = 0.23$) indices did not show significant differences between the injured and uninjured limbs.

The differences in Strut and Spring remained significant after adjusting for multiple comparisons using Bonferroni correction. Gender had a significant effect on the Strut Index ($p = 0.02$), with males showing slightly higher Strut values than females. The interaction between limbs and gender was significant for both the Strut ($p < 0.001$) and Spring ($p < 0.001$) indices, suggesting that the effect of injury on Strut and Spring behaviors varied by gender. Specifically, the effect of injury on these indices was less pronounced in males than in females.

Discussion: The results of this study confirm our hypothesis by demonstrating that both limb injury condition and gender significantly affect the Strut Index in adolescent athletes. Specifically, the injured limb shows a compensatory increase in Strut behavior, which appears to result from a shift in joint mechanics, transitioning from Spring behavior to Strut behavior. This shift indicates that the injured limb, in its attempt to compensate for lost or altered function, may rely more on more rigid joint mechanics (Strut) rather than the elastic, energy-storing properties typical of Spring behavior.

The shift to Strut behavior in the injured limb is likely driven by quadriceps weakness and guarding or avoidance behaviors, which are common impairments after ACL-reconstruction (ACL-r) [3]. These factors may cause the body to reduce the range of motion, and therefore joint work, at the knee to compensate for the loss of normal muscle function and to protect the injured joint. While this may initially stabilize the joint during rehabilitation, it could also lead to maladaptive compensation, potentially causing movement inefficiencies or increasing stress on other tissues. Long-term studies are needed to assess whether these compensatory mechanisms contribute to long term impairments or a heightened risk of re-injury.

Gender differences in the Strut Index suggest distinct biomechanical profiles between males and females following injury, possibly due to differences in strength or neuromuscular control. Males exhibited a less pronounced shift to Strut behavior in the injured limb, indicating they may rely on different compensation strategies compared to females. This is consistent with previous research highlighting that females are at a higher risk of ACL injury [4]. These findings underscore the need for further investigation into gender-specific factors and personalized rehabilitation strategies that address these differences. Tailoring interventions to target specific strength and neuromuscular control deficits may improve rehabilitation outcomes and reduce the risk of maladaptive compensation. These results suggest measuring knee joint functional indices during running could be an appropriate assessment of return to knee joint function in adolescent athletes post ACL-r.

Significance: Overall, this study contributes to a better understanding of biomechanical compensations following ACL-r in adolescent athletes and suggests that functional joint indices may have potential for tracking recovery progress.

References: [1] Kuhman & Hurt. (2019), *J Exp Biol* 222(20); [2] Qiao & Jindrich. (2016), *J Biomech* 49(1); [3] Thomas et al. (2013), *J Athl Train* 48(5); [4] Montalvo et al. (2019), *Br J Sports Med* 53(16).

THE EFFECTS OF A VISUAL DISRUPTIVE TASK ON WALKING GAIT BIOMECHANICS IN THOSE WITH ANTERIOR CRUCIATE LIGAMENT RECONSTURCTION

*Alex Nilius[1], Justin Dennis[1], Tom Birchmeier[1], Troy Blackburn[1]
[1]University of North Carolina at Chapel Hill
*Corresponding author's email: ahewson@unc.edu

Introduction: Those who undergo anterior cruciate ligament reconstruction (ACLR) walk with decreased sagittal knee moments and angles[1]. Patients with ACL injuries also reweigh sensory information, relying more heavily on visual stimuli for lower limb control [2]. The introduction of stroboscopic goggles as a visual-disruptive task may mimic the visual-motor demands of sport and could be used in rehabilitation to reduce dependence on visual stimuli. However, the effects of visual disruption on walking biomechanics in individuals with ACLR are unknown. The objective of this project is to evaluate the acute effects of a visual-disruptive task on walking gait biomechanics in individuals with ACLR. We hypothesized that visual disruption would be associated with decreased sagittal knee moments and angles in both healthy controls and those with ACLR, with a greater level of visual disruption having a greater effect than a lower level of disruption. Due to possible visual reliance in those with ACLR, we also hypothesized that visual disruption would have greater effects in this group compared to healthy controls.

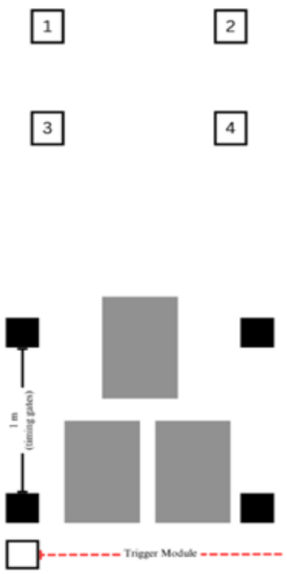

Figure 1: Experimental setup. Lights (1-4) were positioned at the end of the walkway to ensure that any waving motion aimed at turning them off did not influence gait biomechanics.

Methods: Fifteen participants with a history of ACLR and fifteen healthy controls matched for age, sex, BMI and activity level completed an overground gait assessment at 1.3 m/s along a 10 m walkway. Four lights were positioned at the end of the walkway (Figure 1), where one of the lights would randomly turn on as they crossed the force plates. Participants were required to turn off the light by waving in front of it as they passed by. Participants completed this task wearing stroboscopic goggles under three conditions: goggles turned off (CON), and goggles turned on at LOW (100 ms opaque, 100 ms transparent) and HIGH (250 ms opaque, 100 ms transparent) intensities while gait kinematics and kinetics were collected. Peak internal knee extension moment (pKEM), knee flexion angle (pKFA), and vertical ground reaction force (vGRF) were evaluated separately via a mixed-model repeated-measures ANOVA to examine the effects of walking condition (CON, LOW, HIGH) and group (ACLR vs. Control). Means and effect sizes were reported to assess between-group differences.

Results & Discussion: Group means and standard deviations for each outcome under each condition are presented in Table 1. The group x condition interaction effect was not significant for pKEM ($F=1.722$, $p = 0.197$, $\eta^2 = 0.67$), pKFA ($F=0.829$, $p = 0.406$, $\eta^2 = 0.035$), or vGRF ($F=2.654$, $p = 0.081$, $\eta^2 = 1.03$). These findings suggest that neither individuals with ACLR nor healthy controls showed significant changes in the variables of interest under the visual disruptive task, contrary to our hypothesis. The visual disruption task might not have been intense enough to overcome any compensatory mechanisms. Both ACLR patients and healthy individuals may have relied on proprioceptive feedback and other sensory modalities that were not disrupted by the visual manipulation, allowing them to maintain their biomechanics.

	ACLR			Healthy Controls		
	Control	Low	High	Control	Low	High
pKEM	3.29 ± 1.29	3.38 ± 1.32	3.60 ± 1.29	4.24 ± 1.83	4.50 ± 1.75	4.24 ± 1.58
pKFA	14.67 ± 4.53	15.28 ± 5.63	14.97 ± 5.02	14.06 ± 6.99	16.09 ± 6.80	15.22 ± 6.48
vGRF	1.06 ± 0.05	1.04 ± 0.04	1.07 ± 0.04	1.11 ± 0.09	1.13 ± 0.10	1.12 ± 0.09

Table 1: Mean ± standard deviation for each variable of interest.

Significance: Neither the ACLR group nor the healthy control group showed changes in any of the variables of interest under any of the goggle conditions. These findings suggest that neither ACLR patients nor healthy controls were significantly impacted by the visual disruptive task, which may imply that both groups effectively relied on other sensory modalities (e.g., proprioception) to maintain postural stability and execute their movements. These findings have important implications for rehabilitation, suggesting that ACLR patients may benefit from training that enhances proprioceptive and other sensory compensations. Future research with larger sample sizes and more intense visual disruptions could help elucidate these effects more clearly and inform rehabilitation protocols for improved recovery outcomes in ACLR patients.

References: [1]Khandha et al. (2015), *J Orthop Res.* 35 [2] Culiver et al. (2023), *Int J Sports Phys Ther.* 18(1)

EFFECTS OF WATER WEIGHT-INDUCED PERTURBATION ON GAIT CHARACTERISTICS

*Malicki Diallo[1], Nicholas Tom[1], Shawanee' Patrick[1], Ajit Chaudhari[1]
[1] The Ohio State University, Columbus, OH, USA
*Corresponding author's email: malicki.diallo@osumc.edu

Introduction: Since the mid-2000s, perturbation-based balance training has become a key focus in clinical biomechanics research [1]. It is widely regarded as an effective approach in locomotor training, particularly for frail older adults and individuals with neurological disorders. Perturbations are known to impact normal kinematics, kinetics, and muscle activation during both gait and quiet standing. Most perturbation-based training paradigms involve sudden disruptions, such as slips and trips, caused by jerks on the treadmill, cables, and mechanical obstacles in a participant's walking path [1]. Although these training systems provide an advantage in destabilizing participants and creating near-fall situations, the costs of the equipment and the expertise required to operate them may limit their use in clinical settings [1]. The purpose of this study is to determine whether inexpensive water weight perturbations induce gait patterns in healthy young adults that replicate those observed in older adults and individuals with neurological disorders.

Methods: Nine healthy adults (5 Male, 4 Female; 1.80 ± 0.1m; 86.1 ± 10.9kg) from the Ohio State University community participated after providing IRB-approved informed consent. Participants were asked to walk on a self-paced treadmill under three conditions of increasing difficulty: baseline, walking with static weight, and walking with water weight. The static weight consisted of 10 lbs. of metal weights attached to a vest, while the water weight comprised 10 lbs. of water in a Tidal Tank Hydrovest (Catalys, Utrecht, Netherlands). Reflective markers were placed on participants, and five triaxial accelerometers (Trigno Wireless, Delsys, Boston, MA) were positioned on the pelvis, both thighs, and both ankles (medial malleolus). The treadmill was equipped with force plates to measure ground reaction forces. The data was collected in The MotionMonitor XGen (Innovative Sports Training, Chicago, IL) where step length, step width, and gait speed were calculated. Heel strike and toe-off were identified using a modified version of Gurchiek et al.'s algorithm [2] which was used to determine step time. Short-term Lyapunov exponents (STLE) were computed using a modified version of Ihlen et al.'s [3] algorithm in MATLAB 2024b (The MathWorks, Natick, MA). The data were analyzed using repeated measures, one-way ANOVA, and post hoc analysis to compare spatiotemporal parameters across the three conditions in GraphPad Prism 10 (GraphPad Software, San Diego, CA).

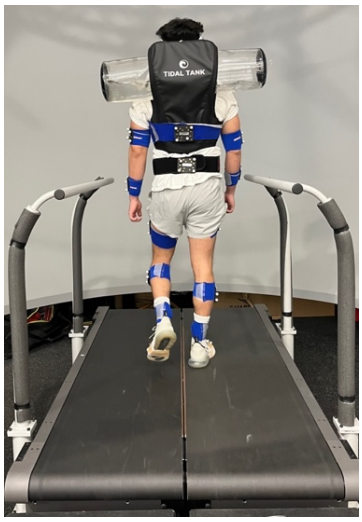

Fig 1. Participant set up with Tidal Tank and reflective markers.

Results & Discussion: Average step length ($p = 0.0023$), average stride time ($p = 0.0129$), and gait speed ($p = 0.0381$) showed significant differences across the conditions. However, post hoc analysis only revealed significant differences between static and water weight for average step length ($p = 0.0016$) and between baseline and water weight in average stride time ($p = 0.0098$). This suggests that the random perturbation induced by the water weight is the primary factor contributing to reduced stride time. However, the changes observed in step length may reflect both the continuous learning effect of walking on a self-paced treadmill and increased comfort with the added weight.

Additionally, step width and dynamic stability, assessed by short-term Lyapunov exponents, showed no significant differences across any of the conditions. The observed faster steps are consistent with previous results from pseudorandom perturbations [4]. While not significant in pairwise post-hoc testing, the difference in mean gait speed between baseline and water weight was at or above previously reported minimal clinically important differences (MCID) [5], [6].

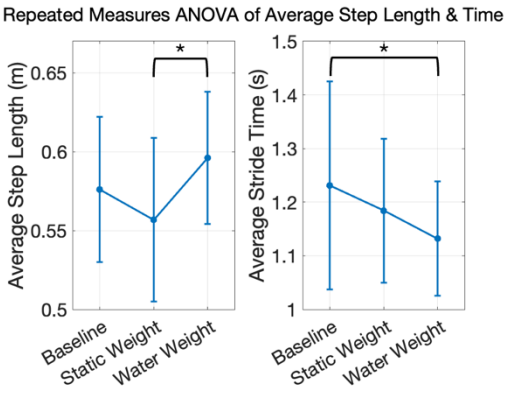

Fig 2. Analysis of variance of average step length and stride time.

Although step width tended to be narrower as the task difficulty increased, this difference was not statistically significant, which contradicts prior research [4], [7]. This discrepancy may be due to using too little added weight, as we added only 10 lbs (approximately 5% of the average adult's body weight). Future studies normalizing the weight to each participant's body mass or strength may provide a more complete understanding of how continuously varying random perturbations, like those induced by the Tidal Tank, affect gait dynamics.

Significance: Water weight-induced continuous random perturbation presents a promising paradigm for gait training due to its affordability, accessibility, and ease of use, making it not only feasible for clinical use but also for home-based therapy, significantly broadening its potential reach. Perturbations induced changes in step length and step time, suggesting that further evaluation with increased challenge and populations at higher risk of falls is worthwhile.

References: [1] McCrum et al. (2022), *Front. Sports Act. Living* 4; [2] Gurchiek et al. (2020), *Gait & Posture* 8; [3] Ihlen et al. (2012), *J Biomech* 45(13); [4] McAndrew et al. (2010), *J Biomech* 43(8); [5] Perera et al. (2006), *J Am Geriatr Soc* 54(5); [6] Bohannon et al. (2014), *Evaluation Clinical Practice* 20(4); [7] Madehkhaksar et al. (2018), *PLoS ONE* 13(4)

IMPACT OF ARM DOMINANCE AND PRACTICE TYPE ON MOVEMENT TASK PERFORMANCE POST SPINAL CORD INJURY

*Rebekah Revadelo[1], Skyler Barclay[1], Andrew Hill[1], Trent Brown[1], Allison Kinney[1], Timothy Reissman[1], Megan E. Reissman[1]
[1]University of Dayton, Dayton, OH, USA
*Corresponding author's email: revadelor1@udayton.edu

Introduction: Task specific training can be an effective rehabilitation technique for people with spinal cord injuries (SCI) and virtual reality (VR) is a useful tool for presenting movement tasks in a controlled and systematic way. Upper extremity rehabilitation is especially important for SCI, which fits with many VR movement tasks [1]. We sought to assess how blocked-task and random-task practice techniques (commonly used in motor learning) would impact task performance. Blocked-task practice involved repeating the same task many times. Random-task practice involves performing multiple tasks in a random order [2]. Prior work suggests that initial randomized practice will have lower performance versus blocked, because task complexity is increased. However, the increased task complexity is thought to drive enhanced learning and skill acquisition [3]. This study uses a blocked trial as a baseline, two random trials as practice, and a final blocked trial as comparison. We hypothesized that performance would decrease between baseline and the first random trial but improve between the first and last blocked trials.

Methods: 7 SCI subjects (5 males, 30.37±15.86 years, 4 C level injuries, 3 T level injuries, 12.44±8.18 years since injury) played the VR game *Beat Saber*. Equipment included a Valve Index headset and 7 HTC VIVE 3.0 trackers. Subjects were instructed to cut through blocks in a specified direction in time to the beat of a song (tasks paced ~2 secs apart). Performance analysis was based on the Cut Offset Error (distance from block center) and Cut Angle Error (matching direction shown) (Fig 1). Tasks were characterized into unilateral (UNI) or bilateral (mirrored (MIR), and opposing (OPP) movements). MIR motions consisted of both arms moving in symmetric motions about the midline. OPP motions consisted of both arms moving in non-symmetric motions about the midline. Based on self report of arm/hand dominance, the dominant (DOM) and non-dominant (NON) arms could also be compared. Blocked (BLOCK) trials consisted of tasks repeated 3 times in a row, while random (RAND) trials consisted of the same tasks in a random order. Subjects played four trials (90 tasks per trial), always in the order BLOCK 1, RAND 1, RAND 2, BLOCK 2. Performance results were extracted from the VR software using a modification package *ScoreSaber*. Data was processed using Python and analyzed in NCSS using a repeated measures ANOVA and Tukey-Kramer pairwise comparisons, with asterisks representing $p<0.05$ in Fig 2 and Fig 3.

Figure 1: Cut Offset Error (left) and Cut Angle Error (right).

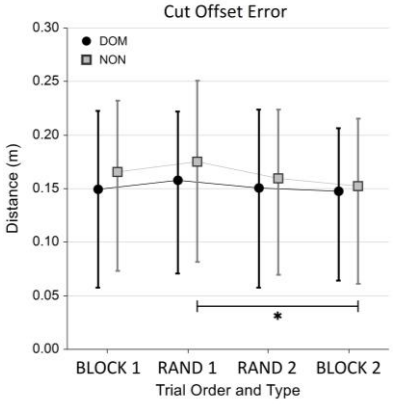

Figure 2: Cut Offset Error comparing trial order and type and hand dominance.

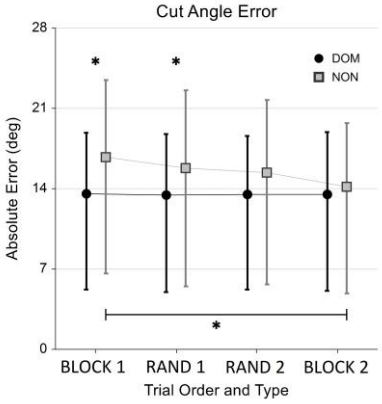

Figure 3: Cut Angle Error comparing trial order and type and hand dominance.

Results & Discussion: Hand dominance was a significant factor in the Cut Offset Error ($p<0.0005$) with the NON side having a larger error compared to the DOM side (Fig. 2). Trial type was a significant factor in Cut Offset Error ($p<0.02$) with BLOCK 2 having a lower error than RAND 1. For the NON side, there was less error in Blocked 2 than Random 1. However, for the DOM side there was no significant difference between trials. This indicates that the practice was more effective in improving the NON side, possibly because the NON side had greater room for improvement compared to the DOM side. Finally, there was a significant difference in Cut Offset Error between the unilateral tasks (UNI) and the bilateral tasks (MIR, OPP), with UNI tasks having a smaller error. This shows that subjects were able to achieve a better performance and cut closer to the center when only using one arm at a time.

Hand dominance was a significant factor in the Cut Angle Error ($p<0.0001$) with the NON side having higher error than the DOM side in the first two trials, but no significant difference in the last two trials (Fig. 3). The DOM side had no significant variation between trials. On average, the NON side decreased in Cut Angle Error in each consecutive trial, with the error being significantly less in BLOCK 2 compared to BLOCK 1. This shows a significant improvement in the NON side between the first and last trial. The decrease in Cut Angle Error suggests that even over a short period of time, the NON side can be trained to perform as well as the DOM side. There was no significant difference in Cut Angle Error between the UNI, MIR, and OPP tasks, showing that task type does not affect Cut Angle Error.

Significance: Results demonstrated performance improvements in BLOCK 2. We expected improvements on both sides, however, changes were driven by the nondominant side, while the dominant side was steady across trials. This task specific training encourages people with SCI to engage their nondominant side, which is likely weaker than their dominant side. Many people with SCI are wheelchair users and rely on upper extremity movements, so maintaining equal bilateral ability is important for their mobility and independence.

Acknowledgments: We acknowledge the funding support that was granted by the Chancellor of the Ohio Department of Higher Education from the Research Incentive Third Frontier Fund.

References: [1] Marryam et al. (2018) *RMJ*; [2] Levin & Demers, (2020) *Disabil Rehabil*; [3] Guadagnoli & Lee, (2004) *J Mot Behav*

STRENGTH IMBALANCES AND SHOULDER PAIN IN MANUAL WHEELCHAIR USERS STRATIFIED BY AGE OF SPINAL CORD INJURY/DISEASE ONSET

*Ashlyn Jones[1], Alyssa Schnorenberg[2], Brooke Slavens[2], Carrie Peterson[1]
[1]Dept. of Biomedical Engineering, Virginia Commonwealth University
[2]Dept. of Mechanical Engineering, University of Wisconsin-Milwaukee
*Corresponding author's email: jonesam10@vcu.edu

Introduction: Shoulder pain is prevalent among individuals with paraplegia who use manual wheelchairs, with 30% to 70% reporting shoulder pain [1]. Predictors of shoulder pain include factors such as age, sex, body weight, wheelchair propulsion techniques, time since injury, the demand of wheelchair activities (e.g., propulsion, transfers, pressure-relief raises), wheelchair design/fit, and upper limb muscle strength and imbalances [1]. The age of spinal cord injury or disease (SCI/D) onset may be important to consider since 48% of adults with pediatric-onset of SCI reported shoulder pain, compared to 84% of adults with adult-onset of SCI despite having more years of wheelchair use [2]. Children who rely on manual wheelchairs are at a unique risk, as their neuro-musculoskeletal systems are developing. However, there are no specific clinical guidelines for pediatric wheelchair propulsion. Further, knowledge of upper extremity strength of pediatric wheelchair users and the relationship between strength and shoulder pain is lacking. This represents a significant knowledge gap as understanding these factors could inform better rehabilitation protocols tailored to pediatric wheelchair users. It is also unknown whether individuals who experience SCI in childhood have different strength-pain relationships compared to those who experience their SCI as adults. The purpose of our on-going work is to determine relationships between strength and strength imbalances with shoulder pain and pathology, and whether these relationships differ based on the age of SCI/D onset. Here, we present shoulder and elbow strength imbalance and shoulder pain data recorded from manual wheelchair users stratified by age of SCI/D onset.

Methods: Forty-seven manual wheelchair users were recruited and participated. Participants were subdivided into one of three subgroups: 12 pediatric participants, 18 adults with pediatric-injury onset, and 17 adults with adult-injury onset. The mean age of the pediatric participants was 13.2 $\pm$ 2.9 years while the mean age for the adult participants was 38.8 $\pm$ 14.5 years. Participants performed maximum voluntary isometric contractions (MVICs) while seated in a Biodex System 3 or BTE PrimusRS to measure maximum isometric joint moments in five different shoulder joint postures, and two elbow joint postures. Each participant performed three maximum contractions for 3-5 seconds for each posture, with at least 30 seconds rest intervals between each trial. To elicit maximum contraction, participants were encouraged and motivated by the researchers. During the contractions, the EMG signals were visually monitored to maintain isolation of the muscle of interest. Shoulder pain was quantified using the Wheelchair User's Shoulder Pain Index (WUSPI) questionnaire, a validated self-report measure. WUSPI scores range from 0 to 150, with a larger score indicating greater pain.

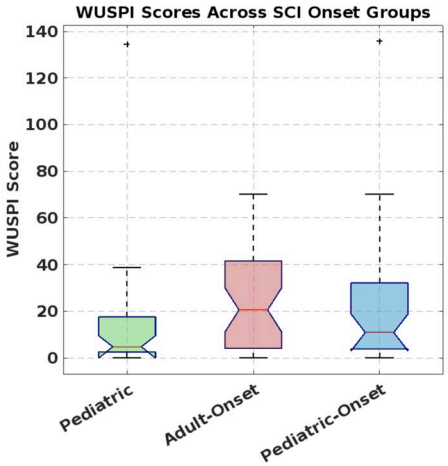

Figure 1: WUSPI scores across MWUs: pediatric, adults with adult-onset SCI/D, and adults with pediatric-onset SCI/D.

Results & Discussion: Qualitative comparison (i.e., preliminary analyses) indicates that shoulder pain was more prevalent in the adults with adult injury-onset group in comparison to the pediatric group and the adults with pediatric injury-onset (Fig. 1). The adult injury-onset group reported a median WUSPI score of 20.58, while the adults with pediatric-onset group reported a median WUSPI score of 10.91. This result is consistent with a previous study that found adults with pediatric injury-onset reported suffering from less shoulder pain compared to adults with adult injury-onset, despite having a greater duration of wheelchair use [3]. The difference in median WUSPI scores between these two groups was beyond the minimal detectable change of 5.1; a change of 10-15 points is considered clinically significant. Our results also suggest that children with paraplegia experience little to no shoulder pain, with a median WUSPI score of 4.76. Elbow flexion/extension moment ratios were highest in the adults with pediatric injury-onset group (Fig. 2). Shoulder external/internal rotation (ER/IR) moment ratios were consistent amongst all three groups.

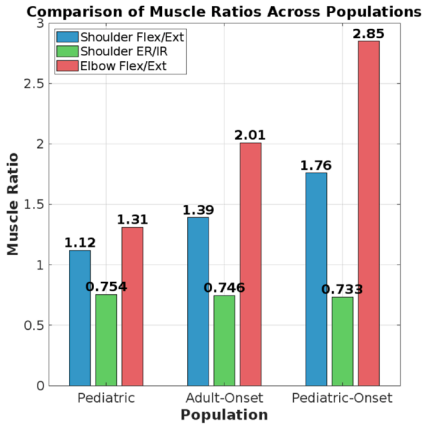

Figure 2: Flexion/extension moment ratios of the shoulder and elbow, and shoulder internal/external rotation moment ratios across the three different injury-onset groups.

Significance: We aim to provide a deeper understanding of how upper limb strength impacts shoulder health across the lifespan, informing approaches to reduce shoulder pain and improve the overall quality of life for manual wheelchair users.

Acknowledgments: Supported by NICHD R01HD098698.

References: [1] Mulroy, S. J., et al (2015). *Physical therapy*, *95*(7), 1027–38. [2] S. W. Brose *et al.*, (2008) *Arch Phys Med Rehabil,* vol. 89, no. 11, pp. 2086-93. [3] Leonardis, et al. (2022). *Arch of rehab research*, *4*(4), 100235

SHOULDER AND WRIST INTRALIMB JOINT COORDINATION ARE AGE AND TRIAL DEPENDENT

Robyn M. Hansen[1]*, Sara L. Arena[1], Robin M. Queen[1]
[1]Department of Biomedical Engineering and Mechanics, Virginia Tech, Blacksburg, VA
*Corresponding author's email: robynh2300@vt.edu

Introduction: Upper limb (UL) joint coordination relies on motor control [1], which improves with age and can classify childhood development as typical or atypical [2]. Joint coordination can be quantified using continuous relative phase (CRP), which measures the phase relationship between two joint angles, with values closer to zero degrees and 180 degrees indicating "in-phase" and "anti-phase" coordination patterns, respectively [3]. As motor learning improves with age [4], joint coordination can change, with younger children relying on visual and proprioceptive inputs (feedback), and older children using internal refinement (feedforward) to improve performance [5]. The purpose of this study was to examine age and trial differences in UL coordination using the mean absolute relative phase angle (MARP) and CRP variability (CRPv) for shoulder-elbow, elbow-wrist, and shoulder-wrist couplings during the Box and Blocks test (BBT). Clinicians commonly use the BBT to assess UL gross manual dexterity [6]. The MARP assesses coordination strategy, while CRPv assesses movement stability [7]. We hypothesize significant interactions between age and trial will exist for all joint couples with post-hoc analyses revealing a significant increase in MARP and CRPv between trials in the younger children, (7- and 9-yr-olds).

Methods: Twenty-one typically developing children aged 7-, 9-, or 11-yr-olds were recruited and signed informed consent. Participants completed three 60-second modified BBT trials, moving blocks to a target as quickly as possible. Kinematics were collected using an 8-camera markerless motion capture system (Theia Markerless Inc.) collecting at 85 Hz, and joint angles were determined using Visual3D (HAS Motion). A custom MATLAB code calculated intra-limb MARP and CRPv for all UL joint pairings for the following joint motions (shoulder abduction/adduction, elbow flexion/extension, and wrist flexion/extension) during the middle 15 successful block movements as well as task completion time (CT), which will be used to measure performance. MARP was calculated by taking the average of the absolute value of CRP and then the standard deviation was calculated to determine CRPv. A linear mixed effects model (α=0.05) was used to determine differences in MARP, CRPv, and CT between age (7yrs, 9yrs, 11yrs), trial (T1, T2, T3), and their interaction. Sex was not assessed due to uneven samples. Height ($p<0.001$) and mass ($p=0.005$) were used as fixed factors due to differences found between age groups. Post-hoc analyses were completed to determine pairwise differences as necessary.

Results: Height and mass did not have a significant effect on the dependent variables. A significant interaction was found for CT, with a significant increase in the 9yr-old group from T1 to T2 ($p<0.001$) and T1 to T3 ($p=0.005$). For the shoulder-wrist coupling, a significant interaction was found for MARP ($p<0.001$) (Figure 1) and CRPv ($p<0.001$), with a significant decrease in the 9yr old group from T1 to T2 (MARP: $p=0.008$, CRPv: $p=0.001$) and a significant increase from T2 to T3 (MARP: $p<0.001$, CRPv: $p<0.001$). For the elbow-wrist coupling, there was an increase in MARP ($p=0.014$) and CRPv ($p=0.011$) between T1 to T3 (MARP: $p=0.003$, CRPv: $p=0.008$) with no differences between ages and no interaction effects. No interaction or main effect differences were found for shoulder-elbow coupling.

Discussion: CT increased for the 9yr-old group over time, demonstrating alterations in movement strategy possibly altering performance. The hypothesis was partially supported with the shoulder-wrist pairing being the only joint couple that showed a significant interaction (Figure 1), likely because younger children struggle to coordinate two highly mobile joints in different planes [8] with the shoulder providing gross movement and the wrist aiding in hand position. Post-hoc tests revealed significant MARP (strategy) and CRPv (stability) changes for the 9yr-olds, who are likely in the transitional phase of motor control [9], meaning they are balancing feedback and feedforward strategies [5]. Feedback strategies result in reduced movement consistency, which would be reflected by significant changes in MARP and CRPv over time, and feedforward control would result in improved consistency [5]. This is also shown in the CT results, showing a strategy shift in 9yr-olds after T1, which changed their performance results more significantly than the other age groups. Additionally, motor development occurs proximal (shoulder) to distal (wrist) [10]. Therefore, 7yr-olds could rely on shoulder and elbow movements, resulting in consistent coordination over time, and 9yr-olds are shifting from the movement stability of the shoulder to exploration of wrist control, reflected in significant coordination changes. This suggests task-driven strategies in the older group that improve performance. Additionally, reduced coordination stability (lower CRPv) was not seen in 7yr-olds as expected, however, this could be due to the lack of feedback provided during the BBT.

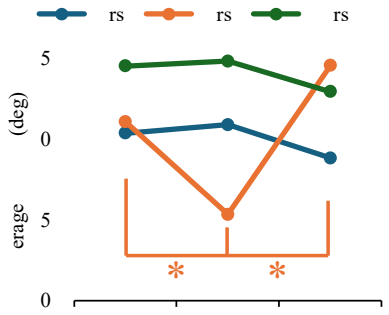

Figure 1. Average MARP for the shoulder-wrist coupling, with significant interactions indicated by corresponding colors. * p-value <0.05

Significance: These results demonstrate differences in motor control strategies in different age groups, which allows us to evaluate motor learning during development. Specifically, 9yr-olds show evidence of active motor learning with movement strategy adaptations and performance alterations. Additionally, this could guide age-specific functional training in clinical populations. Finally, the significant interaction only occurred for the shoulder-wrist coupling demonstrating that this coordination pairing might be a sensitive marker for motor learning development.

References: [1] Hogan et al. (1987), *Exerc Sport Sci Rev* 15; [2] Nemanich et al. (2025), *J Mot Behav* 57(1); [3] Hamill et al. (1999), *Clin Biomech* 14(5); [4] Denckla et al. (1974), *Dev Med & Child Neuro* 16(6); [5] Seidler et al. (2004), *NeuroImage* 22(4); [6] Mathiowetz et al. (1985), *Can J Occup Ther* 52(5) ; [7] Galgon et al. (2016), *J Sports Sci Med* 15(1); [8] Golenia et al. (2017), *Front Psychol* 8; [9] Ozmun et al. (2016), *Adapt. Phys. Ed. Sport. E* 6; [10] Cech et al. (2012), *W.B. Saunders*

SELF-ADAPTIVE PASSIVE HAND EXOSKELETON (SPHEX) FOR HOME-BASED TRAINING POST-STROKE

Thanh Phan[1,2], Mada Alghamdi[1,2], Mary Egwim[1,2], *Sang Wook Lee[1,2,3,4]

[1] Catholic University of America, Washington, DC; [2] National Rehabilitation Hospital, Washington, DC; [3] Korea Advanced Institute of Science and Technology, Daejeon, Korea; [4] Rehabilitation Medicine Department, National Institute of Health, Bethesda, MD.

*Corresponding author's email: leesw@cua.edu

Introduction: Severe hand impairments are commonly observed following stroke, such as flexor hypertonia and extensor weakness, which hinder functional independence [1]. These impairments significantly affect finger coordination and grasp control, often leading to alternative grip strategies [2]. Active robotic exoskeletons can provide intensive rehabilitation but are expensive, complex, and impractical for home use, limiting accessibility [3]. Conversely, passive hand devices can be used outside laboratory (i.e., home use), but they lack adaptability, as they generally provide fixed assistance patterns that do not adjust to individual impairment patterns [4]. We developed Self-adaptive Passive Hand EXotendon (SPHEX), a lightweight, portable exoskeleton that provides adaptive assistance using passive components. Unlike conventional passive devices, SPHEX adjusts assistance based on user intent, detected using force-sensitive resistors (FSRs), switching between grasp and release modes and counteracting angle-dependent flexor hypertonia [5].

Device Functionality and Design: SPHEX is designed to provide adaptive, subject-specific assistance, while allowing users to control its assistance pattern. It consists of a 3D-printed frame and two articulated segments designed to control the movements of the metacarpophalangeal (MCP) and proximal interphalangeal (PIP) joints (Fig. 1), which are actuated by two exotendons (ET_1 and ET_2) that replicate function of two muscles: ET_1 replicates the function of the extensor digitorum communis (EDC), assisting overall finger extension, and ET_2 the function of the intrinsic hand muscles (PIP extension & MCP flexion). The exotendon is pulled by elastic bands, whose tensions are controlled by two linear motors. ET_1 is controlled by the MCP joint movements, and ET_2 by the PIP joint movements.

Two FSRs are embedded on the device to detect user intent, enabling real-time mode switching between the Extension mode that increase exotendon tendon force along extension, and the Flexion mode that reduces assistance to allow users to grasp objects. Angle-dependent threshold values are determined based on differential FSR forces and the joint angle to account for the impact of passive force that changes along with movements. During extension mode, to counteract angle-dependent flexor hypertonia, the assistance level is increased dynamically during extension, and reduced during flexion. This ensures smooth and controlled hand movements while preventing excessive resistance during grasping.

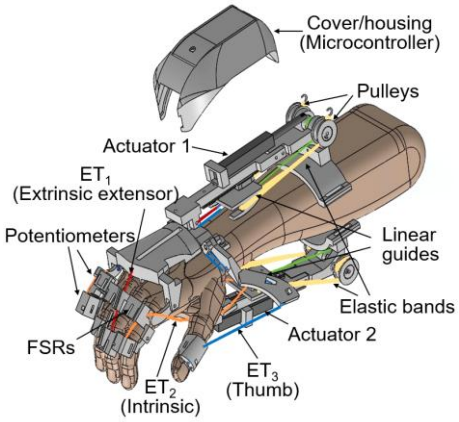

Figure 1: Overall schematics of Self-adaptive Passive Hand EXotendon (SPHEX) device.

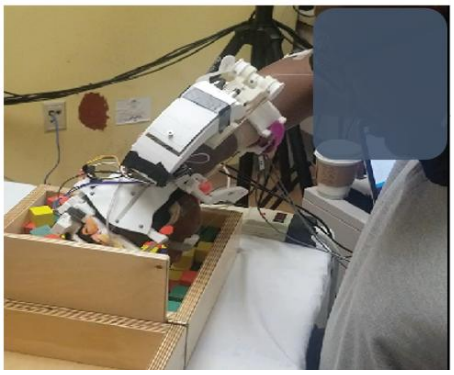

Figure 2: Stroke survivor (S3) performing box and block test with the assistance from SPHEx.

Methods and Results

(1) Experiment 1: Controller Performance Validation

Methods: Five healthy adults performed sequential flexion and extension movements of the PIP and MCP joints while wearing SPHEX. Motion capture, electromyography (EMG), and exotendon force data were recorded to evaluate mode switching and force modulation accuracy. **Results**: FSR-based intent detection successfully identified attempted flexion vs. extension movements in all 20 trials (5 subjects × 2 movements × 4 trials), and the average response times were 615±53ms (MCP) and 577±47ms (PIP). High correlation (mean r = 0.98) between movement intent and exotendon force adjustment (i.e., actuator excursion) confirmed proper modulation of assistance level.

(2) Experiment 2: Functional Assessment in Stroke Survivors

Methods: Eleven stroke survivors performed finger extension tasks and the Box and Block Test (BBT) with and without SPHEX assistance. A subset (n = 3) with intrinsic muscle weakness was tested under two conditions: extrinsic-only assistance (ET_1 activated) and balanced assistance (ET_1 + ET_2 activated).

Results: SPHEX improved finger extension (30° to 45°) and interjoint coordination (MCP-PIP correlation), and the BBT scores increased by +2.6±1.6 blocks (small blocks), +3.0±2.3 blocks (large blocks). Four participants who could not move blocks unaided completed the task with SPHEX. Balanced assistance (ET1+ET2) improved PIP extension with fewer elastic bands, optimizing movement efficiency. These findings confirm that SPHEX enhances functional movement and task performance in stroke survivors.

Conclusion: SPHEX provides adaptive, subject-specific assistance as it can detect user intent, counteracts hypertonia, and improve hand function. By enabling unsupervised home-based training, SPHEX has the potential to enhance accessibility and accelerate functional recovery. Future work will focus on automated calibration, thumb assistance, and long-term at-home studies.

Acknowledgments: This work was supported by National Institute on Disability, Independent Living, and Rehabilitation Research (90REMM0001).

References:[1] Carpinella et al. (2011), J Neuroeng Rehabil 8, 19. [2] García Álvarez et al. (2017), PLoS One 12, e0187608. [3] Lum et al. (2012), Am J Phys Med Rehabil 91, S242-S254. [4] Heo et al. (2012), Int J Precis Eng Manuf 13, 807-824. [5] Seo et al. (2010), Exp Brain Res 202, 891-901.

AGE-SPECIFIC ADAPTATIONS TO MENTAL FATIGUE IN DUAL-TASK WALKING OF VARYING COMPLEXITY

*Hang Qu[1,2], Jinfeng Li[1], Tim Derrick[1], Li-Shan Chou[1]
[1]Department of Kinesiology, Iowa State University, Ames, IA 50011
[2]Neurocognitive and Behavioral Development Laboratory, University of Florida, Gainesville, FL 32603
*Corresponding author's email: quhang116@ufl.edu

Introduction: Mental fatigue, a psychobiological state resulting from prolonged cognitive demands, could significantly impact both cognitive and motor performance in daily activities. While its effects on cognitive functions are well-documented, its influence on gait and balance control, particularly in older adults, remains incompletely understood. Recent evidence suggested that gait requires substantial cognitive resources and is particularly vulnerable to mental fatigue [1]. Previous studies reported that older adults often demonstrated altered gait characteristics and increased instability following mental fatigue compared to younger adults [2], and showed greater dual-task costs in both cognitive and motor domains [3]. This study investigated the differential effects of mental fatigue on cognitive performance and gait characteristics in young and older adults during single-task walking and dual-task walking with cognitive challenges. We hypothesized that: (1) mental fatigue would negatively affect cognitive performance in both age groups, with more pronounced effects in older adults; (2) gait characteristics would be altered following mental fatigue, with older adults showing greater changes particularly under dual-task conditions; and (3) center of mass movement patterns would demonstrate age-specific adaptations to mental fatigue during dual-task walking.

Methods: Twenty-eight participants (14 young: 7F/7M, 23.1±3.4 years, 1.74±0.11m, 70.0±15.1kg; 14 older: 7F/7M, 68.0±6.3 years, 1.74±0.09m, 73.2±14.1kg) completed cognitive and gait assessments before and after a 50-minute mental fatiguing protocol. Cognitive performance was evaluated using digit span tasks (sequencing: arranging numbers in ascending order; reverse: recalling numbers in reverse order) during seated conditions and while walking. Gait was assessed through spatiotemporal parameters (velocity, step length, stride width) and center of mass (CoM) movement during single-task normal walking and dual-task walking with concurrent digit span tasks. A three-way mixed-design ANOVA examined effects of Age (young vs. old), Time (pre-fatigue vs. post-fatigue), and Task (single vs. dual-task conditions) on the dependent variables of cognitive accuracy, gait velocity, and CoM peak velocities at critical gait events.

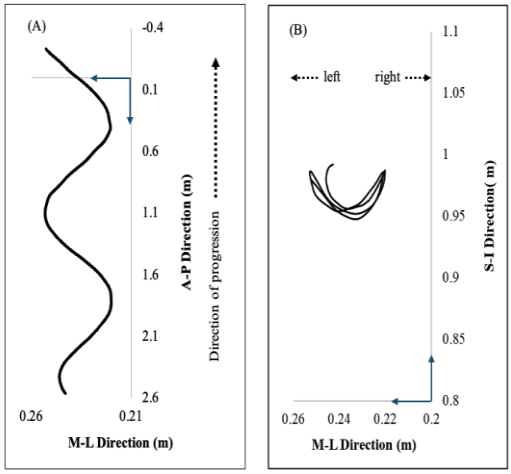

Figure 1: (A) corrected CoM trajectory in transverse plane during gait. (B) M-L CoM trajectories in frontal plane during walking.

Results & Discussion: Older adults, unexpectedly, showed a similar or enhanced performance in single-task sequencing (p=.036) and dual-task walking with reverse (p=.006) post-fatigue. While EEG evidence from our previous work confirmed the effectiveness of our mental fatigue protocol [5], these performance improvements suggest robust compensatory mechanisms rather than insufficient fatigue induction. The results likely reflect cognitive reserve activation and task-specific learning that counteracted fatigue effects [4]. Young adults increased their walking speed in dual-task conditions post-fatigue (sequencing: p=.004; reverse: p=.031), while older adults walked with a similar gait velocity across conditions. This suggests young adults adopted a more assertive walking strategy while older adults prioritized stability when mentally fatigued [1]. Step length also increased significantly for young adults under certain dual-task scenarios (e.g., normal walking with digit span sequencing, p=.003), whereas older adults showed fewer changes, underscoring different adaptation approaches. By contrast, stride width remained largely unchanged across conditions, implying that participants may not need to widen their base of support to preserve balance. The most noteworthy changes were observed in CoM velocity. A three-way interaction (Time × Task × Age) at both heel strike (p=.017) and toe-off (p=.002), demonstrating fundamentally different balance control strategies between age groups under mental fatigue. Young adults exhibited dynamic adaptations with significant increases in CoM velocity during normal walking (p=.001) and dual-task walking with reverse digit span task (p<.001) post-fatigue. In contrast, older adults maintained a similar CoM movement, revealing a conservative strategy prioritizing balance control. These findings challenged prevailing assumptions about age-related vulnerability to mental fatigue and suggested that healthy older adults might utilize different compensatory mechanisms to maintain performance during cognitively demanding conditions.

Significance: Our findings revealed that older adults can effectively use compensatory strategies to sustain both cognitive performance and gait balance under mental fatigue, suggesting individualized interventions may better target those who do exhibit fatigue-related deficits. Furthermore, the interplay between mental fatigue and dual-task walking underscores the necessity of multidimensional assessments—including CoM motion control—to fully capture age-specific adaptations and inform evidence-based fall-risk management.

References:

[1] Yogev-Seligmann G, et al. Mov Disord. 2008;23(3):329–342.
[2] Shortz AE, et al. J Neuroeng Rehabil. 2015;12:115.
[3] Beurskens R, Bock O. Neural Plast. 2012;2012:131608.
[4] Stern Y. Neuropsychologia. 2009;47(10):2015–2028.
[5] Qu H, et al. Med Sci Sports Exerc. 2024;56(10S):327–328.

DUAL-TASK REACTIVE BALANCE CONTROL IN OLDER ADULTS WITH MILD COGNITIVE IMPAIRMENT: THE EFFECT OF COGNITIVE TASK DOMAIN ON COGNITIVE-MOTOR INTERFERENCE

*Jessica Pitts[1], Lakshmi Kannan[1], Tony Szturm[2], Tanvi Bhatt[1]
[1] Department of Physical Therapy, University of Illinois at Chicago, 1919 W Taylor Street, Chicago, IL, USA, 60612
[2] Department of Physical Therapy, University of Manitoba, 771 McDermot Ave, Winnipeg, MB, Canada
*Corresponding author's email: jpitts5@uic.edu

Introduction: Older adults with mild cognitive impairment (OAwMCI) fall 2x more than cognitively intact older adults (CIOA) [1], which often occur while performing a simultaneous motor and cognitive task (i.e., dual tasking) [2]. Dual tasking can lead to cognitive-motor interference (CMI), which results in a deterioration in performance on either or both tasks compared single task [3]. Studies have shown that OAwMCI have higher CMI than CIOA [4], although primarily focused on volitional balance control (i.e., self-initiated movements), rather than reactive balance control (i.e., ability to recover from unpredicted perturbations). Further, it is unknown how different cognitive task domains (e.g., executive function, working memory, visuomotor) affect reactive balance control in OAwMCI, given the multi-domain decline observed in this population. This study compared how four cognitive tasks affected CMI during reactive balance control in OAwMCI vs. CIOA. We hypothesized that OAwMCI would have impaired reactive balance control compared to CIOA in both single task and dual task conditions, although would demonstrate higher CMI than CIOA, and might experience higher CMI for visuomotor tasks than executive function/working memory tasks due to pathology-related decline in visuomotor function [5].

Methods: This study included 38 OAwMCI (Montreal Cognitive Assessment (MoCA): 18-25) and 38 CIOA (MoCA ≥26) (67.7±6.5 yrs; 49 M/27 F). Anterior support surface perturbations were delivered via motorized treadmill in single task and while performing four different cognitive tasks, including two tasks in the visuomotor domain (Target, Track), the Auditory Clock Test (ACT) (visuospatial working memory domain), and the Letter Number Sequencing (LNS) (executive function domain). Cognitive tasks were also completed during unperturbed standing. Reactive balance performance (quantified via fall rate and margin of stability (MOS)) was compared between tasks (single task and four dual tasks) and groups (OAwMCI, CIOA) using a 5x2 Generalized Estimating Equation (GEE) (fall rate) or 5x2 mixed model ANOVA (MOS). 2x2 mixed model ANOVAs were used to compare cognitive performance between tasks (single vs. dual) and groups, and cognitive costs were calculated using the formula: [(single-dual)/single*100].

Results & Discussion: In both single and dual task conditions, OAwMCI had higher fall rate and lower MOS than CIOA ($p<0.05$, ***Fig. 1A***), which suggests that mild cognitive impairment may affect the ability to initiate and/or execute reactive balance responses. In both groups, reactive balance performance was most affected by visuomotor tasks (Target, Track) (**Fig. 1A**), which resulted in a mutual interference pattern (i.e., deterioration in both motor and cognitive performance, $p<0.05$). In comparison, the LNS resulted in motor-related cognitive interference (only cognitive performance deteriorates, $p<0.05$), and the ACT resulted in no interference ($p>0.05$). This suggests that visuomotor tasks may share greater cognitive resources with reactive balance control than executive function/working memory tasks. Lastly, cognitive costs were significantly higher in OAwMCI than CIOA for all tasks ($p<0.05$), with the largest group differences occurring for visuomotor tasks (**Fig. 1B**). OAwMCI may experience greater competition for resources/CMI than CIOA due to pathology-related reductions in the supply of available cognitive resources or difficulty allocating attention between the two tasks. Further, visuomotor tasks may be especially cognitively demanding for OAwMCI due to neural damage in areas responsible for visuomotor processing (e.g., parietal cortex, superior colliculus) [6].

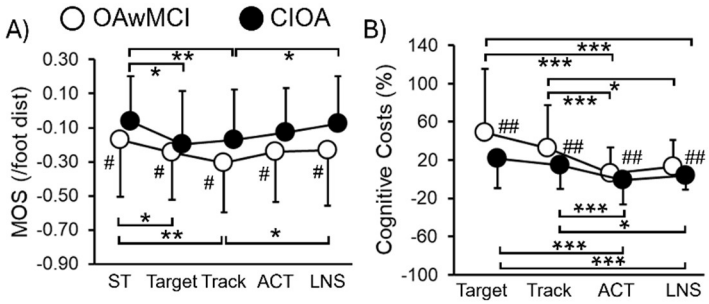

Figure 1: Post-perturbation margin of stability (MOS) (**A**) in older adults with mild cognitive impairment (OAwMCI) and cognitively intact older adults (CIOA) during exposure to a support surface perturbation in single task (ST) and four dual task conditions (Target, Track, Auditory Clock Test (ACT), Letter Number Sequencing (LNS)). Cognitive costs (**B**) are also shown for each task and represent the % change in cognitive performance between single task and dual task. # indicates significant between group difference; * indicates significant within group difference (task effect). */# $p<0.05$; **/## $p<0.01$; ***/### $p<0.001$.

Significance: Dual tasking during daily living can increase fall risk in both CIOA and OAwMCI by interfering with the ability to recover from unexpected, external perturbations. Visuomotor tasks may increase fall risk more than other types of tasks, and are often performed during daily living (e.g., monitoring traffic while crossing the road). Clinicians/researchers may consider incorporating these challenging cognitive tasks into fall prevention training paradigms for older adults, such as reactive balance training (e.g., perturbation-based training). Dual task reactive balance training could be especially beneficial for OAwMCI given their impaired performance in both single and dual task conditions.

Acknowledgments: This work was supported by NIH/NIA (R01AG073152), awarded to Tanvi Bhatt.

References: [1] Shirooka et al. (2018) *Aging Clinical & Exp Research*, 30; [2] Bergland et al. (1998), *Physiotherapy Research Int*., 3(3); [3] Plummer et al. (2013) *Archives of Physical Med & Rehab*, 94(12); [4] Zhou et al. (2023) *Frontiers, Aging Neurosci* 15; [5] Salek et al. (2011) *Eur. Neurology*, 6(5); [6] Barbeau et al. (2004) *Neurology*, 62.

IMPACT OF MILD COGNITIVE IMPAIRMENT ON DYNAMIC GAIT STABILITY IN OLDER ADULTS DURING OVERGROUND WALKING

Caroline Simpkins[1*], Diané Brown[1], Jiyun Ahn[1], Sara Mahmoudzadeh Khalili[1], and Feng Yang[1]
[1]Georgia State University
*Corresponding author's email: claubacher1@gsu.edu

Introduction: Falls are a significant health concern for older adults [1]. Mild cognitive impairment (MCI) is a transitional state between normal cognitive aging and dementia. People with MCI may have impaired balance, gait, and executive functions, which heightens their fall risk [2]. Dynamic gait stability is a novel method to measure a person's fall resistance [3]. Based on a conceptual framework (the Feasible Stability Region theory, or FSR; Fig. 1), dynamic gait stability is quantified by the kinematic relationship between the body's center of mass (COM) and base of support (BOS) [4]. It has been used to quantify dynamic balance in various populations. This study aimed to investigate how MCI affects dynamic gait stability during level walking at self-selected speed. We hypothesized that people with MCI would be less stable than healthy controls (HC) during overground gait due to the MCI-induced sensorimotor dysfunctions.

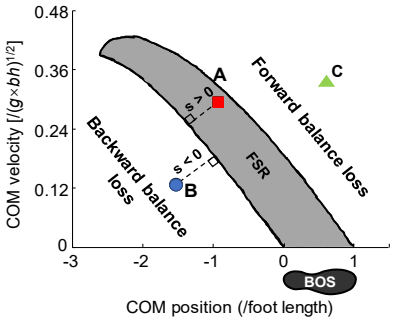

Fig. 1: FSR-based stability (*s*) is calculated as the shortest distance from the COM motion state to FSR's lower limit. The FSR, contained by two limits, represents all possible COM motion states which can maintain balance without altering the BOS (e.g., **A**). A COM motion state below the FSR (**B**) would result in a backward balance loss, and above (**C**) the FSR a forward balance loss.

Methods: Thirty-eight older adults were included: 18 people with MCI (age: 66.44 ± 5.89 years, body height: 1.73 ± 0.09 m, mass: 86.14 ± 18.47 kg) and 20 HC (66.85 ± 6.24 years, 1.69 ± 0.10 m, 73.82 ± 15.75 kg). MCI participants had a Montreal Cognitive Assessment (MoCA) score ≤ 25, and HC participants had scores ≥ 26. Twenty-six reflective markers were applied to participants' bony landmarks. Participants walked two times on an overground 10-meter walkway at their preferred speed. A 9-camera motion capture system (Vicon, UK) collected full-body kinematics from the reflective markers. The second walking trial was analyzed. The two gait events of touchdown (TD) and liftoff (LO) were identified from the foot kinematics. The body's COM kinematics were computed based on joint center data. The COM motion state's two components (velocity and position) were calculated relative to the BOS and normalized by the square root of the product of the body height (*bh*) and gravitational acceleration and the foot length, respectively. Dynamic gait stability (a unitless variable) was calculated as the perpendicular distance from the COM motion state to FSR's lower limit (Fig. 1). The primary outcome measure was dynamic gait stability at TD and LO. Secondary outcomes included COM position/velocity at TD and LO, step length, gait speed, and cadence. Step length was the fore-aft distance between the heels at their TDs. Gait speed was the average instantaneous COM velocity in the walking path's middle section. Cadence was the number of steps per minute. Step length and gait speed were normalized to *bh*. Independent *t*-tests compared normally distributed outcome measures between groups. Mann-Whitney *U* tests analyzed outcomes violating normality. Statistical analyses were performed using SPSS 29.0 (IBM, NY) with $\alpha = 0.05$.

Results & Discussion: Dynamic gait stability at TD ($p = 0.299$) and LO ($p = 0.185$, Table 1) was comparable between groups. COM position was more forward relative to the BOS in MCI than HC at TD ($p < 0.001$) and LO ($p = 0.012$, Table 1). COM velocity was slower in MCI than HC at TD ($p = 0.013$) and similar between groups at LO ($p = 0.109$, Table 1). Step length was shorter in MCI than HC ($p = 0.047$, Table 1). MCI walked at a slower speed ($p = 0.018$) with a lessened cadence ($p = 0.018$, Table 1) than HC. The results revealed people with MCI walked with a shorter step, slower speed, and lower cadence than HC. Despite differing spatial gait parameters, both groups showed comparable stability during walking at TD and LO.

Measurement	Group		*p*-value
	MCI	*HC*	
MoCA (/30)*	22.39 ± 1.82	27.65 ± 1.90	< 0.001
Stability at TD	0.05 ± 0.05	0.04 ± 0.04	0.299
Stability at LO	0.17 ± 0.04	0.16 ± 0.03	0.185
COM position at TD	-0.88 ± 0.18	-1.11 ± 0.11	**< 0.001**
COM position at LO*	-0.45 ± 0.18	-0.56 ± 0.08	**0.012**
COM velocity at TD*	0.29 ± 0.06	0.32 ± 0.04	**0.013**
COM velocity at LO*	0.31 ± 0.06	0.33 ± 0.04	0.109
Step length (/*bh*)	0.37 ± 0.05	0.39 ± 0.02	**0.047**
Gait speed (/*bh*)*	0.67 ± 0.13	0.75 ± 0.01	**0.018**
Cadence (steps/min)*	108.6 ± 10.1	115.6 ± 12.1	**0.018**

Table 1: Primary and secondary outcome comparisons (mean ± SD) between MCI ($n = 18$) and HC ($n = 20$). *: M-W *U* used.

Significance: Our study suggests that older adults with MCI show a cautious gait pattern, but similar stability compared to older people with normal cognition when walking overground at a self-selected speed. These findings provide insight into dynamic stability control among people with MCI during gait and expand our understanding of the control of the dynamic gait balance of human locomotion across populations. It is meaningful to inspect how more advanced cognitive impairment stages impact dynamic gait stability in older adults.

Acknowledgments: This study was partially supported by the National Institutes of Health (1R21-AG077307-01) and the Alzheimer's Association (AARG-NTF-21-852145).

References: [1] James et al. (2020), *Inj Prev* 26. [2] Racey et al. (2021), *BMC Geriatrics* 21(1). [3] Yang et al. (2009), *J Biomech* 42. [4] Yang et al. (2007), *J Biomech* 40.

DOES ADDING A SECONDARY TASK WHILE WALKING ALTER MARGIN OF STABILITY?

Doug Mitchell[1], *Frankie Wade[1]
[1]Biomechanics and Aging Mobility Lab, San Diego State University, USA
*Corresponding author's email: fwade@sdsu.edu

Introduction: Walking requires the full functioning and integration of visual, vestibular, cognitive, and musculoskeletal systems. Activities of daily living necessitate the simultaneous performance of a physical task, such as walking, and a secondary task – whether that is cognitively demanding, such as talking, or physically demanding, such as tray carrying. Those who are unable to successfully perform a simultaneous task while walking are at much greater risk of falls [1]. While the effect of adding a secondary cognitive or motor task to spatiotemporal gait parameters has been established, similar investigations on the instantaneous mechanical stability of walking are missing. Thus, we analyzed margin of stability during the performance of three walking tasks – 1) walking at preferred walking speed, 2) walking while performing a simultaneous cognitive task, 3) walking while performing a simultaneous physical task in adults without mobility restriction. We hypothesized that the addition of a secondary task would increase both anteroposterior (AP) and mediolateral (ML) margin of stability in comparison to the single task walking condition.

Methods: Sixteen adults (age = 41±5 years; height = 1.73±.03m) walked on a single-belt treadmill (Treadmetrix) at their preferred walking speed (BASE), using a previously documented protocol [2], while 9 motion capture cameras (Qualysis) captured the positions of 32 retroreflective markers placed according to a modified Helen Hayes marker set. For the cognitive condition (COG), participants walked while performing a visual-verbal Stroop test, with the screen placed 8ft from the treadmill. For the motor condition (PHY), participants carried a 15lb box (41.9 x 21.6 x 10.75 cm), chosen to replicate the physical demand of carrying a load of laundry or a bag of groceries. Each task lasted 3 minutes, of which the central 2 minutes was used for analysis. All participants provided written consent prior to data collection and were screened for colour-blindness. Margin of stability was calculated using an extrapolated center of mass [3], with the base of support defined by a marker placed on the calcaneus (ML) and 1st metatarsal head (AP). To explore the effect of trial on margin of stability, a repeated measures ANOVA was conducted in SPSS, with $\alpha = 0.05$. All findings are reported as mean ± standard error.

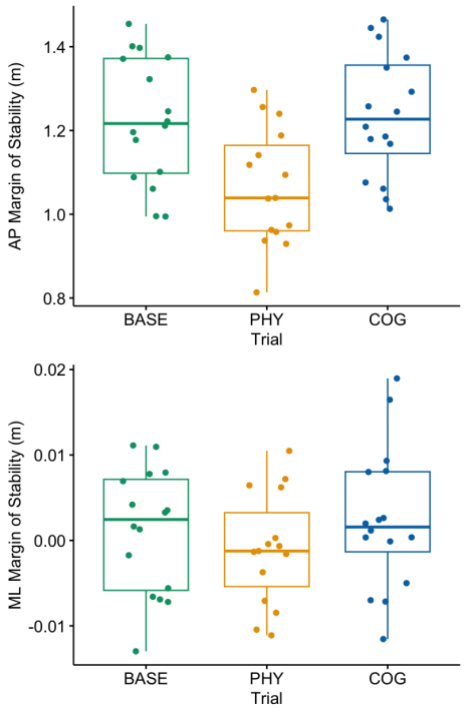

Figure 1: Margin of Stability for baseline (BASE), motor (PHY), and cognitive (COG) tasks in both anterior-posterior (AP, top) and mediolateral (ML, bottom) directions.

Results & Discussion: In partial agreement with our hypothesis, we observed significant reductions in AP margin of stability in the PHY trials compared with both BASE (-.176±.021 m, $p < .001$) and COG (-.186±.024 m, $p < .001$) trials (Fig. 1). This is unsurprising given the box weight was carried anterior to the body, thus moving the center of mass closer to the leading foot. Participants also took shorter steps during PHY (mean difference: .027±.009, $p = .035$) compared with the BASE trial, further reducing the AP margin of stability. When individuals carry loads in daily life, this shifts their center of mass, reducing the margins for displacement and increasing the risk of instability.

Perhaps more surprisingly, there were no differences in ML margin of stability between any trials (all $p \geq .124$; Fig. 1), contrary to our hypothesis. We anticipated that the additional attention required to successfully perform a secondary task would impede walking function, increasing ML instability. A possible explanation was that our secondary tasks were insufficiently challenging for participants. To assess this, we computed the change in accuracy in visual-verbal Stroop performance. We observed a significant reduction in Stroop accuracy from sitting to walking (mean change: 18.1±7.0 %, $p = 0.02$) suggesting that this was a meaningful cognitive load for our participants. While we did not collect ratings of perceived exertion for the PHY task, participants commented on how challenging it was to perform the task. Further limiting our ability to detect the influence of secondary task on stability during walking could be that our participants were healthy and active, with physical activity levels of 11,240 ± 2345 MET-mins per week. However, their average BASE speed on the treadmill was slow (.99±.06 m/s). Our participants may have chosen a slower walking speed to feel more stable initially and have sufficient redundancy in their margins of stability to not need any change with the addition of the secondary task. It would be interesting to replicate this work in older adults at increased risk of falls.

Significance: Our findings suggest that margin of stability during walking is not impacted by simultaneous cognitive tasks but may be by a simultaneous motor task. These findings are important to consider when evaluating an individual's fall risk in activities of daily living and suggest the inclusion of both motor and cognitive dual tasking in assessments of mobility.

Acknowledgments: This work was supported by SDSU Seed Grant Funding (2023-24) and the help of Farah Basmagi was invaluable to data collections.

References: [1] Beauchet et al. (2009), *Eur J Neruo* 16(7); [2] Dingwell & Marin (2006), *J Biomech* 39(3); [3] Hof et al. (2005), *J Biomech* 38(1).

MODELING BRAIN CONNECTIVITY AS A MEDIATOR OF DUAL-TASK PERFORMANCE: PILOT WORK

Jack Manning[1*], Jessica Bernard[2], Joseph Orr[2], Jennifer Yentes[1]
[1] Human Movement Complexity Laboratory; Department of Kinesiology and Sport Management, Texas A&M University
[2]Department of Psychological & Brain Sciences, Texas A&M University
*Corresponding author's email: jackpmanning@tamu.edu

Introduction: The ability to perform a motor task and a cognitive task concurrently, known as dual-tasking, is important for everyday life [1]. Dual-tasking tends to result in poorer performance on either the cognitive, motor, or both tasks. Similarly, aging also tends to result in a degradation of the ability to perform cognitive and motor tasks, both individually and concurrently. Connections from the prefrontal cortex to the striatum (i.e. cortico-striatal), a part of the basal ganglia, are known to be important in both motor and cognitive behaviors. Cortico-striatal functional connectivity has been shown to decrease with advanced aging, reaching a peak in young adulthood and beginning to decline as early as middle age. Dysfunction in cortico-striatal networks has been shown to contribute to both cognitive and motor deficits [2]. Degeneration of the dopaminergic system is thought to be one of the primary reasons for the loss of functional connectivity in the cortico-striatal pathways, which may lead to decrements in both motor and cognitive function [3][4]. As a result, there is typically an increase in activation intensity in regions associated with motor or cognitive tasks being performed, along with activation in regions not typically associated with those tasks [5]. Essentially, more resources are required for older adults to do the same task as a young adult, pushing the older adults closer to their maximal capacity. Understanding the relationship between underlying brain processes and dual-tasking is critical, as it could reveal underlying mechanisms in motor and cognitive decline related to aging. The central hypothesis is that a cognitive task which utilizes the same cortico-striatal network as a motor task should result in a decrement in performance when both are being completed simultaneously during a dual task.

Methods: Eleven older adults were asked to walk on a treadmill at a self-selected speed during four randomized trials: 1) single-task, 2) set-shifting, 3) number naming, and 4) letter naming. During all cognitive tasks, a letter-number combination (e.g. V7) appeared on the screen with either a blue or orange background. If the background was blue, they were asked to verbalize the number; if it was orange, the letter. During set-shifting the background changed randomly, while during number and letter naming the background stayed the same. Each trial was two-minutes in duration, with each prompt appearing for two-seconds. Cognitive task reaction time during the dual-task walking trials was calculated.

During a second visit, structural and functional magnetic resonance images of subject's brains were collected. fMRI data were pre-processed using fmriprep, then processed in CONN Toolbox. Resting-state functional connectivity was assessed by computing the correlation coefficient between the dorsal caudate and the medial prefrontal cortex, which was then Fisher-transformed into a Z-score. To test the hypotheses: 1) simple linear regression was used to determine the direct effect of dual-task on reaction time and 2) a mediation analysis was used to determine the indirect effect of dual-task on cognitive task reaction time with cortico-striatal functional connectivity as a mediator (Fig. 1).

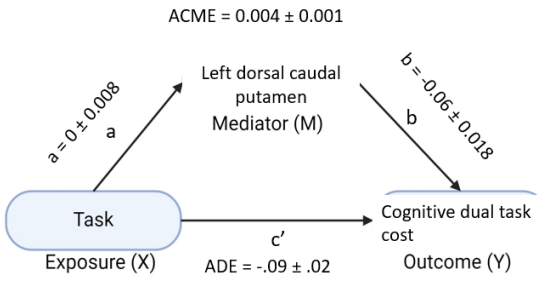

Figure 1: Standard three-path mediation analysis results. Connectivity of the left dorsal caudal putamen (DCP) to the right inferior frontal gyrus pars triangularis (IFGt) does not significantly mediate the relation between task condition and dual-task performance. ACME, average causal mediation effect; ADE, average direct effect. The β ± standard error path coefficients are shown.

Results & Discussion: The simple linear regression indicated a significant relationship between cognitive task and reaction time (β=-0.09, p<0.001). Results of the causal mediation analysis indicate: 1) there is a significant average direct effect of dual-task on cognitive task reaction time (β=-0.09, p<0.001), but 2) there is no average causal mediation effect of dual-task on cognitive task reaction time through cortico-striatal connectivity (β=0.00002, p=0.86). The strength of the resting-state functional connectivity network was used as a proxy for task-related engagement, however, functional connectivity during dual-task performance might differ from resting-state connectivity. It has been shown previously that this connectivity is important for the set shifting task [2]. However, older adults may rely on the activity of alternative brain regions to complete tasks [1]. Thus, it is possible that other networks (e.g. fronto-parietal network) may play a significant role in set shifting tasks if the cortico-striatal network loses its function.

Significance: This study successfully demonstrates a direct dual-tasking cost in cognitive reaction time but fails to support the hypothesis that cortico-striatal connectivity mediates this effect. This raises important factors for future research to consider, such as task-based connectivity and alternative networks, which may be better indicators of dual-task processing in older adults.

Acknowledgments: This work is support by a research SEED grant provided by the Texas A&M School of Education and Human Development's Department of Kinesiology and Sport Management, and a Graduate Research Grant provided by the Sydney and J.L. Huffines Institute for Sports Medicine and Human Performance at Texas A&M University.

References: [1] Leone, C. *et al. Neuroscience & Biobehavioral Reviews* **75**, 348–360 (2017). [2] Bissonette, G. B., Powell, E. M. & Roesch, M. R. *Behavioural Brain Research* **250**, 91–101 (2013). [3] Bell, P. T., Gilat, M. & Shine, J. M. *Brain* **140**, 1174–1177 (2017). [4] Esteban, O. *Nature Protocols* **15**, (2020). [5] Bo, J. *et al. Brain Connectivity* **4**, 166–180 (2014).

CANONICAL CORRELATION ANALYSIS OF MOTOR FUNCTION AND COGNITION

*Haley B. Hentnik[1], Christine B. Phillips[2], Abigail T. Stephan[2], Lesley A. Ross[2], Reed D. Gurchiek[1]
[1]Clemson University, Dept. of Bioengineering, [2]Clemson University, Dept. of Psychology
*Corresponding author's email: hhentni@clemson.edu

Introduction: Declining motor function is a signature feature of aging and is associated with multiple impairments in older adult populations. For instance, reduced gait speed, loss of muscle strength, and reduced balance and dexterity is present in up to 50% of people 65 years or older [1]. Moreover, previous literature suggests that motor decline is prevalent in populations that concurrently exhibit cognitive impairment [2]. While slow and declining usual gait speed can precede the clinical presentation of Alzheimer's disease (AD) by 12 years [2], these gross metrics lack specificity as a digital biomarker for early detection [3]. For example, slow gait speed may result from sarcopenia, cardiovascular dysfunction, or increased metabolic cost of walking. A distinct relationship between cognitive impairment and gait may manifest more strongly in metrics quantifying gait quality and motor control. While identifying this relationship will facilitate development of new digital biomarkers that augment early detection efforts in AD, the complex nature of both gait and cognition complicates their discovery. This study aimed to quantify the multifactorial relationship between cognitive and motor function through canonical correlation analysis. Furthermore, we investigated two categories of metrics quantifying motor function: those characterizing maximal capacity (e.g., maximal strength, maximal gait speed) and those characterizing typical gait.

Methods: Eighty-five middle-age and older adults (average age: 66 years, range: 41-91 years) were assessed on their cognitive and physical function across multiple tests. Cognitive performance was evaluated using the Useful Field of View test (UFOV, subtest 2 for divided attention and subtest 3 for selective attention) and the TestMyBrain (TMB) battery of neuropsychological evaluations. Metrics describing typical gait consisted of usual gait speed and gait similarity, symmetry, smoothness, and stability collected from a sacrum-worn accelerometer (McRoberts MoveTest) [4,5,6]. Metrics describing maximal capacity included maximum gait speed, hand grip strength, timed up-and-go time (TUG), and 5x sit-to-stand time (STS). We performed two canonical correlation analyses (CCA) to determine the relationship between cognition and typical gait and separately between cognition and maximal capacity. This approach identifies a typical gait profile (linear combination of typical gait variables) and a maximal capacity profile that is maximally correlated with a cognition profile. We used the Pearson correlation coefficient to quantify the influence of each variable on the overall profiles.

Results & Discussion: The typical gait profile was more strongly correlated with cognition ($r = 0.70$, $p < 0.01$) than was the maximal capacity profile ($r = 0.57$, $p < 0.01$). While all gait variables contributed to the typical gait profile except gait similarity, gait smoothness had the strongest influence ($r = 0.69$), including more than usual gait speed ($r = 0.42$). The primary metric driving the cognition profile as related to the typical gait profile was divided attention ($r = -0.78$). Likewise, both divided and selective attention (UFOV subtests 2 and 3) had a strong influence on the cognition profile in the relationship with maximal capacity ($r = 0.66$, $r = 0.64$). These results add to the growing body of literature suggesting similar relationships between visual-spatial processing and attention with gait in individuals with mild cognitive impairment. The maximal capacity profile was driven primarily by maximal speed ($r = -0.94$) which further supports the potential for gait analysis to augment screening for cognitive impairment.

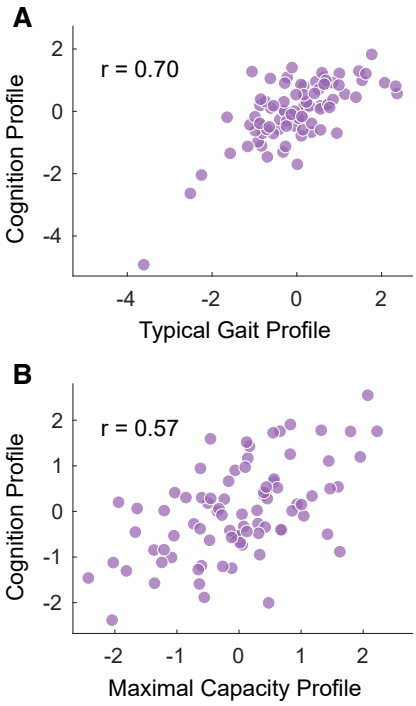

Figure 1: Correlation between cognition profile and typical gait profile (A) and correlation between cognition profile and maximal capacity profile (B).

Significance: These findings suggest that while gait speed may play an important role in predicting cognitive decline, including other measures of gait quality and control could improve the specificity of gait-based digital biomarkers of cognitive impairment. In this context, future research should explore free-living gait analysis given the relationship between cognitive performance and typical gait measures observed in this study. These digital biomarkers could augment other biomarker modalities (e.g., from neuroimaging and phlebotomy) toward improving early detection of AD.

Acknowledgments: This work was supported by Prisma Health Upstate, the Carolina Center on Alzheimer's Disease and Minority Research, the South Carolina Alzheimer's Disease Research Center (SC-ADRC) through the SC Department of Health and Human Services (A202400071A), the NIH (SC-INBRE DRP, P20GM103499), and the Clemson University Dept. of Bioengineering.

References: [1] Buchman & Bennet (2011), *Expert Review of Neurotherapeutics* 11(5); [2] Buracchio et al. (2010), *Archives of Neurology* 67(8); [3] Jayakody et al. (2022), *Journals of Gerontology: Medical Sciences* 77(6); [4] Lamoth et al. (2002), *Gait & Posture* 16(2); [5] Rispens et al. (2015), *JMIR Research Protocols* 4(1); [6] van Schooten et al. (2015), *Journals of Gerontology: Biological Sciences and Medical Sciences* 70(5)

SEX-BASED MACHINE LEARNING MODELS FOR PREDICTION OF ABDOMINAL AORTIC ANEURYSM PATIENT OUTCOMES

Katherine E. Kerr[1], Pete H. Gueldner[1], Indrani Sen[2], Tiziano Tallarita[2], Joseph C. Wildenberg[3], Nathan L. Liang[1,4,5], David A. Vorp[1,4,6-13], Timothy K. Chung[1,10]

[1]Department of Bioengineering, University of Pittsburgh, Pittsburgh, PA, USA [2]Division of Cardiovascular Surgery, Mayo Clinic Health Systems, Eau Claire, Wisconsin, USA [3]Division of Interventional Radiology, Mayo Clinic Health Systems, Eau Claire, Wisconsin, USA [4]Department of Surgery, University of Pittsburgh, PA, USA [5]Division of Vascular Surgery, University of Pittsburgh, Pittsburgh, PA, USA [6]School of Medicine, University of Pittsburgh Medical Center, Pittsburgh, PA, USA [7]McGowan Institute for Regenerative Medicine, University of Pittsburgh, Pittsburgh, PA, USA [8]Department of Chemical and Petroleum Engineering, University of Pittsburgh, Pittsburgh, PA, USA [9]Department of Cardiothoracic Surgery, University of Pittsburgh, Pittsburgh, PA, USA [10]Clinical & Translational Sciences Institute, University of Pittsburgh, Pittsburgh, PA, USA [11]Department of Mechanical Engineering and Materials Science, University of Pittsburgh, Pittsburgh, PA, USA [12]Center for Vascular Remodeling and Regeneration, University of Pittsburgh, Pittsburgh, PA, USA [13]Magee Women's Research Institute, University of Pittsburgh, Pittsburgh, PA, USA

*Corresponding author's email: kak488@pitt.edu

Introduction: Abdominal aortic aneurysm (AAA) is an abnormal focal dilatation of the infrarenal aorta. Although mostly asymptomatic, AAA has up to a 90% mortality rate when ruptured [1]. Despite having a lower AAA prevalence than men, women experience AAA rupture at a rate 3-4 times higher than their male counterparts. Additionally, female patients have higher surgical and post-operative mortality compared to male patients [2]. When a clinician diagnoses AAA, they will proceed based on the maximum transverse diameter, the current gold standard. However, it has been shown that AAA can rupture below the maximum transverse diameter threshold [3]. Our group has shown that AAA patient outcomes can be predicted with better discriminability than maximum transverse diameter using a machine learning (ML) model comprised of clinical, morphological, and biomechanical indices [4]. However, no sex-based differences were accounted for in this model. In this work, we train sex-specific models on only female or male patients and compare them to a general model comprising all patients. Due to the differences in patient outcomes between male and female patients, we expect that training sex-specific models will produce models that have higher discriminability than a general model.

Methods: Patient scans were acquired from University of Pittsburgh Medical Center and Mayo Clinic Health Systems. In total, there were 537 patients, 159 of which were female and 378 of which were male. Segmentation was performed using an automated U-NET classifier. Morphological and biomechanical indices were extracted using an in-house pipeline [4]. Morphological indices were comprised of one-, two-, and three-dimensional indices. Biomechanical indices were comprised of various wall stresses. ML models were trained in MATLAB. The data was split for 20% holdout testing five times to ensure reproducibility in accuracies and area under the receiver-operating characteristic curve (AUC). Due to a smaller number of patients experiencing rupture and clinical intervention in this cohort, these cases were pooled into one "unstable" category, with the assumption that the risk of rupture exceeds the risk of repair for patients who underwent intervention. Feature importance was assessed using Gini feature importance. All accuracies and AUC values reported are from the highest performing model in the testing group.

Results & Discussion: Accuracies and AUC values for the general model and sex-specific model can be seen in **Table 1**. Predictions for both sex-specific models outperformed the predictions for female or male patients in the general model, respectively. All models outperformed maximum transverse diameter. This was consistent with our hypothesis. Looking at the feature importance for this model, we found that there were more biomechanical indices in the top 15 features for the male and general model compared to the female model.

Table 1: Accuracy and AUC values for various trained models as well as diameter. Both the female-specific and male-specific models outperformed the female patients and male patients in the general model, respectively. All models outperformed diameter in predicting patient outcome (stable or unstable)

	Diameter	**General Model**	**Female Model**	**General Model – Female Patients**	**Male Model**	**General Model – Male Patients**
Accuracy	73.0%	77.6%	87.1%	86.2%	74.7%	73.6%
AUC	0.741	0.887	0.946	0.838	0.890	0.775

Significance: Historically, female patients have been understudied in AAA biomechanics, despite having higher rupture rates relative to their male counterparts. In developing ML models, it is important to study potential biases that may arise due to the demographic makeup of your dataset. In this study, we show that striating patients based on sex produces better accuracies and AUCs than a general model and that there were differences in the features prioritized between these models. As ML models are implemented into clinical settings, assessing their generalizability and biases becomes more and more important.

Acknowledgments: This work was supported by the International Society of Women Vascular Surgeons, the Jewish Healthcare Foundation, the Chancellor's Gap Fund, and the Pitt Innovation Challenge. KEK and PHG receive fellowship funding from the NSF.

References: [1] Brown et al. (1990), *Ann Surg* 230(3):289 [2] Malayala et al. (2020), *J Clin Med* 12(12): 794-802
[3] Vorp (2007) *J Biomech* 40(9): 1887-1902 [4] Chung et al. (2024) *Sci Rep* 14(1): 3390

GENERALIZABLE DEEP LEARNING MODEL ENABLES PREDICTION OF FUTURE PHYSIOLOGICAL STATES DURING PERTURBED LOCOMOTION

Sofia Arvelo Rojas[1*], Jennifer K. Leestma[2], Gregory Sawicki[1], Aaron Young[1]
[1]Georgia Institute of Technology, Atlanta, GA
[2]Harvard University, Cambridge, MA
*Corresponding author's email: s.arvelorojas@gatech.edu

Introduction: Falling is the leading cause of injury related death in older adults [1]. Exoskeletons have the potential to augment balance to reduce fall rate, however, classical control strategies are hand engineered and often rely on the cyclic nature of locomotion and are therefore not well suited for transient movements. Recently, a deep learning-based task-agnostic controller based on the user's physiological state was shown to decrease metabolic cost across cyclic and non-cyclic tasks, showing this controller's ability to generalize [2]. However, the effectiveness of this approach for perturbation recovery has not been investigated. We anticipate that the timing of joint moment-driven exoskeleton assistance will differ for approaches that aim to augment balance. Metabolic cost-reducing approaches apply joint moment assistance that is delayed relative to the user's joint moment, while faster-than-human assistance has proven beneficial for balance augmentation [3][4]. The aim of this study is to (1) optimize a deep learning model that predicts future joint moments, enabling faster-than-human control and (2) investigate the ability of this model to generalize to perturbation conditions outside of the training set, to test the robustness of our approach in handing novel perturbations. We hypothesized that (1) estimation accuracy will decrease as forecasting increases and (2) estimation accuracy will be lower for held-out-conditions.

Methods: We collected a training data set of able-bodied individuals (N=17) undergoing translational ground perturbations. The perturbation trials systematically varied perturbation magnitude, onset timing, and direction (Fig. 1A). We collected motion capture, force plates, and inertial measurement unit (IMU) data. We calculated inverse dynamics to obtain frontal and sagittal plane hip moments. The full experimental protocol has been previously described by Leestma et al. [3]. We trained a series of temporal convolutional networks (TCN) that used wearable IMUs (pelvis, torso, and bilateral dorsal foot, shank, thighs) to predict joint moments. First, we trained models that forecasted joint moments 0ms (estimation at current time), 40ms, 80ms, and 120ms into the future. We also conducted a leave-n-conditions-out validation where we held out pairs of directions to test the ability of the models to generalize to unseen perturbation conditions. We computed the estimation accuracy using R^2 and root mean square error (RMSE).

Results & Discussion: As hypothesised, model accuracy decreased as forecasting increased. This is expected as sensor input data is further away from the outcomes we are estimating. Still, most average R^2 values for estimating hip moment across forecasting times were above 0.80 except for frontal plane at our furthest forecasting (Fig. 1B). This accuracy has been previously shown to allow for highly controllable exoskeletons [2]. Contrary our second hypothesis, we found that estimation accuracy was similar when conditions were held out compared to when the full training set was used (Fig. 1C). This might be due to the similarity between the held-out conditions and the ones still included in training. This effectively shows our model's ability to generalize to unseen perturbation directions.

Future work will (1) deploy our forecasting estimators to control a 2-degree-of-freedom hip exoskeleton and (2) further explore the generalizability of our model by excluding different groups based on perturbation magnitude and timing.

Significance: We demonstrate (1) deep learning models can reliably estimate future physiological states which enables faster-than-human exoskeleton assistance and (2) our model can generalize to unseen perturbations. Together, this type of controller shows potential to assist perturbed locomotion in highly dynamic real-world environments.

Acknowledgements: This project was funded by NIH Director's New Innovator Award DP2-HD111709 and Georgia Tech's IRIM student fellowship.

References: [1] Kakara et al. (2023), *MMWR Morb Mortal Wkly Rep;* [2] Molinaro & Scherpereel et al. (2024), *Nature;*[3] Franks et al. (2021), *Wearable Technologies;* [4] Beck et al. (2023), *Science Robotics;* [5] Leestma et al. (2023), *J. Exp Biol.*

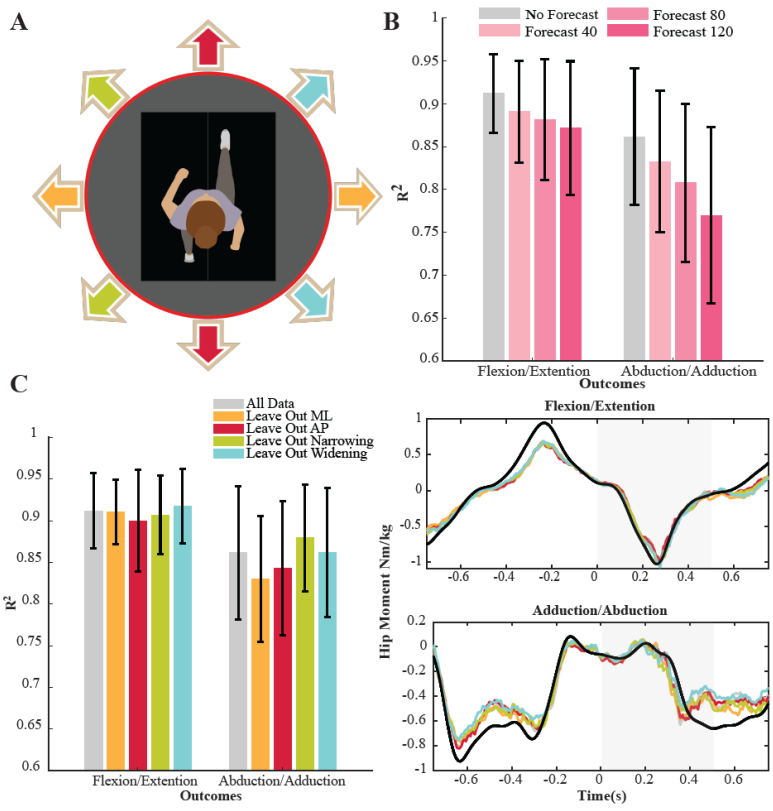

Figure 1: (A) Platform translations were delivered in the mediolateral and anterior posterior directions as well as the respective diagonals. (B) Joint moment estimation R^2 across forecasting times. (C) Joint moment estimation R^2 for direction pairs excluded for the training set. Time series plots show ground truth (black) and estimated (colors) joint moment for a representative trial for the excluded direction pairs. The perturbation happens at time 0 and the shaded area represents the proposed exoskeleton actuation window.

A HYBRID MACHINE LEARNING AND PHYSICS-BASED SIMULATION APPROACH FOR PREDICTING MUSCULOSKELETAL DYNAMICS FROM VIDEO-BASED KINEMATICS

*Emily Y. Miller[1], Tian Tan[2], Scott D. Uhlrich[1]
[1]University of Utah Mechanical Engineering Department, [2]Stanford University Department of Radiology
*Corresponding author's email: Emily.Y.Miller@utah.edu

Introduction: Recent advancements in computer vision and computational biomechanics enable the estimation of motion and musculoskeletal dynamics from video data, enabling injury risk prediction, personalized rehabilitation, and outcomes assessment. For instance, we developed OpenCap, open-source software that estimates 3D motion and musculoskeletal dynamics from two smartphone videos[1]. OpenCap computes kinematics from video, then generates muscle-driven simulations to estimate musculoskeletal dynamics from the kinematics data alone (i.e., without a force plate)[2]. This simulation-based approach yields dynamics estimates that are physically and physiologically plausible, and it is generalizable across varied activities, pathologies, and metrics. However, this flexibility can come at the cost of accuracy on downstream tasks. For example, while OpenCap accurately estimates the knee adduction moment (R^2=0.8), it is less accurate at predicting medial knee contact force (errors of 0.94 bodyweights)[1]. End-to-end machine learning (ML) models can accurately predict quantities like knee loading from video[3–5]; however, they require large, pathology- and activity-specific datasets, thus lacking generalizability. A hybrid ML and physics-based simulation approach could combine the accuracy of ML with the generalizability of simulations, addressing these limitations. The purpose of this study was to develop a hybrid ML-simulation framework for predicting musculoskeletal dynamics from video-based kinematics. We hypothesize that ground reaction forces (GRFs) and joint moments predicted using the hybrid approach will be more accurate than those estimated from both simulation and ML alone.

Methods: We evaluated three approaches for predicting musculoskeletal dynamics using two-camera OpenCap walking kinematics as input: a simulation-based method, a machine learning (ML) + inverse dynamics approach, and a hybrid ML-simulation method. We compared all approaches to an inverse kinematics and inverse dynamics approach using lab-based marker-based motion capture and force plate data[1,6]. The simulation-based approach generated muscle-driven dynamic simulations that tracked video-based kinematics while modelling foot-floor contact using a Hunt-Crossley contact model[1,2]. For the ML approach, we trained a transformer model the AddBiomechanics dataset (n=178 individuals) to predict GRFs and centers-of-pressure from kinematics, which were then used as input for inverse dynamics to estimate joint moments[7]. The hybrid ML-simulation approach incorporated the same simulation framework as the simulation-only method, but it incorporated a cost term to track the ML-predicted GRFs. To assess performance, we evaluated GRFs and joint moments across 15 lower-extremity degrees of freedom using mean absolute error (MAE) and conducted statistical comparisons using a one-way ANOVA. We performed post-hoc pairwise comparisons using Tukey HSD tests to identify significant differences between methods (α=0.05).

Results & Discussion: Compared to the simulation approach, the ML approach had more accurate GRF estimates ($p<0.001$; Figure 1a) but less accurate joint moment estimates ($p<0.001$; Figure 1b). This was largely due to inaccuracy in ML-based center-of-pressure predictions. The hybrid approach also estimated GRFs more accurately than simulation alone ($p=0.004$), and it was not significantly different from the ML approach ($p=0.14$). Joint moments were more accurate for the hybrid approach compared to ML approach ($p<0.001$) and similar between hybrid and simulation only ($p=0.75$).

Our hypotheses were not entirely confirmed. The hybrid approach was not more accurate than both the simulation and ML approaches for both joint moments and GRFs. However, it offered the greatest balance of accuracy across both metrics. While ML had the most accurate GRF estimates, it had the worst joint moment estimations, potentially because the combined GRF and kinematics estimates were not constrained to be physically consistent (i.e., pelvis residuals are allowed in inverse dynamics). Our simulation formulation does not allow pelvis residuals, and thus both our simulation and hybrid approaches produce physically consistent kinematics and GRFs. The hybrid approach effectively balances ML's data-driven strengths with simulation-based models' physical constraints, ensuring both likely and physically consistent dynamic estimates. Further improvements to center-of-pressure accuracy are needed for the hybrid approach to realize improvements in joint moment accuracy that should correspond to more accurate GRFs.

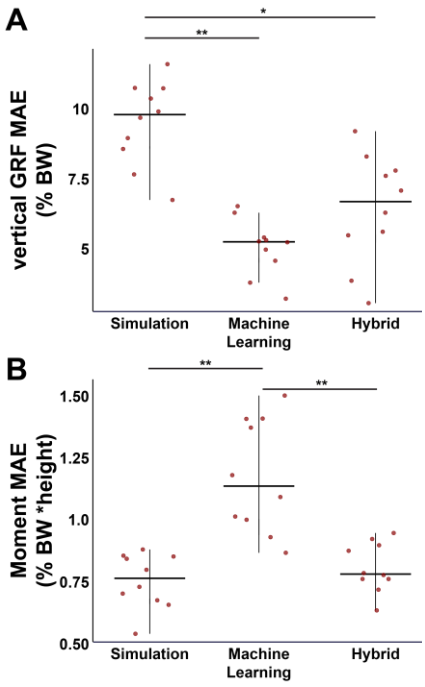

Figure 1: (A) The machine learning (ML) and hybrid ML/simulation approaches more accurately predicted ground reaction forces (GRFs) compared to simulations alone. **(B)** The ML was the least accurate at predicting joint moments, while the hybrid approach performed similarly. (* $p< 0.05$)

Significance: Merging the strengths of physics-based musculoskeletal simulations with machine learning has the potential to improve our ability to accurately estimate musculoskeletal forces from sparse mobile sensor data. Here we demonstrate the strength of this approach and opportunities for development. Accurately estimating both motion and musculoskeletal forces from ubiquitous sensors, like smartphone videos, can accelerate the translation of biomechanical insights into large-scale research studies and clinical practice.

References: [1] Uhlrich SD. et al., PLoS Comput Biol. 2023. [2] Falisse A. et al., bioRxiv. 2024. [3] Xia Z. et al., IEEE Trans Neural Syst Rehabil Eng. 2023. [4] Kidziński Ł. et al., Nat. Commun. 2020. [5] Boswell MA. et al., Osteoarthritis Cartilage. 2021. [6] Seth A. et al., PLoS Comput Biol. 2018. [7] Werling K. et al., PLoS One. 2023.

A machine-learning based, kirigami-inspired shoulder patch accurately predicts shoulder elevation angles

Amani A. Alkayyali[1*], Max Shtein[2], David B. Lipps[1,2]
[1]School of Kinesiology and [2]College of Engineering, University of Michigan, Ann Arbor, MI 48109, USA
*Corresponding author's email: aaalkay@umich.edu

Introduction: Daily monitoring of shoulder kinematics is vital for injury prevention, surgical decision making, and tracking rehabilitation progress. Monitoring shoulder elevation angles can inform individuals about their activities of daily living [1] and monitor shoulder injury progression in athletes undergoing conservative treatment [2]. Accurate measures of shoulder kinematics most often involve optical motion capture systems or inertial measurement units (IMUs). Optical motion capture systems are expensive and require controlled laboratory environments that are not conducive to daily monitoring. IMUs provide a portable solution but are prone to drift over time and require donning multiple sensors to track shoulder kinematics. Advances in sensor technology and machine learning algorithms can improve the accuracy, portability, and affordability of shoulder movement tracking systems. The current study combines a novel, engineered wearable sensor system (**Figure 1A**) with machine learning algorithms to predict shoulder elevation angles. A new class of kirigami-inspired wearable sensors can detect differences in skin deformation corresponding to humeral rotation [3]. Using the design principles of the Japanese art of kirigami (cutting of paper to design 3D shapes), the sensor platform conforms to the shape of the shoulder with on-board strain gauges to measure movement. Our objective was to examine how well this kirigami-inspired shoulder patch, coupled with a machine learning algorithm, could predict shoulder elevation in healthy individuals.

Methods: A custom-developed kirigami-inspired shoulder patch (**Figure 1A**) measured local strain from four strain gauges near the glenohumeral joint as individuals moved their shoulders [3]. 20 participants (5 males, 60.2(18.8) years, 1.78(0.06) m, 82.2(19.5) kg; 15 females, 39.8(20.1) years, 1.65(0.08) m, 64.2(8.27) kg) provided written informed consent to wear the device. From anatomical neutral, participants abducted their right arm along the frontal plane to approximately 45°, 90°, 135°, and 180°, then returned to neutral. Simultaneously, marker-based motion capture recorded movements to determine exact arm angles. The strain gauge data was low-pass filtered (0.001 passband frequency) and compared to ground truth filtered shoulder kinematics from optical motion capture (MotionAnalysis). Congregate group and individual data trained two machine learning models, linear regression and random forest, to predict shoulder elevation angles. Linear regression assumes a linear relationship between inputs and the target, while random forest is a more complex, non-linear method using decision trees to improve accuracy and handle interactions. The models were evaluated with cross-validation, and the coefficient of determination (R^2) and root mean squared error (RMSE) assessed performance.

Results & Discussion: Preliminary machine learning models of congregate group data resulted in an R^2 value of 0.47, suggesting each participant needed its own trained and tested model to account for individual calibration. Machine learning using the random forest models provided better predictions than the linear regression models, with an average(SD) R^2 of 0.96(0.12) and 0.79(0.13), respectively, and an average RMSE of 4.92 (11.3)° and 19.6 (9.61)°, respectively. A random forest model performing better than a linear regression model indicates the sensor data is not quite a linear fit to the ground truth motion capture data. Representative data displaying the relation between the predicted and actual values shows a close relationship and well-performing model (**Figure 1B**). No models were overfitted given the small difference in R^2 values (less than 0.1) between the test and training data. While the R^2 values of both types of models are acceptable, the random forest models had considerably improved RMSE values similar in magnitude to IMU systems [4]. An RSME of 19.6° from linear regression models is poor compared to existing technologies.

Of the kirigami device's four strain gauges for predicting shoulder angles, the strain gauge placed anterior to the acromion was most beneficial for predicting elevation angles, followed by the strain gauge posterior to the acromion. These two locations capture changes in skin deformation from contracting musculature used to abduct the humerus. While the current study supports the ability of kirigami-inspired shoulder patches to predict shoulder angles, further work is needed to determine its calibration and efficacy in real-world environments.

Significance: This study further supports that kirigami-inspired wearables can accurately detect shoulder movement, particularly elevation angles. Given their lower cost and enhanced portability, expanded use of this sensor platform may provide individuals with personalized feedback on their shoulder health and progress during recovery from injury.

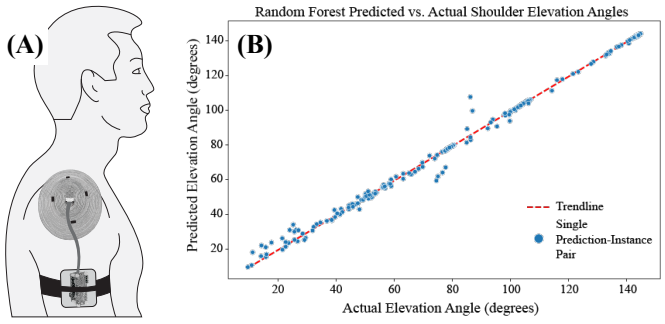

Figure 1: (A) The 9.20cm by 11.20 cm oval kirigami patch, centered on the acromion, measured skin deformation using four strain gauges placed distal, anterior, proximal, and posterior to the acromion. The patch was connected to an armband containing a Bluetooth board and Wheatstone bridge. **(B)** Results from one participant's machine learning random forest model. The actual target range of elevation angles from the dataset is along the X axis, with the model's predicted angles along the y-axis. Each prediction is represented by a blue dot, and the trendline representing best fit for the data is depicted by the red dashed line.

Acknowledgments: National Science Foundation GRFP 1841052; Alanson Sample and Nikola Banovic.

References: [1] Gates et al. (2016) *Am J. Occup Ther.* 70(1); [2] Bolia et al. (2021) *Open Access J Sports Med.* 12; [3] Alkayyali et al. (2024) *Wearable Technol.* 5(e23) [4] Chan et al. (2022) *mHealth* 8.

EVALUATING POST-STROKE UPPER EXTREMITY IMPAIRMENTS WITH POSE ESTIMATION

Kaleb Burch[1,2], Brooke Hall[2], Ryan Roemmich[1,2]
[1]Johns Hopkins School of Medicine, Baltimore, USA
[2]Kennedy Krieger Institute, Baltimore, USA
*Corresponding author's email: kburch4@jh.edu

Introduction: Accurate characterization of motor impairment after neurological injury is essential for assessing motor recovery and guiding clinical treatment. For example, if a person with stroke was unable to flex their fingers, their doctor would prescribe methods such as intensive practice or targeted neuroplasticity to improve this skill [1]. Currently, impairment is best captured by hands-on clinical assessments such as the Fugl-Meyer, but these assessments depend on expert interpretation and record data on coarse scales of just a few increments. Technologies such as optical motion capture provide more accurate and granular data, however, they are too expensive, complex, and time-intensive for clinical translation. If granular movement tracking could be implemented affordably, quickly, and easily, clinical motor assessments would be greatly improved. Pose estimation is a potential alternative approach that meets these criteria; it requires only a simple video recorded with more affordable and familiar technology such as everyday smartphones or tablets. In this experiment, we seek to validate pose estimation as a tool for conducting post-stroke motor assessments.

Methods: We recruited eight participants with chronic stroke to perform motions with both arms. All tasks were video-recorded with Samsung Galaxy Tab A7 tablets and kinematics were recorded with VICON using a 42 marker set. Cameras were placed to the right (90˚), front, and left (90˚) of the participant. Participants performed a series of tasks including rapid hand open/close movements and active shoulder abduction range of motion (ROM). All tasks involved up to 20 repetitions. We tracked kinematics from video recordings using MediaPipe pose estimation [2]. For hand open/close, we calculated finger motion as the average position of all five fingertips and palm position as the average of first knuckle of each finger. We then computed the distance between these two positions to capture hand open/close motion. We then used a Fourier transform and identified the dominant frequency. We compared the agreement between frequencies estimated from all three camera angles using the Bland-Altman method [3]. Camera angles were grouped according to their orientation relative to the active arm: ipsilateral (C_{ipsi}), frontal (C_{front}), and contralalateral (C_{contra}). For shoulder abduction, we computed shoulder angle between the torso axis and the upper arm axis. We calculated average ROM across shoulder abduction repetitions and compared ROM between paretic and nonparetic limbs.

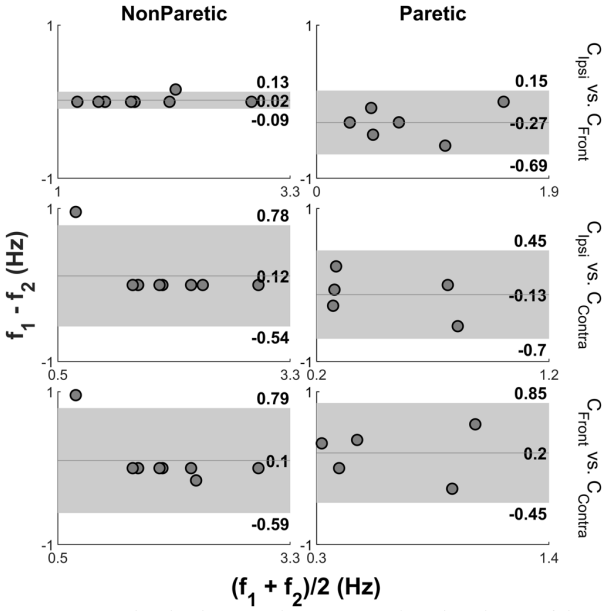

Figure 1: Bland-Altman plots comparing hand open/close frequency across cameras. Left-side plots depict nonparetic results and right-side plots depict paretic results. Dots depict individual subject results, horizontal lines depict mean of differences, and shaded regions show region from lower to upper limits of agreement. Mean of differences and limits of agreement are labelled in text.

Results & Discussion: For the hand open/close task, the group average frequency estimated from C_{front} was 1.83±0.54 Hz for nonparetic and 0.87±0.46 Hz for paretic. There was strong agreement in frequency across cameras for the nonparetic limb: limits of agreement were -0.09 to 0.13 Hz for C_{ipsi} vs. C_{front}, -0.54 to 0.78 Hz for C_{ipsi} vs. C_{contra}, and -0.59 to 0.79 Hz for C_{front} vs. C_{contra}. There was less agreement for the paretic limb: despite lower average frequencies then the nonparetic limb, limits of agreement were -0.69 to 0.15 Hz for C_{ipsi} vs. C_{front}, -0.70 to 0.45 for C_{ipsi} vs. C_{contra}, and -0.45 to 0.85 for C_{front} vs. C_{contra}. Two factors likely reduced accuracy of paretic data: (1) in cases of severe impairment, there was little to no finger motion and (2) hand posture occasionally obscured finger motion. These issues rendered some videos unusable: for three participants, hand/open close frequency could not be computed for at least one camera angle. The overall strength of agreement between cameras demonstrates the potential of pose estimation to capture frequency-based outcome measures in persons with stroke.

For the shoulder abduction task, ROM was 138.1 ±15.0˚ for the nonparetic limb 73.6 ± 46.8˚ for the paretic limb. These results show that pose estimation can capture differences in limb range of motion in stroke patients.

Significance: These preliminary results show the promise of applying pose estimation to characterize post-stroke motor impairments. This study will expand on these results by validating pose estimation against motion capture and by assessing more upper extremity tasks. A validated approach for applying pose estimation to characterize post-stroke arm motion could advance clinical care by enabling practical and reliable means to characterize post-stroke impairments.

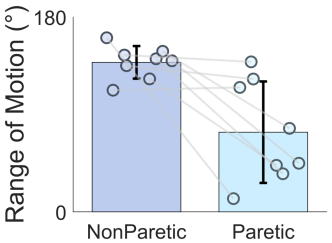

Figure 2: Bar plot comparing shoulder abduction ROM between paretic and nonparetic arms.

Acknowledgments: We acknowledge American Heart Association grant 23IPA1054140 to RTR.

References: [1] Reinkensmeyer et al. (2022), *Brain Comm* 4(6); [2] Zhang et al. (2020), *arXiv* 2006.10214; [3] Bland and Altman (1986), *The Lancet* 327(8476)

PERSONALIZED MUSCULOSKELETAL HAND MODELS: SHOULD WE STRIVE FOR ANATOMIC ACCURACY, PREDICTION ACCURACY, OR BOTH?

*Maximillian T. Diaz[1], Erica M. Lindbeck[1], Joel B. Harley[1], Jennifer A. Nichols[1]
[1]Herbert Wertheim College of Engineering, University of Florida, Gainesville, Florida
*Corresponding author's email: mdiaz40@ufl.edu

Introduction: Personalized musculoskeletal models often improve prediction accuracy [1]. Magnetic resonance imaging (MRI) personalization is considered the most anatomically accurate method, as Hill-type muscle parameters are calculated directly from image data (i.e., segmented muscle volumes, lengths) [2]. In contrast, scaling is the simplest method requiring only measured anthropometrics to adjust length and mass parameters. While MRI and scaling personalization are rooted in anatomical measurements, muscle parameters can also be indirectly estimated by using optimization to calculate parameter sets that provide accurate predictions, even though these tuned parameters may not perfectly match an individual's anatomy. For example, the Neuromusculoskeletal Modeling Pipeline (NMSM) uses a common optimization method of choosing the parameter set that minimizes the error between the predicted joint moments of an electromyography (EMG) driven forwards simulation and the predicted joint moments from an inverse simulation [1,3]. Importantly, both imaging- and optimization-based personalization methods are time-consuming due to the need for complex experimental data. To overcome this barrier, we developed a neural network (NN) that personalizes musculoskeletal hand models using only pinch force data, height, and weight [4]. Here, we evaluate if the prediction accuracy of our NN personalized models is better than MRI, NMSM, scaled, and/or generic models during inverse simulations. We also evaluate muscle parameter accuracy using MRI as the ground truth.

Methods: Healthy individuals [n=30; age 48.6 ± 24 years; 14 male, 16 female] were recruited into this IRB-approved study, with initial analyses performed on 7 participants [age 37.3 ± 22 years; 3 male, 4 female]. Each participant performed 5 trials of 15 tasks [7 range of motion (RoM); 4 isometric at 100% & 50% maximum voluntary contraction (MVC)], while fine-wire EMG (8 thumb muscles), motion capture (44 markers), and time-series thumb-tip force vectors were recorded. Structural MRIs of each participants' arm and forearm (3T axial; ST: 3mm; TR: 3,440 ms; TE: 20 ms; FA: 90º; FOV: 11cm) were collected using a body coil [5].

For each participant, 13 different musculoskeletal models were created in OpenSim 4.4. The generic model consisted of the MoBL-ARMS upper limb and ARMS hand and wrist models [6,7]. The scaled model was generated from static marker data. Five models were created with NMSM by tuning the scaled model with either 50% MVC, 100% MVC, all isometric, all RoM, or all collected tasks. NMSM models were tuned using two randomly selected trials per task, with remaining trials used for evaluation [1]. Five models were made with the NN by using each pinch trial separately to predict parameter sets. An MRI-based model was created by adjusting the scaled model's muscles with the optimal fiber length and maximum isometric force obtained from segmented forearm MRIs [8].

Model performance was evaluated for inverse simulations using measured kinematics as inputs to static optimization to predict muscle activations. Root mean squared error (RMSE) was calculated between measured EMG and predicted activations. Percent differences were calculated between each parameter set and MRI data. Repeated-measures ANOVA and post-hoc comparisons were performed.

Results & Discussion: NN models significantly ($p<0.05$) improved muscle activation predictions (Fig 1A), even though the underlying parameters were significantly different than those measured using MRI (Fig. 1B). Notably, NN model predictions had significantly lower RMSE for 11 of 15 tasks compared to all other models. Across all tasks, the average NN model had the lowest RMSE for 6 of 8 muscles. In contrast, NMSM models had significant differences from generic and scaled models for 3 muscles. When evaluating parameter accuracy, NN models had significantly higher values for maximum isometric force and tendon slack length, and significantly lower values for optimal fiber length across all muscles. NMSM models also had significantly different parameter values than MRI, while there were no significant differences between MRI parameters and generic or scaled models.

The results show that anatomic accuracy of Hill-type muscle parameters is not necessary to improve simulation prediction accuracy. This reflects how different parameter sets can create identical kinematics due to interactions. Of note, a driving factor for NN and NMSM models' improved performance could be their ability to tune tendon slack lengths, as simulations are very sensitive to tendon slack length and it cannot be measured *in vivo* [6,8].

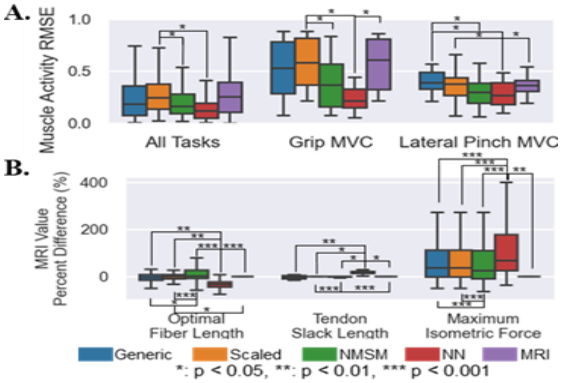

Fig. 1: (a) Model performance predicting activations for one representative muscle (FPL) in 3 representative tasks. Averages across the 5 NN and 5 NMSM models are displayed for readability. (b) Difference between predicted and measured muscle parameters. MRI model parameters (baseline) is included as 0% to visualize significance.

Significance: Our work suggests that personalizing musculoskeletal hand models with neural networks can improve prediction accuracy even though parameter values are significantly different from a participant's anatomical measurements.

Acknowledgments: NIH R21 EB030068, NSF GRFP Grant No. 1842473, and NSF Cooperative Agreement DMR-2128556

References: [1] Akhundov et al. (2022), *PLOS ONE* 17(1); ; [2] Valente et al. (2014), *PLOS ONE* 9(11); [3] Hammond CV et al. (2024), *bioRxiv*; [4] Lindbeck EM et al. (2023), *J. Biomech*., 161; [5] Holzbaur et al. (2007), *J Biomech* 40(4); [6] Saul et al. (2014), *CMBBE* 18(13); [7] McFarland DC et al. (2023), *TBME* 70 [8] Ackland et al. (2012), *J Biomech* 45(8).

AGING ADULTS WITH HIP OSTEOARTHRITIS WALK WITH ALTERED LOWER EXTREMITY JOINT POWER

*Amara G. Sharp[1], K.N. Jochimsen[2,3], A.D. Fain[1], A.A. Mangino[1], S.T. Duncan[1], J.A. Roper[4], M.A. Samaan[1]
[1]University of Kentucky, [2]Massachusetts General Hospital, [3]Harvard Medical School, [4]Auburn University
*Corresponding author's email: amara.sharp@uky.edu

Introduction: Approximately 27% of aging adults have radiographic hip osteoarthritis (OA).[1] Aging adults display a shift in their lower extremity joint power from distal-to-proximal; exhibiting higher hip joint and lower ankle joint contributions for propulsion and support during gait[2] when compared to young adults. It is unknown how this distal to proximal shift impacts hip joint health, but recent work demonstrating that women with hip OA ambulate with similar hip joint power yet less ankle joint power when compared to women without hip OA[3], suggesting that hip joint disease and shifts in joint power may be related. Understanding the relationships between lower extremity joint power and clinical and structural disease severity in aging adults with hip OA may provide insight into clinically relevant targets for gait re-training interventions to mitigate hip OA disease progression. Therefore, the purposes of this study were: 1) To compare sagittal plane lower extremity joint power during walking in aging adults with hip OA and asymptomatic aging adults without radiographic hip OA and; 2) To determine the relationship between joint power and hip OA disease severity.

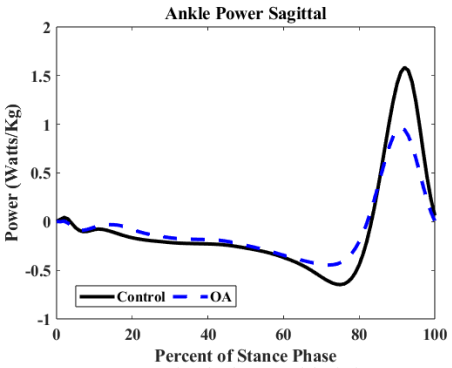

Figure 1: Sagittal plane ankle joint power.

Methods: Fourteen aging adults with radiographic hip OA (7 females, 62±9 years, 25.9±3.38 kg•m^{-2}) and fourteen asymptomatic adults (CONT) without radiographic hip OA (9 females, 56±9 years, 27.0±2.55 kg•m^{-2}) underwent 3D gait analysis on an instrumented treadmill while walking at a self-selected speed. Peak sagittal plane hip, knee, and ankle joint powers, and total power were calculated during the second half of the stance phase (propulsion phase)[2] for the symptomatic limb (Hip OA) or dominant limb (CONT). Total power was calculated by summing the sagittal plane hip, knee, and ankle powers during stance. All participants completed the Hip disability and Osteoarthritis Outcome Score (HOOS) to assess self-reported hip-related outcomes[4]. Participants with hip OA had MR imaging of their symptomatic hip to semi-quantitatively assess hip acetabular and femoral cartilage abnormalities using the Scoring Hip Osteoarthritis with MRI (SHOMRI) evaluation system[3]. Cartilage abnormalities were scored as a 0, 1, or 2 representing no loss, partial thickness, and full thickness loss, respectively, within 4 sub-regions of the acetabular cartilage and 6 sub-regions of the femoral cartilage. The total acetabular and femoral cartilage scores were computed as the summation of cartilage scores within all acetabular and femoral sub-regions, respectively. Welch's t-test was used to assess gait speed, Mann-Whitney U Tests were used to assess age and BMI, and Fisher's exact test used to determine distribution of sex between groups. Between group differences in gait parameters were assessed using separate ANCOVAs, adjusting for gait-speed (Hip OA: 0.76±0.20m·s^{-1}, CONT: 0.91±0.18m·s^{-1}, p=0.04). Kruskal-Wallis tests were used to compare HOOS sub-scores between groups. Associations between significant joint power-related parameters with HOOS sub-scores, as well as acetabular and femoral SHOMRI scores within the hip OA group were measured using partial Spearman's correlations, controlling for gait speed. For all statistical tests, significance was set at α=0.05.

Results & Discussion: Gait-related data are presented as adjusted mean ± standard error. The participants with hip OA walked with significantly lower peak ankle power (Hip OA: 1.25±0.09 Watts·kg^{-1}, CONT: 1.56±0.09 Watts·kg^{-1}, p=0.03) and yet similar peak total power (Hip OA: 1.74±0.15 Watts·kg^{-1}, CONT: 2.15±0.15 Watts·kg^{-1}, p=0.07), peak hip (Hip OA: 0.47±0.04 Watts·kg^{-1}, CONT: 0.45±0.04 Watts·kg^{-1}, p=0.74) and knee power (Hip OA: 0.6±0.1 Watts·kg^{-1}, CONT:0.81±0.1 Watts·kg^{-1}, p=0.16) compared to CONT (Figure 1). The hip OA group reported worse HOOS pain (p=0.02), symptoms (p=0.01), activities of daily living (p=0.02), and quality of life (p=0.02) sub-scores compared to CONT. No associations (p>0.05) were found between peak ankle power, HOOS sub-scores, or SHOMRI scores within the Hip OA group.

Significance: Lower peak ankle joint power may be a primary contributor to lower peak total joint power observed within the hip OA group. Our results also indicate that alterations in ankle joint power exist in both men and women with hip OA. Our future work will seek to determine the relationship between ankle joint power with early biomarkers of cartilage health (i.e. T1rho/T2 mapping) to understand the potential use of ankle joint power as a biomechanical biomarker of hip OA disease severity.

Acknowledgments: NIH (K01-AG073698, K23-AT011922, UL1-TR001998, S10-OD023573)

References: [1] Lawrence et al., (2008), *Arthritis Rheum* 58(1); [2] DeVita & Hortobagyi (2000), *J Appl Physiol* 88(5); [3] Wade et al., (2025), JOR 43(1); [4] Nilsdotter et al., (2003), BMC Musc. Disord 4:10; [5] Lee et al., (2015), *J Magn Reson Imaging* 41(6)

SOLEUS FUNCTIONAL ELECTRICAL STIMULATION ATTENUATES OLDER ADULT DISTAL-TO-PROXIMAL REDISTRIBUTION DURING WALKING

Ningzhen Zhao,* Lisa Griffin, Owen N. Beck
Department of Kinesiology and Health Education, University of Texas at Austin, TX
*Corresponding author's email: l.griffin@austin.utexas.edu

Introduction: The ability to walk relates to older adult health, independence, and quality of life. Unfortunately, walking performance declines with advanced age, concurrent to the age-related increase in metabolic energy expenditure during walking [1][2]. This age-related increase in metabolic energy expenditure is partly because older adults produce less ankle mechanics during walking compared to young adults, and in turn they compensate with increased hip mechanics (distal-to-proximal redistribution) [2]. Yet, older adults still retain the capacity to walk with youthful joint mechanics [3]. Thus, using functional electrical stimulation (FES) to increase ankle extension may help restore more youthful walking mechanics in older adults. Stimulating ankle extensors during walking increases joint output and underlying muscle metabolism. And increasing ankle extensor output reduces hip extension mechanics [4], which consume more metabolic energy to produce joint mechanics than the ankle [5]. Thus, the attenuated distal-to proximal redistribution in leg joint mechanics may offset the metabolic increase of stimulated ankle muscles. We hypothesized that stimulating older adult soleus muscles during walking can attenuate older adult distal-to-proximal redistribution without a detectable increase in whole-body metabolic energy expenditure.

Methods: Twenty adults participated (10 young: 21 ± 2 yrs; 10 older: 77 ± 5 yrs; Avg ± SD). Participants walked on a force-measuring treadmill at 1.25 m/s for familiarization, baseline, and FES trials. Each trial lasted 5-min with a 5-min seated rest preceding each trial. FES was applied over the soleus when the respective leg's propulsive ground reaction force was >10% body weight. We recorded ground reaction forces, motion capture data, and metabolic power during walking. To quantify participant ankle versus hip mechanical use, we calculated Redistribution Ratio = $1-(W_A^+-W_H^+)/(W_A^++W_H^+)$ [6]. W_A^+ represents positive ankle work and W_H^+ represents positive hip work. We conducted a two-way repeated measures ANOVA to test the effects of condition and age group on dependent variables.

Results & Discussion: There was no interaction between walking condition and age group on any dependent variable (all $p \geq 0.129$), so we reported the effect of FES across age groups. Peak ankle moments and mechanical power were greater during walking with FES vs. Baseline (FES: 1.37 ± 0.23, Baseline: 1.32 ± 0.23 Nm/kg, p=0.004; FES: 2.36 ± 0.45, Baseline: 2.17 ± 0.47 W/kg, p=0.004). Peak hip moments and mechanical power did not differ between FES and Baseline (FES: 0.66 ± 0.44, Baseline: 0.70 ± 0.44 Nm/kg, p=0.208; FES: 0.92 ± 0.21, Baseline: 0.95 ± 0.23 W/kg, p=0.138). Collectively, participant Redistribution Ratio decreased 10% from baseline to walking with FES (Baseline: 0.91 ± 0.25, FES: 0.82 ± 0.24, p=0.008). Due to the greater stimulated ankle mechanical output and minimal changes to hip mechanics, walking with FES required 3% more net metabolic power vs. Baseline (FES: 3.11 ± 0.54 W/kg, Baseline: 3.01 ± 0.58 W/kg, p=0.04). FES increased ankle mechanics and metabolic rate during walking in young and older adults. Our findings support the notion that older adults can physically walk with more youthful ankle mechanics, but aging neural strategies contribute to the distal-to-proximal redistribution in joint mechanics.

Significance: FES applied to the soleus during late stance attenuates older adult distal-to-proximal redistribution during walking with a modest metabolic increase. These findings suggest that FES can help restore youthful walking mechanics in older adults.

References: [1] Martin et al. (1985), *J Appl Physiol* 73(1):200-6. [2] Delabastita et al. (2021), Scand J Med Sci Sports 31(5):1036-1047. [3] Browne & Franz (2019), Gait Posture 71:44-49. [4] Fickey et al., (2018), J. Exp. Biol. 221(Pt 22). [5] Fallah & Beck (2025), J Exp Biol. [6] Browne & Franz (2018), *PLoS ONE.*

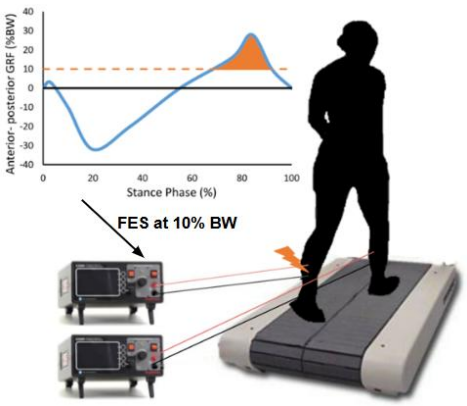

Figure 1. We applied bilateral soleus functional electric stimulation (FES) during walking when horizontal ground reaction force (GRF) was ≥10% body weight (BW).

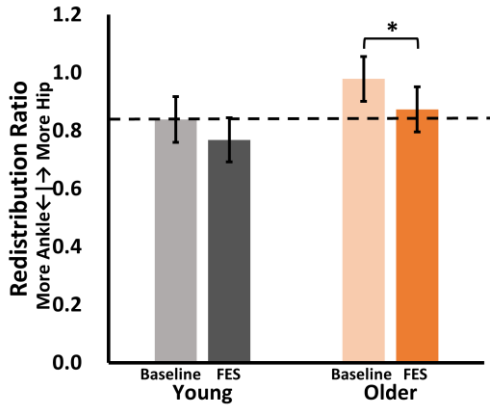

Figure 2. Average (±SE) redistribution ratio for young (gray) and older (orange) adults. Lighter bars show baseline; darker bars show FES.

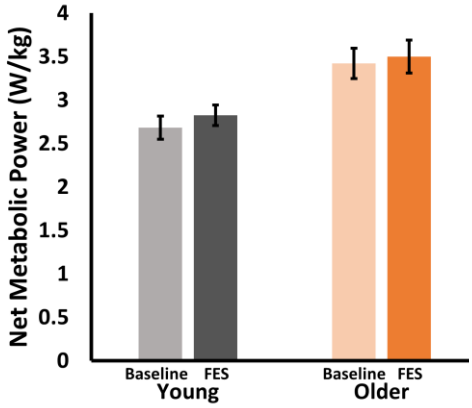

Figure 3. Average (±SE) net metabolic power for young (gray) and older (orange) adults. Lighter bars show baseline; darker bars show FES.

AGE EXPLAINS A SIGNIFICANT PORTION OF THE INCREASE IN LATERAL GASTROCNEMIUS SHEARWAVE VELOCITY DURING PASSIVE STRETCHING

*Andrew Sawers[1], Daniel Ludvig[2], Paige Cordts[2], Eric J. Perreault[2]
[1]University of Illinois Chicago, [2]Northwestern University
*Corresponding author's email: asawers@uic.edu

Introduction: Passive mechanical behavior of skeletal muscle – especially its passive stiffness – is an important yet often overlooked biomechanical property [1]. Increased passive muscle stiffness may raise the risk of injury [2], reduce active force production [3], and impair movement speed and accuracy [4]. Determining if aging increases passive stiffness could enhance our ability to treat age-related declines in mobility. Evidence of muscle stiffening with age is controversial. Animal studies have shown whole-muscle passive stiffness to increase with age [5], while human studies have not [6]. This discrepancy may stem from challenges measuring whole-muscle passive stiffness in humans. Shearwave velocity (SWV) in a passively stretched muscle depends primarily on the stress in that muscle [7]. Given that association, and assuming passive conditions, changes in SWV with joint angle – a proxy for muscle length - can be quantified by the slope of the SWV-joint angle relationship. This slope may serve as a surrogate measure of whole-muscle passive stiffness. The aim of this study was to determine if the slope of the passive SWV-ankle angle relationship varies with age or physical activity level. We hypothesized age would be associated with larger SWV-ankle angle slopes due to known changes in extracellular matrix with aging [8].

Methods: Adults aged 18 to 80 years old with no major neuromusculoskeletal conditions affecting knee or ankle function were recruited. Participants laid prone on an exam table with their knees extended and their foot/ankle secured to rigid footplate. Shear-wave elastography (SWE) (Verasonics, USA) was used to measure SWV of the lateral gastrocnemius (LGAS) across participants' ankle ROM at 10° increments (Fig 1A). Ankle joint angle was measured using a potentiometer affixed to and aligned with the ankle axis on the rigid footplate. The ankle angle where SWV first increased was taken as the slack angle [9] (Fig 1A). Changes in SWV across ankle ROM were quantified as the slope of the SWV-ankle angle relationship from slack angle to maximum dorsiflexion (Fig 1A). LGAS and soleus EMG was recorded each trial to confirm SWV measurements were obtained under passive conditions (i.e., < 3% of MVC). Physical activity level was quantified using the International Physical Activity Questionnaire (IPAQ).

Results & Discussion: Ten unimpaired adults between 19 and 65 years of age participated in the study. In support of our hypothesis, age explained a significant portion of the variance in the passive LGAS SWV-ankle angle slope (R^2=0.45, p=0.03, Fig 1B). Physical activity level (i.e., IPAQ scores) accounted for 33% of the variance, but this association was not significant (R^2=0.33, p=0.08, Fig 1C). Our results are the first to show that age is related to increases in passive SWV across ankle ROM, and possibly whole-muscle passive stiffness in humans. This finding is consistent with previous research on single fibers and fiber bundles in human subjects [2,10] but contrasts with earlier in-vivo studies of whole-muscle passive stiffness [6]. By using shear-wave elastography, our surrogate measure may have detected subtle yet significant differences in whole-muscle passive stiffness that previous studies – which relied on mathematical models to estimate muscle force from net joint torque [6] – could not. Increased passive muscle stiffness may restrict muscles to operating lengths during gait that are shorter than their optimal lengths [11], potentially limiting force production during locomotion that impairs balance and mobility. Greater passive muscle stiffness may also preserve eccentric strength in older adults [3], suggesting a benefit to age-related increases in passive stiffness. Understanding the overall impact of adaptive and maladaptive changes in muscle function driven by increases in passive stiffness is critical to addressing age-related declines in mobility.

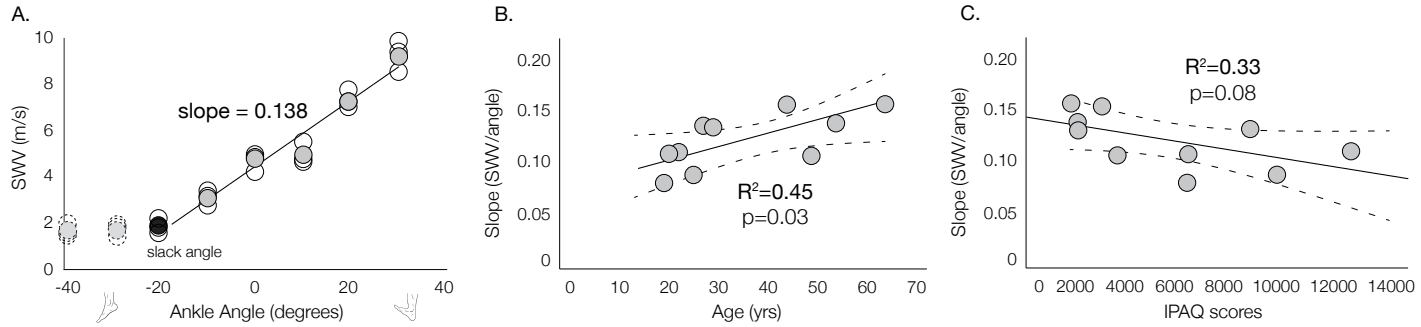

Figure 1. (A) Example of lateral gastrocnemius passive SWV-ankle angle slope for one subject from slack angle (1st increase in SWV) to maximum dorsiflexion (white: single trials, grey: mean). Association between passive SWV-ankle angle slope, age (B), and physical activity level (C).

Significance: Our results indicate aging may increase plantarflexor passive stiffness. Further research into the biological and mechanical basis of these changes, their mobility-related consequences, and the validity of our surrogate measure of passive muscle stiffness is warranted. Given age explained less than 50% of the variance in the slope of the SWV-joint angle relationship, contributions of factors like short-range stiffness and other material properties to muscle stress and passive stiffness should be considered moving forward.

Acknowledgments: Thanks to Tim Haswell and Mahdi Ebrahimkhani for technical assistance. Funding from R01AR071162 to EJP.

References: [1] Noonan et al., (2020); [2] Lim et al., (2019); [3] Zhang et al., (2019); [4] Murtola et al., (2019); [5] Alnaqeeb et al., (1984); [6] Krupenevich et al., (2020); [7] Bernabei et al., (2023); [9] Gillie and Leiber, (2011); [9] Lacourpaille et al., (2013); [10] Pavan et al., (2020); [11] Horner et al., (2025).

OLDER ADULTS FAIL TO MODULATE MUSCLE EXCITATIONS IN ANTICIPATION OF WALKING BALANCE PERTURBATIONS

*Emily K. Eichenlaub[1], Jessica Allen[2], Vicki Mercer[3], Jeremy Crenshaw[4] and Jason R. Franz[1]
[1]Lampe Joint Dept. of BME, UNC Chapel Hill and NCSU, USA, [2]Dept. of Mechanical and Aerospace Engineering, UF, USA,
[3]Division of PT, UNC Chapel Hill, USA [4]Dept. of Kinesiology and Applied Physiology, UD, USA
*Corresponding author's email: emeich@email.unc.edu

Introduction: Age-related declines in muscle activation, strength, reaction time, and cognitive-motor acuity contribute to increased fall risk in older adults by impairing reactive responses to balance challenges. As a potential compensatory mechanism, older adults exhibit heightened agonist muscle activation and antagonist muscle coactivation during walking – something we and others have interpreted as a "generalized anticipatory strategy" [1]. Nevertheless, older adults still exhibit diminished neuromechanical responses following the onset of a balance perturbation [2] that reduce and delay biomechanical responses [3] necessary to mitigate instability. The extent to which generalized anticipatory compensations among older adults would be augmented via overt anticipation of a pending perturbation, and whether age-related differences exist in the complex interplay thereafter between proactive and reactive neuromechanics in governing instability, remain largely unknown. To address these scientific gaps, this study uses: (i) overt anticipation of treadmill-induced perturbations in older and younger adults and (ii) *in vivo* ultrasound imaging to help interpret altered muscle excitations in the context of muscle force output during the preceding, perturbed, and recovery strides. We hypothesized that: (1) independent of anticipation, older adults would exhibit greater generalized anticipatory control - evidenced via greater antagonist muscle coactivation than younger adults; independent of age, (2a) anticipation would increase agonist muscle activation preceding the onset of a perturbation while (2b) unanticipated perturbations would require increased agonist muscle activation during the perturbed and recovery strides that anticipated perturbations; and (3) despite generalized anticipatory control and supplementary proactive adjustments, older adults would still require increased agonist muscle activation than younger adults during the perturbed and recovery strides.

Methods: 19 younger adults (YA; 7M/12F, mean ± standard deviation, 22.7±3.4 yrs, 1.40±0.14 m/s) and 15 older adults (OA; 6M/9F, 73.1±5.7 yrs, 1.28±0.19 m/s) responded to treadmill belt perturbations delivered at the instant of heel-strike in which the belt accelerated or decelerated over 200 ms at 6 m/s^2. We delivered perturbations either unexpectedly (i.e., unanticipated) or at the end of a 3-s verbal countdown (i.e., anticipated). We simultaneously recorded electromyographic (EMG, Delsys) signals and cine B-mode ultrasound images from the tibialis anterior (TA) and medial gastrocnemius (MG). Prior to averaging, we normalized all EMG data to the respective muscle's mean activation over 3 unperturbed strides. We calculated normalized integrated EMG (iEMG) for: early stance (0-50%, ESt), late stance (50-100%, LSt), early swing (0-50%, ESw), and late swing (50-100%, LSw) during the preceding, perturbed, and recovery strides. From ultrasound data (not shown here), we calculated length at heel strike (L_{HS}), maximum change in length (ΔL_{max}), and peak shortening velocity (v_{max}); outcomes used to interpret altered muscle excitations in the context of altered force output. Data were analyzed using multifactorial ANOVAs with age (i.e., younger vs. older) and condition (i.e., anticipated vs. unanticipated) as factors.

Results & Discussion: Proactive adjustments. OA tended to walk with greater MG-TA coactivation than YA in the preceding stride – consistent with a hallmark reliance on generalized anticipatory control. However, independent of perturbation direction, OA did not exhibit any supplementary proactive increase in agonist muscle excitation with anticipation (**Fig. 1B-C**). On the contrary, only YA exhibited proactive adjustments with anticipation via increased MG (i.e., agonist) muscle excitation preceding belt accelerations (p-values<0.001). Reactive adjustments. Independent of their direction, OA exhibited greater MG and TA muscular excitations during the perturbed stride in response to unanticipated than anticipated perturbations, respectively (p-values≤0.014). This was unlike YA, whose anticipatory increases in MG excitations precipitated into the perturbed (LSt, ESw) and recovery (LSt, ESw) strides compared to unanticipated accelerations (p-values≤0.038). There also, despite no measurable increase in proactive TA activity preceding anticipated decelerations, YA also exhibited increased reactive excitations during the perturbed (ESw) and recovery (ESt, LSt, ESw) strides compared to unanticipated decelerations (p-values<0.001).

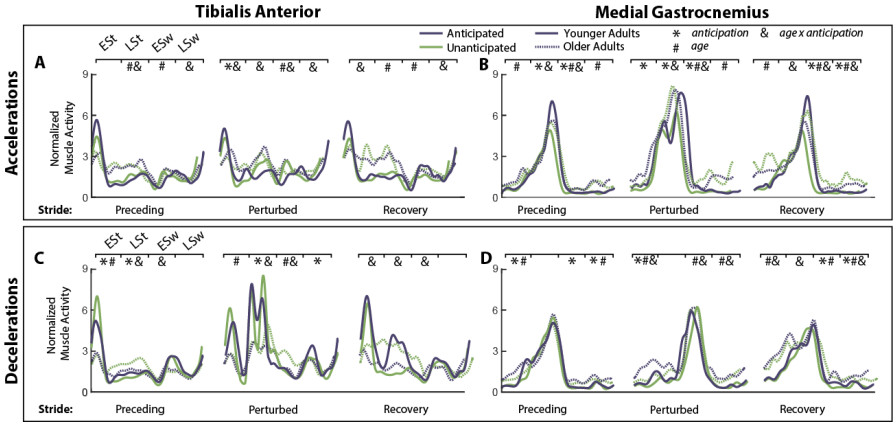

Figure 1. Normalized medial gastrocnemius and tibialis anterior activity during the preceding, perturbed, and recovery strides in response to (A-B) accelerations and (C-D) decelerations.

Significance: Collectively, despite walking with a disproportionate use of generalized anticipatory control than younger adults, older adults failed to modulate distal leg muscle excitations in anticipation of a balance perturbation – an age-related difference that subsequently increased requisite reactive responses.

Acknowledgments: Supported by the National Institutes of Health (F31AG084241-01, R21AG067388).

References: [1] Hortobágyi et al. (2009), *J Gerontol A Biol Sci Med Sci*; [2] Chambers et al. (2007), *Gait & Posture*; [3] Pijnappels et al. (2005)

LOWER-LIMB JOINT KINETICS OF OLDER ADULTS DURING TURNING GAIT

*Erin C. Kreis[1], Zahava M. Hirsch[1], Jun M. Liu[1], Antonia M. Zaferiou[1]
[1]Musculoskeletal Control and Dynamics Lab, Stevens Institute of Technology, Hoboken, NJ, United States
*Corresponding author's email: ekreis@stevens.edu

Introduction: Turning while walking accounts for up to 50% of all steps [1], and falls during turns are about eight times more likely to cause hip fracture in older adults than straight-line gait (SLG) [2]. Thus, the purpose of this study was to characterize how healthy older adults modulate their lower extremity control during turns vs. SLG. Given the increased mechanical demands during turns (i.e., changing facing direction and direction of travel), we hypothesized that turns vs. SLG would be associated with greater frontal and transverse plane lower extremity net joint moments (NJM).

Methods: Healthy female older adults (n=6; 71.8 ± 5.78 years) volunteered for this research in accordance with the IRB. Optical motion capture (Optitrack, 250 fps) and four hidden in-ground forceplates (Bertec, 1000 Hz) were used. Participants performed 12 SLG trials and 12 90-degree leftward turns. If the footfall closest to the intersection was the right foot, it was a "step turn" [3] and included in this analysis. Segment parameters were estimated using Dumas et al. [4]. NJMs are reported with an internal perspective, normalized to body mass, and expressed about each distal segment, from heel-strike to toe-off (**Fig.1**). A two-tailed sign test was used to evaluate differences in maxima (max) NJM between SLG and step turns of the lower-limb joints (α=0.05).

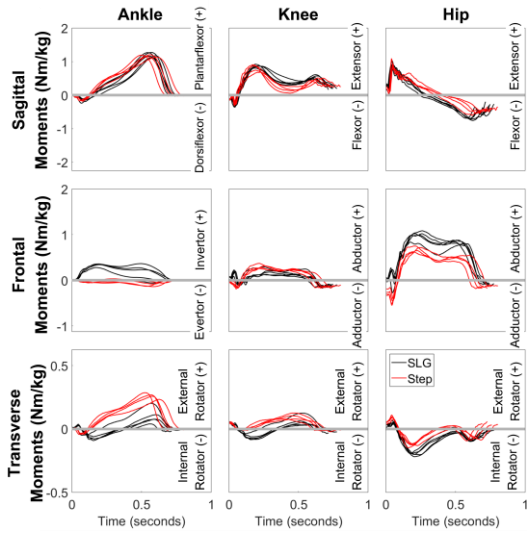

Figure 1: Time series of internal NJM for SLG (black) and step turns (red) across trials for one participant.

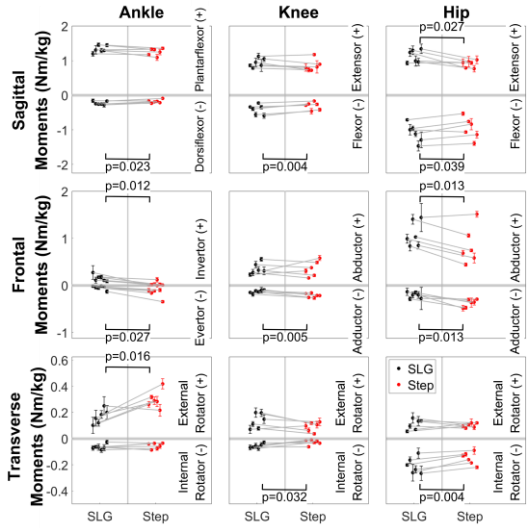

Figure 2: Max NJM comparisons in each direction across tasks, with significant p-values.

Results & Discussion: Significant differences in max NJM in each direction are indicated with displayed p-values (**Fig.2**). **ANKLE**: During step turns, there were significantly smaller max dorsiflexor NJM vs. SLG. However, during both tasks, the max dorsiflexor moment was near zero (**Figs.1-2**), while a majority of the footfall exhibited plantarflexor NJM. In the frontal plane, step turns used significantly greater max evertor and smaller max invertor NJM than SLG. SLG used mostly invertor NJM throughout the footfall duration (**Fig.1**), which suggests that the right ankle could help redirect the body leftward (the turn direction) by *reducing* invertor NJM. In the transverse plane, step turns exhibited significantly greater external rotator NJM than SLG. **KNEE**: Similar to the ankle, there were significantly smaller max flexor NJM during step turns vs. SLG, and these maxima occurred with very small magnitudes during both tasks. In contrast, the knee extensor NJM was predominant. In the frontal plane, there were significantly larger max adductor NJM during step turns vs. SLG. Adductor NJM were brief and much smaller in magnitude than the predominant abductor NJM. In the transverse plane, max internal rotator NJM were significantly smaller during step turns vs. SLG. This makes sense during step turns, where the objective is to rotate in the opposite direction of the planted foot. **HIP**: There were significantly smaller max extensor and flexor NJM during step turns vs. SLG, which is consistent with the global objective to turn. Like the frontal plane for the knee, step turns were associated with larger max hip adductor moments during step turns than during SLG. Adductor NJM were brief and much smaller in magnitude than the predominant abductor NJM. There were also significantly smaller max abductor NJM during step turns vs. SLG. This was surprising, as we expected an increased right hip abductor NJM to facilitate redirecting the body leftward during step turns. In the transverse plane, max internal rotator NJM were smaller during step turns vs. SLG. This makes sense for step turns with the right foot, as it could facilitate leftward rotation. Based on these findings, it is possible that older adults utilize the ankle NJM or transverse plane rotation more than generating hip abductor NJM during this footfall's contribution to step turns. For additional context, footfall duration was significantly longer during step turns than SLG (p=0.033), prompting future study of the *impulse* from each NJM. We will also study how NJMs relate to whole body momenta contexts and compare them to those used by young adults.

Significance: Older adults altered lower-limb joint kinetics between SLG and step turns, prompting further investigation of how older adults can safely utilize these turn strategies in daily life. In many joint planes, the step turn was similar or no more demanding than SLG, which could have clinical value, particularly if future analysis shows larger NJM for other turn strategies.

Acknowledgments: This study was supported by NSF Award#1944207.

References: [1] Glaister, B.C. et al., (2007). *Gait Posture*, 25:289–294 [2] Cumming, R.G. et al., (1994). *J. Am. Geriatr. Soc.,* 42:774– 778 [3] Golyski, P.R. et al., (2017). *J. Biomech.,* 54:96–100 [4] Dumas, R. et al., (2007). *J. Biomech.,* 40:543–553

OLDER ADULTS WALK WITH A LESS EFFICIENT STEP-TO-STEP TRANSTION (STST) THAN YOUNG ADULTS AND MODULATE STST TIMING TO ACHIEVE HIGHER EFFICIENCY AT FASTER SPEEDS

Elham Alijanpour[1], *Daniel M. Russell[1]
[1]Ellmer College of Health Sciences, Old Dominion University
*Corresponding author's email: dmrussel@odu.edu

Introduction: Aging alters step-to-step transition (STST) during gait [1]. Young adults initiate STST before front leg contact [2], while older adults start later, though they may resemble young adults at higher speeds [1]. Efficient STST requires push-off before collision to minimize energy loss, quantified by the Sequence (S) index (0–1), where higher values indicate greater energy loss and cost [3]. S index decreases as the overlap between leg forces diminishes. This occurs when STST is initiated or completed earlier/later than double support. Altered STST has been linked to higher energetic costs, shorter step length, and reduced walking speed [1,3], all major age-related changes to gait [4,5]. Despite its relevance, S index has not been studied in older adults. This study compares S index between age groups across five speeds, hypothesizing that older adults have higher S index, improving with speed by modulating STST timing variables (Fig. 1) to achieve lower values.

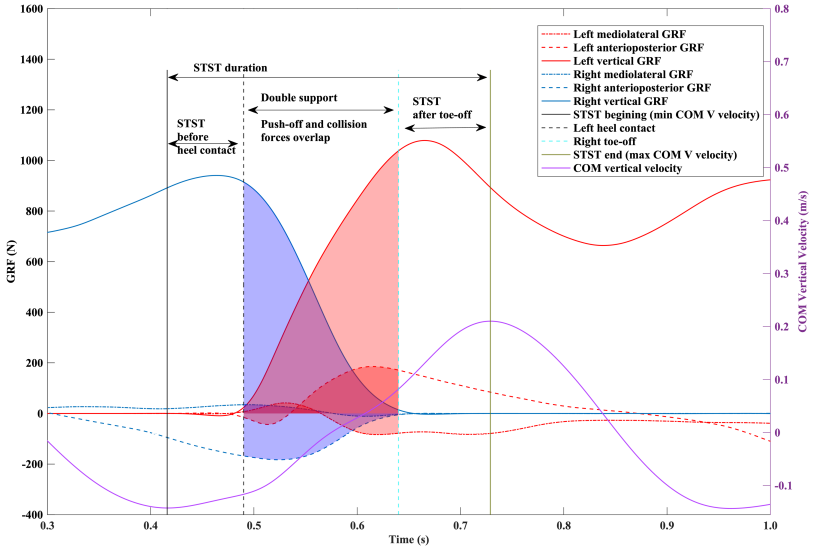

Figure 1: STST timing variables

Methods: Seven young and seven older adults walked at five speeds for three minutes each on an instrumented split-belt treadmill, based on their preferred walking speed (PWS). S index was calculated [2]. To examine strategies for exhibited S index, STST duration, initiation relative to heel contact, completion relative to toe-off, and percentage of STST during double support were computed (Fig. 1). Two-way mixed-design ANOVAs assessed age and speed effects.

Results & Discussion: S index was significantly higher in older adults across all speeds and decreased with increasing speed in older adults and to a lesser extent in young adults (p's < 0.05) (Fig. 2). Higher S index in older adults indicates lower efficiency, aligning with prior findings [4] that reported lower efficiency in older adults calculated from metabolic costs of walking and mechanical work. Younger adults exhibited greater efficiency (lower S index) by having 1) longer STST duration, 2) initiating STST earlier relative to heel contact, 3) extending STST beyond toe-off, 4) dedicating a higher proportion of STST to post-toe-off phases, and 5) allocating less STST to double support at all walking speeds (p's < 0.05) (Fig. 3). These findings show higher S index in older adults arises from altered STST timing. Both age groups reduced S index at higher speeds by primarily extending STST beyond toe-off and, to a lesser extent, initiating STST prior to heel contact (Fig. 3). The importance of initiating STST before heel contact has been previously reported [6] as a key factor in distinguishing age-related deficits in older adults. The present results emphasize that completing STST after toe-off also contributes to the more efficient gait of younger adults and as a mechanism for increasing gait efficiency with speed. Critically, an intervention on step timing of older adults reduced energetic cost of walking [7], suggesting an intervention based on the findings of the current study could further enhance gait efficiency.

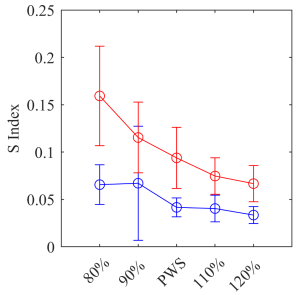

Figure 2: S index mean ± standard deviation for young (blue) and older (red) adults.

Significance: This study reveals that inefficient STST timing drives higher energy loss in older adults. By identifying age-related changes in STST timing variables our findings highlight STST timing as a key target for gait interventions. Future work should explore how changes in S index can change the energetic cost of walking in older adults.

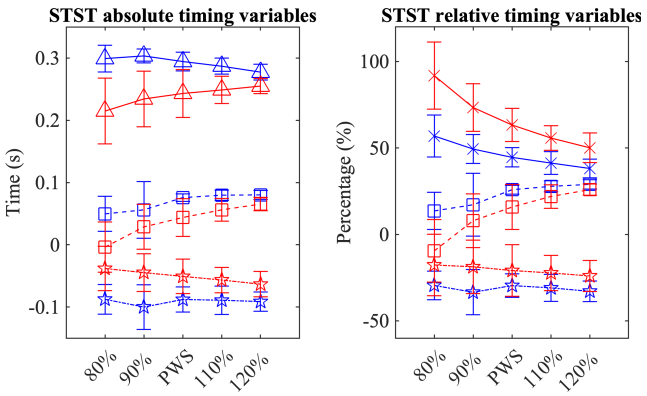

Figure 3: STST timing variables in young (blue) and older (red) adults. Squares and stars show STST timing relative to toe-off and heel contact, respectively. Triangles show duration of STST, and Xs show percentage of STST during double support.

References: [1] Chong et al. (2009), *Neuroscience Letters* 485(1); [2] Adamczyk & Kuo. (2009), *J Experimental Biology* 212(16); [3] Ruina et al. (2005), *J Theoretical Biology* 237(2); [4] Mian et al. (2006), *Acta Physiologica* 186(2); [5] Boyer et al. (2023), *Experimental Gerontology* 173; [6] Meurisse et al. (2019), *PLoS One* 14(8); [7] Collins et al. (2018), *Innovation in Aging* 2(3).

A COMPARATIVE STUDY OF GLOVE USE ON CARPAL TUNNEL PRESSURE RELIEF DURING MANUAL WHEELCHAIR OPERATION: A PILOT STUDY

Kathleen Olmstead[1], Wendy Reffeor[1], Jeanine Beasley[2], *Yunju Lee[1,3]
[1]School of Engineering, Grand Valley State University, Grand Rapids, MI, USA
[2]Department of Occupational Science and Therapy, Grand Valley State University, Grand Rapids, MI, USA
[3]Department of Physical Therapy and Athletic Training, Grand Valley State University, Grand Rapids, MI, USA
*Corresponding author's email:leeyun@gvsu.edu

Introduction: Carpal Tunnel Syndrome (CTS) is a prevalent condition among manual wheelchair users. Approximately 49-73% of individuals with spinal cord injuries rely on wheelchairs for mobility [1]. CTS occurs due to compression of the median nerve as it passes through the carpal tunnel, often resulting in pain, numbness, and reduced hand function [2]. Manual wheelchair users are more susceptible to contracting CTS due to the repetitive use and pressure on their hands during propulsion. Previous research indicated that compression-loaded gel gloves did not significantly mitigate the risk of CTS [3]. However, limited evidence exists on whether gloves can effectively relieve pressure on the median nerve during manual wheelchair operations. Therefore, the purpose of this study was to evaluate pressure distribution across the carpal tunnel and assess whether specific gloves alleviate pressure during manual wheelchair use. We hypothesized that both gloves tested would reduce the pressure across the carpal tunnel, but SHOCK-TEK® would provide the greatest relief due to its specialized design for median nerve pressure reduction.

Methods: Seven able-bodied participants (3 females, 4 males), aged 22-25, all right-hand dominant, completed three different manual wheelchair maneuvers: push-up pressure relief, forward push, and backward push. Each of the maneuvers were performed three times per trial under three conditions: bare hands, Glove A (ATERCEL®), and Glove B (SHOCK-TEK®). The sensor (novel® Elastisens) was attached to the right handrim of a manual wheelchair (Quickie®) to measure the carpal tunnel pressure during the maneuvers. To ensure consistent hand placement across trials, the carpal tunnel location was marked during the bare-handed condition and used as a reference for senor alignment in subsequent trials. A comparative analysis was utilized to evaluate the pressure difference across the carpal tunnel marking for each of the glove conditions and maneuver types. Hand circumference measurements were used for data normalization, and statistical analysis was performed using one-way ANOVAs in R (version 4.4.1), with an overall $\alpha = 0.05$.

Results & Discussion: From the preliminary data of seven participants, the static push-up pressure relief maneuver resulted in the highest normalized average pressure across the carpal tunnel (12.71 kPa/cm), followed by the forward push (3.419 kPa/cm) and backward push (2.203 kPa/cm) (Fig 1). A one-way ANOVA showed that both Glove A ($p < 0.0001$) and Glove B ($p = 0.039$) significantly reduced pressure during the pressure relief maneuver when compared to bare hands. A similar trend was observed in the forward push, where Glove A ($p = 0.0359$) and Glove B ($p = 0.0492$) provided significant pressure relief. However, there was no statistically significant difference between Glove A and Glove B for these two maneuvers. Since the forward push is the most frequent movement for manual wheelchair users, both gloves were recommended as effective options for reducing pressure during this maneuver. For the backward push, ANOVA indicated a significant difference between Glove A and Glove B ($p = 0.0481$). Glove B had the highest normalized average pressure of 2.203 kPa/cm ± 0.795 kPa/cm, while Glove A had the lowest normalized average pressure across the carpal tunnel of 1.566 kPa/cm ± 0.680 kPa/cm (Fig 1). However, neither glove showed a statistically significant difference from bare hands for this maneuver. Given these findings, Glove A is recommended for manual wheelchair users, as it consistently reduces carpal tunnel pressure across all studied maneuvers.

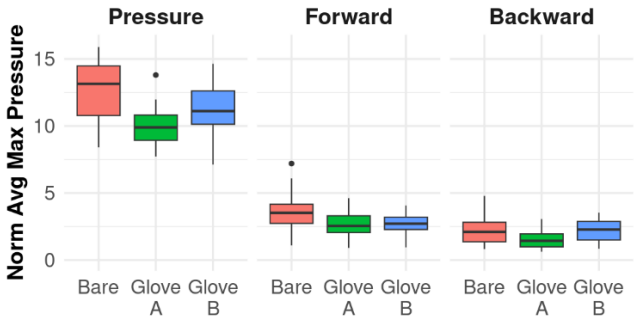

Figure 1: Box plot of normalized average maximum pressure (Norm Avg Max Pressure) for each maneuver performed (Push-up Pressure, Forward, and Backward). The x-axis represents the Glove Type (Bare, Glove A, and Glove B), while the y-axis shows the normalized pressure values in kPa/cm.

Significance: This study provided critical insights into the relationship between pressure distribution during wheelchair maneuvers and the effectiveness of different types of gloves in alleviating that pressure. By identifying the carpal tunnel area, which is the most susceptible to pressure buildup, the study could guide the design of gloves that incorporate strategic padding or other pressure-reducing materials to better protect the carpal tunnel region. Reducing median nerve pressure is essential for preventing carpal tunnel syndrome (CTS), which is a common risk for manual wheelchair users due to repetitive hand propulsion. Furthermore, the study highlighted the need for further research to better understand the effects of carpal tunnel pressure on wheelchair users during their daily activities. Such research could lead to the development of more ergonomic and functional glove designs, ultimately improving user comfort, reducing injury risk, and enhancing the overall quality of life for wheelchair users.

Acknowledgments: We would like to thank the participants for their cooperation and B.T., K.P., and M.G. for their contributions.

References: [1] Yang et al. (2009), *AJ PM&R* 88(12); [2] Padua et al. (2016), *The Lancet Neurology* 15(12); [3] Deltombe et al. (2001), *International Medical Society of Paraplegia* 39

INVESTIGATING THE RELATIONSHIP BETWEEN LOWER EXTREMITY KINEMATICS AND LUMBAR JOINT MOMENTS DURING INITIAL GROUND IMPACT OF MILITARY PARACHUTE JUMPING TASKS

Felicia R. Davenport[1,2], Jazmin M. Cruz[1,2], Peter Le[1]
[1]711th Human Performance Wing (711HPW), Air Force Research Laboratory (AFRL), WPAFB, OH 45433
[2]Oak Ridge Institute for Science and Education (ORISE)
*Corresponding author's email: peter.le.3@us.af.mil

Introduction: Low back pain (LBP) affects about 25% of military parachute jumpers [1], often due to the high compressive loads [2] from jump landings which over time could lead to chronic LBP development and can hinder performance. Among two common parachute training jumps - static line (SL) and military freefall (MFF)- SLs are more impactful to the body than MFFs due to the design of parachute utilized which promotes faster jumps. While simplified jump simulations exist, in-field kinematics and kinetics of military parachute jumpers remain unexplored, despite their potential to better understand the risks of LBP and jumper dismissal. Our protocol addressed this gap by leveraging musculoskeletal (MSK) modelling to analyze in-field wearable sensor data and extract pertinent insights on joint postures, moments, and forces to assess injury risk. This research aims to (1) compare lumbar moments before, during, and after landing, and (2) identify relationships between posture and joint loading in SL and MFFs jump profiles.

Methods: Five military parachutists (93.3 ± 8.0 kg) conducted 3-6 jumps on multiple data collection days. Parachute jump profiles included SL (MC-6), Tactical MFF (RA-1), and Nontactical MFF (Sabre) (Fig. 1A). Parachutists were equipped with 15 six-axis inertial measurement units (IMUs) (Xsens; Movella Inc.) to track kinematics and foot pressure insoles (Tekscan Inc.) (Fig. 1B) to measure ground reaction forces. Motion data were analyzed using OpenSim 4.3, with average L5-S1 joint angles and moments calculated via custom MATLAB scripts. Impact time was determined when the resultant of the first tibial IMU acceleration (filtered) exceeded 50 m/s^2. Pre- and post- impact data were calculated 0.25s before and after impact, respectively.

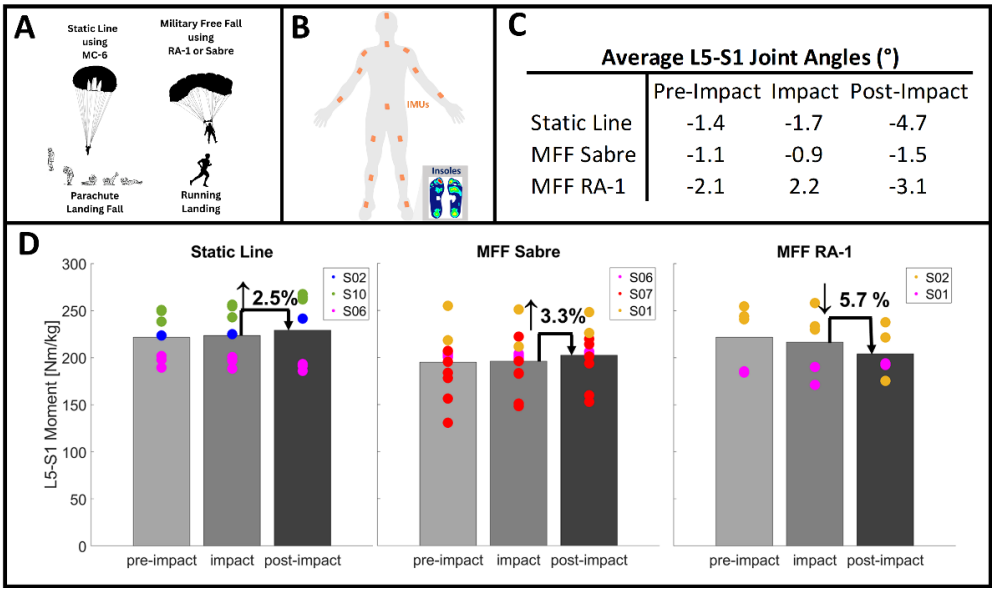

Figure 1: *(A)* Parachute jump profiles performed. *(B)* Wearable sensors parachute jumpers are instrumented with. *(C)* Across-subject averaged L5-S1 joint angles (°) pre-, during, and post-impact for each jump profile. *(D)* Across-subject averaged L5-S1 joint moments (Nm/kg) pre-, during, and post-impact for each jump profile. Individual participant moments shown in color-coded datapoints.

Results & Discussion: SL jumps exhibited the highest joint loads (moments) during and post-impact, followed by MFF RA-1, with MFF Sabre showing the lowest. L5-S1 loads during SL, MFF Sabre, MFF RA-1 were 221.6, 195.1, 221.7 Nm/kg pre-impact; 223.5, 196.0, 216.5 during impact; and 229.3, 202.4, 204.1 post-impact, respectively (Fig 1D). We believed that investigating change in joint moments and postures during and post-impact reveals insights into L5-S1 loading and potential LBP risk. We observed minor changes in lumbar loading (SL: +2.5%, MFF Sabre: +3.3%, MFF RA-1: -5.7%) and varying increases in L5-S1 flexion (SL: 3°, MFF-Sabre: 0.6°, MFF RA-1: 5.1°) (Fig. 1C). The differences in parachute types, designed to influence paratroopers' maneuverability [2] and speed (i.e., MC-6 promotes faster jumps) may attribute to the variation in L5-S1 postures and loading during and post-impact.

Significance: Our results support the capability of effectively simulating in-field wearable sensor data of military parachutists for purposes of monitoring LBP risks across SL and MFF jump profiles. While this work highlights that joint loading during SL jumps could pose a higher risk of injury than MFF jumps, it also introduces the need to be able to properly characterize MSK loading further post-impact which is not currently captured by the pressure insoles. Future work will probe methodologies to improve our understanding and surveillance of lumbar injury risk across military jump profiles.

Acknowledgments: The views expressed in this abstract reflect the results of research conducted by the authors and do not necessarily reflect the official policy or position of the Department of the Air Force, Department of Defense, nor the U.S. Government. This research was supported in part by appointments to the Oak Ridge Institute for Science and Education. The study protocol was approved by the Institutional Review Board (IRB) at the Air Force Research Laboratory (AFRL). Unless otherwise noted, imagery in this document is property of the U.S. Air Force. Distribution Statement A: Approved for Public Release, Unlimited Distribution. AFRL-2025-0802, Cleared 12 FEB 2025.

References: [1] Jiang et al., 2023, *Med. Biol. Eng. Comput.* [2] Y. Bar-Dayan et al., 2004, *Journal of the Royal Army Medical Corps.*

Personalized Muscle Strength Modeling Predicts Larger Joint Contact Impulses in Military Load Carriage

*Anna C. Corman[1], P. H. Sessoms[2], J. T. Sturdy[1], H. N. Rizeq[2,3], C. J. Daquino[2,3], T. T. Whittier[4], A. B. Silder[2], A. K. Silverman[1]
[1]Colorado School of Mines, Department of Mechanical Engineering, Golden, CO
[2]Naval Health Research Center, San Diego, CA; [3]Leidos, Inc., San Diego, CA; [4]Montana State University, Bozeman, MT
*Corresponding author's email: ancorman@mines.edu

Introduction: Injuries in the military are often from overuse, with the greatest numbers occurring in the lower limbs and lumbar spine [1]. Accurate joint contact force predictions from musculoskeletal models can inform injury mechanisms (e.g., [2]), guiding interventions that aim to prevent injuries. In addition, improving physical fitness can reduce some injuries [3] and has been recommended to mitigate injuries from military load carriage [4]. Given that muscle strength is modifiable, it is a key target for interventions that prevent injuries. Individualized modeling of strength has improved joint contact force estimates in weakened populations [5], so having the correct muscle strength is important for estimating joint contact forces. Active duty military personnel tend to be stronger than the general population, suggesting large modifications are needed to personalize generic models. However, how this personalization affects metrics of injury risk from movement simulations of musculoskeletal models is unknown. With greater muscle strength and variation of muscle strength across joints in the military, we hypothesized that personalized models would have significantly different predicted joint contact force magnitudes compared with generic models.

Methods: Sixteen active duty participants' right lower limb and lumbar joint strengths were measured from maximum voluntary isometric contractions (MVICs) (Biodex Medical Systems, Shirley, NY). Two size- and mass-scaled models were developed for each participant from a musculoskeletal model [6]: (1) generic muscle strength and (2) personalized muscle strength. Personalized muscle strength was determined by prescribing the pose and torque from the MVIC test to the generic model. With only the test joint unlocked, modeled muscle group strength was adjusted so that at least one muscle was maximally activated to resist the applied torque [7].

Participants' kinematics (120 Hz; Motion Analysis Corporation, Rohnert Park, CA), ground reaction forces (1200 Hz; Motek Medical, Amsterdam, The Netherlands), and electromyography (min ~1200 Hz; Delsys Inc., Natick, MA) during walking drove and validated simulations of both models under two conditions: (1) no-pack (with personal protective equipment ~6.6 kg) and (2) pack (46-kg load). The muscle recruitment solutions that reproduced the measured kinematics were optimized [7]. Resultant joint contact forces were calculated from the muscle solutions for the lumbar (L4-L5), hip, knee, and ankle. Joint contact impulses (JCIs) were determined over a right stride and normalized to body weight. A two-factor (model, condition) repeated measures ANOVA (α=.05) compared the impulses for each joint.

Results & Discussion: Lumbar, hip, and knee JCIs were greater for personalized strength scaled compared with generic models ($p<.004$) (Fig. 1). Consistent with our hypothesis, there was a difference between the generic and personalized muscle strength scaled model. Personalization resulted in greater JCIs from muscle groups with large scale factors, suggesting that generic models do not well represent active duty participants. This research expands on previous knowledge on the effects of subject-specific muscle strength adjustments on joint contact forces [5].

The pack condition had greater JCIs for all joints compared with no-pack ($p<.001$). The pack condition resulted in greater JCIs due to greater muscle and ground reaction forces to support added pack load. These results build on previous research with larger axial joint contact forces at the lumbar and hips with load carriage [8]. There were no interaction effects. The effect of muscle strength personalization was applicable to multiple conditions with varying levels of muscle recruitment; that is, the effects of personalization are not dependent on the task demands.

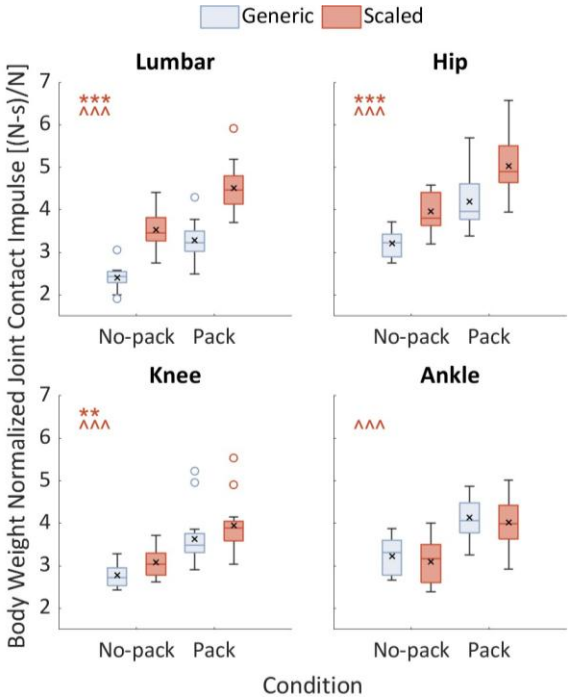

Figure 1: Simulated body weight normalized resultant joint contact impulses over right stride. "X" indicates mean value. Muscle strength scaling significance: 0 < *** < .001 < ** < .01 < * < .05; loading condition significance: 0 < ^^^ < .001 < ^^ < .01 < ^ < .05.

Significance: Personalizing models is important for predicting joint loading to inform injury risk, particularly because different scaling across muscle groups alters muscle recruitment [9]. Personalized strength scaled models can also aid in evaluating training interventions and their effect on overuse injury risk associated with joint loading.

Acknowledgments: This work was supported by the Defense Health Agency under work unit no. N1814. The study protocol was approved by the Naval Health Research Center Institutional Review Board (NHRC.2019.0015) in compliance with all applicable federal regulations governing the protection of human subjects.

References: [1] Hauret (2010), *Am J Prev Med* 38(1 Suppl.); [2] D'Lima (2012), *J Eng Med* 226(2); [3] Knapik (2006), *Mil Med* 171; [4] Knapik (2010) *Load Carriage in Military Operations*, Borden Institute; [5] Knarr (2015), *J Biomech* 48(11); [6] Sturdy (2024), *J Biomech* 163; [7] Thelen (2003), *J Biomech* 36(3); [8] Sturdy (2021), *Appl Ergon* 90; [9] van der Krogt (2012), *Gait Posture* 36(1).

FEASIBILITY TESTING OF BACK EXOSKELETONS FOR LOADS ASSOCIATED WITH PATIENT TRANSFERS

*Madeline Jenkins[1], Joshua Riesenberg[2], Jason Gillette[1]
[1]Iowa State University, [2]Scottish Rite for Children
*Corresponding author's email: mlj2@iastate.edu

Introduction: Over 18% of injuries to healthcare professionals involve the low back [1] and manual patient handling was linked to 89% of these injuries [2,3]. Patient transfers were estimated to exceed the back Compression Design Limit and often exceed the Compression Upper Limit [4]. Previous back exoskeleton research produced varying results for patient transfers, likely due to design differences [5-7]. There is a need to assess evolving back exoskeleton designs as an intervention to reduce back injuries. The purpose of this study was to test back exoskeletons for loads associated with patient transfers. We hypothesized that erector spinae muscle activity and perceived low back exertion would be reduced with back exoskeleton use given they are designed to provide back extensor support.

Methods: Seventeen participants (9 female, 8 male) completed the back exoskeleton assessment. HeroWear Apex Two generates extension moments during trunk flexion through elastic bands (back band exoskeleton) and Ottobock Paexo Back through torsional joints (back torsion exoskeleton). Participants completed a simulated patient transfer by moving a milk crate equipped with a gait belt from a wheelchair to a hospital bed. The milk crate was transferred empty and with 15.9 kg as a realistic, but safe load according to the NIOSH lifting equation [8]. Participants completed the simulated transfer with no exoskeleton, back band exoskeleton, and back torsion exoskeleton. Participants rated their perceived exertion for shoulders, legs, and low back and completed an exoskeleton usability survey. EMG was collected for the lumbar erector spinae, rectus abdominis, latissimus dorsi, and anterior deltoid. Maximum voluntary isometric contractions were collected and used to normalize EMG amplitudes. Kinematic data were collected through reflective markers placed on anatomical landmarks. Knee flexion, hip flexion, shoulder flexion, shoulder abduction, trunk lateral bending, and trunk flexion were calculated. Median and peak (95th percentile) values were determined for EMG amplitudes and joint angles.

Results & Discussion: Peak erector spinae EMG decreased with the back band ($p=0.032$) and back torsion ($p=0.030$) exoskeletons (Fig. 1). Median erector spinae EMG ($p<0.001$) and median abdominal EMG ($p=0.021$) decreased with the back torsion exoskeleton.

Peak shoulder abduction increased for the back band ($p=0.038$) and back torsion ($p=0.013$) exoskeletons. Median shoulder abduction increased with the back band exoskeleton ($p=0.032$). Peak and median hip flexion (both $p<0.001$) decreased with the back torsion exoskeleton.

Perceived exertion decreased with the back band and back torsion exoskeletons for the shoulder ($p=0.003$, $p=0.023$) and back (both $p<0.001$). Perceived exertion decreased for the legs with the back band exoskeleton ($p=0.030$). Participants indicated that the task was easier to complete with the back band exoskeleton ($p=0.007$). When comparing exoskeletons, participants rated the back band exoskeleton more nimble/adaptable/flexible ($p=0.021$), better fit ($p=0.021$), less bulky ($p<0.001$), more useful ($p=0.042$), and higher overall satisfaction ($p<0.001$).

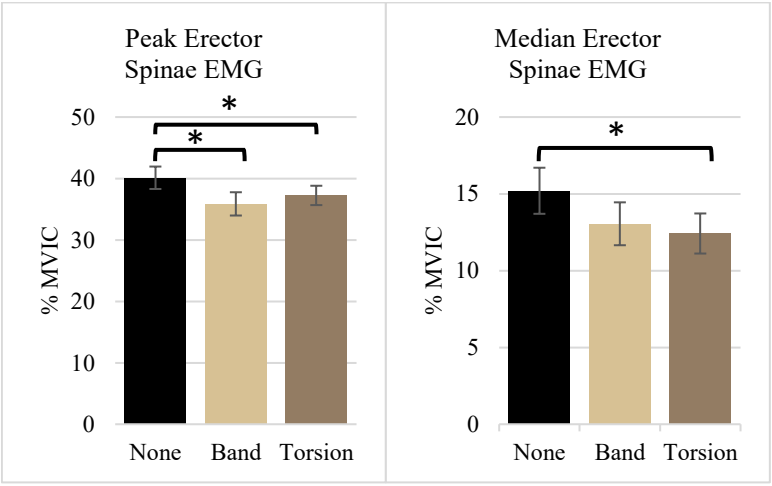

Figure 1: Median and peak erector spinae EMG during simulated patient transfers. * Significant EMG reduction ($p<0.05$)

Our hypothesis that erector spinae muscle activity would decrease with the back exoskeletons was supported by significant reductions in peak EMG amplitudes. Our second hypothesis that participants would perceive reduced low back exertion when wearing the back exoskeletons was supported by significant reductions when lifting the 15.9 kg load. There were increases in peak shoulder abduction with both back exoskeletons, along with an increase in peak hip flexion with the back torsion exoskeleton that may be of concern if not offset by back exoskeleton support. Participants rated the back band exoskeleton higher in usability than the back torsion exoskeleton.

Significance: This study is an initial assessment of whether exoskeletons are a feasible intervention to reduce back injuries associated with patient handling. The results indicated that both exoskeletons reduced low back muscle activity and perceived back exertion during simulated patient transfers. However, the usability of the back band exoskeleton was rated higher by the participants, indicating that the back torsion exoskeleton may not be a practical intervention in a healthcare setting. The next steps in this research line include testing transfers with an individual acting as a patient and if successful, testing actual patient handling with healthcare workers.

Acknowledgments: We would like to thank HeroWear and the Iowa State University Center for Industrial Research and Service for providing the back exoskeletons and the support of the Heartland Center for Occupational Health and Safety at the University of Iowa.

References: [1] Bureau of Labor Statistics; [2] Garg et al. (1992), *J Appl Biomech* 35(9); [3] Edlich et al. (2004), *J Long Term Eff Med Implants* 14(6); [4] Ulin et al. (1997), *SCI Nurs* 14(1); [5] Hwang et al. (2021), *Appl Ergon* 93(6); Miura et al. (2021), *Asian Spine J* 15(1); [7] Erezuma et al. (2023), *J. Appl Biomech* 39; [8] Waters (2007), *AJN* 107(8)

IT'S NOT MY FAULT! RUNG KICKING IS ASSOCIATED WITH THE LADDER DESIGN AND CLIMBING TASK, NOT THE PERSON

*Sarah C. Griffin[1], Violet M. Williams[1], Kurt E. Beschorner[1]
[1]University of Pittsburgh, Department of Bioengineering
*Corresponding author's email: scg57@pitt.edu

Introduction: When climbing ladders, injuries can be caused by adverse events such as kicking a rung, mis-stepping, or needing to adjust one's foot placement. Kicking a rung could be destabilizing by altering the foot trajectory and could either change or delay the subsequent foot placement. Given the role of the feet in supporting body weight during ladder climbing and the impact of foot placement on slip or misstep risk, these kick events are especially relevant to ladder safety [1]. Rung kicks indicate a motor error in swing during climbing [2] yet the causal factors of these events are not well understood.

One potential cause of kick events may be that certain ladder designs or climbing directions put users at risk of kicking rungs. Another possibility is that certain people are at increased risk of kicking due to deficits in motor control or an inclination to climb in a risky manner. The purpose of this work is to determine 1) if environmental or task factors like ladder angle, rung type, or climbing direction influence the likelihood of kicking a rung; and 2) if individual factors like risk propensity, age, or waist-to-height ratio (a metric of obesity) can predict rung kicking. Identifying factors associated with kicking a ladder rung could allow for safer ladder designs or identification of individuals at an increased risk of injury from ladders.

Methods: 87 individuals (42 M, 45 F, 1.7 ± 0.09 m, 27.2 ± 4.3 kg/m^2, 43.2 ± 12.2 years) who regularly climb ladders were included in this work. Participants climbed up and down 5 rungs on a custom modular ladder apparatus fitted with different ladder rungs and situated at multiple angles. This work includes trials in which participants climbed two different designs of flat rungs (thick and thin) with the ladder at two different angles (75º and 90º). Three replicates were completed for each condition, resulting in 24 trials per person. Motion capture video was viewed for each trial to determine if a participant kicked any rungs while climbing. A binary outcome was assigned for each of the eight climbing conditions to indicate if a rung was kicked in any replicate trials.

Participants completed a ladder risk survey which included questions designed to identify a tendency towards unsafe ladder use behaviors (like moving the ladder by hopping it or climbing without using their hands) [3]. Two multiple logistic regression models were generated. The environmental and task factors model included ladder angle, ladder rung, climbing direction, and first-order interactions as independent variables and whether a kick occurred for each condition as the dependent variable. The individual factors model included risk propensity score, age, and waist-to-height ratio, as independent variables and whether a kick occurred during any trial for that participant as the dependent variable.

Results & Discussion: In the 2,021 trials analyzed, a rung kick was identified in 130 trials and 61 of the 87 participants kicked a rung in at least one trial. The environmental analysis created a significant model (χ^2_6 = 30.5, p < 0.001) and climbing direction (χ^2_1 =13.7, p < 0.001), ladder rung (χ^2_1 =6.5, p = 0.011), and their interaction (χ^2_1 =8.6, p = 0.003) were significant predictors, whereas the ladder angle (χ^2_1 = 0.7, p = 0.41) and its interaction with rung type (χ^2_1 =0.7, p= 0.41) and climbing direction (χ^2_1 = 2.9, p=0.09) were not significant. Climbing up the ladder was associated with twice as many kicking incidents as climbing down. The effect of climbing direction on kick propensity may be due to differences in the shoe trajectory between directions that leads to narrower clearances during ascent versus descent. While additional research is needed to understand the impact of rung design, foot trajectory, and the risk of a foot trajectory error (like a kicked rung), the rung and its interaction effect suggests that rung design is a critical factor influencing this kind of risk during ladder climbing.

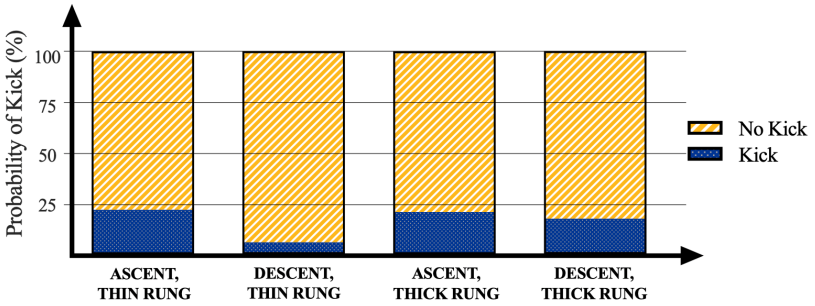

Fig 1. The proportion of trials where a rung was kicked for each rung and direction combination.

The individual factors analysis did not generate a significant model (χ^2_3 = 0.17, p =0.98) and no independent variables were individually predictive of kicking. This result indicates that the hypothesized pathways (individual factors influencing motor control and risk-taking) did not explain the occurrence of kicking events. It is likely that the person themself is not the cause of the incident, but rather their environment causes accidents to occur.

Significance: This work highlights the potential for optimized ladder rung design to reduce kick events during ladder climbing. Although all individuals included in this study were able to recover after the kick, interruptions to foot swing presumably can lead to accidents. Risk due to inadvertently kicking a ladder should not be considered the fault of the climber but rather a result of ladder design and task.

Acknowledgments: This work was funded by NIOSH R01OH011799 and NSF GRFP 2139321.

References: [1] Pliner et al. (2014), *Ergonomics (57)11*. 1739-1747. [2] Williams et al. (2024) *Appl. Ergon (121)* pp. 104371. [3] Hicks et al. (2021) *Int. J. Environ. Res. Public Health (18)* pp. 9799

STROLLER RUNNING ON HILLS: HOW TERRAIN AFFECTS GROUND REACTION FORCES

Joseph M. Mahoney[1*], Teresa B. Reed[2], Amanda Mueller[3], Abby Miller[3], Allison R. Altman-Singles[2,3]
[1] Mechanical Engineering, Alvernia University, Reading PA 19601
[2] Mechanical Engineering, Penn State Berks College, Reading PA 19610
[3] Kinesiology, Penn State Berks College, Reading PA 19610
[*]Corresponding author's email: joseph.m.mahoney@gmail.com

Introduction: Running is a popular activity to maintain physical fitness and mental health. Many runners with young children choose to run with a stroller to help achieve those benefits while caring for their children. Recent research has shown that stroller running may help reduce impact-related overuse injuries by decreasing impact loading [1-2]. However, these in-lab studies use flat, smooth surfaces, which differ from outdoor terrain. It is well established that running uphill without a stroller results in a decrease in impact loading while running downhill results in an increase in impact loading [3-5]. The introduction of a stroller results in a shifted body position that may result in a different response. The purpose of this study is to examine how stroller running affects impact loading on hills. It is expected that stroller running may exaggerate the increase in impact loading downhill and may temper the decrease in impact loading uphill.

Methods: Healthy runners ran a minimum of three trials each on a flat (0% grade), moderate hill (3.33% grade), and steep hill (10.0% grade) sections of road on the Penn State Berks campus. Trials consisted of both uphill and downhill portions and were repeated with and without the stroller. Loadsol-pro (Novel Inc, Pittsburgh, PA) insoles measured ground reaction force (GRF) at 200 Hz. Vertical propulsive peak (VPP) and average vertical loading rate (VALR) were extracted using MATLAB (Mathworks, Natick, MA). VPP and VALR on either the uphill or downhill were compared using a two-factor (stroller and grade) repeated measures ANOVA using MATLAB.

Results & Discussion: Seven runners (35±12 years, 1.69±0.08m, 69±18kg, 3 male, 4 female) completed all flat and incline trials. When running uphill, VPP and VALR did not result in an interaction, but there were significant main effects of both condition (VPP was 6% reduced and VALR was 16% reduced when running with the stroller) and grade (as incline increased, VPP decreased by 5% and VALR decreased by 61%).

When running downhill, both VPP and VALR resulted in a significant interaction effect, indicating that the stroller changes the effect of grade (Figure 1). VPP was 7% reduced when running with a stroller for the medium grade decline, and 9% reduced on the steep decline. Similarly, VALR was 27% increased when running with a stroller on the steep decline. This suggests that the steep decline provided an additional challenge when running with a stroller compared to the control condition.

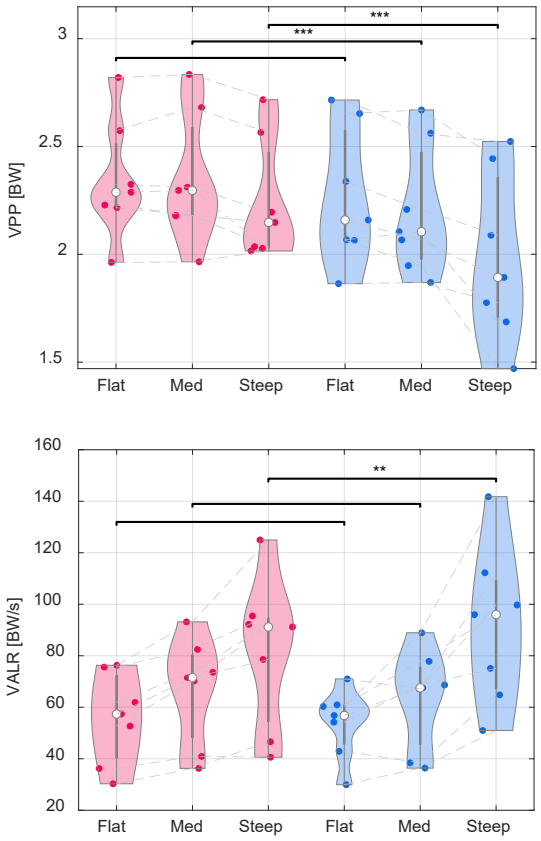

Figure 1: Violin plots of VPP and VALR when running downhill per condition and grade. Red is Control, blue is Stroller. Interaction effect $p<0.01$.

These findings suggest stroller running on uphill terrain reduces vertical loading in both the VPP and VALR, similar to running on a flat surface [1]. The stroller did not change the reduced vertical loading that has been identified as incline increases [3-4]. However, when running downhill, the increased mass of the stroller gains momentum, requiring the runner to lean back and slow their speed, especially on the steep decline. This resulted in a reduced need for propulsion, as observed in the VPP, and an increased need for braking. While the 1D shoe inserts were unable to discern vertical from anterior-posterior force, it is likely that the effects of increased braking also affect the impact loading, and thus the VALR. This exaggerated increase in VALR when running downhill with a stroller could increase the risk of overuse injuries in this potentially vulnerable population [6].

Significance: Running with a stroller on uphill inclines may increase the difficulty of running uphill compared to running without a stroller, however the GRF parameters are similar. Running downhill with a stroller disproportionately increases impact loading and could increase the risk of overuse injuries in runners. Future research should examine long-term effects, consider different stroller designs, and explore strategies to mitigate risk when running downhill.

Acknowledgments: This work would not be possible without a team of undergraduate students, including Brynna Bentz, Jacob Phiel.

References: [1] Mahoney et al. (2022), *NACOB, Ottawa, CA*; [2] Carbajal et al. (2023), *ASB, Knoxville, TN;* [3] Gottschall & Kram (2005) *J Biomech* 38(3); [4] Vernillo et al. (2017), *Sprt Med 47*(4); [5] Hamill et al. (1984), *Med Sci Sprt Exc* 16(2)*;* [6] Davis et al. (2016), *Br J Sports Med* 50.

ASSESSING RELATIONSHIPS BETWEEN ANKLE-FOOT PROSTHESIS STIFFNESS, RESIDUUM-SOCKET INTERFACE PRESSURE, AND SOCKET COMFORT IN UNILATERAL TRANSTIBIAL PROSTHESIS USERS

Michael Jacobson[1], Zachary Hoegberg[1], Ashutosh Tiwari[1], M Sanchez[1], Kiley Armstrong[2], Myunghee Kim[1], *Matthew J. Major[2,3]
[1]University of Illinois at Chicago, [2]Northwestern University, [3]Jesse Brown VA Medical Center
*Corresponding author's email: matthew-major@northwestern.edu

Introduction: One of the most critical issues affecting users' satisfaction with a lower limb prosthesis is their comfort. While the majority of prosthetics clinical encounters are related to the lower limb, previous estimates suggest that between 33% and 57% of lower limb prosthesis users report dissatisfaction with comfort while wearing their prosthesis [1, 2]. Critically, poor prosthetic socket fit as related to discomfort is significantly correlated with prosthesis satisfaction [3]. A survey of Veterans and Service Members with lower limb amputation revealed that prosthesis-related pain was reported as problematic in 37-51% of respondents, with 54-63% reporting residuum skin problems, and 11-14% reporting they could not wear their prostheses due to poor socket fit [3]. As the socket acts as the coupling and hence ground force transmission mechanism between the residuum and prosthesis, user comfort is directly affected by residuum-socket interface pressures [4]. While interface pressures can be affected by transtibial prosthetic socket design and fit, they are also influenced by alignment of distal prosthetic components [5] and possibly by prosthetic foot stiffness according to a recent numerical simulation [6]. However, the relationships between prosthetic foot stiffness, residuum-socket interface pressure, and perceived socket comfort have not been quantified in-vivo. This gap in knowledge limits our understanding of how transtibial prosthesis design and prescription can be optimized to maximize user comfort through manipulation of interface pressure. Therefore, this study aimed to map the in-vivo relationships between prosthetic ankle-foot stiffness, interface pressure, and user comfort for transtibial prosthesis users.

Methods: Eight participants with unilateral transtibial amputation (3 female/5 male, 50±13 yrs, 73.8±15.7 kg, 173.4±9.6 cm, aetiology: 6 trauma / 2 dysvascular, time since amputation: 17±12 yrs) walked on a treadmill while wearing an ankle-foot prosthesis end-effector (Humotech, Pittsburgh, PA) [7] as fitted by a certified prosthetist. The end-effector permitted precise adjustments in the stance-phase torque-angle relationship of the forefoot as controlled through tethered offboard actuation and was used to have participants walk at their self-selected speed at five discrete stiffness conditions for at least two minutes each. Each condition setting was scaled according to their body mass using a scale coefficient (unitless stiffness parameter). At least four minutes of rest was provided between conditions. Residuum-socket interface pressure was recorded through pressure sensors (Tekscan, Norwood, MA) lining the residuum's anterior and lateral sides. For each condition trial, the Socket Comfort Score (0-10) [8] was recorded and interface pressure was quantified based on the pressure-time integral [9], defined by dividing the sum of the pressure measured across the anterior and lateral sensor pads during the trials' last 60 seconds by the average maximum recorded pressure across both pads (*higher value is better, denoting less maximum pressures*). The University of Illinois Chicago and Jesse Brown VA IRBs provided ethical approval.

Results & Discussion: Figure 1 displays the relationships between the socket comfort and stiffness parameter, pressure-time integral and stiffness parameter, and socket comfort and pressure-time integral across participants. While each participant displayed a unique relationship of ankle-foot prosthesis stiffness to perceived comfort and residuum-socket interface pressure (Fig 1A-B), the trends generally suggest that increased forefoot rotational stiffness may yield increased comfort and reduced maximum pressures. Increased forefoot stiffness may provide the needed support against body weight as the prosthetic limb transitions from midstance into pre-swing, thereby requiring less gait compensatory mechanisms that would increase load demand on that limb. Clinically, increased perceived comfort would encourage prosthesis use while reductions in normal pressure might help minimize risk of pain and tissue trauma. Accordingly, there appeared to be a strong correlation between increased socket comfort and reduced interface pressures (Fig 1C), supporting evidence that perceived comfort during prosthetic gait is partially a function of experienced pressures [4].

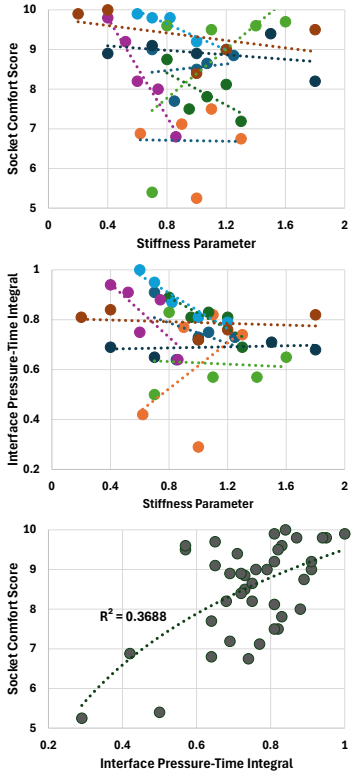

Figure 1: Relationships for comfort and stiffness (A), pressure and stiffness (B), and comfort and pressure (C). Linear trend displayed for each participant denoted by different color (A, B), and a logarithmic trend applied to all data (C).

Significance: Our results suggest that a transtibial prosthesis user can experience better socket comfort and interface pressure distribution through optimization of prosthetic ankle-foot stiffness. Such individual optimization can be achieved through clinical selection and tuning of prosthetic components, which would support patient satisfaction and long-term use of a prosthetic leg.

Acknowledgments: We thank Stefania Fatone, PhD, BPO(Hons) for her contributions. Funding was provided by the U.S. Dept of Veterans Affairs (RX004077) and VA Chapter 31. Views expressed do not reflect the policy of the VA or U.S. Government.

References: [1] Pezzin et al. (2004), *Arch Phys Med Rehab* 85. [2] Dillingham et al. (2001), *Am J Phys Med Rehab* 80. [3] Berke et al. (2010), *J Rehab Res Dev* 47. [4] Binedell et al. (2023), *PMR* 15. [5] Jia et al. (2008), *Disab Rehab* 3. [6] McGeehan et al. (2022), *J Rehab Assist Tech* 9. [7] Wen et al (2020), IEEE IROS. [8] Hanspal (2003), *Disab Rehab* 25. [9] Dou et al. (2006), *Clin Biomech* 21.

INTRAMUSCULAR EMG AND REGENERATIVE PERIPHERAL NERVE INTERFACE (RPNI) SIGNALS IMPROVE INTUITIVE PROSTHETIC CONTROL OF MULTI-GRIP HAND AND WRIST PROSTHESIS

*Ziyad Emara[1], Mira E. Mutnick[1], Dylan Wallace[1], Cynthia Chestek[1], Paul Cederna[1], Deanna Gates[1]
[1]University of Michigan, Ann Arbor, MI
*Corresponding author's email: zemara@umich.edu

Introduction: Commercially available myoelectric hand prostheses use surface electromyography (EMG) from electrodes embedded in the socket to control movement of the terminal device. To provide users with increased functionality, some prostheses are equipped with multi-grip control, allowing the user to perform a variety of functional grips. However, intuitive control of these hands is still limited. The state-of-the-art control approach is to use pattern recognition (PR) to decode EMG from a large number of electrodes in the socket into grips. This approach is limited by movement of the socket, which can impact signal consistency of the signals, and reduce muscle specificity due to placement. These limitations lead to frequent recalibration [1] and limit grip selection accuracy.

To address poor surface EMG signal reliability and increase specificity, intramuscular electrodes can be implanted into residual muscles [2]. To increase the number of independent control inputs, electrodes can also be placed in regenerative peripheral nerve interfaces (RPNIs). RPNIs are small pieces of reinnervated muscles created from free nerve endings in the residual limb. Prior work has found that use of RPNIs consistently improves multi-grip classification accuracy [3]. The purpose of this study was to determine if the use of signals from intramuscular EMG and RPNIs improves the ability to control both a hand and wrist, intuitively, compared to surface-based approaches.

Methods: Our participant was one 58-year-old female with transradial limb loss and four RPNIs constructed during her amputation procedure. One year post amputation, eight bipolar electrodes were implanted into five residual muscles and three RPNIs (NCT03260400). In two 3-hour sessions, linear discriminant analysis (LDA) PR classifiers were trained to decode functional grips and wrist rotation on either eight pairs of surface EMG signals (Surface-PR) or the eight channels of intramuscular EMG electrodes (RPNI-PR). We verified that the classifiers had an offline accuracy of over 90% before testing. In one session she used Surface-PR and in the other she used RPNI-PR in the other to control an iLimb Quantum (Ossur, Reykjvik, Iceland) with a wrist rotation unit. In each session, she performed the Clothespin Relocation Test (CRT) [4] to assess wrist rotation and the Coffee Task [5] to assess sequential grip transitions. For the CRT, the latter half of the trials were performed concurrently with the Controlled Oral Word Association Test (COWAT) to assess cognitive load [6]. We calculated the percentage of clothespins dropped in each CRT trial (failure rate), separated into CRT alone versus COWAT + CRT. The Coffee Task was divided into a continuous (CCT) section and segmented (SCT) section. CCT recorded trial times with a maximum of 150 seconds, while SCT measured grip errors, with a maximum of 25. At the end of each session, the participant completed the Prosthesis Task Load Index (PROS-TLX) [7], which we scored with two modifications: (1) a 21-point Likert scale was included and (2) dividing by 25 (the number of comparisons) instead of 8 (the number of factors) to ensure a score out of 100.

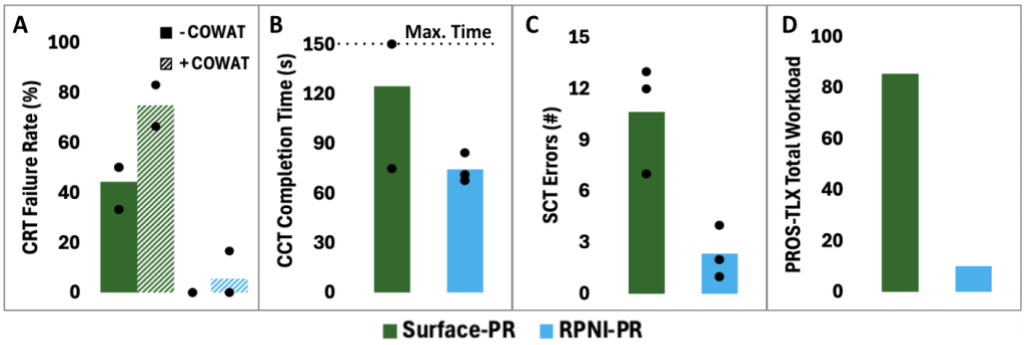

Figure 1: A. CRT, no COWAT versus with COWAT. B. Average trial time for CCT. C. Average SCT errors. D. Cognitive load measured post-sessions.

Results & Discussion: For CRT alone, the participant had zero errors with RPNI-PR (0%) compared to a high failure rate with Surface-PR (44.4%). With COWAT, the participant showed a slight increase in failure rate for RPNI-PR (+5.7%), but a large increase for Surface-PR (+30.6%). The participant completed the CCT much faster with RPNI-PR (74.5s) than with Surface-PR (124.9s). In SCT, the participant was more accurate at grip switches with RPNI-PR (2 errors) than with Surface-PR (11 errors). Finally, the participant had a much lower perceived workload using RPNI-PR (10 pts) compared to Surface-PR (85.4 pts) (Fig. 1).

Significance: Overall, the participant improved in all assessments of function across both tasks when using RPNI-PR. The participant reported RPNI-PR to be less of a cognitive burden than Surface-PR, which is further supported by her CRT + COWAT performance. This data suggests that RPNI-PR is a more intuitive and accurate method of controlling a prosthetic hand and wrist than Surface-PR.

Acknowledgements: This work was supported by the National Institutes of Health under Award R01NS105132. The opinions expressed in this article are the authors' own and do not reflect the view of the National Institutes of Health. We would like to thank Ossur for the use of the prosthetic hand, and Sara Isgro and Grace Li for their assistance with data processing and analysis.

References: [1] Atzori and Müller. (2015), *Frontiers in System Neuroscience,* vol. 9. [2] Dewald et al. (2019), *J Neuroeng Rehabil.* 16(147). [3] Vu et al. (2023), *J Neuroeng Rehabil.* 20(026039). [4] Hussaini et al. (2016), *Prosthetics and Orthotics International* 41(3):294-302. [5] Lee et al. (2024), *J Neuroeng Rehabil.* 21(1):21. [6] Ross et al. (2007), *Archives of Clinical Neuropsychology* 22(4). [7] Parr et al. (2023), *PloS One*, 18(5).

METABOLIC COST OF WALKING IS LOWER IN HIGH-FUNCTIONING TRANSFEMORAL PROSTHESIS-USERS WITH BONE-ANCHORED PROSTHESES VS. SOCKET-BASED PROSTHESES

*Ross H. Miller[1], Gauri A. Desai[1], Jae Kun Shim[1]
[1]University of Maryland, College Park, MD, USA
*Corresponding author's email: rosshm@umd.edu

Introduction: Individuals with lower limb loss typically have a high metabolic cost of walking compared to able-bodied individuals. For transfemoral limb loss, this high cost appears to be unavoidable: very high-functioning users still on average have a high metabolic cost [1-3], motivating a focus on how or if prosthesis characteristics can affect metabolic cost. Most transfemoral prostheses are attached using a socket, and this non-rigid interface presents a potential source of mechanical energy loss that must be restored through muscular force and/or work to locomote periodically. Bone-anchored prostheses attach directly and rigidly to the residual limb, removing a potential source of energy loss. Bone-anchoring is typically a surgical revision for prosthesis users who have poor outcomes with a socket. Longitudinal (pre- vs. post-surgery) data support a causal effect for bone-anchoring reducing the metabolic cost of walking vs. using a socket [4]. However, these data are complicated by confounders like weight loss and the outcomes of surgery and rehabilitation, which can independently affect metabolic cost. Comparisons between individuals with bone-anchored vs. socket-based prostheses who are all fit, mobile, and high-functioning could help isolate the effect of bone-anchoring *per se* and complement these longitudinal data. The purpose of this study was therefore to compare metabolic cost of walking between high-functioning transfemoral prosthesis users with and without bone-anchoring. Due to suspected mechanical energy loss by the socket, we hypothesized that individuals with bone-anchored prostheses would walk with lower metabolic cost than individuals with socket-based prostheses. We further checked this suspicion using optimal control simulations of walking with different degrees of freedom at the residual limb-prosthesis interface.

Methods: Twenty-four participants (43±11 years) with unilateral transfemoral limb loss were recruited, 12 with socket-based prostheses and 12 with bone-anchored prostheses. Each group had eight men and four women. The minimum detectable difference in metabolic cost with long-term error rates $\alpha = 0.05$ and $\beta = 0.20$ was ~2% for typical means and variance in this population [1,2]. Participants were included if they were at least 18 months post-surgery, able to walk unassisted for at least 20 minutes with their definitive prosthesis and no other aids, had a Medicare K-level of at least 3, and had no other health complications known to affect metabolic cost. All participants self-reported frequent participation in at least one additional form of recreational sport or exercise including cycling, running, hiking, swimming, tennis, weightlifting, CrossFit, wrestling, football, and/or basketball.

Participants walked while fasted on a level motorized treadmill at a belt speed of 1.0 m/s for 10 minutes. Respiratory gasses were measured using a metabolic part (Parvo Medics, UT, USA). Gasses were averaged over the final three minutes and converted to metabolic power, neglecting protein metabolism [5]. Body mass including the prosthesis mass was measured using a force platform (Kistler, Switzerland). Metabolic power was divided by speed and body mass to determine metabolic cost (J/m/kg). Due to the small sample sizes, metabolic cost was compared between groups using a Wilcoxon rank sum test (threshold $p < 0.05$).

Optimal control simulations of walking were performed using a three-dimensional full-body OpenSim model with the right leg modified to emulate a bone-anchored transfemoral prosthesis [3] (Fig. 1). Here different versions of the model were created that attached the prosthesis non-rigidly with spring-dampers allowing 1-6 degrees of freedom (DoF). OpenSim Moco was used to optimize muscle excitations and prosthesis stiffness and damping parameters to minimize the sum of (i) metabolic cost of walking and (ii) deviations from able-bodied gait mechanics [3]. Mechanical energy lost in the limb-prosthesis interface was then correlated with the model's gross metabolic cost of walking using Pearson's *r*.

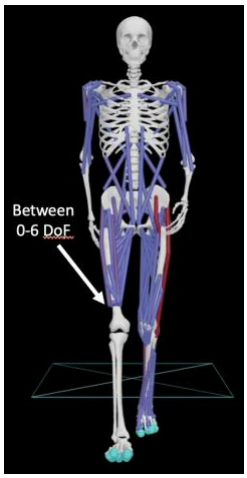

Figure 1: The OpenSim model walking with a transfemoral prosthesis.

Results & Discussion: Metabolic cost averaged 11.4% lower in bone-anchored users vs. socket-based users ($p = 0.035$; Fig. 2). In the simulations, metabolic cost increased progressively as more DoF were added to the limb-prosthesis interface. The full six-DoF model had 8.7% greater metabolic cost than the zero-DoF model. Metabolic cost in these simulations correlated strongly with mechanical energy loss in the limb-prosthesis interface ($r = 0.90$). Prosthesis mass averaged 4.6 kg for both groups.

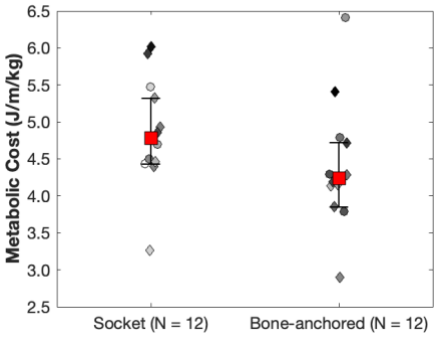

Figure 2: Metabolic cost of walking at 1.0 m/s for human participants with socket-based and bone-anchored prostheses. Square symbols are medians with 95% confidence intervals. Diamonds/circles are men/women. Darker symbols were older in age.

Significance: The present results support previous findings that bone-anchored prosthesis users have a lower metabolic cost than socket-based users [4,6] and suggests this economy results from reducing mechanical energy losses in the prosthetic limb.

Acknowledgments: Funded by CDMRP (HT9425-23-1-0103). The authors thank Chioma Ezeajughi and John Pope for assistance with data collections.

References: [1] Jarvis et al. (2017) *APMR* 98(7); [2] Russell Esposito et al. (2018) *Pros Orth Int* 42(2); [3] Miller et al. (2024) *PeerJ* 12:e16756; [4] Van de Meent et al. (2013) *APMR* 94(11); [5] Brockway (1987) *Hum Nutr* 41(6); [6] Kooiman et al. (2023) *Gait Posture* 103:12-18.

TRANSTIBIAL PROSTHESIS USERS EXHIBIT DIFFERENT PATTERNS OF HIP MUSCLE CO-CONTRACTION THAN CONTROLS IN BOTH THEIR RESIDUAL AND INTACT LIMBS

*Hannah D. Carey[1], Andrew Sawers[1]
[1]University of Illinois Chicago, Department of Kinesiology
*Corresponding author's email: hdcarey@uic.edu

Introduction: Transtibial prosthesis users (TTPU) users walk with a higher metabolic cost. Increased antagonist co-contraction may contribute to gait inefficiency and therefore be a potential target for rehabilitation. Greater ankle and knee muscle co-contraction has been reported in the residual limb [1] of TTPUs, but has yet to be characterized in the hip. Whether co-contraction in TTPUs is adaptive or maladaptive is unknown; characterizing hip muscle co-contraction patterns is the first step in determining whether co-contraction is modifiable, or whether modifications are desirable. As an initial step in understanding the patterns and purpose of hip muscle co-contraction, our objective was to identify periods of the gait cycle where co-contraction in TTPUs is significantly different from controls. We hypothesized that intact and residual limbs would exhibit periods of higher co-contraction than control limbs.

Methods: Bilateral bipolar surface EMG signals were collected at 1200 Hz from the gluteus maximus (GMAX), gluteus medius (GMED), rectus femoris (RFEM), and adductor magnus (ADMG) of six traumatic unilateral TTPUs (5 male, age: 52±21 yrs, time since amputation: 24±11 yrs) walking for 1 minute at their preferred speed (1.1±0.23 m/s) and six unimpaired controls (1 male, 30±8 yrs). Processed EMG signals were amplitude normalized to within-task maximums and each gait cycle was time normalized. Co-contraction between the ADMG and GMED, and the RFEM and GMAX was calculated across the gait cycle using Rudolph's co-contraction index (CCI) [2]. Unlike other common CCIs that yield a single discrete co-contraction value, Rudolph's CCI generates a co-contraction value at each timepoint in the gait cycle, providing a measure of when and how much co-contraction occurs. The resulting co-contraction time series were averaged across gait cycles for each participant and leg. Separate wavelet-functional ANOVAs (wfANOVA) [3] were run to test for significant differences in hip co-contraction between the control, residual, and intact limbs in each muscle pair.

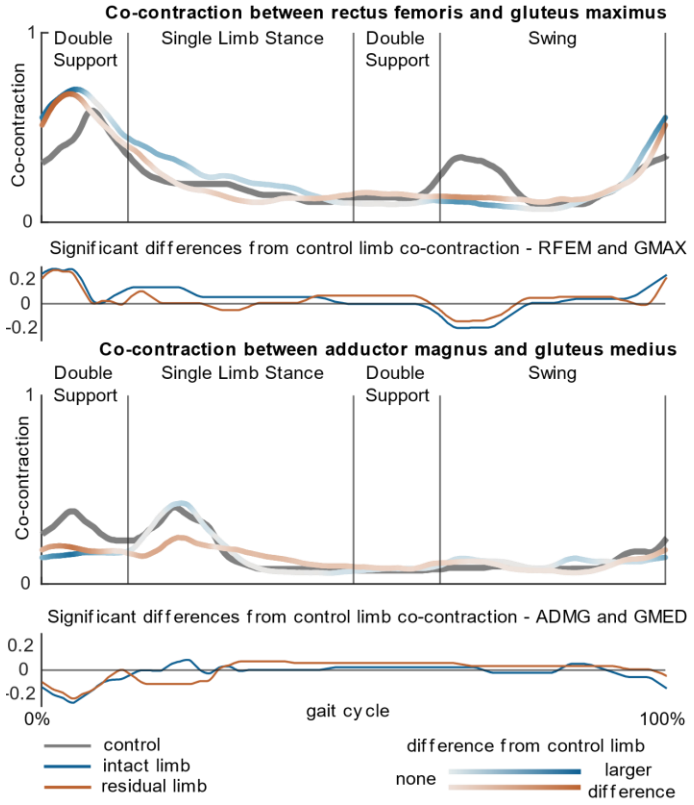

Figure 1: Average co-contraction in control (gray), intact (blue) and residual limbs (red), between RFEM and GMAX (1st panel), ADMG and GMED (3rd panel). Darker shading indicates larger difference from control limb, also plotted in second and bottom panels.

Results & Discussion: We found significantly different hip muscle co-contraction patterns in TTPUs compared to controls, possibly reflecting the different biomechanical demands on the hip and reduced capacity of residual limb muscles after amputation [4,5]. Co-contraction between GMAX and RFEM was greatest during late swing and early stance in all limbs, potentially serving to stiffen and prepare the hip for weight acceptance. The peak of GMAX/RFEM co-contraction was significantly larger and earlier in the intact and residual limbs compared to controls. Increased co-contraction in the residual limb could reflect smaller quadriceps contributions during early to mid-stance [5], rather than purposeful co-contraction. The smaller peak observed in early swing among controls was not present in TTPU; however, the presence of this peak varied widely among controls. Co-contraction between ADMG and GMED in controls exhibited two peaks, one in early and one in mid-stance, potentially providing mediolateral stability to the pelvis during the transition from double- to single-limb support. TTPU's intact limb exhibited the mid-stance, but not the early-stance peak; ADMG/GMED co-contraction in the residual limb was low overall. We observed substantial stride-to-stride and between subject variability in residual limb co-contraction patterns, suggesting subject-specific adaptations to walking with a prosthesis.

Significance: TTPUs exhibit different patterns of hip muscle co-contraction than controls in both their residual and intact limbs, potentially reflecting differences in muscle capacity and the mechanical demands of walking with a prosthesis. Hip muscle co-contraction in TTPUs was not consistently greater, suggesting it may not be a primary contributor to increased metabolic cost. These results motivate further experiments and simulations to probe the role of early-stance hip muscle co-contraction in amputee gait and investigate whether co-contraction is maladaptive and modifiable.

Acknowledgments: Funding from DoD award # HT9425-24-1-0212. Authors thank Moaz Tobaigy for help with data collection.

References: [1] Seyedali et al. 2014. *JNER* (9). [2] Rudolph et al. 2000. *Knee Surg Sports Traumatol Art* 8(5). [3] McKay et al. 2013. *J Neurophys* 109(2). [4] Prinsen et al. 2011. *Arch Phys Med Rehabil.* 92. [5] Silverman & Neptune 2012. *J Biomech.* 45(13).

TRANSTIBIAL PROSTHESIS USERS ARE MORE FATIGABLE THAN UNIMPAIRED ADULTS

*Julie Ferrell-Olson[1], Dan Junquera[1], Brian J. Hafner[2], Andrew Sawers[1]
[1]University of Illinois Chicago, [2]University of Washington
*Corresponding author's email: jferre26@uic.edu

Introduction: Activity-induced fatigue is often reported by lower limb prosthesis (LLP) users prior to a fall [1] and has been shown to increase the odds a fall will be injurious [2]. Given their high fall rate, identifying LLP users' susceptibility to activity-induced fatigue and its impact on stability is paramount. Self-report surveys that measure overall fatigue do not exhibit expected differences between LLP users and controls [3] likely because they do not measure fatigue relative to the performance of specific physical tasks [4]. Likewise, assessing fatigue via changes in gait speed alone during timed walk tests does not account for self-pacing strategies LLP users adopt to avoid fatigue [5]. Locomotor fatigability indices overcome these limitations by contextualizing fatigue-induced changes in gait speed during a timed walking test relative to the total distance walked [6]. These indices have not yet been used to evaluate the effect of amputation on locomotor fatigability. Consequently, despite the potential influence of locomotor fatigability on falls and fall-related injury, it remains unknown if transtibial amputation increases locomotor fatigability or how an acute fatiguing locomotor task affects gait stability in LLP users [7]. The objectives of this study were to determine if traumatic transtibial amputation increases locomotor fatigability, and if said fatigability reduces LLP users' stability while walking. We hypothesized that, due to the loss of ankle plantarflexion power, traumatic transtibial prosthesis users (TTPU) would be more fatigable than controls, and that greater locomotor fatigability would be correlated with reduced gait stability.

Methods: Data from 18 participants with unilateral traumatic amputation (2 females; 42.6 ± 12.4 yrs old; 12.7 ± 11.2 yrs since amputation) collected in a prior study [7] were compared to 12 unimpaired controls (2 females; 34.1 ± 8.71 yrs old) collected for this study. Locomotor fatigability was quantified as the ratio of change in gait speed to total distance walked during a standardized 6-min walk test [5]. Gait stability was inferred from changes in spatiotemporal variables related to walking stability (e.g., step width, % double support) [8] recorded on a 5-meter electronic walkway (ProtoKinetics LLC, Havertown, Pennsylvania) during the 6-min walk test. An independent-sample t-test was used to assess differences in locomotor fatigability scores between TTPUs and controls and test our hypothesis that traumatic transtibial amputation increases locomotor fatigability. A common language effect size was calculated to interpret the magnitude of between-group differences. Pearson correlation coefficients were calculated between locomotor fatigability scores and changes in spatiotemporal gait variables to test our hypothesis that increased locomotor fatigability reduces gait stability.

Results & Discussion: Locomotor fatigability scores were significantly greater in TTPU than controls (TTPU: $\bar{x}$=1.76 ± 0.23; CONT: $\bar{x}$=1.39 ± 0.14; $t(28)=4.97$, $p<.001$, Fig 1). A common language effect size of 0.90 indicates there is a 90% probability that a randomly selected TTPU would have greater locomotor fatigability than a randomly selected control. Based on the higher fatigability scores among TTPUs than controls, coupled with the absence of any significant co-morbid conditions among the TTPUs that typically accompany lower limb amputation, we can infer that: i) traumatic unilateral transtibial amputation increases locomotor fatigability; ii) the locomotor fatigability index [5] used here possesses initial evidence of validity, making it a feasible and acceptable method for assessing the impact of more proximal amputation levels and additional etiologies, and iii) the loss of ankle plantarflexion power - the primary biomechanical difference between TTPU and controls - is likely a key contributor to TTPUs locomotor fatigability. Among the spatiotemporal gait variables related to walking stability, only percent time in double support was moderately and significantly correlated with locomotor fatigability (r_s=-0.55, p=0.019). This indicates that TTPUs who were more fatigable reduced the amount of time spent in double support at the end of the 6-min walk test relative to the start of the test. Given that increasing time in double support is a common strategy for promoting stability in walking, the observed decrease in percent double support with increasing locomotor fatigability suggests that walking-induced fatigue may render TTPUs' gait less stable, making them more susceptible to falls.

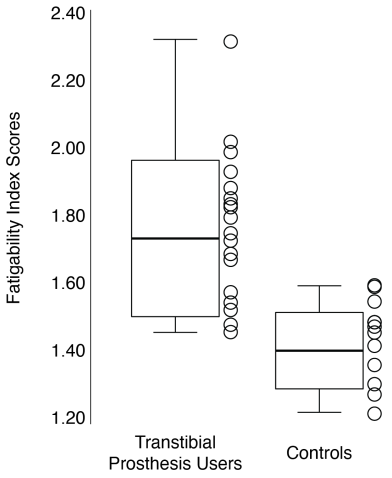

Figure 1: Fatigability Index scores for TTPU and Controls. Center line represents the mean, boxes ±1 SD. Dots represent individual subjects.

Significance: Our results indicate that TTPUs are more fatigable than controls and that increased locomotor fatigability may challenge their locomotor stability. Given reports of activity-induced fatigue prior to a fall [1] and evidence that such fatigue raises the odds of a fall being injurious [2], our results represent an important first step in connecting locomotor fatigability with stability and fall risk in LLP users. Determining how activity-induced fatigue impairs balance and balance recovery could improve our assessment and treatment of fall risk in LLP users. Additional research into the biomechanical, physiological, and prosthetic-specific factors underlying TTPUs' locomotor fatigability and its consequences is warranted.

References: [1] Sawers et al. (2022), *PloS One*.17(7); [2] Tobaigy et al. (2023), *PM&R*.15(4); [3] Amtmann et al. (2015), *APMR*. 96(8); [4] Glynn and Qiao (2023), *Fatigue.* 11(2-4); [5] Eldadah (2010), *PM&R*. 2(5); [6] Schnelle et al. (2012), *JAGS.* 60(8); [7] Morgan et al. (2018), *PloS One*. 13(2); [8] Sinitski et al. (2019), *Disab and Rehab*.16(1)

IN-SOCKET MECHANICS ARE ASSOCIATED WITH PATIENT-REPORTED COMFORT AND FUNCTION IN INDIVIDUALS WITH TRANSFEMORAL AMPUTATIONS

*Paige Paulus[1,2a], Tom Gale[2a], Rishabh Shetty[2a], Justin Elder[2b], Yulia Yatsenko[2a], Gina McKernan[2b], Goeran Fiedler[2c], and William Anderst[2a]

[1]Northwestern University, Department of Physical Medicine and Rehabilitation, [2]University of Pittsburgh, [a]Department of Orthopaedic Surgery, [b]School of Medicine, [c]Department of Rehabilitation Science and Technology

*Corresponding author's email: paige.paulus@northwestern.edu

Introduction: Despite advancements in prosthetic technology, individuals with lower limb loss face persistent challenges, including residual limb skin problems and low back pain, due, in part, to poorly fitting prosthetic sockets [1]. Prosthetists aim to optimize socket design to enhance function while minimizing discomfort. However, there is limited quantitative data to support this optimization process, resulting in heavy reliance on patient feedback and clinical expertise. Additionally, there is limited information available on the relationship between socket design and in-socket mechanics and how these mechanics influence patient-reported comfort and function. It has been theorized that reducing residual femur and skin motion improves socket function, but there is limited quantitative data to support these assumptions [2]. This project aims to determine the relationship between in-socket mechanics and patient-reported comfort and function and to identify clinical measurements that are related to research grade data that can inform socket design considerations. We hypothesized that the amount of residual bone motion and peak skin strain are associated with patient-reported comfort and function. Additionally, we hypothesized that x-ray imaging during static standing will correspond to dynamic residual femur motion.

Methods: Individuals with unilateral transfemoral amputations provided written informed consent to participate in this IRB approved study. Participants were casted and fitted by a licensed prosthetist for up to seven prosthetic sockets which were altered to reflect the standard socket adjustments made in a clinical setting. These modifications included changes to brim height, volume, cross-sectional geometry, and material stiffness. Thirty to 50 radio-opaque beads were adhered in a grid pattern to participants' distal residual limb prior to donning sockets. Participants walked on a treadmill in each socket, and three trials of synchronized biplane radiographs were collected per socket at 100 images/sec for 2.0 sec (max 90 kV, 200 mA, 1 ms pulse width). Additionally, one static, weightbearing image was collected per socket for static analyses and baseline measurements. Participants provided feedback on the comfort and function of each socket relative to their current socket using a global rating of change (GROC) scale at the end of each socket configuration [3]. CT scans of each participant's the residual femur were obtained (average 0.57 × 0.57 mm in-plane resolution, 1.25 mm slice thickness) and used to create subject-specific bone models. Residual femur motion relative to the socket was tracked using a previously validated volumetric model-based tracking system with submilimeter accuracy [4], and residual limb skin strain was measured using a previously validated bead tracking technique and FEBio analysis [5]. Dynamic data was interpolated to percent stance phase and peak values were identified and averaged per participant and socket type. Generalized linear models (GLM) were employed for statistical analyses [6], allowing for the assessment of in-socket mechanical parameters' effects on patient-reported outcomes.

Results & Discussion: Eight individuals with traumatic unilateral transfemoral amputations (1F, age: 57±14 years, height: 180.1±6.6 cm, weight with prosthesis: 80.9±15.5 kg) were included in this analysis. The overall model to predict comfort, which included peak skin strain at the lateral and medial socket wall, and average strains at the central anterior, lateral, and distal lateral socket aspects was significant, $F(5,20)=4.278$, $p=.008$. Peak skin strain, specifically in the central anterior region, was a significant predictor of comfort $F(1,20)=10.677$, $p=.004$, accounting for the largest amount of variability in comfort score, $\beta=31.445$, 95% CI [11.371-51.52]. Additionally, femur orientation from static imaging was correlated with peak residual femur motion during gait (Table 1). Overall, the data indicates that peak residual femur motion is more related to static femur orientation than skin strain, but skin strain is most predictive of comfort and function.

Table 1: *Correlation coefficients from analyses of the relationship between residual femur orientation in static imaging and peak dynamic residual femur motion during gait. ** p<0.01 * p<0.05*

		Peak Dynamic Motion					
		Anterior Tilt	Internal Rot.	Varus	Lateral Trans.	Piston	Anterior Trans.
Static Orientation	Anterior Tilt	0.28	0.12	0.26	0.25	0.52**	0.18
	Internal Rotation	0.51**	0.85**	0.02	-0.24	0.04	0.68**
	Varus	-0.43**	-0.17	0.82**	0.11	0.80**	-0.33*
	Lateral Trans.	0.03	-0.47**	-0.00	0.95**	0.41**	-0.23
	Piston	-0.33*	-0.24	0.68**	0.43**	0.99**	-0.39**
	Anterior Trans.	0.36*	0.64**	-0.03	-0.27	-0.02	0.83**

Significance: The findings from this analysis provide support to the theory that within socket mechanics are associated with prosthetic socket satisfaction. Additionally, they provide insights into clinically accessible metrics which are associated within socket mechanics that typically can only be evaluated using research-grade instrumentation.

Acknowledgments: The research was supported by the DoD Office of the Congressionally Directed Medical Research Programs through the Restoring Warfighters with Neuromusculoskeletal Injuries Research Award under award number W81XWH2010914.

References: [1] Amtmann D, er al. (2015), *APM&R*; 96(8); [2] Wernke MM, et al. (2017), *AWC*; 6(7); [3] Jaeschke R, et al. (1989), *CCT*; 10(4); [4] Gale T, et al. (2020), *J Biomech*; 112; [5] Gale T, et al. (2021), *J Biomech*; 129; [6] McCullagh P. (2019); *Rout.*

PASSIVE MECHANICS OF SKELETAL MUSCLE DEMONSTRATE SEXUAL DIMORPHISMS

*Timothy McGinley[1] and Benjamin I Binder-Markey[1,2]
[1]School of Biomedical Engineering, Science and Health Systems & [2]Department of Physical Therapy & Rehabilitation Sciences, Drexel University, Philadelphia Pa
*Corresponding email: tm3292@drexel.edu

Introduction: Sexual dimorphisms, systematic differences between sexes of the same species, are well-documented phenomena in various biological systems. Previous studies have shown that male skeletal muscles generally exhibit greater muscle mass and physiological cross-sectional area (PCSA) compared to female muscles [1, 2]. These size differences are often attributed to differences in sex hormones, such as testosterone and estrogen, which play significant roles in muscle development and maintenance [3]. However, once normalized for size the specific tension between sexes remains the same, indicating that intracellular fiber mechanisms and mechanics remain consistent across sexes [4]. Despite these findings, there is a notable gap in research specifically addressing sexual dimorphisms in skeletal muscle passive mechanical properties. Understanding these differences is crucial as they can influence muscle function, injury susceptibility, and rehabilitation outcomes. Joint-level mechanics literature demonstrates male joints tend to exhibit higher stiffness compared to female joints [5]. Yet this discrepancy may be due to the lack of normalizing of size across individuals, and they don't isolate the muscles' mechanics from joint and ligament properties. Therefore, the purpose of this study is to directly measure passive mechanical properties in the skeletal muscles of male and female mice to determine if there are sexual dimorphisms in the passive mechanics. We hypothesize that male skeletal muscles will exhibit higher passive stresses compared to female skeletal muscles. This research aims to fill the existing gap by providing a comprehensive analysis of the passive mechanical characteristics of male and female muscles, contributing to a deeper understanding of sex differences in muscle mechanics.

Methods: Passive mechanical characteristics across four hind-limb muscles, differing in structure and function, of both male and female 12- to 16-week-old C57BL6 mice were collected. Muscles collected were the rectus femoris (RF), semimembranosus (SM), lateral gastrocnemius (LG), and tibialis anterior (TA). Fresh muscles were dissected from their proximal to distal bony insertions, placed in a physiological bath, and mechanically tested. Each muscle was lengthened in ~5% whole muscle strain increments from 0%-50% in a stepwise function with a 3-minute hold at each strain. Force and displacement at the end of each hold were recorded. Following testing, we recorded the sample's muscle mass. Muscle passive forces were normalized to PCSA [6]. The force-strain data and normalized passive stress-strain data were fit using a non-linear regression and that line was averaged across samples [7]. The normalized stiffness and mass were compared across sexes.

Results & Discussion: Aligning with previous studies, female muscles demonstrated significantly lower mass (Table 1). Yet males did not demonstrate significantly larger passive muscle forces (graph not shown). Furthermore, when the forces were normalized to PCSA, the stress-strain curves demonstrated significantly higher stress profiles in the female samples across all the muscles (Fig. 1). This result is the opposite of our initial hypothesis. These data suggest male and female muscles have different passive mechanical properties at the tissue level, whereas their intrinsic active properties remain similar.

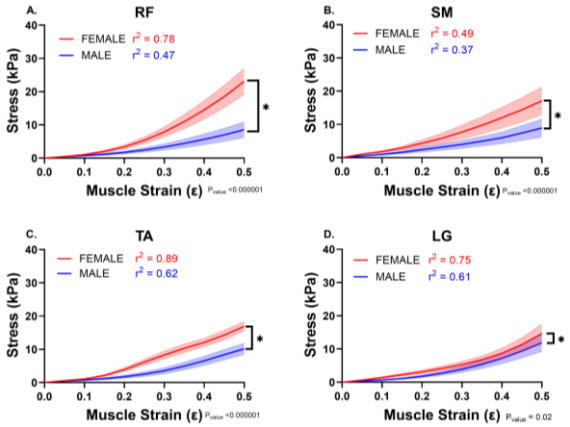

Figure 1: Normalized stress-strain curves for female (red) and male (blue) 12-16 week old C57BL6 mice. Data shown as averages±SD. Overall r^2 for each condition. * *and bracket indicate* $p<0.05$; $n_{female}=5$; $n_{male}=7$-8

Significance: We have demonstrated in 12 to 16-week-old sexually mature mice that the passive mechanics of male and female skeletal muscle differ, which is not a result of increased muscle mass and volume. These differences can influence muscle function, injury susceptibility, and rehabilitation outcomes and thus must be accounted for in future studies. Future studies will explore how these dimorphisms change with age and ovulation cycle. In addition, collagen content analysis will be performed to determine the differences in connective tissue between sexes. Overall, these findings contribute to a deeper understanding of sex differences in passive muscle mechanics and could have implications for developing sex-specific training and rehabilitation programs.

Acknowledgments: Individual Researcher Biomedical Award from The Hartwell Foundation and Foundation for Physical Therapy Research

Table 1: *Averaged physiological properties of female and male muscle *=p<0.05 compared to female muscle*

	Mass (mg)	
	Female	**Male**
RF	68.36 ± 4.60	98.44 ± 13.83*
SM	85.34 ± 7.40	135.20 ± 20.17*
TA	44.12 ± 6.63	60.10 ± 8.51*
LG	46.12 ± 6.97	86.87 ± 10.59*

References:

[1] Emmert et al. (2024), J Appl Physiol 137(2):274-299; [2] Gartych et al. (2021) Front. Neuroanat. 15:734555; [3] Plotkin et al. (2024) J. Endocr. Soc 8(10); [4] Haizlip et al. (2015) Physiol. 30(1):30-39; [5] Glenmark et al. (2004). Am. J. Physiol. Endocrinol. 287(6) 1125-1131; [6] Binder-Markey et al. (2021), J Biomech 129; [7] Ward et al. (2020), Front Physiol. 11.

SHARED SIGNATURES OF FOOT PLACEMENT CONTROL FOR STABLE LOCOMOTION ACROSS SPECIES

*Antoine De Comite[1], Nidhi Seethapathi[1]
[1]Department of Brain and Cognitive Science, MIT, Cambridge, MA, USA
*Corresponding author's email: adecomit@mit.edu

Introduction: Stable locomotion is a fundamental motor skill for many legged animals. Foot placement control, i.e. placement of the swinging leg in a manner that corrects recent errors, is a primary control mechanism for stable locomotion in humans. However, it remains unclear whether such error-based foot placement is shared across species. Indeed, two different theoretical control structures are used to model how animals achieve stable locomotion. A feedforward-only controller (Model 1), thought to dominate in smaller animals, assumes forward velocity-dependent foot placement patterns (Figure 1, red). A feedback controller (Model 2) that uses body state error-dependent control to modulate foot placements is thought to dominate in humans, but lacks evidence in other species (Figure 1, blue). Here, we put forth a unified feedforward-feedback controller structure, developing a data-driven model to test empirical support for these two control hypotheses. By comparing their predictions to the statistical dependencies observed during overground locomotion in flies, mice, and humans, we find shared signatures of feedforward-feedback control across species.

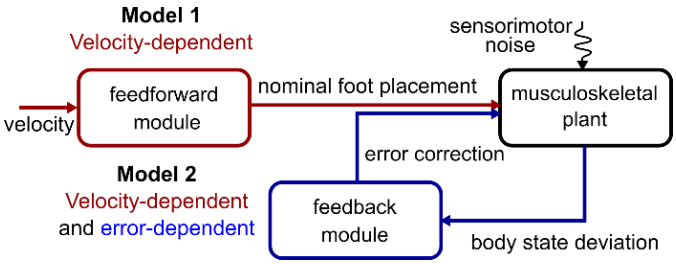

Figure 1: Two alternative control models for foot placement

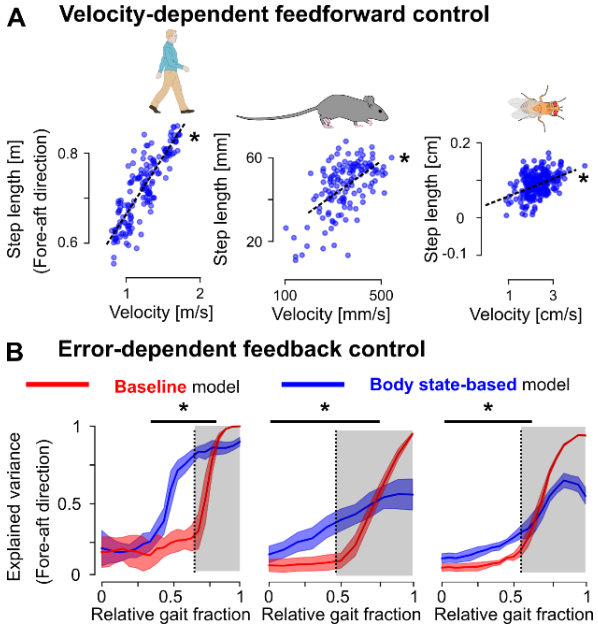

Figure 2: The fore-aft foot placement (A) is explained by velocity whereas the lateral foot placement (B) is explained by body state errors in humans, mice, and flies.

Methods: We unify two alternate hypothesized control structures (Figure 1) testing signatures of their components in large-scale locomotion data in humans [1], mice [2], and flies [3]. The phase-locked positions of the limbs as well as positions of the body were analysed while individuals were freely moving. The initiations of the stance and swing phases of each limb were defined respectively as the maximum and minimum of the fore-aft position of that limb, expressed with respect to the body marker. The contact locations were then defined as the average location of the limbs during their stance phase. We regressed the contact location against the movement velocity to extract signatures of velocity-dependent foot placement. We regressed the deviations in foot placement relative to nominal velocity-dependent foot placement, against the body deviations relative to the nominal body states to identify signatures of the body state error-dependent foot placement.

Results & Discussion: The fore-aft foot placement was correlated with velocity (Figure 2A), but the lateral foot placement was not in humans, mice, and flies. The variability in lateral foot placement was better predicted by the body deviations than by a baseline model that predicts foot placement using the variability in foot kinematics (blue and red in Figure 2B, respectively), even before the initiation of leg swing (gray rectangles in Figure 2B). These results provide empirical support for the hypothesized feedforward-feedback control structure, demonstrating the existence of both velocity-dependent and body state error-dependent control signatures across species. These signatures also reveal a decoupling between control of the fore-aft and lateral foot placement across species.

Our data-driven model reveals that humans, mice, and flies exhibit velocity- and error-dependent foot placement control, but also that these different species use different control amplitudes, captured by the increase in R^2 relative to the baseline, for such foot placement control.

Significance: This work reveals previously unknown common signatures of stabilizing control during locomotion across species, finding that flies, mice, and humans exhibit body state error-dependent foot placement. By suggesting the existence of error-dependent control in neuroscientifically accessible animals, we open a new avenue for investigating the neural basis of locomotor stability in natural variability. These cross-species findings also highlight how diverse nervous systems and body mechanics achieve a common functional goal. This work could potentially lead to cross-species diagnostics as well as inform the development of animal-inspired control strategies for legged robots.

Acknowledgments: ADC is supported by a fellowship of the K. Lisa Yang ICoN Center at MIT.

References: [1] Yang et al. (2014), *Biology Letters*, **10(9)**: 20140405; [2] Camargo et al. (2021). *J. Biomech*, **119**: 110320; [3] Klibaite et al. (2022), *Molecular Autism* **13**:12 [4] DeAngelis et al. (2019) *Elife*, **8**: e4640.

IN VIVO ESTIMATES OF SHEAR PROPERTIES IN CAT SOLEUS MUSCLE

***Ridhi Sahani**[1,2], Qifeng Wang[1], Hendrik Dewald[1,2], Amr Mahrous[1], Matthieu Chardon[1], Kenneth Shull[1], Daniel Ludvig[1,2], Eric Perreault[1,2]
[1]Northwestern University, Illinois, USA
[2]Shirley Ryan AbilityLab, Illinois, USA
*Corresponding author's email: ridhi.sahani@northwestern.edu

Introduction: The material properties of skeletal muscle are essential for muscles' ability to produce the forces required for movement and posture. Alterations in these complex properties are implicated in muscle dysfunction, and it is important to develop methods to characterize the full material properties of muscle to understand the underlying causes of muscle dysfunction. While the tensile properties of muscle have been extensively studied, few studies have characterized muscles' response to shear loading. The shear properties of skeletal muscle are important for force transmission within muscle and during injury [1,2] but have not been characterized in active muscle or *in vivo*. Shear wave elastography (SWE) is a promising method for noninvasively estimating shear moduli, but SWE varies with stress and activation in muscle [3] and direct measures of shear moduli are necessary for validating and improving SWE methodology. The goal of our study was to develop a method to estimate the shear moduli of active and passive muscle with varying levels of stress. To do so, we performed *in vivo* experiments in cat soleus muscles using a micro-indentation technique to estimate shear moduli in the direction of muscle fibers (u_{II}) and in the plane perpendicular to muscle fibers (u_T). We hypothesized that the shear moduli (u_{II} and u_T) would increase with active and passive stress. This would suggest that muscles' resistance to shear loading *in vivo* is dependent on the stress within muscle, which may explain conditions in which injury due to shearing is more likely.

Methods: The hindlimbs of anesthetized cats were placed in a 37C saline bath with knee and ankle joints fixed. The soleus and its distal tendon were dissected from surrounding tissues, remaining connected to a bone chip of the calcaneus (Fig 1A). Force-length properties were characterized by systematically lengthening the muscle and measuring force by stimulating a distal branch of the sciatic nerve (40Hz). Four active and four passive lengths corresponding to 25-100% optimal force (F_{max}) were selected. At each fixed length, isometric force was measured and used to calculate stress, accounting for the changing cross-sectional area [4]. Rapid changes in muscle-tendon length (2mm at 2m/s) were applied to measure the short-range stiffness of the muscle tendon unit and calculate Young's modulus parallel to muscle fibers (E_{II}) [3]. The shear moduli were estimated using a coupled micro-indentation and finite-element modelling approach to fit material properties based on the force-displacement data from indentation, along with the measured E_{II}. This method was validated in gel phantoms with known material properties where direct measurements of shear moduli were possible (10% accuracy). The indenter blade was positioned in the mid-belly region of the muscle, oriented either parallel or perpendicular to muscle fibers. A linear (2mm at 2m/s) and sinusoidal (0.2mm at 10Hz) indentation was applied to estimate the shear modulus parallel (u_{II}) and perpendicular (u_T) to muscle fibers. During indentation, an ultrasound probe was used to align the indenter blade and measure contact area between the blade and muscle in the perpendicular configuration. Individual linear regressions were performed on the relationships between shear moduli and stress, with data shown from one cat (Fig 1).

Results & Discussion: From preliminary results in one cat, we found that the shear modulus parallel to muscle fibers (u_{II}) increased with active stress (p=1.4e-3), while the shear modulus perpendicular to muscle fibers (u_T) increased with passive stress (p=1.1e-6) (Fig 1B). The estimates of u_T were derived directly from the micro-indention, while the estimates of u_{II} also relied on the measured E_{II} and thus have greater levels of noise. Future studies will determine the consistency of these trends across cats. If these trends hold, this may help to explain why SWE measurements vary between active and passive muscle at macthed stress levels [3].

Significance: To our knowledge, this is the first study to estimate the shear moduli of active muscle, which is particularly important for force transmission during movement. Our measurements of *in vivo* muscle properties can also be used to compare with estimates of muscle stiffness from non-invasive methods such as SWE that could have significant clinical impact.

Acknowledgments: Thank you to our funding sources (R01 AR071162, T32 HD07418).

References: [1] Huijing, P., et al. (1998). *J. Exp. Biol.* **201**, 683–691 [2] Järvinen, T. A., et al. (2014). *Muscles Ligaments Tendons J.* **3**, 337–345 [3] Bernabei, M et al. (2023). *J. Appl. Physiol.* **134**, 941–950 [4] Cui L. et al. (2008). *J. Biomech.* **41**, 1945

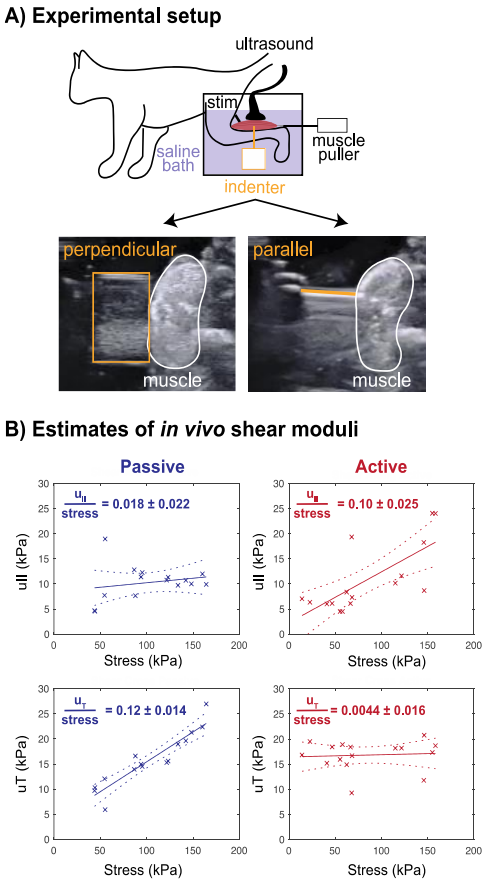

Figure 1: A) Experimental setup with indentation perpendicular and parallel to muscle fibers. B) Estimates of shear moduli vs. stress with linear regressions and 95% confidence intervals.

DEVELOPMENT OF A SMALL ANIMAL DEVICE FOR MEASURING IN VIVO MUSCLE-TENDON LOADING

*Alex Reiter[1], Patrick Hinkle[1], Fuad Al Hasan Bin Enam[1], Koyal Garg[1]
[1]Department of Biomedical Engineering, Saint Louis University, Saint Louis, MO
*Corresponding author's email: alex.j.reiter@slu.edu

Introduction: Animal models allow for the characterization of muscle-tendon mechanics during any stage of development, homeostasis, disease, or injury. However, their usefulness is limited due to the lack of a noninvasive, direct measure of in vivo tissue loading. *In vivo* techniques utilizing implantable devices are invasive [1], while noninvasive methods measuring joint torque do not assess tissue-level function [2]. Shear wave tensiometry has been introduced as a noninvasive technique for direct assessment of in vivo muscle-tendon loading in humans [3-5]. Loading is quantified by tracking the vibrational behavior of propagating shear waves in the tissue. The purpose of this study was two-fold: (1) develop tensiometry for rodent models demonstrating the predicted analytic solution in healthy animals, and (2) characterize reductions in tissue loading due to a traumatic muscle injury.

Methods: Female Sprague Dawley rats (10-12 weeks old, 225-275g, Inotiv) were subjected to a traumatic muscle injury ($n = 4$) or served as age-matched controls ($n = 3$). For the injury group, animals were subjected to a surgically induced volumetric muscle loss injury in the gastrocnemius muscle; approx. ~20% of the muscle's mass was removed. After four weeks, the function of the right triceps surae muscle-Achilles tendon unit was tested via shear wave tensiometry simultaneously with a typical ankle torque measurement device (806D, Aurora Scientific). The custom-built tensiometer consisted of a piezoelectric actuator (PK4FQP2, Thorlabs) for superficially inducing shear wave vibrations in the Achilles tendon and two miniature accelerometers (352C23, PCB Piezotronics) for measuring the vibration wave traveling through the tendon (Fig. 1). Wave speeds were computed using the time delay between accelerometer signals estimated using a cross-correlation approach as described previously [3]. To prepare for tensiometer and torque measurements of the right hindlimb plantarflexor complex, animals were anesthetized, and the peroneal branch of the sciatic nerve was transected surgically. Animals were laid prone with the foot strapped to the foot pedal of the ankle torque measurement device and the ipsilateral knee fixed in an adjacent clamp; the tensiometer was placed over the Achilles tendon. Two platinum electrodes were inserted around the sciatic nerve and isometric contractions were initiated with varying stimulation frequencies (20Hz-100Hz, 20Hz intervals, 2 min. rest between contractions). Statistical differences between control and injured muscles in terms of wave speed and torque production were analyzed using two-way ANOVA with Sidak post-hoc tests if significant interactions or main effects were detected. Wave speed and ankle torque were normalized to animal body mass; significance was set at $p \leq 0.05$.

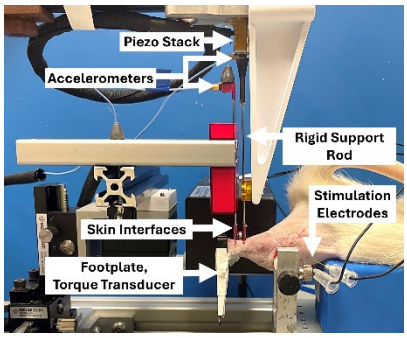

Figure 1: The tensiometer and corresponding components measuring tendon wave speed in an animal.

Results & Discussion: During isometric contractions, tensiometry was able to capture wave speed measurements with similar time series trends as torque data, including the rising edges with contraction onset, loading plateaus within the contraction region, and falling edges upon relaxation (Fig. 2). Injured muscles showed a significant reduction in wave speed and torque (main effect, $p<0.001$) relative to control muscles (Fig. 3). The stimulation frequency also significantly affected the measured wave speed and ankle torque (main effect, $p < 0.001$). No interaction was detected for wave speed ($p = 0.250$) or torque ($p = 0.089$). Post-hoc tests revealed differences in control and injured animals at 60-100 Hz for wave speed and 40-100 Hz for torque. The results show that tensiometry can be reliably and noninvasively scaled to detect expected time-series trends during contraction, linear relationships between wave speed and loading predicted by the analytical model, and reductions in tissue loading due to injury. By capturing tissue-specific loading rather than net plantarflexor torque, tensiometry could provide further insight into in vivo triceps surae force-frequency relationships in healthy and injured muscle not possible with ankle torque measurement. Although peroneal nerve transection enabled exclusive plantarflexor complex recruitment, future work will assess tensiometry as a true noninvasive, longitudinal technique. Ongoing work is also testing additional healthy and injured animals, tracking longitudinal changes following injury, and determining sex-based differences in both cases.

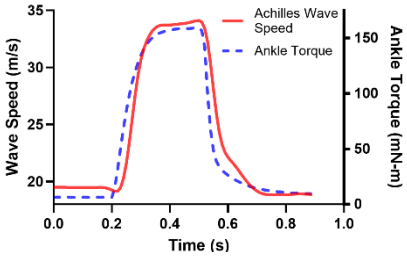

Figure 2: Representative time series wave speed and torque during isometric contraction at 100Hz stimulation.

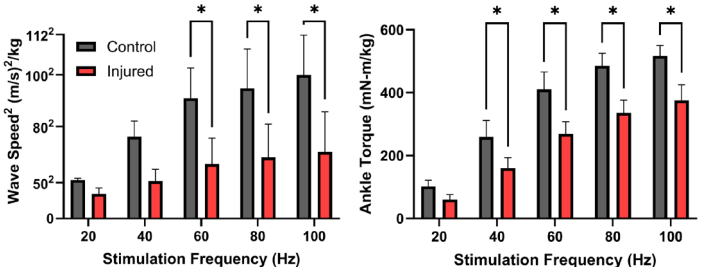

Figure 3: Squared wave speed (left) and ankle torque (right) vs stimulation frequency for control and injured animals. (*$p \leq 0.05$)

Significance: This work has translational significance. Novel treatments for muscle and tendon injury and disease are extensively studied in animal models before clinical use. Tensiometry has the potential to quantify the efficacy of such treatments noninvasively at the tissue level in animal models, with a clinical version under development allowing for translational research.

Acknowledgments: Funding from NIH (R03HD115731 and 1R15GM129731-02).
References: [1] Herzog et al., *J Biomech* 26(8), 1993. [2] West et al., *Am J Physio Cell*, 2023. [3] Martin, *Nat Com*, 2018. [4] Keuler, *Sci Rep*, 2019. [5] Acuña, *Phys Rep*, 2019.

PEAK STRESS AND PEAK STRAIN LOCATIONS ARE DIFFERENT IN A PORCINE ACHILLES TENDON FOLLOWING APPLICATION OF BIOLOGICAL LOADS

*Zoe M. Moore[1], Christopher P. Curry[1], Jayden J. Weaber-Heagele[1], Julianna C. Simon[2], Meghan E. Vidt[1,3]
[1]Biomedical Engineering, Pennsylvania State University, University Park, PA, USA
[2]Graduate Program in Acoustics, Pennsylvania State University, University Park, PA, USA
[3]Physical Medicine and Rehabilitation, Penn State College of Medicine, Hershey, PA, USA
*Corresponding author's email: zmm5238@psu.edu

Introduction: Tendon injuries affect ~7 million adults worldwide, with increased prevalence in tendons that are subjected to repetitive loading or high load bearing [1]. Tears decrease the mechanical integrity of the tissue, resulting in decreased tissue function [1]. Prior work suggests that tendon tears develop at locations of peak stress and peak strain [2, 3]. However, little work has examined these trends in the Achilles tendon, a tendon susceptible to tearing that regularly experiences high loads. The objective of this work was to develop and implement a finite element model of a healthy porcine Achilles tendon to examine the tendon mechanical response to loading. This model will improve our understanding of tear development in tendons that are susceptible to injury. It is hypothesized that peak stress and peak strain will increase with increased magnitude of load applied, and that peak stress and peak strain locations in response to the applied load will both occur at the enthesis region.

Methods: Magnetic resonance images of a porcine hind limb were segmented to create a 3D mesh that was imported into COMSOL software (v.6.2, COMSOL AB, Stockholm, Sweden). The bone, enthesis, tendon, aponeurosis, and muscle regions were defined in the model. Material properties for each region were defined using prior literature [4, 5, 6] and prior experimental data. The model was validated by applying 2 forces along the force-displacement curve from experimental data to the centroid of the enthesis in the direction of the muscle belly to replicate the mechanical testing set-up. The differences between modelled and experimental displacements were examined. After model validation, forces that were multiples (0.4x, 1x, 2.5x, 4x, and 9x body weight) of average body weight (64 kg) of pigs from a prior experimental study were applied to the centroid of the aponeurosis in the direction of the muscle belly to represent biological loading conditions [7, 8, 9]. Peak principal stress and peak principal strain magnitudes and locations within the model were identified. A linear regression analysis was performed to separately determine the relationship between body load and peak principal stress, peak principal strain. Analyses were performed in MATLAB (Mathwork, Natick, MA, USA) with significance set at $p<0.05$

Results & Discussion: Model predicted displacements were not different than the experimental displacements for both force inputs ($p=0.985$, $p=0.100$), indicating that the model was validated. There was a positive linear relationship between peak principal stress and applied body load ($p<0.0001$), and between peak principal strain and applied body load ($p=0.00014$) (Figure 1A, B). However, at the lower applied loads (0.4x, 1x, and 2.5x), a toe region in peak principal strain was observed. This toe region resulted in a non-linear relationship between peak principal strain and applied body load ($p=0.1789$). The toe region seen for peak principal strain could be due to the viscoelastic behaviour of the tissue or the high Poisson's ratio of porcine Achilles tendon [9]. Ongoing work continues to examine these trends to better understand the effects of load magnitude on the internal strain response. Peak principal stress locations for all 5 applied body loads were located at the distal end of the aponeurosis on the posterior side of the tissue (Figure 1C). This result suggests that tendon rupture should develop at the aponeurosis in an Achilles tendon. Peak principal strain locations for all of the applied body loads were located at the distal end of the tendon toward the enthesis boundary (Figure 1). This result is consistent with clinical presentation of tendon rupture and suggests that tear development is likely to occur at the enthesis. The diverging results in peak principal stress and peak principal strain locations indicate that more work is needed to improve our understanding of how load is localized in and contributes to tendon injury.

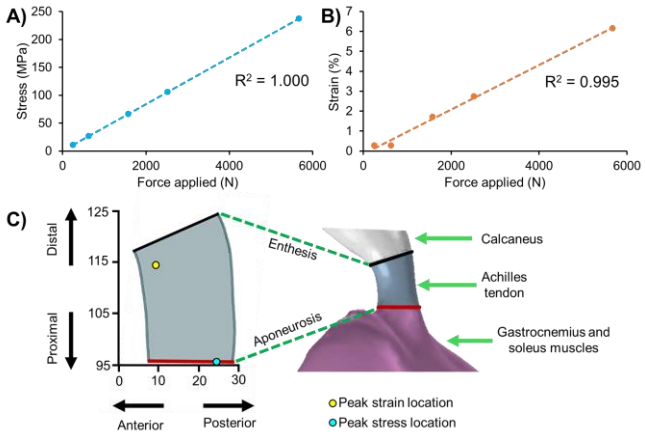

Figure 1: A) Model predicted peak principal stress and **B)** peak principal strain for the 5 applied body loads**. C)** Model predicted locations of peak principal stress and peak principal strain within the tendon in the coronal plane.

Significance: This work developed and implemented a finite element model of a healthy porcine Achilles tendon that included regions of bone, enthesis, tendon, aponeurosis, and muscle. Results provided insight into mechanisms of injury development during normal biological loading conditions. The model developed here can be used for further investigation of the internal stress and strain response and how these parameters may influence development of injury. In the future, this model can be used to inform clinical populations on the mechanisms of injury development and can be used to investigate novel treatments for tendon injury.

Acknowledgments: NIH-R01EB032860 (Simon)

References: [1] Thomopoulos et al. (2015), *J. Orthop. Res.* 33(6); [2] Miller et al. (2019), *Ann. Biomed. Eng.* 47; [3] Thunes et al. (2015), *J. Biomech. Eng.* 137; [4] Genin et al. (2009), *Biophys. J.* 97; [5] Gatt et al. (2015), *Acta Biomater.* 24; [6] Kato et al. (1998), *Hosp. Jt. Dis*. 57(4); [7] Clayton and Hobbs (2019), *J. Equine Vet. Sci.* 76; [8] Thorup et al. (2007), *Animal* 1; [9] Griffin et al. (2004), *J. Exp. Biol.* 207

The design of a bighorn sheep horn bioinspired impact mitigation system

Bryce H. Reimer[1], Chiara Vessicchio[1], Benjamin B. Wheatley[1]
[1]Bucknell University, Department of Mechanical Engineering
*Corresponding author's email: bhr009@bucknell.edu

Introduction: Traumatic brain and musculoskeletal injuries occur daily due to automotive accidents, athletic impacts, and falls. Chronic traumatic encephalopathy (CTE) can cause functional deficits ranging from memory loss to severe depression and anxiety [1]. Studies show that approximately 5% of all athletes and 8% of American football players exhibit CTE, with prevalence rising to nearly 90% in players with a history of brain trauma. While the exact mechanisms remain unclear, brain cavity accelerations and excessive brain tissue strain are strongly linked to concussions and neurodegeneration [2]. Despite frequent high-energy collisions, bighorn sheep show little to moderate evidence of CTE [3]. The unique tapered spiral shape of their horns reduces brain cavity accelerations through directional oscillations after impact that store and dissipate impact energy [4]. Computational models suggest that these spirals can lower the head injury criterion (HIC) by over 50%, it remains unclear if the native animal horn shape can be optimized for improved energy dissipation [5]. We aim to develop bioinspired impact-mitigation system based on bighorn sheep skulls and horns, which first requires the development and validation of a computational model of horn-like oscillating structures.

Methods: Initial modeling of the bioinspired impact mitigation system was conducted using SolidWorks to design simplified horn-like geometries. Customizable splines refined geometry and allowed for targeted modifications to the horn's curl and excursion, allowing a range of configurations for impact analysis. These geometric models were then incorporated into a finite element modeling workflow in Abaqus (Figure 1A). Specifically, two models were studied in this work – one horn-like tapered spiral, and one-half sphere (as a control). In parallel, an experimental impact system was developed with a silicone horn-like oscillating structure, shock absorbing springs, and instrumentation to measure acceleration of the top plate of the system (Figure 1B). A silicone half sphere was dropped from three different heights and impacted the top plate, initiating oscillations of the horn-like structure. Simulation parameters, including impact velocities corresponding to experimental drop heights and spring stiffness were set to match the physical system. The area under the acceleration curve of the top plate was compared between experimental measures and computational predictions for model validation.

Results & Discussion: Results include noticeable differences in the impact performance of the two geometries—the horn-like tapered spiral and half-sphere—across varying drop heights and impact velocities. Computationally, the horn demonstrates a lower average area under the curve (AUC) for the acceleration profile, while experimentally the differences in horn and half sphere accelerations were dependent on drop height, although similar (Figure 1C). The model reasonably predicted acceleration behavior, suggesting validation (Figure 1C). However, with further tuning and calibration of certain parameters, such as the model springs and dashpots, we could further improve the model's predictive accuracy and better align it with real-world experiments. This is the first time that a model of a designed horn-like oscillator has been directly validated against experimental data, giving us confidence in this approach moving towards optimized geometries. A validated model enables an optimization process to systematically explore key design parameters, such as horn curl, excursion, and material properties. Through parametric analysis, we aim to identify the optimal configuration for minimizing impact forces and improving energy dissipation. Specifically, a design of experiments approach will be employed to systematically vary five key parameters—horn excursion, curl, impact velocity, core inclusion, and material properties—across multiple levels, with 20 additional simulations planned to assess their influence on performance. The results from these simulations will inform the optimization of the geometry for impact mitigation.

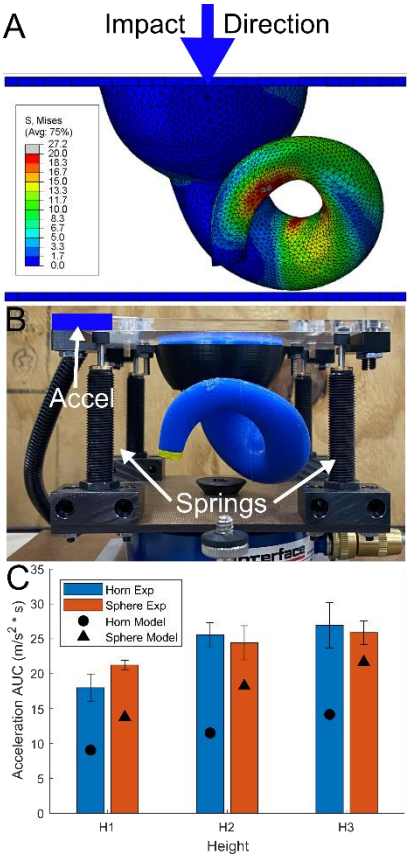

Figure 1. A) Finite element model of horn-like oscillator, showing impact direction. B) Experimental impact system of horn-like oscillator, with springs and accelerometer. C) Validation of model acceleration (circle and triangle markers) to experimental data (bars with standard deviation).

Significance: The significance of this project lies in its potential to create a groundbreaking technology for impact mitigation that could transform multiple industries. This technology could be applied to improve football helmets, reducing the risk of brain injuries by better absorbing and distributing impact forces. With the ability to optimize and tailor the system for different scenarios, this project lays the foundation for a versatile and scalable solution with wide-ranging implications for both consumer safety and industrial applications.

Acknowledgments: Funding provided in part by Bucknell Healthcare Technologies Inventor's Program (HTIP).

References: [1] Bieniek, K. F. et al. *Brain Pathology* 30, 63–74 (2020); [2] Meaney, D. F. & Smith, D. H. *Clin Sports Med* 30, 19–vii (2011); [3] Ackermans, N. L. et al. *Acta Neuropathol* 144, 5–26 (2022). [4] Drake, A. et al. *Acta Biomaterialia* 44, 41–50 (2016); [5] Wheatley, B. B., et al. *Bioinspir. Biomim*. 18, 026005 (2023)

INTERLIMB NEURAL COUPLING DURING GAIT: COHERENCE AND DIRECTIONALITY ANALYSIS WITH RHYTHMIC HAPTIC CUEING IN ARM SWING TRAINING

Ines Khiyara[1*], Babak Hejrati[2]
[1]Department of Mechanical Engineering, The Biorobotics and Biomechanics Lab, University of Maine, Orono, 04469, United States of America
*Corresponding author's email: ines.khiyara@maine.edu

Introduction: Walking relies on coordinated upper and lower limb movement, with interlimb neural coupling playing a key role in gait adaptability. However, the nature of this coupling—whether driven by a common neural drive or influenced by directional interactions between the arms and legs—remains unclear. Although gait training usually focuses on the lower limbs, arm swing plays a crucial role in balance and proper gait mechanics. Recent studies have examined upper limb involvement, with rhythmic haptic cueing shown to modulate arm swing [1], but its impact on interlimb neural coupling during gait is not well understood. This study examines how haptic cueing influences interlimb connectivity, analyzing coherence (COH) and directionality between upper and lower limb muscles across alpha (8–15 Hz), beta (15–30 Hz), and gamma (30–60 Hz) bands, which correspond to subcortical and cortical motor control. By distinguishing forward (legs influencing arms), reverse (arms influencing legs), and zero-lag (common drive) interactions, we aim to determine whether haptic cueing alters neural synchronization patterns and gait control.

Methods: Seventeen older adults (mean age: 73.2 ± 6 years) completed walking trials under three conditions: (1) Baseline walking, (2) Cueing Condition 1 (C1) with a 20% reduced arm swing cycle time (CT), and (3) Cueing Condition 2 (C2) with a 20% increased CT. A smartphone app-driven system [1] with vibrotactors provided rhythmic haptic cues to modify arm swing CT, assuming a 1:1 frequency ratio between arm and leg swings [1]. Surface EMG data were recorded at 1926 Hz from the right and left anterior deltoid, posterior deltoid, rectus femoris, and biceps femoris. Signals were high-pass filtered (5 Hz FIR), rectified, and segmented based on right foot heel strikes detected via IMUs for 30 gait cycles per subject. Time-warping via linear interpolation aligned all cycles to each individual's average gait cycle duration. EMG envelopes were normalized and smoothed using a 10-ms moving average filter. Time-dependent COH was analyzed using a 200-ms sliding window with a 50-ms step size [3]. Directionality analysis decomposed COH into forward, reverse, and zero-lag components using Fourier-based decomposition with pre-whitening to eliminate autocorrelations [3]. Statistical comparisons were conducted using Wilcoxon signed-rank tests, with p-values adjusted via the Benjamini-Hochberg procedure.

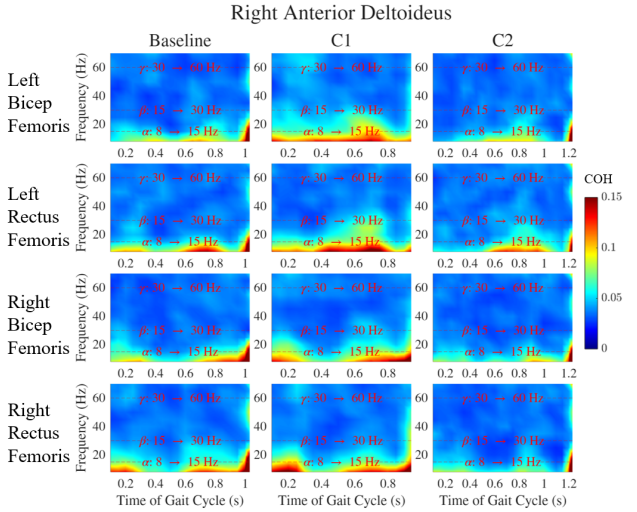

Figure 1: Time-frequency COH between the right anterior deltoideus and lower limb muscles across gait conditions (Baseline, C1, C2), with key frequency bands labeled.

Results & Discussion: At Baseline, COH was strongest in the alpha band, reflecting a reliance on intrinsic rhythmic generators, while beta and gamma COH were minimal, suggesting limited cortical involvement. Zero-lag COH (common drive) dominated across all muscle pairs, except for one, which exhibited reverse-lag COH in the gamma band ($p = 0.015$), suggesting a pre-existing top-down influence from the upper limbs on lower limbs. During faster cueing (C1), COH increased across all frequency bands, reinforcing subcortical-driven rhythmic control (alpha) and greater cortical involvement (beta/gamma) in gait adaptation. Despite this increase, zero-lag COH remained dominant across all muscle pairs. The same muscle pair that showed reverse-lag COH at Baseline again showed this pattern in the gamma band ($p = 0.024$), suggesting that faster cueing enhanced this localized top-down modulation (Fig. 2). Slower cueing (C2) maintained COH patterns similar to Baseline, with alpha COH remaining dominant and minimal presence in beta and gamma, reinforcing subcortical-driven synchronization. Zero-lag COH continued to dominate, confirming a common driver. These findings suggest common drive dominates interlimb coupling across conditions, with C1 increasing cortical contributions.

Significance: This study shows that rhythmic haptic cueing modulates interlimb neural coupling, supporting its use in gait rehabilitation and home-based training.

Acknowledgments: This work was supported by the National Science Foundation under Grant 2145177.

References: [1] Khiyara, I., Sidaway, B., Hejrati, B., 2024, *Ann. Biomed. Eng.*; [2] Weersink, J. B., de Jong, B. M., Halliday, D. M., Maurits, N. M., 2021, *J. Physiol.* 599(8), 2283–2298.

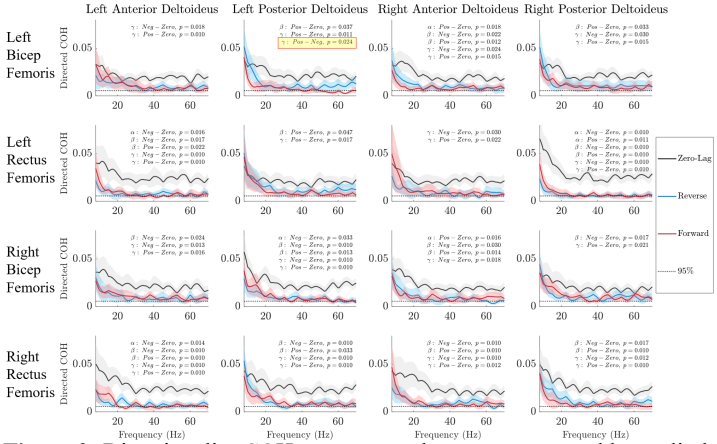

Figure 2: Directionality COH components between upper and lower limb muscles for C1. Shaded regions represent 95% confidence limits, with statistical comparisons highlighting significant differences.

VECTOR CODING QUANTIFYING WHOLE-BODY COORDINATION DURING FUNCTIONAL MOBILITY IN PEDIATRIC CEREBRAL PALSY

*Guilherme M Cesar[1], Ligia Y Mochida[1], David Williams[2], Clayton Wauneka[3], Kira Flanagan[1], Paulo RP Santiago[4], Bruno LS Bedo[5]
[1] Department of Physical Therapy, University of North Florida, FL, USA
[2] School of Engineering, University of North Florida, Jacksonville, USA
[3] Brooks Motion Analysis Center and Clinical Research Center, Brooks Rehabilitation, Jacksonville, USA
[4]School of Physical Education and Sport of Ribeirao Preto, University of São Paulo, Brazil
[5]Technology and Sports Performance Analysis Laboratory, School of Physical Education, University of São Paulo, Brazil
*Corresponding author's email: g.cesar@unf.edu

Introduction: Traditional balance assessments rely on center of pressure metrics and posturography, which primarily evaluate static postural control but overlook whole-body responses, such as segmental coordination, needed during dynamic tasks. While static balance contributes to postural control, dynamic balance – heavily reliant on intersegmental coordination – is essential for mobility and engagement in life activities [1], and its impairments increase fall risk, particularly for those with neuromotor disorders. Recently, vector coding, a technique that quantifies instantaneous phase relationship between segments, was used during translational perturbations [2]. However, its use in pediatric neurology remains unexplored, particularly during dynamic conditions. Children with cerebral palsy (CP) exhibit hindered postural control and often use compensatory patterns that reduce adaptability and efficiency compared to typically developing (TD) peers [3]. Considering functional mobility tests, the Timed Up and Go (TUG) is widely used for children with disabilities, especially CP [4]. While this test involves standing, walking, and turning, the turning phase is key for evaluating whole-body coordination. Yet, quantification of intersegmental coordination during TUG is lacking in CP research. This study applied vector coding to investigate thorax-pelvis coordination during the turning phase of TUG in children with CP and contrasted findings with TD peers.

Methods: Two children with CP (4 years old; 0.9 and 1.0 m; 14 and 17 kg) and two TD children (10 and 5 years old; 1.4 and 1.0 m; 40 and 14 kg) performed TUG test three times. The two gait cycles (one right, one left) during the turning phase were analyzed. Vector coding quantified transverse plane trunk-pelvis coordination. Descriptive representation of this metric was displayed via trunk-pelvis joint angles and coupling angle per child. Percentage of coordination patterns [in-phase (thorax and pelvis rotating together), anti-phase (segments rotating independently), pelvis-only and thorax-only rotations] were quantified per group and contrasted using Cohen's d effect size.

Results & Discussion: Joint and coupling angles per child are shown in Fig 1. When considering coordination patterns, *large effect sizes* indicated differences between CP and TD. While both groups predominantly exhibited in-phase coordination, TD showed higher (Cohen's d 1.3) percentage (86.5%) than CP (73.3%), suggesting greater segmental synchronization. In contrast, children with CP relied more on isolated segmental movements, exhibiting higher pelvis-only (11.7% vs. 3.5%, Cohen's d 1.1) and thorax-only (11.2% vs. 5%, Cohen's d 1.1) rotations, suggesting a reduced ability to dynamically integrate trunk-pelvis motion. Also, CP exhibited slightly higher anti-phase coordination (3.8% vs. 1.8%, Cohen's d 1.5), which may reflect compensatory attempts to manage stability challenges during turning. These findings suggest that while TD employ adaptable task-oriented intersegmental control strategies, children with CP exhibit more constrained movement patterns [5]. The segmental isolation in children with CP during the turning phase may contribute to inefficient movement transitions, decreasing balance control during dynamic conditions.

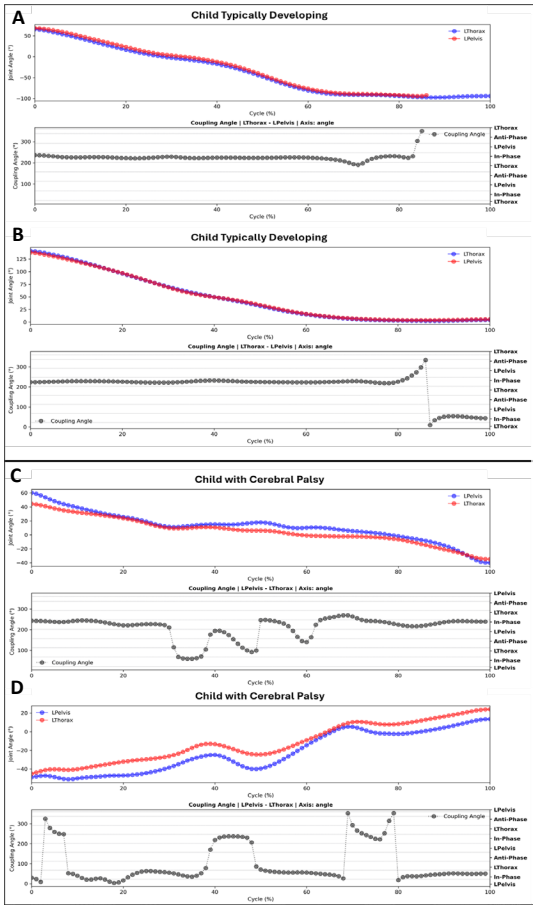

Figure 1: Trunk and pelvis transverse plane angles and coupling angles for a representative trial of older (A) and younger (B) children TD, and children with CP (C, D) during the turning phase of Timed Up and Go test.

Significance: This study quantified intersegmental coordination strategies for balance control during a clinically relevant mobility task. Findings revealed thorax-pelvis coordination differences that offer biomechanical evidence for interventions enhancing movement efficiency and dynamic balance control in children with CP. This pilot work is innovative as it uniquely applies vector coding to evaluate whole-body coordination during a functional mobility task, expanding its use in pediatric CP research.

Acknowledgments: Eunice Kennedy Shriver National Institute of Child Health & Human Development of the National Institutes of Health (R03HD114548); Pediatric Physical Therapy Research Grant from the Foundation for Physical Therapy Research.

References: [1] Cesar et al., 2024, *Front Neurol*; [2] Taleshi et al., 2022, *Scientific Reports*; [3] Özal et al., 2022, *Pediatr Health Med Ther*; [4] Carey et al., 2016, *Pediatr Phys Ther*; [5] Newman et al., 2018, *J Appl Biomech*.

EFFECTS OF BACK MUSCLE FATIGUE AND MODIFIED TRUNK INERTIA ON LUMBAR KINEMATICS, KINETICS, AND MUSCLE ACTIVITY DURING WALKING

*Benjamin Sibson, PhD[1], Andrew Yegian, PhD, Ali Yawar, PhD, Daniel Lieberman, PhD
[1]Center for Advanced Orthopaedic Studies, Beth Israel Deaconess Medical Center, Boston, MA 02155
*Corresponding author's email: bsibson@bidmc.harvard.edu

Introduction: Back muscle endurance is a strong predictor of low back pain [1], but the mechanisms of this relationship are not clear. Because fatigue reduces muscles' capacity to generate force [2], less endurance may increase spinal loading and trunk muscle co-contraction. Using a novel apparatus and fatiguing protocol, we investigated the effects of modified trunk inertia and back fatigue on lumbar kinematics, kinetics, and muscle activity during walking. We first hypothesized back fatigue would increase lumbar angles and moments, increase max abdominal muscle activity, and decrease max back muscle activity. Our second hypothesis was increased trunk inertia would reduce lumbar angles, increase lumbar moments, and increase max back and abdominal muscle activity. We also investigated associations of back endurance with fatigue-induced changes in lumbar kinematics, kinetics, and muscle activity. We tested two alternative hypotheses: that less back endurance is associated with either greater fatigue-induced increases in lumbar angles and moments, or greater fatigue-induced increases in max back and abdominal muscle activity.

Methods: 12 adults (6 F, 6 M) participated. The novel apparatus was a frame backpack with two rods bolted perpendicular to each other and at 45˚ to the sagittal plane of the pack as worn (Fig. 1). 3% body mass weights were added distally to the rods. Four Biering-Sørensen tests [3] fatigued participants' backs before no-pack and pack walking trials and assessed fatigue. Participants walked at 0.2 Froude [4] (1.37±0.04 m sec^{-1}) in four conditions: no-pack and pack (randomized), pre- and post-fatigue. 24 reflective markers plus five tracking clusters were placed on the upper body and pelvis, with positions sampled at 200 Hz and low pass filtered 4 Hz. Surface electromyography (EMG) was recorded from lumbar erector spinae (ES) and rectus abdominus (RA) at 2,000 Hz, bandpass filtered 20-500 Hz, and rectified. A lumbar joint between the trunk and lab frame permitted sagittal pitching, coronal rolling, and transverse yawing motion, corresponding to flexion-extension (FE), lateral bending (LB), and axial rotation (AR) moment inverse dynamics solutions [5]. Kinematic and kinetic amplitudes and max muscle activity were calculated per stride. Back fatigue and endurance were measured with EMG median frequency analysis [6]. Linear mixed effects models with Tukey *post hoc* comparisons tested for differences in amplitudes and max muscle activity among conditions. Ordinary least squares regression models with Pearson's product-moment correlation coefficients (r) tested for associations between back endurance with changes in amplitudes and max muscle activity with fatigue.

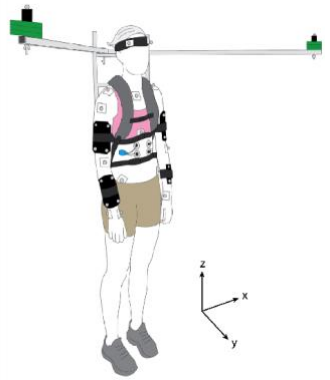

Figure 1: Schematic of modified frame backpack.

Results & Discussion: Back fatigue had no effect on kinematics, kinetics, or muscle activity across conditions. Increased trunk inertia caused decreases in amplitudes of roll angle by 36% and yaw angle by 69% (both $p<0.001$), increases in amplitudes of FE moment by 46% ($p<0.001$), LB moment by 13% ($p=0.019$), and AR moment by 426% ($p<0.001$), and an increase in max lumbar ES activity by 78% ($p<0.001$). For the no-pack condition, back endurance was positively associated with the change in max lumbar ES activity ($r=0.69$, $p=0.013$; Fig. 2A), negatively associated with the change in max RA activity ($r=-0.72$, $p=0.008$; Fig. 2B), and negatively associated with the change in FE moment amplitude ($r=-0.62$, $p=0.031$) with fatigue. Overall, individuals with less back endurance showed increases in max abdominal muscle activity post-fatigue whereas individuals with higher back endurance showed the opposite response, increasing max back muscle activity more post-fatigue (Fig. 2). Less back endurance was also associated with increased loading – namely higher lumbar FE moment amplitudes – post-fatigue.

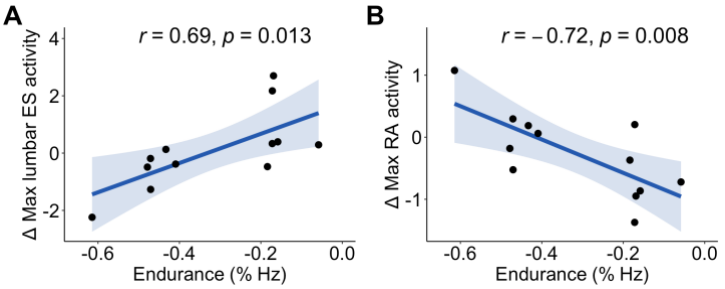

Figure 2: Least squares regression fits with 95% CI shading of back endurance with the change in max muscle activity due to fatigue.

Significance: For individuals with less back endurance, increased RA activity during walking may be a protective mechanism for stabilizing the trunk in response to increased sagittal lumbar loading due to fatigue. For individuals with high back endurance, it would appear the lumbar ES is still able to generate sufficient force to properly balance lumbar spine loads during walking. Global trends of reduced spinal loading and back muscle activations, and associated less back endurance [7], may increase susceptibility to low back pain, as these results suggest back endurance affects lumbar kinetic and neuromuscular strategies during walking with a fatigued back.

Acknowledgments: This work was supported by the American School of Prehistoric Research.

References: [1] Alaranta et al. (1995), *Clin Biomech* **10**, 323-324; [2] Enoka & Duchateau (2008), *J Physiol* **586**, 11-23; [3] Biering-Sørensen (1984), *Spine (Phila Pa 1976)* **9**; [4] Alexander & Jayes (1983), *J. Zool*. **201**, 135–152; [5] Winter (2009), *John Wiley & Sons, Inc.* **4th Edition**; [6] Mannion & Dolan (1994), *Spine (Phila Pa 1976)* **19**(11); [7] Sibson et al. (2024), *PLoS one* **19**(11)

REACTIVE ARM SWING DURING BALANCE RECOVERY IS RELATED TO SLIP DIRECTION AND MAGNITUDE

Gracie Zimmer[1], Matthew Zintek[2], Seongwoo Mun[3], Abderrahman Ouattas[3], Nathaniel H. Hunt[3], *Corbin M. Rasmussen[1]
[1]Department of Exercise Science and Pre-Health Professions, Creighton University, Omaha, NE, USA
[2]Department of Biology, Creighton University, Omaha, NE, USA
[3]Department of Biomechanics, University of Nebraska at Omaha, Omaha, NE, USA
*Corresponding author's email: corbinrasmussen@creighton.edu

Introduction: Slips are a common cause of falls, thus understanding effective strategies to recover from a slip and prevent a fall is important to reducing their burden on society. One recovery strategy is to utilize arm swing, which can shift the center of mass and reduce angular velocity to extend recovery time [1]. However, arm swing reactions after slips on curvilinear paths have not been examined, despite non-straight walking paths comprising up to 45% of our daily gait patterns [2] and posing greater fall risk [3]. Because angular momentum during turning is naturally elevated compared to straight walking [4], effective use of the arms may be especially important to balance recovery after slips. Based on similar work during straight walking, we hypothesized that the arm swing reactions employed by both the ipsilateral and contralateral arm after an unconstrained slip during curvilinear walking would be tailored to the slip mechanics experienced, indicating specificity of the response to the instability rather than a general startle response. Specifically, we expected arm swing directions to correlate with slip directions and arm swing magnitudes to correlate with slip distances.

Methods: 21 healthy young adults (mean±SD 24.57±4.74 years, 1.72±0.12 m, 71.72±18.17 kg, 10 females) were fitted with a fall-arresting safety harness and full-body marker set that was measured with a 17-camera motion capture system at 100 Hz. All participants walked at an average velocity of 1.3±0.1 m/s [5] along 180° curved paths of either 1.0 m or 2.0 m radius. Unconstrained slips were delivered during gait with the Wearable Apparatus for Slip Perturbations [6] at every combination of early, mid, or late stance to either the inside or outside foot relative to one of two path curvatures. Arm swing reactions were calculated as humeral elevation and azimuth angles at compensatory step touchdown. For both angles, the origin was set at the acromion marker, and the angle of the vector connecting the acromion and lateral epicondyle markers with heading (azimuth) and with vertical (elevation) were derived. We used the humeral azimuth angle to represent arm swing direction and the humeral elevation angle to represent arm swing magnitude.

For this analysis, all slip onset phase and path curvature conditions were pooled together to obtain a broad range of slip mechanics to correlate with the arm reactions employed in response. Ipsilateral and contralateral arms relative to the slipping foot were analysed separately due to their disparate reaction magnitudes after a slip during straight walking [7]. Similarly, inside and outside foot slips were analysed separately because of their qualitatively different slip directions [3]. Spearman's rank correlation coefficients were calculated between 1) slip directions and humeral azimuth angles, both relative to heading, and 2) slip distances and humeral elevation angles for ipsilateral/contralateral arms within inside/outside foot slips. For all correlations, the critical alpha was set at $\alpha=0.05$.

Results & Discussion: Outside foot slips showed the strongest relationship between slip and arm swing directions, with significant, strong correlations for both arms (Ipsi: $\rho(118)=-0.565$, $p<0.001$; Contra: $\rho(118)=0.608$, $p<0.001$). These results indicate that the direction of reactive arm swing may be tightly controlled in response to outside foot slips on a curved path. For inside foot slips, we found a significant moderate correlation between slip direction and humeral azimuth angle relative to heading in the ipsilateral arm ($\rho(95)=-0.376$, $p<0.001$) and a significant yet weak correlation in the contralateral arm ($\rho(95)=0.256$, $p=0.011$). Inspection of the contralateral arm azimuth angles across inside foot slip directions reveals little variation from 150° in azimuth, which would be generally behind the individual. This suggests a twisting motion when paired with the trend of the ipsilateral arm to concurrently cross the body midline (i.e., negative azimuth angles) as slip directions become more contralateral and anterior, which would reorient the trunk toward the falling direction and may result in a more advantageous position to take a compensatory step.

In terms of slip distance and arm elevation, the strongest correlations between the two were found after inside foot slips (Ipsi: $\rho(97)=0.478$, $p<0.001$; Contra: $\rho(97)=0.530$, $p<0.001$). This indicates that as slips became more severe in terms of magnitude, the magnitude of the arm swing response also tended to increase. Outside foot slips also exhibited significant, moderate correlations between slip distance and arm elevation (Ipsi: $\rho(118)=-0.299$, $p<0.001$; Contra: $\rho(118)=0.440$, $p<0.001$). Notably, ipsilateral arm responses tended to decrease as slip magnitude increased, suggesting that ipsilateral elevation may be harmful to the odds of regaining balance.

Significance: Understanding the recovery strategies like arm swing that are utilized in response to slips can provide targets for fall prevention. To our knowledge, this is the first investigation of arm reactions during slip recovery on non-straight walking paths, which comprise a significant portion of our daily walking patterns [2]. The unique relationships between arm reactions and slip mechanics for inside and outside foot slips illustrate the specificity of the responses to the context of the slip. Broadening our knowledge of balance recovery to other walking contexts like curvilinear walking can inform a more comprehensive approach to slip-and-fall prevention.

Acknowledgments: This work was supported by grants R15AG063106 and P20GM109090 from the National Institutes of Health.

References: [1] Cheng et al. (2014), *Hum Mov Sci* 38; [2] Glaister et al. (2007), *Gait Posture* 25; [3] Rasmussen et al. (2024), *J Exp Biol* 227; [4] Nolasco et al. (2019), *Gait Posture* 70; [5] Bohannon & Andrews (2011), *Physiotherapy* 97; [6] Rasmussen & Hunt (2019), *J Neuroeng Rehabil* 16; [7] Lee-Confer et al. (2022), *J Biomech* 133.

HOW DOES HANDS-FREE STROLLER RUNNING AFFECT THE GROUND REACTION FORCE?

Allison R. Altman-Singles[1,2*], Naomi Fay[1], Amanda Mueller[1], Abby Miller[1], Teresa B. Reed[2], Joseph M. Mahoney[3]
[1] Kinesiology, Penn State Berks College, Reading PA 19610
[2] Mechanical Engineering, Penn State Berks College, Reading PA 19610
[3] Mechanical Engineering, Alvernia University, Reading PA 19601
[*]Corresponding author's email: ara5093@psu.edu

Introduction: Running is a popular activity that can result in physical and mental health benefits. Running with stroller requires constant manual manipulation to maintain direction, speed, and control. Previous research has speculated that holding onto the stroller may alter mechanics, through reducing impact loading [1], increasing torsion under the foot [2], and encouraging forward lean [3]. While reduced impact loading may mitigate the risk of injury in this population [4], increased torsion increases injury risk [5]. Thus, it is important to better understand the effects of using the hands to control a stroller.

Products that tether the runner to the stroller allow for hands-free stroller running. This permits more natural trunk rotation and arm swing, to more closely replicate running without a stroller. The use of these products may make running with a stroller more enjoyable, encouraging more runners to take advantage of this beneficial activity. Thus, the purpose of this study was to investigate the effect of a tethered stroller mechanism on the ground reaction force during running. It was expected that a tethered system would result in mechanics similar to those found when running without a stroller.

Methods: Healthy runners were recruited to run across an 18 m force plate (Bertec, Columbus, OH) instrumented runway under three conditions: holding and pushing a stroller (Thule Urban Glide 2, Thule, Malmo, Sweden), running tethered (StrollRunner, Burlington, VT) to the stroller, and running without a stroller (control). Five trials were collected per condition.

Force data were sampled at 2000 Hz and trimmed to stance phase. Vertical impact peak (VIP), vertical propulsive peak (VPP), vertical average loading rate (VALR), and vertical instantaneous loading rate (VILR) were extracted using custom MATLAB (Mathworks, Natick, MA) code. Median values for each subject in each condition were compared within subjects using bootstrapped, paired t-tests to assess statistical significance. Holm Bonferroni correction was used to correct the *p*-values for multiple comparisons.

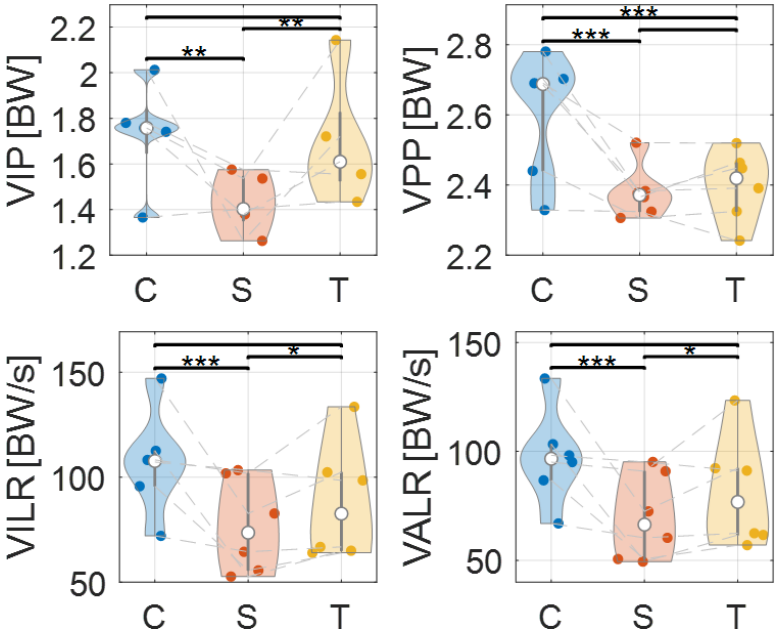

Figure 1: Violin plots of force (top) and loading (bottom) metrics from **C**ontrol, **S**toller, and **T**ethered running. One star indicates $p < 0.05$, two stars indicate $p < 0.01$, three stars indicate $p < 0.001$.

Results & Discussion: Six runners (21±3 years, 1.64±0.05m, 62±7kg, 1 male, 5 female) completed all stroller, tether, and control trials. When comparing stroller to control conditions, VIP (18.4%), VPP (8.86%), VALR (33.7%), and VILR (33.4%) decreased, similar to previous work [1]. VIP, VALR, and VILR were not significantly different when running with the tethered stroller compared to the control, but VPP remained 8.13% reduced. When stroller was compared to tethered condition, VIP (16.0%), VALR (13.6%), and VILR (14.5%) were increased (Figure 1).

These findings suggest that the tethered system restores a more natural running form, returning VIP, VALR, and VILR to control values. However, this may not be a positive change, as higher impact loading, characterized by VIP, VALR, and VILR, has been associated with increased injury rates [4]. The similarities of the tethered running to the control condition may mean that torsional loading is also decreased in this condition, but this has yet to be confirmed in this early experimental stage. VPP with the tethered condition more closely resembled the stroller condition, indicating that the increased load of the stroller plays a more important role in propulsion than the load distribution through the hands.

Significance: The results of this study indicate that a tethered stroller running system may help to restore normal running mechanics. This may result in a more enjoyable experience for runners, freeing their hands to facilitate arm swing and non-stroller-related tasks. However, this may eliminate the reduced force and loading benefits that traditional stroller running has been shown to provide.

Acknowledgments: StrollRunner LLC donated the *StrollRunner® - Complete Hands-Free Running System* but had no involvement in the protocol, data collection, or writing.

References: [1] Mahoney et al. (2022), *NACOB, Ottawa, CA*; [2] Mahoney et al. (2024) *ASB, Madison, WI*; [3] O'Sullivan et al. (2016) *Gait Posture 43*; [4] Davis et al. (2016), *Br J Sports Med* 50; [5] Milner (2006) *J BioMech* 39.

GAIT BIOMECHANICS DIFFER BETWEEN TRANSFEMORAL AND TRANSTIBIAL AMPUTATIONS

*Nikou Nikoumanesh, Shradha Sudhir, Karma C. Foucher, Lindsay S. Hannigan
University of Illinois Chicago
*nniko@uic.edu

Introduction: Approximately 150,000 individuals in the United States undergo lower limb amputation (LLA) annually. LLA significantly impacts mobility and gait performance, resulting in reliance on their intact limb. The level of amputation significantly impacts post-surgery symptoms and physiological demands. Individuals with transfemoral amputations (TF) require more energy to walk compared to those with transtibial amputations (TT) [1]. Changes in gait following LLA may play a role in increased reported proximal joint pain, however there is limited information comparing gait behaviors in those with LLA to older adults without LLA. We hypothesized that those with LLA would demonstrate similar gait behaviors, with increased frontal and transverse plane motion towards the intact limb, compared to older persons.

Methods: Nine participants with unilateral TF (80.90±12.58 kg, 1.73±0.12 m, 56.81±13.30 yrs), 10 individuals with TT (85.40±16.40 kg, 1.75±0.13 m, 56.80±15.15 yrs) amputations and 13 older persons (OP) without history of amputation (96.98±32.09 kg, 1.70±0.09 m, 62.71±9.74 yrs) walked at a self-selected speed on an instrumented treadmill while wearing reflective clusters on the thorax, sacrum, thighs, shanks, and forefeet. Low-pass Butterworth filters with 8-Hz and 12-Hz frequencies were applied to the marker trajectories and the ground reaction force data, respectively. Kinematic data were reduced to 101 points to represent 0-100% of the gait cycle, with 60% representing toe-off during walking. Heel strike was defined as the point when vertical ground reaction forces exceeded 20N. Mean differences and associated pooled standard deviations were calculated for periods of the gait cycle when 90% confidence intervals did not overlap for three or more consecutive points.

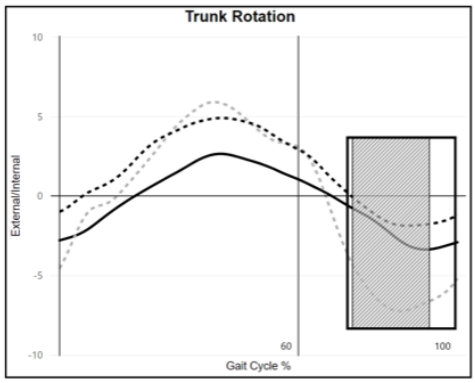

Figure 1: Mean kinematic data changes in the amputated side during 0-100% of gait cycle. The solid line represents the OP group, the black dashed line represents the TT group, and the gray dashed line represents the TF group. The areas of significant difference between the OP and TF groups are shown with dashed blocks and between the TF and TT groups with black thick-bordered blocks.

Results & Discussion: Vertical ground reaction force was significantly lower in the TF group compared to the OP (-1.99±1.58N/kg) during the loading response on the amputated side. The TF group also showed higher vertical ground reaction forces during midstance compared to TT (1.21±0.97N/kg) and OP groups (1.03±0.77N/kg). The TF group had greater ipsilateral trunk rotation toward their intact side **(Figure 1)** during the stance phase compared to the OP (5.44±4.15°) and TT (6.60±4.52°) groups. The TF group also demonstrated increased trunk rotation towards the intact side during the swing phase compared to TT (4.92 ±4.02°) and OP (4.35±3.64°). The TT group demonstrated more lateral trunk flexion towards the intact side during initial contact (4.60±4.16°) and swing phase (4.81±3.93°) compared to OP. Similarly, The TF group showed greater trunk lateral flexion during terminal stance towards the non-amputated side (2.97±2.86°). The TF group had greater hip adduction on their amputated side during the swing phase than the OP group (3.56±3.75°) and greater knee adduction during initial contact on the intact limb than OP (2.01±2.32°). The TT group demonstrated greater knee internal rotation on the intact side compared to the OP group during mid-stance (3.23±3.11°) and terminal stance (4.14±3.53°).

The results suggest that individuals with TT have a gait pattern that is more similar to OP than the TF group. The TF group demonstrated greater lateral trunk flexion and rotation toward the intact side, demonstrating weakness in the hip muscles on the amputated side. The results of this study show that individuals with LLA adopt different compensatory strategies depending on the level of amputation, leading to distinct load patterns on the knee, hip, and lower back joints. For example, individuals with TF amputations are at a greater risk of developing knee osteoarthritis due to differences in the gait biomechanics of their non-amputated side [2], while individuals in the TT group are more likely to suffer from lower back pain due to their prolonged trunk movements. Individuals with LLA may benefit from rehabilitation to improve muscle strength in the hips, abdominals, and trunk, leading to improved gait patterns and decreased risk of lower back pain and knee osteoarthritis. In addition, improving gait patterns, reducing pain, and increasing activity would also reduce the risk of cardiovascular disease and overall mortality [3].

Significance: This research enhances the understanding of gait biomechanics in individuals with LLA and offers further insight into the gait compensatory strategies employed by this population. These data also support that the risk profile for joint disease may be dependent on the level of amputation, with individuals with TF demonstrating gait patterns that may lead to knee osteoarthritis on the intact side and individuals with TT demonstrating gait patterns that may lead to low back pain. Individuals with LLA may benefit from rehabilitation focusing on gait and muscle strength in individuals with LLA.

Acknowledgments: This study was funded by the American Heart Association grant #20CDA35310419.

References: [1] Molina Cs, et al. (2022), *StatPearls*; [2] Russell Esposito, et al. (2015), *Clin Biomech*;[3]Stern, et al. (2017), *Ann Vasc Surg*

TEST-RETEST RELIABILITY OF PASSIVE ANKLE QUASI-STIFFNESS IN YOUNG ABLE-BODIED ADULTS

*Nicole K. Rendos[1,2], Jorjie M. Wilson[2], Kristen L Jakubowski[2,3], Mark Lyle[2], Trisha M. Kesar[2], Jason Franz[4]
[1]Florida Institute for Human and Machine Cognition, Pensacola, FL; [2]Emory University, Atlanta, GA; [3]Georgia Institute of Technology, Atlanta, GA; [4]Univeristy of North Carolina at Chapel Hill and North Carolina State University, Chapel Hill, NC
*Corresponding author's email: nrendos@ihmc.org

Introduction: Ankle joint quasi-stiffness is an aggregate biomechanical parameter relevant to ankle joint leverage for propulsion during gait which facilitates adaptability across different environments. Ankle quasi-stiffness represents a composite measure of both active (voluntary and stretch-reflex mediated muscle contraction) and passive (in-series viscoelastic properties) muscle-tendon mechanics. Assessing passive ankle quasi-stiffness can thereafter help differentiate active and passive contributions to overall quasi-stiffness during gait. Furthermore, the viscoelastic nature of the plantarflexor muscles and Achilles tendon convey velocity-dependent properties [1], making comparisons between gait and seated measurements difficult. Prior studies have made estimates at an angular velocity of 30°/s as an approximation of midstance phase of walking [1-3]; though lower angular velocities have also been employed [4]. The objective of the current study was to address an important barrier for comparisons by evaluating the test-retest reliability and intra-individual variability of passive ankle quasi-stiffness measurements across different testing sessions.

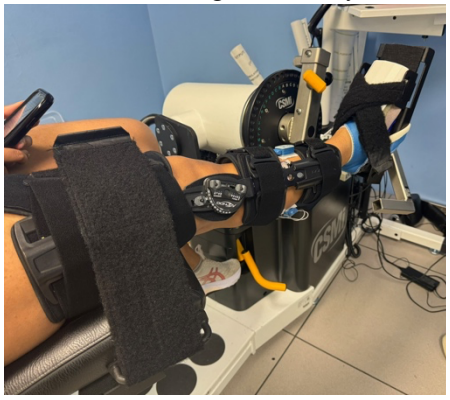

Figure 1. Experimental set-up for the measurement of barefoot passive ankle quasi-stiffness on the isokinetic dynamometer.

Methods: Nineteen young able-bodied adults (10 male, 9 female, age = 25.6 ± 2.4 years) were seated with their foot rigidly secured to an isokinetic dynamometer, and knee fixed at 10° flexion (Figure 1). Surface electromyography (EMG) was recorded for the tibialis anterior, medial and lateral gastrocnemius, and posteromedial soleus. Participants performed two maximum voluntary isometric contractions (MVIC) into dorsiflexion (DF) and plantarflexion (PF) at ankle neutral. Neutral ankle position (90°) was determined using a goniometer by an experienced clinical examiner. For each ankle stiffness trial, the dynamometer passively rotated the ankle for 5 repetitions through a full range of ankle PF and DF motion as the participant remained relaxed. Three trials were performed at 10°/second and 30°/second with (shod) and without (barefoot) shoes. The order of conditions was randomized among participants. Participants returned to the laboratory for a second analogous day of testing 8.6 ± 4.2 days later. Trials were excluded from the analyses if EMG activity exceeded 5% of MVIC. Repetitions 3 and 4 from the final trial for each condition were averaged. Passive ankle quasi-stiffness was calculated as the slope of the torque-angle relationship between 10° PF and 15° DF, or maximum DF if less than 15°. Two-way mixed effects model with absolute agreement intraclass correlation coefficients (ICCs) were calculated for each condition between Day 1 and Day 2. ICC values < 0.5, between 0.5 and 0.75, between 0.75 and 0.9, and > 0.9 indicate poor, moderate, good, and excellent reliability, respectively [5]. To evaluate day-to-day variability, a one-sample repeated measures *t*-test was conducted to determine if intra-individual differences between Day 1 and Day 2 significantly deviated from zero.

Results & Discussion: Of the 19 participants, 15 pairs of Day 1 and Day 2 testing data were suitable for analysis; while the remaining data were excluded for excessive muscle activation, signal noise, or collection errors. The means and standard deviations (SD), intra-individual differences, ICCs, and 95% confidence interval are presented in Table 1. ICCs of each condition ranged from good to excellent. While the ICC was high, with low group level differences across days, the one-sample *t*-tests revealed significant differences in intra-individual variability of passive ankle quasi-stiffness measures between Day 1 and Day 2 across all conditions ($p \leq .001$).

Condition	Day 1 Mean ± SD N·m/rad	Day 2 Mean ± SD N·m/rad	Intra-individual Difference N·m/rad	ICC	95% CI
Barefoot 10°/s	15.47 ± 8.96	15.60 ± 9.20	3.33 ± 2.42	0.947	[0.833, 0.983]
Barefoot 30°/s	25.05 ± 10.22	25.07 ± 10.81	5.75 ± 3.71	0.882	[0.643, 0.961]
Shod 10°/s	15.41 ± 7.88	15.81 ± 8.10	2.87 ± 30.3	0.928	[0.786, 0.976]
Shod 30°/s	25.23 ± 9.41	25.35 ± 9.71	4.68 ± 3.66	0.895	[0.682, 0.965]

These findings suggest that while individual-level variability exists between Day 1 and Day 2 measurements, this variability is not evident at the group level.

Significance: The high reliability (good to excellent) of passive ankle quasi-stiffness measurements supports confidence in group-level analyses. However, significant day-to-day variability is observed at the individual level. Potential contributors to this variability may include inter- and intra-rater inconsistencies in determining ankle neutral position using a goniometer [6], variations in the time interval between data collection sessions, and the absence of standardized activity protocols between testing days.

Acknowledgments: This work was supported by NIH NICHD K01HD107294. The content is solely the responsibility of the authors and does not necessarily represent the views of the NIH.

References: [1] Lamontagne et al. (1997) *J Orthop Sports Phys Ther*; 26: 244-252. [2] Krupenevich et al. (2020) *J Appl Biomech*; 36: 209-216. [3] Mentiplay et al. (2018) *Gait Posture*; 65: 190-196. [4] Theis et al. (2012) *J Electromyogr Kinesiol*; 22(6): 947-53. [5] Koo and Li. (2016) *J Chiropr Med*; 15(2): 155-163. [6] Konor et al. (2012) *Int J Sports Phys Ther*; 7(3): 279-287.

A GENERALIZED COHERENCE FRAMEWORK FOR QUANTIFYING INPUT CONTRIBUTIONS IN MULTI-INPUT BIOMECHANICAL SYSTEMS WITH CORRELATED OR UNCORRELATED INPUTS

*Nolan H. Howes[1], Matthew S. Allen[1], Dario Farina[3], Steven Charles[1,2]
[1]Mechanical Engineering and [2]Neuroscience, Brigham Young University
[3]Bioengineering, Imperial College London
*Corresponding author's email: nolan.howes@byu.net

Introduction: Multiple-input systems are common in nature and engineering, and it is often desirable to understand how much each input contributes to an output. Examples include biomechanical applications (such as tremorogenic activity in multiple muscles producing tremor at the hand) as well as non-biomechanical applications (such as vehicle vibrations generating noise and seismic motions deforming structures). Estimating individual input contributions, known as contribution analysis, is a common problem.

For uncorrelated inputs, contribution analysis can be performed using ordinary coherence, which measures the linear relationship between two signals in the frequency domain [1]. However, when inputs are correlated, as occurs naturally in many systems, contribution analysis becomes much more challenging. Existing coherence measures (such as ordinary, partial, and multiple coherence) can be applied in special cases but do not accurately estimate input contributions in the general case of correlated inputs. Hence, the purpose of this work was to develop a new method of contribution analysis that accounts for correlation between inputs [2].

To validate our new contribution analysis method, we applied it to a simulated 3-input system with known input-output relationships. Finally, we demonstrate the new method by applying it to an important but previously unsolved question in the management of upper-limb tremor: which muscle(s) contribute most to a person's tremor?

Methods: To bridge the gap in existing coherence measures, we derived a novel coherence measure, component coherence, that optimally (least-squared error) decomposes output power into distinct components, each of which can be interpreted physically in terms of either power from a given input or cross power due to interference between a pair of inputs (Fig. 1). By strategically summing component coherence terms, we can determine contributions from individual inputs. These contributions were defined as either excluded coherence (the portion of the output removed if a given input is excluded) or isolated coherence (the portion of the output that remains if a given input is isolated).

To showcase the effectiveness of these new coherence measures and compare them with existing ones, we simulated a mass-spring-damper model with three force inputs. The system comprised four masses, with three serving as force input sites, and the displacement of the fourth mass representing the system output. A parallel spring and damper connected all masses to each other and to ground. For inputs with various amounts of inter-input coherence and noise, we calculated the mean and root-mean-square errors for each coherence measure (ordinary, partial, multiple, excluded, and isolated) relative to the true contribution.

For application to tremor, we recorded surface sEMG in the four major wrist muscles (inputs) and translation of the hand in three degrees of freedom (outputs) from 14 subjects with Essential Tremor (ET) as they attempted to maintain neutral wrist posture. In data segments that exhibited definitive tremor and high multiple coherence (>0.5) between the set of inputs and each output, we calculated component coherence at the tremor frequency and then all coherence measures for each muscle.

Results & Discussion: Validating the new contribution analysis method with the mass-spring-damper model, we found that excluded coherence had negligible mean error for excluded contributions, and isolated coherence had negligible mean error for isolated contributions, independent of the level of input correlation. Similarly, excluded coherence had the lowest RMS error for excluded contributions, and isolated coherence had the lowest RMS error for isolated contributions, regardless of input correlation. In contrast, ordinary and partial coherence only predicted input contributions accurately when input correlation was minimal (and multiple coherence was incapable of attributing contributions to individual inputs).

Applying this new method to tremor, we found that correlation between inputs was high (≥0.7), suggesting that only excluded and isolated coherence would accurately estimate true contributions. Isolated coherence values showed that isolating ECR would retain most tremor power, whereas isolating FCU or ECU would retain little. Excluded coherence indicated that eliminating ECR would reduce tremor power by 80%, while excluding FCU/ECU would actually increase tremor (because they provided destructive interference)!

Significance: Together with existing measures, these novel coherence measures form a generalized coherence framework (Fig. 1) that allows for general contribution analysis of multiple-input systems with correlated or uncorrelated inputs.

Acknowledgments: This study was funded by NIH grant R15NS087447.

References: [1] Bendat and Piersol (2010). *Random Data*. Hoboken, NJ, Wiley. [2] Howes et al. (2025). *Biomed Signal Process Control* 104: 107522.

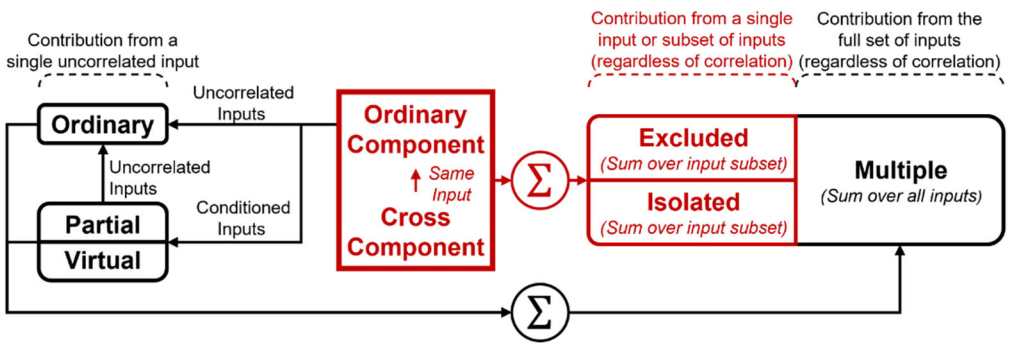

Figure 1: Generalized coherence framework, with existing coherence measures in black and novel coherence measures in red.

DETERMINING THE EFFICACY OF SHORT-SEPARATION CHANNELS FOR FNIRS MOTION ARTIFACT CORRECTION

*Alexandra C. Lynch[1], Ka'Jean Tallette[2], Corey A. Pew[1], Keith A. Hutchison[1], and Scott M. Monfort[1]
[1]Montana State University; Bozeman, MT, USA, [2]Howard University; Washington D.C, USA
*Corresponding author's email: alexandra.lynch@montana.edu

Introduction: Functional near-infrared spectroscopy (fNIRS) is a neuroimaging technique that leverages the optical properties of blood in the cerebral cortex to measure neural activation using near-infrared light. The lightweight and low-cost design make it ideal for biomechanics laboratory and field experiment designs [1]. The presence of motion artifacts is a major challenge when integrating fNIRS into biomechanics paradigms that include dynamic movements. Short-separation (SS) channels have been used to measure non-neural artifacts by isolating measurement to extracerebral regions [2]. Although previous works have assessed the validity of SS channels in stationary settings (e.g., sitting at a computer), their use in movement paradigms, such as those seen in biomechanics research, is underdeveloped [3]. It is unclear if SS channels provide robust utility against the inertial effects of intracranial fluids (e.g., interstitial fluid, blood) during activities involving large head movements. Critically, failing to address motion artifacts could lead to spurious findings [4]. Therefore, the purpose of this study was to evaluate the effectiveness of SS channels across varying hemodynamic response strengths in motion paradigms using a novel, dynamic optical phantom. We hypothesized that SS channels would show improved discriminative ability in detecting simulated neural signals amidst motion artifacts across various neural signal levels compared to analysis without SS channel regression.

Methods: *Phantom Development* – An optical phantom (epoxy resin, TiO, contents of blood and bovine tissue) mimicking the light scattering and absorption properties of the human brain was constructed with an internal fluid reservoir that allowed fluid movement [5]. *Motion Artifact Testing* – A dynamic platform rotated the phantom uniaxially (amplitude of 6.3 mm, and a frequency of 0.133 Hz) to introduce motion artifacts similar to repeated head tilting. An fNIRS device (NIRSport 2; 8 sources, 7 detectors, 8 SS channels) was secured to the dynamic phantom. fNIRS data were collected for five 30-second movement blocks, each preceded by 30 seconds of stillness, mirroring human study paradigms. *Data Processing* – Data were processed using a custom Matlab (Mathworks; R2022b) script to implement functions from the Brain AnalyzIR Toolbox [6]. The collected fNIRS signals in all source-detector channels were considered motion artifact, as the phantom generated no actual neural response. A known simulated hemodynamic response was superimposed over half of the (non-SS) channels with predefined (true) β values of varying strength (β = 1, 3, 5, 7, 9) using the 'SimData' function in the toolbox [7]. Optical density and modified Beer-Lambert Law toolbox functions were used. *Statistical Analysis* – Autoregressive, iteratively reweighted least squares regression models with and without SS channels as regressors were used to estimate the oxygenated hemoglobin hemodynamic response, with the magnitude represented by the calculated β values. Receiver operating characteristic (ROC) analysis was also performed to assess the ability of this processing method to discriminate between simulated (true) signal and motion artifact (from phantom) [7]. Area under the curve (AUC) values were calculated for ROC analyses performed at each true β. Higher AUC indicates better performance.

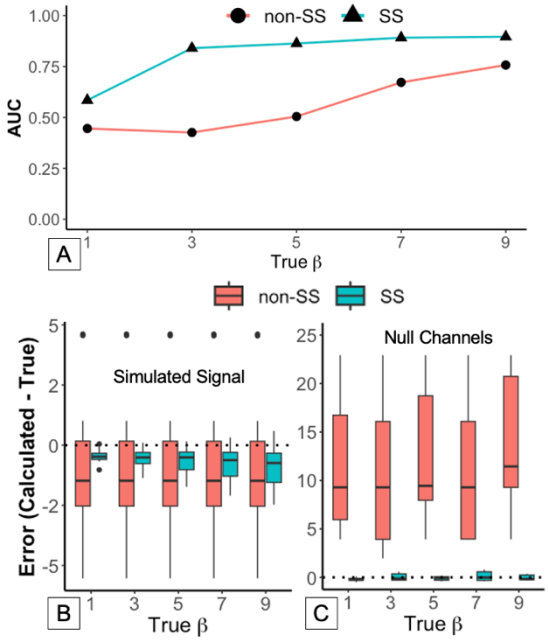

Figure 1: A) AUC for SS and non-SS channels calculated at each true β value. B) Error of measurement channels with simulated data across true β values. C) Error of measurement channels without simulated data (β = 0) across true β values. One error outlier in null channels for each true beta which was removed for visualization.

Results & Discussion: ROC analyses indicated that SS channels consistently had increased AUC across all β values compared to non-SS channels (Fig. 1A), supporting the hypothesis of SS channels enhancing discriminative ability in the presence of motion-induced fNIRS signal artifact. AUC values generally increased with larger simulated signal magnitude, suggesting that SS channels may play a larger benefit for low-moderate hemodynamic responses. Further investigation into individual channel error (calculated β – true β) for both signal (Fig. 1B) and null (Fig. 1C) channels revealed clear trends for all true β values. SS channels consistently had increased accuracy (i.e., mean error closer to zero) and precision (i.e., decreased variance) in estimating the hemodynamic response. The drastic reduction in β value error for null channels highlights the SS utility against spurious findings. These findings align with previous work noting improved signal isolation with SS channel regression [2,7] and extend them into a scenario that reflects large-scale motion artifacts. Testing across various frequency, amplitude, and phantom content combinations is still needed to provide deeper insight.

Significance: These preliminary results corroborate suggestions that SS channels may aid in motion artifact reduction through protection against false positive and false negative neural activation in the presence of motion artifact, providing support for their utility in multimodal applications involving biomechanics and neural activation analyses.

References: [1] Vanderwert et al. (2013) Funct. Infrared Spectrsc. FNIRS, 85(1). [2] Gagnon et al. (2011) NeuroImage, 56(3). [3] Noah et al. (2021) Neurophotonics, 8(1). [4] Oliveira et al. (2016) J. Neural Eng, 13(3). [5] Swartling et al. (2003) Appl.Opt, 42(22). [6] Santosa et al. (2018) Algorithms, 11(5). [7] Santosa et al. (2020) Neurophotonics, 7(3).

DISTAL FEMUR FRACTURE DISPLACEMENT FIELDS FROM WEIGHTBEARING COMPUTED TOMOGRAPHY

*Eric D. Thorhauer[1,2], William D. Lack[1,3], Elmer Vazquez[1,4], Joseph Davis[1,4], Sam Nelson[1,4], Aerie Grantham[1], Scott Telfer[1,2,3], William R. Ledoux[1,2,3]
[1]Center for Limb Loss and MoBility (CLiMB), VA Puget Sound Health Care System, Seattle, WA
Departments of [2]Mechanical Engineering and [3]Orthopaedics & Sports Medicine, and the [4]School of Medicine, University of Washington, Seattle, WA
*Corresponding author's email: ericthor@uw.edu

Introduction: Distal femur fractures are challenging to treat and occur at an incidence of 8.7/100,000 person-years [1]. Although nonunion is estimated in 5 to 10% of long bone fractures, healing complications have been reported for up to 32% of distal femur fractures [2]. Mechanoregulation of fracture healing has been demonstrated to be important clinically [3], but inability to quantify the temporospatial relationships of in vivo interfragmentary motion, strain and fracture healing has limited translation of knowledge into clinically actionable interventions [4]. Our laboratory has developed a technique for quantifying distal femur fracture motion on cadaveric specimens and human subjects using weightbearing computed tomography (WBCT) scans. In this study, we present distal femur fracture displacement field patterns (normal and shear) across different fixation types (e.g. nail or plate) and materials.

Methods: Cadaveric full femur specimens (n=7) underwent removal of a 1cm thick section of the distal femur via an osteotomy 5cm proximal to the medial epicondyle. The specimens were fixated with either lateral plates or femoral nails by an orthopaedic trauma surgeon. The specimens were axially loaded and scanned via WBCT while loading was increased from 0N to 222.5N in 44.5N increments. Subject-specific volumetric bone fragment models from pre-fixation CT (devoid of metal artifact) were segmented and used to track the dynamic response of the fracture between non-WBCT and WBCT using our custom model-based bone registration software suite. Displacement maps representing the resultant relative normal and shear motion between opposing proximal and distal sides of the fracture surface were generated.

Results & Discussion: We have generated an initial preliminary representation of this technique using three osteotomized cadavers, each with a different fixation type: titanium plate, stainless steel plate, and titanium nail. For the plate fixations, higher compression was observed on the medial side of the fracture (Figure 1), while the lateral side of the proximal segment exhibited higher posterior shear relative to the distal (Figure 2). Nail fixation produced the least normal and shear motion overall, with the proximal segment moving slightly anterolateral relative to the distal. In both plate and nail constructs, the differing shear directions medially and laterally suggest rotation about the femoral long axis. The titanium plate showed the largest overall motions—particularly lateral shear and medial compression—despite having a bridge span less than a third of the stainless-steel plate. The titanium nail exhibited slightly greater lateral shear than the stainless plate. This indicates that material properties (especially titanium's lower modulus) may exert more influence on fracture site motion than bridge span. Nail fixation appears to yield more uniform and predictable fracture site motion, which could have important implications for healing. Finally, these findings corroborate the clinically observed tendency for asymmetric callus formation (more medial than lateral) under plate fixation, possibly due to variable shear inhibiting lateral callus development.

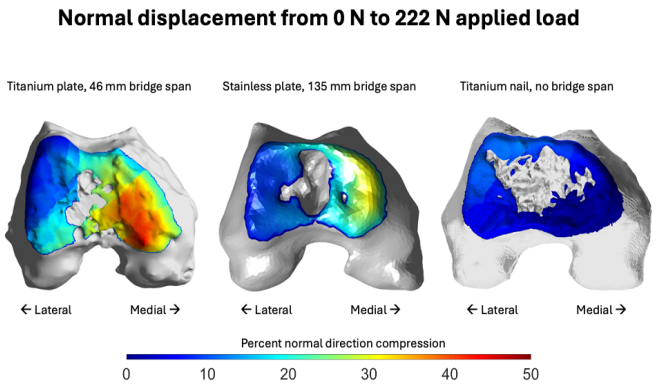

Figure 1: Normal relative motion between non-WBCT and WBCT conditions for three fixation types.

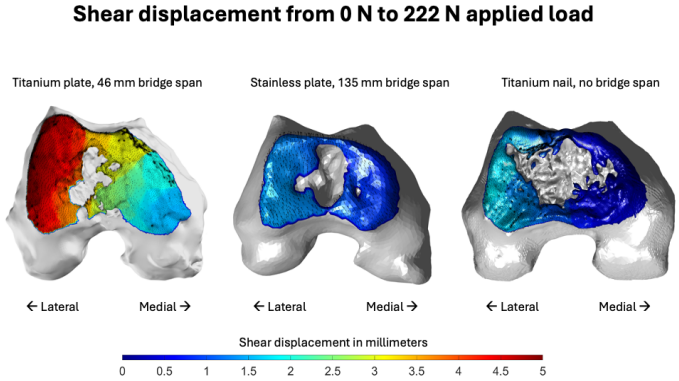

Figure 2: Shear relative motion (mm) between non-WBCT and WBCT conditions for three fixation types.

Significance: Non-invasive temporospatial assessment of complex post-operative interfragmentary motion has been described as critical to understanding "mechanically-induced tissue reactions" involved in fracture healing [5] and to translating knowledge of mechanoregulation into clinical practice [4, 6].

Acknowledgments: This work was partially supported by US Department of Veterans Affairs Grants RX003608 and RX002970.

References: [1] Elsoe, R., et al., Int Orthop, 2018. 42(1): 191-6.; [2] Henderson, C.E., et al., J Orthop Trauma, 2011. 25 S1: S8-14.; [3] Kenwright, J. and A.E. Goodship, Clin Orthop Relat Res, 1989(241): 36-47.; [4] Inacio, J.V., et al., J Orthop Res, 2023. 41(5): 1049-59.; [5] Hente, R.W. and S.M. Perren, J Biomech, 2021. 125; [6] Pivonka, P. and C.R. Dunstan, Bonekey Rep, 2012. 1: 221.

MARKERLESS MOTION CAPTURE CAN RELIABLY ASSESS CERVICAL AND SHOULDER RANGE OF MOTION

*Morgan A. Lamarre[1], Matin Jahani Jirsaraei[1], Yonathan Assefa[1], Abhishek Aher[1], Reihana A. Akhwand[1], Kirubel B. Tadesse[1], Yu-Lin Hsu[2], Benjamin Seiyon Lee[2], William F. Rosenberger[2], Secili DeStefano[1], Jay P. Shah[1], Lynn H. Gerber[1], Siddhartha Sikdar[1], Samuel A. Acuña[1]

[1]Department of Bioengineering, George Mason University, Fairfax, VA, USA

[2]Department of Statistics, George Mason University, Fairfax, VA, USA

*Corresponding author's email: mlamarre@gmu.edu

Introduction: Clinicians use range of motion (ROM) assessments to determine musculoskeletal condition severity and monitor patient progress. Musculoskeletal conditions, such as chronic myofascial pain, can affect the maximum ROM patients can achieve, especially in the upper body [1]. Traditional assessment methods, such as visual estimation and goniometers, are examiner-dependent and time-consuming [2]. Optical marker-based motion capture is highly accurate for quantifying human kinematics but not typically used in clinical settings due to length set-up and calibration requirements [3]. Markerless motion capture offers a promising alternative, providing automated, standardized, and non-invasive measurements with reduced human error [4-5]. These remove the need for marker placement, instead using machine learning algorithms to identify anatomical landmarks and body orientations from human movement video [5]. ROM value variability can arise from changes in fatigue, pain levels, recent activity, and, for markerless motion capture, clothing fit and lighting conditions [6-9]. This emphasizes the need for reliable measurement tools that can consistently capture accurate ROM data. The purpose of this study was to assess the reliability of cervical and shoulder ROM values measured using a markerless, single-camera, portable motion capture system.

Methods: Participants (22 normal, not experiencing chronic myofascial pain) performed cervical and shoulder movements while joint kinematics were recorded using a single-camera markerless motion capture system (Kinotek, Portland, ME, USA). Cervical movements consisted of cervical extension, flexion, side flexion, and rotation. Shoulder movements consisted of shoulder abduction, flexion, external rotation, and internal rotation (**Fig. 1**). Six of the movements, excluding cervical extension and flexion, provided bilateral ROM information. Each of the eight movements was performed three consecutive times within a 30-second time frame. The maximum ROM values reached during each of the three repetitions were extracted from the time series data provided of the movement. Intraclass Correlation Coefficients (ICC) were calculated for each movement. ICC values between 0.75 and 0.9 were interpreted as indicating good reliability and values above 0.9 were interpreted as indicating excellent reliability [10].

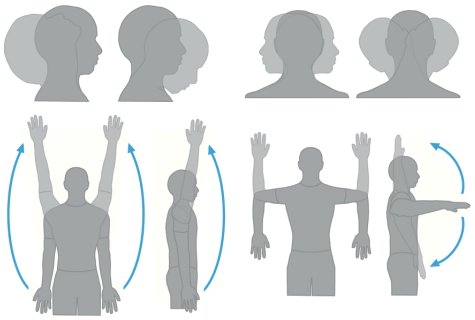

Figure 1: Eight movements tracked using the Kinotek camera.

Results & Discussion: ICCs were calculated for each movement, first considering individual participants, then including side (left vs. right) as random effects. For cervical extension and flexion ICCs were calculated using only individual participants as random effects, as these movements lack a bilateral component. ICC values for all movements except shoulder flexion improved when side was included, suggesting some of the variability in the ROM measurements is attributable to differences between the left and right sides of the body. ICCs were greater than 0.8, indicating good reliability, for all movements except for shoulder flexion (**Table 1**). This was expected and is consistent with our hypothesis that markerless motion capture would demonstrate high reliability in measuring ROM values across repeated trials for upper body movements. The ICC for shoulder abduction was found to be greater than 0.9, indicating excellent reliability. This outcome was anticipated, as shoulder abduction involves a large, well-defined movement performed directly facing the markerless motion capture camera. This positioning likely facilitates the machine learning algorithm's ability to accurately identify body poses and calculate ROM. Shoulder flexion, however, was found to have an ICC below 0.75, indicating poor reliability. This may be because, when performing shoulder flexion, the participant raises their arms in front of them, obscuring part of the body from the camera's view. This may have hindered the algorithm's ability to accurately detect joint angles and could be addressed by incorporating a second camera or adjusting the participant's positioning.

Table 1: ICC values for four cervical and four shoulder movements

Movement	ICC	
	No side random effect	**With side random effect**
Cervical Extension	0.891	NA
Cervical Flexion	0.824	NA
Cervical Side Flexion	0.773	0.864
Cervical Rotation	0.577	0.854
Shoulder Abduction	0.886	0.948
Shoulder Flexion	0.644	0.626
Shoulder External Rotation	0.850	0.887
Shoulder Internal Rotation	0.804	0.816

Significance: This study demonstrates the potential of markerless motion capture as a reliable tool for cervical and shoulder ROM assessment in clinical and research settings, offering a non-invasive and efficient alternative to traditional methods.

Acknowledgments: Efforts are sponsored by the Government under Other Transactions Number NIH HEAL 1R61AT012286.

References: [1] Alvarez & Rockwell (2002), *Am Fam Physician*; [2] Hanks & Myers (2023), *Int J Sports Phys Ther*; [3] Salisu et al. (2023), *Diagnostics*; [4] Pottorf et al. (2023) *Int J Sports Phys Ther*; [5] Wade et al. (2022), *PeerJ*; [6] Cortes et al. (2014), *Gait Posture*; [7] Moromizato et al. (2016), *J Physiol Anthropol*; [8] Muir et al. (2010), *North Am J Sports Phys Ther*; [9] Ray et al. (2024), *Front Comput Sci*; [10] Koo & Li (2016), *J Chiropr Med*

ACCURACY OF 2D VIDEO-BASED MOVEMENT ANALYSIS TOOLS FOR THE STUDY OF HUMAN FALLS AND IMPACTS

Kitaek Lim[1], Junwoo Park[1], Seyoung Lee[1], Soyeon Yoon[1], Sungmin Chun[1], Donggeon Kim[1], Woochol Joseph Choi[1]*
[1]Injury Prevention and Biomechanics Laboratory, Dept of Physical Therapy, Yonsei University, South Korea
*Corresponding author's email: wcjchoi@yonsei.ac.kr

Introduction: Video analysis tools are available for the kinematic analysis of movements, and human falls and impacts are analyzed with MediaPipe Pose Estimation (MPE) or Kinovea [1,2]. However, the 2D video-based analysis has an inherent limitation, "perspective error", which arises when the point of interest moves out of the calibrated plane of movement, which commonly occurs during human falls and impacts (i.e., body rotation during descent and impact). While improved technology (i.e., machine learning, auto tracking, auto calibration, etc) seems to help minimize the error, the accuracy needs to be studied, particularly for human falls. We compared the accuracy of the 2D video-based analysis tools with a 3D motion capture system.

Methods: Eight healthy young adults (4 males, 4 females) participated in falling experiments, where they fell sideways voluntarily ("self-initiated fall"), and slipped unexpectedly via a linear motor ("motor-induced fall"). For the self-initiated falls, they mimicked typical sideways falls of older adults on a 40 cm-thick mattress. For the motor-induced falls, they stood on a carpet placed over the mattress, which was suddenly, without a cue, translated horizontally at a velocity of 2.3 m/s via a linear motor (SL280, Sewoo Industrial Systems, Ansan, South Korea).

During trials, reflective markers were placed on the wrists, knees, and pelvis to record the kinematics of body segments using an 8-camera motion capture system (MOCAP) (Vero v2.2, VICON, Oxford, UK) at a sampling rate of 200 Hz. Trials were also video recorded with an iPhone 12 Pro at a sampling rate of 30 Hz and a resolution of 1920 × 1080 pixels. Three trials were acquired for each falling condition and averaged for data analysis.

To calculate outcome variables (peak vertical and horizontal velocities of the pelvis at impact), we used MPE software (version 0.10.21, Google, CA, USA) for automatic detection of body segments during a fall (Fig. 1a). We also used Kinovea software (version 2023.1.2, Spectator Sports, Bordeaux, France) for manual digitization of body segments during a fall, which was conducted by SY, DK, and SC with a moderate to good inter-rater reliability (ICC (2,1) = 0.84 and 0.7 for vertical and horizontal velocity, respectively) (Fig. 1b). To calibrate and minimize errors caused by image distortion, a calibration panel (dimension 148 cm × 182 cm, 8 × 8 grid of 1.4 cm diameter circular markers spaced 20 cm apart) was used (Fig. 1c). We also used MOCAP data as a standard (Fig. 1d).

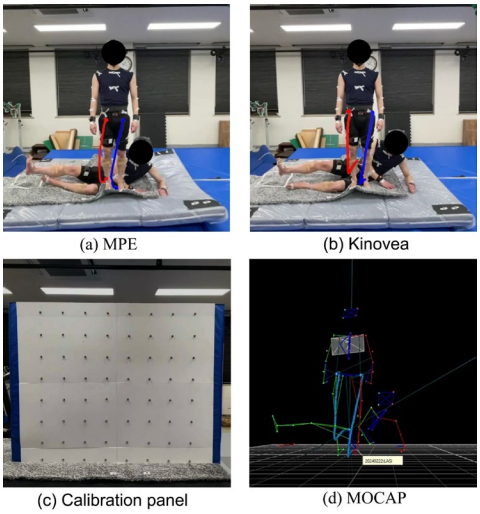

Figure 1: Tracking of the pelvis using (a) MPE, and (b and c) Kinovea along with a calibration panel, and (d) MOCAP during sideways fall.

Paired t-tests were used to examine the accuracy of the analysis technique (MPE, Kinovea) when compared to MOCAP.

Results & Discussion: In self-initiated falls, our t-test suggested that, when compared to MOCAP, the peak vertical impact velocity of the pelvis was 34.5% and 20.7% smaller in Kinovea and MPE, respectively (2.9 versus 1.9 m/s; 2.9 versus 2.3 m/s, respectively) ($t = 8.389$, $p < 0.0005$; $t = 2.667$, $p < 0.05$, respectively). Similarly, the peak horizontal impact velocity of the pelvis was 35.7% smaller in Kinovea (1.4 versus 0.9 m/s; $t = 6.304$, $p < 0.0005$) (Fig. 2a).

In motor-induced falls, our t-test suggested that, when compared to MOCAP, the peak vertical impact velocity of the pelvis was 25.8% and 22.6% smaller in Kinovea and MPE, respectively (3.14 versus 2.3 m/s; 3.1 versus 2.4 m/s, respectively) ($t = 4.016$, $p < 0.005$; $t = 2.802$, $p < 0.05$, respectively). Similarly, the peak horizontal impact velocity of the pelvis was 45.5% smaller in Kinovea (1.1 versus 0.6 m/s; $t = 4.425$, $p < 0.005$) (Fig. 2b). These results indicate that video-based kinematic analysis tools have a limitation in accuracy, particularly for human falls and impacts.

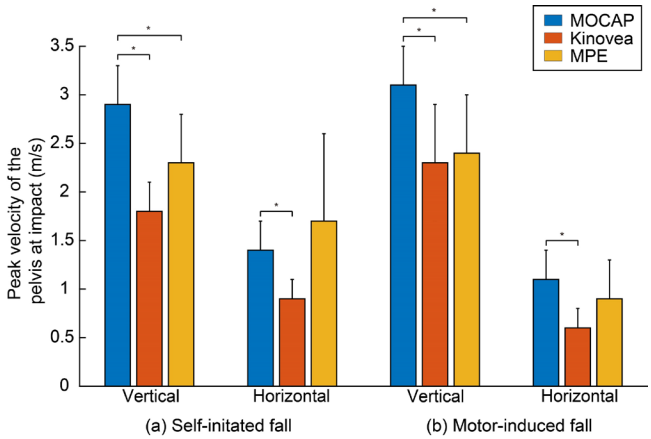

Figure 2: The peak velocity of the pelvis at impact during (a) self-initiated falls and (b) motor-induced falls.

Significance: We have examined the accuracy of 2D video-based movement analysis tools. Despite improved technology, their estimation on the impact velocity of the pelvis during a fall was 30.8%, on average, lower when compared to a gold standard. Clinicians and researchers should be advised when they study on human falls with video-based movement analysis tools.

Acknowledgments: This research was supported by Basic Science Research Program (RS-2023-00270689) and by the Brain Korea 21 FOUR Project, the Korean Research Foundation

References: [1] Shishov et al. (2021), *PLoS One* 16(10); [2] Kibet et al. (2024), *Sensors* 24(24).

RELATIONSHIP BETWEEN FOOT MECHANICAL POWER AND WHOLE-BODY METABOLIC POWER IN OLDER AND YOUNGER ADULTS

*Christopher L. Long[1], Daniel J. Davis[1], Jason R. Franz[2], Kota Z. Takahashi[1]
[1]Department of Health and Kinesiology, University of Utah, Salt Lake City, UT
[2]Lampe Joint Department of Biomedical Engineering, UNC Chapel Hill & NC State University, Chapel Hill, NC
*Corresponding author's email: christopher.long@utah.edu

Introduction: The metabolic energy cost of walking is approximately 17% higher in older adults than in younger adults [1]. Furthermore, older adults lose more mechanical energy via the foot and generate less power at the combined ankle-foot system [2]. These functional deficits coincide with morphological changes such as weaker and smaller toe flexor muscles [3]. We reason that energy lost at the foot must be compensated for elsewhere, possibly at joints with less efficient muscle-tendon architecture, such as the hip [4]. If true, greater foot mechanical energy loss could contribute to the higher whole-body metabolic demand of walking in older adults. However, this relationship remains unclear. To address this gap, we examined the association between foot mechanical power and whole-body metabolic power during level, barefoot walking in younger and older adults. We hypothesized that: (1) greater negative net foot power (i.e., a higher rate of mechanical energy loss) would be associated with greater metabolic power, and (2) this relationship would be more pronounced in older than in younger adults. As a secondary analysis, we also examined the relationships between positive and negative foot power and whole-body metabolic power, as net foot power reflects overall energy loss but does not distinguish whether that loss results from reduced power generation or increased power absorption/dissipation.

Methods: To date, 8 older adults (6F/2M, 66.5 ± 3.3 yrs, 65.9 ± 11.3k g) and 23 younger adults (12F/11M, 25.1 ± 3.3 yrs, 67.5 ± 12.1 kg) have walked barefoot on an instrumented treadmill at 1.2 m/s. We calculated foot mechanical power for each stride using unified deformable (UD) segment analysis, which captures the summed mechanical power contributions of all structures distal to the hindfoot center of mass [5]. We calculated positive and negative work by integrating the respective areas under the foot power curve, which we summed to calculate net foot work. We converted work to average power (positive, negative, and net) by dividing by stride duration. We then averaged power across strides and normalized it to body mass.

We calculated gross whole-body metabolic power (W/kg) from gas exchange rates and converted it to net metabolic power by subtracting the metabolic power measured during standing. To examine the relationship between net foot power and net metabolic power and whether this relationship differs by age group, we employed a multiple linear regression model with net foot power and age group as predictors. As a secondary analysis, we ran two additional regression models, replacing net foot power with positive and negative foot power, respectively.

Results & Discussion: Net foot power was not significantly associated with whole-body net metabolic power ($p = 0.278$), and this relationship did not change between age groups, failing to support our hypothesis (Fig. 1A). Negative foot power also showed no association ($p = 0.614$). However, positive foot power was negatively associated with net metabolic power ($B = -7.753$, $p = 0.002$), regardless of age group. This result indicates that individuals who generated less positive power at the foot walked with higher net metabolic power. Specifically, for every 0.03 W/kg decrease in positive foot power, metabolic cost increased by approximately 9% relative to the group average (Fig. 1B). Since prior studies have shown reduced energy generation at the foot in older adults [2], our current findings suggest that decreased positive foot power may be linked to the increased metabolic energy cost of walking in older age. Future studies should investigate whether this relationship is driven by compensatory energy generation at proximal joints.

Significance: Our preliminary results suggest that reduced energy generation at the foot is associated with increased whole-body metabolic cost during walking. Therefore, these findings may motivate interventions aimed at increasing positive foot power (e.g., footwear modifications or foot muscle strengthening) to reduce the metabolic energy cost of walking in older adults.

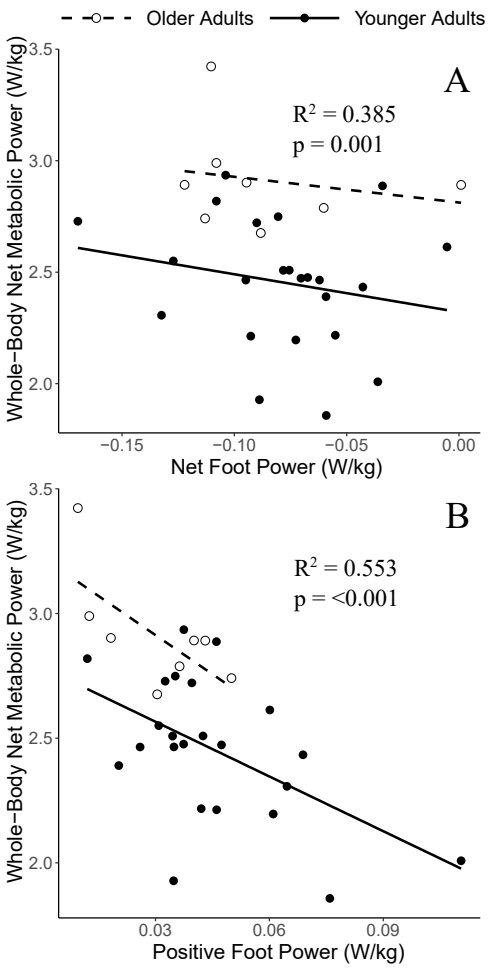

Figure 1: The relationship between net foot power (A), positive foot power (B), and net whole-body metabolic power during walking at 1.2 m/s. A line of best fit is displayed for each age group.

Acknowledgments: This work was supported by NIH R01AR081287 awarded to KZT and JRF and NIH T32TR004394 awarded to DJD.

References:

[1] Das Gupta et al. (2019), *Sci Rep*, 9; [2] Krupenevich et al. (2021), *J Biomech*, 123; [3] Mickle et al. (2016), *J Orthop Sports Phys Ther*, 46(12); [4] Devita & Hortobagyi (2000), *J Appl Physiol*, 88(5); [5] Takahashi et al. (2017), *Sci Rep*, 7(1).

EFFECTS OF PASSIVE STRETCH TRAINING ON PLANTARFLEXOR FUNCTION AND GAIT SPEED IN PATIENTS WITH PERIPHERAL ARTERY DISEASE

*Logan Faux-Dugan[1], Jocelyn Delgado Spicuzza, Judy M. Muller-Delp[2], Carl J. Ade[3], Stephen J. Piazza[1], David N. Proctor[1]
[1]Department of Kinesiology, The Pennsylvania State University, University Park, PA, USA.
[2]Department of Anatomy and Physiology, Kansas State University, Manhattan, KS, USA.
[3]Department of Kinesiology, Kansas State University, Manhattan, KS, USA.
*Corresponding author's email: fauxdugan@psu.edu

Introduction: Peripheral artery disease (PAD) is a pathological condition characterized by poor circulation, muscular atrophy, and reduced mobility, which is brought on by atherosclerotic blockages often occurring in the lower limbs [1]. Current interventions, such as supervised treadmill exercise, have low compliance rates. Recent evidence suggests that passive stretch training, an intervention with high compliance, may be used to improve the microcirculation and walking speed of patients affected by PAD [2]. Additionally, static stretch training has also been found to increase fascicle length and muscle strength and power in healthy individuals [3]. However, the effects of a stretching intervention on plantarflexor function in PAD patients are unknown.

In the present study, we investigated the impact of four weeks of passive stretch training on the structure and function of the plantarflexors and walking performance in patients with PAD. We hypothesized that stretch training of the plantarflexors would increase the static fascicle length and normalized fascicle excursions of the medial gastrocnemius during walking at a preferred speed. It was also hypothesized that the patients would walk faster after the stretching intervention.

Methods: PAD patients (n=9) engaged in stretch training, in which they passively stretched their plantarflexors for 30 minutes/day, five days/week, for four weeks.

Pre- and post-stretching measurements were made to assess walking performance and medial gastrocnemius architecture. Static fascicle lengths were measured using ultrasonography (LF9-5N60-A3; Telemed, Lithuania) with the patients lying prone. Total distance and continuous speed were recorded from a six-minute walk test. Lastly, ultrasonography was used to measure normalized fascicle excursions of the medial gastrocnemius during treadmill walking at the patients' preferred speed, which was taken as the average continuous walking speed during the walk test.

Results & Discussion: After stretching, the patients walked significantly farther during a walking test (316 ± 93 m vs. 336 ± 89 m; $p = 0.002$), and they had significantly longer static gastrocnemius fascicles (Figure 1A; 45 ± 3 mm vs. 48 ± 4 mm; $p = 0.003$) and normalized fascicle excursions (Figure 1B; 0.54 ± 0.15 vs. 0.68 ± 0.21; $p = 0.010$) during treadmill walking. These findings suggest passive stretch training can improve the structure and function of the plantarflexors, which may contribute to improvements in the walking of individuals with PAD. Further testing of additional patients is ongoing at this time.

Significance: Passive stretch training may be useful for improving the structure and function of the plantarflexors and walking performance in patients with peripheral artery disease.

Acknowledgments: Funding for this study was provided by the American Heart Association (AHA-23IPA-1053325), and we would like to thank the Penn State Clinical Research Center for providing the staffing, facilities, and expertise necessary for the completion of this research thus far.

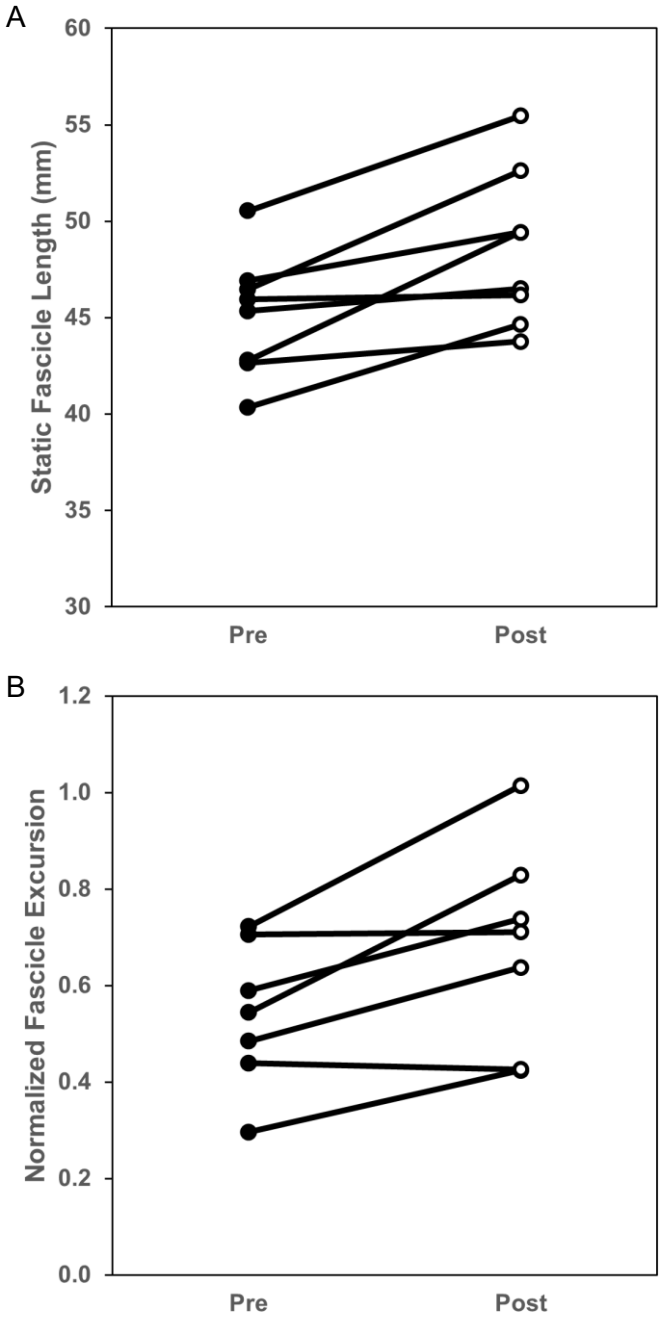

Figure 1: A) static fascicle lengths and B) normalized fascicle excursions of the medial gastrocnemius before and after a four-week passive stretching intervention.

References: [1] McDermott et al. (2020), *Arterioscler Thromb Vasc Biol* 40(11); [2] Hotta et al. (2019), *Cardiovasc Revasc Med* 20(8); [3] Arntz et al. (2023), *Sports Med* 53(3).

AGE-RELATED CHANGES IN THE BIOMECHANICS OF THE LOWERING PHASE OF A PUSH-UP: IMPLICATIONS FOR ARRESTING A FORWARD FALL

Rebecca Go[1], James Borrelli[1]*
[1]Enginering, Math, and Physics, Stevenson University
*Corresponding author's email: jborrelli@stevenson.edu

Introduction: Maintaining balance requires careful management of the relationship between the center of mass (*CoM*) and pressure (*CoP*). Arresting a fall requires similar management of the *CoP* and *CoM*. Upon impact in a forward fall, rapid loading of the arms is required to orient the *CoP* with respect to the *CoM* such that the fall energy is arrested. The aim of this work was to develop a framework for analyzing forward fall with a focus on the *CoM* and *CoP* relationship, time to contact, and stability. As a secondary aim, we hypothesize that older adults, because of decreased energy absorbing capacity of the arms [1-3], will challenge themselves to a lesser extent than younger adults and it will be evident by considering the stability of the movement.

Methods: Twenty-three healthy adults (12 older adults (4 females, 72 (7) yrs) and 11 younger adults (3 females, 23 (11) yrs)) performed a single push-up 'as fast as possible.' The instructions were meant to induce the most unstable state that participants were willing to take on. Summing moments around point *O* (figure 1), assuming small angles, and simplifying gives

$$vGRF \cdot u - mgx = mL\,\ddot{y}. \quad [1]$$

An equation for *y(t)* is obtained after integrating equation [1] twice,

$$y(t) = \frac{1}{2}(vGRF \cdot u - mgx)t^2 + v_0 t + y_0 \quad [2]$$

An estimate for the time when the body will impact the ground, or the time to contact (τ) can be derived by solving equation [2] for *y(t)*=0,

$$\tau_{1,2} = \left[-v_0 \pm \sqrt{v_0^2 - 4y_0\left(\frac{vGRF}{mL}u_0 - \frac{g}{L}x_0\right)}\right] \Big/ \left[2\left(\frac{vGRF}{mL}u_0 - \frac{g}{L}x_0\right)\right]$$

where y_0, v_0, x_0, and u_0 are the height of the *CoM*, vertical velocity of the *CoM*, horizontal location of the *CoM*, and horizontal position of the *vGRF*. In order to avoid impact with the ground, the *CoP* must move forward of the *CoM*. A margin of stability (*MoS*) can be estimated by taking the product of the time to contact and velocity (v_0) [4]. The lower panel in figure 1 shows the relative position of the *CoM* and *CoP* for an example trial. The *CoM* and *CoP* are the same distance from the feet prior to beginning a push-up (lower panel in figure 1). The lowering phase requires the *CoP* to move closer to the feet, accelerating the body downward before moving closer to the shoulder to arrest the downward motion and eventually accelerate upward during the elevating phase. We chose to analyze the time point when the *vGRF* under the hands is a minimum which results in the largest downward acceleration (see equation [1] above).

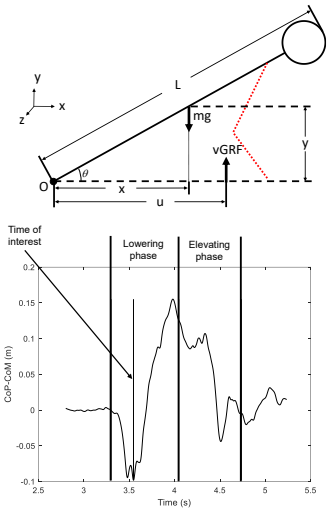

Figure 1: Free body diagram of a push-up modeled as an inverted pendulum (top). Plot of position of the *CoP* relative to the *CoM* during the lowering phase and elevating phase of a push-up (bottom). Analysis was performed on the time point when the force under the hands was a minimum.

Table 1: Significant differences (*p*-values<0.05) are highlighted in bold.

	Younger adults	Older adults
$vGRF_{min}$ (%BW)	**38(19)**	**52(11)**
$vGRF_{max}$-$vGRF_{min}$ (%BW)	**64(30)**	**34(19)**
y_0 (m)	0.40(0.05)	0.39(0.04)
v_0 (m/s)	**-0.13(0.11)**	**-0.06(0.05)**
u_0-x_0 (m)	**-0.18(0.16)**	**-0.07(0.08)**
τ (s)	**0.34(0.12)**	**0.52(0.21)**
MoS (m)	**-0.039(0.025)**	**-0.027(0.018)**

Results & Discussion: Younger adults performed the lowering portion of the push-up (780 (258) s) more rapidly than older adults (1123 (650) s). The minimum *vGRF* under the hands ($vGRF_{min}$) was significantly lower for younger adults and increased to a greater load than older adults (Table 1). The lowering velocity was greater and the relative position of the *CoP* (u_o-x_0), the time to contact, and the *MoS* smaller for younger adults. The differences reported here may be explained by participants only moving as quickly or allowing as large a *CoP*-*CoM* displacement as they are able to arrest without impacting the floor. Age-related declines in energy absorbing capacity of the arms may explains older adults accelerating themselves to a lesser degree, as evidenced by the smaller difference in *CoP* and *CoM*.

Significance: In an actual fall, the velocity of the body will be larger than reported here. Future work is required to evaluate the use of this framework in actual and simulated falls. However, this model provides a means to evaluate fall biomechanics taking relevant parameters and combining them into a single measurand. The framework provides a novel avenue for investigating fall arrest strategies and as part of a feedback control model for use in a fall simulator developed by the authors.

Acknowledgments: The authors acknowledge a support from the Kahlert foundation and the Stevenson Summer Scholars Research Program.

References: [1] DeGoede et al. (2003), *J Biomech* 36(7); [2] Lattimer et al. (2017), *JAPA* 25(3); [3] Borrelli et al. (2022), *Hum Mov Sci* 81; [4] Hof et al. (2005), J Biomech 38(1).

THE EFFECTS OF INCONTINENCE TYPE ON BALANCE IN ADULT WOMEN

*Sydney L. Lemley, Sarah A. Hudacheck, Haley Hartman, Marlee Scott, Robert Shapiro, Corrie Mancinelli,
Omar D. Garcia, and Jean L. McCrory
School of Medicine, West Virginia University, Morgantown WV
*Corresponding author's email: sll00002@mix.wvu.edu

Introduction: Many women with urinary incontinence (UI) experience issues with balance [1]. UI can be classified into three types: stress, urge, and mixed [2]. Stress UI (SUI) is attributed to weak pelvic floor musculature [3]. Uncontrolled urination could result from forceful movements such as coughing, sneezing, or exercise. Balance issues possibly arise in stress and mixed UI from weakened pelvic floor musculature, as the pelvic floor muscles have been shown to play a part in postural stability due to their role in stabilizing the pelvic girdle [4]. Urge UI (UUI) is uncontrolled urination before the toilet is reached and is due to a distended bladder or overactive bladder [5]. Mixed UI (MUI) is a combination of stress and urge UI [2]. The purpose of this study was to observe which medically-diagnosed incontinence type has a greater impact on postural stability in adult women.

Methods: Twenty-one women diagnosed with UI (10 SUI [49.3±13.0yrs, 1.6±0.1m, 77.4±13.9kg]; 4 UUI [66.3±6.2yrs, 1.6±0.1m, 71.2±14.5kg], 8 MUI [61.3±15.4yrs, 1.7±0.1m, 78.5±14.5kg]) participated. Subjects were recruited from WVU University Town Centre Women's Clinic. Exclusion criteria included: medication that affects balance, current or recent pregnancy, uncontrolled blood pressure, any musculoskeletal issue or injury that affected gait or load bearing, back surgery <1 year, vertigo, or any neuromuscular impairment.

An Inertial Measurement Unit was secured on an elastic band wrapped around each subject's chest at the lower bra strap. Subjects completed the Modified Clinical Test of Sensory Integration in Balance (CT-SIB) that involved a series of balance tests: a) standing on firm surface with eyes open (EO), b) standing on firm surface with eyes closed (EC), c) standing on foam with eyes open (EOF), and d) standing on foam with eyes closed (ECF). Subjects were also tested on single leg balance (SLS) on their dominant leg with eyes open. Triaxial linear acceleration and angular velocity data (1125 Hz) were processed using MATLAB. To capture sway, we determined the root mean square (RMS) and standard deviation (STDV) of the following parameters: anteroposterior, mediolateral, and vertical linear accelerations, and frontal, sagittal, and transverse plane angular velocities. Normalized path length (NPL) for the anteroposterior acceleration was determined for each condition [6]. Statistical analyses were performed in SPSS. A two-factor ANOVA (Group x Condition) was performed on each outcome variable. Tukey post-hoc analyses were performed when appropriate ($\alpha = .05$).

Results & Discussion: RMS of angular velocity and linear accelerations were greatest in the SLS condition. Group x Condition interactions were significant such that frontal plane angular velocity (Fig.1a) was greatest in SLS in the UUI group ($p<.001$). STDV of vertical axis linear acceleration was significantly greater for the SLS condition in the UUI group ($p<.001$). Moreover, STDV of vertical acceleration was significantly greater for the EO condition in the SUI group vs. the UUI and MUI groups ($p<.001$) (Fig.1b).

The finding that UUI sway was the greatest during the SLS condition could be due to a decrease in the strength of pelvic floor muscles (PFM) from less frequent mobility activities, as other authors reported that women with UUI tend to stay near a toilet to avoid leaks and falls due to a slower gait, thus further impairing balance [2,7]. If PFM training increases the strength of the PFMs for UUI, then disuse would decrease PFM strength and thus balance [8]. The increased sway along the vertical axis during the EO condition is interesting, as it was only found to be significantly higher in women with SUI. This could be due to weakness of the PFMs [9,10] and/or increased contraction of the PFMs and trunk musculature, as other authors have reported women with SUI have increased contraction in these areas which can cause less trunk flexibility. This decreased flexibility/responsiveness of the trunk to a change in the body's position can hinder balance control and increase sway [11,12]. However, one author found no balance impairment in SUI when comparing SUI to UUI [2]. Thus, more research is needed to understand these differing results.

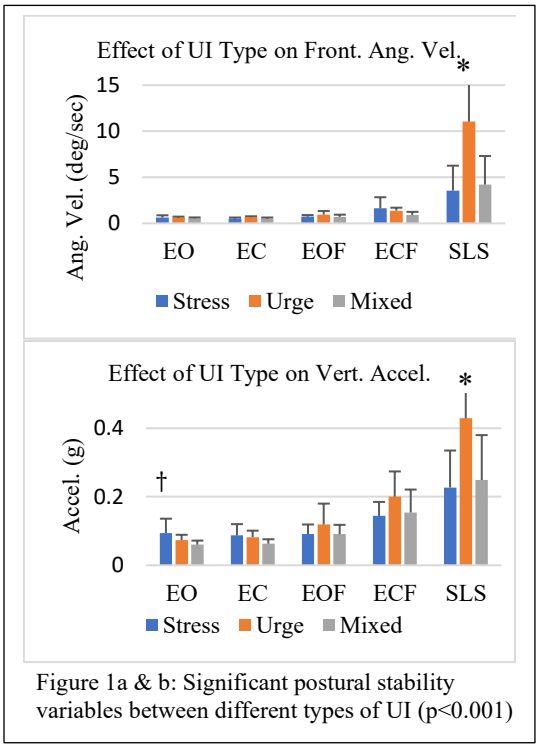

Figure 1a & b: Significant postural stability variables between different types of UI ($p<0.001$)

Significance: Women with pelvic floor dysfunction have an increased risk of falling compared to unaffected women [1]. Others have reported differences in fall risk between the different pathological causes of UI [1,7,11]. This study is the first to report on postural stability differences between women with different UI diagnoses. The results obtained can assist with providing improved care to women with UI.

References: [1] Chmielewska et al. (2017), *Neurourol Urodyn* 36(8), [2] Fritel et al. (2013), *BJOG: An Int. Journ. of Obst. & Gyn.*120(12), [3] Ghaderi et al. (2016), *Urology* 93, [4] Hodges et al. (2007), *Neur. Urodyn.* 26(3), [5] Kim et al. (2010), *Int Neuro. J* 14(4), [6] Alkathiry et al. (2018) *J Athl Train.* 53(12), [7] Chahal et al. (2024), *Continence* 12, [8] Mont-Briant et al. (2023), *Continence* 7, [9] Sun et al. (2022) *BMJ Support Palliat. Care*12(1), [10] Lee et al. (2024) *American Jour. of Obst. and Gyn.,* [11] Smith et al. (2007) *Neurourol. and Urodynamics* 26(3), [12] Smith et al. (2008) *Neurourol. and Urodynamics* 27(1)

INTRAINDIVIDUAL VARIABILITY IN SIMPLE REACTION TIME IS ASSOCIATED WITH BALANCE AND FALLS IN OLDER CANCER SURVIVORS

*Shores CMV[1], Bell SG[2], Hehir MK[3], Rosano C[4], Richardson JK[5], Kolb N[5], Redfern MS[1], McNeish BL[6]
[1]Department of Bioengineering, University of Pittsburgh
[2]Department of Obstetrics and Gynecology, University of Pittsburgh
[3]Department of Neurological Sciences, University of Vermont
[4]Department of Epidemiology, University of Pittsburgh
[5]Department of Physical Medicine and Rehabilitation, University of Michigan
[6]Departement of Physical Medicine and Rehabilitation, University of Pittsburgh
*Corresponding author's email: CMS402@pitt.edu

Introduction: Intraindividual reaction time variability (IIRV) is associated with physical function and falls in older cancer-free adults but has been minimally studied in aging cancer survivors [1, 2]. The aims of this study were (1) to assess the association of IIRV with physical function and falls in chemotherapy-treated cancer survivors, (2) to determine if this relationship varied between middle-aged and older cancer survivors, and (3) to determine if any associations are independent of reaction response central tendency (i.e., total reaction accuracy) and locomotor impairment.

Methods: Fifty cancer survivors (n=28 with age≥ 65 years, 88% women) post chemotherapy treatment were included in this cross-sectional study. IIRV was defined as the standard deviation of simple reaction time from stick drop paradigm and separately total accuracy, a measure of executive function central tendency, was evaluated with a go/no-go stick drop paradigm. (Fig. 1). Physical function was measured by time to complete five sit-to-stand (5STS), number of sit-to-stand repetitions in thirty seconds (STS30), and unipedal stance time (UST). Self-reported recurrent and injurious falls in the past year were recorded as secondary outcomes. Bivariate analyses were conducted between IIRV measures and physical function variables in middle-aged and older aged cancer survivors. Multivariable models were used to examine the associations of simple IIRV with UST and falls outcomes. Included covariates were age, total reaction accuracy, a measure of central reaction tendency, and presence of a locomotor risk factor (obesity or neuropathy).

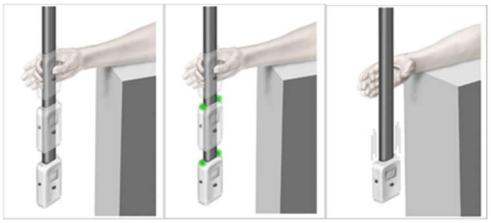

Figure 1: ReacStick Testing: (A) Simple mode for determining simple reaction time (SRT). The device was released, after random time delays, and the participant grasped the falling device as quickly as possible. (B, C) To evaluate total accuracy the mode on the device was changed to Complex after which the lights affixed to the top illuminated, randomly, at the instant of release for 50% of the trials. Complex reaction times were recorded on correct trails when lights illuminated "On trials" and incorrect "Of trials." total accuracy was

Results & Discussion: In older aged cancer survivors, Spearman correlations demonstrated significant inverse relationships of IIRV with UST (r=-0.52) and STS30 (r=-0.41), but not 5STS. In multivariable models, the interaction of age ≥65 years with increasing levels of simple IIRV was independently associated with worse UST (B -0.919, 95% CI -1.68, -0.159, p=0.02), increased recurrent falls (OR 1.29, 95% CI ,1.04 1.61, p=0.02), and injurious falls (OR 1.30, 95% CI ,1.04 1.63, p=0.02). IIRV was independently associated with balance and falls outcomes in older chemotherapy-treated cancer survivors. The relationship of IIRV to balance and falls did not extend to middle-aged cancer survivors, suggesting that IIRV may be of greater importance for cognitive motor control in older cancer survivors.

Significance: The current study identifies two key aspects of executive function- total accuracy, reflecting the central tendency of complex reaction responses, and IIRV, measuring sustained attention variability- as independent determinants of balance and falls in the presence of locomotor risk factors. While longstanding research has shown that chemotherapy-induced peripheral neuropathy affects balance and mobility, our findings expand the conceptual model of balance in chemotherapy-treated cancer survivors by incorporating IIRV in addition to executive function central tendency. This is particularly relevant, as effective central sensorimotor integration likely requires both sustained (low IIRV) and accurate (high total accuracy) integration of sensory input and this may confer mobility resilience in the context of known deficits in CIPN [3] and vestibular dysfunction [4]. Additionally, emerging research suggests that IIRV may serve as a biomarker for chemotherapy-related cognitive dysfunction (CRCD) [5], raising the possibility that CRCD may contribute to mobility impairments in chemotherapy-treated cancer survivors. Finally, targeting central sensorimotor integration control could provide a unique opportunity to improve mobility dysfunction that is multifactorial from both peripheral (e.g., peripheral neuropathy and vestibular dysfunction) and central (e.g., chemotherapy-related cognitive dysfunction) sources.

Acknowledgments: The work was supported in part by P30AG02482 from University of Pittsburgh Claude D. Pepper Older Americans Independence Center to BLM.

References: [1] McNeish et al. (2023), *J Geriatr Oncol* 14 (8); [2] Jayakody et al. (2021), *Gait Posture* 89; [3] McCary et al. (2019), *J Natl Compr Canc Netw* 127 (21); [4] Medina et al. (2021), *Cancer* 127 (21). [5] Yao et al. (2017), *Pyschooncology* 26 (12).

Heart Rate Dynamics During Motor Function: A Marker of Frailty

Mohammad Hosseinalizadeh[1,2], Kübra Akbaş[2], Alexandria Jean L. Rufin[2], Nima Toosizadeh*[2]
[1]Department of Biomedical Engineering, School of Graduate Studies, Rutgers University
[2]Department of Rehabilitation and Movement Sciences, School of Health Professions, Rutgers University
*Corresponding author's email: nima.toosizadeh@rutgers.edu

Introduction: Frailty is a common syndrome in older adults, marked by reduced strength, endurance, and physiological reserve, which can lead to an increased vulnerability to stressors [1]. Frailty has been linked to autonomic nervous system (ANS) dysfunction, with heart rate variability (HRV) identified as a key marker [2]. This study aims to establish and validate a platform for simultaneous motor and cardiac function execution to evaluate heart rate (HR) dynamics, HR changes due to physical activity, as a potential marker for frailty in community-dwelling older adults. Given the limitations of HR assessment during walking, such as motion artifacts, space constraints in clinical settings, and mobility restrictions in some older adults, we utilized a previously validated upper extremity function (UEF) test. This test involves rapid elbow flexion, to assess motor performance based on slowness, weakness, inflexibility, and fatigue [3]. We hypothesized that HR dynamics during and after UEF would be significantly associated with frailty.

Methods: Older adults were recruited from three diverse cohorts. Inclusion required the ability to walk, and exclusions included severe motor or cognitive impairments (MMSE ≤23) and conditions affecting HR (e.g., arrhythmia and β-blocker use) [4]. Frailty was classified using the Fried phenotype criteria [1]. During the UEF test, wearable motion sensors (BioSensics LLC, 100 Hz) captured elbow angular velocity, and UEF motor scores were computed using previously established methods [5]. HR was continuously recorded using an ECG system (Mega Electronics, 1000 Hz). RR intervals were extracted via the Pan-Tompkins algorithm. HR outcomes included resting HRV (e.g., RMSSD) and HR dynamics (HR increase during UEF and HR decrease during recovery). ANOVA models assessed differences in HR features and UEF motor score across frailty groups, adjusting for age, sex, and BMI.

Results: A total of 140 participants were recruited, including 26 non-frail (age=71.61±9.88 years), 93 pre-frail (age=77.55±9.46 years), and 21 frail (age=78.81±9.56 years). Demographic variables (age, sex, BMI) did not differ significantly between groups (p>0.10). The UEF motor score differed between groups (p=0.0021), which demonstrated lower performance in pre-frail and frail individuals. HR dynamics also differed (Figure 1, p=0.0341), as well as HR recovery post-task (Figure 1, p=0.0231), with pre-frail and frail participants showing lower responses in those outcomes. The HR increase rate during the task was also different among frailty groups (p=0.0412), while the HR recovery rate (p=0.2639) and RMSSD were not significantly different between groups (p=0.8545, Table 1).

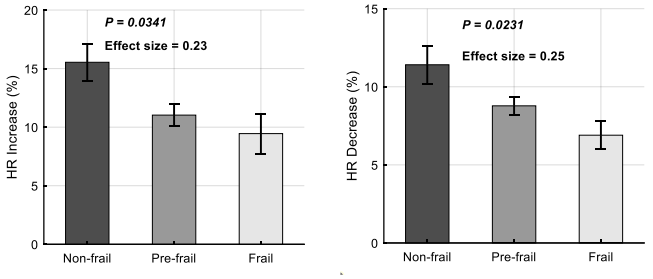

Figure 1) Differences in mean HR dynamic outcomes in response to UEF among non-frail, pre-frail, and frail participants. Error bars represent standard errors. p-values are obtained from the ANOVA model, adjusted for age, sex, and BMI.

Table 1) Results for ANOVA models (adjusted with age, sex, and BMI), representing differences in UEF motor score and baseline HR and HR dynamics. *: Significant difference

Parameters	Non-frail (n=26)	Pre-frail (n=93)	Frail (n=21)	p-value (effect size)
UEF motor score, 0-100 (SD)	36.5 (15.97)	53.36 (25.37)	60.62 (17.06)	0.0021 (0.34)*
HR percent increase, % (SD)	15.54 (8.01)	11.03 (8.72)	9.45 (7.41)	0.0341 (0.23)*
HR percent decrease, % (SD)	11.41 (6.11)	8.78 (5.40)	6.90 (3.88)	0.0231 (0.25)*
HR increase rate (SD)	0.24 (0.23)	0.15 (0.16)	0.10 (0.13)	0.0412 (0.25)*
HR recovery rate (SD)	0.14 (0.13)	0.14 (0.21)	0.07 (0.12)	0.2639 (0.13)
RMSSD (SD)	24.65 (20.29)	35.78 (66.64)	40.82 (63.02)	0.8545 (0.09)

Discussion: As hypothesized, significant associations were observed between frailty status and HR dynamics during and after the UEF test. Frail individuals exhibited a diminished HR response, characterized by a smaller HR increase during activity and a slower HR decrease during recovery, indicating impaired autonomic regulation and reduced cardiac reserve. Our results suggest that HR dynamics during activity may provide a more sensitive marker of frailty than HRV during resting state. This supports the notion that frailty is a result of multisystem dysregulation rather than impairment in a single physiological domain. Given the feasibility of measuring HR responses during a simple motor task, integrating cardiac and motor assessments could enhance frailty prediction in clinical settings.

Significance: This study highlights the potential of HR dynamics during the UEF task as a sensitive marker of autonomic function and physiological reserve. Our findings suggest that HR dynamics could be integrated into future frailty assessments for individuals with heart-related conditions. This approach captures both cardiac and motor function in a clinical setting within less than two minutes of physical task while seated. These measures could be incorporated into accessible devices like smartwatches, enabling frailty assessment and remote monitoring in clinical and home settings.

Acknowledgments: This research was supported by one award from the National Institute of Aging (NIA/NIH-1R01AG076774-01A1) and one award from the National Science Foundation (NSF 2236689—CAREER).

References: [1] Fried LP, et al. J Gerontol A. 2001;56(3):M146-M157; [2] Moghtadaei M, et al. J Physiol. 2016;594(23):7105-7126; [3] Toosizadeh N, et al. PLoS One. 2017;12(2):e0172766; [4] Folstein MF, et al. J Psychiatr Res. 1975;12(3):189-198; [5] Toosizadeh N, et al. BMC Geriatr. 2017;17:1-7.

SHOE HEEL-TOE DROP AFFECTS RUNNING ECONOMY

Kaleigh Renninger[1]* & Owen N. Beck[2]
[1]Walker Department of Mechanical Engineering, The University of Texas at Austin, TX
[2]Department of Kinesiology and Health Education, The University of Texas at Austin, TX
*email: kaleigh.renninger@utexas.edu

Introduction: Distance-running performance depends on the athlete's rate of metabolic energy expenditure (running economy) [1]. Athletes can enhance their running economy, and their running performance, by improving their running mechanics [2]. Researchers can further advance shoe design to improve user running mechanics and economy by adjusting shoe features, such as adding carbon-fiber plates to the midsole [3]; however, it is unestablished how shoe heel-toe drop affects running biomechanics and economy.

Shoe heel-toe drop affects user's ankle angle during stance. A higher heel-toe drop likely improves the ankle's effective mechanical advantage (EMA), thereby decreasing leg muscle-tendon force. Yet, muscle fascicle force may not systematically change due to a higher heel-toe drop. That is because a higher heel-toe drop likely shortens muscle fascicle operating lengths and increases pennation angles. The effect of better EMA and more rotated fascicles may elicit similar fascicle force across shoe heel-toe drops, causing muscle fascicle operating length to drive metabolic changes [4]. Thus, we hypothesized that a higher heel-toe drop would increase user metabolic energy expenditure during running.

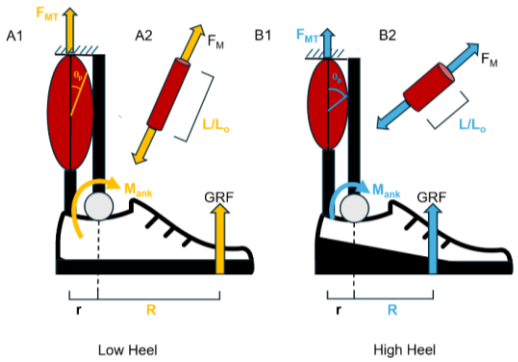

Figure 1: Prediction of how shoe heel-toe drop alters user running biomechanics.

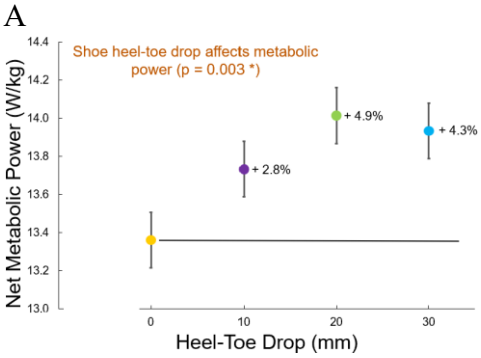

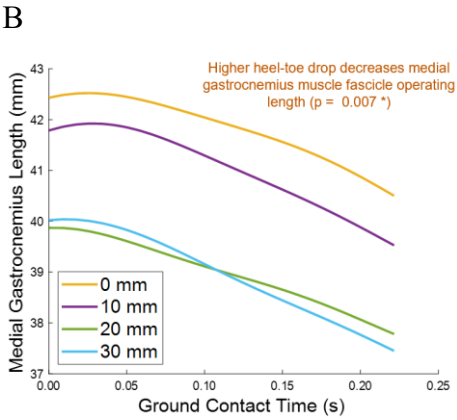

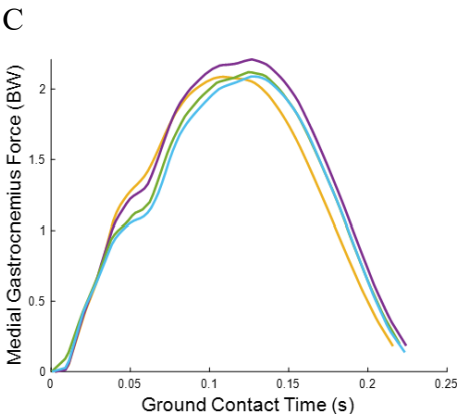

Figure 3. Higher heel-toe drop A. increases metabolic power, B. decreases muscle fascicle length, and C. elicits similar muscle force (n =2).

Methods: 20 runners participated. Participants performed a treadmill familiarization trial in their own shoes followed by 4 x 5-min running trials at 3.5 m/s. In each experimental trial, participants ran in a different pair of custom Nike Pegasus shoes that differed in their heel-toe drop: 0, 10, 20, & 30 mm (Fig. 2). We randomized shoe conditions and provided ≥ 5-min seated rest between trials. We computed net metabolic power, mechanics, and leg muscle activity during running in each shoe.

Figure 2: The running shoes we tested varied in heel-toe drop and were mass normalized with an EVA foam midsole.

Results & Discussion: Consistent with our hypothesis, higher shoe heel-toe drop increased user metabolic power ($p<0.001$). Running in shoes with a 30 vs. 0 mm heel-toe drop increased net metabolic power >4% (Fig. 3). There was not a systematic relationship between medial gastrocnemius (MG) force and shoe heel-toe drop, consistent with the trade-off between the contrasting effects of EMA and pennation angle. A higher shoe heel-toe drop shortened MG fascicle operating lengths at touch-down, toe-off, and on average during stance ($p\leq0.025$) (Fig. 3). Shoe heel-toe drop did not affect MG average or peak muscle fascicle velocity during stance ($p\geq0.081$). Running in higher heel-toe drop shoes decreased the average vertical ground reaction force ($p = 0.014$), lengthened ground contact time ($p = 0.015$), but did not affect stride frequency ($p = 0.682$). Across all shoe conditions, stride average tibialis anterior muscle activation did not change; however, in higher vs. lower heel-toe drop shoes, stride average lateral gastrocnemius muscle activation decreased ($p=0.067$) while soleus muscle activation increased ($p=0.235$).

Significance: Running in shoes with a lower heel-toe drop enables calf muscles to operate at longer, more economical lengths [4]. Accordingly, shoes with a lower heel-toe drop reduce user metabolic energy expenditure during running, and in turn likely improves their distance-running performance.

References: [1] Daniels (1985), Med Sci Sports Exerc. [2] Moore (2016), Med Sci Sports. [3] Hoogkamer et al. (2018), Sports Med. [4] Beck et al. (2022), J Appl Physiol.

DETERMINING THE EFFECTIVENESS OF FOOTWEAR AS AN INTERVENTION FOR PLANTAR FASCIITIS IN FEMALE RECREATIONAL RUNNERS

*Kristyne Wiegand
[1]Eastern Washington University, Cheney WA, USA
*Corresponding author's email: kwiegand1@ewu.edu

Introduction: One of the most common overuse injuries in running is plantar fasciitis (PF). [1] Despite this high prevalence, the mechanisms that underlie the development, progression, and treatment of PF are not fully understood. Increased mechanical loading as a result of foot structure, training, and footwear, is considered a major risk factor. [2] Females have higher incidence rates, which may be due in part to a thinner plantar fascia, [3] potentially increasing the mechanical load on the tissue and thus elevating injury risk. Current treatments vary but include medication, physical therapy, surgery, or custom orthotics. An accessible and cost-effective alternative is the strategic use, and regular replacement of, footwear. Although existing research on footwear as a PF treatment is limited, especially within athletic female populations, appropriately selected and regularly replaced shoes have been found to alleviate PF pain. [4,5] Further, despite potential benefits to pain levels, there is mixed research on the effects of highly cushioned footwear on loading. [6,7] Therefore, the overall aim of the current study was to determine the efficacy of a footwear-based intervention for female recreational runners with PF. Specifically, this study assessed the differences in loading rate and subjective measures of pain during a 12-week footwear intervention comparing a neutral-cushion shoe to a high-cushion shoe. We anticipated that with the introduction of new shoes, both groups would experience a pain reduction throughout the intervention period. We also hypothesized greater pain reductions in the highly cushioned shoe despite greater instantaneous vertical loading rate (VLR) compared to the neutral shoe.

Methods: Twelve female recreational runners (41±8 y) diagnosed with plantar fasciitis, with self-reported pain in the past 30 days, participated. All were otherwise healthy with no recent lower extremity injuries and were running at least 10 miles per week. Data collection occurred over a period of 12 weeks, with a pre- and post-intervention testing session. Participants were assigned to high-cushion (MAX) or neutral-cushion (NEU) shoes in a counterbalanced manner. At pre-testing, participants completed a running and injury questionnaire and ran overground at a preferred pace in both their own and study shoes while kinetic data (1200 Hz) were collected. During the intervention, participants maintained training while logging weekly mileage and pain (0-100 scale). After 12 weeks in the new shoes, participants reported for post-testing, during which they ran in the study shoes only. Kinetic data were filtered with a fourth-order zero-lag Butterworth filter (50 Hz), and instantaneous VLR was calculated from the first 50 ms of stance. VLR was analyzed using a 2 (group) × 2 (time) mixed ANOVA and an independent t-test for habituated vs. new shoes at pre-test (α=.05). Visual trends of weekly pain levels were assessed, and pain scores were compared pre- and post-intervention with paired samples t-test (α=.05).

Results & Discussion: Based on reported pain levels in the pre- and post-intervention surveys, the introduction of new footwear significantly reduced pain over 12 weeks, regardless of shoe type ($p = .0006$). This supports previous findings that regular footwear replacement may mitigate plantar fasciitis symptoms. However, pain reduction in the MAX group was not significantly different than NEU. These results suggest that shoe cushioning was not fully responsible for the observed pain reduction. With regard to weekly pain levels, there was high variability in reported pain among participants, and individually from week to week (Figure 1). Further, there was no significant difference in VLR between habituated and new shoes during pre-testing ($p > .05$), indicating that the immediate transition to new footwear did not alter loading rate. There was also no significant interaction, nor group or time effects ($p > .05$) on VLR, thus MAX did not alter loading compared to NEU. These results align with previous equivocal findings regarding cushion and loading. [6,7] Additionally, there was no change in VLR from pre- to post-intervention. Overall, although replacing footwear may be an effective, low-cost strategy for managing plantar fasciitis symptoms, cushioning level does not appear to alter loading rate or provide additional pain relief. Future research should focus on individual factors influencing pain response or develop longer-term adaptations to footwear interventions.

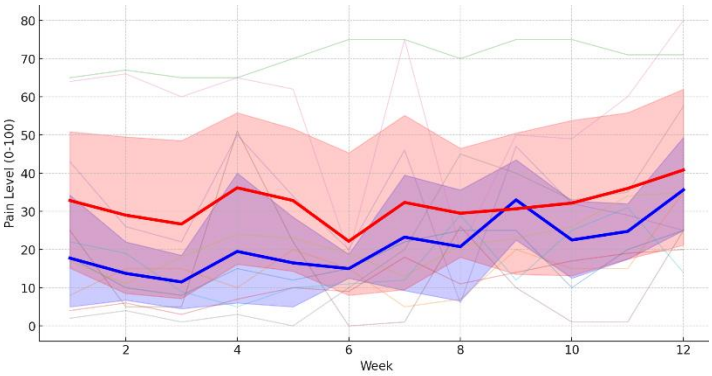

Figure 1: Pain levels over the 12-week intervention. Faded lines represent individual weekly reported pain, while the solid lines signify group averages (red = NEU; blue = MAX). Shaded areas represent 95% CI for each group.

Significance: In general, a reasonable approach to reducing plantar fasciitis pain lies in a focus on individual needs and preferences. Further, focusing on regular footwear replacement, regardless of shoe type, is a reasonable and easy-to-implement approach. Based on the lack of differences in vertical loading rate, pain relief is not linked solely to mechanics. These findings support the importance of individualized recommendations and the utilization of a variety of treatment approaches, tailored to a specific runners' needs.

Acknowledgments: Funding for this study was supported by the **ASB Junior Faculty Research Award.**

References: [1] Sobhani et al. (2013), *Scand J Med Sci Sports* 23(6); [2] Bolgla et al. (2004) *J Athl Train* 39(1); [3] Shiotani et al. (2019) *J Biomech* 85; [4] Umar et al. (2022) *J Fam Med Prim Care* 11(7) [5] Bishop et al. (2018) *BMC Musculoskelet Disord* 19(1); [6] Kulmala et al. (2018) *Sci Rep* 8(1); [7] Ogston (2019) *Footwear Sci* 11(1)

THE INFLUENCE OF RUNNING CADENCE MANIPULATION ON KNEE CARTILAGE DEFORMATION IN DISTANCE RUNNERS

*Ryan J. Evans[1], Harry S. Battersby[1], Tom Boers[1], Richard W. Willy[2], Derek N. Pamukoff[1]
[1]Western University, London ON
[2]University of Montana, Missoula MT
*Corresponding author's email: revans44@uwo.ca

Introduction: Patellofemoral pain (PFP) is a common injury in runners, [1] and may be linked to patellofemoral joint force (PFJF) and patellofemoral joint stress (PFJS). Increasing running cadence by 10% contributes to lower single step PFJF and PFJS. [3] As such, cadence manipulation has been used as an intervention for runners with PFP. However, it is unclear how running cadence manipulation influences acute cartilage response within the patellofemoral joint. We examined the influence of running cadence manipulation on femoral cartilage deformation in runners. It was hypothesized that (1) there would be greater cartilage deformation observed following the habitual cadence compared to high cadence run, and (2) that greater deformation would be associated with higher PFJF and PFJS.

Methods: Twenty-two runners participated (8 females and 14 males; Height=1.74±0.08m, Mass=67.3±7.8kg, Age=22.05±3.3years, Running Experience=6.2±3.4years, Self-Selected Running Speed=3.34±0.3m/s, Weekly Running Amount=51.9±29.1km, Habitual Cadence=162.8±6.2spm). Runners were included if they 1) ran at least 3 times per week for at least 16km 2) injury free for the preceding 6 months and 3) had a habitual cadence of ≤170 steps per minute. Participation began with a screening session to determine habitual cadence during a self-selected speed 10-minute run followed by 2 counterbalanced running sessions. The sessions included 30 minutes of supine rest, ultrasound imaging of femoral trochlear cartilage, a 5-minute warmup and 30-minute run with a metronome playing the cadence for each session (Habitual and +10%), and post-run cartilage ultrasound imaging. Participants ran at their self-selected speed on a Bertec force instrumented treadmill surrounded by an 8-camera motion capture system and were outfitted with lab standard shoes and reflective markers. Kinematic (240 Hz) and Kinetic (2400 Hz) data were sampled for 10 seconds every 5 minutes. Cartilage images were obtained with the participants knee in 140° of flexion. Three images were collected, and a custom MATLAB script was used to trace the femoral cartilage, and thickness was measured from the medial, central and lateral regions by an investigator blinded to running condition. Cartilage deformation was calculated as the difference between pre- and post – thickness measurements, and a positive value indicates greater deformation. A musculoskeletal model using an inverse-dynamics approach accounting for hamstring and gastrocnemius co-contraction was used to calculate peak PFJF and peak PFJS. [4] A 2 (condition) x 2 (time) ANOVA with repeated measures compared cartilage thickness between conditions. Spearman's rho assed the association between peak PFJF, PFJS and cartilage deformation; and a paired sample t-test compared peak PFJF and PFJS between conditions to confirm a difference in loading.

Results & Discussion: Paired sample t-tests revealed that peak PFJF ($p=0.004$) and peak PFJS ($p<0.001$) were lower in the high cadence (PFJF: 3.71 ± 0.94BW's, PFJS: 10.34 ± 2.90 mPA) compared to habitual cadence (PFJF: 4.49 ± 0.9BW's, PFJS: 12.35 ± 3.12 mPA) condition, which is consistent with previous literature. [3] No condition-by-time interactions (medial: $F_{1,21}=0.322$, $p=0.570$, central; $F_{1,21}=0.101$, $p=0.754$; lateral: $F_{1,21}=0.256$, $p=0.618$) or main effect of condition (medial: $F_{1,21}=947$, $p=0.341$; central: $F_{1,21}=0.114$, $p=0.739$; lateral: $F_{1,21}=0.580$, $p=0.455$) were found for cartilage thickness. As such, increasing running cadence may not influence acute cartilage deformation despite lower peak PFJF and PFJS. A main effect of time was found for medial ($F_{1,21}=6.575$, $p=0.018$) cartilage thickness, but not central ($F_{1,21}=2.572$, $p=0.124$), or lateral ($F_{1,21}=0.497$, $p=0.489$) cartilage thickness (Table 1). Regardless of running cadence condition, the medial region of cartilage underwent a similar deformation. Habitual cadence peak PFJF and peak PFJS were not associated with the change in cartilage thickness in the medial, central, or lateral regions (all rho <0.183, p>0.415). High cadence peak PFJF was not associated with the change in cartilage thickness (all rho <0.359, p>0.101). However, peak PFJS was associated with change in medial (rho=0.511, p=0.015) cartilage thickness, but not the change in central or lateral cartilage thickness (all rho <0.111, p>0.623). Therefore, peak PFJS may only influence cartilage in the medial region during high cadence running, which may be due to different kinematics and joint contact patterns when utilizing high cadence running.

Table 1: Cartilage Thickness Pre- and Post- Running Sessions (Mean ± SD)

	Habitual Cadence		High Cadence	
	Pre	Post	Pre	Post
Medial (mm)	2.09 ± 0.31	2.02 ± 0.32	2.05 ± 0.31	1.96 ± 0.3
Central (mm)	2.58 ± 0.41	2.62 ± 0.37	2.55 ± 0.39	2.61 ± 0.43
Lateral (mm)	2.17 ± 0.42	2.13 ± 0.41	2.13 ± 0.37	2.12 ± 0.37

Significance: Lower peak PFJF and PFJS were observed during high compared with habitual cadence running, but no differences in cartilage response was observed between conditions. Both running conditions contributed to cartilage deformation that may benefit joint health as it may facilitate the diffusion of new nutrients into the cartilage matrix for positive adaptations to occur. A higher peak PFJS may contribute to greater medial cartilage deformation in high cadence running.

Acknowledgments: This project received funding from the Natural Sciences and Engineering Research Council of Canada (RGPIN-2022-04804, PI: DN Pamukoff), the Canadian Foundation for Innovation John R. Evans Leader Fund (Project ID: 42110, PI: DN Pamukoff) and the Ontario Graduate Scholarship 2024-2025 (RJ Evans).

References: [1] Kakouris N et al. (2021) *J Sport and Health Sci* 10(5). [2] Eijkenboom JFA et al. (2018) *Bone Joint Res* 7(9). [3] Lenhart RL et al. (2014) *Med Sci Sports Exerc* 46(3). [4] Messier SP et al. (2011) *Osteoarthritis and cartilage* 19(3).

EFFECTS OF RUNNING SPEED ON LIMB COORDINATION WITHIN THE FRAMEWORK OF THE UNCONTROLLED MANIFOLD ANALYSIS

Joelle F. Dick [1*], Alena M. Grabowski [2], Young-Hui Chang[1]
[1] School of Biological Sciences, Georgia Institute of Technology, Atlanta, GA, USA
[2] University of Colorado Boulder, Boulder, CO
*Corresponding author's email: jdick7@gatech.edu

Introduction: Running is a complex motor skill requiring precise control of multiple body segments. Speed may alter key biomechanical variables, imposing constraints on limb coordination strategies. Prior research indicates that increased speed reduces dynamic limb stability [1]. Although the effects of speed on biomechanics and physiological responses have been studied, the relationship between these responses and performance remains unclear. This study aims to quantify the effects of speed on motor coordination strategies by analyzing variance in joint kinetics. We hypothesized that as task constraints increase, joint torque variance is structured to stabilize task-relevant variables (i.e. vertical ground reaction force).

Methods: 14 participants participated in the Intermountain Healthcare IRB approved protocol. *Experimental Data collection:* Participants were instructed to run on an instrumented treadmill (Treadmetrix, Park City, UT) at a range of speeds up to maximum speed. We incremented speed from 3 m/s to maximum speed in 1 m/s increments until participants approached maximum speed and then smaller increments were employed. Motion capture (300 Hz) data (Motion Analysis Corporation, Santa Rosa, CA), ground rection force (1000 Hz) data, and Visual3D software (C-Motion, Inc., Germantown, MD) were used to calculate joint kinematics and kinetics.
UCM Kinetic Model: A 3-segment kinetic MATLAB model was created to determine whether joint torques were coordinated to stabilize force within the stance phase of a stride cycle [2]. A Jacobian matrix was derived using segment angles and joint torques averaged over the entire cycle. IMA (Index of Motor abundance) values were calculated for the running speeds of 3.0m/s up to 9.0m/s. The IMA for each speed were averaged across subjects.

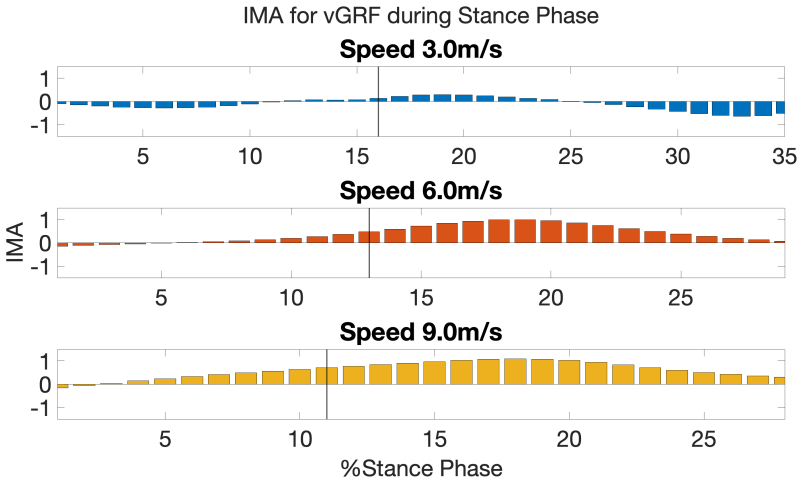

Figure 1: Index of Motor Abundance (IMA) strategies for running at **3.0 (n=12), 6.0 (n=12) and 9.0m/s (n=6)** running. Stabilization of vertical ground reaction force (vGRF) occurred when IMA was greater than zero. Black vertical line indicates time of peak vGRF.

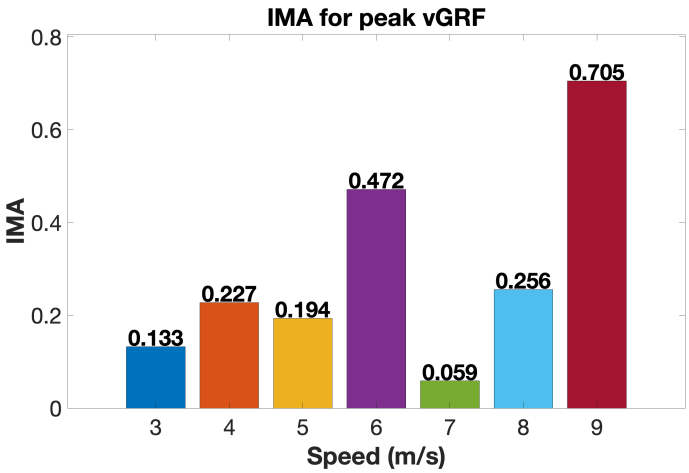

Figure 2: IMA at peak vGRF for running at **3.0 (n=12), 4.0 (n= 14), 5.0 (n=13), 6.0 (n=12), 7.0 (n=11), 8.0 (n=7) and 9.0 m/s (n=6)**.

Results & Discussion:
A UCM analysis revealed that joint torque variance was structured to stabilize vertical ground reaction force (vGRF) at mid- and late- stance and on average was greater at 9 m/s versus 3 m/s, as indicated by an IMA value greater than zero (Fig. 1). At 9.0 m/s, the IMA value at peak vGRF increased versus the slower speeds measured (Fig. 2), suggesting improved vGRF control despite more variable joint torques. The increase in IMA with faster running speed indicates that runners adopt a flexible coordination strategy, structuring their joint torque variance to maintain vGRF stability. Further analysis will extend to participants with a transtibial amputation who use running prostheses to determine whether similar strategies are employed or if unique adaptations emerge due to prosthesis use.

Significance: These preliminary results provide additional context on how athletes coordinate limb dynamics to maintain control of performance during running and sprinting. Sprinters must increasingly use coordinated joint torque combinations that stabilize limb force as they run at greater speeds; a strategy that may be less accessible by runners with a leg amputation

References: [1] Look et al. (2013), Chaos 23(4)., [2] Yen et al. (2009), Exp Brain Res. 196(3):439-51.

EFFECTS OF SPEED, LOAD, AND SURFACE ON TIBIAL BENDING AND STRESS

Thomas A. Wenzel[1*], Eric B. Francis, Tyler N. Brown[1]
[1]Department of Kinesiology, Boise State University, Boise, ID
*Corresponding author's email: thomaswenzel@u.boisestate.edu

Introduction: Tibial stress fracture is a destructive overuse injury commonly suffered by runners and military personnel. Tibial stresses that produce bone microdamage accumulation and eventual injury may stem from hazardous tibial bending. Resultant tibial bending, which reportedly bends the bone in posterior and medial directions, is purportedly responsible for 70–80% of tibial stress [1]. Considering tibial bending is attributed to both internal (i.e., muscle and related joint moments) and external (i.e., joint reaction) forces, factors like speed, body borne load, and surface that increase these forces may produce greater resultant tibial bending and elevate bone stresses [1]. But, the impact of specific locomotion factors on tibial bending is not yet fully understood. We hypothesize that locomotor speed and body borne load will increase tibial bending and stress, while an uneven surface will decrease resultant tibial bending.

Methods: 14 recreational runners had lower limb biomechanics quantified during a jog (3.0 m/s) and run (4.5 m/s) over a flat and uneven surface with and without 15 kg body borne load. The flat surface consisted of wood panel, while the uneven surface consisted of wood panel with rock-climbing modules secured randomly. For the 15 kg load, participants wore a weighted vest. During each trial, synchronous 3D marker trajectories and GRF data were collected using ten high-speed optical cameras (240 Hz) and a single force platform (2400 Hz). Then, lowpass filtered (12 Hz, 4th order Butterworth) and processed in Visual3D obtain lower limb biomechanics.

Custom Matlab code was used to estimate tibial stress. Specifically, axial stress at the distal third of the tibia and bending moments along with their AP and ML components were calculated according to the methods described by [2], using internal muscle forces and external joint reaction forces according to [3]. The resultant magnitude of the previously calculated AP and ML moments and stress was calculated to represent off-axis bending at the distal third of the tibia.

Total axial stress and the AP, ML components of both stress and bending, and the resultant bending moments and stresses were submitted to repeated measures ANOVA to determine the effect of speed and surface, with alpha level was 0.05.

Results & Discussion: In agreement with our hypothesis, the increase in speed and addition of body borne load lead to greater tibial bending and stress. Specifically, AP, ML, and resultant bending moments and stress increased 12-15% during the run and 7% with the 15 kg body borne load (all: $P < 0.001$) (Fig. 1). These large increases in resultant bending and tibial stresses may increase bone microdamage and stress fracture risk at faster speeds and with body borne load.

Supporting our hypothesis, the uneven surface decreased peak bending moments and tibial stress. Participants exhibited a 5-9% decrease in peak bending moments and tibial stress on the rocky surface (all: $P<0.022$) (Fig 1). Running over an uneven surface, such as the chosen uneven surface, shifts lower limb muscular work production away from the ankle, up the kinetic chain [4]. This reduction in ankle work stems may result in decreases in force from the associated musculature when traversing uneven surfaces. Considering internal, i.e., muscular, ankle forces are the largest contributor to tibia stresses and bending moments the irregular, uneven surface may shift work production up the distal chain, and result in the observed decreases tibial stress and bending [4]. But, considering mean tibial stresses and bending moments did not significantly decrease ($P = 0.061$) on the uneven surface, further study is needed to determine if the smaller peak tibial bending reduce bone microdamage accumulation, lowering tibial stress fracture risk.

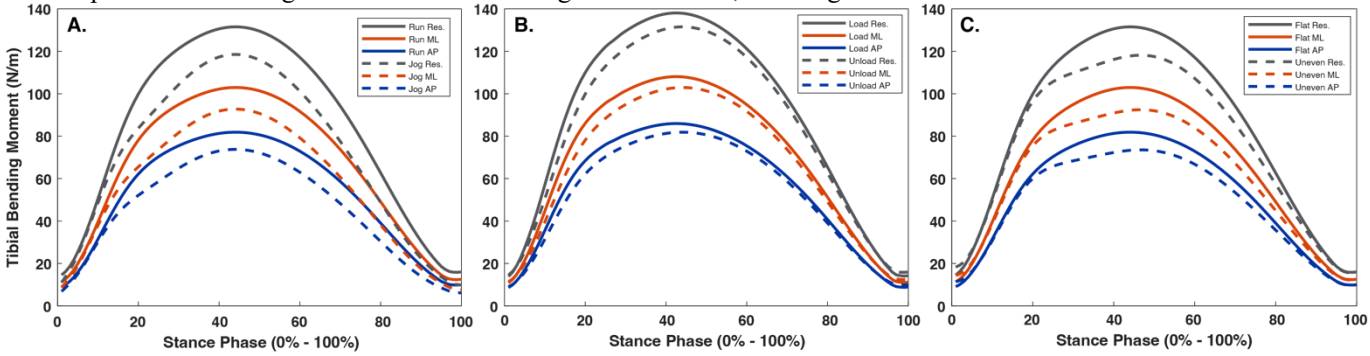

Figure 1: Depicts bending stress moment for the resultant, AP and ML axis for differing speeds (A), load (B), and surface (C).

Significance: An increase in locomotor speed and addition of body borne load increase tibial stress and subsequent injury risk. But, locomotion over uneven surfaces may not increase peak resultant bending and tibial stress. Bone stress injuries are a large issue for recreational runners. Although training at faster speed or with borne load may increase tibial stress fracture risk, performing training activities on irregular, uneven surfaces, such as trails or uneven paths, may not further elevate injury risk. Considering the external factors that increase tibial stress and bending during training activities may be necessary for a beneficial reduction in the occurrence of these common running injuries for recreational runners and military personnel.

Acknowledgments: NIH NIGMS (2U54GM104944, P20GM109095, P20GM148321) supported this work.

References: [1] Derrick et al. (2016), *J Biomech* 49; [2] Rice et al. (2019), *MSSE* 51(11); [3] Hamner et al. (2010), *J Biomech* 43(14); [4] Schrøder et al. (2022), *J Biomech* 141.

BIOMECHANICAL ADAPTATIONS IN RUNNERS WITH MEDIAL TIBIAL STRESS SYNDROME AND TIBIAL STRESS FRACTURES: A GROUND REACTION FORCE AND LOAD RATE ANALYSIS

Ryan M. Nixon[1,2*], Sharareh Sharififar[1,2], Matthew S. Martinson[1,2], Kevin R. Vincent[1,2], Heather K. Vincent[1,2]
[1]Department of Physical Medicine and Rehabilitation, [2]UF Health Sports Performance Center
*Corresponding author's email: ozswinem@ufl.edu

Introduction: Medial tibial stress syndrome (MTSS) and tibial stress fractures (TSF) are among the most prevalent running-related injuries, and both are believed to arise from insufficient adaptation to mechanical loading. Differences in the ground reaction force (GRF) and load rate (LR) characteristics during loading and unloading may provide insight into injury-specific responses. Traditional GRF analysis often focuses on discrete metrics such as peak impact forces and LR magnitudes in specific regions of interest; however, such approaches may overlook critical timing and waveform characteristics that reflect injury status. To improve GRF analysis, we implemented a double-Gaussian model for high-resolution time series force data [1]. This approach examines GRF waveforms in more detail, capturing the biphasic loading pattern of running. The study aimed to characterize multidimensional GRF features, including net force, medial and lateral ground reaction forces, full LR waveforms, and force redistribution strategies. These metrics were compared across four groups: uninjured controls (control), runners with symptomatic MTSS, and those recovering from TSF (either unilateral [UL] or bilateral [BL]; 4-8 months post).

Methods: A total of 80 runners were analyzed, including symptomatic MTSS (n=21), recovering TSF (n=19; UL n=14 and BL n=5), and matched healthy controls (n=40). GRFs were measured at 1200 Hz as participants ran at a self-selected speed on a zero-grade instrumented treadmill. Raw net GRF data were normalized to body weight and stance time, then averaged over at least 10 steps per participant. A double-Gaussian function was employed to model the biphasic force pattern of running gait, distinguishing between the initial impact phase (lower extremity striking the ground) and the active phase (bodyweight loading and unloading). The Gaussian parameters were used to describe the relative differences and shape change based on injury conditions. LR was calculated using the central difference numerical derivative of the raw normalized net force data. A one-way ANCOVA was performed to compare key GRF and LR characteristics across groups.

Results & Discussion: Significant GRF and LR metric differences were observed across the four groups (all $p<0.05$). MTSS had higher than average max medial forces, and BL TSF runners exhibited nearly double the maximum medial forces compared to controls ($p<0.001$), reflecting altered mediolateral loading strategies that may contribute to stress redistribution along the tibia. Compared to uninjured controls, the MTSS and UL TSF groups exhibited significantly lower peak LR values ($p<0.01$), suggesting a potential protective adaptation to reduce tibial loading. Conversely, the BL TSF group demonstrated elevated peak LR ($p<0.01$), suggesting a compensatory response to this previous injury. Temporal characteristics of LR also varied across groups. Controls and UL TSF subjects exhibited distinct early stance unloading (negative LR) during the braking phase, whereas MTSS and BL TSF runners showed continuous loading throughout this period (Fig. 1.B). Asymmetries in GRF timing and LR waveforms further differentiated injury subgroups. The BL TSF group displayed significant inter-limb discrepancies in the timing of active phase loading and secondary LR peaks, whereas UL TSF participants maintained more symmetrical loading patterns ($p<0.05$). These findings suggest that unilateral stress fractures may promote localized compensatory adjustments, but bilateral injuries elicit broader alterations in gait mechanics that could predispose runners to persistent loading imbalances.

Significance: These findings highlight the unique biomechanical characteristics associated with MTSS and TSF recovery. The observed differences in GRF waveforms and medial loading underscore potential diagnostic applications and intervention opportunities. Runners with symptomatic MTSS and recovering from BL TSF may benefit from rehabilitation strategies to reduce excessive medial reaction forces.

Acknowledgments: The UH Health Sports Performance Center and the UF Strategic Funding Initiative, Sports Collaborative, supported this work.

References: [1] *Alternative preprocessing techniques may unveil distinctive ground reaction force dynamics related to the presence of running-related injury*, Nixon et al. ASB 2024

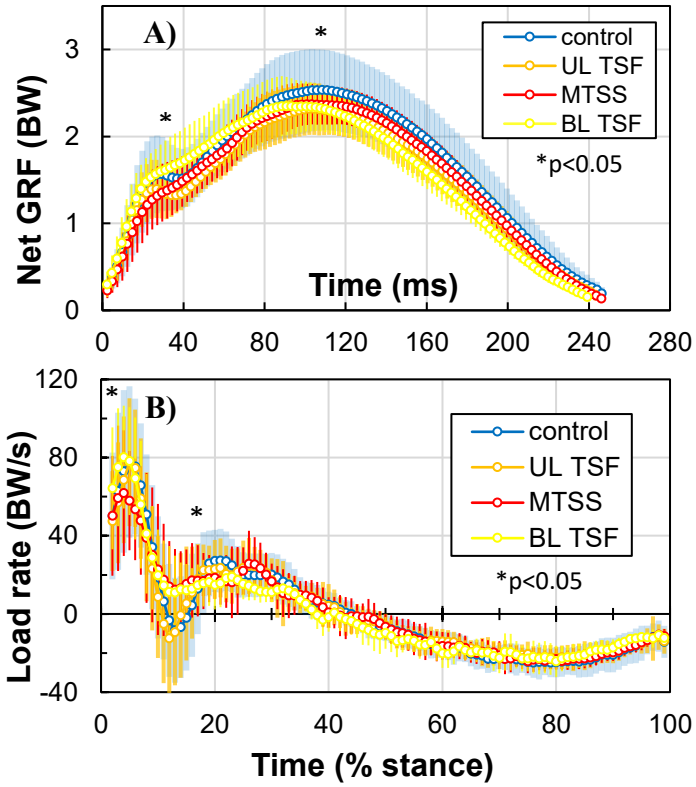

Figure 1: A) Net GRF vs time; means shown with error bars ±SD **B)** Load rates for the entire stance phase; regions of significant variance indicated with an asterisk

DISTAL RESIDUAL LIMB SOFT TISSUE STRESSES IN TRANSFEMORAL AMUPTEES ARE ASSOCIATED WITH MODIFIABLE PROSTHETIC SOCKETS GEOMETRY PARAMETERS

*Tom Gale[1], Paige Paulus[1], Goeran Fiedler[2], William Anderst[1]
[1]Biodynamics Lab, Department of Orthopaedics, University of Pittsburgh
[2]School of Health and Rehabilitation Sciences, University of Pittsburgh
*Corresponding author's email: tom.gale@pitt.edu

Introduction: There are approximately 29,000 cases of above knee amputations recorded in the United States every year [1]. Artificial limbs are generally connected to the residual limb with a socket prosthesis that facilitates weight bearing, suspension, and force coupling. Prolonged loading of soft tissue adjacent to bone has been shown to lead to degeneration of surrounding muscle tissues [2]. For socket prosthetic users, this type of soft tissue loading is inevitable. Although a previous study has measured skin movement within the socket prosthesis [3], deeper soft tissue mechanics have not been sufficiently quantified, especially during everyday activities. It is also unknown to what degree socket geometry, which is the most modifiable parameter in patient-prosthetic relationship, influences these internal stresses. This ongoing study aims to determine if internal soft tissue stress of the distal residuum correlates to specific key socket design parameters. It was hypothesized that proximally supportive and looser socket designs will increase localized internal soft tissue stresses compared to distally supportive tighter socket designs due to differences in restriction of distal femur motion.

Methods: Following institutional review board approval and informed consent, persons with unilateral transfemoral amputations were enrolled in the study [4]. A key inclusion criterion was the ability to ambulate without the use of assistive devices. Participants were cast and fitted for 4 custom check sockets by a licensed prosthetist. One check socket was modified during the lab visit to create two additional sockets, yielding a total of 6 socket fits (standard of care (SoC), 6% under volume, sub-ischial (SI), ischial containment (IC), quad, and pliable material). Approximately 40-60 radio-opaque beads (1.6-2.0mm diameter) were glued to the participants' residual limb, then usual donning of the liner and socket was performed. The beads and the distal residuum-socket interface were imaged using biplane radiography (100 images/sec, 80kV, 125mA maximum, 1ms pulse width, 2s trial duration) while participants walked at a self-selected pace (0.77±0.20 m/s) on a treadmill. CT scans of the residual limb were also obtained. The bead locations were tracked using radiostereometric analysis (RSA) and processed as previously described [3]. The residual bone motion was tracked using previously validated model-based tracking technique [5]. FEBio was used to create a finite element model of the distal residuum including skin, fat, muscle, and bone (Figure 1). Skin deformation was modeled from the bead positions, the muscle and bone were segmented from the CT scan, and the remaining space was filled with the fat material. Skin motion calculated from the beads and the residual femur motion from the model-based tracking were input into FEBio as boundary conditions, creating a displacement driven model. Material properties of each tissue were set to values from literature for similar soft tissues [6, 7], and bone was set as a rigid body. The residual limb was divided into anatomic quadrants (anterior, posterior, medial, and lateral) and the peak compressive 1st principal stress over the first 30% of stance phase, per quadrant, was calculated. Generalized estimating equations (GEE) were used to test the effects of socket designs on regional maximum stresses of both skin and muscle.

Results & Discussion: Data from 19 sockets across 4 participants was included in this interim analysis. The maximum stress in the lateral region of the muscle for the ischial containment socket was significantly greater than the sub-ischial socket (0.029±0.003MPa vs 0.021±0.006MPa; $p<0.001$). The maximum stress in the posterior region of the skin for the under-volume socket was significantly greater than the standard of care socket (0.079±0.027MPa vs 0.049±0.009MPa; $p=0.004$). The difference in lateral region muscle stress may be related to the lateral movement of the distal femur during the early portions of stance, which has been previously reported [6]. Ischial containment type sockets rely on the proximal lip to provide stability of the socket-residuum interface, whereas sub-ischial sockets by design provide stabilization of the residuum using more distal geometric features. This proximal stabilization could reduce the amount of distal area stabilization required, increasing localized stress from excessive distal bone movement. The increase in skin stress from reduction of the socket volume was expected simply from fitting the residuum into a reduce volume.

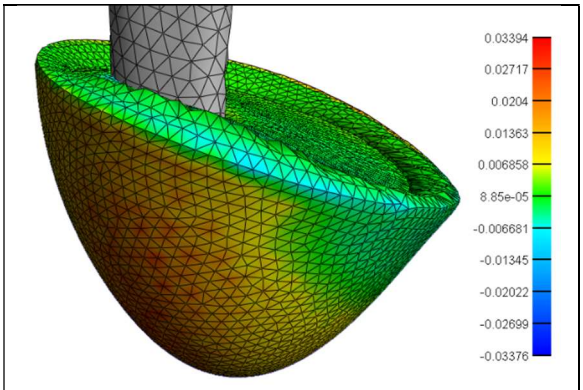

Figure 1: Example output model with 1st principal stress shown at foot strike. The higher compressive stress on the left side of the image represents the lateral quadrant and the right side of the image represents the posterior quadrant.

Significance: The present study is the first to combine radiostereometric analysis and model-based tracking techniques to create dynamic models of the residual limb within a socket during an activity of daily living. Refinement and validation of the model may lead to models that can predict differences in soft tissue response to socket design change, which will reduce time to creation for a patient's final socket, reduce cost, and reduce focused areas of high tissue loading leading to improved residual limb health.

Acknowledgments: This work was supported by the Department of Defense Office of the Congressionally Directed Medical Research Programs (CDMRP) through the Restoring Warfighters with Neuromusculoskeletal Injuries Research Award (RESTORE).

References: [1] U.S. Department of Health & Human Services (2021); [2] Ceelen et al. (2008), *J Biomech*; [3] Gale et al. (2021), *J Biomech*; [4] Anderst et al. (2022), *Trials*; [5] Anderst et al. (2003), *J Biomech Eng*; [6] Comley et al. (2010), *Int J Solids Struct*; [7] Feng et al. (2018), *Sci Rep*; [8] Gale et al. (2020), *J Biomech*.

OPTIMAL POWERED ANKLE PROSTHESIS TORQUE PROFILE TO REDUCE KNEE JOINT LOADING DURING WALKING FOR INDIVIDUALS WITH UNILATERAL TRANSTIBIAL AMPUTATIONS

*Eric H. Hu[1], Glenn K. Klute [2], Richard R. Neptune[1]
[1]Walker Department of Mechanical Engineering, The University of Texas at Austin, Austin, TX
[2]Center for Limb Loss and MoBility, Department of Veterans Affairs, Seattle, WA
*Corresponding author's email: eh32733@my.utexas.edu

Introduction: Prosthetic devices provide valuable assistance for individuals with unilateral transtibial amputations (TTA) to effectively engage in daily activities. However, commonly prescribed passive prostheses do not provide sufficient ankle push off work, which has been found to increase intact limb (IL) loading during walking that can lead to an increased risk of knee joint osteoarthritis [1]. In addition, repetitive high loads at the socket-residual limb (RL) interface can increase the risk of soft tissue injury [2]. Commercial powered devices have demonstrated a reduction in indirect measures of IL knee joint loading over different walking speeds [3]. However, it is unclear whether there is a prosthetic ankle torque profile that can directly reduce knee joint loading for both limbs. Predictive simulations can identify causal relationships between torque profiles and the resulting joint loads that are difficult to obtain experimentally. Therefore, the objective of this study was to optimize the ankle torque profile of a powered prosthesis that minimizes IL and RL knee joint loading for individuals with TTA using a predictive forward dynamics simulation framework. We expected that an optimal torque profile exists that reduces both knee joint loads.

Methods: A 2D musculoskeletal model was modified within SCONE [4] to represent an individual with a unilateral TTA (9 degrees of freedom, and 20 Millard-type muscles). Muscle activations were described as a combination of a rise-fall pattern feedforward controller [5] and a muscle reflex feedback controller [6]. A coordinate actuator replaced the muscles spanning the right ankle joint and was controlled with an optimizable transient function and a proportional derivative control mechanism. Three optimizations were performed to optimize the actuator parameters for each of the following conditions: 1) a passive prosthesis tracking individuals with TTA experimental kinematic and ground reaction force (GRF) walking data to provide a baseline (PASS) [7], 2) a powered prosthesis tracking able-bodied experimental data (POW) [8], and 3) a powered prosthesis tracking able-bodied experimental data while minimizing the maximum knee joint loads (POWJL). The optimized prosthetic torques, peak knee joint loads and net prosthetic work were compared across conditions.

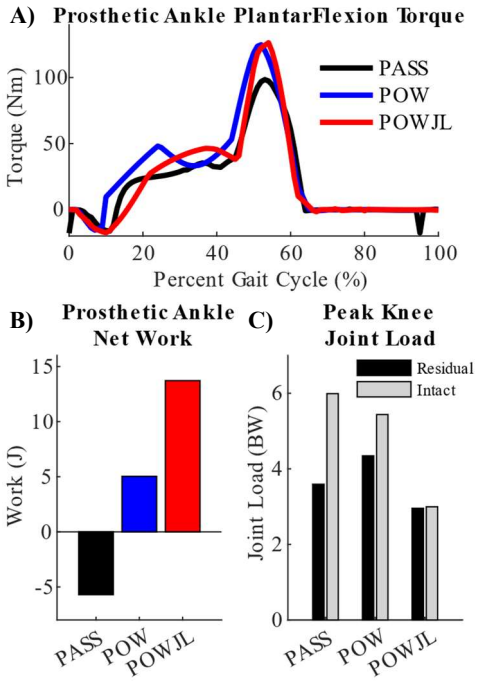

Figure 1: (A) Optimized prosthetic ankle torque, **(B)** net prosthetic ankle work and **(C)** peak knee joint load for passive prosthesis (PASS), powered prosthesis tracking able-bodied experimental data (POW) and powered prosthesis tracking able-bodied experimental data while minimizing max knee joint load (POWJL).

Results & Discussion: All simulations tracked the experimental kinematics and GRF data within two standard deviations of the mean. The optimal torque profiles for the powered conditions exhibited an overall increase in plantarflexion torque compared to the PASS condition during mid- and late-stance, while the timing of the plantarflexion torque varied in early and mid-stance between the three conditions (Fig. 1A). The PASS condition produced negative net work, which was consistent with other studies [9]. In contrast, the net work from the powered conditions was positive and increased nearly three-fold from the POW to POWJL condition (Fig. 1B). The increase in net work led to a decrease in the peak IL knee joint load (Fig. 1C). This result is consistent with previous research suggesting increased mechanical work from a prosthetic ankle can potentially reduce IL joint loads [1, 3]. The peak RL knee joint load increased from the PASS to POW condition, but the difference in joint loads between limbs decreased. This suggests that individuals with TTA walking with an able-bodied gait pattern does not necessarily reduce the joint loads on both limbs, but rather it improves joint load symmetry. For the POWJL condition, the additional increase in net work provided a further reduction in knee joint loading while also improving the joint load symmetry between limbs.

Significance: Findings from this study highlight the importance of the timing and magnitude of the torque profile to reduce knee joint loading with a powered ankle prosthesis. Although an optimal torque profile was found to exist, further prosthesis design considerations are needed to accommodate the increase in net work. Overall, this work provides a framework for developing more elaborate and customized controllers for powered prostheses to improve other biomechanical quantities in individuals with TTA gait.

Acknowledgments: This work was supported by the VA RR&D Service (RX003138 & RX002974).

References: [1] Morgenroth et al. (2011), *Gait Posture.* 34(4); [2] Mak et al. (2001), *J Rehabil Res Dev.* 38(2); [3] Grabowski et al. (2013), *J Neuroeng Rehabil.* 10(49); [4] Geijtenbeek (2019), *JOSS. 4*(38); [5] Ding et al. (2018) *Sci Robot. 3*(15); [6] Geyer and Herr (2010), *IEEE Trans Neural Syst Rehabil Eng. 18*(3); [7] Ardianuari et al. (2024), *J Biomech. 177*(112385); [8] Molina et al. (2023), *J Biomech. 157*(111731); [9] Fey et al. (2011), *Clin Biomech*. 26(10).

GLENOHUMERAL SECONDARY KINEMATICS AND JOINT CONTACT DURING UNLOADED TASKS: A SIMULATION STUDY

Morgan Dalman, M.S.[1*], Katherine R. Saul, Ph.D.[1]
[1]Department of Mechanical and Aerospace Engineering, North Carolina State University, Raleigh, NC, USA
*Corresponding author's email: ksaul@ncsu.edu

Introduction: Many clinical assessments of the shoulder use standardized planar motion (flexion/extension, abduction/adduction, internal/external rotation)[1], and as a result, many biomechanical analyses have examined glenohumeral loading and contact in the context of these motions. However, daily tasks engage the glenohumeral joint differently given the complex and three-dimensional nature of shoulder movement. Joint loading and contact are known factors in development of osteoarthritis and other shoulder pathologies[2,3], but difficult to assess clinically. Exploring glenohumeral contact in dynamic, multi-directional movement patterns is critical to understanding shoulder function and influence on potential pathology. Thus, the goal was to evaluate glenohumeral humeral head translation in an upper limb model during multiplanar unloaded upper limb tasks.

Methods: An existing upper limb musculoskeletal model representing a 50th percentile male adult[4,5] was augmented to include GH joint contact between the glenoid fossa and the humeral head with surfaces defined from MR images. Blankevoort ligaments[6] representing the coracohumeral, superior, medial, and inferior GH ligaments were included.[7] In addition, 13 representative ligaments for the glenohumeral capsule were included. Linear stiffness was defined from previous tensile strength studies.[8–10] Glenohumeral joint contact between the glenoid fossa and the humeral head was incorporated using the elastic foundation method.[11,12] Bone surfaces were duplicated, reduced, and meshed with triangles, then enlarged to create ~2 mm spacing to account for cartilage thickness on the humerus and glenoid.[13] The glenoid and humeral head articular cartilage were assigned an elastic modulus 2.2 and 4.2 MPa, respectively[14,15] and a Poisson's ratio of 0.45.[15]

Kinematic data for scaption, axilla wash, forward reach, hair comb, and upward reach to 115° movements previously collected were used for this study.[16,17] A set of 100 models were created using a trajectory method to select parameters for limb length, limb mass[21] and strength of the model.[18] Parameter ranges were determined from prior experimental data (Height: 150-190 cm; Weight: 110-220 lbs; Shoulder Strength: 40-85 Nm; Elbow Strength: 40-105 Nm)[18–22]. These models were used for simulations of the tasks using COMAK to predict humeral head translation. Statistical analysis was conducted using one-way Anova (GraphPad Prism 10, α=0.05).

Results & Discussion: The hair comb movement generated the greatest overall superior/inferior translation and was statistically different from all other movements ($p<0.0001$). Upward reach and axilla wash movements resulted in the greatest overall anterior/posterior translation and were statistically different from scaption, forward reach, and hair comb ($p<0.0001$).

Significance: This work provides insight into predicted humeral head translation during a variety of unloaded upper limb tasks relevant to activities of daily living. The outcomes of this work represent a critical step in understanding how the glenohumeral joint functions internally, and suggests that functional tasks require more glenohumeral translation than planar movement often used in clinical and lab settings.

Predicted Humeral Head Translation During Upper Limb Tasks

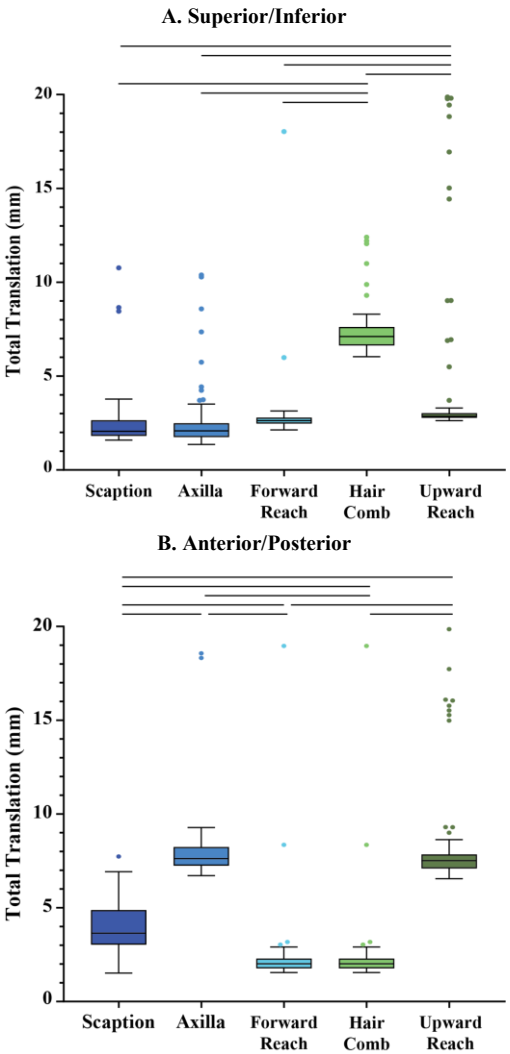

Figure 1: Total range of predicted humeral head translation for different unloaded upper limb tasks. Hair comb resulted in the greatest superior/inferior translation. Axilla wash and upward reach movements resulted in the greatest anterior/posterior translation and forward reach and hair comb movements resulted in the least amount of anterior/posterior translation.

Acknowledgements: Support was provided by NIH F31 (AR081691-02).

References: 1. Fenton, et al. 2022. *Trauma* 36(3). **2.** Jacxsens, et al. 2016. *J. Shoulder Elbow Surg.* 25(10). **3.** Paletta, et al. 1997. *J. Shoulder Elbow Surg.* 6(6). 4. Holzbaur, et al. 2005. *Ann. Biomed. Eng.* 33(6). **5.** Saul, et al. 2015. *Comput. Methods Biomech. Biomed. Engin.* 18(13). **6.** Blankevoort et al. 1991. *J. Biomech. Eng.* 113(3). **7.** Yang, et al. 2010. *Clin. Biomech.* 25(2). **8.** Bigliani, et al. 1992. *J. Orthop. Res.* 10(2). **9.** Boardman, et al. 1996. *J. Shoulder Elbow Surg.* 5(4). **10.** Moore, et al. 2005. *J. Biomech.* 38(6). **11.** Bei, et al. 2004. *Med. Eng. Phys.* 26(9). **12.** Smith, et al.. 2018. *Comput. Methods Biomech. Biomed. Eng. Imaging Vis.* 6(5). **13.** Schleich, et al. 2017. *Cartilage* 8(2). **14.** Huang, et al. 2005. *J. Biomech.* 38(4). **15.** Lenhart, et al. 2015. *Ann. Biomed. Eng.* 43(11). **16.** Vidt, et al. 2018. *Clin. Biomech.* 60. **17.** McFarland, et al. 2020. *J. Appl. Biomech.* 36(4). **18.** Holzbaur, et al. 2007. *J. Biomech.* 40(11). **19.** Holzbaur, et al. 2007. *J. Biomech.* 40(4). **20.** McFarland, et al. 2019. *J. Biomech. Eng.* 141(5). **21.** Saul, et al. 2015. *J. Appl. Biomech*. 31(6). **22.** Vidt, et al. 2012. *J. Biomech.* 45(2).

The Sensitivity of Glenohumeral Joint Arthrokinematic Variables to Different Calculation Methods

Stacey Chen, Marcie Harris-Hayes, Michael D. Harris, Rebekah L. Lawrence*
Program in Physical Therapy, Washington University School of Medicine, St. Louis, Missouri, USA
*Corresponding author's email: r.lawrence@wustl.edu

Introduction: Maintaining dynamic glenohumeral joint (GHJ) stability, defined as controlled movement of the humerus on the glenoid, is important for shoulder function. Impairments in GHJ stability may be key biomarkers of mechanical function in clinical populations [1]. One way to assess GHJ stability is through joint arthrokinematics, or the interaction between two joint surfaces during movement. However, the literature is highly variable regarding the extent to which arthrokinematics are impaired in clinical populations [2, 3]. The heterogeneity in findings could be substantially affected by the different methods used to calculate joint arthrokinematics [2, 4-6]. Hence, the purpose of this study was to investigate the sensitivity of GHJ arthrokinematics calculations to four published calculation methods.

Methods: This study utilized existing data of the dominant shoulder in asymptomatic individuals (n=54). Motion analysis was conducted during scapular plane abduction using a biplane videoradiographic system [7]. The humerus and scapula were segmented from CT scans and reconstructed into 3D surface meshes. 3D distance maps were calculated between the articular surfaces of the humerus and glenoid across all frames of data. A contact center was calculated on the glenoid using 4 methods: constrained unweighted centroid [2], constrained weighted (binned) centroid [4], constrained weighted (inverse square) centroid [5], and unconstrained unweighted minimum distance [6]. Constrained measures limited the contact center to a specific surface area on the glenoid (e.g., closest 200 mm^2), while unconstrained measures considered the entire surface. Weighted measures either biased the contact center towards mesh faces closer to the humerus (binned) or towards mesh faces that were closer and larger (inverse square). Unweighted measures considered the minimum distances to all mesh faces equally. The following GHJ arthrokinematics variables of interest were calculated across the motion trial and normalized to glenoid size: cumulative contact path length, average anterior-posterior (AP) and superior-inferior (SI) contact center position, and AP and SI contact center position range (Fig. 1). Preliminary results are provided descriptively (n=10). Once the full sample is processed (n=54), calculation methods will be compared using repeated measures ANOVAs or statistical parametric mapping ANOVAs based on the nature of the variable (e.g., scalar, time series).

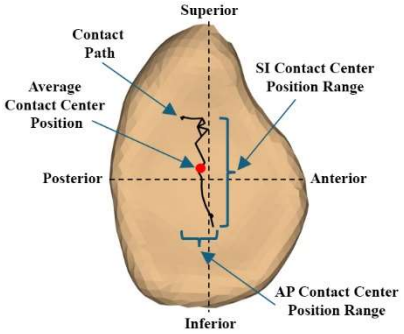

Figure 1. GHJ arthrokinematic variables. Solid line represents the excursion of the contact center during the motion.

Results & Discussion: The 3 centroid methods were descriptively comparable across methods while the minimum distance method tended to result in larger values (e.g., longer path, contact center farther from the glenoid center) (Table 1). This may reflect the nature of the calculation in that the minimum distance location is defined by a single point on the 3D distance map while the centroid is calculated as the weighted or unweighted average of many points across the surface. Thus, the contact center calculated using centroid methods may undergo less excursion across the glenoid during movement (i.e., shorter path length, smaller contact position range). Differences between centroid calculations may exist, especially in variables that are more cumulative in nature (e.g., path length) compared to temporal average measures (i.e., average contact center position) or instantaneous measures (e.g., contact center range). For example, the contact path length differed by up to 20% of the glenoid height across centroid methods, while the average contact position differed by less than 2%. Additionally, the difference between contact center position ranges differed by up to 5% of the glenoid height between the two constrained weighted centroid measures (binned and inverse square). Although the clinical meaningfulness of these differences remains unclear caution may be warranted when comparing the results of studies that use different calculation methods.

Table 1. GHJ arthrokinematics variables calculated using each calculation method normalized to glenoid size (mean ± standard error). Positive values represent anterior and superior directions relative to the glenoid center; negative values represent posterior and inferior directions.

	Calculation Method			
Variable	**Constrained Unweighted Centroid**	**Constrained Weighted (Binned) Centroid**	**Constrained Weighted (Inverse Square) Centroid**	**Unconstrained Unweighted Minimum Distance**
Contact Path Length	96.0% ± 12.2%	76.4% ± 9.2%	86.6% ± 13.3%	418.0% ± 54.5%
Average Contact Center Position				
Anterior/Posterior	-6.2% ± 2.0%	-5.1% ± 1.7%	-6.7% ± 2.1%	-8.1% ± 2.7%
Superior/Inferior	9.3% ± 2.7%	8.2% ± 2.7%	10.0% ± 2.8%	12.0% ± 4.1%
Contact Center Position Range				
Anterior/Posterior	14.2% ± 1.8%	13.4% ± 1.3%	15.4% ± 3.1%	36.0% ± 5.5%
Superior/Inferior	25.5% ± 3.5%	22.0% ± 2.7%	27.8% ± 3.7%	48.6% ± 5.3%

Significance: Descriptions of GHJ arthrokinematics may be sensitive to the calculation method used. These variations pose a challenge when synthesizing findings across studies that used different methods or when applying these methods to compare clinical populations (e.g., intact to torn rotator cuff) or to assess the effect of treatment (e.g., GHJ stabilization exercises).

Acknowledgements: This project was supported by the NIH (K99/R00-AR075876) and the Foundation for Physical Therapy Research.

References: [1] Lawrence, *J Biomech,* 2020;109. [2] Baumer, *OSJM,* 2016;4(9). [3] Miller, *J Shoulder Elbow Surg,* 2016;25(4). [4] Anderst, *J Biomech*, 2003;36(9). [5] Lawrence, *JoVE*, 2021;169. [6] Soslowsky, *JOR*, 1992;10(4). [7] Chen *Ann Biomed Eng*, 2024.

MULTIPLE, NOT SINGLE, RECIPIENT MUSCLE TENDON TRANSFERS ACCOMPLISH EVERYDAY GRASPING TASKS: A SIMULATION STUDY WITH APPLICATION TO POST-SCI GRASP-RESTORATIVE PROCEDURES

Oliver Garcia, *Joseph D Towles[1]
[1]Department of Engineering, Swarthmore College
*Corresponding author's email: joseph.towles@swarthmore.edu

Introduction: Grasp-restorative tendon transfer surgical procedures are performed to restore lateral pinch grasp after flaccid, cervical spinal cord injury (SCI) [1]. Post-surgical outcomes, however, have been mixed with pinch strength in individuals varying from approximately 150 g of force to ten times as much [2, 3]. We believe this is the case because such tendon transfer procedures only engage the flexor pollicis longus (FPL) muscle [1]. Flexor pollicis longus's intrinsic musculoskeletal properties are such that the muscle produces an endpoint force that is more directed toward slip during contact than maintaining the contact [4]. Previous tendon transfer simulation work in our group has shown the benefits of using a multiple-recipient-muscle tendon transfer approach to improve thumb-tip force production, as compared to that of FPL, during lateral pinch grasp [5]. In the multiple-recipient-muscle tendon transfer approach, the donor muscle is attached to multiple recipient muscles and the muscle force it generates is distributed across the recipient muscles and the resultant of that distribution is the grasp contact force. To date, it has not been shown that such a tendon transfer approach can produce endpoint forces that accomplish functional tasks, e.g., holding a fork. The goal of this study was to determine whether multiple-recipient-muscle tendon transfers could produce endpoint forces that accomplish activities of daily living (ADL). We hypothesized that such tendon transfers could do so because endpoint force production characteristics generally improve with more muscles involved [6].

Methods: We simulated 3D narrow-grip lateral pinch force production following multiple-recipient-muscle tendon transfer surgery–in which the donor muscle was attached to small groups of paralyzed muscles–using nonlinear optimization and in-situ, 3D measurements of individual muscle endpoint forces previously published [4, 5]. One hundred twenty-six groups of 4 muscles were formed from all possible 4-muscle combinations of the thumb's 9 muscles. The nonlinear optimization algorithm searched for all muscle combinations that accomplished the 12 ADL tasks or a subset of them described in Smaby et al. [7]. Example ADL tasks were pressing a TV remote control button, pulling a key out of its door-knob insert and inserting a fork into food. Each task, which was associated with frictional contact between the digits involved and the object of interest [8], posed 3D force magnitude and directional requirements on the grasp force and also the forces that each recipient muscle transmitted from the donor muscle. In the context of accomplishing each task, the optimization algorithm sought to minimize the difference between the produced tangential force and the force required for slip at the contact.

Results & Discussion: We found that 57 of 126 muscle groups accomplished one or more of the ADL tasks, as we hypothesized (Fig. 1). Notably, 23 muscle groups accomplished the most number of tasks, i.e., 9 of 12 tasks, up to and including inserting a fork into food ("Fork" ADL). These 23 muscle groups are a subset of the larger pool of groups that satisfied the endpoint force requirements of each activity shown to the left of "Fork" in Fig 1. Those 8 activities are completed by more muscle groups than "Fork" because they have less limiting force requirements than "Fork", that is, a smaller force magnitude in the direction required to complete the task (i.e., object force in Fig. 1), and/or a larger ("less slippery") frictional coefficient value. We would expect the group of 23 muscle groups, 3 of which are highlighted in the table insert (Fig. 1), to be capable of producing lateral pinch force vectors that can complete any activity with less stringent requirements than those investigated. The 3 remaining activities ("H Zip Close", "Plug Out", "Plug In") had more restrictive requirements than "Fork" and were not completed by any muscle group. Activities with limiting characteristics are completed by few groups because they require endpoint lateral pinch force vectors that are strong and nearly aligned with the palmar direction (Fig. 1).

Significance. With respect to long-standing guidelines for the design of tendon transfers [9], this study challenges the common notion that the donor muscle should attach to a recipient muscle(s) in a straight line fashion. Computational musculoskeletal and cadaveric surgical simulation tools make it tractable to consider this novel multiple-recipient-muscle tendon transfer approach where the lines of actions of donor and recipient muscles could intersect at an angle. This novel surgical approach has the potential for improved grasp-restorative surgeries after SCI.

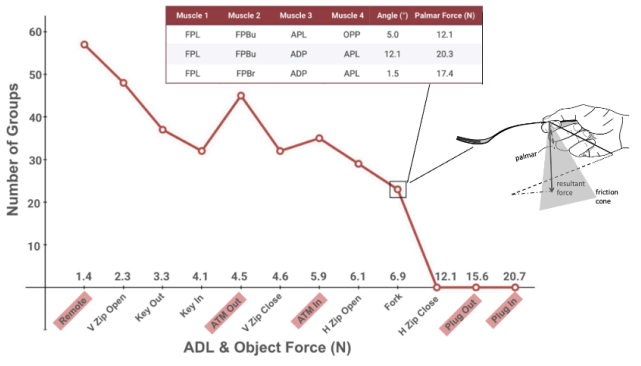

Figure 1. ADL Completion Frequencies. The number of muscle groups that completed each activity (vertical axis); associated object forces (horizontal axis), e.g., the force required to press a button on a remote control or the force required to insert a plug into an outlet; and frictional coefficient values are presented/indicated. The tasks highlighted in red have a frictional coefficient of 0.5 (plastic) while the others have a coefficient of 0.33 (aluminum) [8]. The table shows 3 example groups that completed 9 activities (up to "Fork"). The angle and palmar component of the grasp force vector, each group generates, are shown. The picture of the hand and fork is an illustration of the concept of the novel, simulated multiple-recipient-muscle tendon transfer in which the donor muscle is attached to multiple recipient muscles. The donor muscle force is distributed across each of the recipient muscles to produce a well-directed endpoint force to accomplish inserting a fork into food.

References: [1] Fox KI et al (2018), *Topics Spinal Cord Inj Rehabil*, 24(3). [2] Johanson ME et al (2016), *Arch of Phys Med Rehab*, 97. [3] Waters R et al (1985), *J Hand Surg [Am]*, 10A. [4] Towles et al. (2008), *Clin Biomech* 23(4). [5] Towles (2023), *Annu Int Conf IEEE Eng Med Biol Soc*. [6] Sharma, N, & Venkadesan, M (2022), *PNAS* 119(12). [7] Smaby et al. (2004), *J Rehab Res Dev* 41(2). [8] Buchholz et al. (2007), *Ergonomics*, 31(3). [9] Gardenier J et al (2020), *Indian J Plast Surg 53.*

HIGH-RESOLUTION NEUROMECHANICS OF THE HUMAN EYELID

Jinyoung Kim[1], Ashley Shirriff[2], Jordan Cornwell[2], Ereni Delis[1], Sophia Wang[1], Daniel Rootman[2], *Tyler R. Clites[1]
[1]Department of Mechanical and Aerospace Engineering, University of California, Los Angeles
[2]Stein Eye Institute, University of California, Los Angeles
*Corresponding author's email: clites@ucla.edu

Introduction: Crucial eyelid functions are driven by the *orbicularis oculi* muscle (OOM). The remarkably diffuse innervation of this complex muscle allows for precise sequencing of contraction required for wetting and protecting the eye, pumping tears to the outflow systems and maintaining complex facial expressions [1]. The complex activation-contraction dynamics of the OOM, which enable the large variety of eyelid behaviors, have not yet been rigorously studied due in part to technological limitations in the spatial and temporal resolution of measurement devices. Activation dynamics have primarily been measured via surface electromyography (EMG), which is prone to cross-talk and limited to low-electrode-count systems [2]. Furthermore, prior attempts to measure kinematics of eyelid using magnetic search coils [3], and high-speed video [4] typically focused on a single point on the eyelid margin. As a result, it is still not known how segmental activation differs between eyelid behaviors, nor how changes in activation produce the differential kinematics that are specific to each behavior.

To address these limitations, we present a novel strategy built on a combination of three-dimensional kinematics, high-speed video, and intramuscular EMG from a distributed array of fine-wire electrodes in both the upper and lower eyelid (Fig. 1A). This enables precise detection of segmental and sequenced OOM activation, synchronized to the resulting eyelid kinematics.

Methods: Distributed electromyography (EMG) and three dimensional kinematics were recorded from the eyelids of 8 persons without eyelid paralysis. Fourteen bipolar EMG fine wire electrodes were inserted into the upper and lower pretarsal and preseptal OOM (Fig. 1A), and EMG was recorded during five distinct eyelid activities (spontaneous blink, voluntary blink, reflexive blink, soft closure, and forced closure). Kinematics were tracked simultaneously with EMG at 5 points across the upper eyelid margin using a five-camera optical motion tracking system (Vantage, Vicon Inc., Oxford, UK). Key features were extracted from kinematics and EMG, and compared across behaviors. Muscle excursion was also estimated from strain between markers; this is uniquely possible in the eyelid margin because the OOM is attached to the skin along its length.

Results & Discussion: Significant differences in key kinematic features (onset medial traction and reverberation) were found between behaviors, corresponding to specific functions associated with those behaviors (Fig. 1B). These differential kinematics were explained by distinct sequences of muscle patterns that varied significantly between behaviors (Fig. 1C). Activation patterns also varied significantly across the eyelid, in a manner that could not be explained via single-point innervation. Spontaneous and voluntary blinks tended to activate medially, with subsequent lateral propagation. Reflexive blink and forced closure tended to activate equally across the eyelid, with significantly higher activation peaks and more transience in reflexive blink. These results show that the OOM is driven by complex sequences of segmental activation that differ between behaviors.

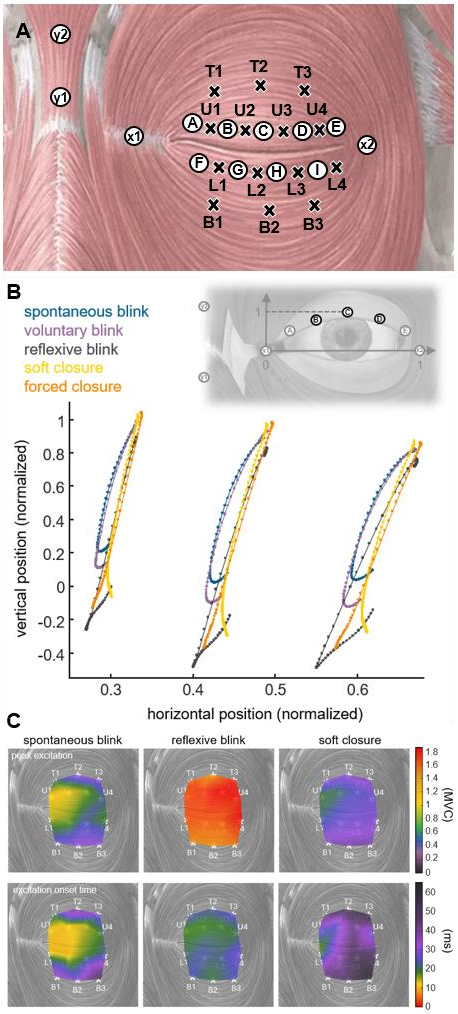

Figure 1: (A) Electrode (x) and marker (circle) placement in the *orbicularis oculi* muscle. (B) Inter-subject average upper eyelid kinematics for each behavior. (C) Map of peak excitation (top) and excitation onset time (bottom) for a selection of the behaviors.

Significance: Our approach has enabled us to study eyelid neuromechanics with unprecedented spatial and temporal resolution, shedding new light on the neurophysiology of this fundamental structure. Our results show that critical differences in eyelid behavior are driven by distinct activation sequences, which in turn drive distinct kinematic trajectories. This knowledge has critical implications for the diagnosis and treatment of eyelid paralysis, including the development of neuroprosthetic systems to restore eyelid function. For instance, artificial recreation of natural eyelid motions will likely require precise segmental recruitment of OO fibers, with independent control of activation timing and intensity. Current "all-at-once" stimulation approaches [5] are likely to create motions that mimic the protective functions of reflexive blink, rather than the natural wetting and tear-clearing functions of spontaneous blink. We anticipate that this work will also serve as a starting point for robust mechanistic models of eyelid function.

Acknowledgments: This work was supported in part by the NIH National Eye Institute (award #1R21EY036680-01)

References: [1] Rodriguez et al. (2018). Current Eye Research 43(1); [2] Frigerio et al. (2014). JAMA Facial Plast. Surg. 16(5); [3] Perez et al. (2011). Journal of Modern Optics. 58(19); [4] Kwon et al. (2013). J. R. Soc. Interface. 10(85). [5] Somia et al. (2001). Microsurgery. 21(6).

Thank you to our Sponsors

AMTI
FORCE AND MOTION

BIOEX
CONSULTING
EXCELLENCE · EXPERIENCE · EXPERTISE

THE BIOMECHANICS
INITIATIVE

MAYO
CLINIC

novel

University of Pittsburgh | Swanson School of Engineering Bioengineering